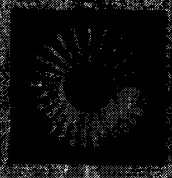

UNITED TECHNOLOGIES
SIKORSKY AIRCRAFT

Stratford, Connecticut 06601

UNITED TECHNOLOGIES
SIKORSKY AIRCRAFT

TITLE A Rotorcraft Flight/Propulsion Control Integration Study

DOCUMENT NUMBER SER-760606 (NASA CR-179574)

PREPARED UNDER Contract NAS3-24343

DOCUMENT DATE November, 1986

PERIOD COVERED June 1984 - June 1986

THIS DOCUMENT IS APPLICABLE TO THE FOLLOWING AIRCRAFT MODEL(S).

MODEL

PREPARED BY D.G.C Ruttledge CHECKED BY J.J. Howlett

APPROVED BY R.D. Murphy

REV.	CHANGED BY	REVISED PAGE(S)	ADDED PAGE(S)	DELETED PAGE(S)	DESCRIPTION	DATE	APPROVAL

A Rotorcraft Flight/Propulsion Control Integration Study

SER-760606

Contract NAS3-24343

November, 1986

D.G.C. Ruttledge

Sikorsky Aircraft

E.J. Hammon

Chandler Evans Inc.

D.R. Gilmore

General Electric

FORWARD

This report was prepared by the Sikorsky Aircraft Division of United Technologies Corporation for the National Aeronautics and Space administration, Lewis Research Center, Cleveland, Ohio, under Contract NAS3-24343.

Additional material from the Control Systems Division of Chandler Evans Inc. and the Aircraft Engine Business Group of General Electric Co., who were subcontractors to Sikorsky Aircraft for this contract, is incorporated throughout this report.

This contract, to conduct a study to identify benefits associated with an integrated flight/propulsion control system for rotorcraft, was funded and administered by the National Aeronautics and Space Administration, Lewis Research Center. Mr. J.R. Mihaloew was the Technical Monitor.

The authors wish to acknowledge the help of Messrs. E. Ackerman, I. Alansky, G. Clemence, F. Ebert, G. De Los Reyes and B.T. Wachter from the three companies, during the performance of this contract.

SUMMARY

An eclectic approach was taken to a study of the integration of digital flight and propulsion controls for helicopters. The basis of the evaluation was the current Gen Hel simulation of the UH-60A BLACK HAWK helicopter with a model of the GE T700 engine supplied by NASA.

A list of flight maneuver segments to be used in evaluating the effectiveness of such an integrated control system, was composed, based on past experience and an extensive survey of the recently acquired U.S. Army Air-to-Air Combat Test (AACT Contract D318) Data.

A number of possible features of an integrated system were examined and screened. Those that survived the screening were combined into a design that replaced the T700 fuel control and part of the control system in the UH-60A BLACK HAWK Gen Hel simulation. This design included portions of an existing "Pragmatic Adaptive" fuel control design by the Chandler-Evans company and an LQR based N_p governor design by the General Electric company, melded with changes in the basic Sikorsky Aircraft designed control system.

Some assessment of the design is presented here - the integrated system exhibited improved total system performance in many areas of the flight envelope. An expanded investigation is to be carried out on the VMS facility at NASA (Ames) in the near future.

TABLE OF CONTENTS

SA 1174

LIST OF FIGURES

LIST OF FIGURES (Cont'd)

LIST OF SYMBOLS

AACT	Air to Air Combat Tests
AFCS	Automatic Flight Control System
AGAIN	Np Governor Gain Adjustment
ALT	Altitude
A_R	System Coefficient Matrix Used in Observer in Np LQR
ASE	Automatic Stabilization Equipment (part of MGH controls module)
BCQDOS	A Rotor Stall Severity Indicator
B_R	Input Coefficient Matrix Used in Observer in Np LQR
BRMR	Flapping Angle of #1 Rotor Blade
C_D	Aerodynamic Drag Coefficient
CDP	Compressor Discharge Pressure
CLUEG	Engine Drive Clutch Engagement Flag
C_R	Output Coefficient Matrix Used in Observer in Np LQR
D318	Contract Number Colloquialism by which AACT results are known
DNPRAT	Rotor Decay Anticipation Increment on NPRATP in Np governor
DNPREF	Total Increment in Reference Np Value
ECU	Electronic Control Unit (isochronous part of baseline T700 fuel control)
EFCS	Electronic Flight Control System (employed on BLACK HAWK)
FPS	Flight Path Stabilization (outer loop part of EFCS)
g	Acceleration due to gravity
GEN HEL	A colloquialism for Sikorsky originated General Helicopter Simulation Program
i.c.	Initial conditions (e.g. for helicopter trim)
IHMUSE	Code to indicate logic state of baseline T700 fuel control
JEMAX	Number of engines simulated independently
Kp	A general factor
LGMR	Lagging angle of rotor blade #1
LQR	Linear Quadratic Regulator
$L\beta$	Coefficient of rolling moment due to sideslip (dihedral effect)
MCEP	Maneuver Criteria Evaluation Program
MGH	Master Generic Helicopter simulation system
NDOTDC	Decel. schedule output
NDOT, $\dot{N}g$ XNGDTE	Acceleration of gas generator
NG, PCNGC, XNGE	Gas generator speed
NGD	Winning input to $\dot{N}g$ governor
NGDGOV, NGTOP	Ng topping input to $\dot{N}g$ governor
NGDTL	Temperature limit input to $\dot{N}g$ governor
NMR	Average equivalent rotor tip speed estimated by observer in LQR
NPINTE	Trimmed i.c. on Np governor
Np, NPMEAS, N2RFE	Power turbine output speed
NR	Rotor speed
NZ	Normal acceleration of aircraft center of gravity
OMR.MR	Acceleration of rotor shaft
OMRMR	Speed of rotor shaft

SA 1114

LIST OF SYMBOLS (Cont'd)

OPSTAT	Operational status flag (for emergency high power engine conditions)
P	Aircraft roll rate
P2	Engine inlet pressure
PAS	Power Available Spindle angle (Pilot's cockpit control)
PHIB	Aircraft bank attitude
PI	Proportional plus Integral
PSIB	Aircraft heading
Q	Aircraft pitch rate
QHBMR, QMR	Torque absorbed by main rotor
QPTE1	Power turbine output torque
R	Rotor radius or aircraft yaw rate
RMODE	Code to indicate logic state of integrated fuel control
SAS	Stability Augmentation System
$T_{4.5}$, T45E, T45MEA	Temperature at power turbine inlet
THETAB	Aircraft pitch attitude
THETTR	Tail rotor collective pitch
Va/c, VKT	Aircraft airspeed
Vc	Aircraft climb speed
V_E	Aircraft ground speed in easterly direction
v.g.	Variable Geometry of engine compressor inlet guide vanes
V_{LOC270}	Blade tip speed at azimuth 270° (left side)
V_{LOC90}	Blade tip speed at azimuth 90° (right side)
VMS	Vertical Motion Simulator (at NASA Ames)
VYB	Aircraft velocity toward right
WF, WFCE	Fuel flow into engine
WFBG	Fuel flow requested by N_G Bottom governor
WFDEC	Fuel flow requested by N_G DECEL limiter
WFDMND	Fuel flow command from controller into stepper motor
WFHI	Fuel flow selected
WFNG	Fuel flow requested by $\dot{N}g$ governor
WFNP	Fuel flow requested by Np governor
XA+1, XAPC	Lateral stick movement
XB+1, XBPC	Longitudinal Stick Movement
XC+1, XCPC	Collective stick movement
XP+1, XPPC	Directional control pedal movement
X_R	Vector of state variables in LQR observer
Y_R	Vector of output variables in LQR observer
α	Local angle of incidence
β_E	Engine collective pitch anticipation
δ	Ambient pressure ratio
θ	Ambient temperature ratio
Ω	Rotor speed

SA 1114

1.0 INTRODUCTION

At the inception of this contract (June 1984), current helicopter design practice was to use fast microprocessors on a piecemeal basis to solve particular design problems. Sikorsky had successful operational digital Stability Augmentation Systems (SAS) and digital Automatic Flight Control Systems (AFCS). General Electric was involved in a contract (NAS3-22763) to provide the LQR design used at NASA (Lewis) in a full authority digital electronic control on the NASA T700 test engine. Chandler Evans had just finished its work on the digital EMC-85 control system for the Army 800 SHP Advanced Technology Demonstrator Engine (ATDE) developed by Detroit Diesel Allison, and as a follow-up was continuing to develop and test the adaptive control system simulations of the twin Allison C-30 engined Sikorsky S76 helicopter as well as flight testing it in an Allison owned and powered Bell 206L helicopter.

The engineering work in this contract attempted to indicate how the various sub-systems might be brought together (not necessarily in the sense of being in one micro-processor, but in the use and sharing of sensor data and computation of functions which might serve more than one purpose, or to which a priority hierarchy might be attached) in such a way as to promote the synergism of the total system. Thus, the objective was to identify the benefits of integrated flight/propulsion control for rotorcraft.

The tool used to establish, first a basis of comparison, then the possible system improvements, was Sikorsky's Master Generic Helicopter (MGH) simulation of the UH-60A BLACK HAWK helicopter powered by a NASA simulation of twin T700-GE-700 gas turbine engines. These are described in section 2 together with brief outlines of the basic aircraft and engine and an ancilliary simulation used during development.

Before attempting any design work, some effort was expended in identifying a series of generic mission task segments that would be used to quantify the benefits of such an integrated flight/propulsion control system, by measuring the system's performance as it was "flown" by a simulator through the maneuver. The criterion for these segments or maneuvers, was that they should involve a sudden large torque change in the rotor load. If they involved an autorotative rotor state with declutching of the power turbine and possible spool-down of the gas generator, they would be most likely to lead to problems in subsequent recovery from the maneuver and therefore have the most room for improvement in any synergistic system that included control of both engine and airframe. The identification of these generic mission tasks is dealt with in section 3.

Section 5 contains descriptions of a number of schemes that for one reason or another were rejected during the screening of all the features that preceded the design integration process.

Section 6 is an evaluation of the differences in performance between the basic BLACK HAWK/T700 system in production and the same airframe/engine equipped with the designed integrated flight/propulsion control system. This evaluation was done using the MGH simulation model. A further evaluation using the Vertical Motion Simulator at NASA Ames and their Gen Hel BLACK HAWK model, was to have followed immediately. This is dealt with in section 7.

2.0 SIMULATION TOOLS

The basic simulation tool used for this study was Sikorsky's current MGH (Master Generic Helicopter) digital computer program which has been evolving within the company over a period of at least twenty five years. The last major revision of this simulation occurred in 1980 when the older General Helicopter or "GEN HEL" simulation programs were rigorously modularized. The resulting modules were placed in a protected library, an executive program was written and is used in conjunction with an efficient debugger. The result has been an extraordinarily flexible simulation system. This system is under continual development using the modular format and library to preserve the integrity of previous work.

Sikorsky has on occasion entered into contracts (notably with NASA) to provide the means of simulating its aircraft on other than in-house simulators. When this has been done, Sikorsky has provided the equations for the simulation which have then been coded by the on-site simulator personnel. This work is typified by References 1 and 2 which are formal documentations of the equations used in the real-time simulation at NASA (Ames) of the RSRA and UH-60A BLACK HAWK aircraft respectively. These transferred simulations and their documentation have come to be known as the "GEN HEL" simulations. They differ from Sikorsky's MGH simulations in the ease of use conferred by the modularity of MGH and the operating environment, the large array of utilities available with MGH, particular ways of handling repeatable I.C.s and of course, subsequent development of detailed modelling. NASA's GEN HEL simulations are characterized as having a multi-rigid-blade rotor representation with freedoms in rotor speed and blade flapping and lagging, transferring total forces and moments through a hub to a six degree-of-freedom body. Aerodynamic forces and moments are represented by coefficient maps while rotor downwash is a first harmonic approximation. Since no linearization is performed, nor any small angle assumptions made, the Gen Hel simulation provides a good basis for any increase in sophistication in modelling that may be deemed necessary for particular problems.

MGH is oriented toward the handling qualities, real-time, pilot-in-the-loop type of investigation. Constraints imposed by the real-time requirement on one hand and a determined effort to "show the physics of the problem" on the other, have led to some compromises in the modelling methods presently used. As computational speeds increase, new modules can be expected to be written which will increase the band-width of the total simulated system by increasing the sophistication of the modelling in some areas. The present MGH model has been correlated with flight test data for most Sikorsky aircraft. In trim, the small number of blade segments and lack of performance correction "tricks" prevents its use for predicting performance to within performance guarantee levels, however trim attitudes and control positions are adequately forecast (Ref 3). Dynamically, MGH shows good correlation with aircraft motion taken from flight test data. The MGH simulation system is routinely used for the successful prediction of design values for primary control systems, SAS and 1st engine-rotor torsional oscillation and other aircraft coupled and uncoupled motions.

2.1 MGH (Master Generic Helicopter)

Reference 2 is a very complete documentation of the specific BLACK HAWK GEN HEL simulation program as received at NASA (Ames) in 1981. It was to a large extent due to the existence of this program and its documentation that NASA (Lewis) chose to specify the BLACK HAWK as the simulation vehicle for this study.

The developed MGH version of the BLACK HAWK simulation differed from the Reference 2 model at NASA in several respects, both models have been revised during the course of this study and are now substantially similar again. For NASA, the main gearbox and engine clutch interface has been rewritten to be the same as the rigid shaft version on MGH (the flexible shaft MGH version is extremely marginal in real-time computations and was not warranted in this study). This newer version allows for the correct summing of the tail rotor drive torque and accessory drive torques in both engine clutched and de-clutched conditions. The tail rotor module has been extended to include a torque calculation (Wheatly-Bailey method) rather than the formerly used factor on the main-rotor figure which can be substantially in error. Both of the above changes were transmitted to NASA for the RSRA X-wing simulation and very little work was required to adapt them to the BLACK HAWK simulation. R.S. McFarland of NASA (Ames) has done a considerable amount of investigation into the Gen Hel rotor algorithms as programmed for the VMS, including the re-introduction of terms previously dropped from the flapping equation and, more significantly, a temporal correction to the blade lagging acceleration term (Ref 4). These corrections have been incorporated into MGH.

The maneuver segments were "flown" on the simulation, using one of the three available modules from the MGH Library. These are:

i INPUTA
ii PROPLT
iii MANUVF

INPUTA consists of specifying input levels on any input variable as functions of time. Steps, pulses, doublets and sinusoids are available as well as an arbitrary function. This form of input is adequate for the very simplest of maneuvers e.g. autorotational recoveries, but the input specification rapidly gets out of hand when a particular flight path is required.

PROPLT was written as an improvement on INPUTA when flight path profiles were required to be flown. The module requires the flight path profiles to be specified as time histories, and a control variable to be assigned to control each profile. Gains are then specified for application to rate, proportion and integral of the error between the profile flown by the simulation and that specified. Some experience is necessary in picking both reasonable profiles and appropriate gains. All in all, the "profile pilot" is quite effective in giving a reasonable solution for a given level of effort - it was used for most of the maneuvers performed during this study. Its weakness is that it cannot cope at all well if appreciable control cross-coupling is present.

MANUVF was written most recently to alleviate the cross-coupling problem and provide a means of flying a specified maneuver. The module is a partial model following system in which a flight profile time history is specified and passed through a series of filters which shape a required vector of time-varying variables ("the model response") which would smoothly accomplish the required maneuver if flown by the helicopter. The controls required to fly the maneuver are found by passing the model response vector through the inverse of the A and B matrices of derivatives which describe the linearized behavior of the helicopter at that particular airspeed--this constitutes a feed forward loop. A feedback loop is formed by using the error between the actual and modelled (desired) flight profile variables and placing proportional and integral gains on those signals. There is provision for stick position limits and (to make the controller behave more like a pilot) many kinds of performance limiters may be built in (e.g. attitude and rate limiters). This module is very versatile and once set up, can fly a specified maneuver in a convincing manner provided that the profile is not too complex. It does however require significant effort to set it up; data describing the aircraft's approximate second order response, actuator dynamics, suitable PI gains in each control channel, in addition to a full array of derivatives varying as a function of airspeed, must all be specified. The controller is not capable of flying the more subtle aspects of maneuver techniques (e.g. the deliberate holding on of large sideslips in order to slow down more quickly), nor can it compensate for SAS saturation effects.

2.2 NASA's T700 Engine/Fuel Control Model

The other major change from the Reference 2 simulation was in the modelling of the T700 Engine and Fuel Control. The original linearized model documented in the reference was replaced by a detailed non-linear thermodynamic model supplied by NASA (Lewis). Unfortunately, development problems on this real-time model with its extremely demanding operational frequency range, precluded its use in the initial design of the integrated control system. When the NASA model (detailed in reference 5) did become available, its heat sink feature (modelled to account for discrepancies in transient response where significant quantities of energy are stored or released by metallic mass temperature changes over short periods), was incompatible with the simpler excess torque model used in the initial design. This is discussed further in § 4.3 q.v. Subsequent design iterations were performed with the heat-sink feature turned off.

The model described in Reference 5 was separated into engine and fuel control modules so that the latter part could be replaced by the designed integrated control at will.

2.3 COPTR Simulation Model

As mentioned in §2.2, the initial design work of the fuel control based parts of the integrated control was not performed with MGH and the NASA T700 model. Instead, Chandler-Evan's COPTR simulation was used. COPTR is a simulation of a generalized twin engine powered helicopter employing a highly detailed and flexible fuel control, fuel transfer and engine model coupled to rather more rudimentary but adequate airframe model representing the rotor torque loading.

The microprocessor-based control system is modeled using sampled data techniques. The inputs to the control are sampled at their individually unique sampling rates. Control algorithms, however, operate in simulated continuous time (0.002-second integration increment) to allow the system designer to introduce dynamic compensation, etc., without concern for the dynamic accuracy of the model. The output of the control is both delayed and updated at a time increment equal to the microcomputer cycle time of the actual hardware. Thus, control logic and effects of microcomputer cycle time, a parameter which tends to increase with more complex adaptive controls, can be investigated.

The pump and fuel metering model contains the stepper motor interface, the overspeed solenoid interface and a representation of the dynamics associated with fuel metering. The stepper motor equations are updated every 2 milliseconds to simulate the fixed 500-step/second rate of the actual hardware. The dynamics of the fuel metering section and overspeed solenoid models are representative of test data obtained for these devices. There exists the capabilty of varying pump and fuel metering performance, fuel type, etc., to investigate these effects on overall propulsion/helicopter system performance.

The engine is modeled by the excess torque method whereby steady state relationships for fuel flow, burner pressure, temperature, etc., are supplemented by partial derivatives with respect to excess torque (or fuel flow) for transient operation. The full operating range of the engine from startup to maximum power at various altitudes and ambient temperatures is covered. The starting characteristics of the engine include options for a variable delay to simulate filling a fuel manifold and also a variable delay to represent delays in lighting off the engine. The gas temperature partial derivatives can be tailored to match a particular engine starting characteristic and to produce hotter than normal starts for control mode studies. The starter motor is represented by a decreasing torque input to the engine model that reaches zero at the point that the motor would normally decouple from the engine. This torque input can be scaled down to represent a weak starter/battery condition. The engine relationships can be individually altered to simulate wear, damage, etc., and to mismatch engines in twin installations. (The latter features were not used in the study, since the NASA T700 model did not have such capabilities).

The rotor drive is comprised of a five inertia, four spring rate model which includes a gearbox, clutch and centrifugal main rotor shaft for articulated rotors. The primary main rotor and tail rotor resonant modes out to 10 Hz are well-represented. Rotor loads are determined from a combination of static main and tail rotor characteristics involving the collective pitch and rudder pedal inputs and aerodynamic effects dependent on aircraft motion. The model can be altered to simulate various stages of degradation such as drive shaft failure, lag damper failure, etc.

The airframe representation is for two-dimensional flight in the vertical/longitudinal plane. Rotor lift is apportioned into vertical and longitudinal components by cyclic pitch. These components of force are used to accelerate or decelerate the inertia of the aircraft to a velocity at which drag and gravity forces on the fuselage match the thrust components. The rate of change of energy of the aircraft is conserved by feeding back to the rotor system an aerodynamic torque which drives the rotors in a descent and acts as an additional drag during a climb.

Although restricted to two-dimensional flight, the airframe model results in aerodynamic loads on the rotor similar to those which exist during actual flight. Simulated rotor and free turbine speed transients have correlated quite well with flight test data. It is possible to widen the range of application beyond the two-dimensional vertical plane by feeding flight test load traces from lateral maneuvers on an aircraft, into the model as external disturbances.

COPTR was used extensively in the preliminary design of the integrated control, particularly in the integration of the LQR N_p governor into the system.

2.4 The UH-60A BLACK HAWK

The BLACK HAWK helicopter (Figure 2.4.1) is a conventional single main rotor helicopter, designed in the early seventies to meet the Army's UTTAS mission requirements. The, then, unconventional stability and control design features were the canted tail rotor and stabilator. The canted tail rotor was adopted for design purposes other than handling qualities and required extra compensation to be provided in the various (digital) EFCS subsystems. As the design process continued, it becomes clear that about half the extra compensation (e.g. lagged side acceleration) was required in the stabilator circuit, not directly because of the canted tail rotor but to compensate for the assymetric spanwise flow distribution across the rather large stabilator. This effect is approximated in the simulation model by adding $Y\beta$, $L\beta$ and $M\beta$ terms. In order to meet transportability requirements, the helicopter is fairly short-coupled. This leads to the empennage areas being fairly large. In particular, it requires that a moving stabilator be provided rather than a fixed stabilizer, to cope with the low speed rotor wake shift phenomenon. The stabilator is programmed to give efficient cruise operation at one design condition (and has reasonably good performance over the whole design range).

The digital EFCS provides; a trim system to give the pilot a force feel; a pitch bias actuator to improve the static stick/speed gradient; a limited authority, three axis SAS; an attitude/altitude hold; a heading hold; a coordinated turn capability above 60 Kt; and a stabilator schedule which is a function of airspeed, pitch rate, lateral acceleration and collective pitch setting.

Flight tests have shown that the large horizontal tail surface yields a longitudinal response with natural damping of about 0.2, with SAS on, this improves to about 0.7. The large vertical tail surface together with the 11 ft. diameter tail rotor, yield an unaugmented Dutch Roll damping of about 0.15. With SAS on, this improves to just about dead-beat.

2.5 The General Electric T700-GE-700 Engine

The T700-GE-700 engine is a front drive, turboshaft engine featuring a single-spool gas generator section consisting of a five-stage axial, single-stage centrifugal flow compressor, a through flow annular combustion chamber, a two-stage axial flow gas generator turbine, and a free or independent two-stage axial flow power turbine, see Figure 2.5.1. The power turbine shaft, which has a rated speed of 20,900 rpm, is co-axial and extends to the front end of the engine. The engine also incorporates modular construction throughout, an integral inlet particle separator, a top-mounted accessory package, an engine-driven fuel boost pump, a self-contained lubrication system, condition monitoring-diagnostic provisions, a hydromechanical gas generator control system, and an electrical power control system providing power turbine speed control, dual engine load sharing, and redundant power turbine overspeed protection.

SA 1114

The engine control system incorporates all control units necessary for the proper and complete control of the engine. The system provides for the more common functions of fuel handling, computation, compressor bleed and variable geometry control, power modulation for rotor speed control, and overspeed protection. The system also incorporates control features for torque matching of multiple engine installation, and overtemperature protection.

The T700 control system was designed to be a system requiring a low level of pilot attention. The system performs many of the controlling functions formerly performed by the pilot, allowing him to direct his attention to the prime task at hand, completing his mission. This has been done by providing:

- Isochronous power turbine and helicopter rotor (N_p/N_R) governing
- Automatic load sharing
- Automatic limiting of power turbine inlet temperature
- Rapid engine transient response through collective compensation
- Automatic starting

The basic system operation is governed through the interaction of the electrical and hydromechanical control units. In general, the hydromechanical control unit provides for gas generator control in the areas of acceleration limiting, rapid response to power demand and variable geometry actuation. The electrical control unit trims the hydromechanical control unit to satisfy the requirements of the load so as to maintain rotor speed and load sharing and also to limit engine power turbine inlet temperature.

3.0 Generic Mission Tasks

A list was composed, of simple segments of maneuvers that could be reasonably easily simulated on MGH and that would highlight the advantages of an integrated flight/propulsion control system. The list was based on two sources: past experience of helicopter design problems and a search of the air-to-air combat (AACT) data base. Maneuvers that entailed rapid changes in torque loading on the main rotor were sought because this is the area where flight/propulsion control schemes are likely to be useful. The typical control problem is that given a maneuver in which the main rotor torque load changes rapidly, the engine is unlikely to be able to respond quickly enough to keep the rotor speed (Ω) constant. Control power is a function of Ω^2, so a droop of 5% in rotor speed can cause a 10% change in stick sensitivity - this makes for great difficulties in precision flying. In extreme cases of autorotational recoveries, droops of 15% have been recorded, over 25% reduction in control results, and although precision maneuvering may not be required, even maintaining a loose flight profile is difficult.

The list of Table 3.0.1 was compiled and is the result of (i) reviewing past design experience and (ii) searching the AACT data base.

These two sources are discussed separately in sections 3.1 and 3.2 below.

Table 3.0-1 Definition of Generic Mission Tasks

1	Classic autorotation recovery
2	Bob-up and remask
3	Quick stop
4	Quick turn/deceleration
5	Engine failures
6	Side accelerations
7	Roll reversals

The figures that accompany these sections are taken mainly from the AACT results (§3.2 q.v.), others are from published flight test results. Because the BLACK HAWK is relatively benign in behavior, largely due to its heavier rotor, and the objective is to illustrate the problem, the figures pertain to a variety of helicopters.

3.1 Sikorsky Engineering Experience

The first five items in Table 3.0.1 were all the result of gathering together comments from pilots and designers at Sikorsky on the type of maneuvering discussed in §3.0 and grouping them into maneuvers that it was felt could be amenable to simulation on MGH, using the maneuver controller code available there.

The first maneuver is a classic autorotation (or steep approach) recovery, in which a pilot, having established a steady split needles autorotative descent (with engines operative but in a de-clutched, zero HP output flight idle condition) decides to abandon the descent and return to powered flight. He does this by pulling up on the collective pitch lever. The maneuver can be broken down into four main types, each having different detail characteristics dependent upon the particular engine/airframe combination. The rough classifications are: Fast collective pull (< 1 sec); slow pull (> 1 sec); from large split (i.e. % rotor speed more than 5% greater than % engine speed); from small split (< 5% speed difference). The "split needles" refers to the pilot's instrumentation on which a triple tachometer mounted in one case, commonly moves three pointers (needles) over a single scale marked in %. In autorotation, the normally superimposed pointers separate to show the two engine speeds (governed to 100%) and the main rotor speed.

The small split, long pull (Figure 3.1.1) is the easiest for a pilot to perform as the responses are slow and predictable. If from the same small split, the collective is pulled much faster, the engine, despite the collective anticipation link, has no time to spool up the gas generator in preparation for the increasing torque load at the power turbine. The result is often the worst rotor speed droop seen

in flight test for that aircraft (Figure 3.1.2). From large splits, a fast collective pull is somewhat less severe than the aforementioned small split case because there is more time for Ng to spool up before the engine/rotor clutch is engaged, simply because the speeds were further apart in the beginning (Figure 3.1.3). A slow pull from a large initial split introduces another phenomenon--the engine governor may cut back the engine fuel flow at just the wrong instant because the engine turbine has overspeeded in response to the collective anticipation, but before the rotor speed has fallen enough to engage the clutch and apply the load to the engine. The result is significant droop and often overshooting of the rotor speed response (Figure 3.1.4).

The bob-up and remask maneuver is a precision hover task in which altitude and heading control are at a premium. From a trimmed hover, collective is pulled to gain height (to clear an obstacle), the height is then stabilized and probably a heading change made (aiming or observing) and stabilized. The remask is a fast descent to the original hover condition. Problems arise if the torque demand on the engine is too large, in which case rotor speed droop will occur and the attendant changes in control power and damping make control more difficult (Figure 3.1.5). This is a case where the engine/fuel control inhibits the pilot from exploiting the full airframe potential and can lead to the aircraft being exposed from terrain cover for longer than necessary.

The quickstop is a straight forward longitudinal manuever in which speed is lost by holding the nose high and thus forcing the lift vector to slow down the aircraft as a component is directed back along the flight path. In order to avoid ballooning up as the nose is raised, collective pitch must be lowered at the same time. The rotor swiftly moves into an autorotative regime which of itself, is no great problem although the brief 16% overspeed causes increased sensitivity and pedal compensation for the torque load change is required. The difficulties, if any, occur in the eventual recovery from the maneuver, where as in the autorotation recoveries, the engine may be declutched. In fact, the maneuver seems to be either more benign or flown more gently than the auto recoveries. Flight test (Figure 3.1.6) show large excursions in rotor speed during the auto entry, but no particular control problems are observed through the eventual entry into hover. Another reason for the apparent comparative ease of flying this maneuver is probably the long time period over which it is flown. The so-called quickstop is not the fastest method of losing speed.

The quick turn or turning deceleration is another (faster) way of losing speed. This is really a combination of two objectives into one maneuver; for the quick turn, the fastest way to achieve a large heading change is to slow the aircraft down as much as possible and then apply yaw control; if a speed loss is desired and there is flight room, the fastest way to achieve that, is to load the rotor up as much as possible. By allowing the rotor to load up as far as the sustained g limit of the flight envelope, a large force can be

directed back along the flight path and thus a higher deceleration achieved than in the "quickstop". To avoid altitude changes and sustain the g for a longer period, it is usual to pull into a banked turn for this speed loss maneuver. An added bonus is that it is relatively easy for a pilot to hold on a substantial sideslip during the turn, increasing drag and thus deceleration (and also increasing sideforce and therefore turn rate). Again, recovery from this maneuver may pop the rotor through an autorotative state with possible attendant droop and control problems. Figure 3.1.7 shows an example.

Engine failures are limiting in low speed flight (indeed their finite probability gives rise to he familiar "deadman curves" of the helicopter pilot's handbook which designate combination of height and airspeed which must be avoided). They can also be a problem at high speeds; the abrupt removal of driving torque to the main rotor may cause large sideslips to occur on an aircraft with marginal directional stability (exacerbated by the slowing of both main and tail rotor rotational rates). The sideslip in turn, causes large roll excursions through the dihedral effect $L\beta$. Figure 3.1.8 illustrates just such a response. If a canted tail rotor is involved, a pitch response adds to the complexity of the subsequent motion.

3.2 AACT Data Search

The recent U.S. Army air-to-air combat test (AACT) involved the flying of, and recording of data from, well instrumented helicopters of various designs by personnel for the Army's Applied Technology Laboratory, the U.S. Navy Test Pilot School and industry. The flight tests, flown at the Naval Air Test Center, Patuxent River, Maryland, consisted first of flying the aircraft individually through a list of prescribed aggressive maneuvers (the Maneuver Criteria Evaluation Program or MCEP maneuvers) and secondly, in pairs, in simulated one-on-one air combat, in both loosely prescribed and free-form maneuvers, taking turns to be aggressor, than defender.

The data (often referred to by the Contract number, D318) includes time histories of control positions, airspeed, angular rates and positions, load factor, sideslip, rotor speed, engine torque, fuel flow and spatial position. This vast quantity of data is routinely referenced by a digital program "DATAMAP" which serves as a data manager, making it possible to plot particular time histories or cross-plot test parameters at will.

Our search was concentrated on maneuvers that exhibited a rotor speed excursion of more than 5% on any aircraft. All such maneuvers were then classified by type and further studied in an attempt to understand the underlying cause of the excursion and assess whether it was configuration dependent or not.

This search and classification reaffirmed the significance of the first four items in Table 3.0-1 and added the sixth and seventh.

The side acceleration maneuver shows signs of excessive rotor speed excursions especially when flown aggressively. The more conventional method of flying the maneuver consists of rolling the aircraft to some modest bank angle and then applying collective pitch to accelerate sideways while controlling heading with pedals. This performance is generally within the capabilities of the engine/fuel controls of the test aircraft and the added torque required by the collective pull is met smoothly and without droop. The aggressively flown maneuver (Figure 3.2.1) is accomplished by applying full pedal and then as much collective pitch as the aircraft will take to maintain heading, while controlling altitude with bank angle. This involves compensating for both engine/fuel control and airframe response and, while it might serve as an ideal integrated control maneuver, it requires great skill on the part of the pilot to fly it. The recovery from the side velocity involves the banking of the aircraft in the opposite direction to the flight path in order to remove the velocity. This reversal of bank angle pushes the rotor into an autorotative state but because the engine has been at high torque throughout most of maneuver, the autorotation recovery problems due to a spooled-down gas generator, do not occur. Some speed excursions of the rotor are quite common however.

The roll reversal maneuver occurs frequently in terrain avoidance tasks and also during evasive maneuvering. The segment considered here consists of a swiftly applied bank angle of some fifty or sixty degrees in one direction, followed by a roll through level attitude to a similar bank angle in the opposite direction, finally concluded by a roll back to level again. The maneuver, particularly during an evasive task, was often not co-ordinated - indeed a "false turn" was sometimes deliberately flown to evade a helicopter whose design compelled its pilot to commit to a turn when banking by pulling load factor. The more agile machines could bank briefly without load factor and then bank and turn in the other direction, pulling load factor. This was less decisive in the D318 tests than it sounds, since pilots soon learned the characteristics of all the aircraft and could hold off committment if necessary. The characteristic of the maneuver that caught the eye was a sharp torque spike that occurred when helicopters rolled from right to left, but that was hardly noticeable when rolling from left to right. The spike was severe enough to overtorque the gearbox of one aircraft and for this reason, inhibited its pilot from maneuvering to the airframe limits. There is some difference of opinion over the cause of the phenomenon, but it seems likely that most of the increase is caused by the assymetry of the rotor in forward flight. The left side of the disk (on counter-clockwise rotating rotor U.S. helicopters) operates at a higher angle of attack on average then the right side, since it has to balance the moments and less total dynamic pressure is available at the blade [on left, $V_{LOC270} = \Omega R - V_{a/c}$ while on right $V_{LOC90} = \Omega R + V_{a/c}$]. The effect of roll rate ($\dot{p}$) is to add a component of velocity in the vertical direction proportional to p, which is positive on the right side when rolling right to left. The effect on

SA 1114

α, the local blade angle of attack, of an equal but oppositely signed vertical velocity is quite different on each side of the rotor disk, since a tangent function is involved]$_1$ Very roughly, $\Delta\alpha_{left} = \tan^{-1}(Kp/(\Omega_R - V_{a/c}))$ while $\Delta\alpha_{right} = \tan^{-1}(Kp/(\Omega R + V_{a/c}))$]. In turn, the effect of the greater α change on the left drives the change in local blade drag even more markedly (since C_D is a function of α squared). Thus a roll rate to the left can be expected to increase the (already higher) local blade incidence and hence C_D on the left side, much more than the corresponding smaller α (and hence C_D) on the right side. The net C_D change is reflected as a rotor torque change. Conversely a roll rate to the right will decrease the left side α (although the decrease in C_D will be less than before since a flatter part of the $C_D \sim \alpha$ relationship is involved) and increase the right side α and C_D by little more than the previous case. The net effect (which can be shown on MGH) is a torque increase of only about a third as much when rolling left to right than when rolling right to left. Figures 3.2.2-3 show examples from the AACT flight tests. Some aircraft seem more susceptible to this phenomenon than others, but the above simplistic explanation would seem to account for this also, since the sensitivity is clearly a function of blade loading - which varied greatly among the D318 test machines. This speculation has not been substantiated by any further inquiry however, other than to verify that the change in mean rotor torque with roll rate in an otherwise steady general trim is about three times more for left roll rate, than right.

4.0 INTEGRATED FLIGHT/PROPULSION CONTROL DESIGN

The following ~~concept~~ sections highlight each ~~concept~~ of the integrated control design and explain its purpose and the techniques used to integrate the feature into the overall system. Because the design is presently a computer simulation, no attempt was made to decide which piece of code belongs on which processor or the optimal routing of sensor signals between sensors, actuators and processors. The majority of the code is propulsion control oriented and as such, fits neatly into the fuel control module of MGH, with some unavoidable additions and changes in the ASE/Controls module. On an implemented design, one might expect to the see more of the coding in a flight controller processor and less in the fuel control. For example, the engine failed detection is an obvious choice to remain in the fuel control processor, but subsequent actions to be take (§4.6) could be expected to be placed in the flight controller. In this code, they are all in the integrated control (situated in the fuel control module). Similarly, memory requirements and execution speeds were not considered.

That part of the code which represents what would be coded onto one or another processor (as opposed to the code that represents hardware) has been arranged to be able to operate at a different time scale to the rest of MGH. Thus, the MGH code may be cycling 100 Hz to simulate a continuous system, while the simulator processor may cycle at 40 or 50 Hz, representing an actual processing delay (c.f. §4.1 & 4.2 for more details).

SA 1174

A brief summary of the integrated control is presented here, a detailed description follows in the numbered subsections. For the most part, the concepts are discussed in the subsections in non-programming terms, but where necessary (e.g. the executive and sampling modules), a programmer's approach is used.

The core of the controller is an isochronous Np governor whose reference speed may be modulated by various combinations of variables representing present or anticipated airframe/engine states (e.g. load factor). The Np governor itself consists of a linear quadratic regulator state feedback algorithm in which rotor tip speed is estimated by a Kalman-Bucy filter. Additional adaptive logic is used to anticipate rotor decay and help recovery from the declutched state. The traditional collective pitch to load demand spindle anticipator in the fuel control is retained but in digital form. The (equally traditional) collective pitch to tail rotor collective link is replaced by a measured engine torque to tail rotor collective link. An indication of power available to hover is provided for the pilot. A cue for inhibiting the application of collective stick while the fuel control is on its acceleration schedule is provided by a logic signal. A variety of stick movements following engine failure, depending on height and velocity, are available. A switchable fuel consumption minimizer operating in conjunction with added loops in the AFCS is also available.

The subroutine shells or even complete coding for various other functions which were not developed as a useful part of this study but were retained as being worthy of investigation in an other-than-BLACK HAWK environment are also described, albeit minimally.

Reference 6 is a formal documentation of the digital computer code used to simulate the Integrated Flight/Control System.

4.1 Executive For Integrated Flight/Propulsion Control Module

This is the framework module for the integrated system - a block diagram (Figure 4.1.1) shows the program flow. On entry, the sensor modelling is computed, followed by a sampler routine which decides whether the elapsed time since the last sample was taken, is sufficient to require that another should be taken (signalled by flag LLSFLG). The stepper motor simulation module is then executed and if flag LLSFLG is false, an exit route from this executive model is taken. Thus the only parts which are always computed at the MGH frequency are the sensor, the stepper motor fuel pump and the sampling decision timer.

If the sampler indicates that an integrated control computation should be performed, all the other modules are executed in the order indicated in the figure. While the aircraft is being trimmed in 1g flight, there is no interest in the failure mode or performance or dynamic enhancers, so these are skipped. Also four of the modules need only be executed after all engines have been computed for that time step, (separate parts of a dual engine installation are provided

for, so that single engine degradation can be studied, or, the engine torque from one computation can be doubled) so they are skipped until the engine counter setting (NE) reaches the number of engines to be computed (JEMAX). The limit fuel flow logic is then performed, "losing" integrators are reset by backtracking (q.v. §4.4) and finally the tail rotor collective link variable is calculated. The time step in the sampler routine is solely responsible for the operating frequency of the integrated control.

4.2 The Sampler Routine

Figure 4.2.1 is a flow diagram of the sampling routine used to

(a) regulate the execution frequency of the integrated control, and

(b) to interpolate sampled values of sensor variables at the appropriate time.

The sampler keeps a running total of elapsed time in terms of both MGH time and its own internal clock. If at a given pass, it is predicted that the MGH time total at the next following pass will be greater than the internal elapsed time, (Figure 4.2.2), a temporary sample of the sensed variables is taken and the flag to execute the integrated controller is switched on. The integrated control uses not the temporary sample just taken, but the interpolated values calculated when the sampler and integrated control were last active together. On the next pass, the flag is turned off, another set of samples taken and the values are linearly interpolated on a time basis for an estimated value at the precise sampling time. The interpolated values are then held until the integrated control is again active. Thus the sampler allows a true representation of the time lapse of a cycling processor provided that the sensor is accurately modelled and the cycle time includes the digital conversion time.

To prevent a build up in round-off error, the two running clock times are resynchronized when they fall to within 0.01% of each other.

4.3 Linear Quadratic Regulator Power Turbine Speed Governor

The purpose of a power turbine governor for a helicopter application is to maintain constant power turbine speed (Np) in the presence of torque load changes in the helicopter propulsive system. Such governors have in the past used feedback of Np error from some reference value to regulate fuel flow to the engines. The so-called "droop" governor which allowed a droop of about 10% of Np to generate enough error signal and therefore fuel flow, to hold Np to a 100% reference value under high load conditions - and 110% under no load, was an early example of such a governor. An improvement on this design was to add an integrator to the error loop, so that the steady state error could be removed, resulting in an isochronous governor (a position plus integral or PI governor) that maintained speed at the

SA 1114

reference value under all loads (apart from transient load changing conditions which then became all-important).

A limitation on this form of governor is caused by the existence of two torsional resonances in the drive train system (usually, but not always, well damped modes). The resonances are caused physically by the engine and drive-train rotational freedom working against the blade lagwise direction freedom (for an articulated rotor, across the blade lagging hinges). The BLACK HAWK's main rotor blade/drive system torsional resonance occurs at a frequency of the order of 2.7 Hz, the tail rotor blade/drive system torsional resonance higher at about 7 Hz. Hydraulic lag dampers are provided across the main rotor hinges to add damping to the system (these dampers are sized by ground resonance conditions rather than the pure first torsional mode). To avoid exciting these modes, Np governors have employed band-width limiting designs which cut off considerably below the first torsional frequency. This of course limits the speed of response of the engine/fuel control - which is then often too sloppy to allow good tight aircraft response during rotor torque load changing maneuvers. It should be emphasized that the rotor load change referred to is a torque loading change, not a rotor thrust change. While a change in rotor thrust almost always results in a change in rotor torque load, the reverse is not true - the rotor may be supporting the aircraft in one g flight under maximum power conditions (e.g. high speed climb) or in zero power conditions (autorotational descent), in either case, the total rotor thrust is very similar, the torque loads quite different.

The advent of all-digital controls has made the PI governor easier to implement but also opens the door to more sophisticated mathematical techniques for overcoming the torsional mode problems. Reference 12 showed a successful implementation using a higher order notch filter to attenuate response at the first torsional frequency. General Electric's approach here is to employ an LQR design. This allows the bandwidth to be increased and thus improves the response time of the system.

GE provided a high performance power turbine speed governor, designed for a recent technology turboshaft engine (the T700) coupled to an advanced, articulated helicopter rotor system (the BLACK HAWK). Modern control system design techniques were used to obtain a higher-bandwidth system than previously achievable. The Linear Quadratic Regulator (LQR) technique was used to design the governor, and a Kalman Filter was included in the control system to estimate the helicopter main rotor blade velocity used in the LQR governor. The design method is fully described in Reference 7. The effect of the LQR governor in the frequency domain is to attenuate the resonant peak caused by the interaction of the helicopter main rotor and the power turbine (the first torsional mode). The LQR governor provides adequate phase and gain margins for good stability and robustness. The resonant peak attenuation, combined with large phase margin, allows the system gain to be higher and results in the increased bandwidth.

SA 1114

The LQR design method applied to the T700 fuel control uses a five state model to represent the system c.f. Figure 4.3.1. The states are:

- Ng — Gas Generator speed (measured).
- Np — Power turbine speed (measured).
- Wf — Output fuel flow of the governor (calculated).
- QMR — Main rotor torque load transmitted across flap-lag hinge combination - (approximated by engine shaft torque).
- NMR — Average tip velocity of a main-rotor blade (reconstructed by an observer).

NMR and QMR are rotor states that cannot be measured directly. NMR is an approximation to the average blade tip velocity which should better reflect a change in torque loading than shaft speed, since the aerodynamic loads are a function of the former. Since NMR is a variable outboard of the lagging hinge, it cannot be measured directly without more instrumentation, so a closed loop system containing a model of this rotor velocity is used to estimate it. This system is called an observer and is designed separately from the main LQR governor loop.

A schematic of an observer is shown in Figure 4.3.2. the observer system must meet the usual requirements of stability and performance with the added requirements that it calculates the estimated states of interest fast enough so that the performance of the main loop is not affected. If the model of the system used in the observer is observable, all of its poles can be placed arbitrarily in the s-plane, with the restriction that complex poles be placed as complex conjugate pairs. Main rotor blade velocity is observable in the T700 system from power turbine speed. More discussion on observability can be found in Reference 8. The Kalman Filter algorithm places the system poles in a specific manner.

The rotor model used for the observer is the simplified model of Figure 4.3.3 that neglects the tail-rotor dynamics. The power turbine inertia is not lumped as part of the transmission as is done for the complete engine and rotor system. The rotor model was put into state-space form given generically as:

$$\dot{X}_R(t) = A_R X_R(t) + B_R U_R(t) \qquad (1a)$$

$$Y_R(t) = C_R X_R(t) \qquad (1b)$$

where $X_R(t)$ is the rotor state vector, $U_R(t)$ is the input to the rotor, Y_R is the output vector, and A_R, B_R, and C_R, are the system coefficient matrices. Model validity around a steady-state value is implied.

SA 1114

The states for the observer are main rotor angular velocity, $\hat{NMR}$, a main-rotor torque state, $\hat{QMR}$, and transmission speed, $\hat{NP}$. The transmission speed is approximated as power turbine speed, NP, because of this simple model, the coupling between the power turbine and transmission is assumed rigid. The caret (Λ) above the state variables indicates that these are estimated states from the observer rather than measured states. The input, $U_R(t)$, to this system is engine shaft torque, Q shaft. The output vector, Y consists of $\hat{NP}$ and $\hat{QMR}$. An assumption was made that Q shaft was a good approximation to QMR.

The LQR Preliminary design was performed as follows:

The LQR NP governor was analyzed in the frequency domain using standard Bode plot techniques to determine the system stability margins, speed of response, and disturbance-rejection characteristics. These techniques are valid since the final LQR design is single input (WF) and single output (NP). The primary stability analysis was done with the loop broken at the WF input to the engine. A sinusoidal WF was input to the engine model and the resulting WF feedback was measured. This is shown schematically in Figure 4.3.4. This point in the loop is important because WF is the main driver of the engine, and also it is affected by all the engine states by the definition of full-state feedback. WF is also affected by the Kalman Filter. The turbine governor is a regulator that functions to reject disturbances to the power turbine. The controller reacts to these disturbances through WF when they appear in power turbine speed or shaft torque. In the frequency domain, the magnitude of the open-loop transfer function at WF should be as large as possible over the frequency range where the disturbances occur so that they will be attenuated more effectively.

The system closed-loop frequency response was calculated for sinusoidal inputs at the gas generator speed (NG), shaft torque, and power turbine speed (NP) sensors to determine the noise rejection characteristics of the system. The disturbance rejection characteristics of the system were analyzed by putting a sinusoidal torque disturbance input to the closed-loop system through the helicopter main and tail rotors.

As mentioned, the power turbine governor is a regulator that maintains power turbine speed constant in the presence of disturbances. The primary sources of disturbances are the helicopter main and tail rotors. The frequency response of the closed-loop LQR and T700 baseline systems was calculated for a main rotor torque disturbance and a tail rotor torque disturbance to analyze the effects on power turbine speed and helicopter main rotor speed. The simulated disturbance was a sinewave frequency sweep. The parts in the rotor system where the disturbances were input are shown in Figure 4.3.5. Each disturbance was input separately. The response of power turbine speed to a main rotor disturbance is shown for the LQR governor and

SA 1174

for the T700 baseline governor in Figure 4.3.6. The amplitudes in the figure indicate that disturbances are rejected better by the LQR NP governor than by the T700 baseline governor. This better attenuation of disturbances is seen in the time responses, also (e.g. Figure 4.3.7).

The helicopter main-rotor centrifugal spring constant can be considered proportional to the square of the main rotor speed. From steady state operation, this variable was considered a constant because rotor speed is governed at 100% speed. During a transient, however, the rotor speed will vary from 100%, and the centrifugal spring constant will also vary. To assure that stability margins are maintained at extreme variations from 100%, the spring constant was varied up and down corresponding to a ± 10% change in helicopter rotor speed. The spring constant is proportional to speed squared, so the constant was increased 21% and decreased 19%. The frequency response results for increased and decreased spring constant showed that the system remains stable under both conditions.

The frequency response of the LQR Np governor was calculated with only one engine driving the helicopter rotor system, simulating the loss of one engine. Stability was not adversely affected but the bandwidth of the system was lowered from about 8-10 rad/sec to about 5 rad/sec.

The LQR governor did not attenuate the main rotor resonant peak when the lag-hinge damping was reduced to zero. Performance degradation and instability could result in this situation. It is possible that an LQR governor could be designed to perform well in this situation and in the normal-damping situation.

The detailed GE engine large transient simulation limit cycled when run with the LQR controller. The limit cycle was eliminated when the engine heat soak model was disabled. The heat soak model was designed to account for the effects of heat absorption by the engine metal mass during large transients. Analysis revealed that this specific heat soak model contributed 25 degrees of phase lag and 4.5 dB attenuation at 4 rad/sec for small perturbations. This dynamic effect along with other non-linearities was sufficient to cause the system to limit cycle. Engine tests and comparison of the frequency domain effects of this heat soak model with other similar models indicate that the phase lag is excessive. A lead compensator was added to the Wf output of the LQR controller to restore sufficient stability margin when run with the heat soak simulation. Since the lead had a minimal effect on performance without the heat soak model, the lead had been used during all transient simulations.

The higher bandwidth translates directly into better performance in the time domain. The first transient considered is a simulated wind gust (40 ft/sec ramped in over a distance of 200 feet) which causes a load disturbance in the rotor system. The LQR Np governor reduces

the NP droop from 3.25% to 1.3% which is a 60% reduction as shown in Figure 4.3.7. The specific wind gust selected ends with gas generator speed Ng (curve labeled PCNGC) at 87% which is the point of minimum system stability margin. This is most evident in the rate of change of Ng signal, NDOT (curve labeled XNGDOTE). The baseline control has several small oscillations before the system stabilizes. The LQR Np governor virtually eliminates these oscillations demonstrating its better phase margin.

Two additional transients are also shown demonstrating the responsiveness of the LQR Np governor. During both of these transients other integrated control functions which can effect system response either do not operate or have been disabled. Figures 4.3.8 & 9 show a roll reversal and a high g turn, respectively. In both cases Np is held closer to 100% with the LQR governor than with the baseline control. It is also noted that fuel flow (curve labeled WFCE) varies over a smaller range with the LQR Np governor than with the baseline Np governor. This indicates that the LQR governor is more efficient in that it makes better dynamic use of energy.

The CECO pragmatic adaptive system complements the basic LQR control adding large transient logic and additional governors. Integration of the original LQR design into the basic CECO pragmatic adaptive control format was quite complex.

Since the LQR power turbine governor uses fuel flow as an output, the basic structure of the pragmatic control had to be changed. The adaptive control used NDOT/CDP as the demanded set point into the proportional-plus-integral controller. The output of each mode was NGDOT/CDP so the lowest/highest wins gates were comparing variables with the same units. On inserting the LQR governor directly into the adaptive control, this was no longer true.

In order to keep as much of the adaptive control intact as possible, a compromise fuel control was designed. The core engine control uses NDOT control through a proportional-plus-integral controller. Both the acceleration limiter and deceleration limiter use NDOT/CDP schedules for compatibility with the surge detection and recovery features. The NDOT governor consists of the top governor, acceleration limiter, and temperature limiter. The output of the NDOT governor is in ratio units, WF/CDP, which is then multiplied by CDP to get fuel flow. This NDOT fuel flow is compared with the LQR governor fuel flow, and the lowest fuel flow wins. The winning fuel flow is compared in a "highest wins" situation with the fuel flows from the bottom governor and the NDOT deceleration limiter. The integrated control block diagram is shown in Figure 4.3.10.

The integrated control nominally operates on the LQR power turbine governor. In extreme maneuvers, it will be limited on the top end by the NDOT governor and on the low end by the bottom governor and NDOT

deceleration limiter. On each computer cycle these limits determine the upper and lower extremes of the allowable fuel flow.

The structure of the integrated control is more complicated than that of the adaptive control as it involves three integrators: the LQR governor, the acceleration limiter, and the deceleration limiter. Reset logic was designed in such a way that the integrators not in the winning path would not wind up. The reset logic calculates backward through the control modes using the winning fuel flow value. The non-winning integrator values are reset as if they had produced the winning fuel flow. In this manner, the fuel flow limits will always be appropriate for the current fuel flow and mode changes will be smooth.

The adaptive features which affected the power turbine set speed of the original Pragmatic Adaptive Control are applied to the power turbine speed setpoint in the LQR governor. These features include torque sharing, rotor decay anticipation, rotor droop recovery, and load factor enhancement. Collective rate anticipation was not included since the LQR governor had its own collective pitch maps.

The LQR governor is essentially a small disturbance device. In particular, it was not designed to handle a decoupled rotor system and the pragmatic adaptive controller has to deal with such situations. For the autorotational rotor decay anticipation, the adaptive control provides a flag which signals when the system goes into autorotation. This flag is set by comparing the power turbine speed and the rotor shaft speed, when the difference between the speeds is greater than a deadband, the autorotational flag is set. This flag is used by the LQR governor to decrease the gain in its loop by a factor of 10 and switch out the rotor tip speed, shaft torque, and core speed paths. These paths add no information to the LQR in autorotation. Through this modification, the LQR is temporarily converted into a proportional-plus-integral controller with a low gain.

Figure 4.3.11 shows the operation of the rotor decay anticipator during a slow collective pull recovery from a large split autorotation. The Ω and N2RFE traces meet after about 1 second at 112% N_R, indicating that the engines came back on-line at that time. The DNPRAT trace shows the incremental Np_{REF} signal that the decay anticipator is generating, RMODE indicates that the controller is on the accel. schedule most of the time. Figure 4.3.12 shows the same recovery with the decay anticipator switched off. The engine does not come on-line until 0.5 seconds later than before and the rpm has sunk to 110%. The Np governor does not cut back on the fuel flow due to overspeed until just after the clutch has re-engaged so the usual droop does not occur (but c.f. Figure 5.3.2 for what happens when that limit does cut in at the wrong moment when running with a standard T700 control). The overall response is very little different between these cases-- some further tuning of the gains would probably help and might better illustrate the worth of this feature.

SA 1114

A further problem occurred when the rotor decay anticipation tried to increase the power turbine speed to recouple the system because the gain in the LQR is reduced during autorotation. To avoid this, the gain in the rotor decay anticipation path had to be proportionately increased to keep the complete path loop gain constant.

Figure 4.3.13 shows the working of the other non-linear large perturbation compensation part of the pragmatic adaptive control system, the droop compensator. The logic of this subsystem is to detect that a droop has occurred and inhibit the likely torque (and therefore Np) overshoot that will follow, by deliberately delaying the governor demanded fuel flow. On the figure, DNPREF is the signal that reduces the Np_{REF} governed value as the droop starts to diminish. The rotor decay anticipation signal is active during this fast pull recovery from a large split autorotation, but doesn't have time to spool up the engine to meet the torque demand, because the rotor speed decreases so rapidly when a full 70% of collection is impressed on the rotor with a consequent severe torque load; the rotor (and engines) then droop. Just after the lowest shaft speed is reached, DNPREF is activated and a smooth recovery to 100% Np then takes place. Figure 4.3.14 shows the overspeed that occurs in the same situation when the droop compensator is switched off. Figure 4.3.15 shows the baseline T700 controller response--both droop and overspeed are rather worse.

A final complication arose when the fuel control was on the top N_G governor (c.f. §4.4 following). This could happen if the pilot decreases power by using the power available spindle (PAS). An interactive loop formed with the core speed path in the LQR governor and the top governor. While the fuel control should operate through the NDOT governor, the LQR governor could take command through this interaction. Therefore, the LQR is switched to a proportional-plus-integral controller whenever the PAS is moved from its "flight" setting. The core speed path of the LQR is no longer active, and the top governor keeps control.

4.4 Pragmatic Adaptive Fuel Control Elements

The adaptive fuel control designed and under development by CECO is fully described in References 9 and 10. It was designated as a "pragmatic" adaptive controller by Sikorsky, to distinguish its behavior from a controller designed using the adaptive control concepts of modern control theory. CECO's controller recognizes an off-design condition in a practical way and compensates for it using a prescribed logic decision set; it is not a linear system algorithm.

The version used in this integrated control design has had the PI Np governor (referred to at the beginning of §4.3), removed and replaced by GE's LQR design. As explained in §4.3, this entailed some redesign of the pragmatic controller. Figure 4.3.10 is a block diagram of the integrated control. The rest of this section (4.4) expands somewhat on the summary given in §4.0 and is an explanation of the other fuel flow governor features of the control, all of which derive from the pragmatic adaptive design.

The acceleration schedule is the usual control which seeks to inhibit compressor surge by allowing the gas generator to accelerate in a pre-programmed fashion with maximum acceleration being a function of gas generator speed decided upon by the engine manufacturer. CECO has incorporated their adaptive surge margin compensation (c.f. §5.5) and also uses a lagged compressor discharge pressure rather than the more conventional engine inlet pressure, P_2, as a multiplier in the limiting fuel flow path gain, to further stabilize surge recovery. The NGTOP action simulates the action of the pilot controller PAS in acting as an upper limit throttle on N_G (and thus maximum engine power output) at all settings below 103%. The intent of this limiter on the original T700 fuel control is to give the pilot some control if the (separate) ECU should fail. Its retention here gives similar control but the failure mode that would warrant its use is less clear. It does of course serve as an absolute N_G and corrected N_G limit.

The TLIM section is a straight-forward digital implementation of a $T_{4.5}$ limiter. A logic switch OPSTAT which is triggered by the engine failed status flag of the other engine in a twin engine installation, can boost the allowable temperature for emergency power situations.

The lowest output of the above three governor sections (ACCEL., NGTOP and TLIM) is passed to the $\dot{N}g$/PC section which produces an error signal from the difference between its integrated value and the sampled Ng value and then calculates a weighted PI type gain which it multiplies by lagged compressor discharge pressure. The resulting fuel flow is the Ng governor fuel flow which is compared with the Np governor flow on a 'lowest wins' basis. The three components of the Ng governor thus serve as alternative top limits to the fuel flow. The integration in this governor is back calculated when the top limits are not being used, to the value corresponding to the actual fuel flow value selected by the complete system and the $\dot{N}g$ value measured at the corresponding time. Thus any transition onto the limits is smoothly negotiated by the integrator.

A prescribed deceleration schedule set by the engine manufacturer to ensure sufficient margin from flame out (in a basically similar way to the acceleration schedule) is provided. This path has an integrator in it, which is controlled by back-calculation in an exactly similar way to the $\dot{N}g$ governor while it is not actually govenoring the fuel flow.

An NGBOTTOM governor which prevents the gas generator speed from falling below a prescribed self-sustaining lower limit, is also supplied.

The last two low flow limits (deceleration and NGBOTTOM) are compared on a 'highest wins' basis with the (possibly limited by $\dot{N}g$) Np governor demand. The resulting fuel flow (after subjection to further absolute maximum and minimum limits) is the demanded fuel flow value that is passed to the stepper motor which regulates the pumping of fuel into the engine very precisely. An Np actuated overspeed switch cut-off value is present on the engine side of the stepper motor to deal with runaways. (e.g. shaft failures)

SA 1114

Thus the fuel flow delivered by the controller to the engine via a stepper motor is subjected to various limitations from other parts of the controller. On increased power demand, the Np governor fuel/flow requirement may be limited by the lowest of three limit governors:

NGTOP — a variable limit which protects the engine by limiting the speed of the gas generator part as a function of power available lever angle (PAL) chosen by the pilot - usually set in "Fly" position but can be used as a rather simple throttle in an emergency override condition as on the actual BLACK HAWK.

ACCEL — An $\dot{N}g$ acceleration limiter with built in adaptability to avoid compressor surge and stall after a first occurrence.

T LIMIT — An engine turbine inlet temperature limiter.

If the lowest fuel flow form any of these three governors is lower than that of the Np governor, it will be given precedence.

On decreasing power demand, the engine is protected by two other limit governors:

NG BOTTOM — gives a low fuel flow limit which is a function of ambient temperature and the compressor state. This is a sustaining "engine alight" limit.

NDOT DECEL — limits the maximum deceleration rate for the gas generator.

If the fuel flow from either of these two limiters is higher than that from the Np governor, it will be given precedence.

After these limits have been applied, an overall maximum and minimum fuel flow limitation is imposed, followed by a final Np overspeed shut off.

Three further subsystems can influence the fuel flow by changing the Np reference signal in the Np governor. The first is a dual installation torque sharing device - the digital equivalent of the present T700 controller which (indirectly) speeds up the gas generator of the low torque engine to match the output of the non-degraded engine, by applying an incremental Np reference signal proportional to the torque error, to the lower engine.

The second subsystem is the minimum fuel consumption optimizer. This is an extremely simple algorithm which when switched on in cruise, samples the fuel flow at intervals and perturbs the Np reference signals to change the rotor speed. Once the required direction of rotor speed change is established, the system makes successively smaller changes until either the authority limit is reached or small changes about the optimum value are continually made. This is an

SA 1114

extremely long term action, with a time constant measured in minutes rather than seconds due to the long soak times taken by the engine before settling down. The EFCS of the simulated BLACK HAWK had to be modified for this system. Figure 4.4.1 shows the results achieved by the simuated system. Since the attitude hold was inappropriate, it was switched off and an altitude hold introduced in its place. The airspeed hold outer loop FPS action was retained, thus allowing the FPS to counter the trim changes induced by changing rotor speed and maintain a trimmed flight path (airspeed and altitude). Because of the significant effect of rotor speed on control power, there is room for improvement in the FPS gain selection when performing these duties - time and budget restraints precluded any further investigation.

The third subsystem is the Load Factor Enhancement. In general, it is possible to increase the aerodynamic load factor capability of a helicopter by increasing the rotor speed. If the local blade incidence (α) is in stall, the increase in speed many reduce it to below stall and the increased total dynamic pressure will produce more lift. If the rotor is power limited, the decrease in α and hence C_D may allow the increased lift to be obtained for almost no power increase. (At high speeds where the C_D is largely a Mach No. dependent phenomenon, this is no longer true). Figure 4.4.2 shows the order of magnitude of the effect as predicted by MGH. A simple increase in N_{PREF} was conceived as a part of the original pragmatic adaptive controller, triggered on load factor rising above a threshold value and being proportional to load factor, with overlapping switching steps to try to prevent ratcheting. Because the load factor signal is so noisy, ratcheting did occur; substituting the product of pitch rate (q) and airspeed (v) for n_z smoothed the signal but the changes in Np still looked far too abrupt to be anything but unsettling to a pilot.

The final form of this subsystem involved ramping in an increment in N_{PREF} proportional to the product of body pitch rate and aircraft velocity and keeping it on for a set time after the load factor is removed. This tends to keep the engine spooled up longer and better able to deal with a large torque increased should the rotor pop in and out of an autorotative state. This is one area where it rapidly became apparent that a pilot-in-the-loop is essential for evaluation.

It should be noted that in all cases where the operating Np was deliberately altered, no effort was made to assess the resultant vibratory loads. Modern aircraft have self-adaptive vibration absorbers that work well over a range of rotor speeds: the BLACK HAWK helicopter, designed in the early 1970's, has absorbers that are tuned to the design reference speed. The self-adaptive type would be required for the integrated design.

SA 1114

4.5 Other Pragmatic Adaptive Features

The flame-out detector relies on the accuracy and constancy of the relationships between an $\dot{N}g$ deceleration and the Ng at which flame-out occurs and the range of Ng decelerations at given Ng's which are part of normal operations. Figure 4.5.1 shows the relationships, the flame-out boundary being determined by the engine manufacturer. The detection boundary is the line that appears to give adequate clearance to avoid false signals at legitimate $\dot{N}g$ decels while giving as much warning time as possible.

The logic failure signal is arranged to give a visual cockpit warning and may initiate other actions detailed in §4.6 under the EFFPR heading. The power available to hover (PATH) computation uses nominal maps of corrected engine torque and power turbine inlet temperature to calculate the maximum torque available from the engine. These maps are continually updated to include any engine degradation. The engine deterioration is stored into computer memory by modifiers of these maps. Thus, the maximum torque available signal is diminished if the engine performance is degraded. The torque required to hover is calculated from a map of the ratio torque-reqired-to-hover/torque-required-to-cruise versus airspeed (See Figure 4.5.2). While loitering at constant airspeed, the current torque is used to determine the torque required to hover for the current conditions. Maximum torque available is then compared against torque required to hover. A positive difference indicates a surfeit of available torque, and a hover condition is feasible.

Figure 4.5.3 shows the kind of indicator that might be provided in the cockpit. The power available pointers move up and down the outside of the ribbon engine torque percentage indicators. The power required pointer moves up and down between the two ribbons, it is illuminated in red when above the power available indicators and green when below. At airspeeds above 50 knots, the illumination of all three pointers is turned off.

4.6 Airframe Originated Features

As mentioned briefly in §4.0, the collective pitch to tail rotor collective link has been removed in the integrated control in favor of a sum of engine output torques to tail rotor collective link. In maneuvering situations, where the torque load on a rotor can change very quickly as the attitude and airspeed change, collective pitch becomes a misleading guide to the rotor torque load and thus also the compensation required in the yaw axis. The ideal link would be one which produced a yawing moment proportional to the main shaft torque load - unfortunately, the shaft torque is very difficult to measure and the production of yawing moment via manipulation of a tail rotor

collective pitch mechanism is not truly linear, making the proportionality property equally difficult to achieve. The integrated control solution is to use the sum of the engine output torques as an approximation to the main rotor shaft torque and live with the nonlinearities inherent in the tail rotor collective yaw controls.

The gearing of this linkage was chosen to yield pedal trim positions similar to the present BLACK HAWK controls. Figure 4.6.1 is an example of the trim positions through the level flight speed range, at a fairly light weight. An exhaustive investigation of trim position and margins was not undertaken. This linkage is destabilizing to the natural Dutch Roll mode without SAS augmentation, but not noticeably so with augmentation on.

Another feature programmed into the control is the use of the fuel control status flag c.f. pg. 37 (value $\geq$ 67 signalling that the engine is on its accel. schedule and is increasing output torque at the highest rate possible) to inhibit the pilot from applying increasing torque loads via the collective pitch lever, faster than the engine can absorb them without allowing droop to occur. The status flag signals an electric clutch mechanism on the collective lever, which adds about 12 lb of stick force when the lever is moved in the upward direction. The pilot can override 12 lb of stick force very easily if he feels it to be necessary. In use, a pilot would pull the collective until he felt the force increase and then maintain a steady pressure which would allow the stick to step upward in very small increments as the controller switched rapidly on and off the accel. schedule. The collective pitch control thus increases at the optimal rate constrained by constant rotor shaft speed. Figure 4.6.2 shows the response obtained in an autorotative recovery, by simulating the pilot's collective stick pull limiter with a simple integrater switched on and off by the accel. schedule status flag. The contrasting figure without the inhibiter control is 6.1.2.

The framework for a torque spike response inhibitor was written when the phenomenon (c.f. §3.2 pp 12-13) was first noted. However, in all the cases run, the simulated LQR Np control on the BLACK HAWK dealt adequately with the roll reversal torque load, so the extra compensation planned to be applied when bank angle was positive and roll rate negative, via the engine load demand spindle was never required and further development was not undertaken.

The last feature under this heading is that of automatic control action to be taken after single or dual engine failures. There are four separate facets of this problem, two at high speed and two at low speeds or hover. Section 3.1 and figure 3.1.8 illustrate the response to a throttle chop (simulating failure) at high speed of a modern helicopter. The BLACK HAWK does not respond to anywhere near the same degree, the relatively heavy rotor keeping the shaft speed higher, and large fin area, coupled with more effective tail

rotor (because rpm is maintained) make the directional stability much greater, hence sideslip never develops and the roll response due to the dihedral effect is very mild. Since no problem existed on the BLACK HAWK and changing rotor mass to provoke it, would have such a large effect throughout the design, no further studies were conducted. It seems quite possible however that if needed, the engine flame-out warning flag could be used at higher airspeeds to impress a tail rotor pitch input early enough to prevent the yaw and consequent roll response seen in Figure 3.1.8. The other high speed problem is merely that of low altitudes, the undercarriage must not be allowed ground contact above a speed consistent with its strength. To avoid this, the speed-altitude prohibition curves in the pilot's handbook include a forbidden zone of below 25 feet at all speeds higher than 55 knots. No automatic means of decreasing this area is envisaged, although for a machine designed primarily for nap-of-the-earth missions, the undercarriage would probable be sufficiently strengthened to move the prohibited area out to 80 knots or so anyway. The safe procedure in such circumstances is to flare the aircraft by pulling up the nose, until enough speeds is lost to make a safe landing possible--a quickstop maneuver without the hover recovery.

The low speed facets are the familiar "deadman's curves" of most pilot's handbooks. At low speeds, for given atmospheric conditions and gross weight, there are two critical altitudes beyond which, after an engine failure occurs and is recognized by the pilot and action taken, recovery is not possible. The lower altitude limit is that above which the vertical velocity cannot be reduced enough to prevent ground contact at above the critical rate for the strength of the undercarriage. The upper altitude limit is that below which the pilot cannot fly away on one engine without ground contact or, in the case of dual failure, make a controlled autorotational descent and landing. A large part of the prohibited area is created by the requirement to allow the pilot time to recognize the problem and react to it (commonly 3 seconds). The automatic control envisioned would recognize the height-velocity area in which failure(s) occurred and take the appropriate action immediately on perceiving the failure flag(s).

The application of cyclic (forward) and collective (down or held still) would depend on the area on the H-V diagram where failure occurred and would be preprogrammed-or possibly use the power to hover and performance mapping information of the pragmatic fuel controller to make the logical decisions. The stick would be moved by clutch mechanisms which could be overriden by a pilot using stick force alone. The movement-causing forces would be faded out after five seconds or so. Pilot-in-the-loop simulation is the only way of assessing such schemes.

5.0 Screened-Out Integrated Control Concepts

This section lists those concepts that were not proceeded with in this study and the rationale for the decision. Concepts that were retained are dealt with in section 4 preceeding.

The reasons for screening out of this study fall for the most part under three headings viz:

Impracticability
Modelling Limitations
Inappropriateness for BLACK HAWK

The first reason is somewhat subjective and was used sparingly. The second is perhaps less obvious but more definite - for example the variable geometry of the T700 inlet guide vanes was not modelled as a separate freedom in the engine model, but was included as an integral part of the performance curves, where a fixed schedule was assumed. A major rework of the engine simulation model would have been required to separate this freedom and it was not performed. (c.f. §5.3 for further details on v.g.). The third reason is the perhaps unfortunate result of having to take what is available: the T700 engine model and BLACK HAWK simulations were specified in the contract because of their availability, and the choice fitted very well with the overall eclectic approach. The fact that this engine-airframe match happens to be a particularly harmonious combination, tends to ameliorate factors that have caused problems on other helicopters and since resources are limited, some concepts that did not appear to be particularly rewarding for the BLACK HAWK were not pursued even though application might be appropriate to other aircraft (In some cases, empty "shells" were left in the final design coding to allow for development at a later date. In others, coding was left in place even though it was not strictly part of the integrated control, or could not be practically tested due to modelling limitations).

5.1 Dutch Roll/Torsional Mode Tuning

It is well established that a fuel control system can theoretically influence the Dutch Roll mode of single main rotor helicopters (Ref. 11). When body rate signals are fed back additively to the Np reference signal, the resultant fuel flow changes can cause engine torque output changes which apply yawing moments to the aircraft and thus alter the characteristic motions, particularly in the lateral and directional modes. Signal shaping allows the designer some control on phase as well as magnitude of the feedback and of subsequent changes in both the Dutch Roll (which is typically an oscillatory motion in which the aircraft fuselage both rolls and yaws with a frequency of the order of 0.2 Hz, damping varying between $\zeta = 0.5$ to zero or even negative (unstable on some helicopters) and the first torsional drive train mode (in which the main rotor blades' lagging

SA 1114

motion is in opposition to the drive train (main shaft) motion. The frequency is an order of magnitude higher at 2 - 3 Hz, the damping, provided almost entirely by the installed blade lag dampers on an articulated rotor, is normally high at 0.5 or so). It has usually been found that an improvement in damping in one of these modes by the introduction of shaped feedback, has resulted in a decrease in the stability of the other. However, there is often room for improvement in one mode which can be bought without giving up too much in the other.

The BLACK HAWK characteristics are quite satisfactory as simulated. The augmented (SAS on) Dutch Roll is well damped throughout the speed range and even at high speed, where lag dampers usually spend more time in saturation and thus tend to yield a lower net damping, the first drive train torsional mode is very hard to measure because of the rapid decay of this highly damped mode. Also, the LQR Np governor (q.v. § 4.3) deals adequately with the torsional mode.

In the case of the BLACK HAWK, this concept had little application, but to demonstrate its feasibility, a short sensitivity analysis was undertaken. Figure 5.1.1 summarizes the results of this work; the effects of implementing an N_{PREF} feedback link driven by roll rate, pitch rate and yaw rate individually, in turn, with gains of ±0.1 are shown, together with the base case Dutch Roll root. Positive pitch and roll feedback increase the damping, while negative feedback decreases damping, (to the point of instability in the case of roll rate). A negative yaw rate gain increases the damping, while the effect of positive gain is to reduce the stiffness (frequency) of the Dutch Roll mode. The code for this analysis is complete but the input parameters for BLACK HAWK are all zero. Application to a less well matched airframe/engine system would be straight forward.

5.2 Stabilator Setting and Fuel Minimisation

In level flight trim, a helicopter main rotor will have assumed an attitude and steady rates relative to the air, which results in balancing all forces and moments - this is the definition of trim. In particular, the lift force of the rotor balances the weight and any aerodynamic lift on the rest of the aircraft, while the rotor propulsive force balances the drag forces and the hub pitching moment balances the pitching moments. It is reasonable to assume that if the drag of the aircraft can be reduced, a savings in fuel consumption should result. On aircraft fitted with stabilators such as the BLACK HAWK, a means to change drag is available. Adjustment of the stabilator incidence in high speed flight, causes a redistribution of pitching moments between rotor and fuselage resulting in the changes of attitude shown in Figure 5.2.2(a). In addition to the reduction of drag of about 1600 lbs with the raising of the aircraft nose, a further advantage of less fuselage download occurs - the net effect being a reduction in the total force vector generated by the rotor of about 1.6%. Sketches 5.2.1 a-c illustrate the trimmed rotor forces with the stabilator positioned at +6°, + 1.01° (design position) and at -4°. Figure 5.2.2(b) illustrates the effect of these

changes on the fuel flow. The changes are quite small, indicating weak sensitivity and the figure shows the programmed stabilator yielding an efficient level flight trim condition at high speed. A salient disadvantage is that the longitudinal stick position (Figure 5.2.2(c)) moves forward beyond allowable margins. It had been proposed that a fuel minimization scheme consisting of an on-line Kalman-Bucy filter which would continuously identify a system whose outputs were stabilator angle and governed rotor speed to achieve a minimum fuel flow. The weakness of the stabilator function together with the unacceptable stick margins and the difference in speed of stabilator/fuselage response (compared with rotor speed adjustments) combined to reject this solution to fuel minimization. An independent attitude hold (seeking zero in level flight) and working on stabilator only, was at first added to the FPS but was removed when the stick margin problem surfaced. The original CECO long term Np_{ref} adjustment and fuel flow sampling was retained. This slow loop (with a settling time measured in minutes rather than seconds) is the Np_{ref} adjustment described in the integrated control section (4.4).

5.3 Engine Variable Geometry Investigation

It was known before the start of this contract that NASA's simulated T700 Engine would not be able to model a compressor variable geometry (v.g.) that was not controlled to the standard design schedule (conditions referred to as "off-schedule"). Since such operation (under the control of an integrated system) seemed likely to show promise, a limited investigation into possible benefits was undertaken by General Electric Co., using their own transient cycle deck and judicious extrapolations. That investigation is reported in this section since it obviously could not become a part of the integrated control design.

G.E.'s transient cycle deck represents v.g. effects up to ± 5° off-schedule. That data was extrapolated to provide trend rate for the larger transients examined here.

The compressor airflow required for a given output power level is a function of Ng, the gas generator speed, and the compressor flow area controlled by the v.g. The v.g. is altered (on schedule) by small fast actuators and the response is crisp. For Ng to change, the gas generator inertia must be overcome - a process that introduces significant lags into the engine response. In a system optimized for transient response, Ng would remain constant throughout a power change maneuver and the quick response of the v.g. actuation mechanics would yield a significantly faster engine response than the present combined Ng and scheduled v.g. arrangement. However, the present T700 control system was designed to yield (i) adequate stall margins, (ii) good specific fuel consumption figures and (iii) operation below any aeromechanical stress limits throughout all conditions. Implementation of off-schedule v.g. control strategies might be limited by failure to meet such criteria.

The first part of this study concentrated on the evaluation of an autorotation recovery transient with the various off-schedule v.g. arrangements shown in Figure 5.3.1 (a-e). The base case (a) (scheduled) v.g. is seen to hold the v.g. closed to 30.5° until $Ng/\sqrt{\theta}$ reaches approx. 78%, v.g. is then opened linearly until it reaches 0° at about 98% $Ng/\sqrt{\theta}$. The resulting Np droop during the autorotation recovery maneuver is shown in Figure 5.3.2 (full line) to reach 11.5%.

Case (b) moved the v.g. off schedule by a further 5° of closure at zero HP output (which now occurred at 72.6% corrected Ng as opposed to 71.2% of the base case). The v.g. remained constant until $Ng/\sqrt{\theta}$ of 78% was reached, whereupon it returned abruptly to the base schedule. The resultant Np droop (not illustrated) was 9.8% (i.e. a incremental 1.7% improvement over the base case).

Case (c) extended the v.g. off schedule closure to 9° at zero HP output (occurring now at $Ng/\sqrt{\theta}$ = 74.2%). Again, the v.g. is returned to schedule abruptly when 78% $Ng/\sqrt{\theta}$ is reached. This response is the broken line on Figure 5.3.2. The droop Np figure is seen to be 8.8% (an incremental 2.7% improvement over the base case). It can also be seen that the 2.5-3% increase in $Ng/\sqrt{\theta}$ created by the v.g. closure at zero HP, is maintained over the whole maneuver, increasing the available power and therefore decreasing droop throughout.

Case (d) considered the effect of using the 9° closure at zero HP together with a revised schedule that would open the v.g. at the same rate as the base case, but starting from 39.5° at $Ng/\sqrt{\theta}$ = 78% rather than the scheduled 30.5°. Keeping the v.g. closed by the extra 9° throughout the transient resulted in more N_p droop than the base case (by 1%).

Case (e) differed from (d) in that an abrupt opening of v.g. occurred at 78% $Ng/\sqrt{\theta}$. The v.g. remained at 4° further open than the base schedule throughout the transient. This arrangement resulted in the Np droop decreasing to 8.5% (an incremental 3% improvement over the base case).

The results are summarized in the table below.

SA 1114

Table 5.3.1 Effect of Off-Schedule v.g. During Autorotation Recovery

Case	v.g.	% Np Droop	Δ Improvement Over Base Case
a	Baseline Schedule	11.5	--
b	5° Closure at OHP, on Schedule after 78 % Ng	9.8	+1.7
c	9° Closure at OHP, on Schedule after 78 % Ng	8.8	+2.7
d	9° Closure at OHP, &9° more closed than Schedule after 78 % Ng	12.5	-1.0
e	Closure at OHP, &4° more open than Schedule after 78 % Ng	8.5	+3.0

The above results demonstrate that significant reductions in Np droop, during autorotation recovery, can be obtained by closure of v.g. at zero horsepower. The over closure of v.g. increased Ng at zero horsepower. The increased Ng will reduce the time required to accelerate to the same high power and therefore reduce the rotor droop. The second part of the study deals with maintaining Ng constant during a transient by using a vertical v.g. schedule as shown in Figure 5.3.1f. The vertical v.g. schedule is the limiting case of the above where there is sufficient range to hold Ng constant for varying horsepower. There are however stress and other considerations that prohibit large v.g. closure with redesign of the T700 engine. In this second part of the study the v.g.'s are scheduled open loop as a function of horsepower.

Bursts and chops of shaft horsepower instigated by changes in the collective pitch compensation were used to evaluate the effect of the vertical schedule. The large v.g. off-schedule migrations required these v.g. effects to be approximated to establish trends. Figure 5.3.3 shows a typical burst response comparison between the base schedule and the vertical schedule. In the base case, the Ng increase is being limited for one second while the controller is on its acceleration schedule; in the vertical schedule case, Ng is virtually constant throughout and fuel flow does not reach acceleration schedule level. Also notable is the smaller torque overshoot in the vertical v.g. schedule case. However, since this overshoot is influenced by the control system as well as the v.g. effect and no effort was applied to design other than the simple open loop v.g. schedule, it cannot be assumed that this particular aspect of the performance can be met in general. The net effect is a faster engine response as is shown in the summarizing table below (5.3.2).

SA 1114

Table 5.3.2 Engine Transient Response Time

Case	Base Schedule Transition	Vertical Schedule Transition	% Improvement
	Time (Sec)	Time (Sec)	
Burst 240-950 HP	.68	.54	21
Burst 510-950 HP	.30	.19	37
Chop 950-240 HP	.89	.59	34
Chop 950-510 HP	.28	.18	36

The conclusions of this short study were:

(i) Overclosure of v.g.'s at zero horsepower can reduce the usual droop of the main rotor speed below the governed reference after initiating autorotational recovery, by up to 25%.

(ii) Normal power transient times which are limited by accel. or decel. schedules can be reduced by 20% or more by scheduling v.g.'s to maintain constant Ng for varying shaft horsepower output.

(iii) The specific fuel consumption is adversely affected during steady state operation by most schemes that require significant off scheduling of the variable geometry.

(iv) Implementation of any off-schedule v.g. control may be limited by system and hardware constraints including reduction of stall margin and aeromechanical stress limits.

5.4 Engine Bleed

Various non-flight-critical functions use air bled from the engine compressor stages. This is known by the engine manufacturers as customer bleed and it can reduce the available power at intermediate rating by up to 10%. An obvious precaution would be to include an automatic shut-off for customer bleed under emergency maximum power conditions, within an integrated control. This was not included in the control of section 4 because customer bleed is not dealt with separately in the engine model.

SA 1114

5.5 Engine Surge Avoidance

One of the main features of CECO's pragmatic adaptive fuel control scheme was the means of modifying the individual controller's accel. Schedule when surging occurred due to deterioration or damage (Ref, 10). On detecting a surge (evidenced by a rapid spiking drop in compressor discharge pressure (CDP) and coincidental spikes of higher gas temperatures), the fuel flow would be regulated by a signal proportional to the accel. schedule N/CDP at the operating Ng, multiplied by a lagged CDP signal. This provided a reduced fuel flow and suppressed multiple surges as compared to the more conventional N/PT2 schedule which tends to increase fuel flow (which in turn increases the likehood of multiple surges). In CECO's scheme, the memory of the fuel control retains a modifier at the Ng at which surge occurred and restores the surge margin by reducing the local accel. schedule at and close to the surge point. Subsequent accelerations through that Ng range should be surge free unless further deterioration occurs. Subsequent examination of the surge modifier values when servicing the engine/fuel control would give valuable information on engine deterioration or damage.

The scheme was thought attractive enough to leave in the integrated control despite the fact that the NASA T700 Engine model could not emulate the real characteristics of a compressor surge. No testing of the code has been performed beyond ascertaining that it matches the performance of the original development when artificial spikes are injected into the CDP sensor signals. Actual compressor surge is an extremely complex phenomenon and it is likely that the seemingly promising CECO approach will be tested on a hardware implementation before the correct engine response is successfully simulated. Meanwhile the code and memory requirements are representative of this approach to surge protection and thus worth retaining in the integrated control.

6.0 EVALUATION

The evaluation of the integrated flight/propulsion control system was to be conducted in two phases, the first as part of this contract on in-house MGH simulation facilities, the second on the V.M.S. simulation with a pilot in the loop at NASA Ames.

6.1 Evaluation Using MGH

The mission segment tasks listed in Table 3.0.1 were simulated using various control strategies from the MGH control library. Whichever piloting method was chosen for a particular maneuver, was maintained as the control strategy for both baseline and integrated control equipped cases. It proved extremely difficult to "fly" the aircraft anywhere near the aerodynamic boundaries of capability because even the quite sophisticated "maneuver controllers" were not sufficiently adaptable to deal adequately with the changes required of them in the course of flying the more complex maneuvers. The MGH evaluation therefore concentrated on flying each maneuver in as simple and repeatable way as possible, in order to make comparisons between baseline and integrated systems, leaving a complete "wringing out" of the new control system to the V.M.S. stage of evaluation where a human pilot could be expected to make a more complete assessment.

The integrated control design was to have been iterated upon several times, once it became available for evaluation on the MGH simulation. Owing to the delay in receiving the working version of the T700 engine model from NASA, and subsequent heat sink problems, only one partial design iteration was possible. There is room for improvement in detail performance of several aspects of the integrated design presented here.

The evaluation was performed as indicated, by "flying" the simulation through a series of maneuvers. Each maneuver employs various items in the integrated control to different extents--where the behavior is similar, it is not enlarged upon, but reference is made to the first descriptive occurrence.

In general, the BLACK HAWK simulation was flown with SAS 'on' but FPS 'off'. Both sub-systems could be expected to be incorporated in an integrated design, and SAS 'on' is a way of acknowledging that incorporation. The FPS functions of the BLACK HAWK were largely inappropriate for this study. The coordinated turn feature was provided by the maneuver controller and leaving the FPS feature 'on', caused interference with the controller operation, so was not done. The attitude hold feature was the opposite of what was required for the fuel minimization scheme, and an altitude hold for that function is not featured in the UH-60A EFCS package. (An outer loop closure was written for that task, switched and coded outside the MGH EFCS module).

The integrated control cycle time was varied between 1¼ and 25 millisecs for the autorotation recoveries; no performance differences were discernable, so the standard 10 millisecs was reverted to for all other cases.

Both baseline and integrated fuel controls were provided with a coded variable to define the operational status of the control at all times. These are:

SA 1114

For Baseline control, IHMUSE = 1 Np governor
2 Minimum Idle
3 Decel. Limit
4 Accel. Limit

For Integrated control, RMODE = 20 Decel. Limit
30 Ng bottom governor
40 Ng top governor
50 Np governor
60 Temp Limit
70 Accel. Limit

Additionally, 3 is added to RMODE when on minimum flow stop, subtracted when on maximum flow stop (i.e. 47, 53).

In each of the section 6 Figures (6.1.1 thru 6.1.10), the following information is plotted as a time history:

ALT	The flight path altitude starting from an arbitrary zero (Sea Level, standard conditions)
VC	aircraft climb velocity
VKT	aircraft airspeed
VE	aircraft groundspeed in easterly direction
NZ	Aircraft normal load factor at the center of gravity
P	aircraft roll rate
Q	aircraft pitch rate
R	aircraft yaw rate
PHIB	aircraft bank angle
THETAB	aircraft pitch attitude
PSIB	aircraft heading, starting from north
BCQDOS	"degree of rotor stall" indicator
XAPC, XBPC, XCPC, XPPC	control positions, lateral longitudinal, collective and rudder pedal respectively
QHBMR	filtered torque load generated by the main rotor
OMRMR	the main rotor shaft speed
OMR.MR	acceleration of the main rotor shaft

SA 1114

N2RFE	engine power turbine output speed
THETTR	collective pitch angle at the tail rotor
BRMR	flapping angle of a reference main rotor blade
LGMR	lagging angle of a reference main rotor blade
PAS	power available spindle angle (cockpit signal to engine)
QPTE	#1 engine power output torque
T45E	gas temperature at engine power turbine inlet.
PCNGC	engine gas generator speed
XNGDTE	engine gas generator acceleration
WFCE	engine fuel flow
RMODE	coded status of integrated control governor
IHMUSE	coded status of original T700 fuel control
CLUEG	engine-main rotor shaft clutch status
T45MEA	temperature at engine power turbine inlet (as measured by a simulated sensor)
NDOTDC	output of the integrated governor decel. schedule
AGAIN	gain applied to the LQR Np governor
WFNP	fuel flow requested by integrated N_P governor
WFNG	fuel flow requested by integrated N_G governor
WFHI, WFDMD	'winning' fuel flow passed to stepper motor
WFDEC	fuel flow requested by integrated $\dot{N}_G$ decel. governor
WFBG	fuel flow requested by integrated $\dot{N}_G$ BOTTOM governor
DNPRAT	rotor decay anticipator increment in integrated Np governor
DNPREF	total increment to Np_{REF} in integrated Np governor
NGDGOV	rate of change of N_G in integrated NG topping governor
NGDACC	rate of change of N_G in integrated $\dot{N}_G$ accel. governor

SA 1114

NGDTL — rate of change of N_G in integrated temperature limiting governor

NGD — rate of change of N_G in 'winning' N_G governor in integrated controller

Not all of these variables are actively contributing during each maneuver.

The dashed lines represent the baseline BLACK HAWK T700 simulation, the full lines represent the integrated flight/propulsion control version.

Figures 6.1.1. through 6.1.4 are the simulated autorotational recoveries for each of the four types discussed in 3.1. The splits are 17% and 2%, the collective lever pull times are 3.0 and 0.5 seconds. In each case, the collective pitch is pulled up to 70%, resulting in a final climb rate of over 3000 ft/min (from an initial descent-rate of just under 3000 ft/min). The cases were flown by applying a ramped collective input while allowing the maneuver controller to act as a full authority rate damper in roll and yaw axes. Thus the pedal activity necessary to counteract the large changes in main rotor torque load while keeping the yaw rate small can easily be seen and the two systems compared. (The heading hold was not used as it sometimes interfered with the maneuver controller). The standard SAS (limited authority rate dampers) was switched on. The solid lines on the plots are for the integrated control, the dashed lines for the baseline control.

Figure 6.1.1 shows the recovery from a 17% split, using a 3 second pull. The rotor speed droop (OMRMR, Figure e) is reduced from 10.5% to 2%. The normal load factor N_Z bias is higher than the baseline by about 0.25g, presumably due to both direct and indirect effects of the higher OMRMR. The direct effect is to produce more lift, the indirect one is to produce more pitching moment which allows the nose of the aircraft with integrated control to pitch up more and sooner (THETAB, c). The rate of climb (Vc,a) reflects the increased lift between 2.0 and 8.0 seconds. The amount of pedal and reversals of their direction (XPPC, d) required to keep the rate of yaw (R, b) small is seen to be less for the integrated control while the applied control at the tail rotor (THETTR, f) is much the same. It is not particularly clear from the power turbine output shaft speed plot (N2RFE, e) but can be seen on the engine clutch state (CLUEG, h) that the integrated controller causes that engine to engage with the main shaft much earlier (and at higher speed) than the baseline - this is due to the rotor decay signal (DNPRAT, k) producing a fuel flow to speed up the gas generator as well as the collective pitch (LDS) link. Once engaged, the LQR Np governor takes over (AGAIN, i goes to 1.0), detects that the NP is overspeeding and puts the controller onto its decal. schedule by demanding a large decrease in fuel flow. Eventually, the Np governor requires short bursts on the accel. schedule before it copes in its own range with a quite smooth recovery. In contrast, the baseline controller detects the N2RFE (e)

overspeed (caused by the LDS link) and switches to its decel. schedule (IHMUSE, h) before the clutch engages (CLUEG, h). Details of the baseline fuel demands are not plotted, but the net result of the cut back at the wrong time is a droop in rotor speed of 10.5%.

Figure 6.1.2 shows the same recovery using a much faster (0.5 second) pull. This time, there is much less difference in behavior, droop being reduced from 8% to 7%. the nose still goes higher with slightly more g pulled and the rudder pedal activity clearly favors the integrated controller. Basically, the fast LDS input slams both controllers onto their accel. schedules immediately and the rotor load increases so quickly (causing the shaft speed to decline swiftly), that the power turbines do not have time to overspeed, nor does the rotor decay compensation have time to speed up the gas generator. The result is that each system has to wait for the accel. schedule to allow the engine to produce enough torque to overcome the droop. The integrated control then makes a much better job of the subsequent recovery, allowing no overspeeding (as opposed to 4% from the baseline control).

Figure 6.1.3 shows slow (3.0 second) pull recovery from the small split autorotation condition. The integrated control is rather worse than the baseline, allowing 4% droop as against 1%. This is largely because, after clutch engagement, which occurs at about 0.9 secs on each version, the integrated control cycles on and off its decel. schedule with N2RFE of 102.5% - this seems to be a sensitivity problem which could be solved with another design iteration but for which there was insufficient time. It is noted that even with the slightly larger droop, the integrated control requires less pedal motion, XPPC.

Figure 6.1.4 is the corresponding small split recovery using a fast (0.5 second) pull. The integrated control is again marginally worse than the baseline (16% droop as against 15%) while the overspeed recovery is much better (0.5% overspeed versus 4%). The pitch response is unrealistically severe, pilot action would have been taken long before the nose rose to 30°. Basically, once again both controllers slam on to the accel. schedule and stay there (the basic control for too long, since it caused an overspeed at 4.5 seconds while still on the accel. schedule). The integrated control comes off its accel. schedule at 2.2 seconds and the subsequent recovery is smooth.

These autorotational recovery performances are summarized in table 6.1.1 below. A set of figures for a 1 second pull (not illustrated) has been added.

SA 1114

Table 6.1.1. Droop Levels During Autorotational Recovering

	Large Split (17%)			Small Split (2%)		
Pull Time (Sec)	.5	1.0	3.0	.5	1.0	3.0
Droop [Baseline]	-8.0	-6.5	-10.5	-15.0	-10.0	-1.0
Overshoot	+4.0	+0.5	+3.0	+4.0	+4.0	0
Droop [Integrated]	-7.0	-1.5	-2.0	-16.0	-9.0	-4.0
Overshoot	0	0	0	+0.5	0	0

Figure 6.1.5 is the simulated pop-up and remask maneuver flown using the maneuver controllers. A 5% overrun in collective pitch was not corrected. The height change is 55 ft, achieved in 6 seconds, pulling a load factor in hover of about 1.9. The engine cannot respond quickly enough despite each control going onto its accel. schedule almost immediately and a 6% droop occurs. The baseline control stays on its accel. schedule for a full second longer than the integrated control, with attendant overshoots twice as large. The LQR Np governor deals with the situation more smoothly once the initial accel. limited response is completed. This is further confirmed by the pedal movement plot where compensation is initially required because the rotor torque load comes on before the engine response, later in the maneuver, the compensation comes smoothly off until, briefly on the remask, the rotor load again changes faster that the engine response while on the decel. schedule.

Figure 6.1.6 is the simulated straight line quickstop without altitude gain. The speed change is from 145 knots to 10 knots in 30 seconds. This was flown by the profile autopilot holding the nose up at 15° with longitudinal stick until the speed had dropped, while maintaining nominally zero rate of climb by dropping, then slowly increasing, the collective pitch. The baseline governor goes onto its accel. schedule for 2.5 seconds and allows about 2% rotor speed droop. The LQR Np governor deals with the loads without permitting any droop (there is a momentary drop onto the decel. schedule as collective pitch comes down very fast at the 2 second mark).

Figure 6.1.7 is the simulated sideward accel/decel maneuver. It was flown by the profile autopilot developing 40° of bank in one direction over 30 seconds reversing to 40° opposite bank in a further 2 seconds, then rolling back to a recovery in hover. The bank angle was not left on for an appreciable time, so only about 60 ft is traversed although roll rates of 60°/second were developed. Neither controller has much difficulty with the loads developed although each allows about 1.5% variation in Np. The integrated control hits the maximum fuel flow limit and pops onto the accel. schedule briefly as the stick is moved left at 3.7 seconds to remove the right bank. The pedal yaw rate compensation is slightly more abrupt for the integrated control because the collective pitch compensation for constant altitude tends to help the baseline linkage whereas the engine torque phase lag tends to hinder the integrated control.

Figure 6.1.8 shows the simulated high g turn/deceleration maneuver, flown by initiating and holding a 60° bank left turn for a 180° heading change, bleeding off speed from 145 to 80 knots. The autopilot gains were rather higher than optimal, causing some unnecessary 1 Hz input excitation during initiation and recovery. There may also have been some undesireable coupling into the load factor enhancer which is later (at and after the 2 second mark) seen to be holding Nr about 7% above nominal during the turn thus allowing the 'g"' pulled to approach 2.25). A 2% droop is seen for both controls during the final recovery.

Figures 6.1.9 and 6.1.10 show the simulated roll reversals, 50° right to 50° left and 50° left to 50° right respectively, flown by the profile autopilot. The LQR Np governor exhibits good control during both these maneuvers allowing just 1% droop during the most severe load change at 8 seconds on the 6.1.9 plots when the negative roll rate peaks at -45°/sec.

6.2 Using VMS Simulator of NASA (Ames)

A series of recommendations for VMS experiments to evaluate the integrated control were made and were published as Reference 13. For various scheduling reasons, this work has not yet been undertaken. A full evaluation can only be performed with a real-time pilot-in-the-loop motion simulation such as that available at NASA (Ames).

7.0 CONCLUSIONS

i. A set of standard maneuvers which exhibited potential for improvement using an integrated flight/propulsion control system, was established.

ii. Frameworks and protocols were set up whereby externally supplied Fortran coded simulations of engines and fuel controls can be converted into MGH modules fairly easily.

iii. A list of desirable concepts for an integrated control was established.

These were:

LQR Np Governor
Engine Performance Mapping/Power Available to Hover
Fuel Consumption Minimization in Cruise
Engine Failure Detection - Contingency Power
Tail Rotor Pitch Link to Engine Torque
Rotor Speed Scheduling in Maneuvering Flight
Collective Pitch Rate Limiter
Torque Spike Anticipation in Roll Reversals
Flight Path Response after Engine Failure

SA 1114

iv. A further list of possible features and required changes in the simulation to accommodate them was also established.

These were:

Dutch Roll/Torsional Mode Tuning
Stabilator Setting and Fuel Consumption Minimization
Engine Variable Geometry
Engine Bleed
Engine Surge Avoidance

v. An MGH module containing the features of item # iii was written and in slightly modified form, sent to NASA for incorporation in the Ames 'Gen Hel' BLACK HAWK VMS simulation. This module was written in strict ANSI Fortran IV for maximum transportability and contains the means for changing the simulated microprocessor execution time as well as the main execution time for maximum flexibility.

vi. The integrated flight/propulsion control scheme was evaluated using MGH and found to be an improvement to the basic control in most areas, even though the latter is a harmonious match of engine and airframe which exhibits few of the problems of other aircraft (or on a much diminished scale as seen in the AACT data). Therefore, it would be expected that less well matched systems could benefit more from such integration.

vii. While MGH provides a useful tool for the preliminary investigation of this control approach, the essence of the evaluation has to be a pilot-in-the-loop motion simulation because the critical factor is the extent to which rotor speed droop affects control power and how a pilot copes with the subsequent control problem. To this end, a preliminary schedule for a set of simulation experiments to be carried out on the VMS at NASA (Ames) has been prepared (Reference 13).

viii The eclectic approach of selecting versions of concepts already existing, results in many design compromises that should not have to be made. It is strongly recommended that airframe, engine and control manufacturers establish a small integrated design team at the start of a helicopter project to deal with all aspects of the required integration schemes.

ix. There are several interesting schemes that were not examined at all because of the (perhaps self-imposed) restrictions of BLACK HAWK and the T700. They might well be studied, at least in a preliminary fashion, using a linearized approach. They should include auxiliary propulsion devices (probably employing some form of convertible engine).

REFERENCES

1 Houck, J. et al: Rotor Systems Research Aircraft Simulation Model. NASA TM78629 November 1977.

2 Howlett, J.J.: UH-60A BLACK HAWK Engineering Simulation Vols I & II. NASA CR 166309 December 1981.

3 Kaplita, T.T.: UH-60A BLACK HAWK Engineering Simulation Model Validation and Proposed Modifications. NASA CR 177360 June 1986.

4 McFarland, R.E.: Establishment of a Rotor Model Basis NASA TP 2026 June 1982.

5 Ballin, M.G.: A High Fidelity Real-Time Simulation of a Small Turboshaft Engine. NASA TN (to be published).

6 Ruttledge, D.G.C.: Description of Digital Computer Subroutine Simulating a Flight/Propulsion Control Integration Scheme FORNAS.FOR SER-760604 Revision 1 November 1986.

7 de los Reyes, G., and Gouchoe, D.R.: The Design of a Turboshaft Speed Governor using Modern Control Techniques. NASA CR 175046 Feb 1986.

8 Kwakernaak, H. and Sivan, R.: Linear Optimal Control Systems. New York. Wiley Interscience 1972.

9 Howlett, J.J., Morrison, T and Zagranski, R.D.: Adaptive Fuel Control for Helicopter Applications. AHS Journal Vol 29, No. 4, October 1984.

10 Morrison, T., Zagranski, R.D. and White, A.J.: Adaptive Fuel Control Feasibility Investigation. USAAVRADCOM-TR-83-D-1 May 1983.

11 Kuczynski, W.A. et. al: The Influence of Engine/Fuel Control Design and Dynamics and Handling Qualities. AHS 35th Annual National Form Paper 79-37.

12 Alwang, J.R. and Skarvan, C.A.: Engine Control Stabilizing Compensation-Testing & Optimization. JAHS Vol. 22 No. 3 July 1977.

13 Ruttledge, D.G.C.: Recommendations for VMS Experiments to Evaluate a Flight/Propulsion Control Integration Scheme. Sikorsky Engineering Report - SER-760605. April 1986.

SA 1114

UNITED TECHNOLOGIES
SIKORSKY AIRCRAFT

SER 760606

UH-60A BLACK HAWK

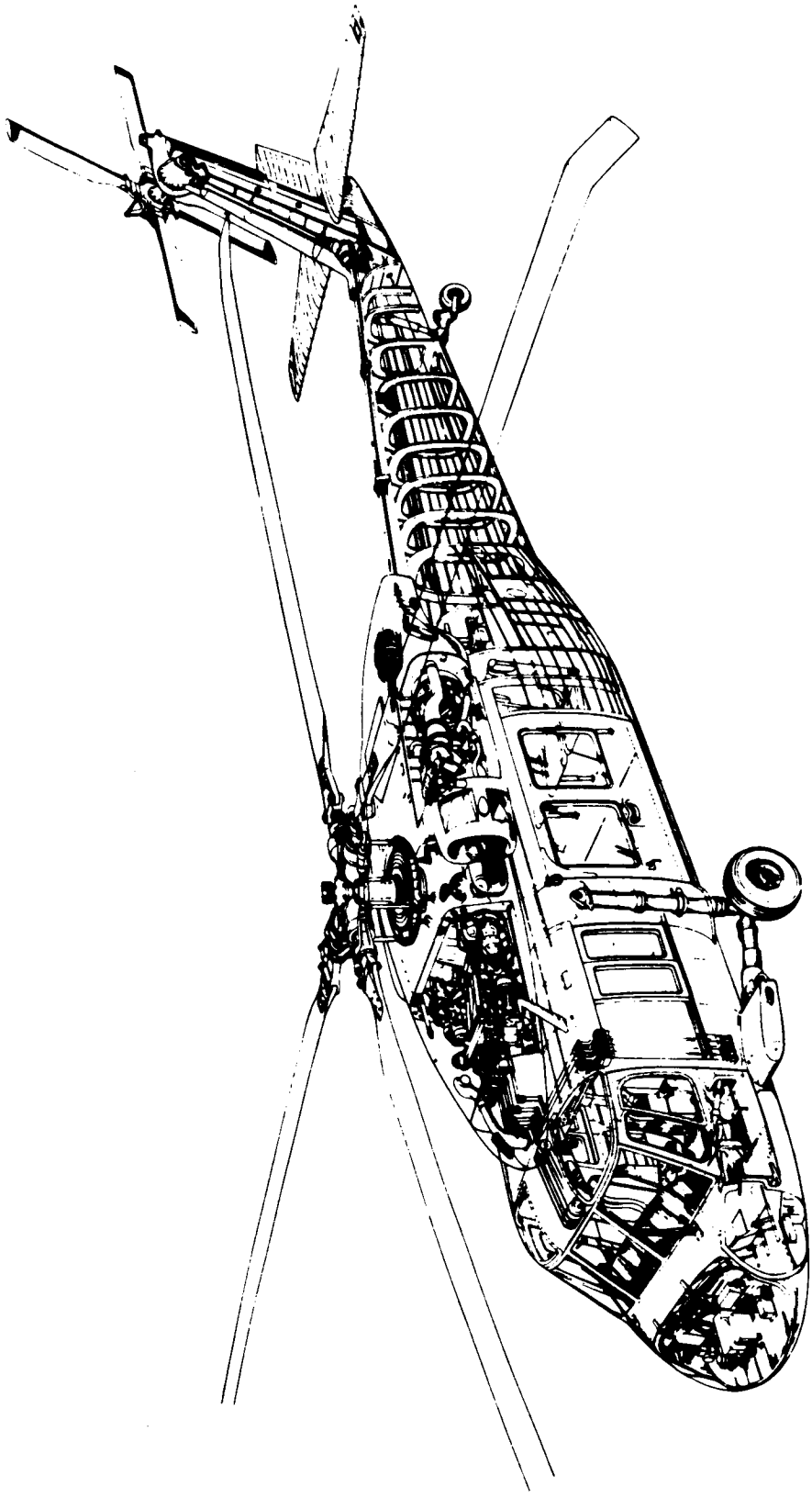

SA 1114

FIG. 2.4.1

UNITED TECHNOLOGIES SIKORSKY AIRCRAFT

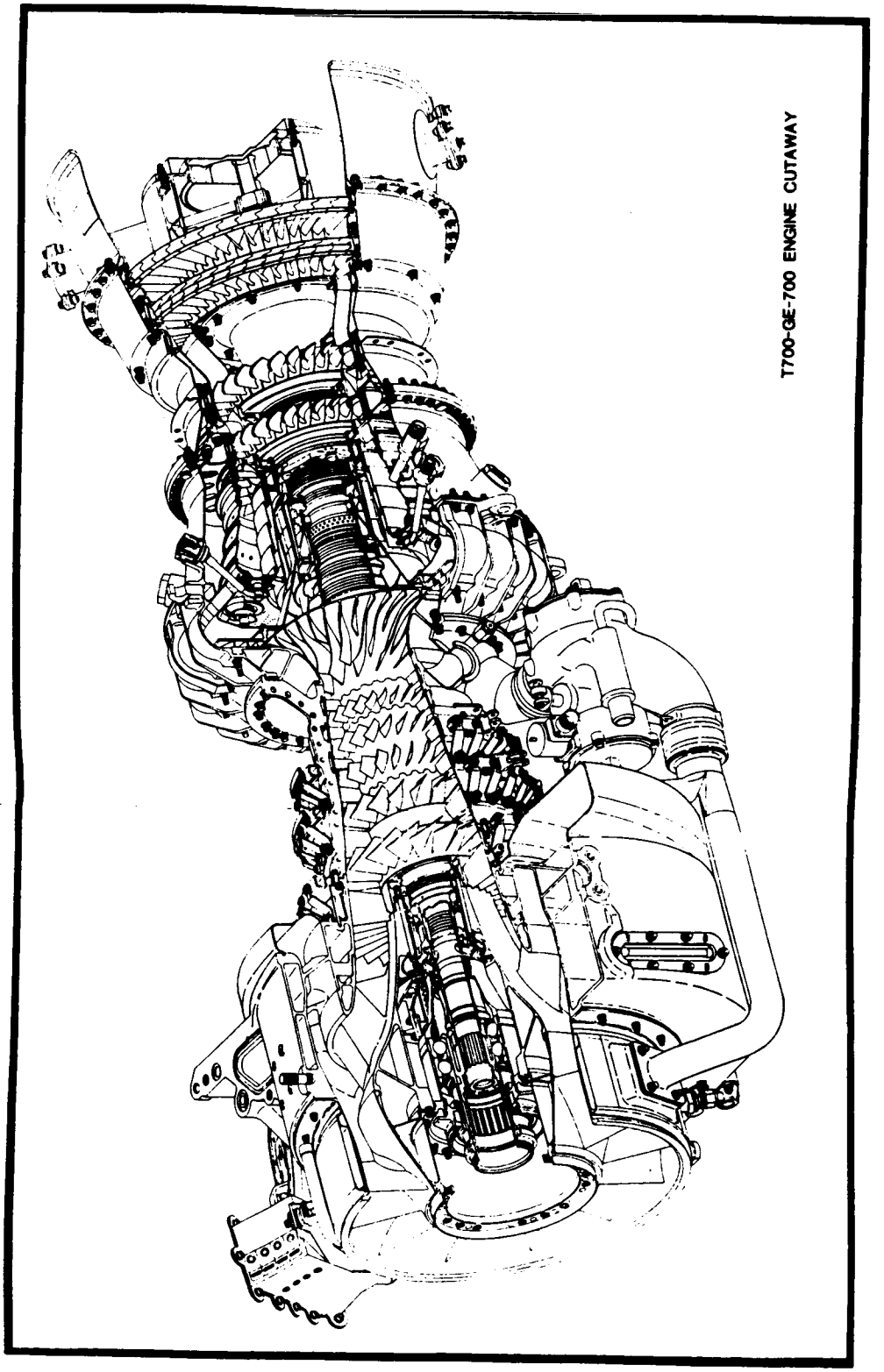

SA 1114

FIG. 2.5.1

UNITED TECHNOLOGIES
SIKORSKY AIRCRAFT

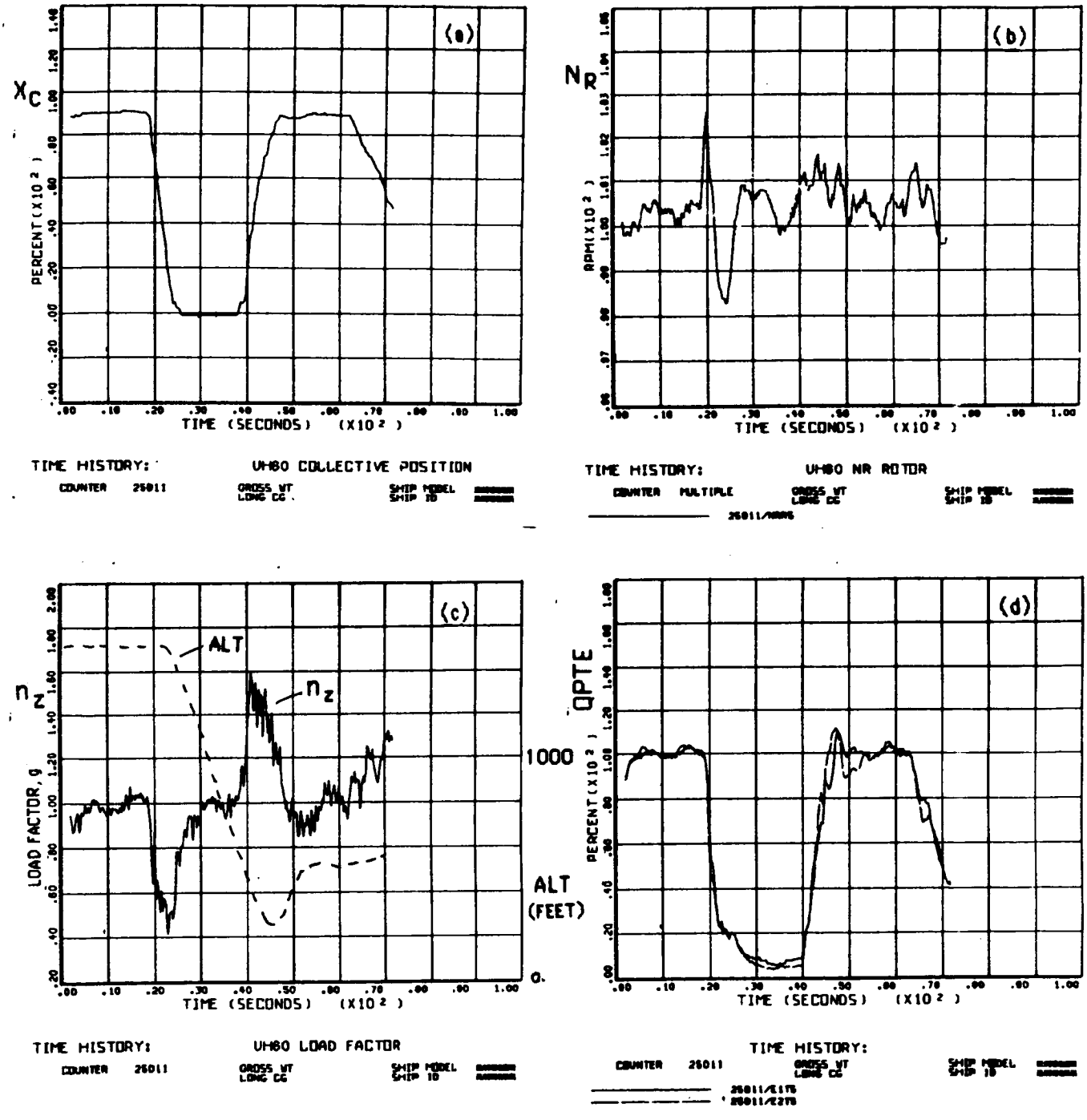

SA 1114

FLIGHT TEST: AUTOROTATION RECOVERY (SMALL SPLIT, SLOW PULL)

FIG.3.1.1

UNITED TECHNOLOGIES SIKORSKY AIRCRAFT

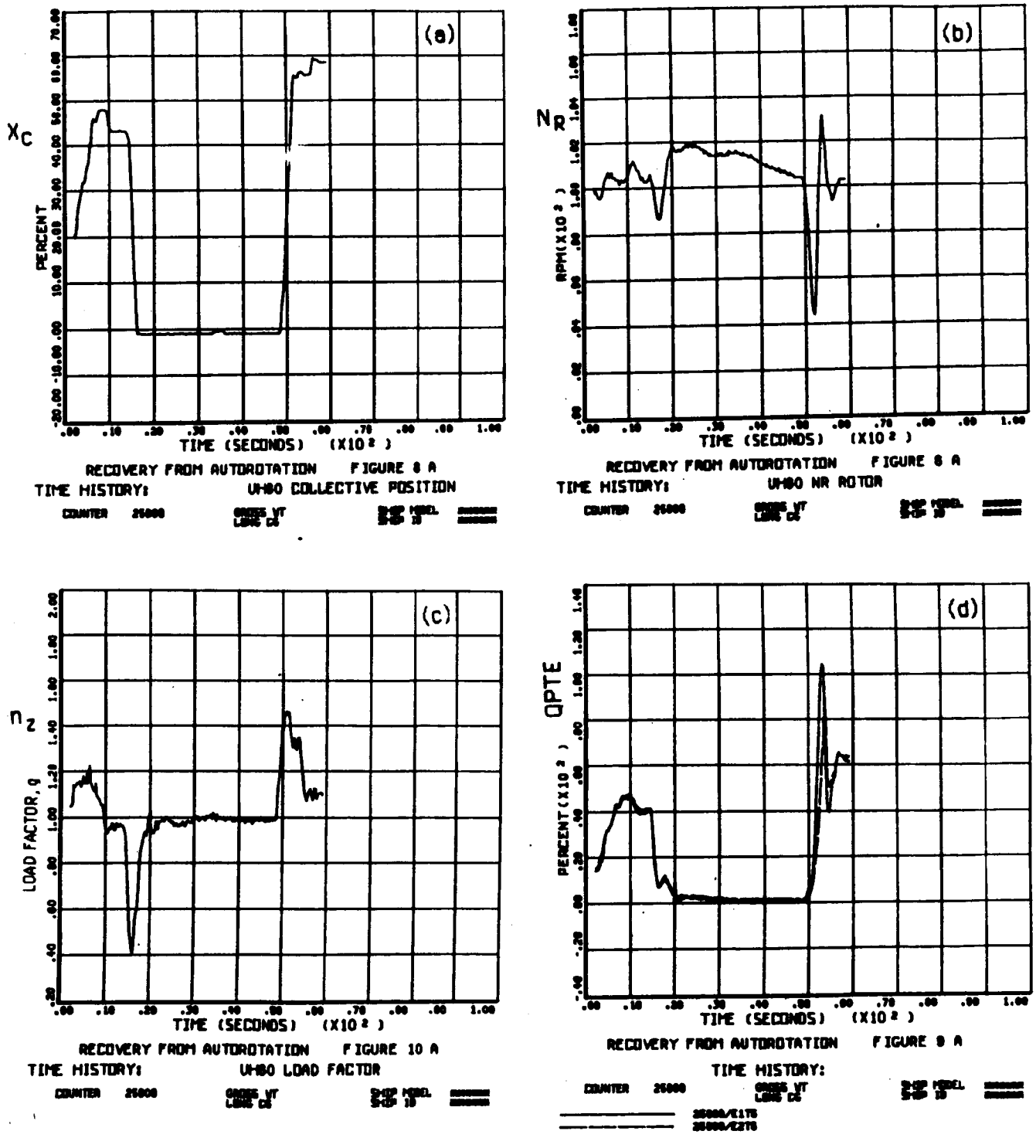

SA 1114

FLIGHT TEST: AUTOROTATION RECOVERY (SMALL SPLIT, FAST PULL)

FIG.3.1.2

UNITED TECHNOLOGIES
SIKORSKY AIRCRAFT

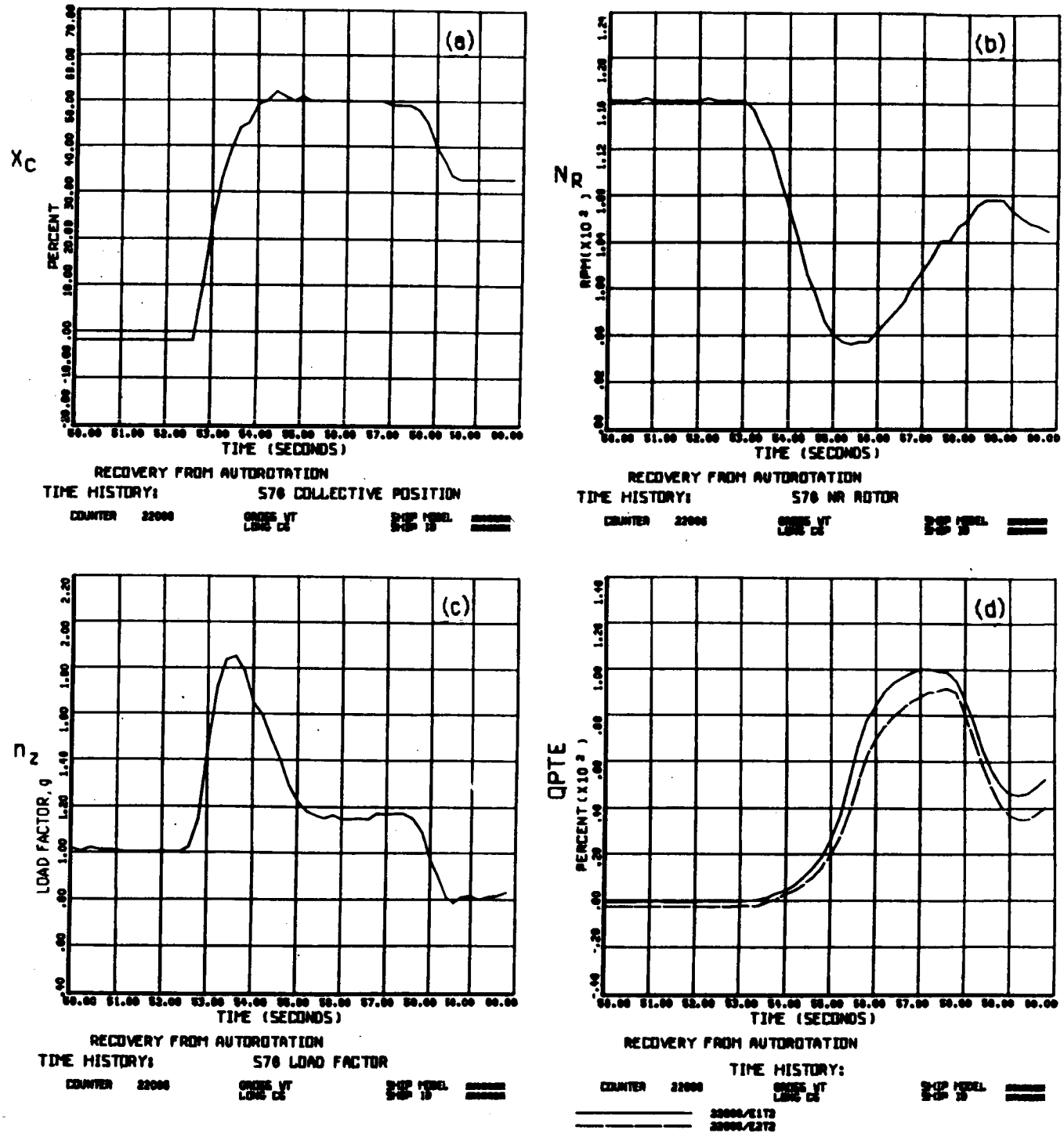

SA 1114

FLIGHT TEST: AUTOROTATION RECOVERY (LARGE SPLIT, FAST PULL)

FIG.3.1.3

UNITED TECHNOLOGIES
SIKORSKY AIRCRAFT

ORIGINAL PAGE IS
OF POOR QUALITY

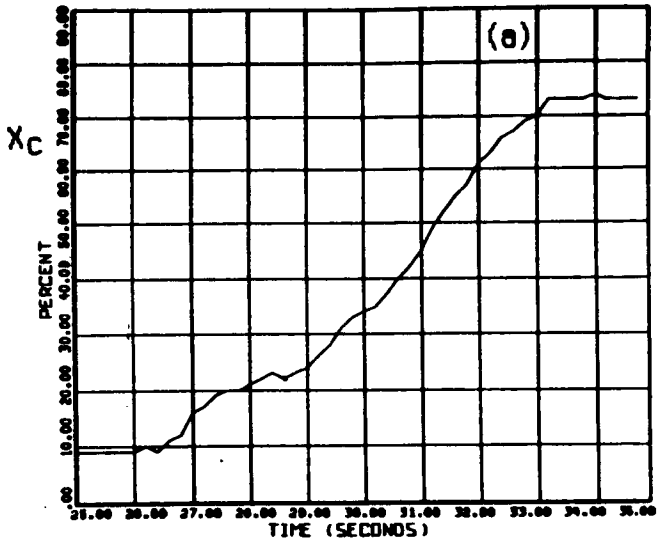

TIME HISTORY: 576 COLLECTIVE POSITION
COUNTER 22008

22008/COL2

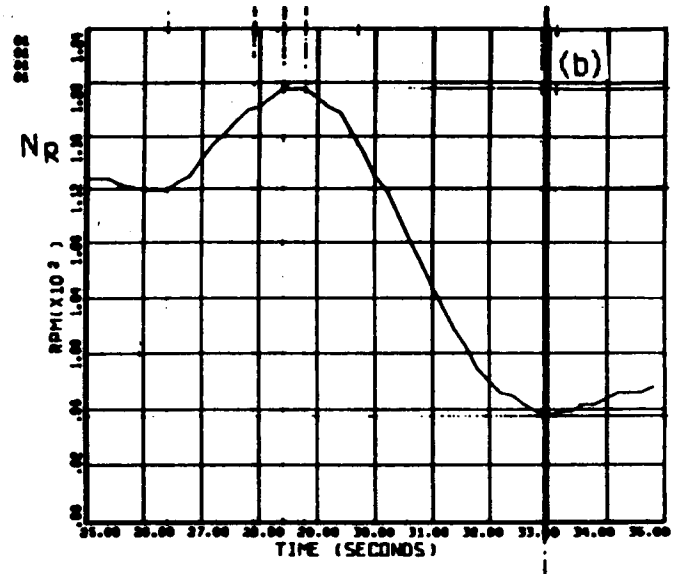

TIME HISTORY: 576 NR ROTOR
COUNTER 22008

22008/NRR2

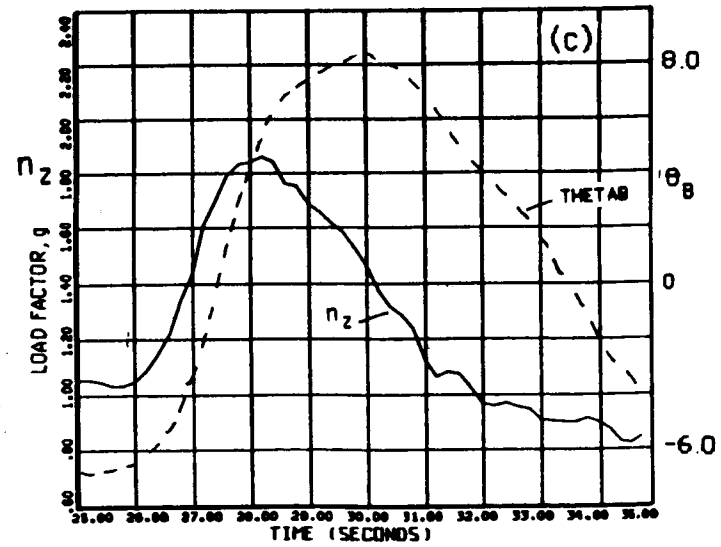

TIME HISTORY: 576 LOAD FACTOR
COUNTER 22008

22008/GGG2

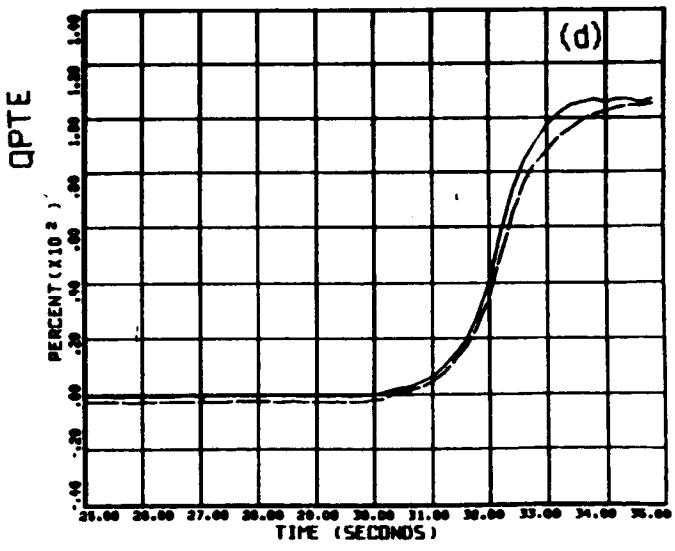

TIME HISTORY:
COUNTER 22008

22008/E1T2
22008/E2T2

SA 1114

FLIGHT TEST: AUTOROTATION RECOVERY (LARGE SPLIT, SLOW PULL)

FIG.3.1.4

ORIGINAL PAGE IS
OF POOR QUALITY

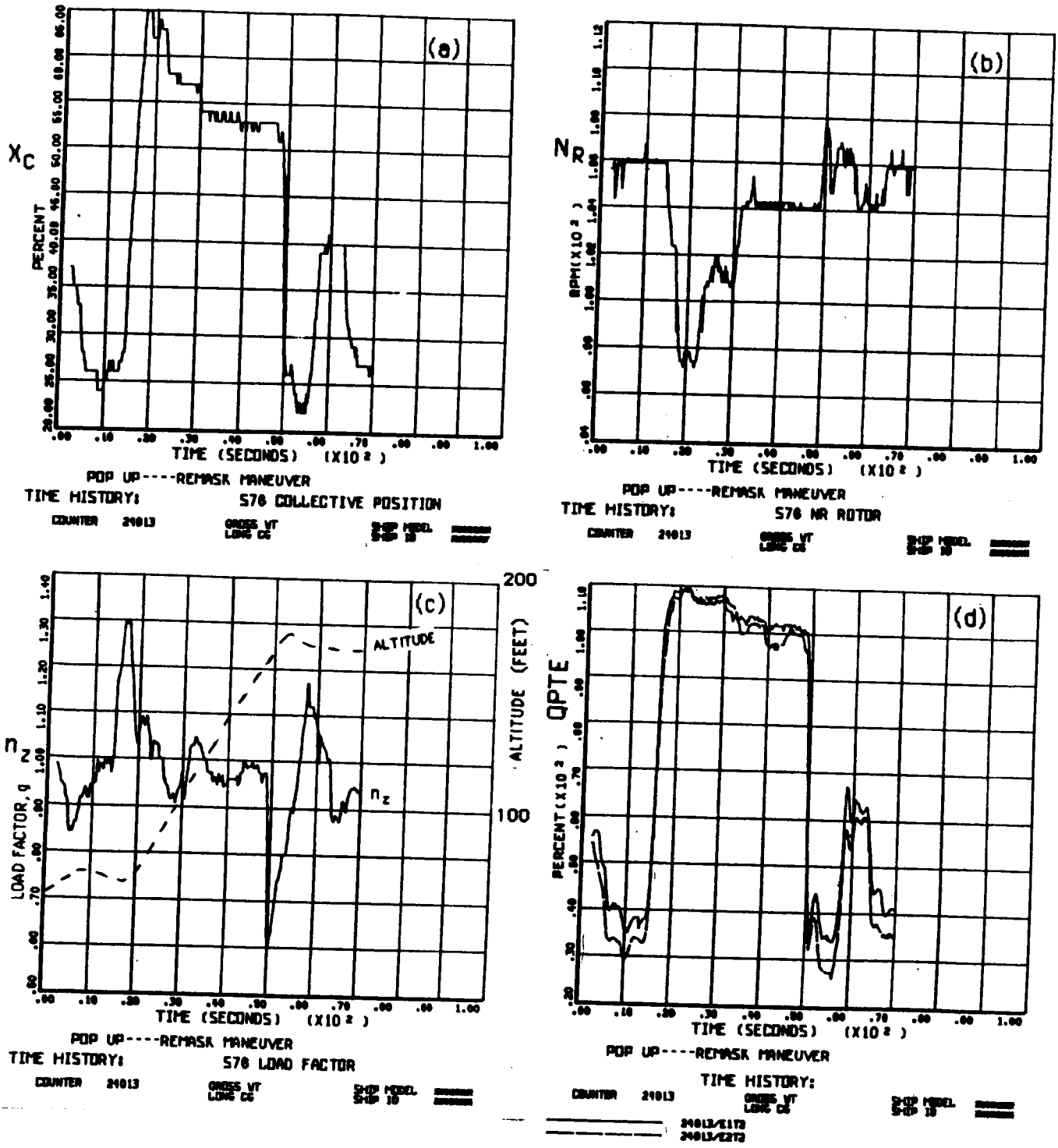

FLIGHT TEST: POP-UP AND REMASK

FIG. 3.1.5

UNITED TECHNOLOGIES
SIKORSKY AIRCRAFT

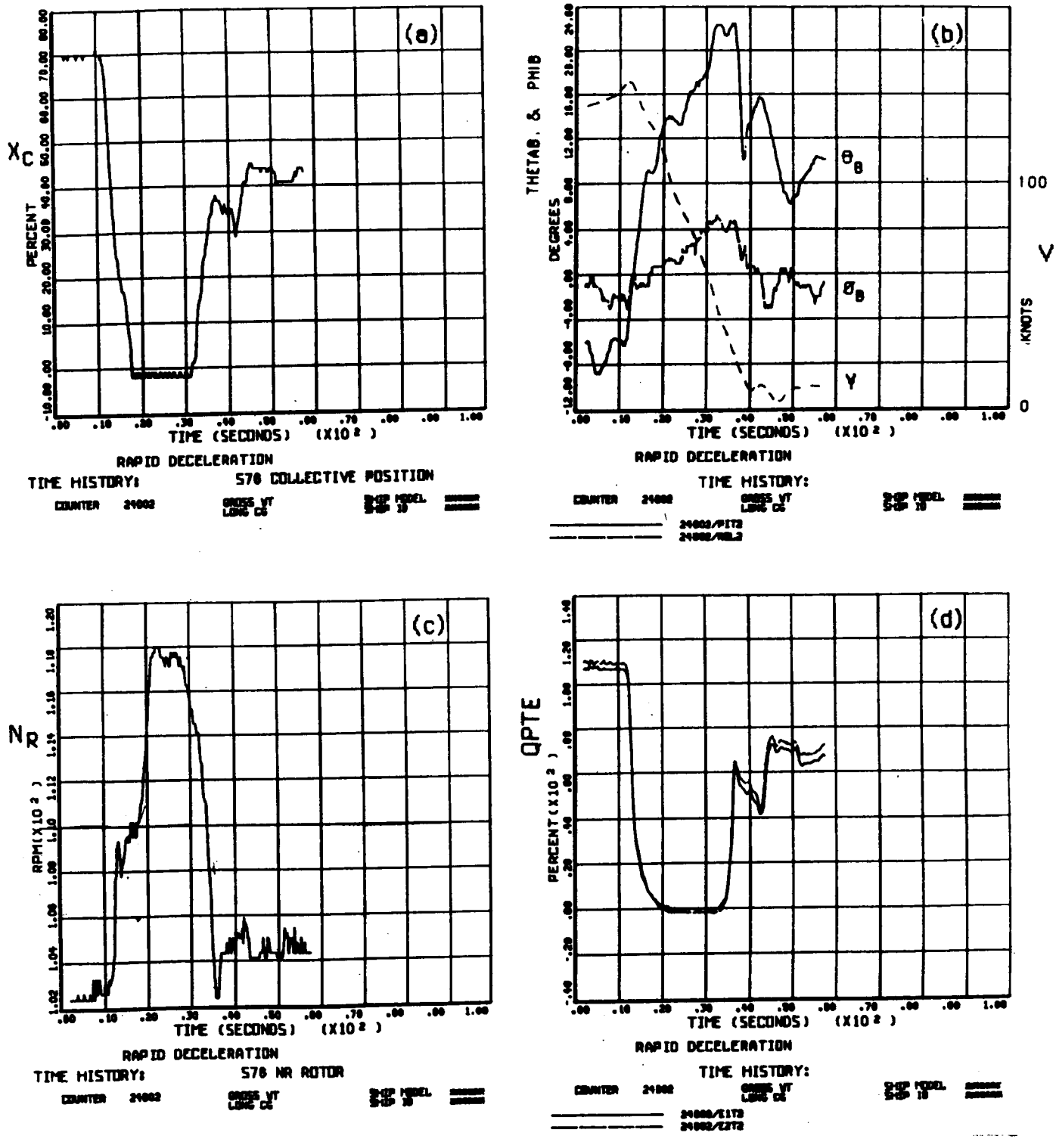

SA 1114

FLIGHT TEST: QUICKSTOP

FIG. 3.1.6

UNITED TECHNOLOGIES
SIKORSKY AIRCRAFT

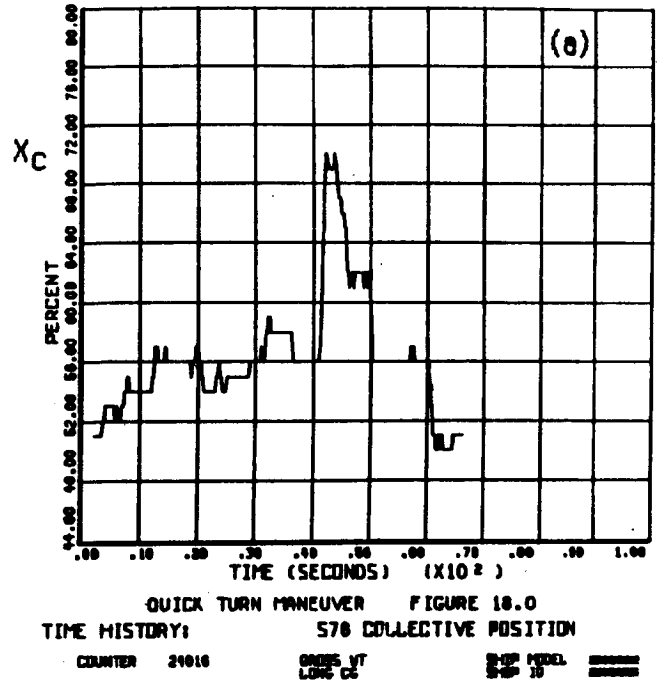

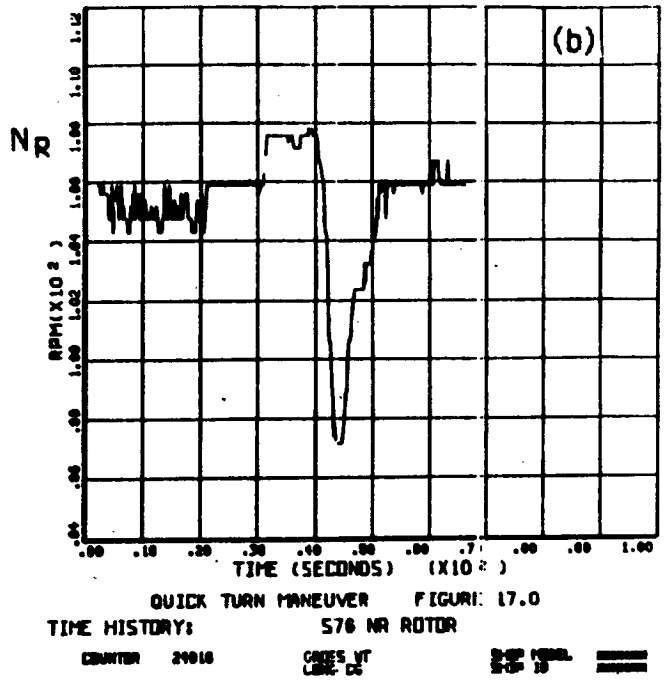

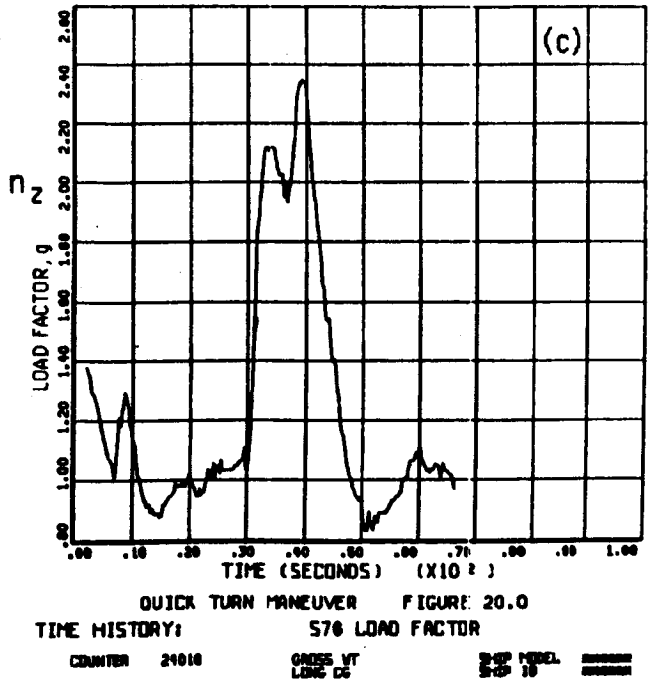

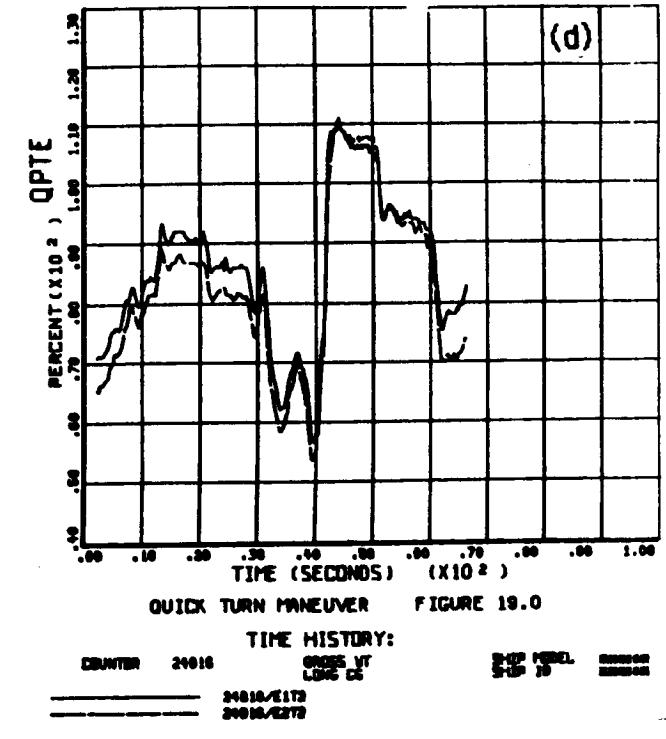

SA 1114

FLIGHT TEST: QUICK TURN / DECELERATION

FIG. 3.1.7 a - d

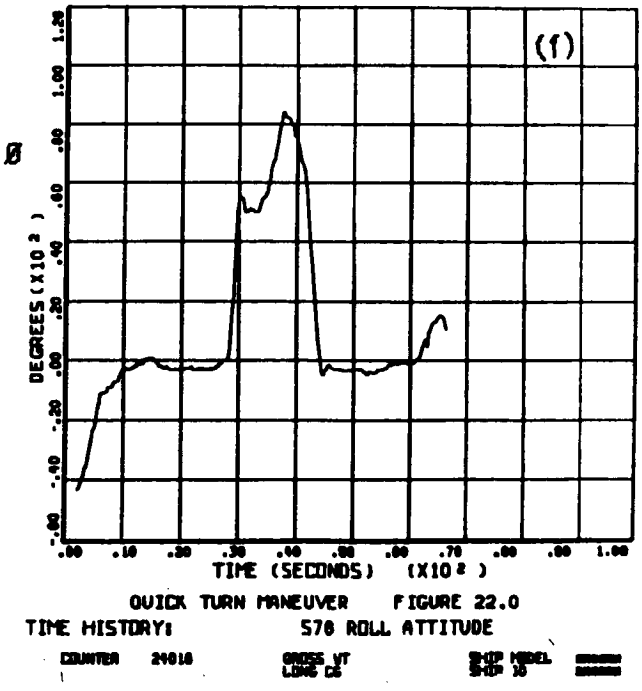

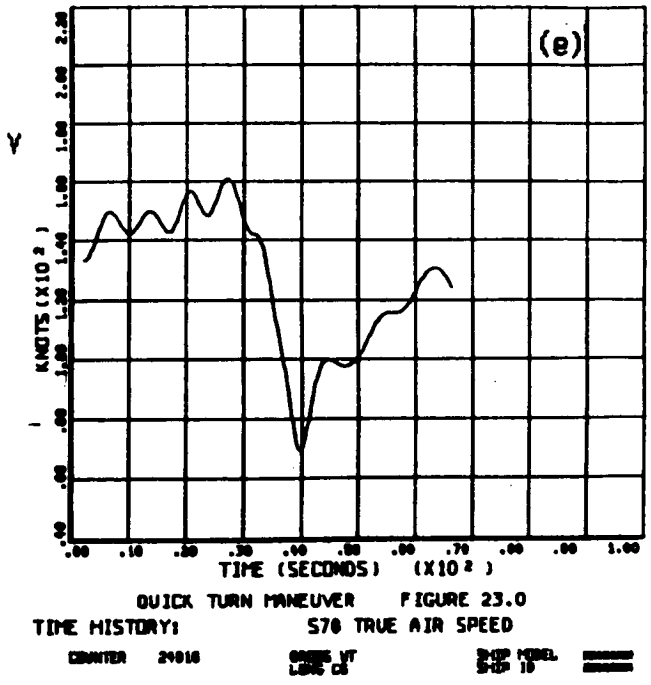

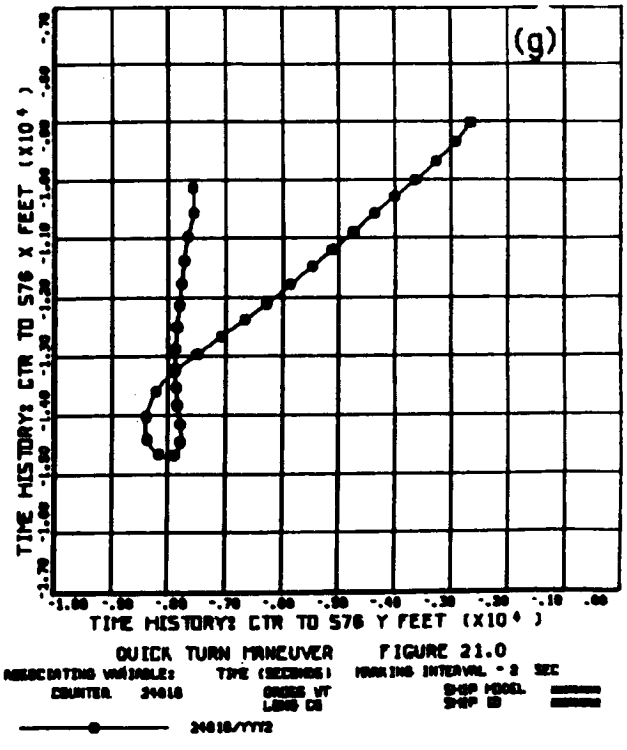

SA 1114

FLIGHT TEST: QUICK TURN / DECELERATION

UNITED TECHNOLOGIES SIKORSKY AIRCRAFT

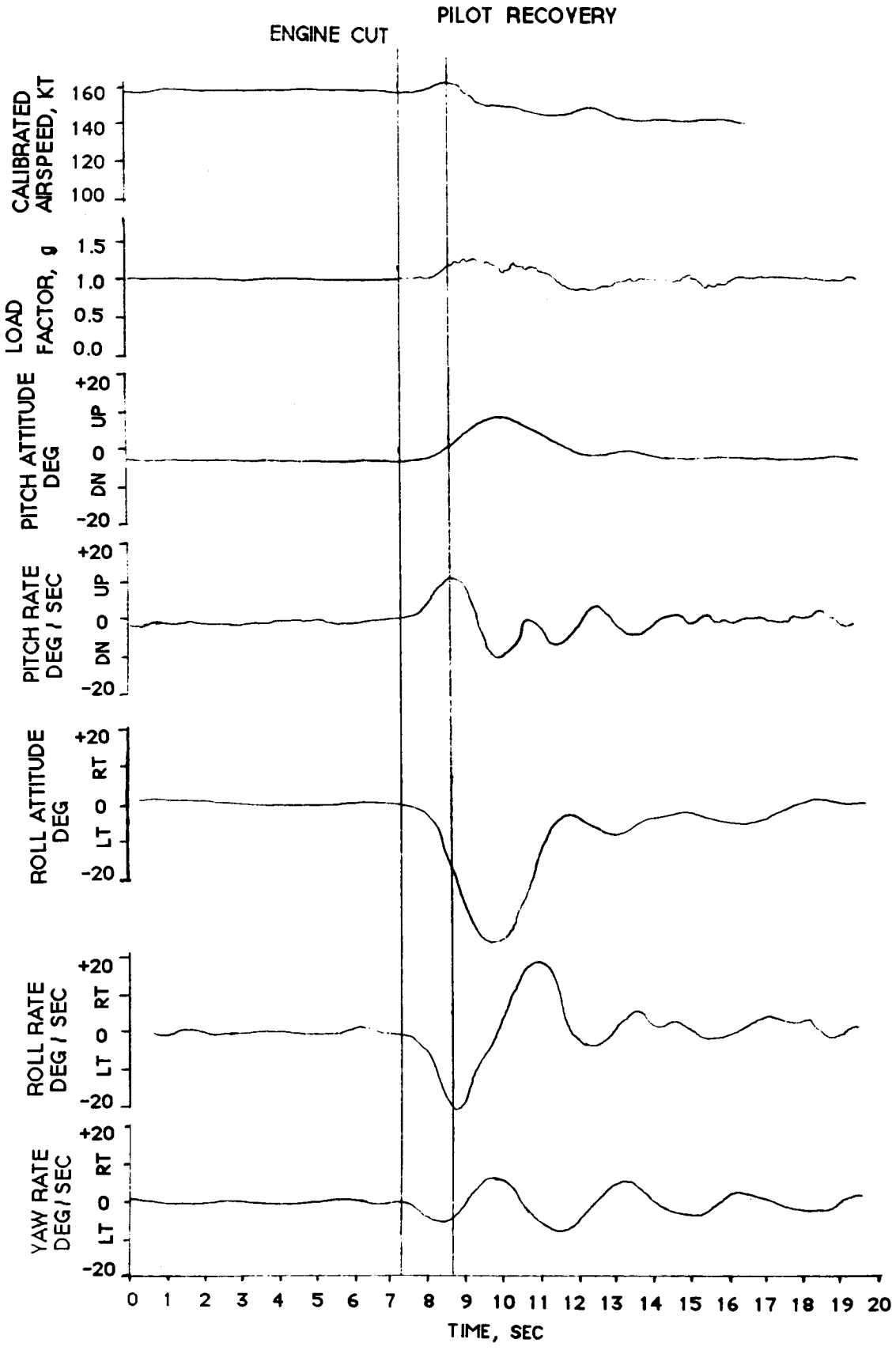

FLIGHT TEST: THROTTLE CHOP

FIG. 3.1.8

UNITED TECHNOLOGIES
SIKORSKY AIRCRAFT

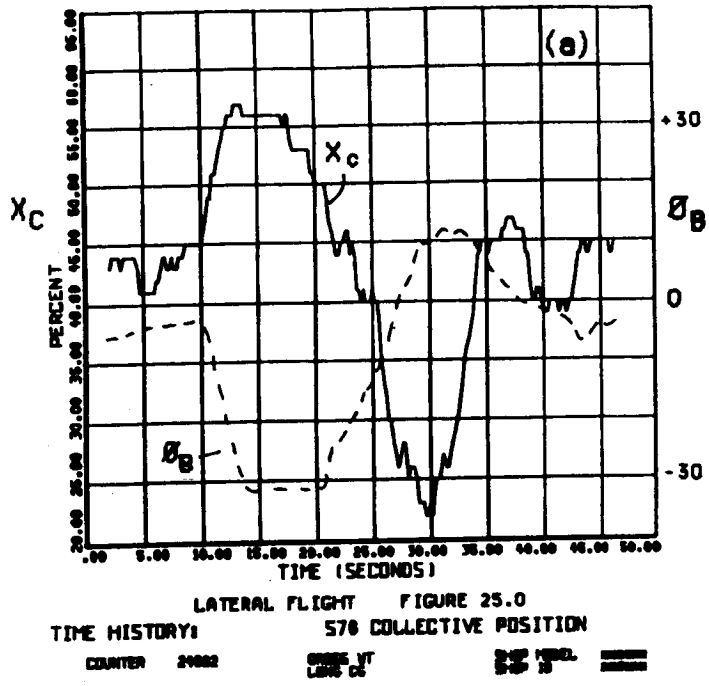

LATERAL FLIGHT FIGURE 25.0
TIME HISTORY: 578 COLLECTIVE POSITION

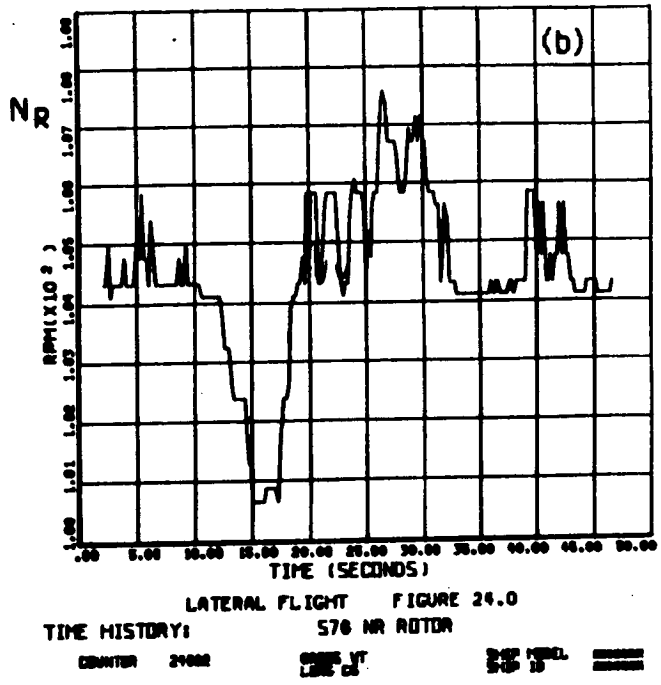

LATERAL FLIGHT FIGURE 24.0
TIME HISTORY: 578 NR ROTOR

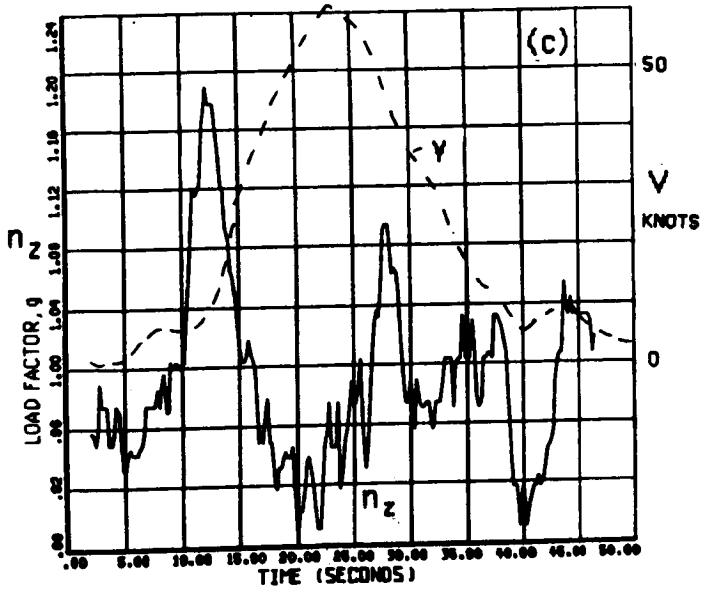

LATERAL FLIGHT FIGURE 27.0
TIME HISTORY: 578 LOAD FACTOR

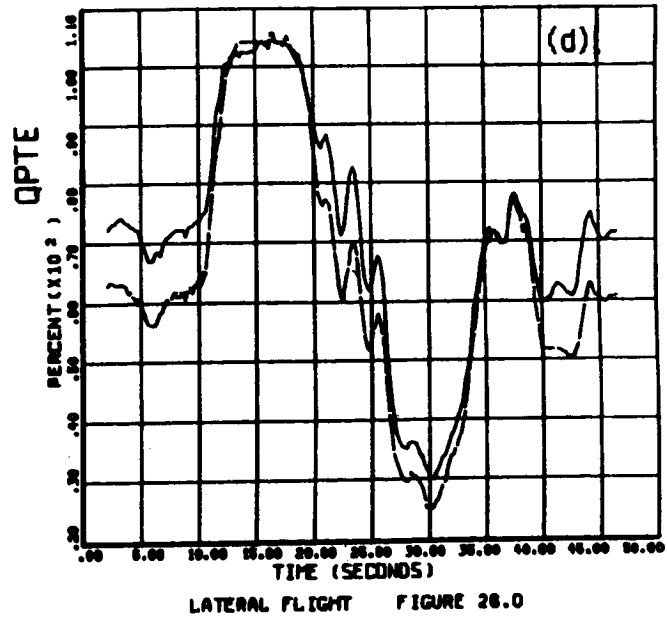

LATERAL FLIGHT FIGURE 26.0
TIME HISTORY:

SA 1114

FLIGHT TEST: SIDEWARD ACCELERATION/DECELERATION

FIG. 3.2.1

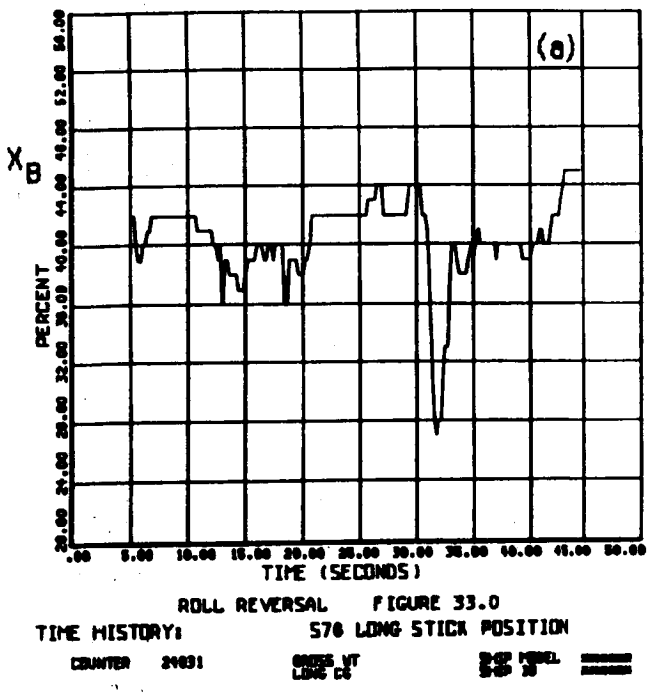

ROLL REVERSAL FIGURE 33.0
TIME HISTORY: 578 LONG STICK POSITION

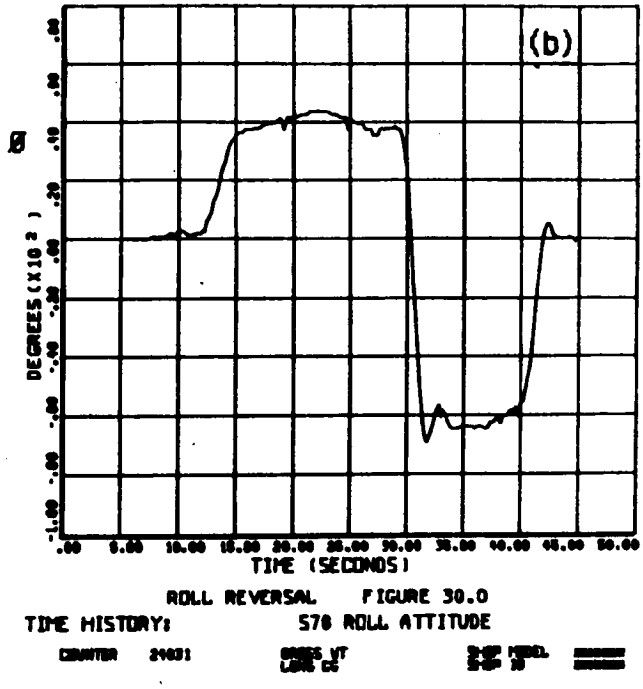

ROLL REVERSAL FIGURE 30.0
TIME HISTORY: 578 ROLL ATTITUDE

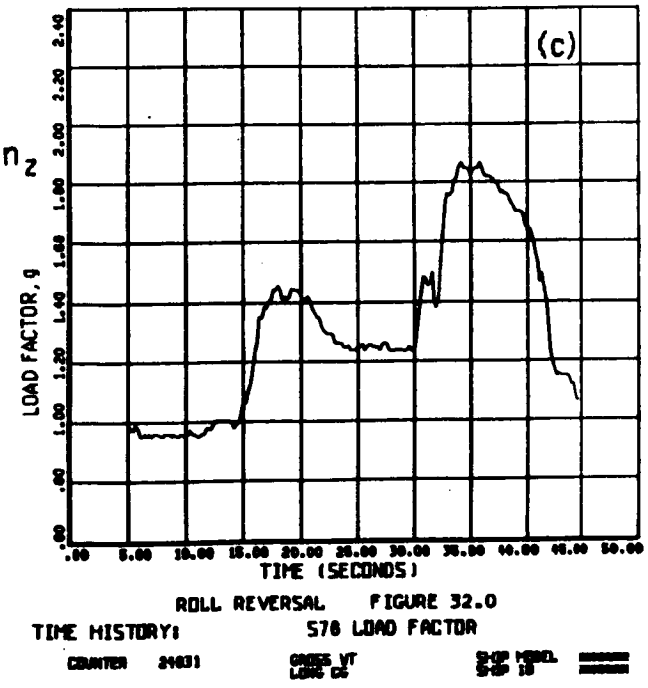

ROLL REVERSAL FIGURE 32.0
TIME HISTORY: 578 LOAD FACTOR

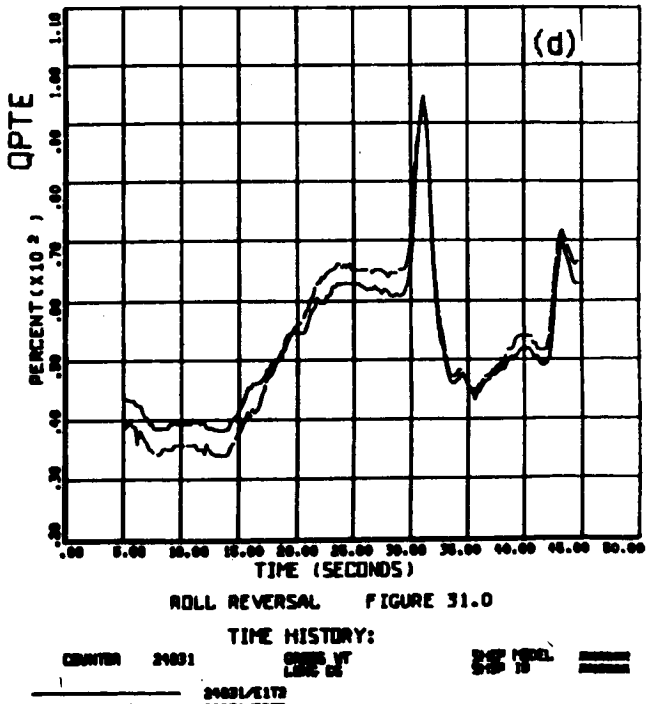

ROLL REVERSAL FIGURE 31.0
TIME HISTORY:

SA 1114

FLIGHT TEST: ROLL REVERSAL (RIGHT-LEFT-RIGHT)

UNITED TECHNOLOGIES SIKORSKY AIRCRAFT

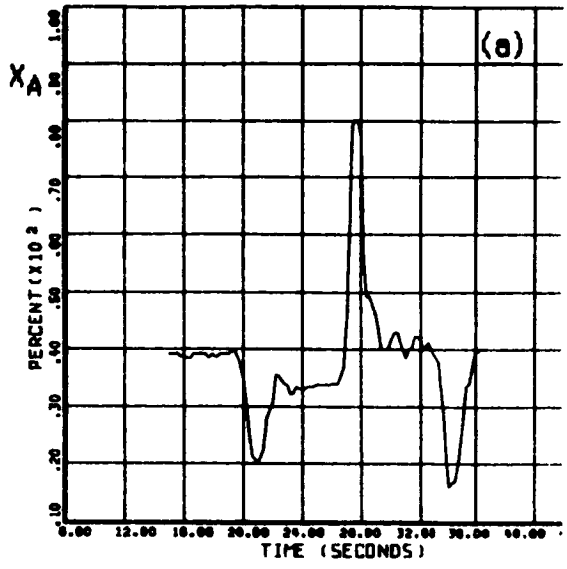

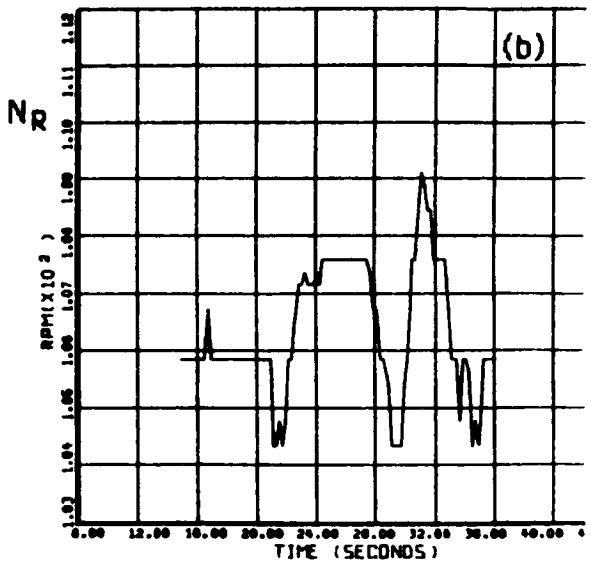

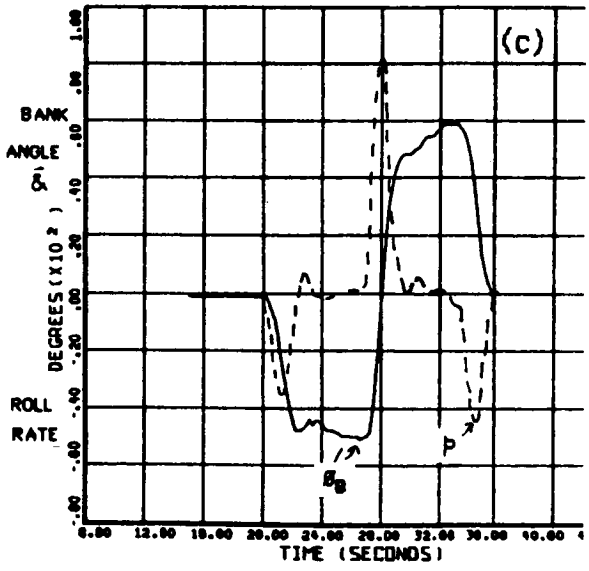

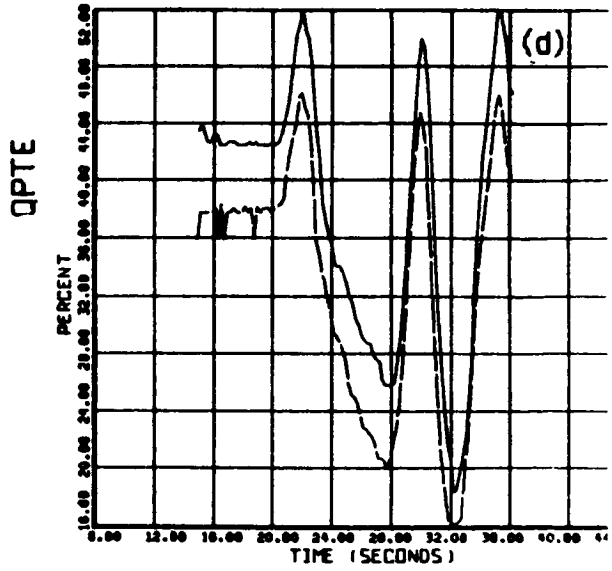

SA 1114

FLIGHT TEST: ROLL REVERSAL (LEFT-RIGHT-LEFT)

FIG. 3.2.3

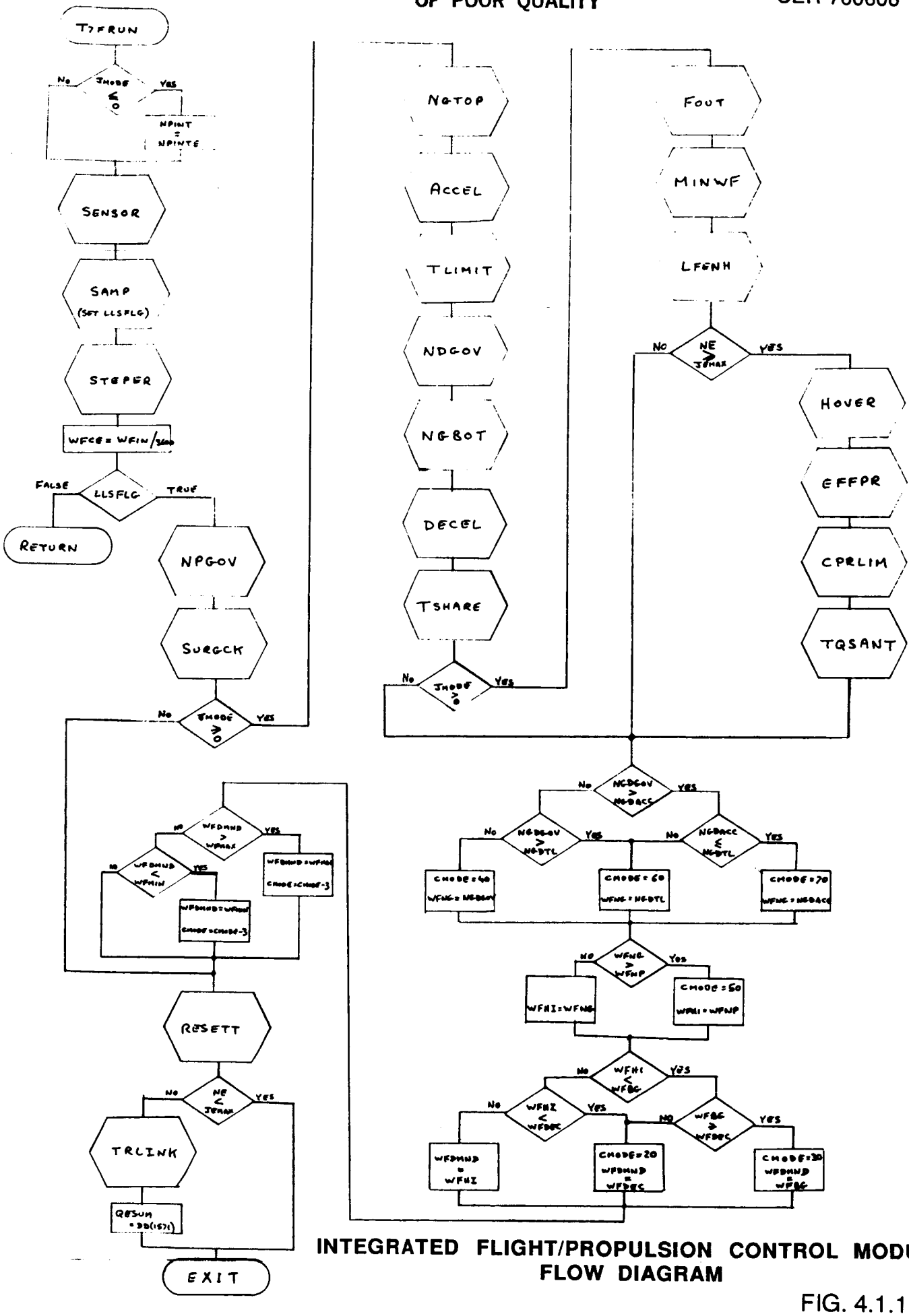

INTEGRATED FLIGHT/PROPULSION CONTROL MODULE FLOW DIAGRAM

FIG. 4.1.1

UNITED TECHNOLOGIES SIKORSKY AIRCRAFT

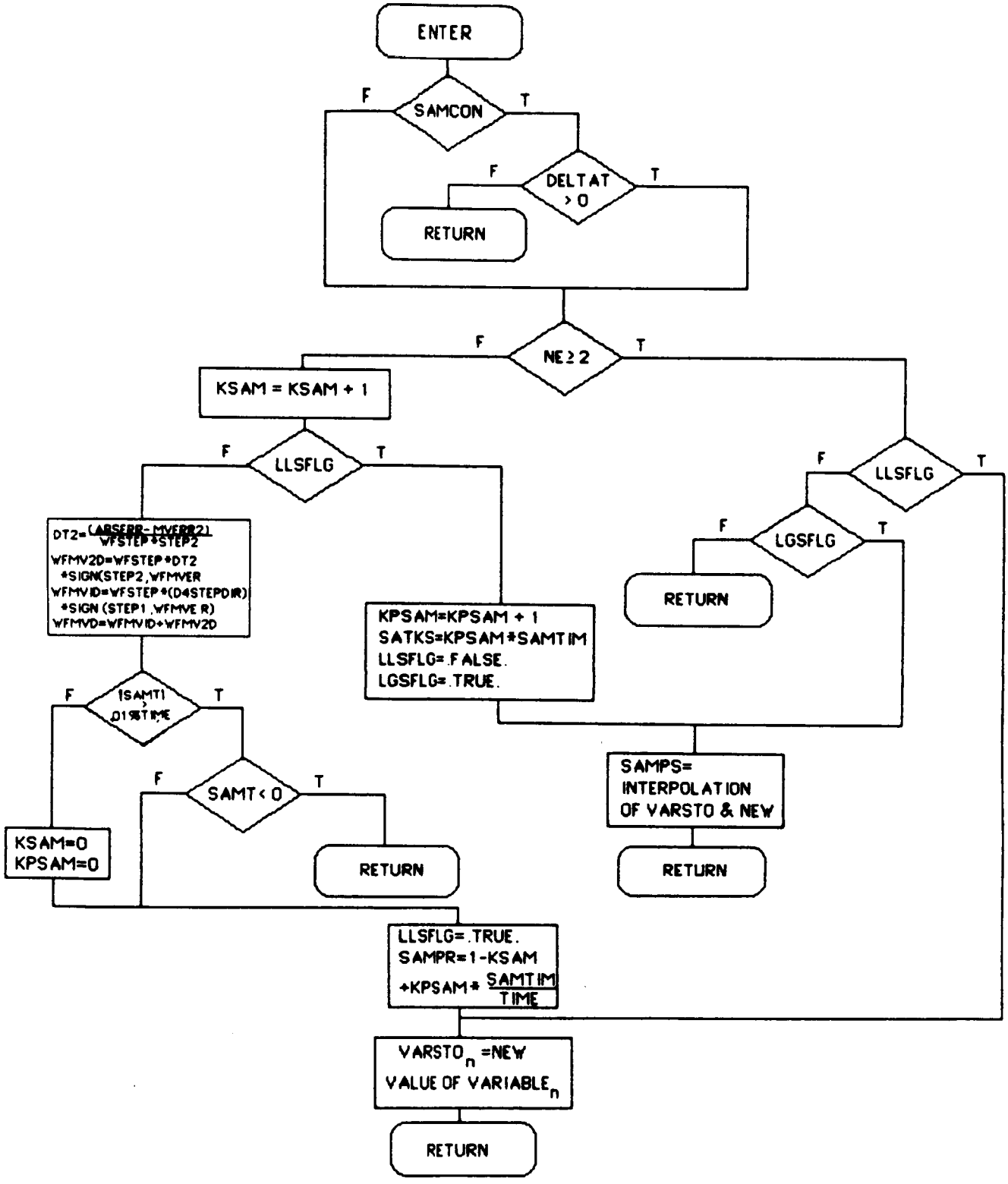

SAMPLING ROUTINE FLOW DIAGRAM

FIG. 4.2.1

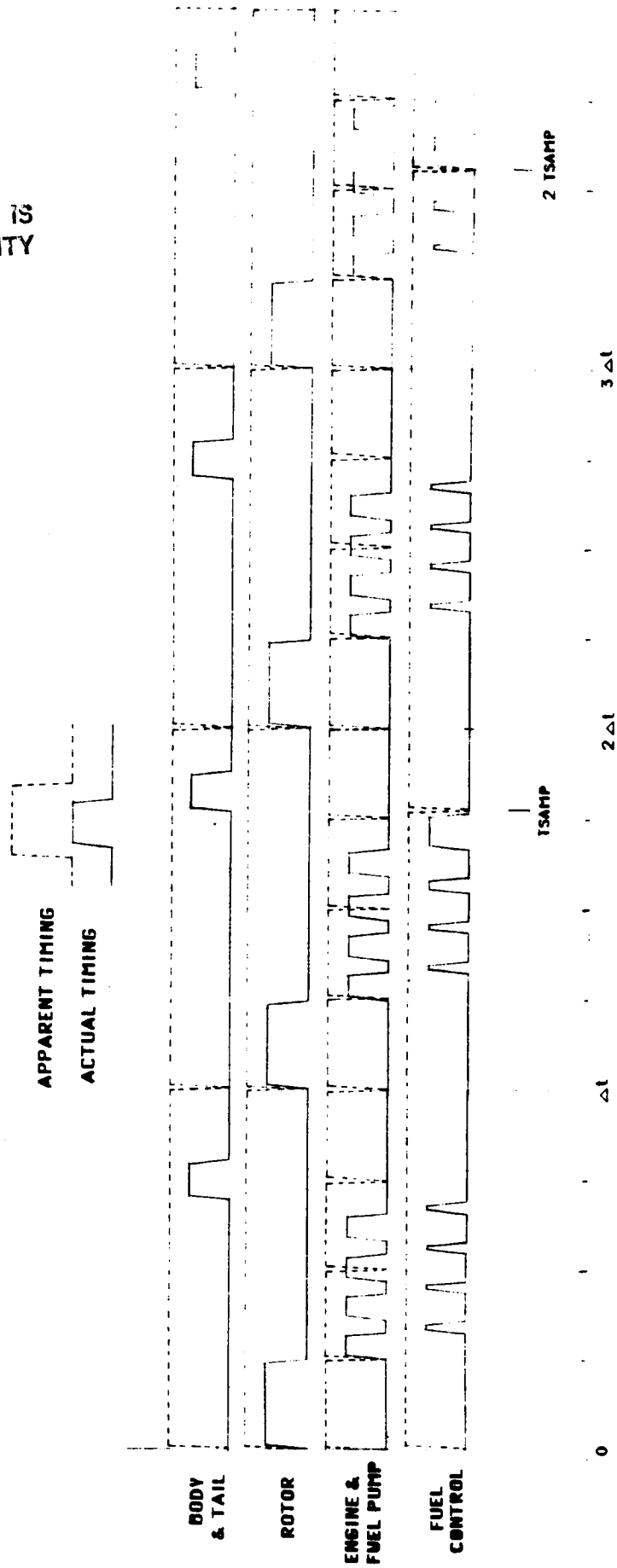

MGH TIME SCALES

FIG. 4.2.2

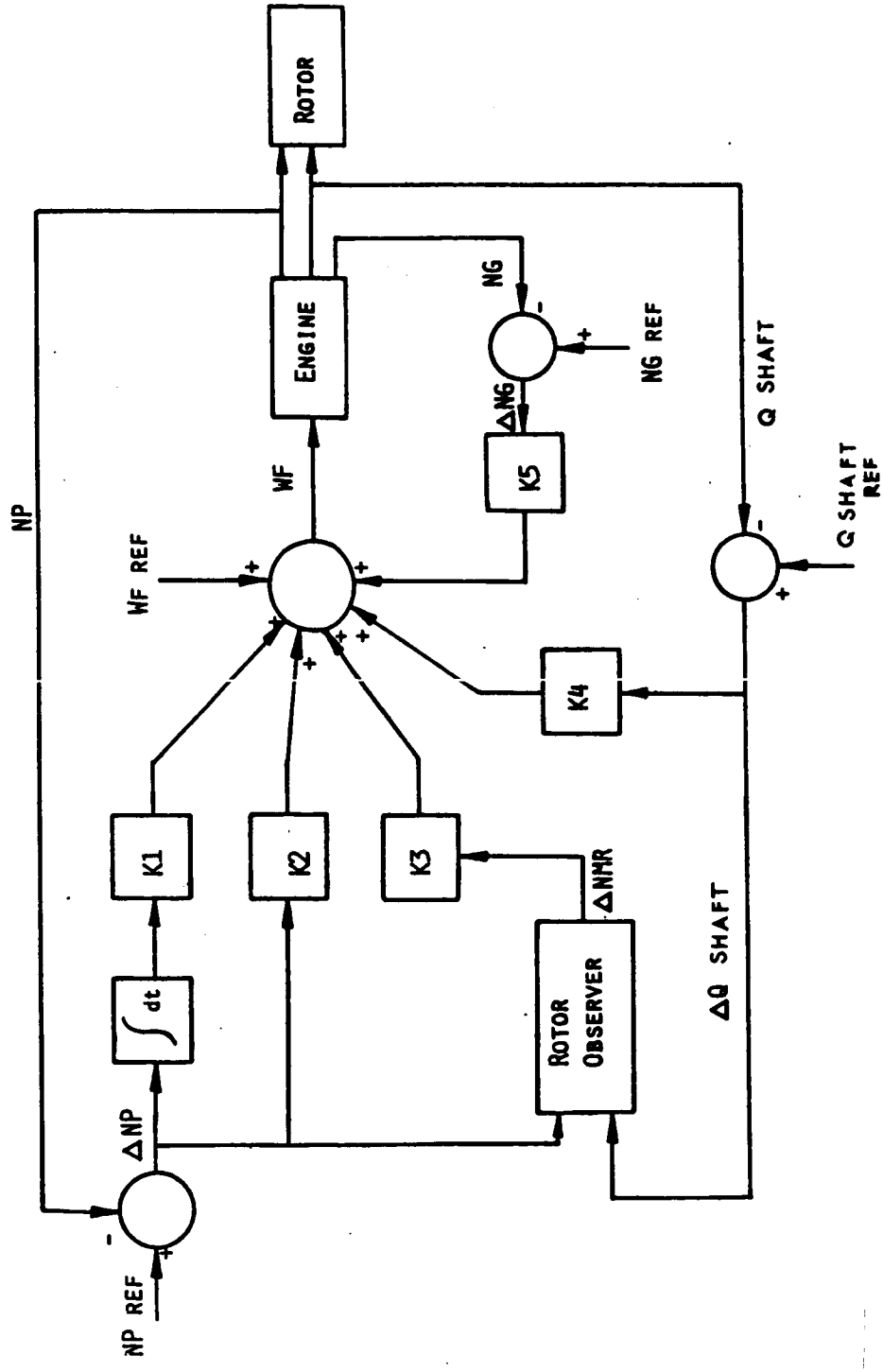

SA 1114

BLOCK DIAGRAM OF ENGINE & HELICOPTER WITH LINEAR STATE FEEDBACK

FIG. 4.3.1

UNITED TECHNOLOGIES
SIKORSKY AIRCRAFT

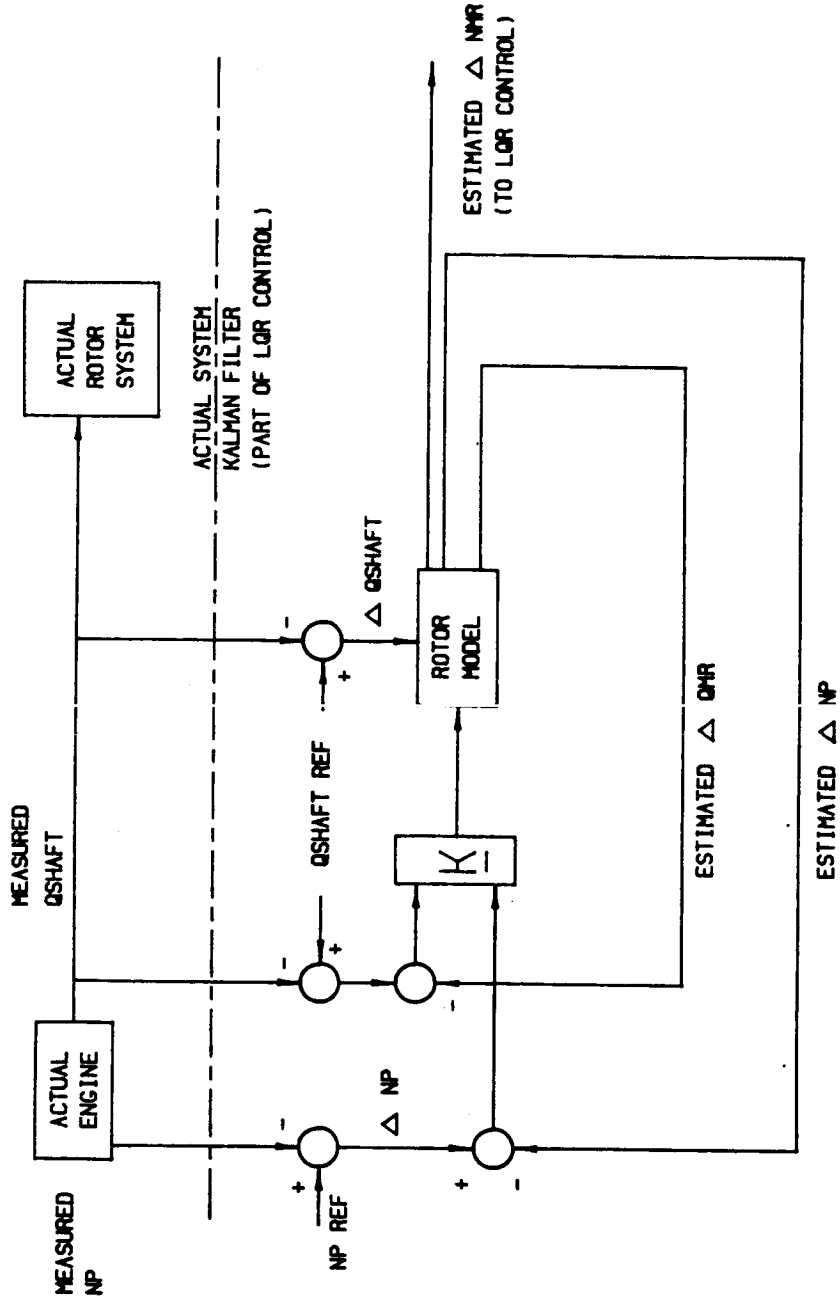

SCHEMATIC DIAGRAM OF OBSERVER (ESTIMATOR FOR LMR)

SA 111

FIG. 4.3.2

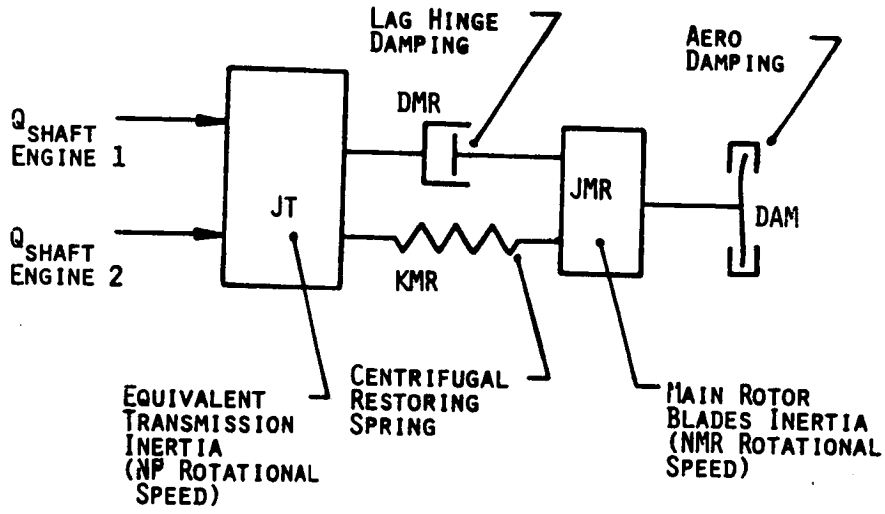

SIMPLIFIED LINEAR HELICOPTER/ROTOR MODEL USED IN OBSERVER DESIGN

SA 1114

FIG. 4.3.3

UNITED TECHNOLOGIES SIKORSKY AIRCRAFT

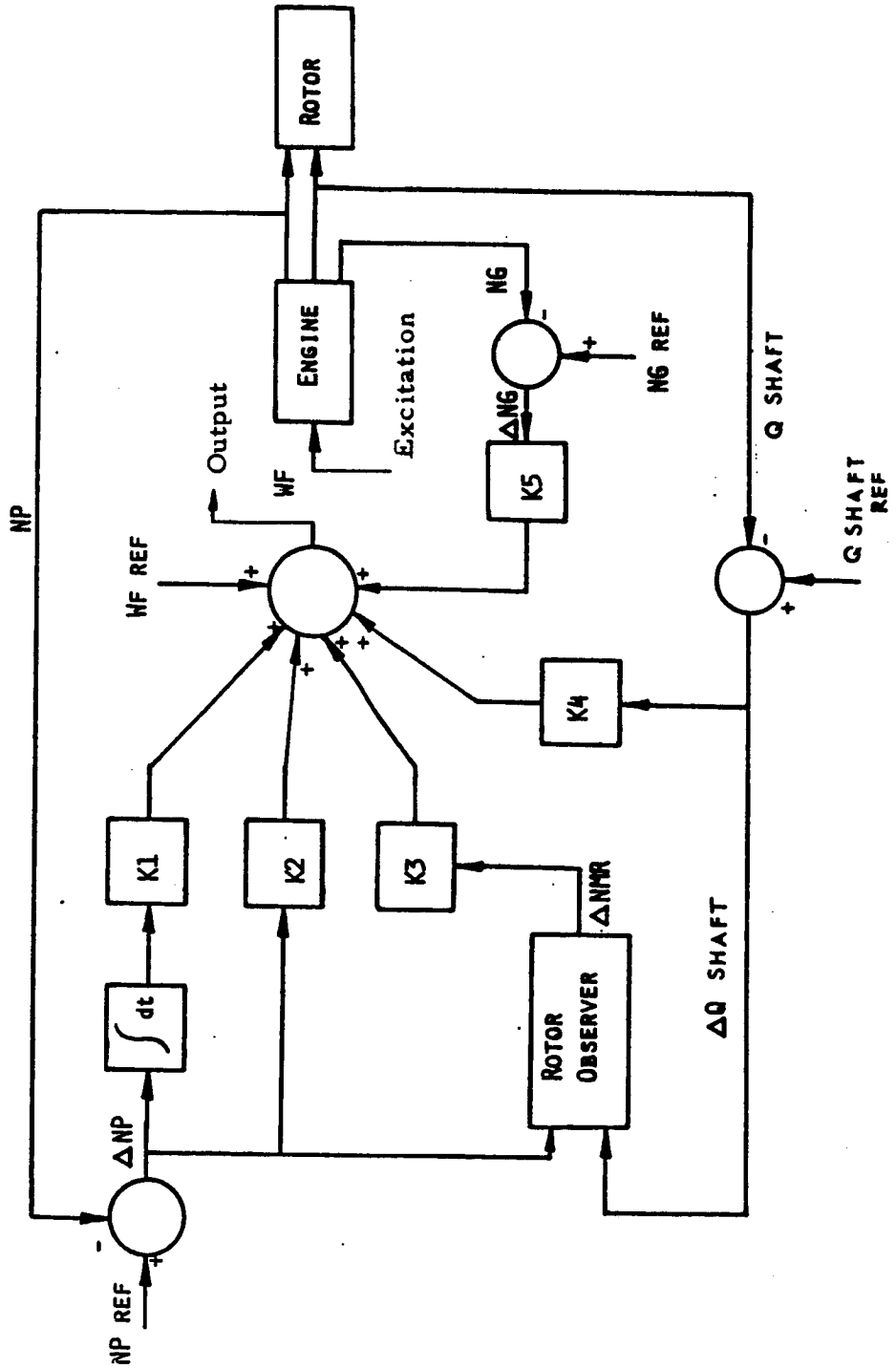

SA 1114

SCHEMATIC OF ENGINE, ROTOR & LQR, SHOWING WF I/O

FIG. 4.3.4

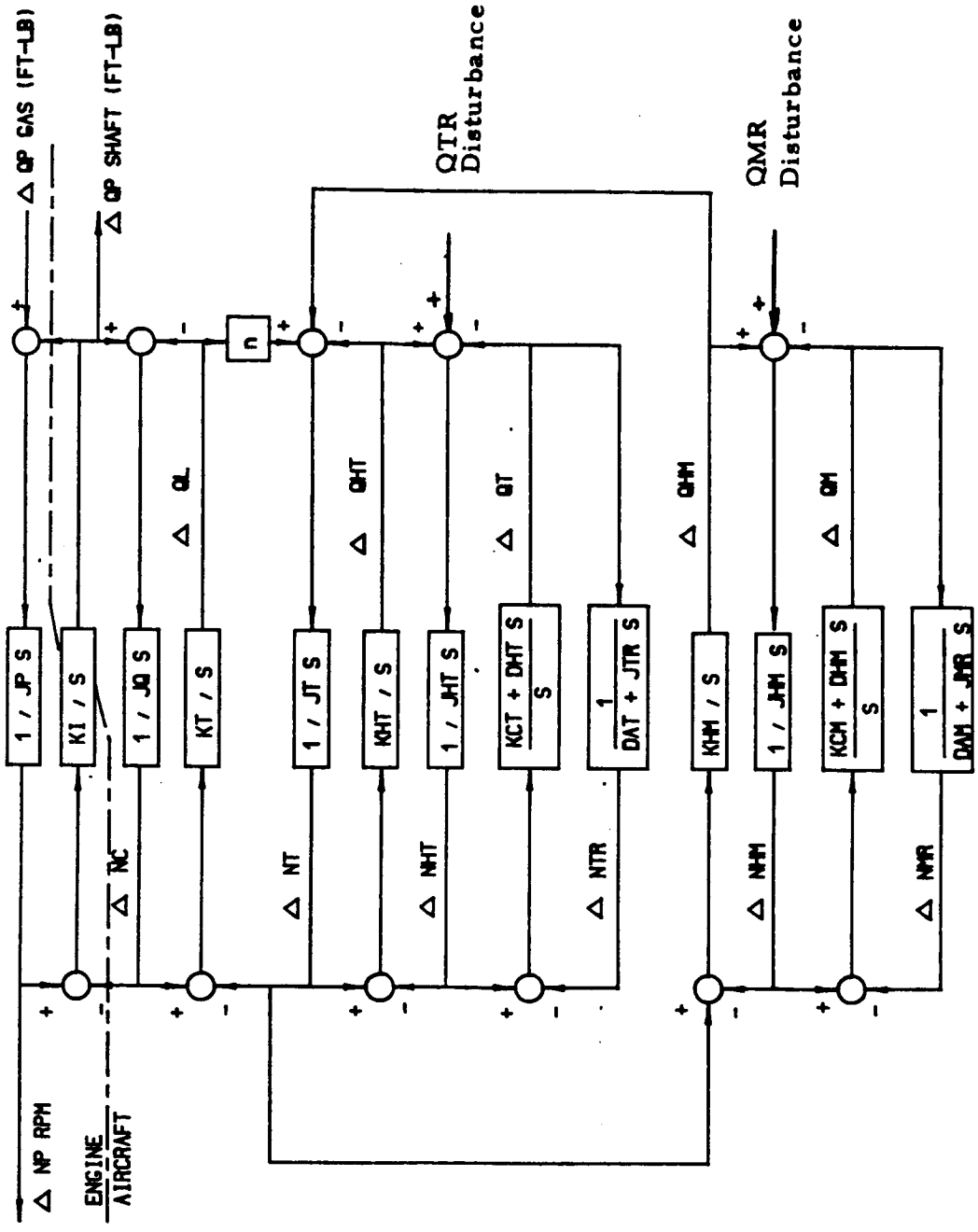

SCHEMATIC OF ROTOR SYSTEM SHOWING DISTURBANCE I/O

SA 1114

FIG. 4.3.5

UNITED TECHNOLOGIES
SIKORSKY AIRCRAFT

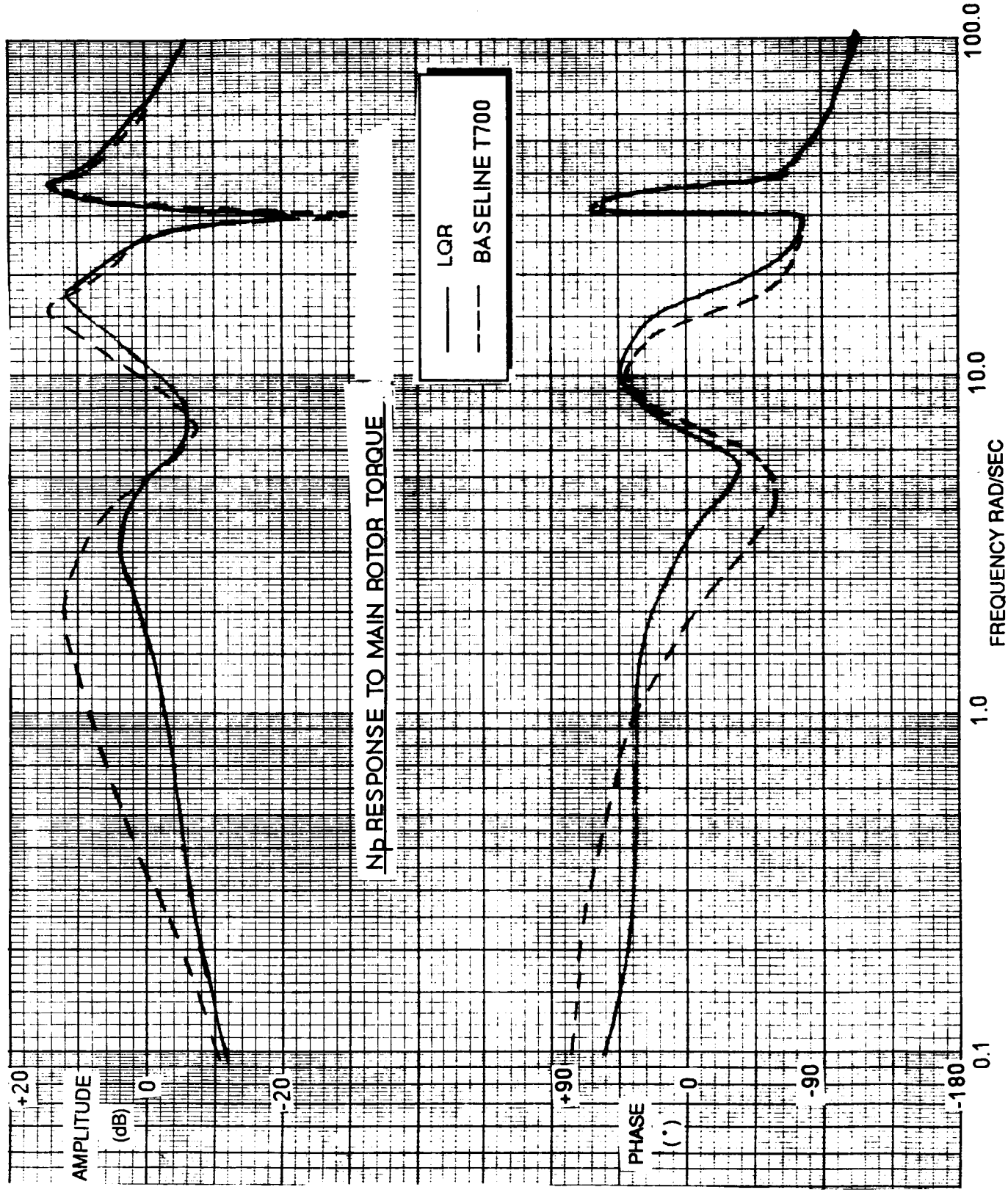

SA 1114

BODE PLOT OF BASELINE AND LQR NP GOVERNORS

FIG. 4.3.6

60A - BLACK HAWK

FGUST - DISCRETE GUST, 40 FT/SEC OVER 200 FT
INTEGRATED F/C

XA+1	5.8226444	XB+1	-3.3737828	XC+1	6.5916135	XP+1	3.2155248
THETAB	-2.1876235	VKT	135.00308	PHIB	0.	VYB	-1.5665258
XNGE	41779.404	NPINTE	1.3107440	VC	-.15807E-2	WEIGHT	16638.000
OMRMR	0.9999999	NPMEAS	99.999999				

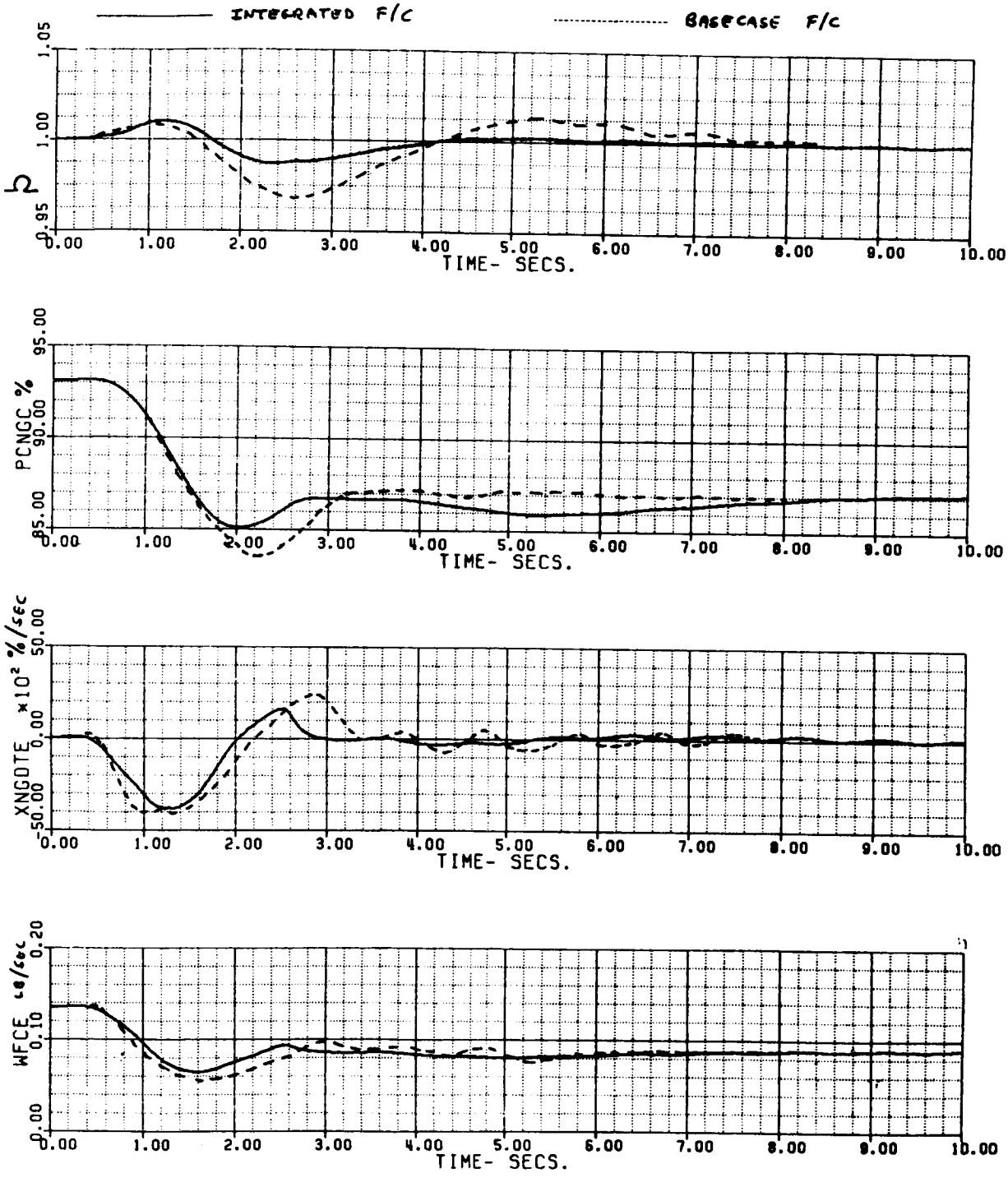

SIMULATED DISCRETE GUST RESPONSE USING LQR

FIG. 4.3.7

60A - BLACK HAWK

FROLRE - ROLL REVERSAL, INTEGRATED FUEL CONTROL
ROLL RIGHT THEN LEFT

XA+1	5.8205497	XB+1	-3.3702563	XC+1	6.5933595	XP+1	3.2153668
THETAB	-2.1869954	VKT	135.00311	PHIB	0.	VTB	-1.5477484
XNGE	41784.030	NPINTE	1.3116747	VC	.116586E-2	WEIGHT	16638.000
OMRMR	0.9999999	NPMEAS	99.999997				

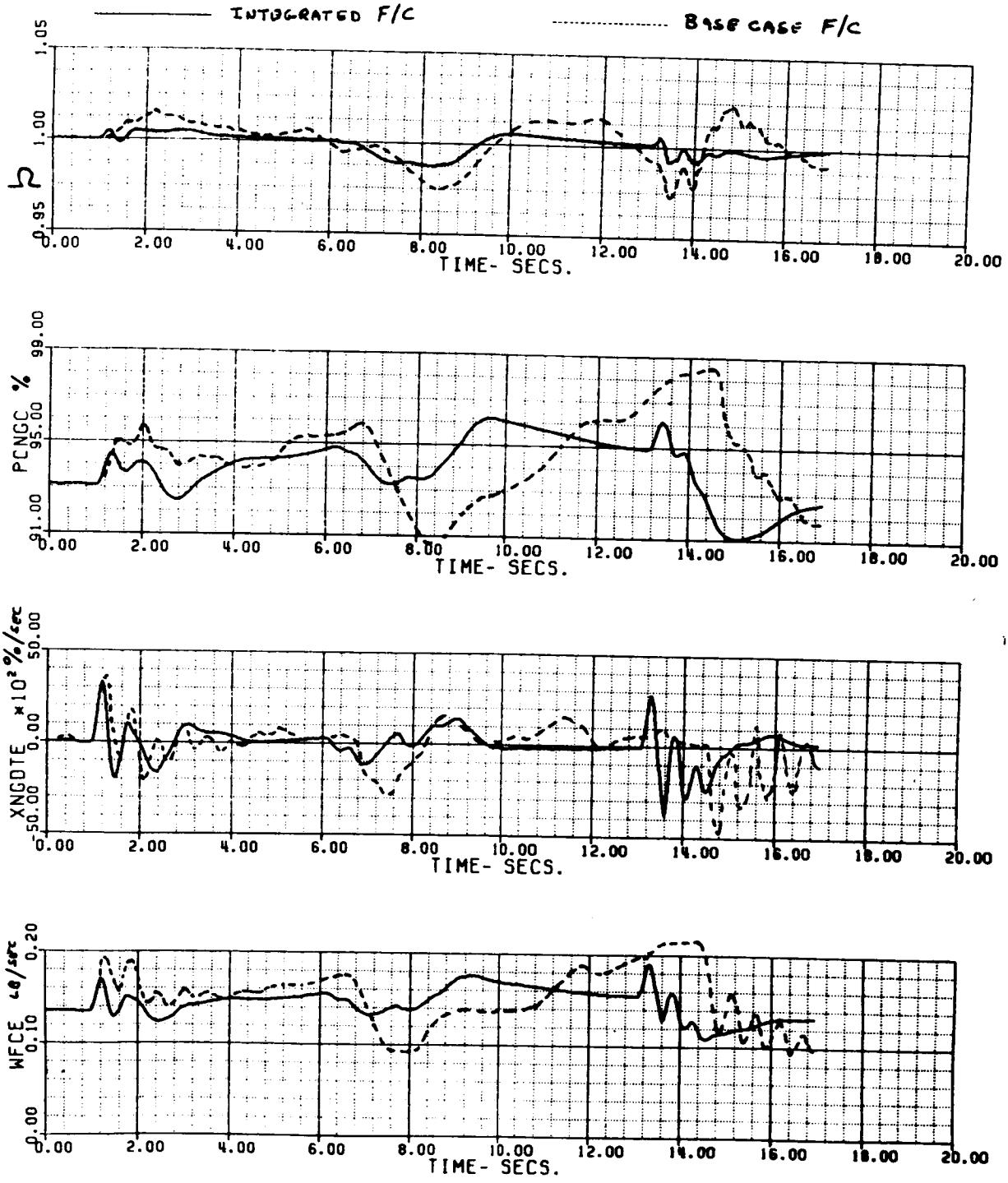

SIMULATED ROLL REVERSAL USING LQR

FIG. 4.3.8

60A - BLACK HAWK

FHIGTRB - HIGH G TURN WITH LFENH OFF
INTEGRATED CONTROL

XA+1	5.7934504	XB+1	-3.5048361	XC+1	6.2285295	XP+1	3.1972200
THETAB	-1.7015953	VKT	129.99821	PHIB	0.	VTB	-1.5543622
XNGE	41510.471	NPINTE	1.3307189	VC	-.58650E-3	WEIGHT	16638.000
OMAMR	0.9999999	NPMEAS	99.999999				

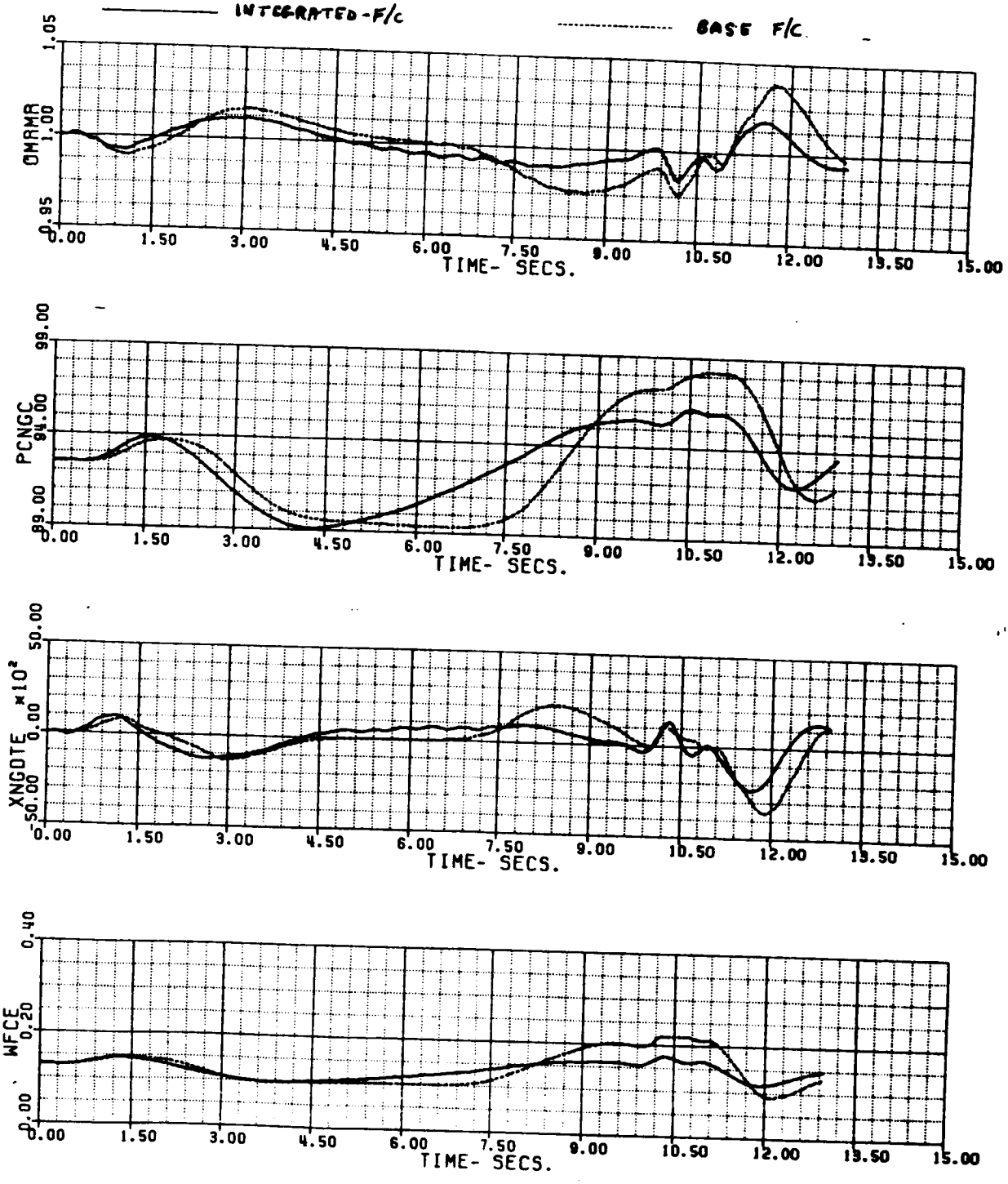

SIMULATED HIGH G TURN USING LQR

FIG. 43.9

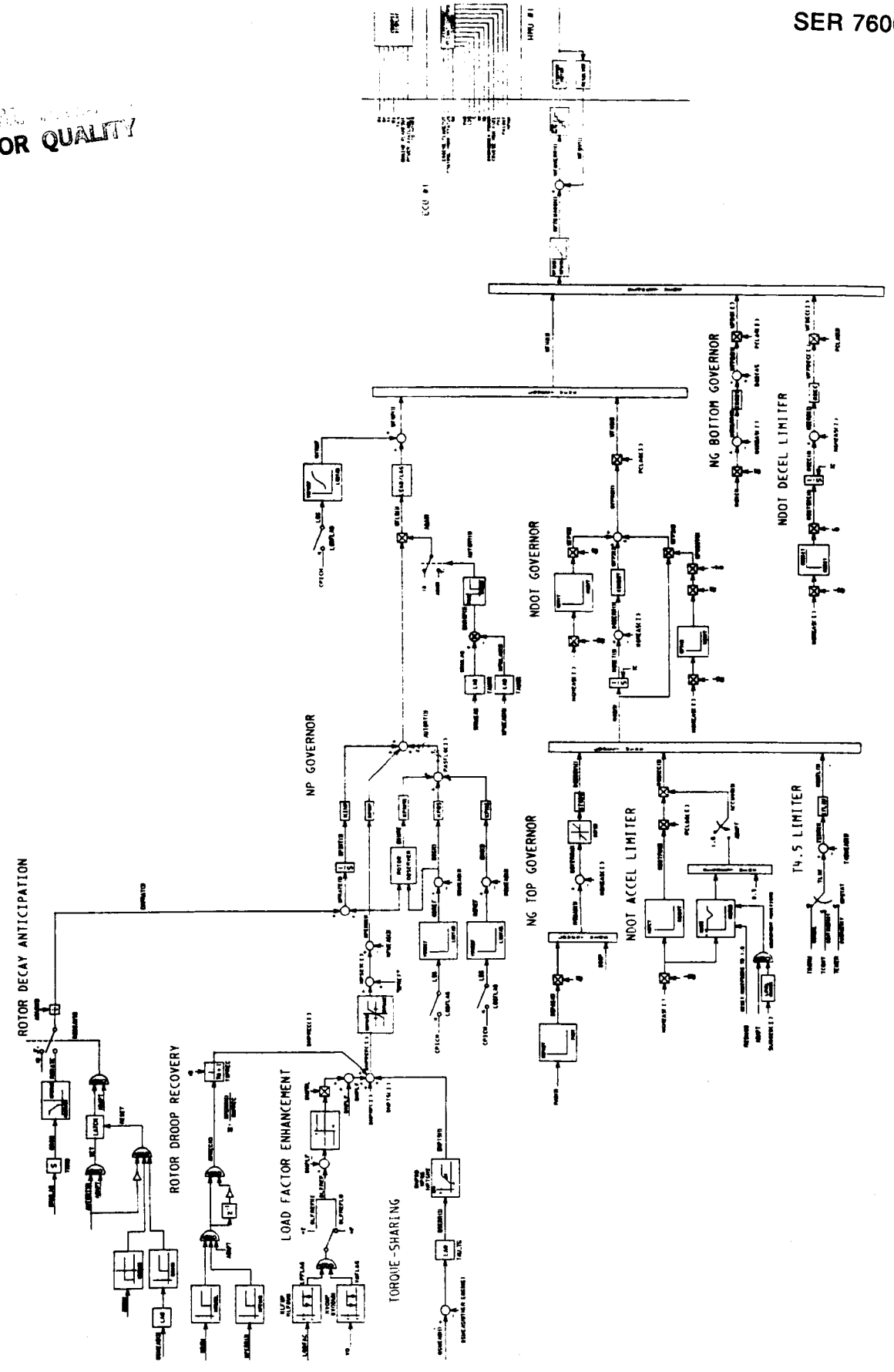

BLOCK DIAGRAM OF INTEGRATED CONTROL

FIG. 4.3.10(a)

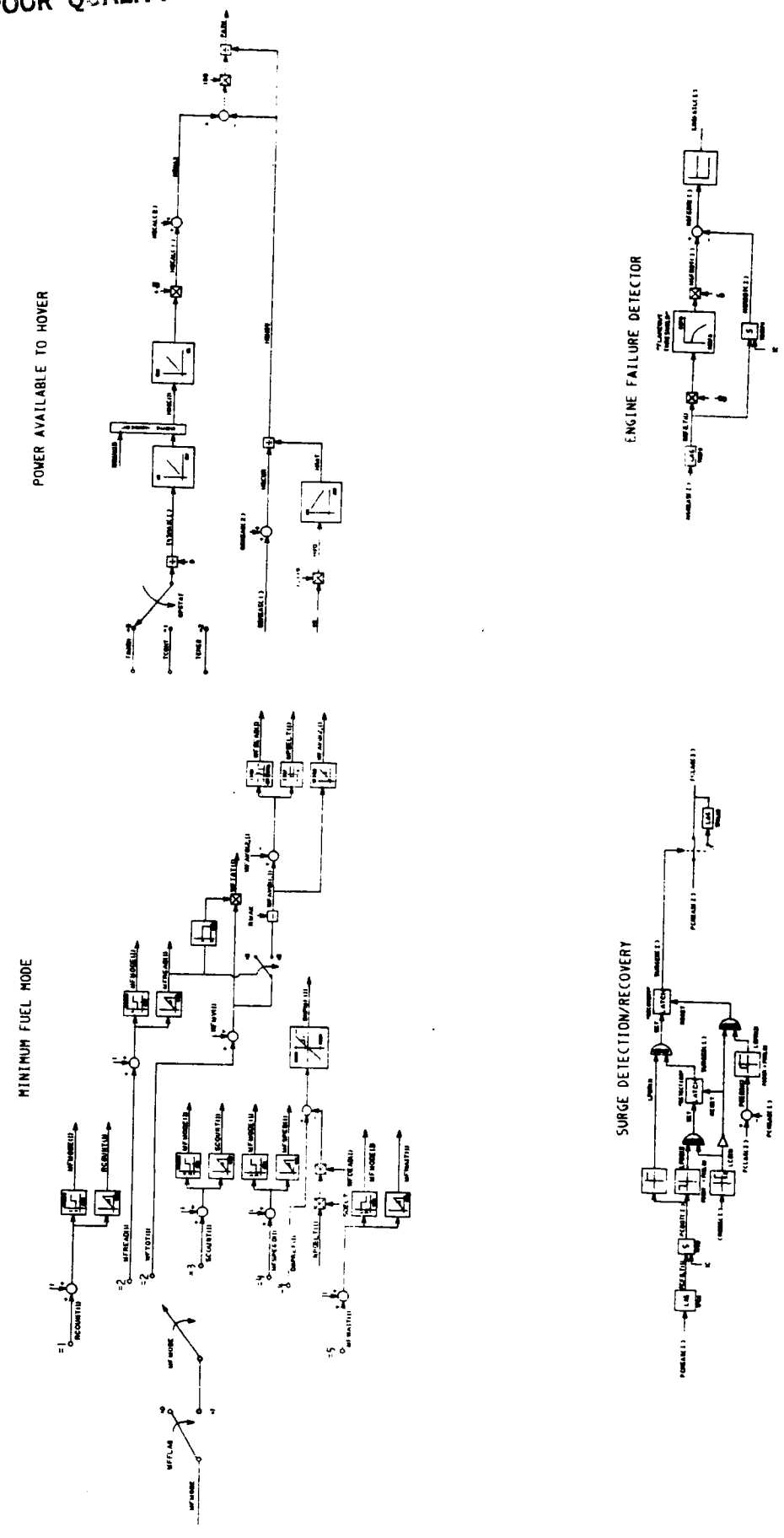

BLOCK DIAGRAM OF INTEGRATED CONTROL

FIG. 4.3.10(b)

60A - BLACK HAWK

SER 760606

FAUTOL - AUTOROTATION RECOVERY, LARGE SPLIT, INT. F/C
70% XC IN 3 SEC. ADAPT = -1

XA+1	5.0569677	XB+1	-5.6562455	XC+1	-.23504E-1	XP+1	3.5084966
THETAB	0.3639957	VKT	79.996621	PHIB	0.	VTB	-11.785354
XNGE	33718.873	NPINTE	7.3990915	VC	-2657.0983	WEIGHT	16638.000
OMRMR	1.1699999	NPMERS	99.974205				

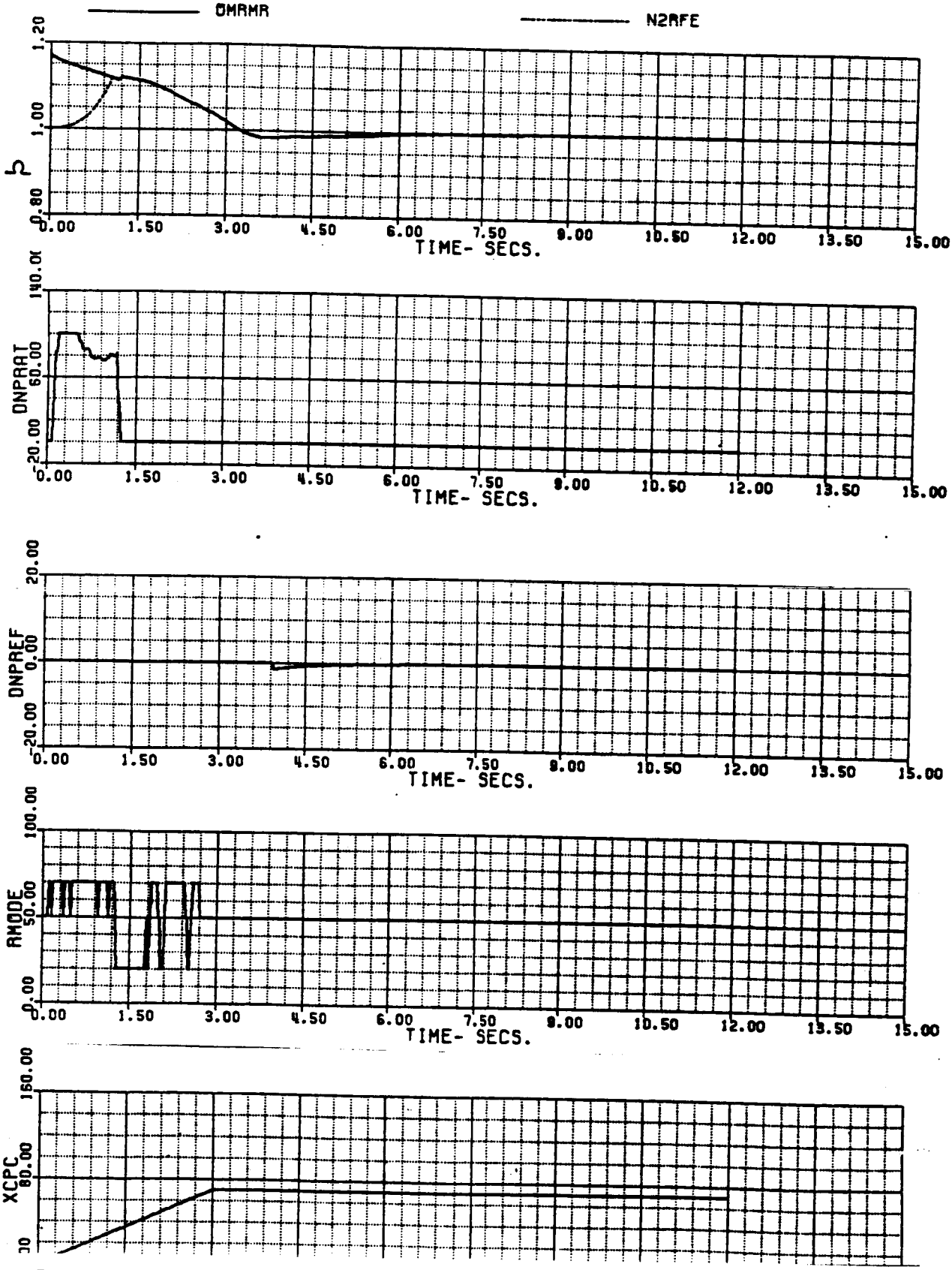

SIMULATED AUTO RECOVERY, DECAY ANTICIPATION ON

FIG. 4.3.11

60A - BLACK HAWK

FAUTOL - AUTOROTATIVE RECOVERY,LARGE SPLIT. INT F.C.
70% XC IN 3 SEC. ADAPT=0

SER 760606

XA+1	5.0597396	XB+1	-5.6463754	XC+1	-.81637E-2	XP+1	3.5047419
THETAB	0.3666584	VKT	79.995915	PHIB	0.	VYB	-11.718003
XNGE	33626.880	NPINTE	7.8543024	VC	-2648.0592	WEIGHT	16638.000
OMRMR	1.1699999	NPMEAS	99.974205				

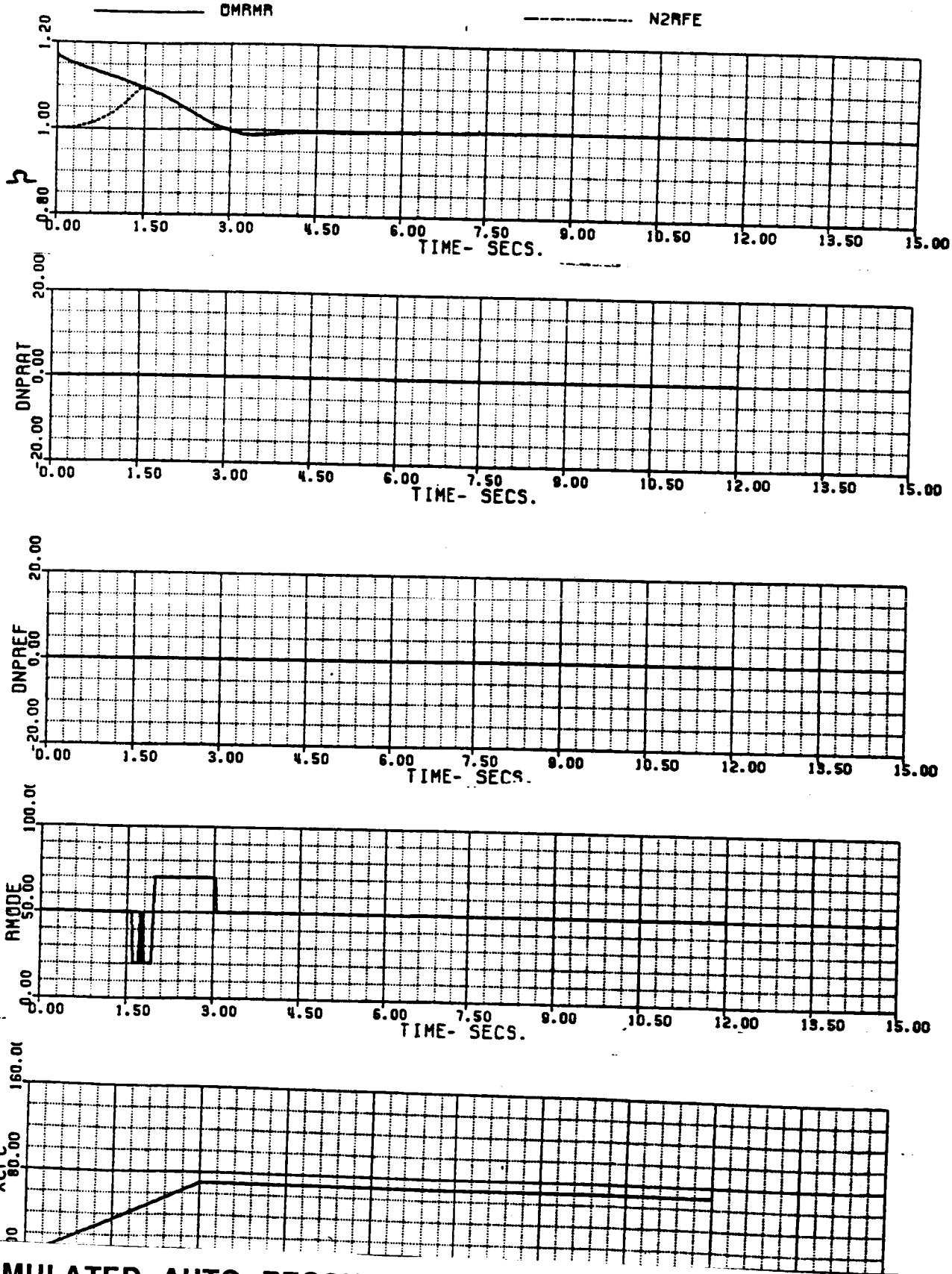

SIMULATED AUTO RECOVERY, DECAY ANTICIPATION OFF

FIG. 4.2.12

60A - BLACK HAWK

SER 760606

FAUTOL - AUTOROTATION RECOVERY, LARGE SPLIT, INT. F/C
70% XC IN .5 SEC, ADAPT = -1

XA+1	5.0568549	XB+1	-5.6564609	XC+1	-.23656E-1	XP+1	3.5085098
THETAB	0.3639475	VKT	79.996625	PHIB	0.	VTB	-11.765136
XNGE	33718.472	NPINTE	7.3856667	VC	-2657.1674	WEIGHT	16638.000
OMRMR	1.1699999	NPMEAS	99.974205				

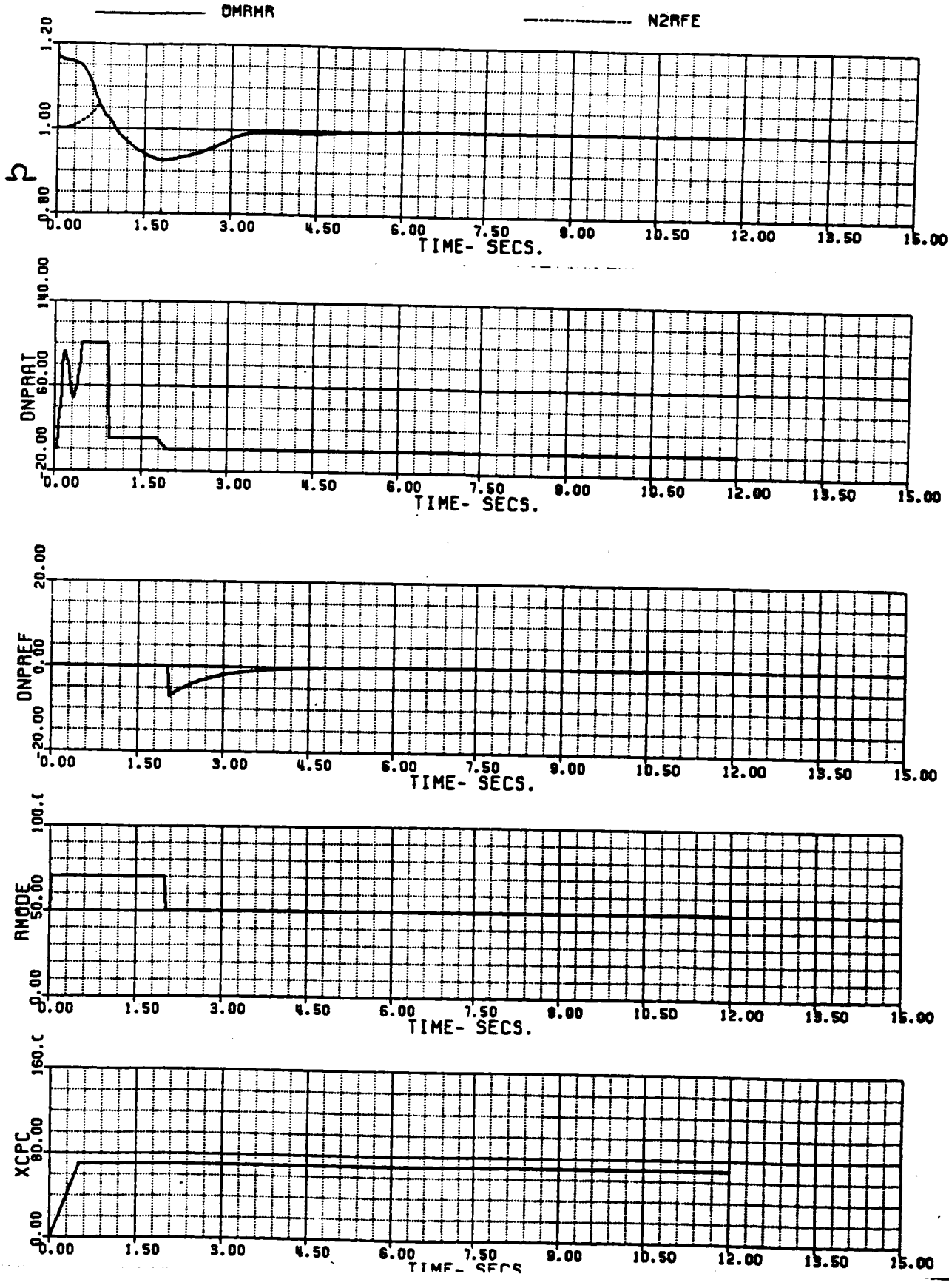

SIMULATED AUTO RECOVERY, DROOP RECOVERY ON FIG. 4.3.13

60A - BLACK HAWK

SER 760606

FAUTOL - AUTOROTATIVE RECOVERY. LARGE SPLIT. INT.F.C.
70% XC IN .5 SEC., ADAPT=0

XA+1	5.0597377	XB+1	-5.6479475	XC+1	-.90494E-2	XP+1	3.5060552
THETAB	0.3695894	VKT	79.995893	PHIB	0.	VTB	-11.748589
XNGE	33630.224	NPINTE	7.8225337	VC	-2647.3590	WEIGHT	16638.000
OMRMR	1.1699999	NPMEAS	99.974205				

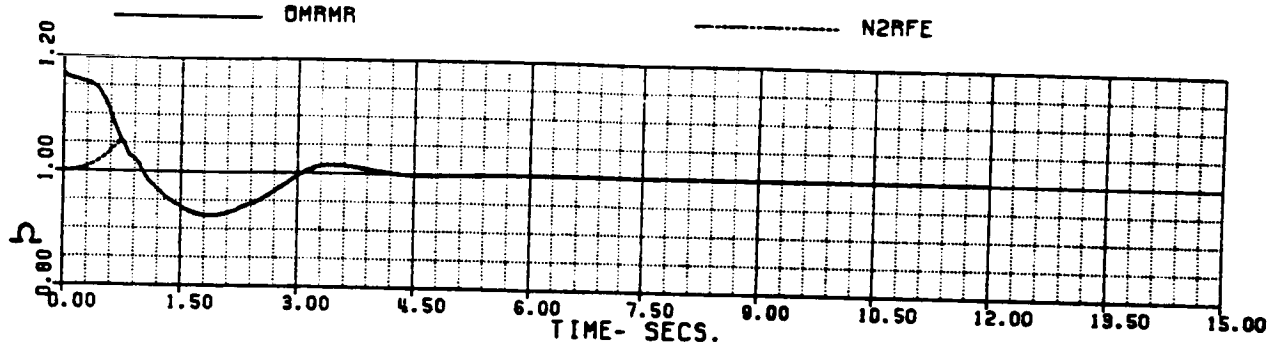

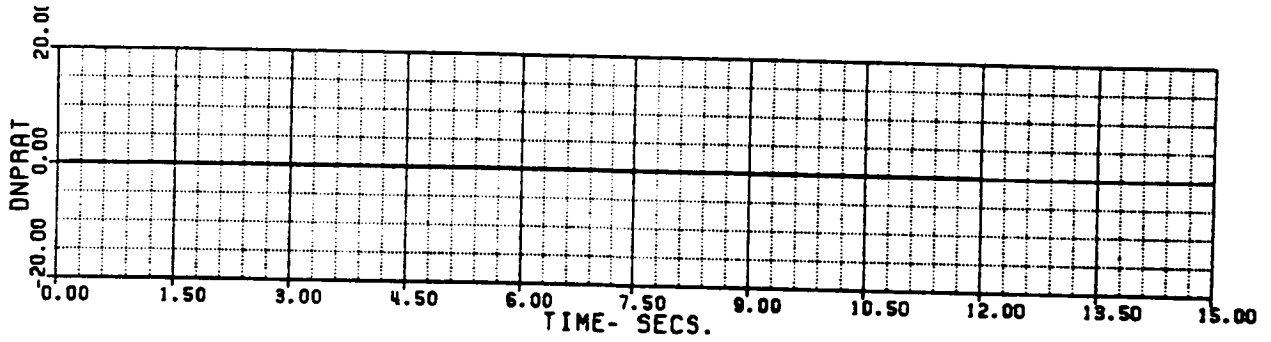

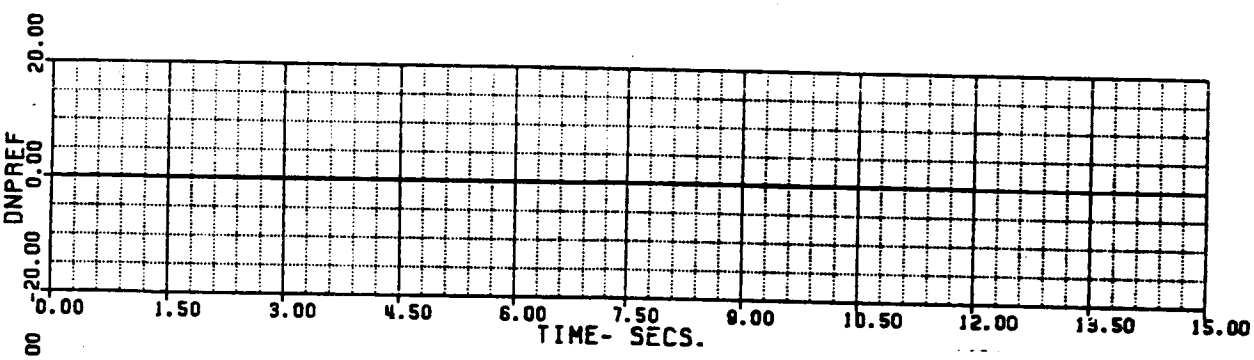

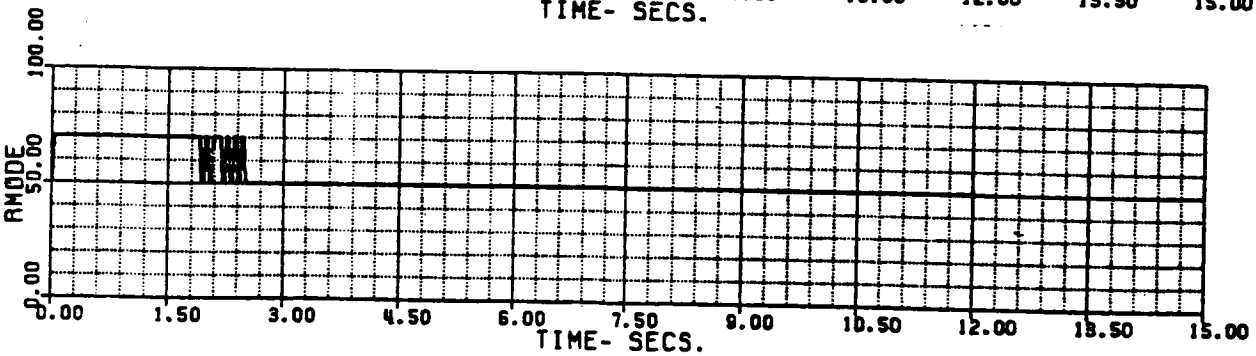

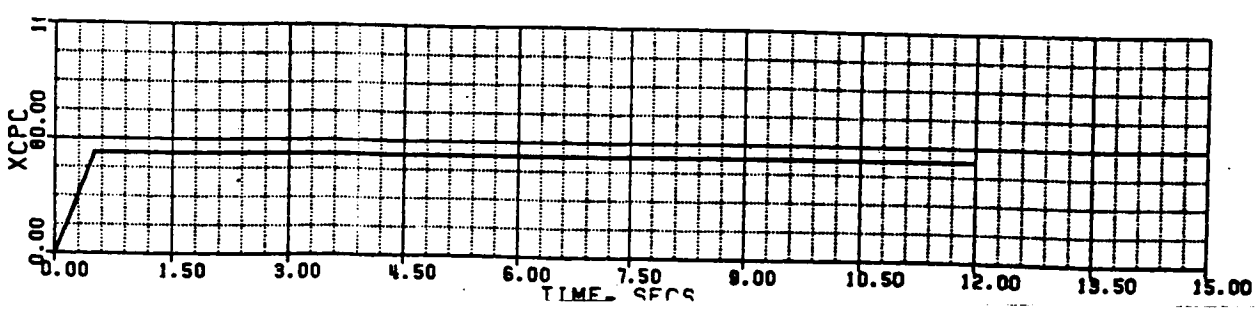

SIMULATED AUTO RECOVERY, DROOP RECOVERY OFF FIG. 4.3.14

60A - BLACK HAWK

HAUTOL - AUTOROTATION RECOVERY, LARGE SPLIT, 70% XE IN 3 SEC
BASE CASE WITH UPDATED ECU & HMU

XA+1	5.0597541	XB+1	-5.5022587	XC+1	-.94179E-2	XP+1	3.2520557
THETAB	0.3692555	VKT	79.995894	PHIB	0.	VTB	-11.762901
XNGE	33586.252	SPDSI	1.6957209	VC	-2647.4306	WEIGHT	16638.000
OMRMR	1.1699999						

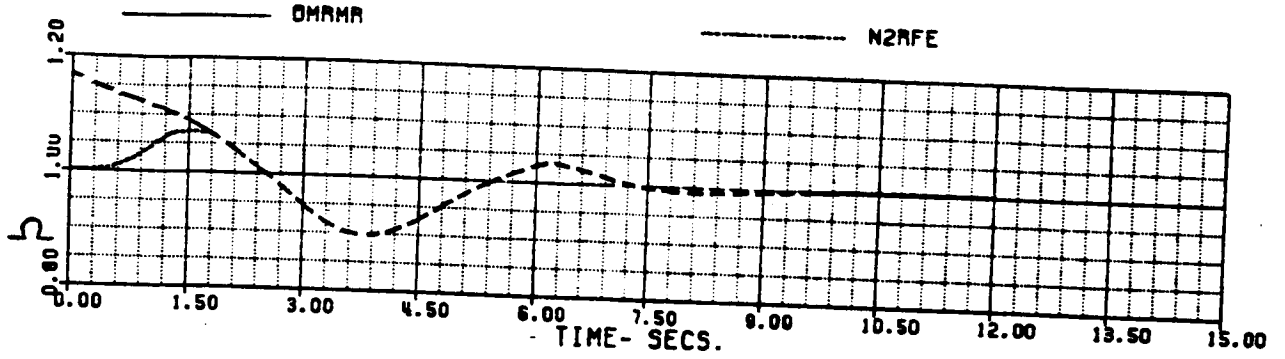

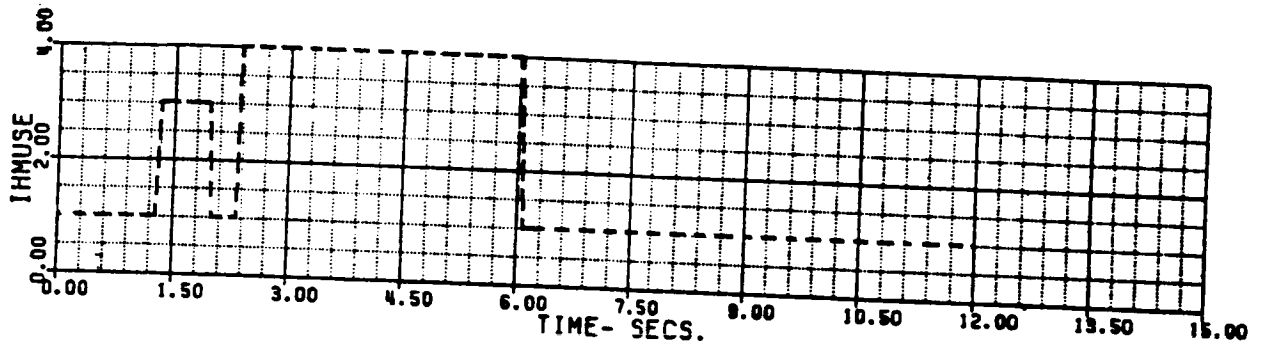

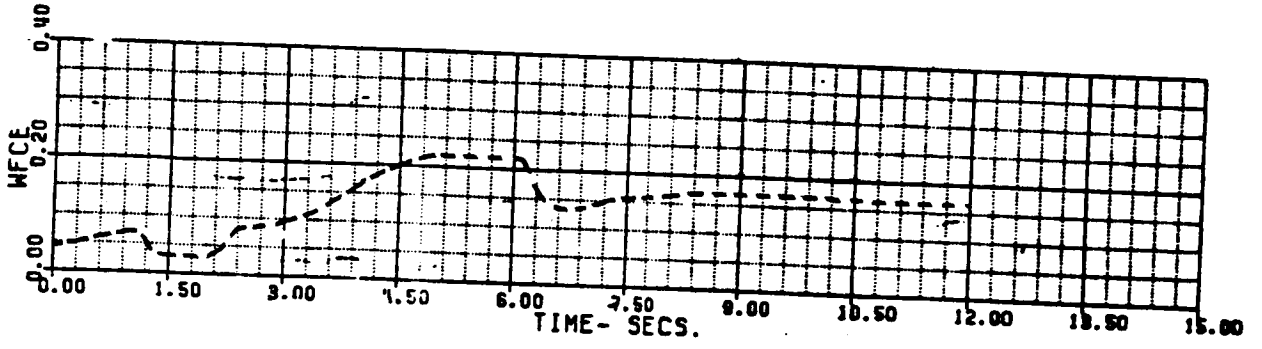

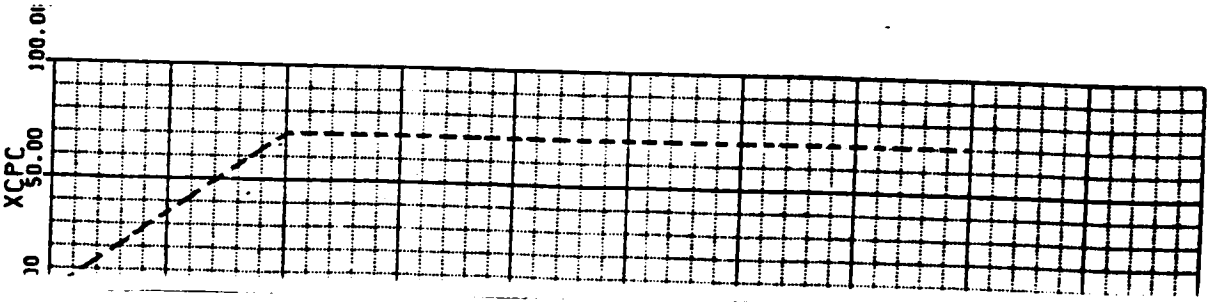

SIMULATED AUTO RECOVERY, BASELINE CONTROL

FIG 4.2.15

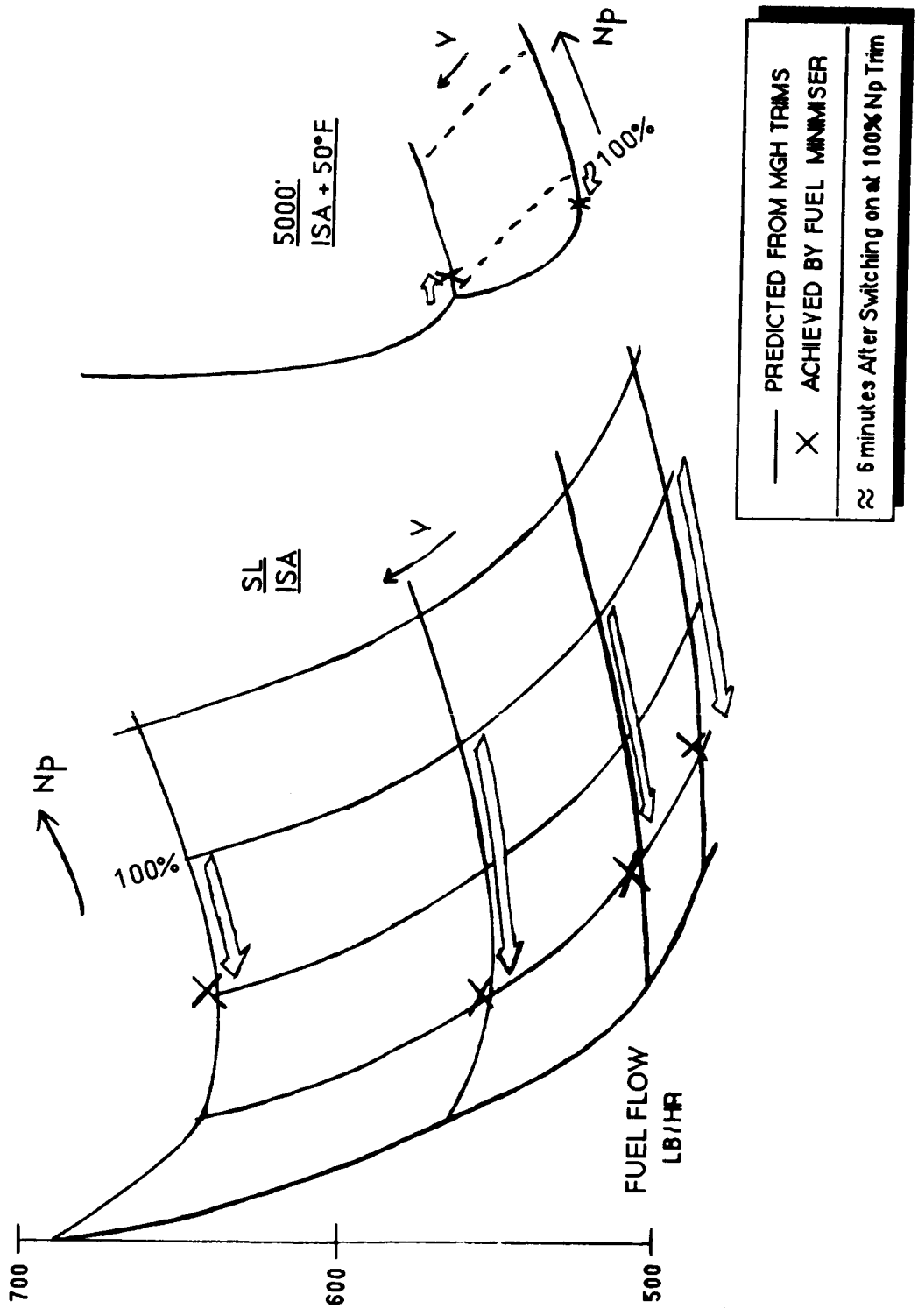

FUEL FLOW RATE ~ NP ~ V

FIG. 4.4.1

PULL-UP TIME HISTORIES

GEN HEL BLACK HAWK

LOW G. W. 140 K_T

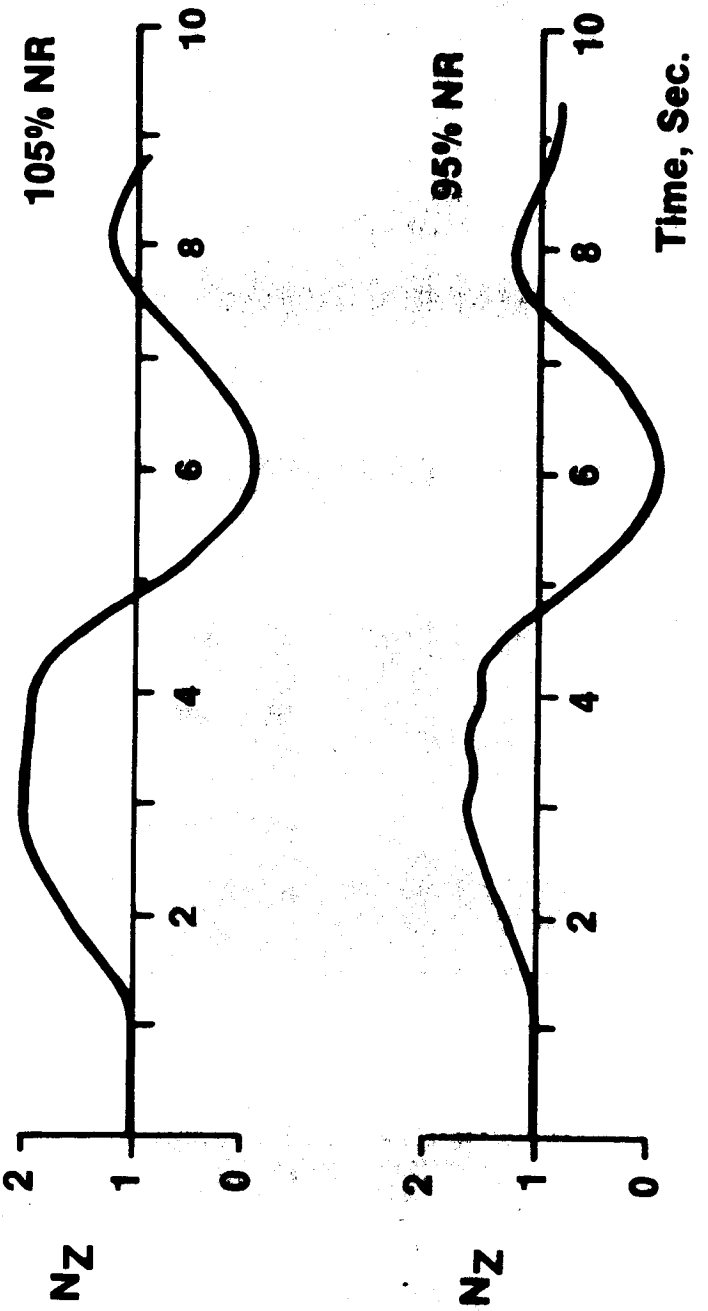

SIMULATION OF PULL-UP G's $\sim N_R$

FIG. 4.4.2

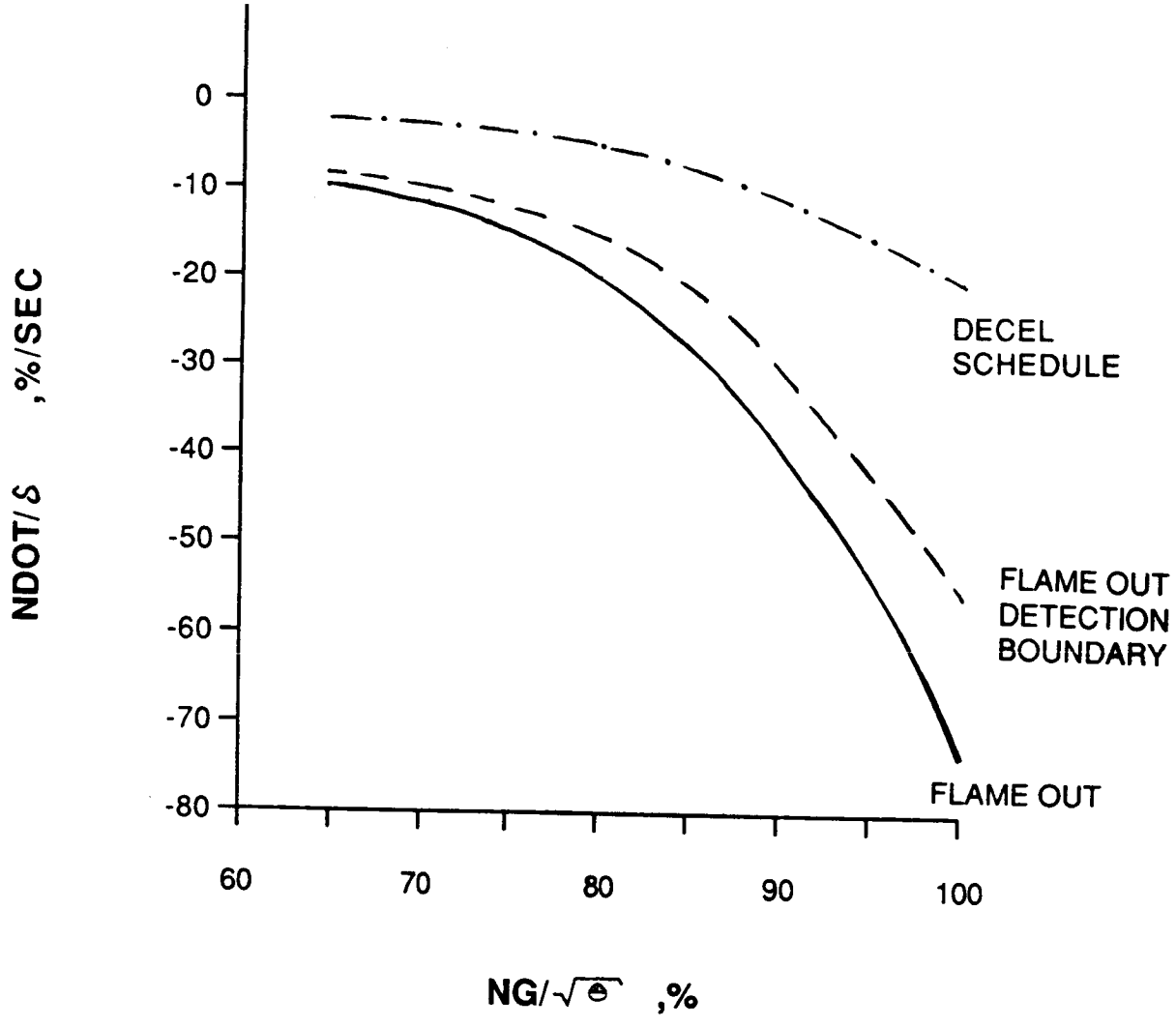

TYPICAL FLAME OUT DETECTION DATA

FIG. 4.5.1

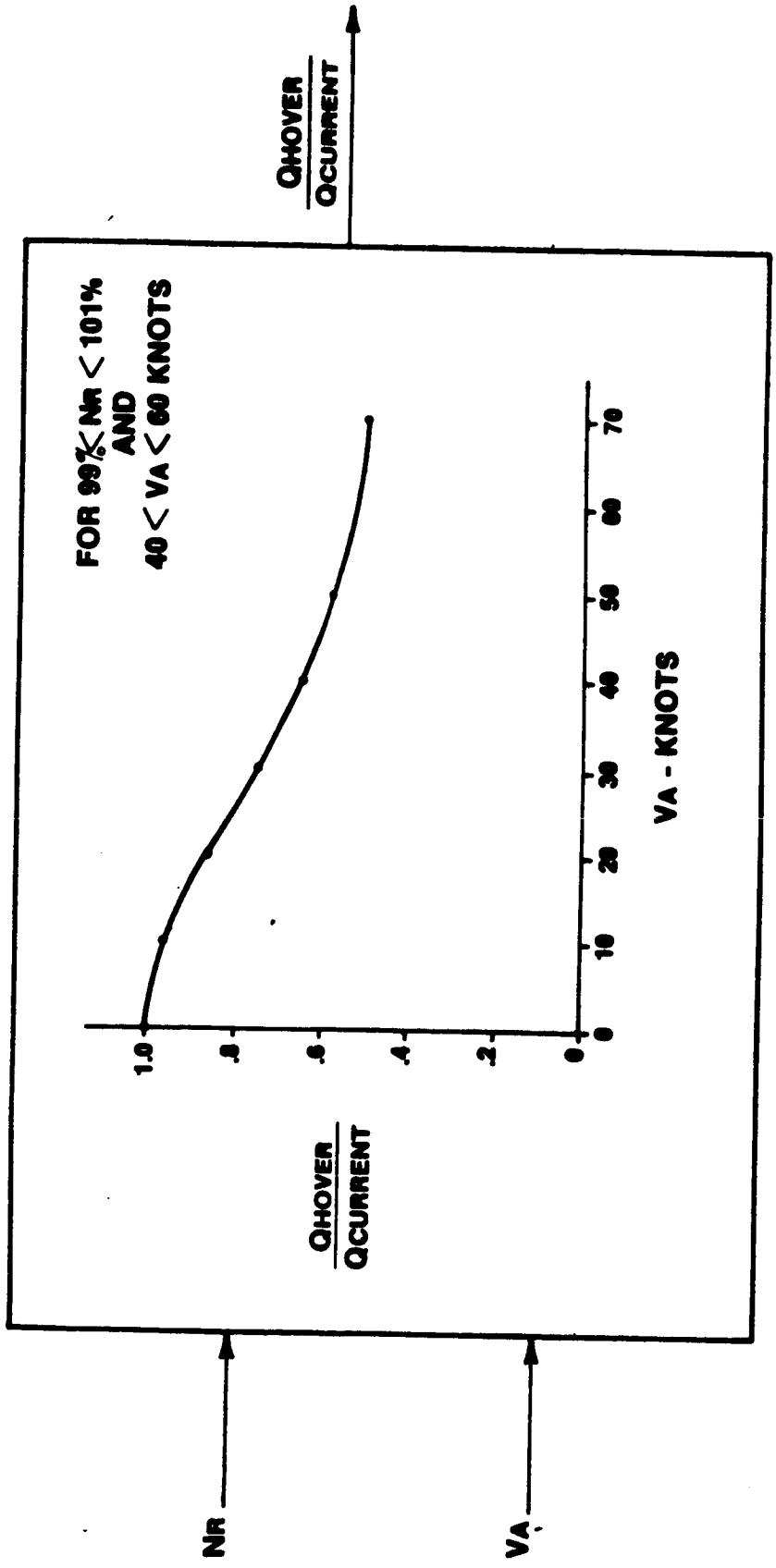

PREDICTED HOVER TORQUE RATIO

PREDICTED TORQUE REQUIRED TO HOVER
RATIOED TO CURRENT OPERATING TORQUE

FIG 4.5.2

POWER AVAILABLE TO HOVER

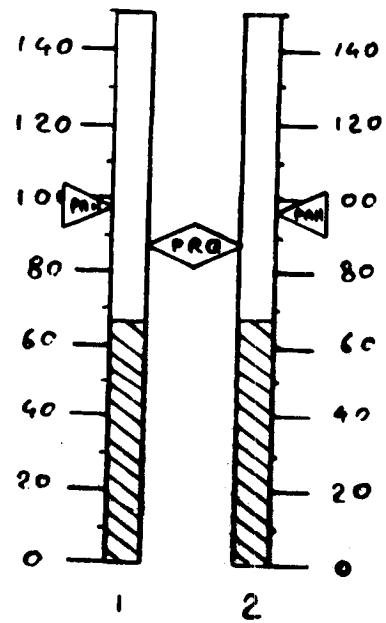

TORQUE

PRQ - % Torque Required to Hover

PAH - % Torque Available at Hover

UNITED TECHNOLOGIES SIKORSKY AIRCRAFT

PEDAL POSITION IN HIGH SPEED TRIM

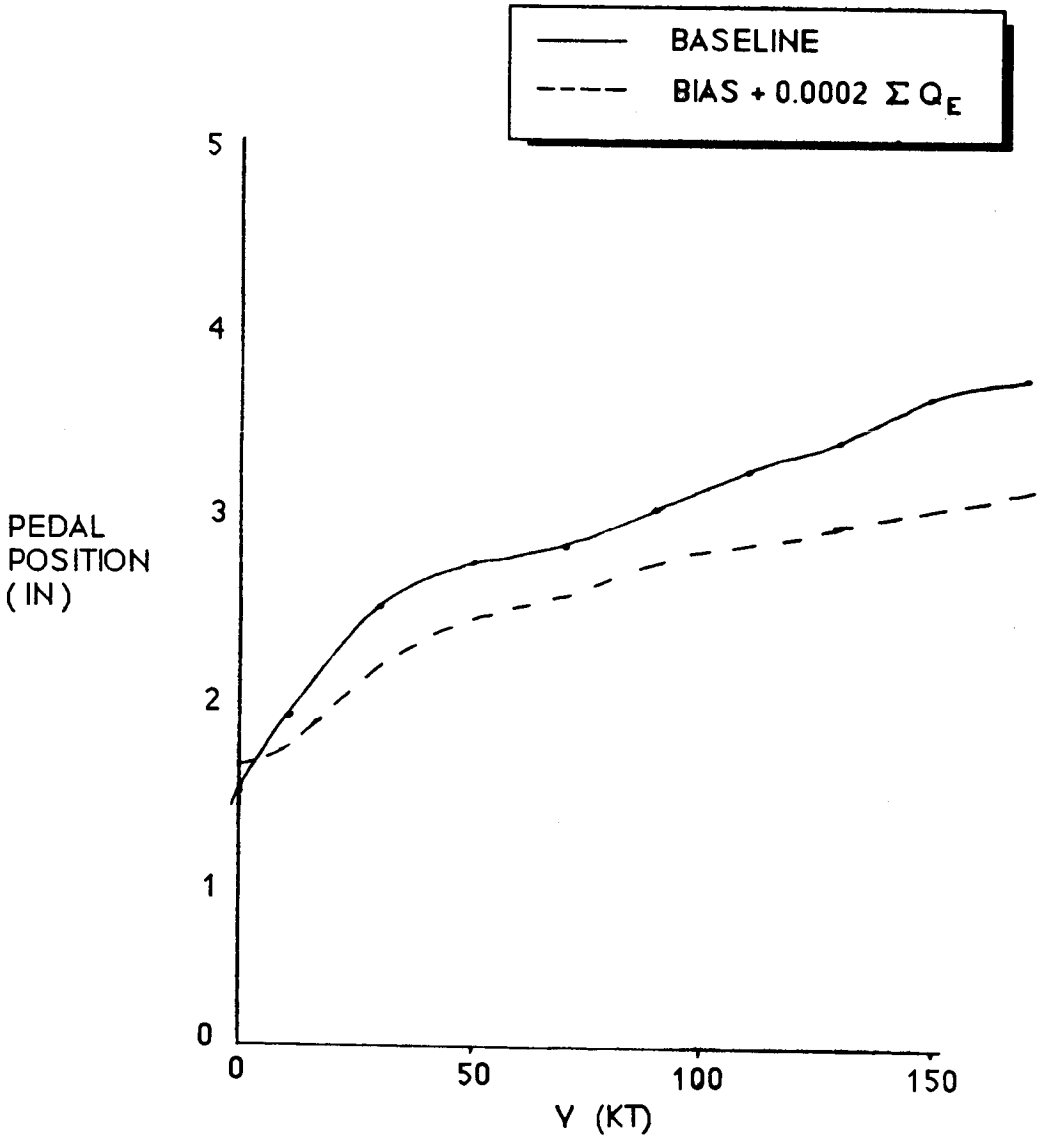

LINKING PEDAL POSITION TO SUM OF ENGINE TORQUES

FIG. 4.6.1

60A - BLACK HAWK

FAUTOS - AUTOROTATION RECOVERY, SMALL SPLIT, INT. F/C
70% XC IN 0.5 SEC - LIMITED WHEN F/C ON ACCEL. SCHED.

XA+1	5.0212293	XB+1	-5.9145290	XC+1	-.25941E-2	XP+1	3.6174507
THETAB	0.8433573	VKT	79.993820	PHIB	0.	VYB	-12.519340
XNGE	33592.203	NPINTE	8.2331274	VC	-2776.3938	WEIGHT	16638.000
OMRMR	1.0199999	NPMEAS	99.974205				

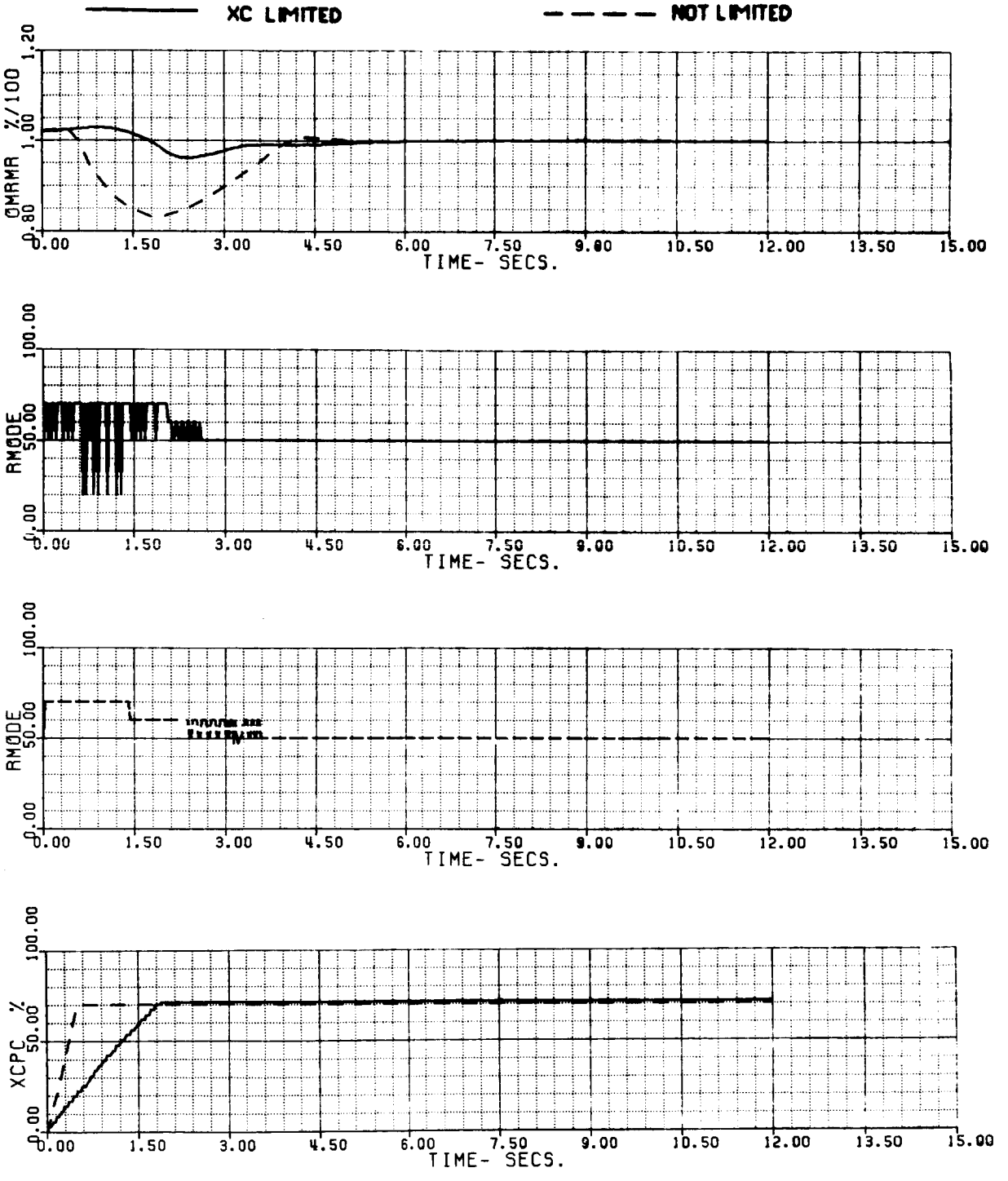

SIMULATED AUTO RECOVERY, XC LIMITED WHEN ON ACCEL. SCHEDULE

FIG 4.6.2

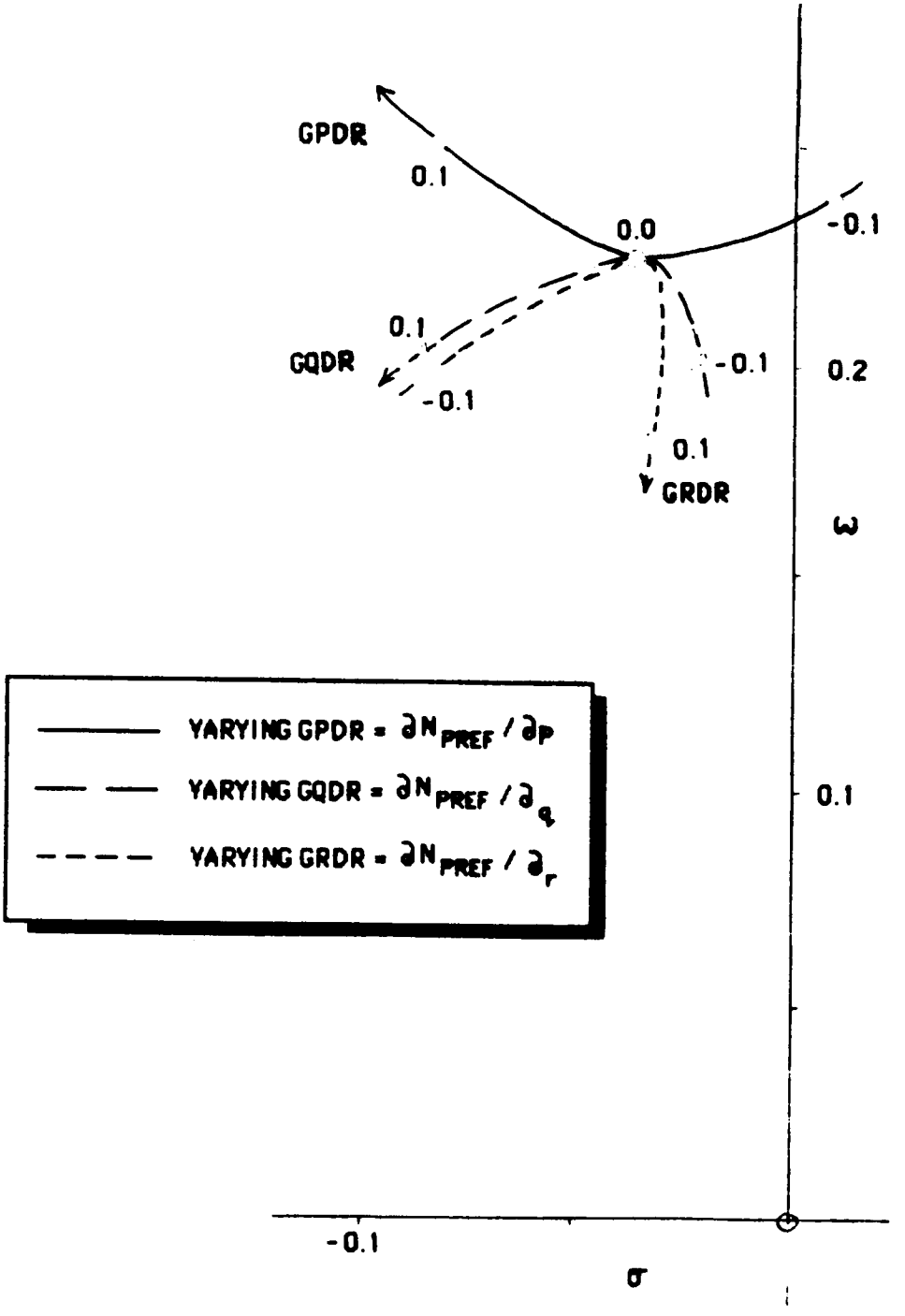

EFFECTS ON DUTCH ROLL MODE OF FEEDING BODY RATES TO NP REF

SA 1114

FIG 5.1.1

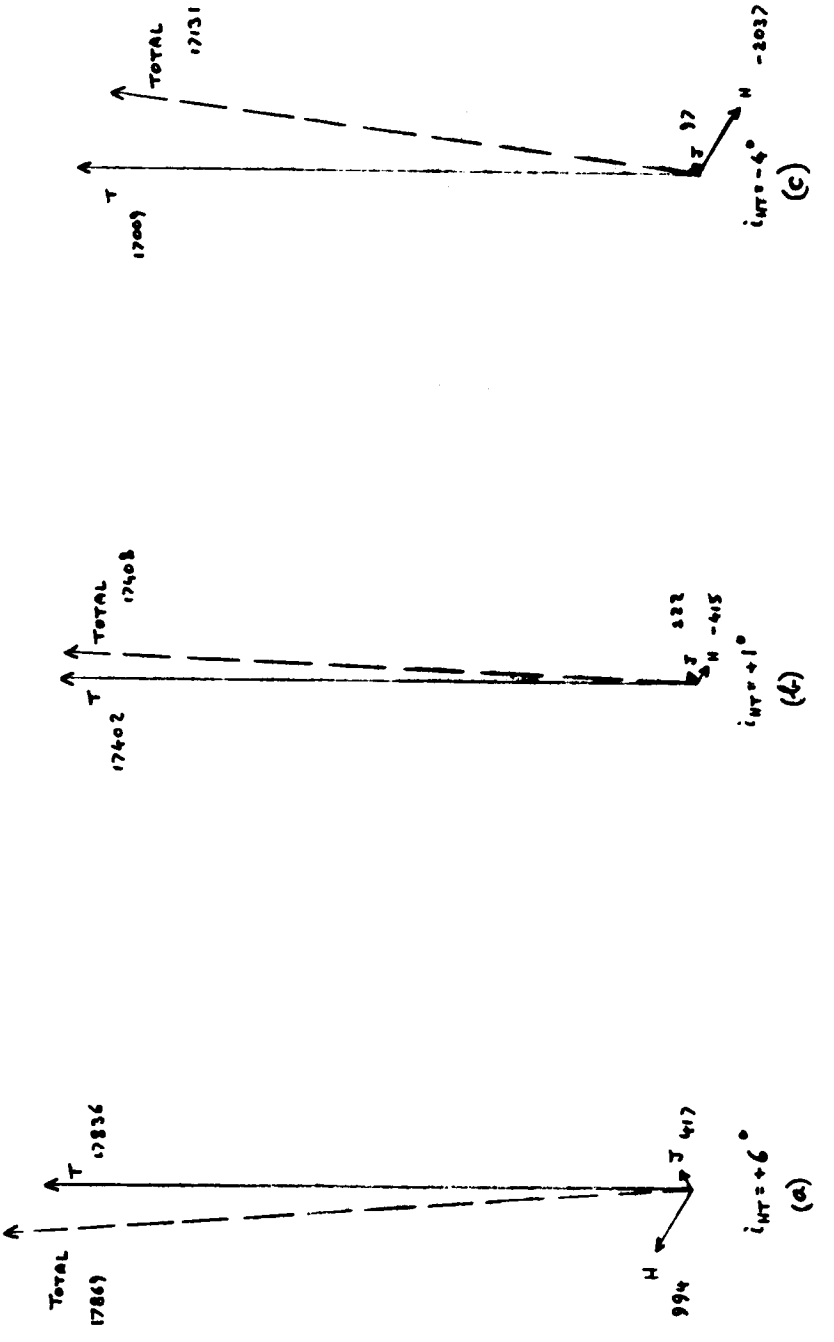

MEAN TRIMMED ROTOR FORCES AT DIFFERENT STABILATOR ANGLES

SA 1114

FIG 5.2.1

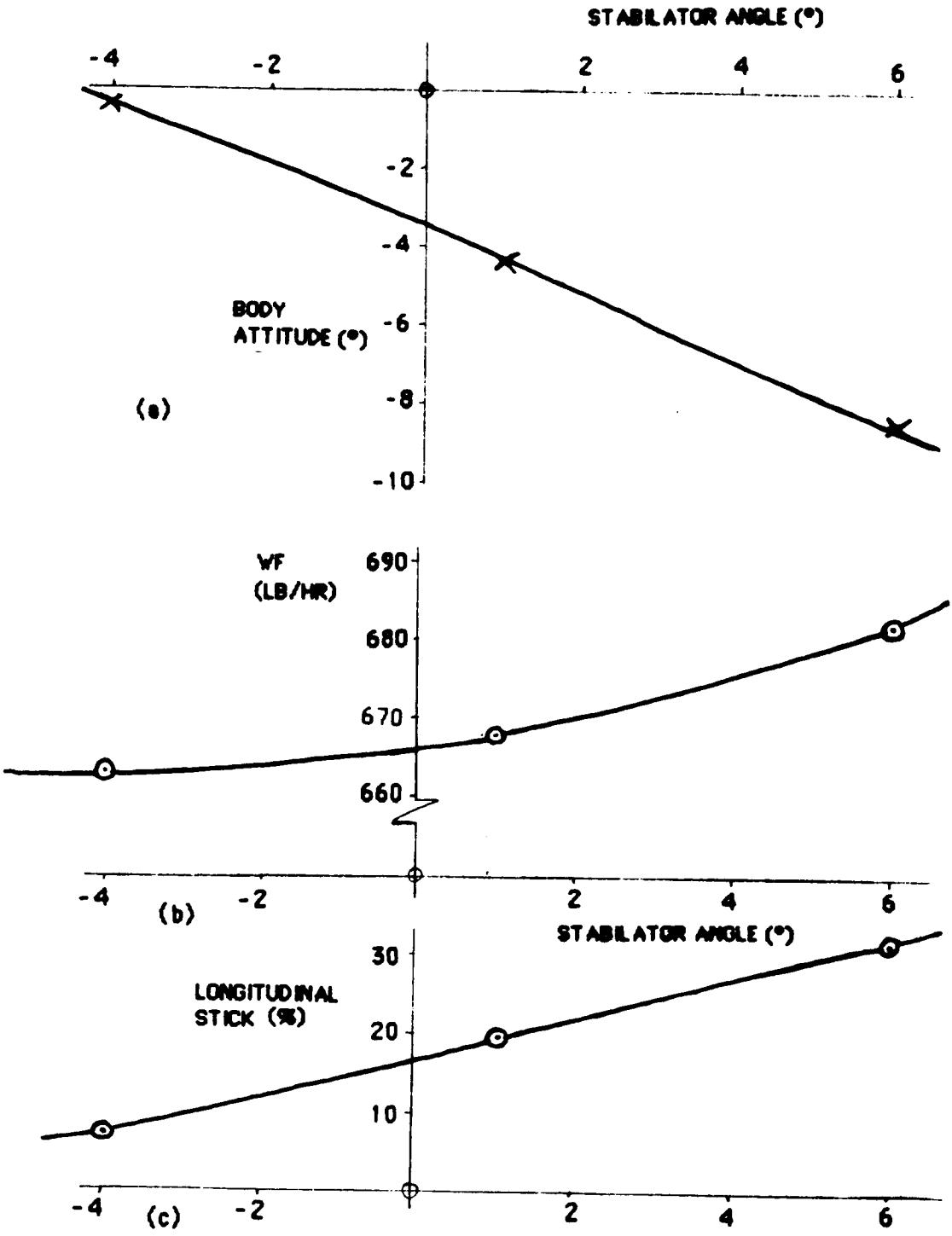

TRIM PARAMATERS ON MGH UH60A
AT HIGH SPEED ~ STABILATOR ANGLE

FIG 5.2.2

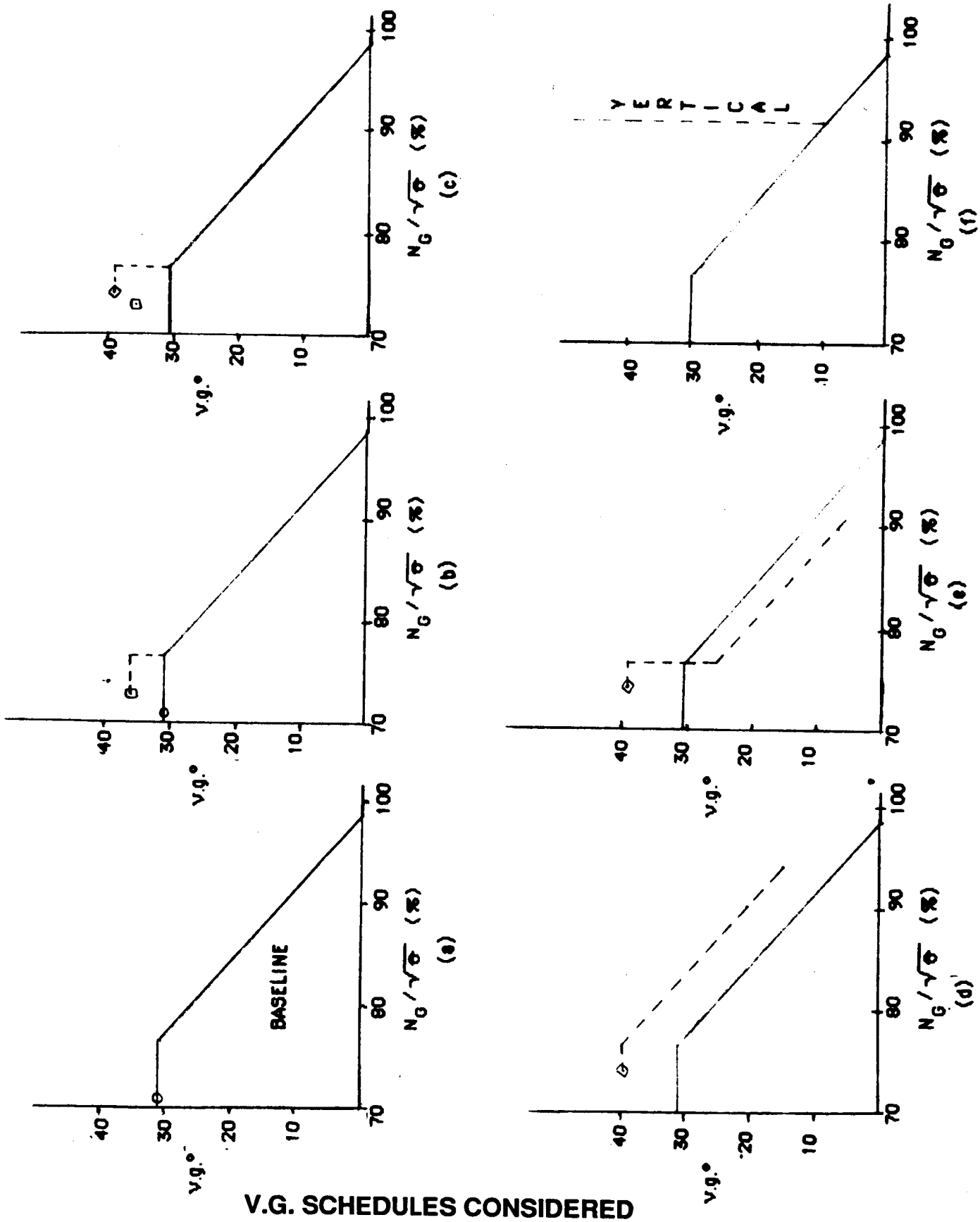

SA 1114

V.G. SCHEDULES CONSIDERED

C-2

FIG 5.3.1

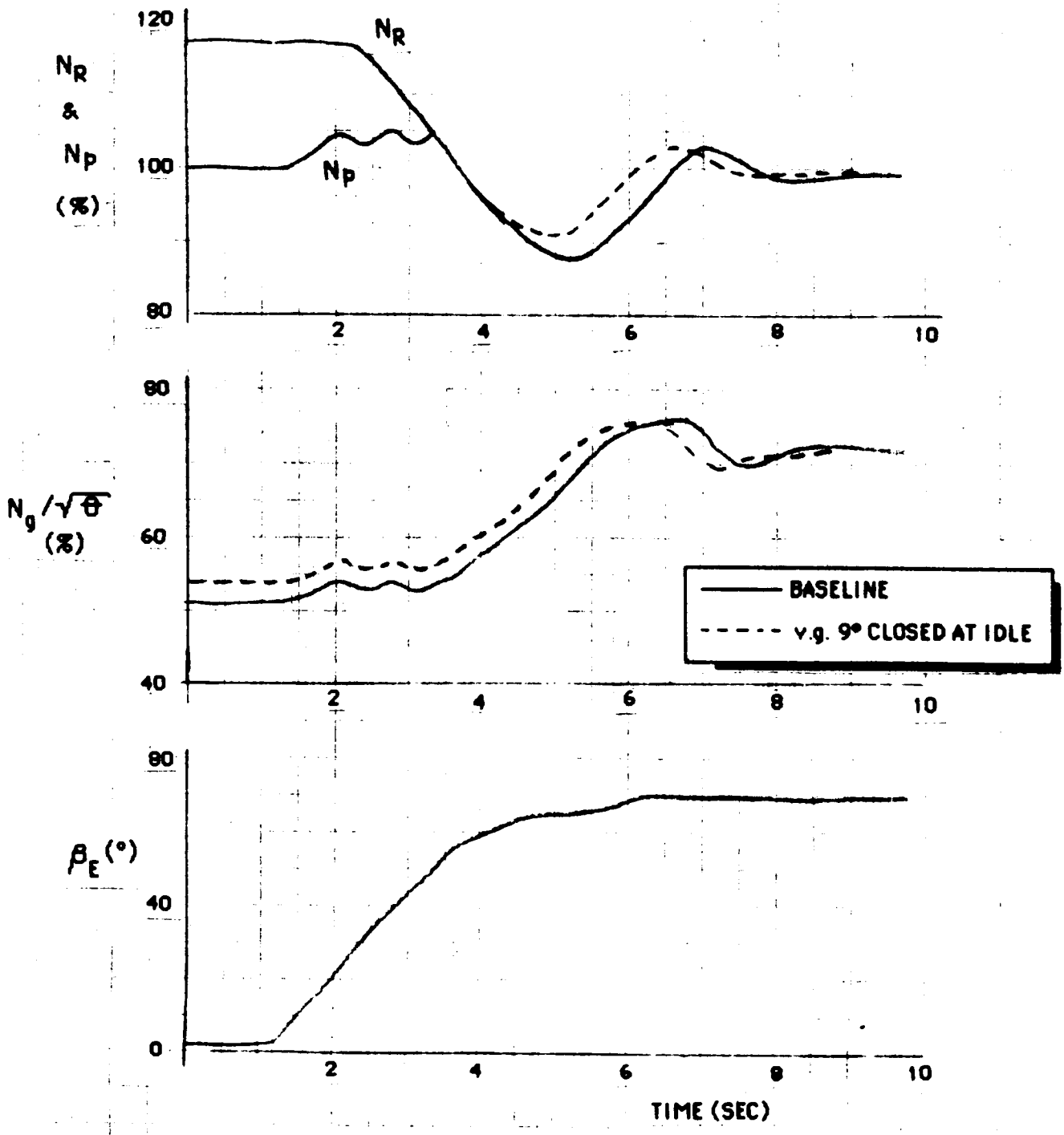

SIMULATED AUTO RECOVERY

(BASE & V.G. 0° CLOSED AT IDLE)

Sikorsky Aircraft

ORIGINAL PAGE IS
OF POOR QUALITY

SER 760606

REPORT NO.

MODEL

FIGURE NO. 5.3.3

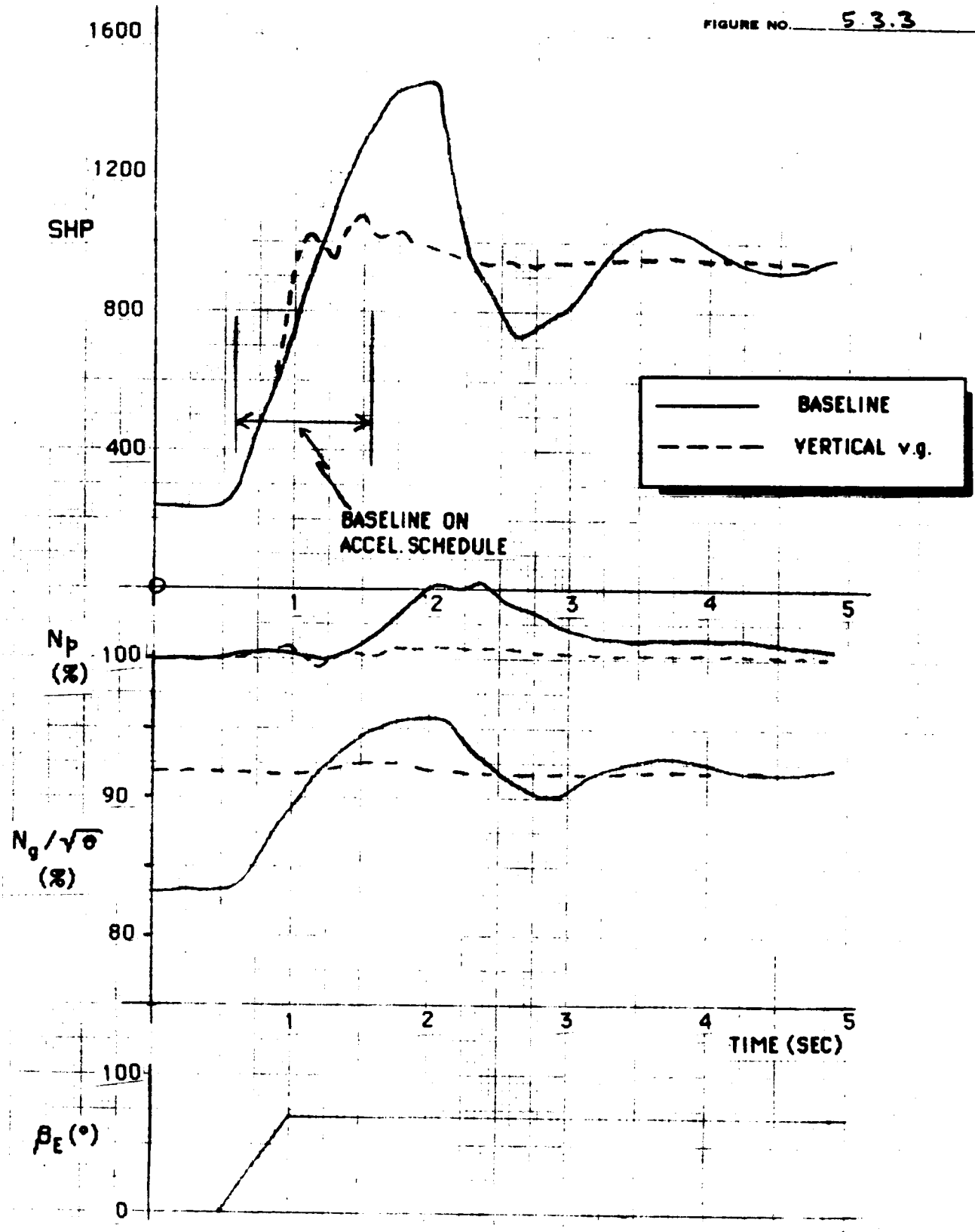

SIMULATED POWER BURST

(BASE & VERTICAL V.G. SCHEDULE)

SA 31 REV C

FIG 5.3.3

60A - BLACK HAWK

FAUTOL - AUTOROTATION RECOVERY, LARGE SPLIT, INT. F/C
70% XC IN 3 SEC, ADAPT = -1

XA+1	5.0569677	XB+1	-5.6562455	XC+1	-.23504E-1	XP+1	3.5084966
THETAB	0.3639957	VKT	79.996621	PHIB	0.	VYB	-11.785354
XNGE	33718.873	NPINTE	7.3990915	VC	-2657.0983	WEIGHT	16638.000
OMRMR	1.1699999	NPMEAS	99.974205				

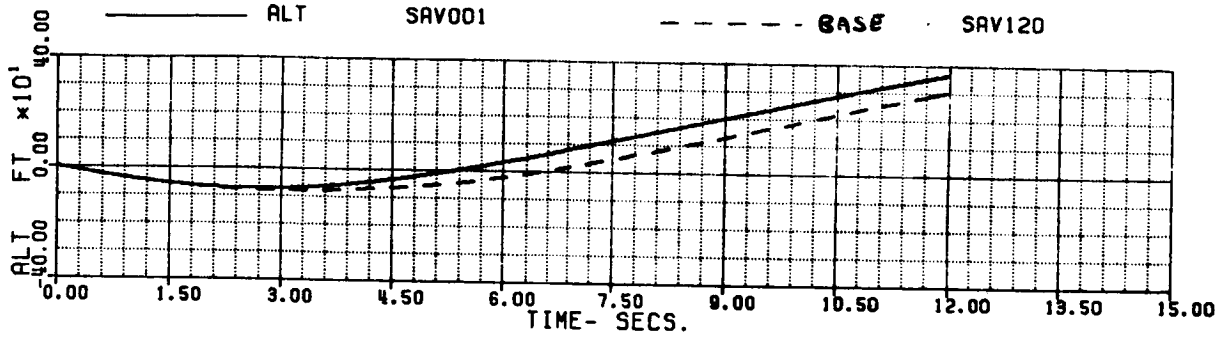

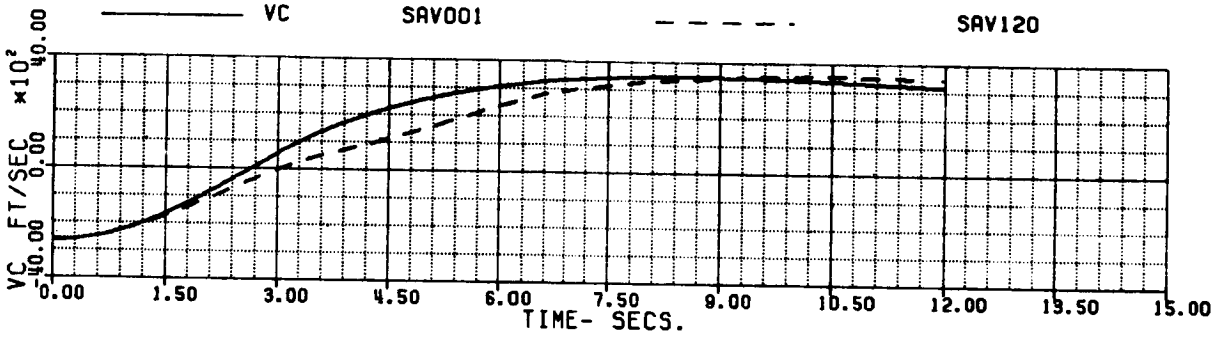

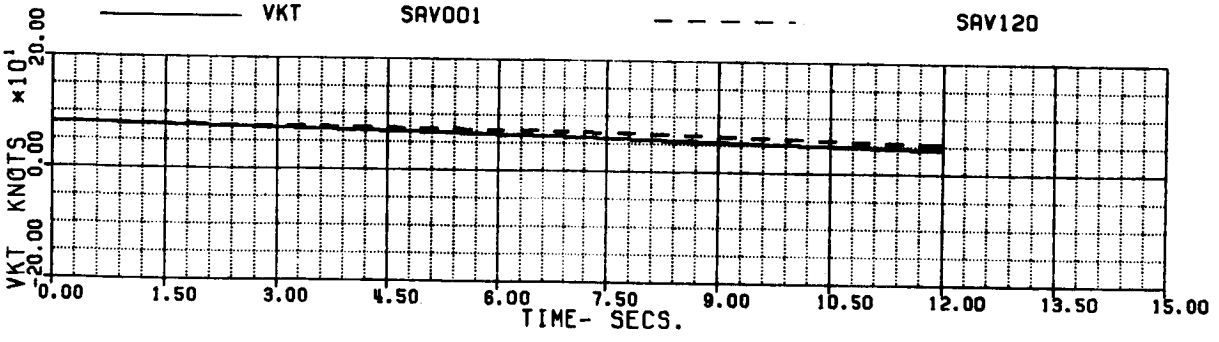

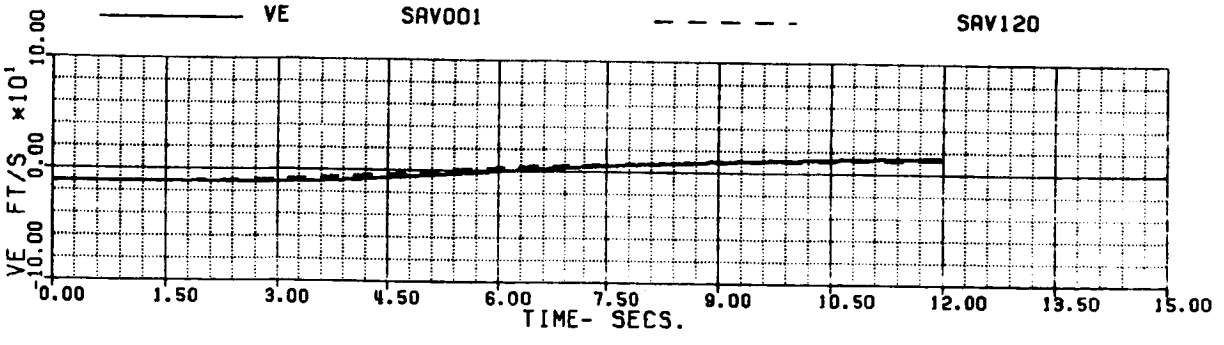

SIMULATED AUTOROTATION RECOVERY

(LARGE SPLIT, SLOW PULL)

FIG 6.1.1 (a)

60A - BLACK HAWK

FAUTOL - AUTOROTATION RECOVERY, LARGE SPLIT, INT. F/C
70% XC IN 3 SEC, ADAPT = -1

XA+1	5.0569677	XB+1	-5.6562455	XC+1	-.23504E-1	XP+1	3.5084966
THETAB	0.3639957	VKT	79.996621	PHIB	0.	VYB	-11.785354
XNGE	33718.873	NPINTE	7.3990915	VC	-2657.0983	WEIGHT	16638.000
OMAMR	1.1699999	NPMEAS	99.974205				

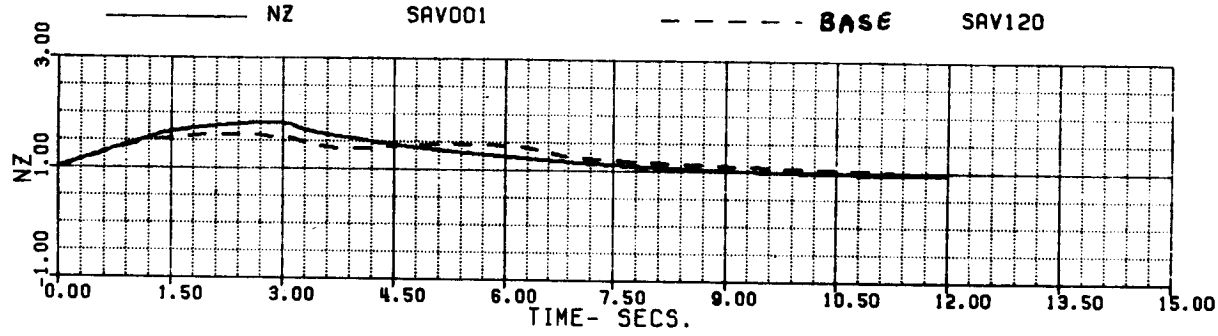

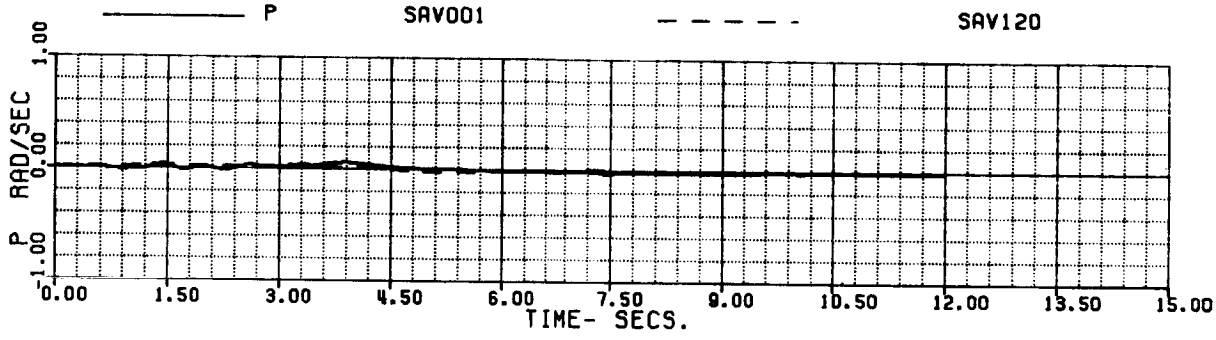

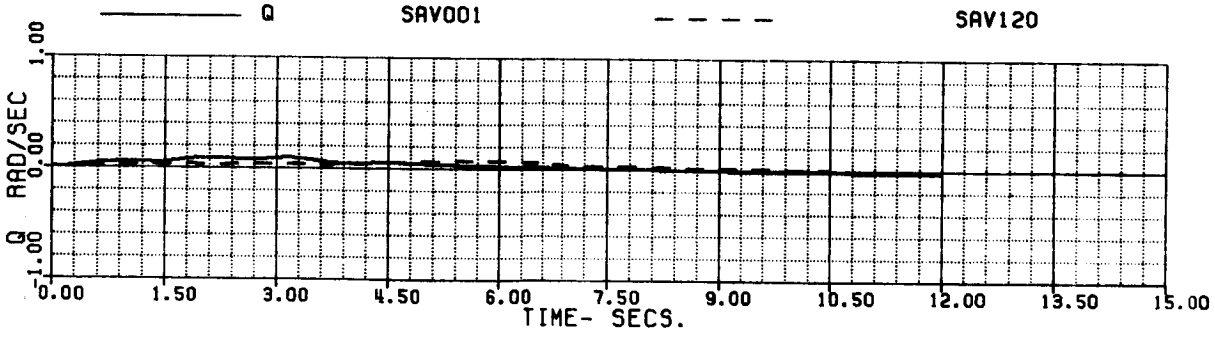

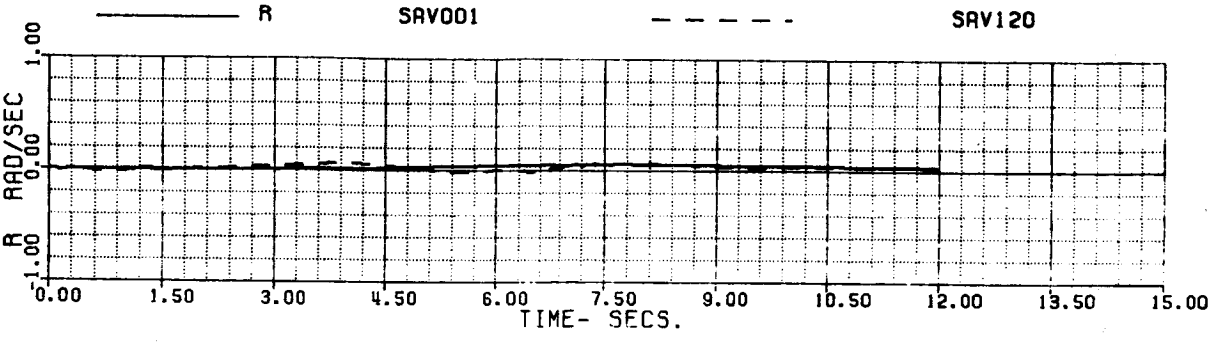

FIG 6.1.1 (b)

60A - BLACK HAWK

FAUTOL - AUTOROTATION RECOVERY, LARGE SPLIT, INT. F/C
70% XC IN 3 SEC, ADAPT = -1

XA+1	5.0569677	XB+1	-5.6562455	XC+1	-.23504E-1	XP+1	3.5084966
THETAB	0.3639957	VKT	79.996621	PHIB	0.	VYB	-11.765354
XNGE	33718.873	NPINTE	7.3990915	VC	-2657.0983	WEIGHT	16638.000
OMRMR	1.1699999	NPMEAS	99.974205				

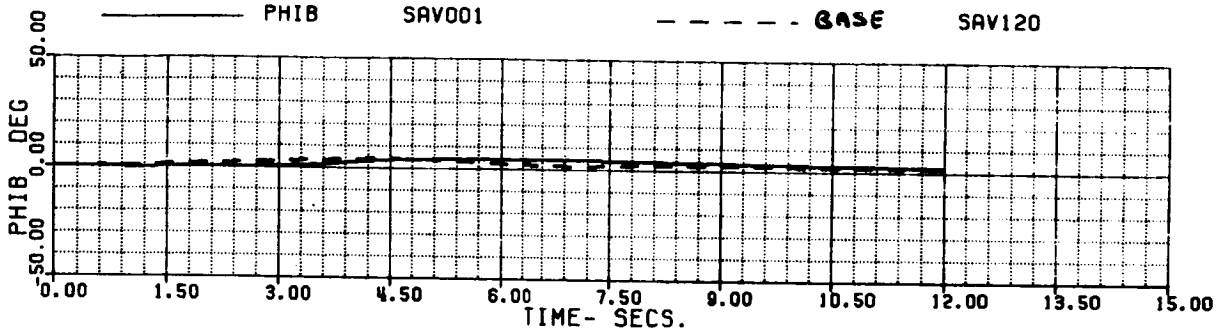

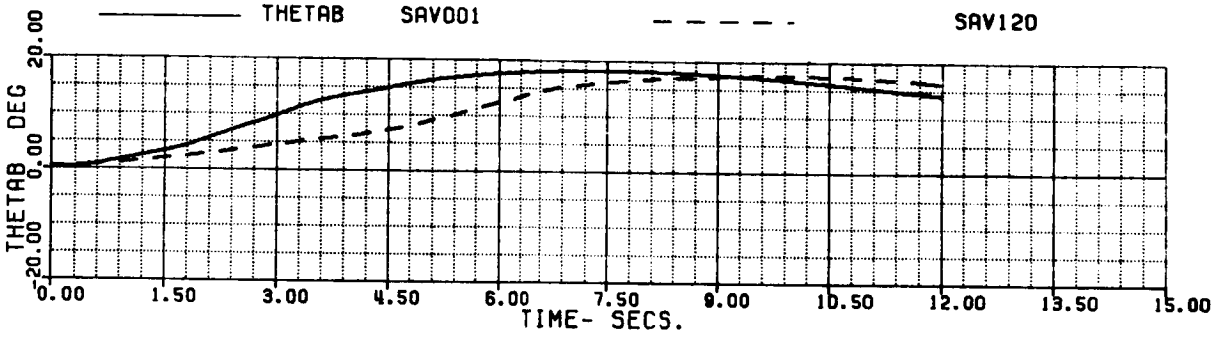

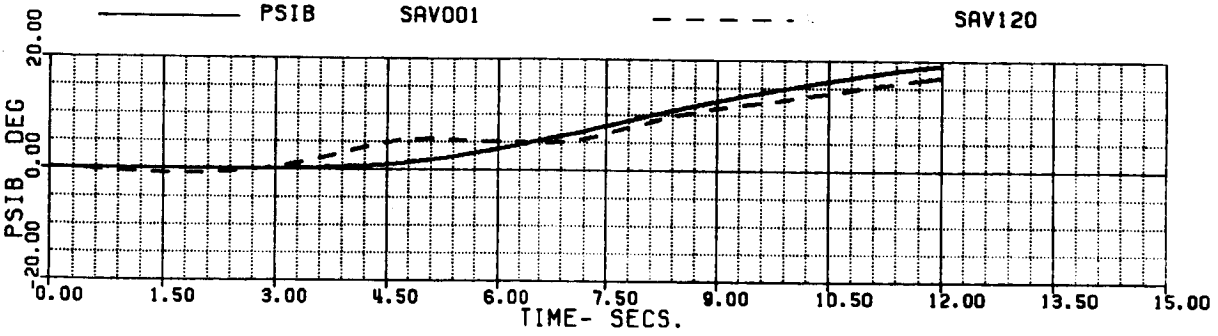

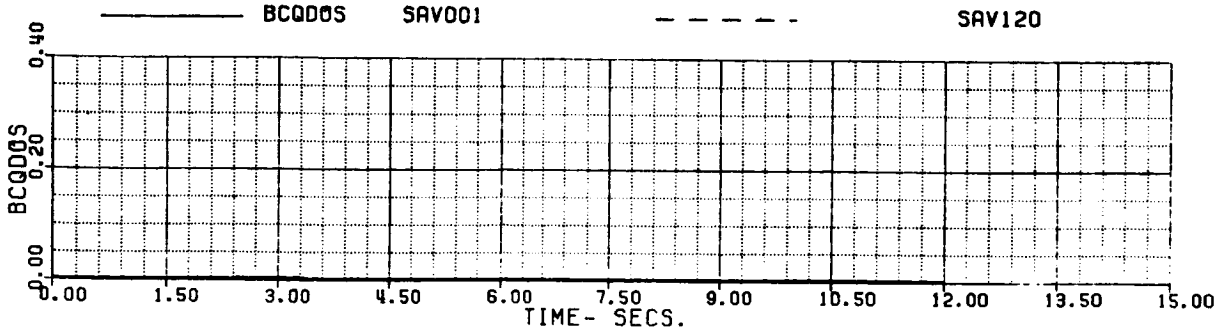

FIG 6.1.1 (c)

60A - BLACK HAWK

FAUTOL - AUTOROTATION RECOVERY, LARGE SPLIT, INT. F/C
70% XC IN 3 SEC, ADAPT = -1

XA+1	5.0569677	XB+1	-5.6562455	XC+1	-.23504E-1	XP+1	3.5084966
THETAB	0.3639957	VKT	79.996621	PHIB	0.	VYB	-11.785354
XNGE	33718.873	NPINTE	7.3990915	VC	-2657.0983	WEIGHT	16638.000
OMRMR	1.1699999	NPMEAS	99.974205				

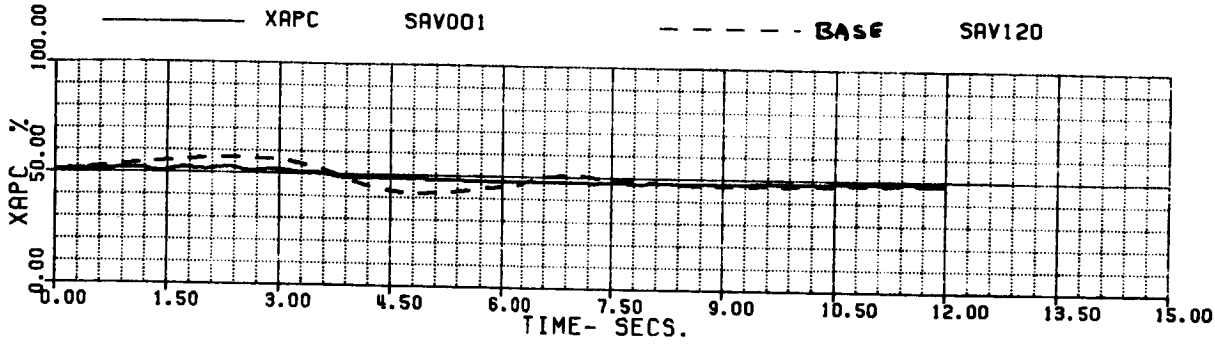

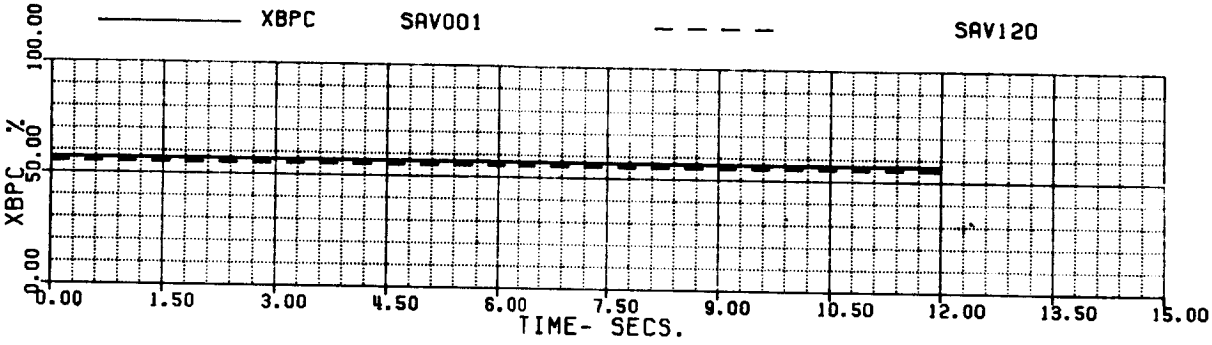

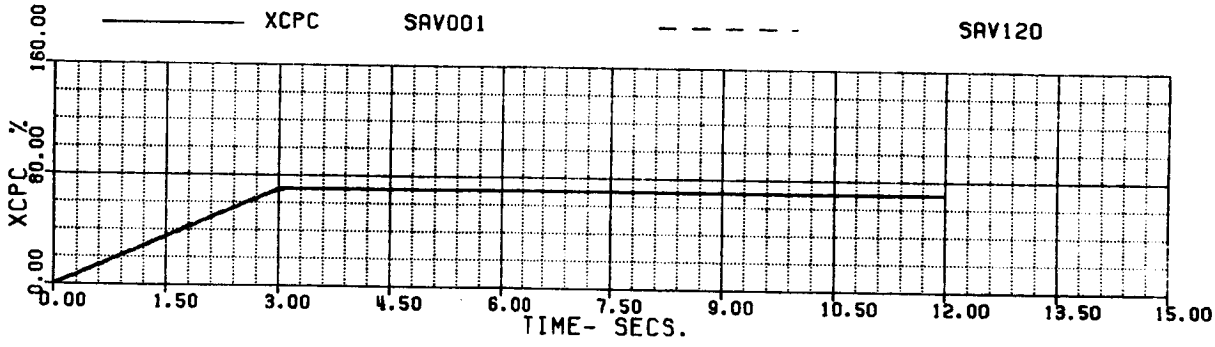

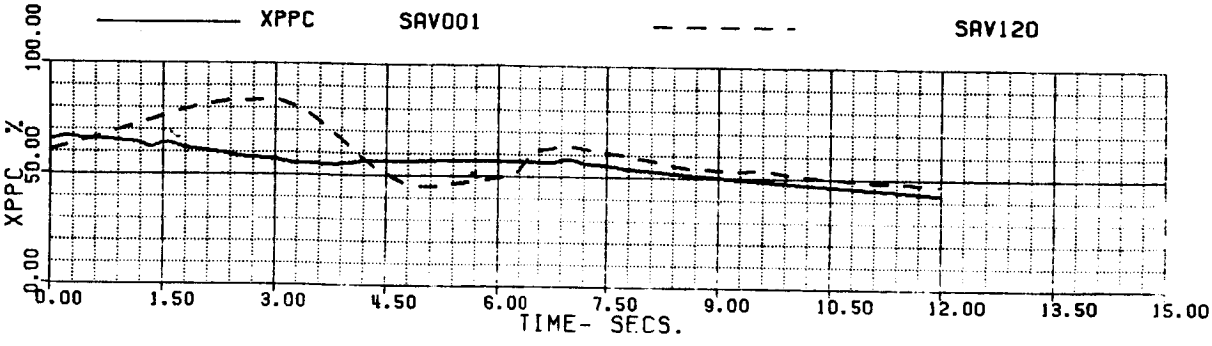

FIG 6.1.1 (d)

60A - BLACK HAWK

FAUTOL - AUTOROTATION RECOVERY, LARGE SPLIT, INT. F/C
70% XC IN 3 SEC, ADAPT = -1

XA+1	5.0569677	XB+1	-5.6562455	XC+1	-.23504E-1	XP+1	3.5084966
THETAB	0.3639957	VKT	79.996621	PHIB	0.	VYB	-11.785354
XNGE	33718.873	NPINTE	7.3990915	VC	-2657.0983	WEIGHT	16638.000
OMRMR	1.1699999	NPMEAS	99.974205				

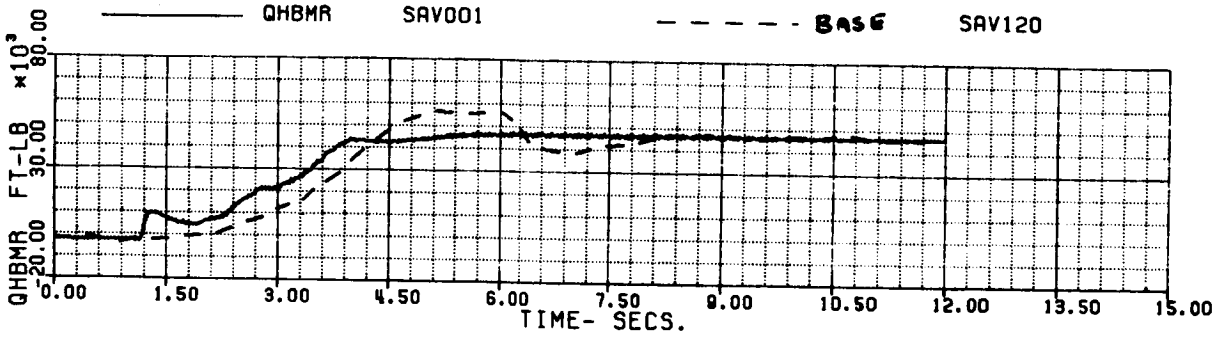

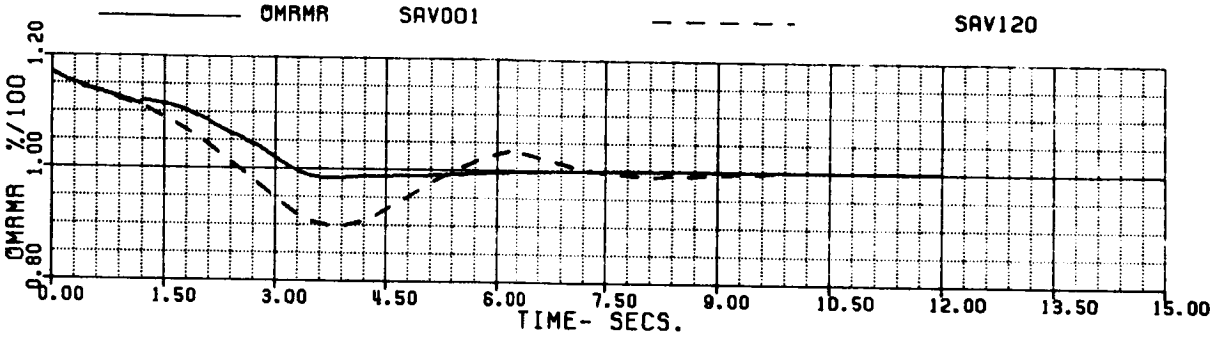

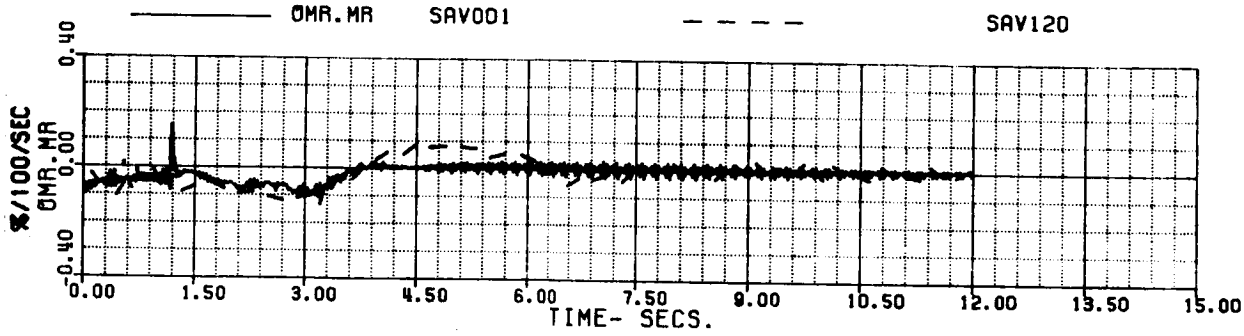

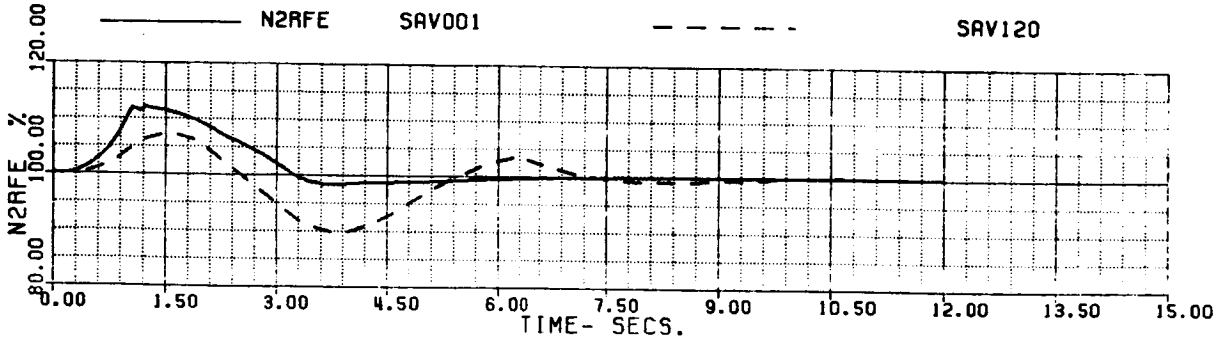

FIG 6.1.1 (e)

60A - BLACK HAWK

FAUTOL - AUTOROTATION RECOVERY, LARGE SPLIT, INT. F/C
70% XC IN 3 SEC, ADAPT = -1

XA+1	5.0569677	XB+1	-5.6562455	XC+1	-.23504E-1	XP+1	3.5084966
THETAB	0.3639957	VKT	79.996621	PHIB	0.	VYB	-11.785354
XNGE	33718.873	NPINTE	7.3990915	VC	-2657.0983	WEIGHT	16638.000
OMRMR	1.1699999	NPMEAS	99.974205				

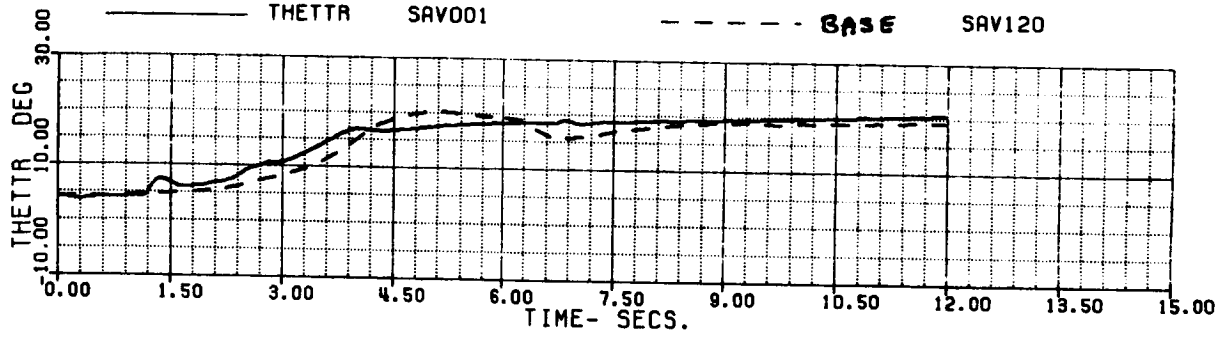

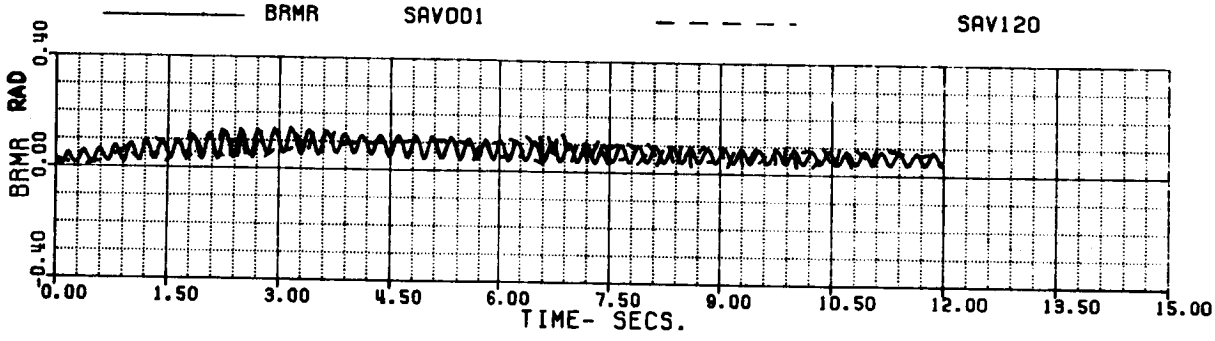

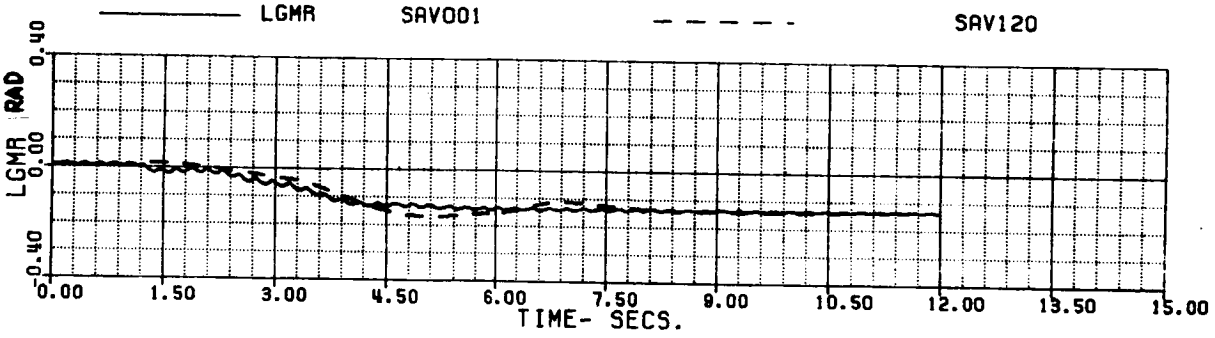

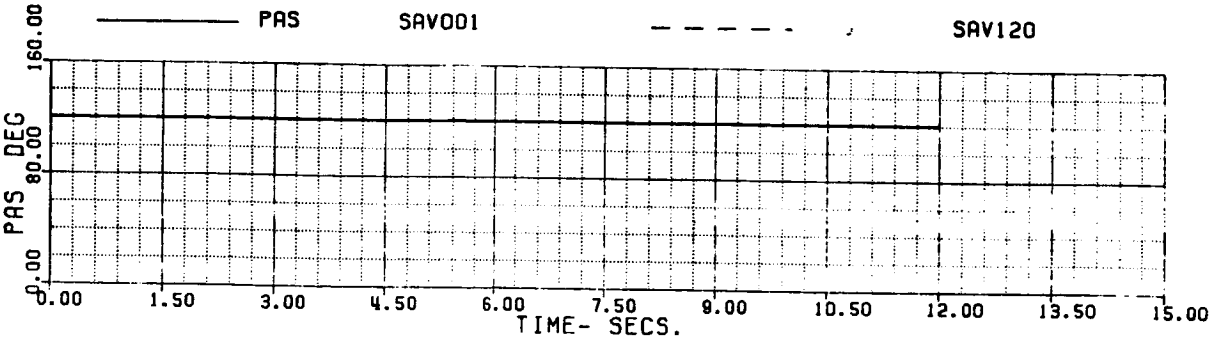

FIG 6.1.1 (f)

60A - BLACK HAWK

FAUTOL - AUTOROTATION RECOVERY, LARGE SPLIT, INT. F/C
70% XC IN 3 SEC. ADAPT = -1

XA+1	5.0569677	XB+1	-5.6562455	XC+1	-.23504E-1	XP+1	3.5084966
THETAB	0.3639957	VKT	79.996621	PHIB	0.	VYB	-11.785354
XNGE	33718.873	NPINTE	7.3990915	VC	-2657.0983	WEIGHT	16638.000
OMRMR	1.1699999	NPMEAS	99.974205				

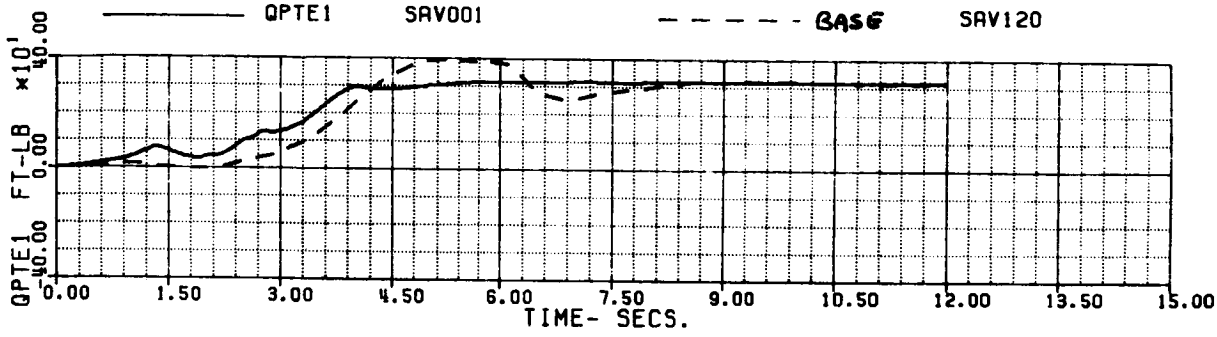

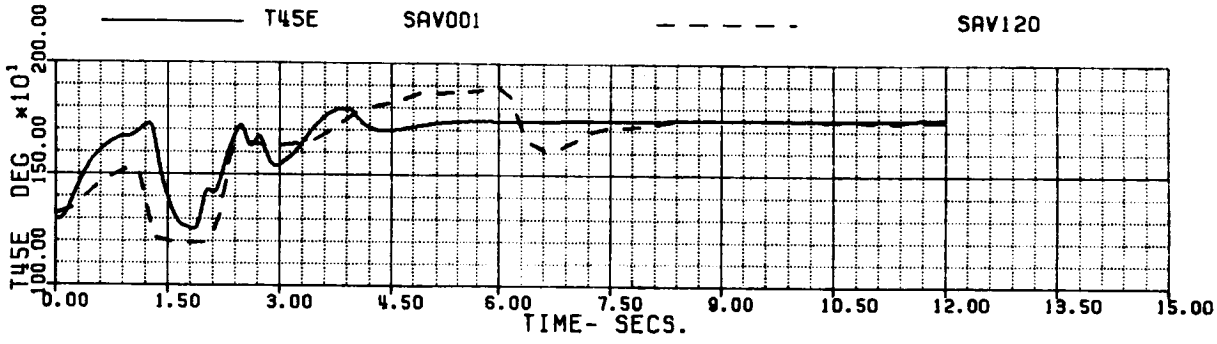

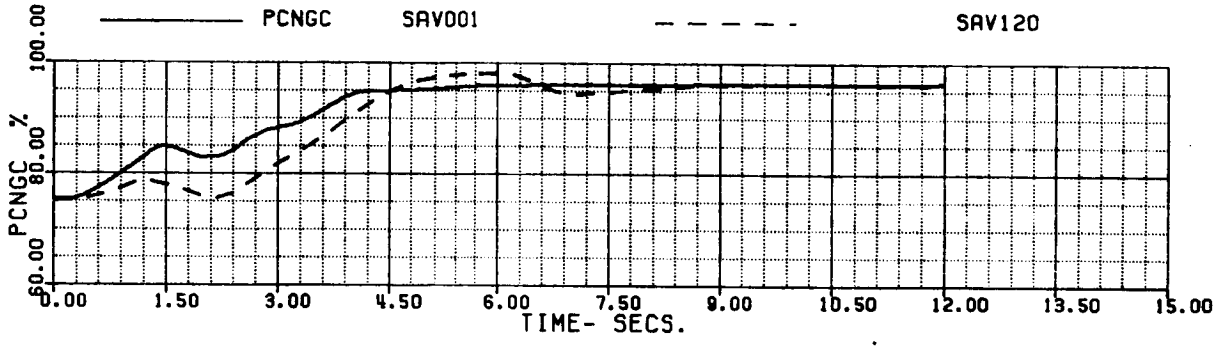

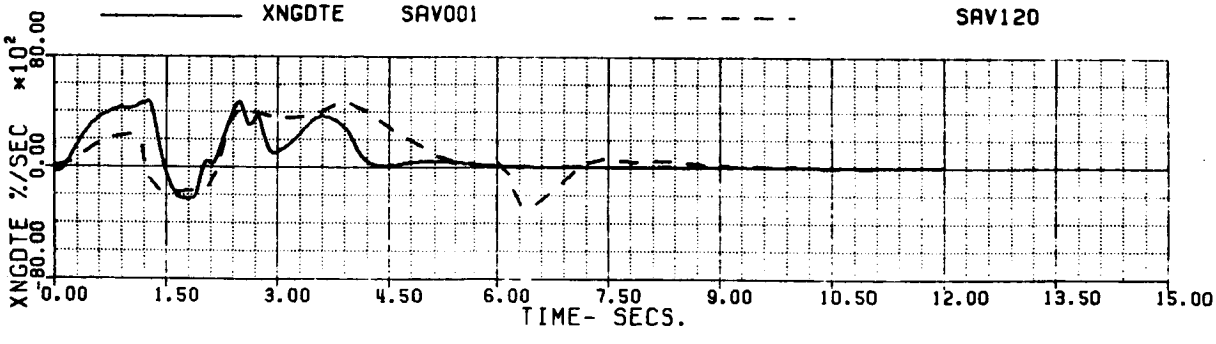

FIG 6.1.1 (g)

60A - BLACK HAWK

FAUTOL - AUTOROTATION RECOVERY, LARGE SPLIT, INT. F/C
70% XC IN 3 SEC. ADAPT = -1

XA+1	5.0569677	XB+1	-5.6562455	XC+1	-.23504E-1	XP+1	3.5084966
THETAB	0.3639957	VKT	79.996621	PHIB	0.	VYB	-11.785354
XNGE	33718.873	NPINTE	7.3990915	VC	-2657.0983	WEIGHT	16638.000
OMRMR	1.1699999	NPMEAS	99.974205				

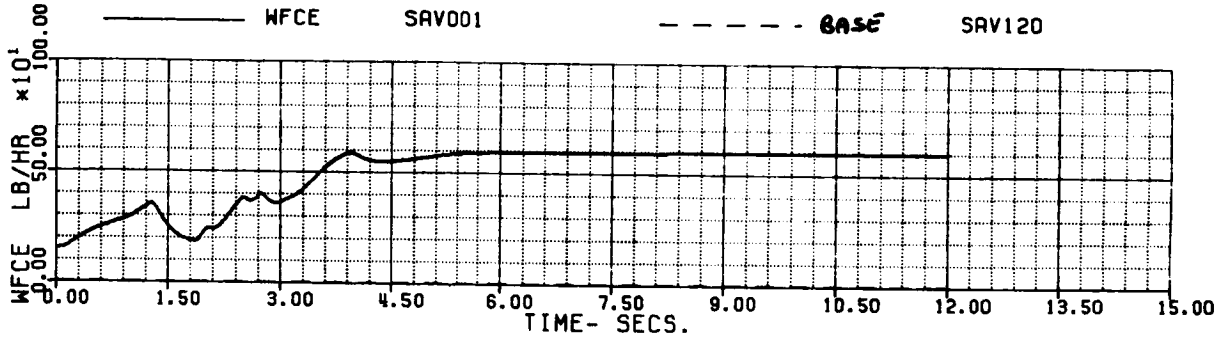

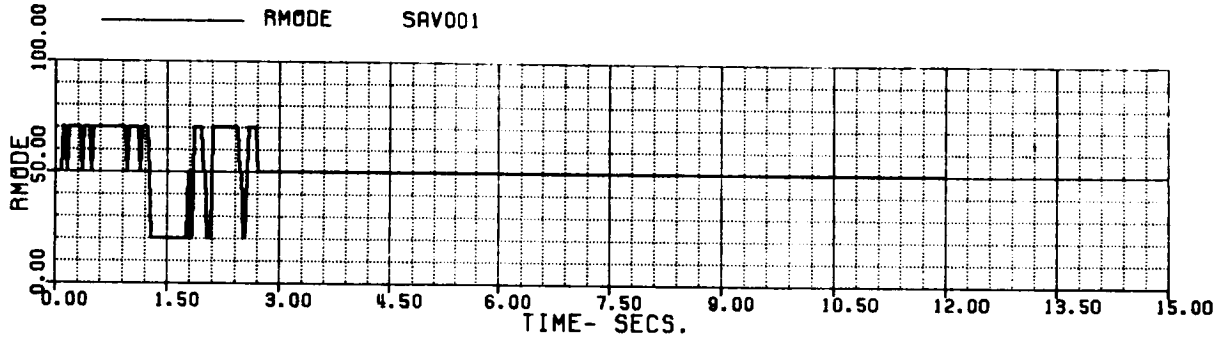

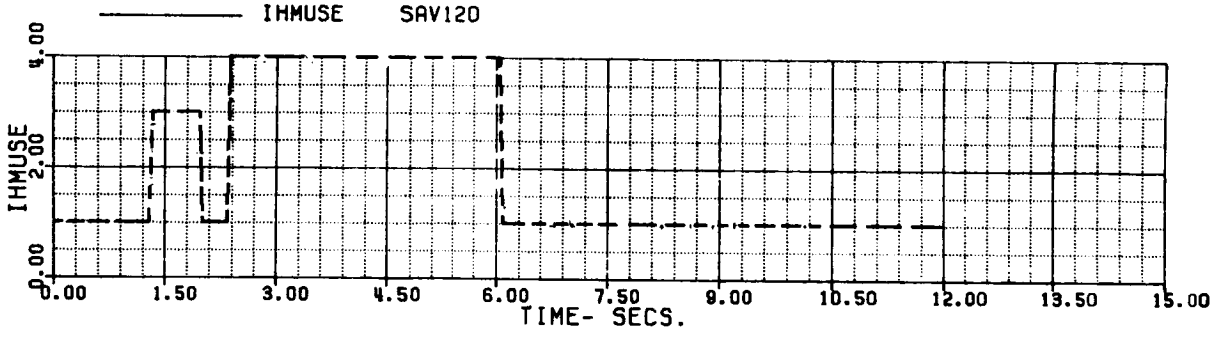

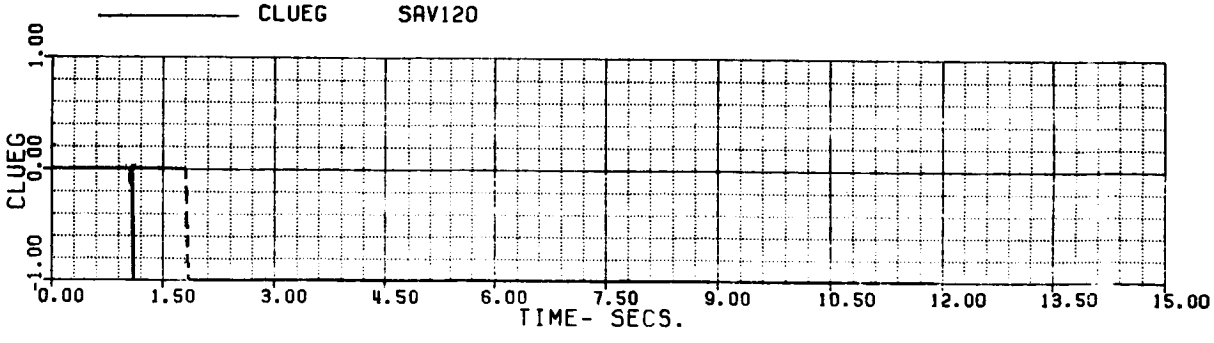

FIG 6.1.1 (h)

60A - BLACK HAWK

FAUTOL - AUTOROTATION RECOVERY, LARGE SPLIT, INT. F/C
70% XC IN 3 SEC, ADAPT = -1

XA+1	5.0569677	XB+1	-5.6562455	XC+1	-.23504E-1	XP+1	3.5084966
THETAB	0.3639957	VKT	79.996621	PHIB	0.	VYB	-11.765354
XNGE	33718.873	NPINTE	7.3990915	VC	-2657.0983	WEIGHT	16638.000
OMRMR	1.1699999	NPMEAS	99.974205				

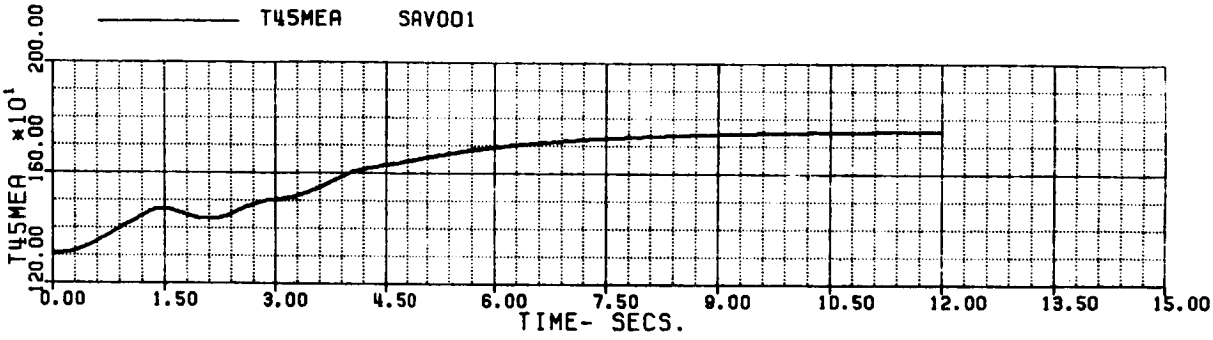

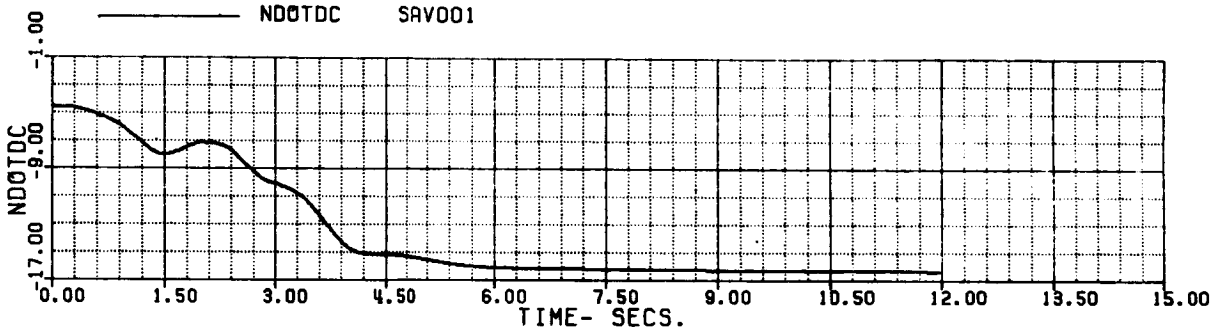

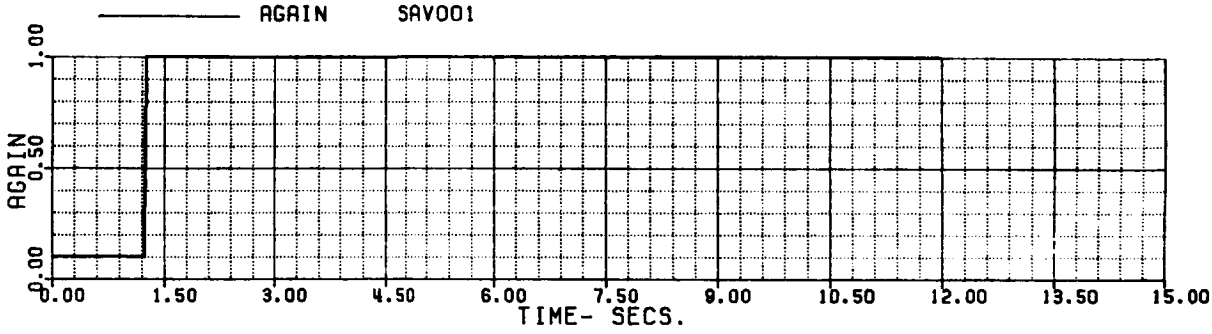

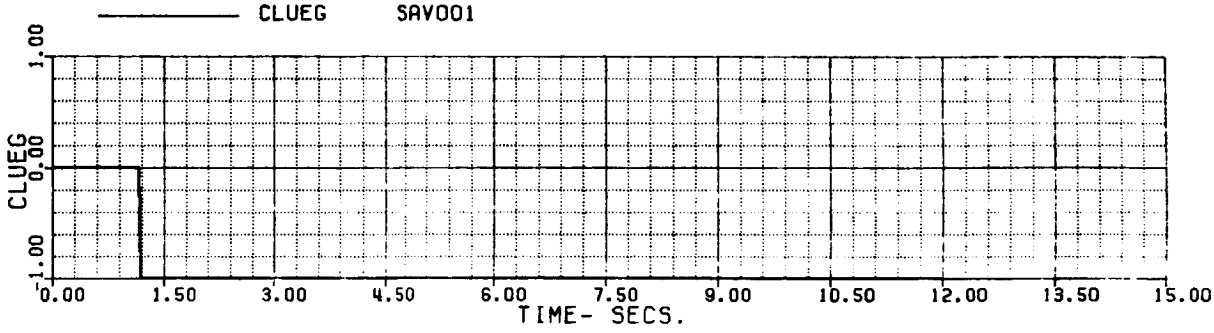

FIG 6.1.1 (i)

60A - BLACK HAWK

FAUTOL - AUTOROTATION RECOVERY, LARGE SPLIT, INT. F/C
70% XC IN 3 SEC, ADAPT = -1

XA+1	5.0569677	XB+1	-5.6562455	XC+1	-.23504E-1	XP+1	3.5084966
THETAB	0.3639957	VKT	79.996621	PHIB	0.	VYB	-11.7853
XNGE	33718.873	NPINTE	7.3990915	VC	-2657.0983	WEIGHT	16638.00
OMRMR	1.1699999	NPMEAS	99.974205				

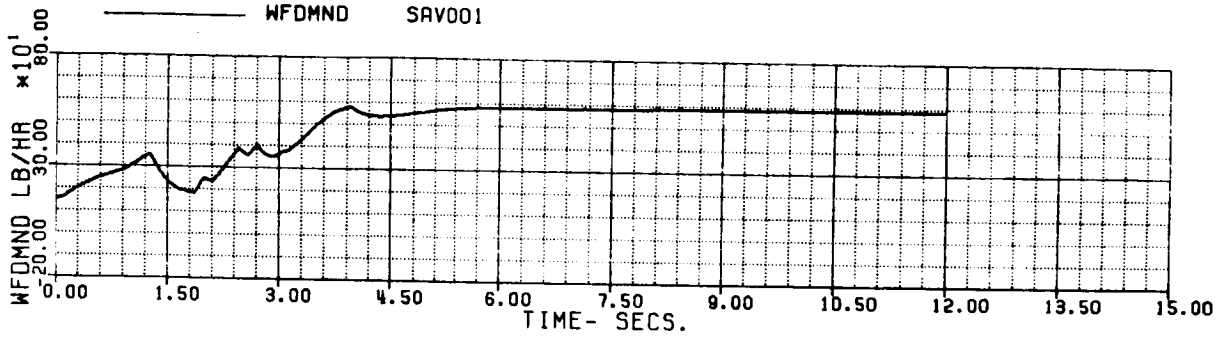

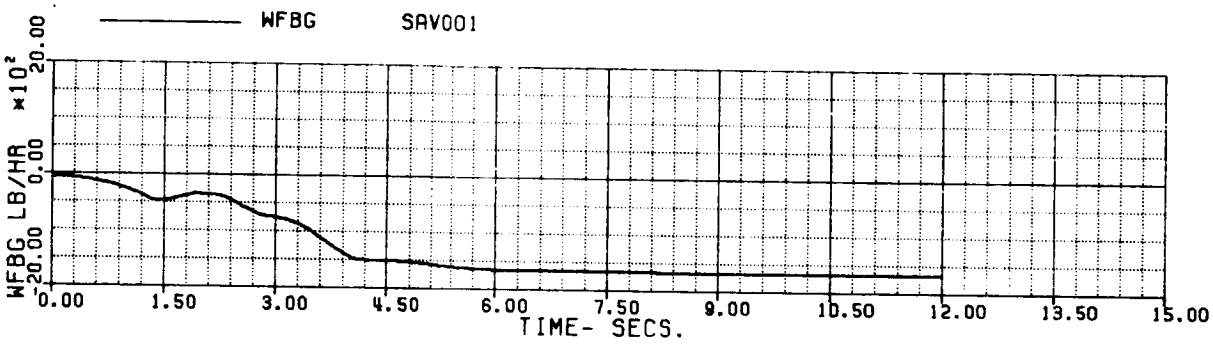

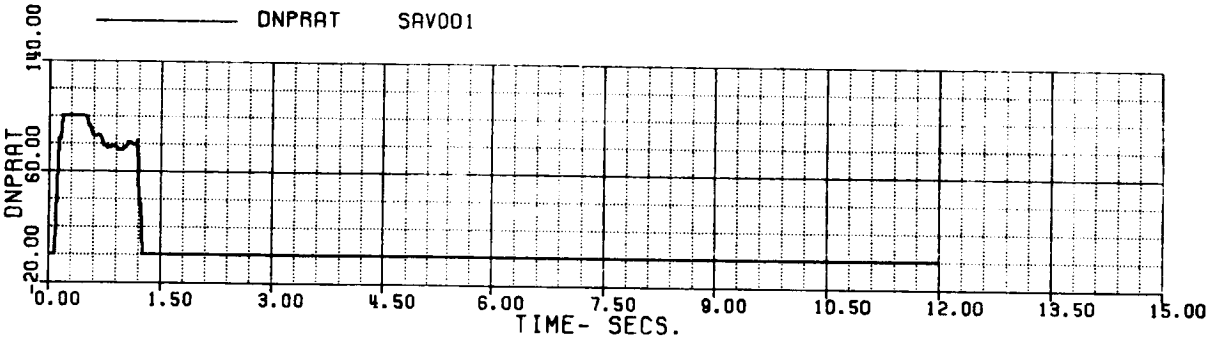

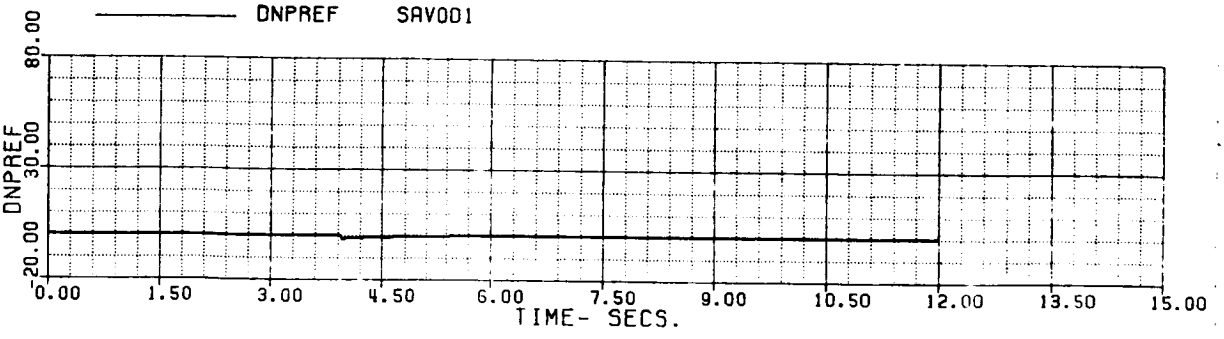

FIG 6.1.1 (j)

60A - BLACK HAWK

FAUTOL - AUTOROTATION RECOVERY, LARGE SPLIT, INT. F/C
70% XC IN 3 SEC, ADAPT = -1

XA+1	5.0569677	XB+1	-5.6562455	XC+1	-.23504E-1	XP+1	3.50849
THETAB	0.3639957	VKT	79.996621	PHIB	0.	VYB	-11.785
XNGE	33718.873	NPINTE	7.3990915	VC	-2657.0983	WEIGHT	16638.0
OMRMR	1.1699999	NPMEAS	99.974205				

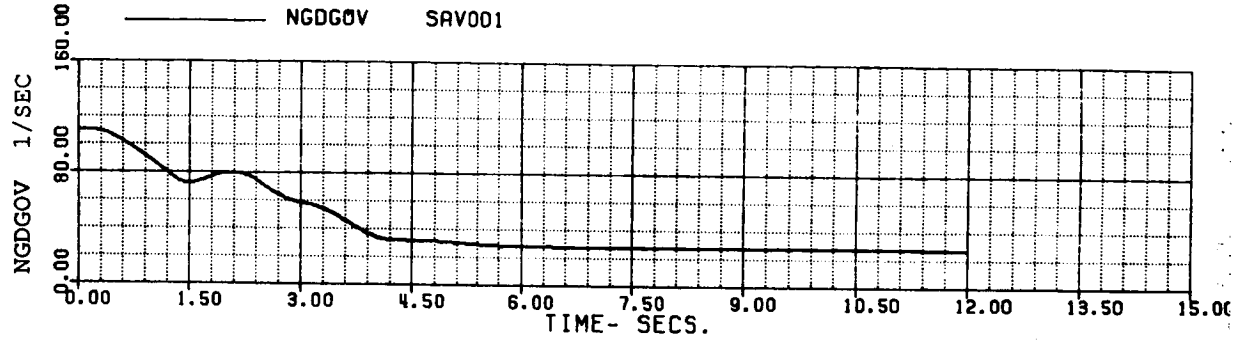

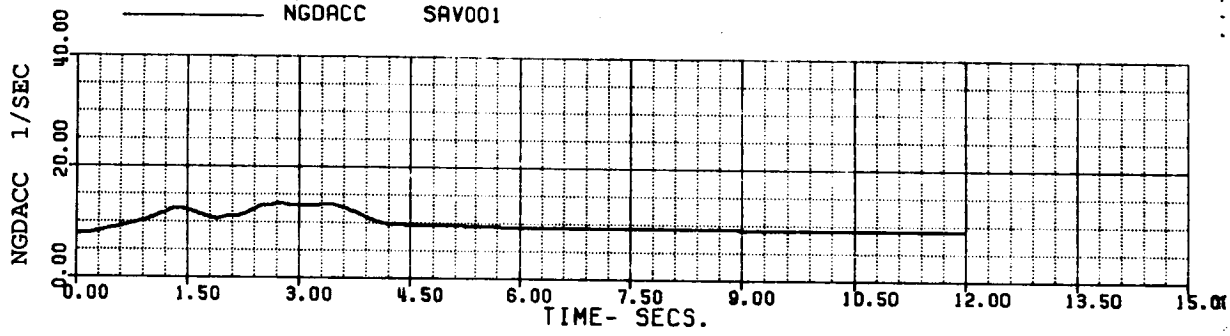

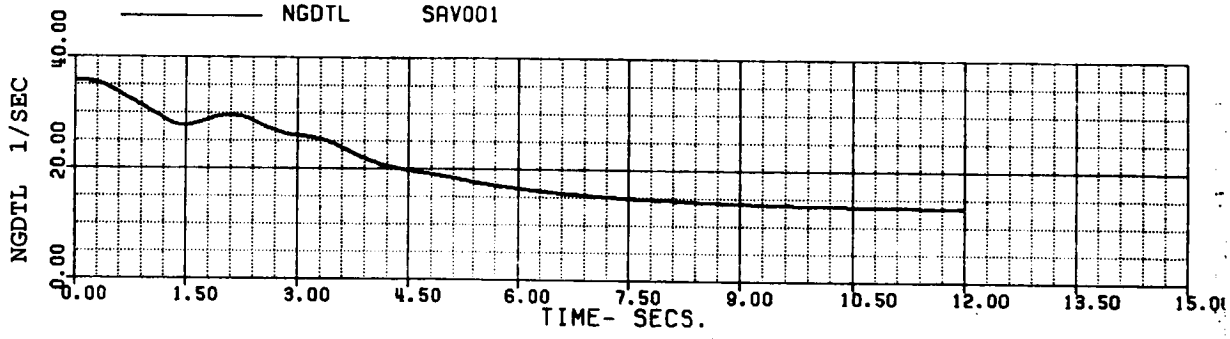

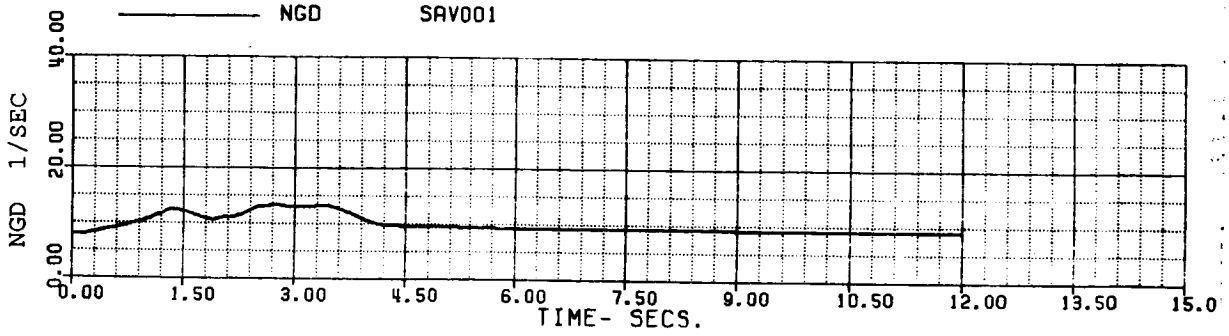

FIG 6.1.1 (k)

60A - BLACK HAWK

FAUTOL - AUTOROTATION RECOVERY, LARGE SPLIT, INT. F/C
70% XC IN .5 SEC, ADAPT = -1

XA+1	5.0568549	XB+1	-5.6564609	XC+1	-.23656E-1	XP+1	3.5085098
THETAB	0.3639475	VKT	79.996625	PHIB	0.	VYB	-11.785136
XNGE	33718.472	NPINTE	7.3856667	VC	-2657.1674	WEIGHT	16638.000
OMRMR	1.1699999	NPMEAS	99.974205				

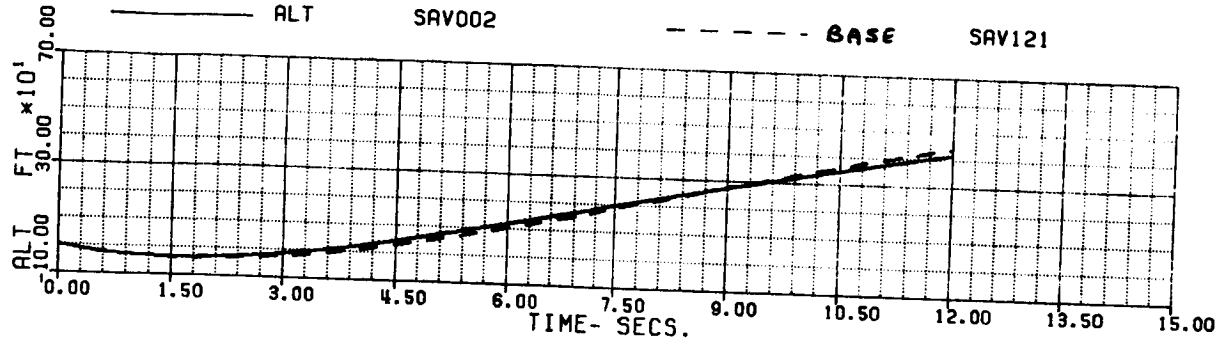

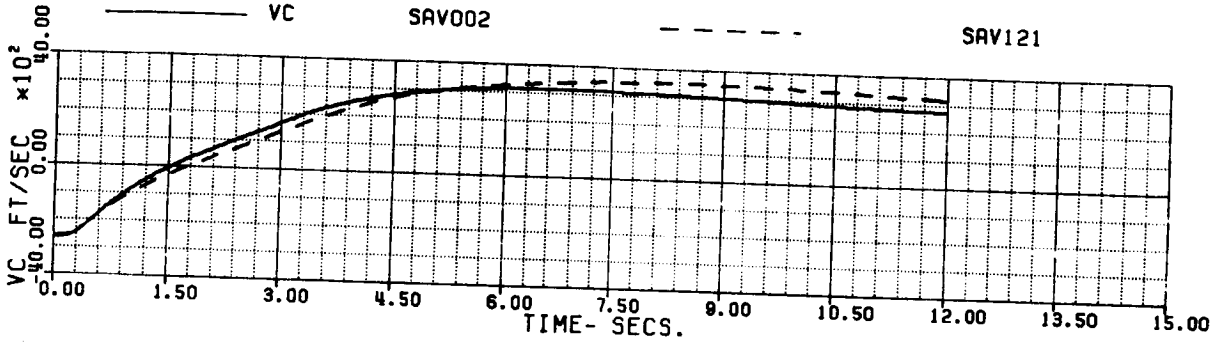

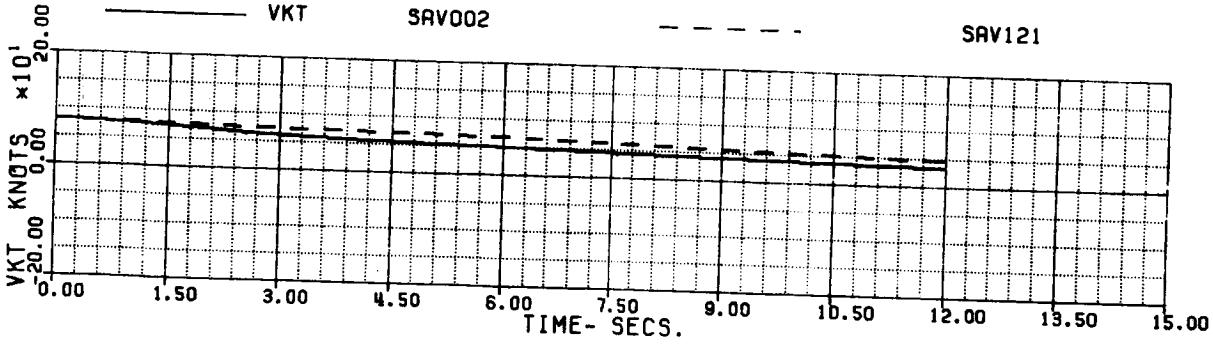

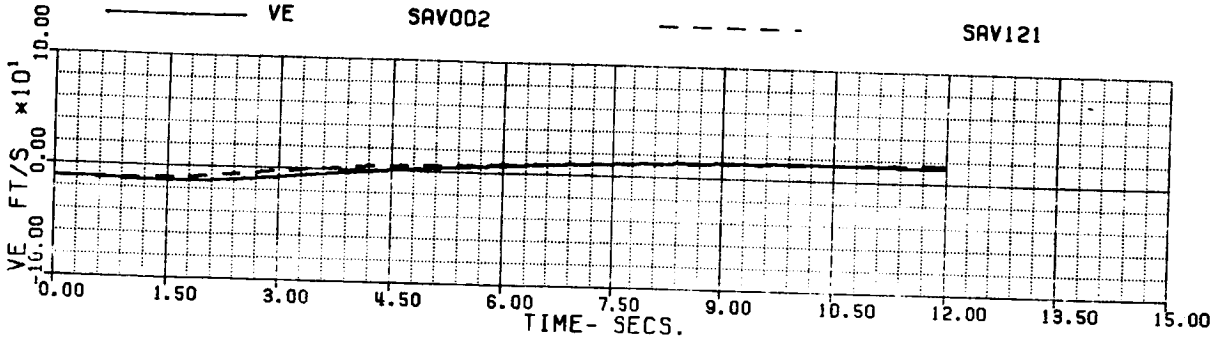

SIMULATED AUTOROTATION RECOVERY
(LARGE SPLIT, FAST PULL)

FIG 6.1.2 (a)

60A - BLACK HAWK

FAUTOL - AUTOROTATION RECOVERY, LARGE SPLIT, INT. F/C
70% XC IN .5 SEC, ADAPT = -1

XA+1	5.0568549	XB+1	-5.6564609	XC+1	-.23656E-1	XP+1	3.5085098
THETAB	0.3639475	VKT	79.996625	PHIB	0.	VYB	-11.785136
XNGE	33718.472	NPINTE	7.3856667	VC	-2657.1674	WEIGHT	16638.000
OMRMR	1.1699999	NPMEAS	99.974205				

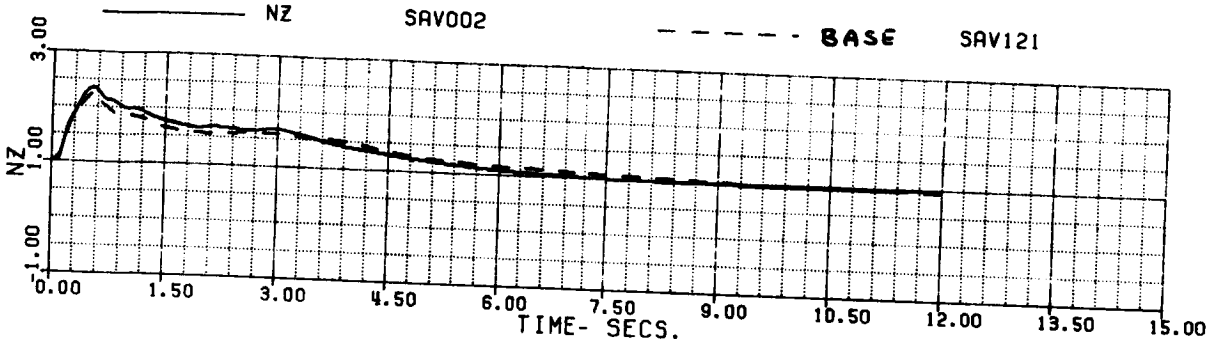

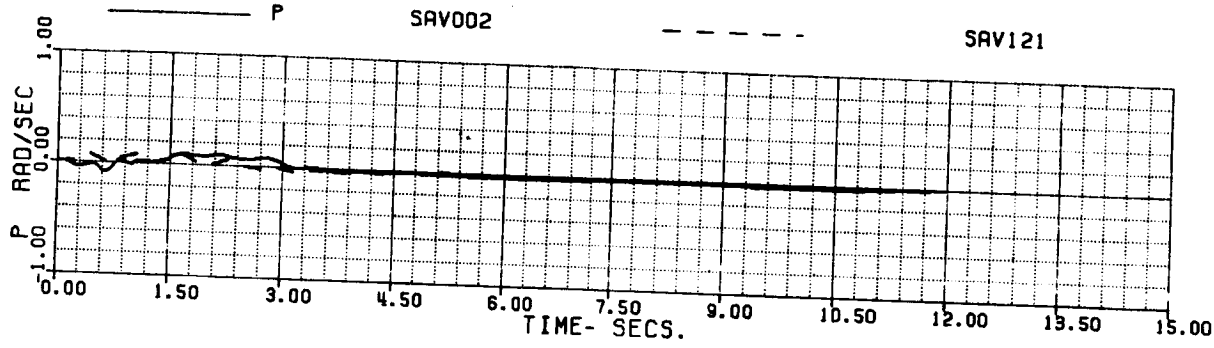

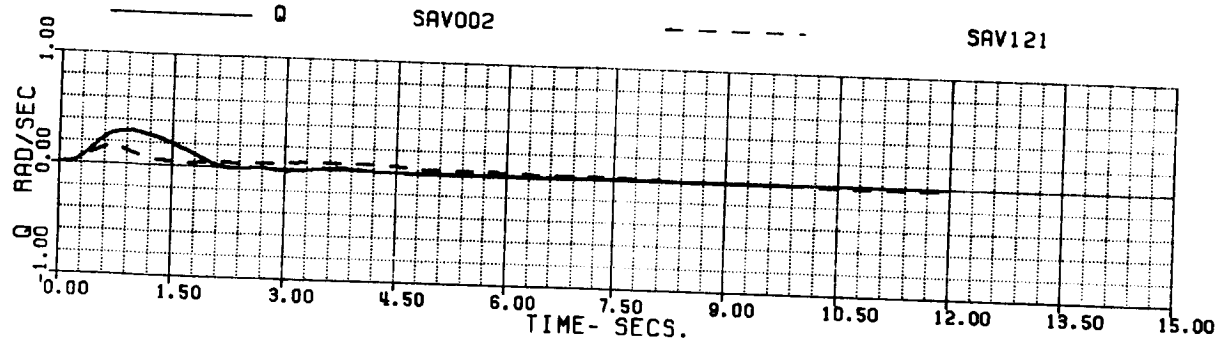

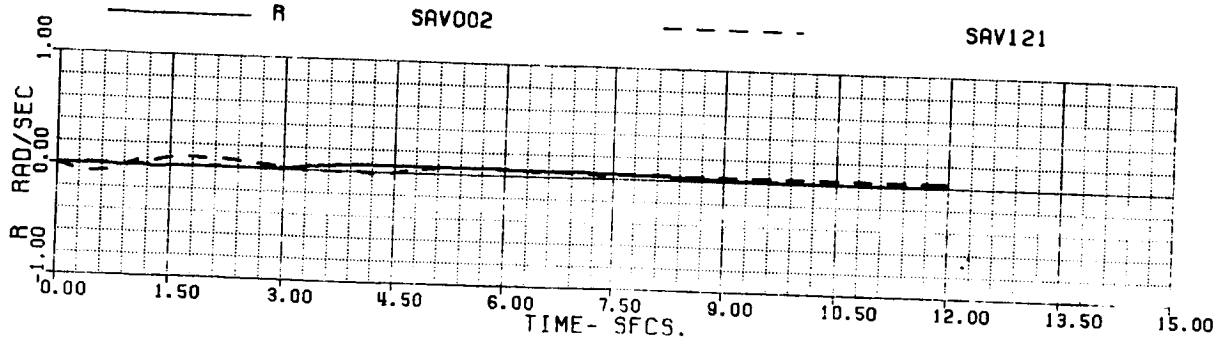

FIG 6.1.2 (b)

60A - BLACK HAWK

FAUTOL - AUTOROTATION RECOVERY, LARGE SPLIT, INT. F/C
70% XC IN .5 SEC, ADAPT = -1

XA+1	5.0568549	XB+1	-5.6564609	XC+1	-.23656E-1	XP+1	3.5085098
THETAB	0.3639475	VKT	79.996625	PHIB	0.	VYB	-11.785136
XNGE	33718.472	NPINTE	7.3856667	VC	-2657.1674	WEIGHT	16638.000
OMRMR	1.1699999	NPMEAS	99.974205				

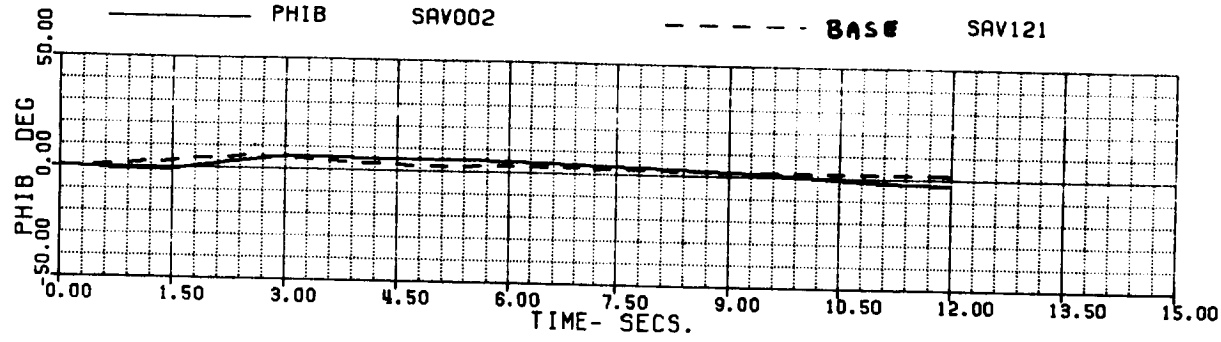

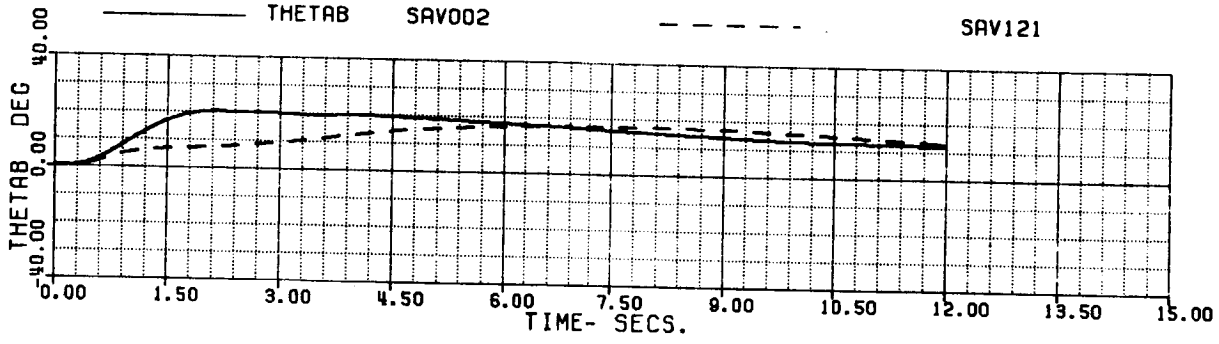

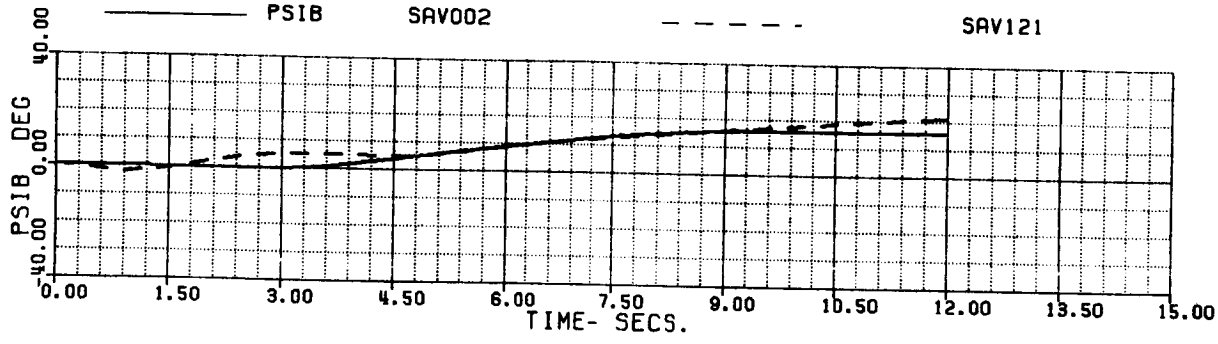

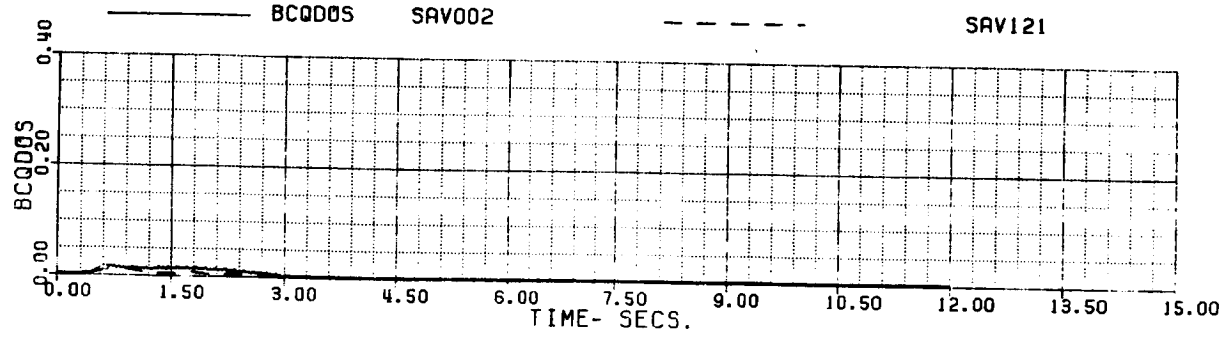

FIG 6.1.2 (c)

60A - BLACK HAWK

FAUTOL - AUTOROTATION RECOVERY, LARGE SPLIT, INT. F/C
70% XC IN .5 SEC, ADAPT = -1

XA+1	5.0568549	XB+1	-5.6564609	XC+1	-.23656E-1	XP+1	3.5085098
THETAB	0.3639475	VKT	79.996625	PHIB	0.	VYB	-11.785136
XNGE	33718.472	NPINTE	7.3856667	VC	-2657.1674	WEIGHT	16638.000
OMRMR	1.1699999	NPMEAS	99.974205				

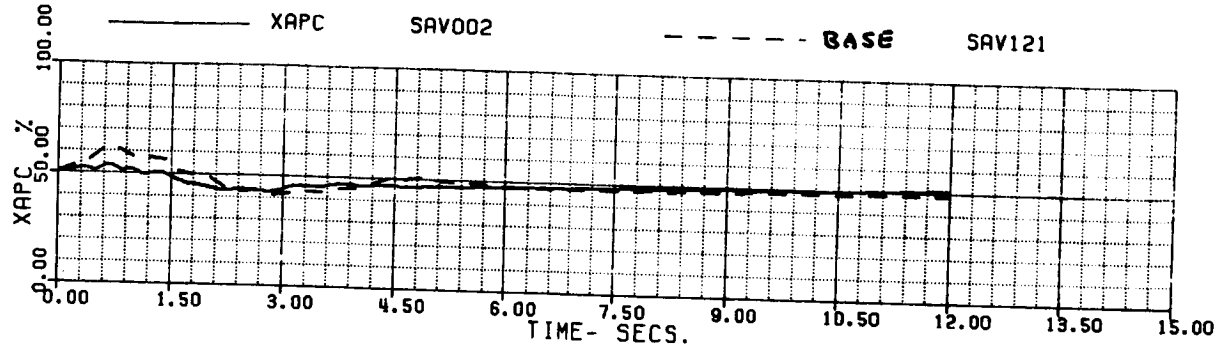

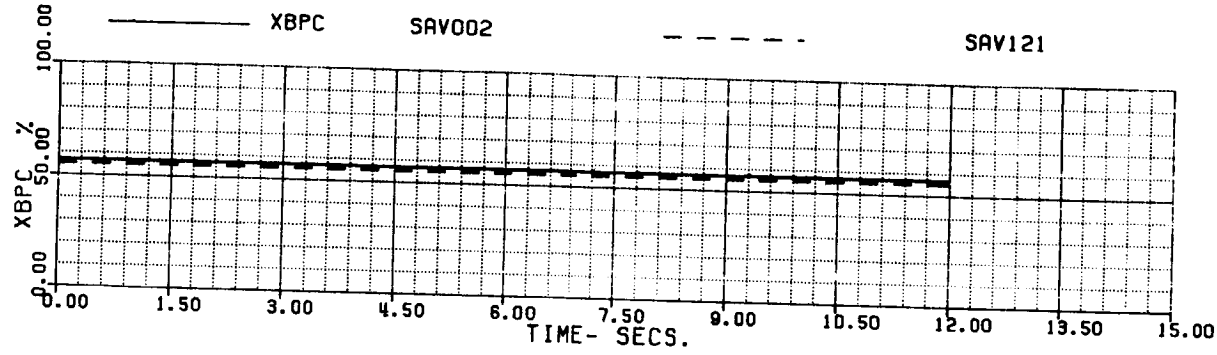

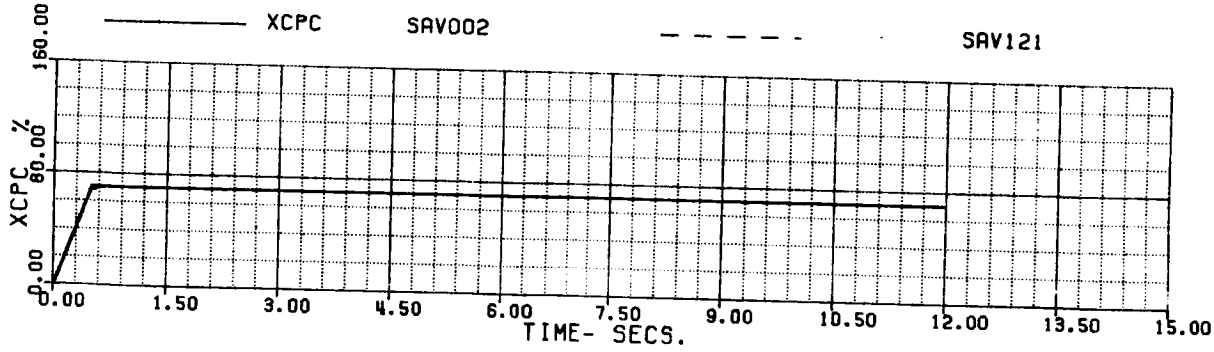

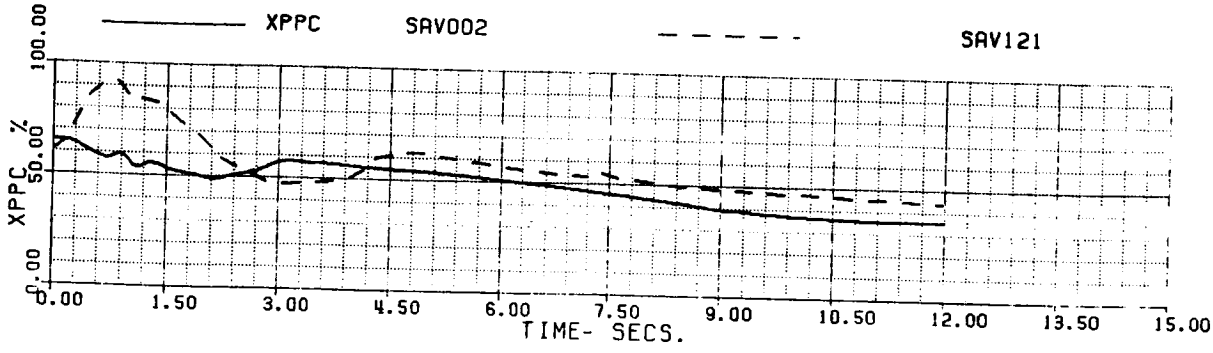

FIG 6.1.2 (d)

60A - BLACK HAWK

FAUTOL - AUTOROTATION RECOVERY, LARGE SPLIT, INT. F/C
70% XC IN .5 SEC, ADAPT = -1

XA+1	5.0568549	XB+1	-5.6564609	XC+1	-.23656E-1	XP+1	3.5085098
THETAB	0.3639475	VKT	79.996625	PHIB	0.	VYB	-11.785136
XNGE	33718.472	NPINTE	7.3856667	VC	-2657.1674	WEIGHT	16638.000
OMRMR	1.1699999	NPMEAS	99.974205				

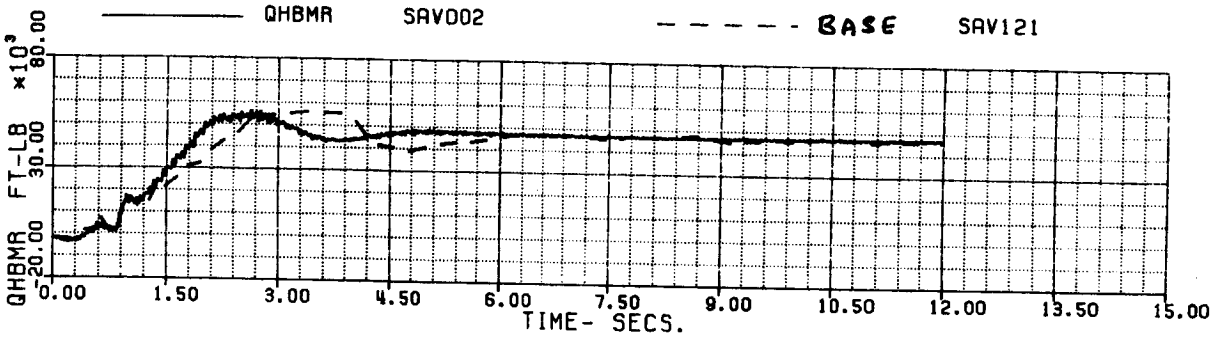

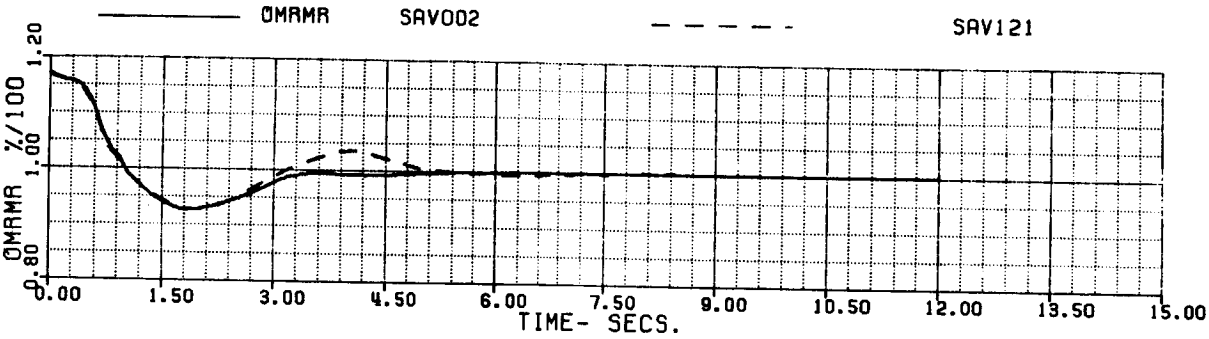

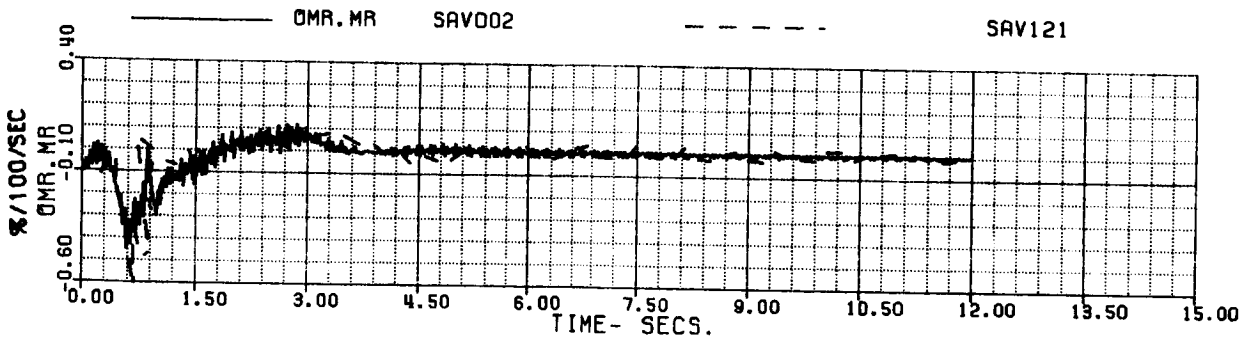

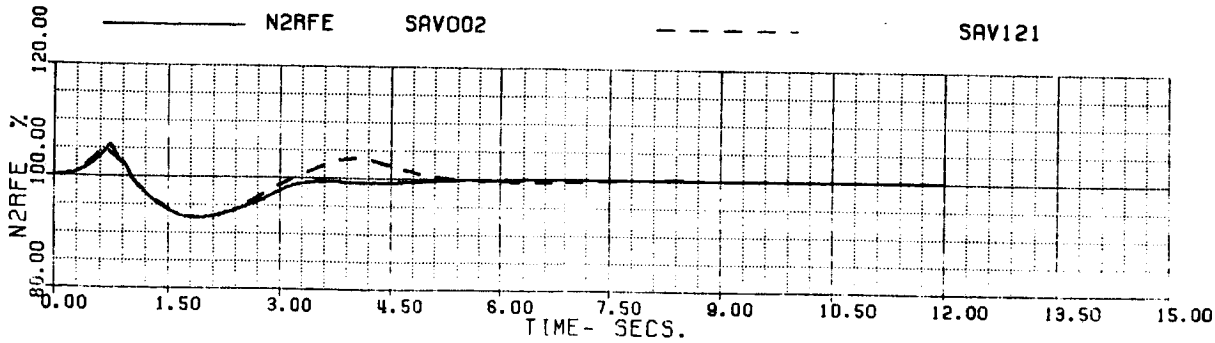

FIG 6.1.2 (e)

60A - BLACK HAWK

FAUTOL - AUTOROTATION RECOVERY, LARGE SPLIT, INT. F/C
70% XC IN .5 SEC, ADAPT = -1

XA+1	5.0568549	XB+1	-5.6564609	XC+1	-.23656E-1	XP+1	3.5085098
THETAB	0.3639475	VKT	79.996625	PHIB	0.	VYB	-11.785136
XNGE	33718.472	NPINTE	7.3856667	VC	-2657.1674	WEIGHT	16638.000
OMRMR	1.1699999	NPMEAS	99.974205				

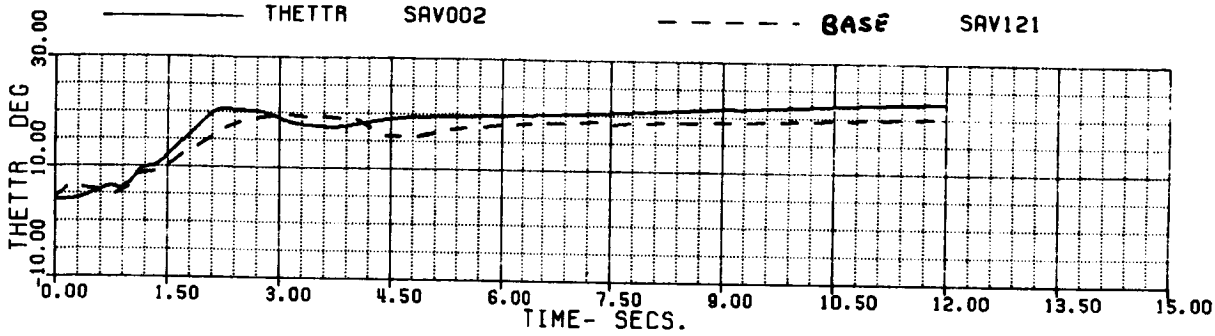

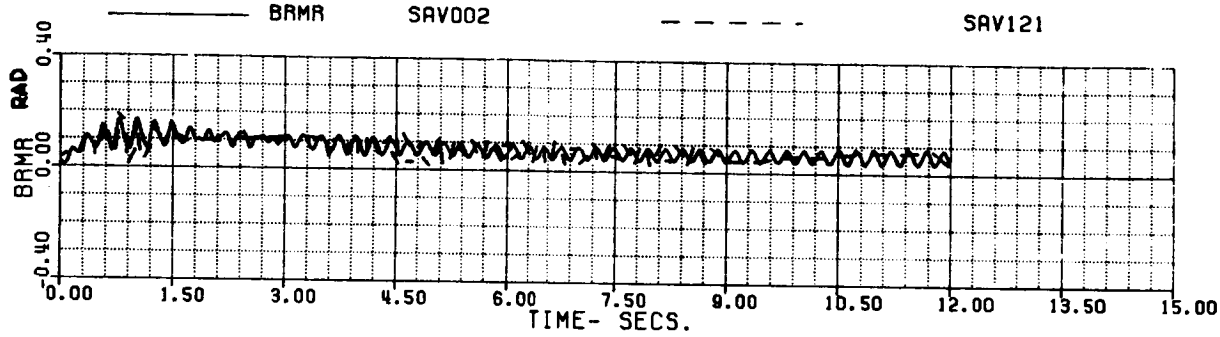

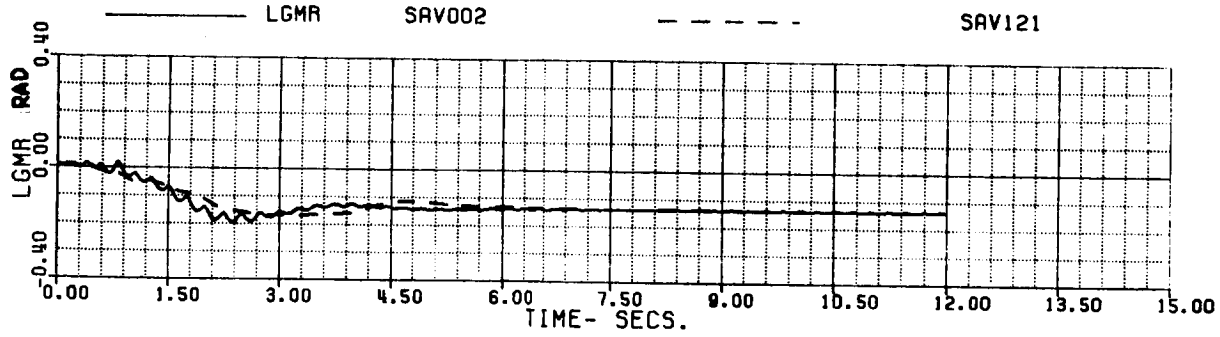

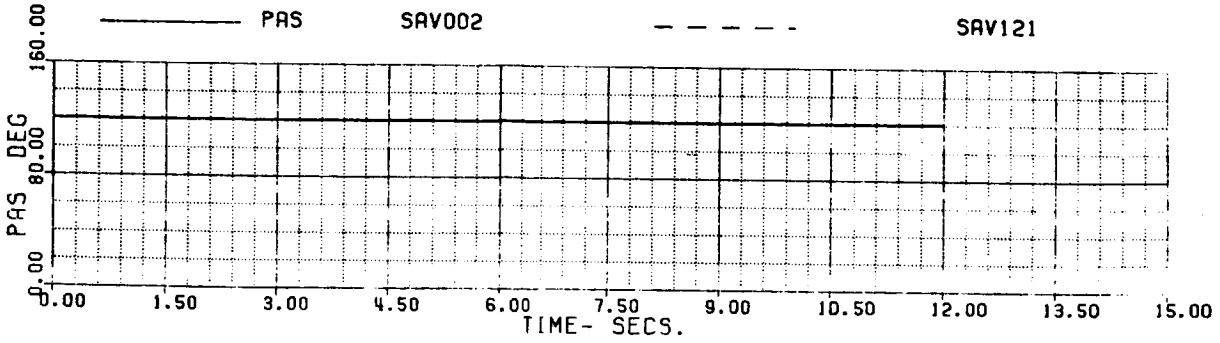

FIG 6.1.2 (f)

60A - BLACK HAWK

FAUTOL - AUTOROTATION RECOVERY, LARGE SPLIT, INT. F/C
70% XC IN .5 SEC, ADAPT = -1

XA+1	5.0568549	XB+1	-5.6564609	XC+1	-.23656E-1	XP+1	3.5085098
THETAB	0.3639475	VKT	79.996625	PHIB	0.	VYB	-11.785136
XNGE	33718.472	NPINTE	7.3856667	VC	-2657.1674	WEIGHT	16638.000
OMAMR	1.1699999	NPMEAS	99.974205				

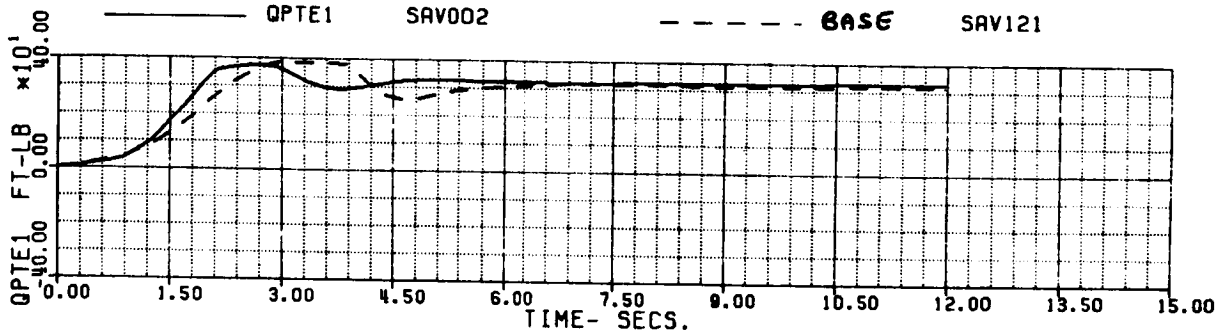

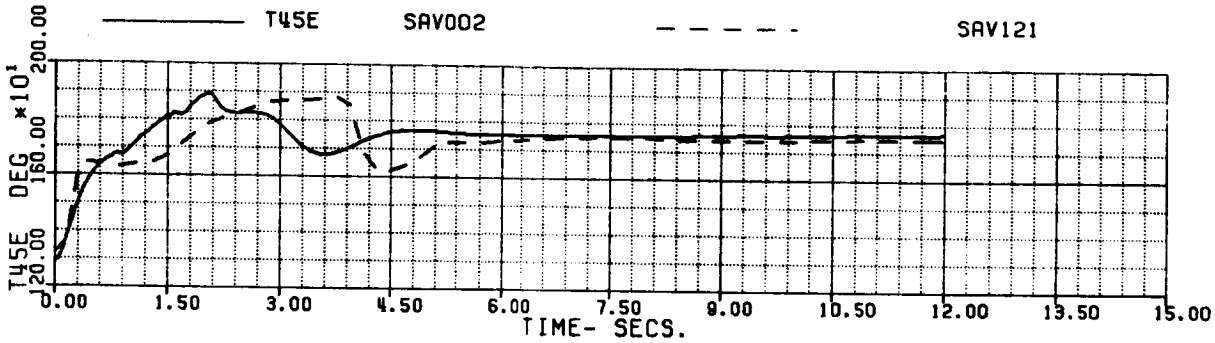

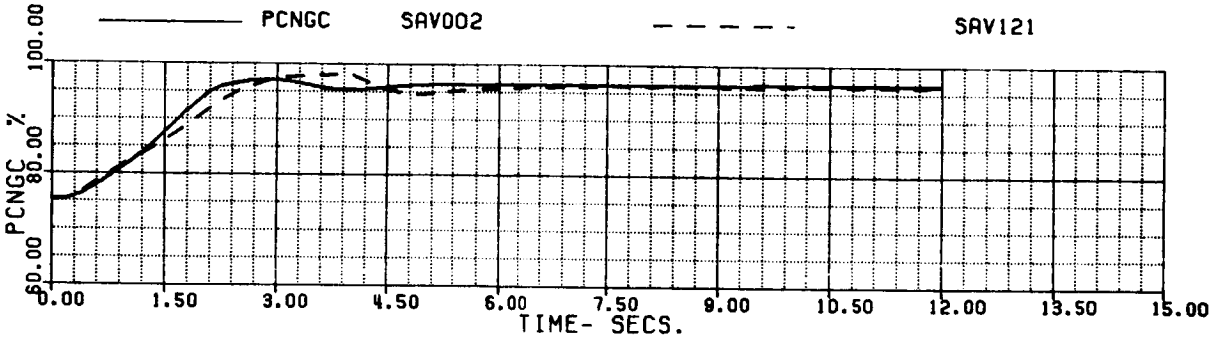

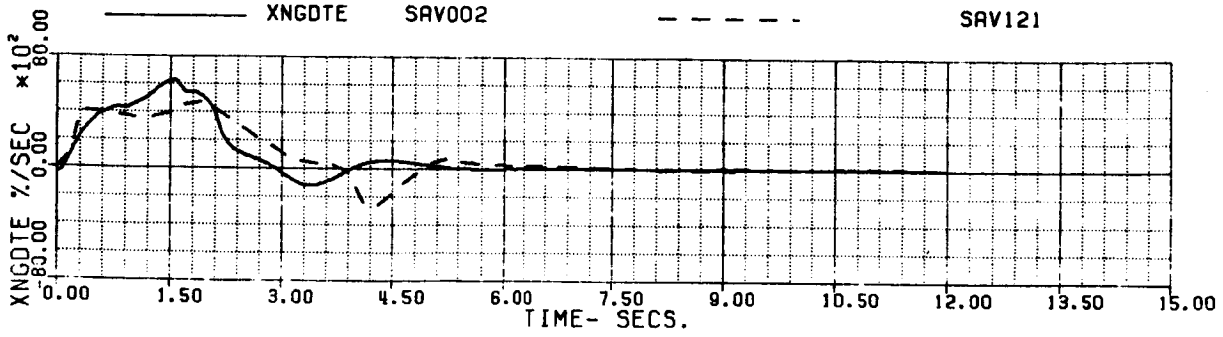

FIG 6.1.2 (g)

60A - BLACK HAWK

FAUTOL - AUTOROTATION RECOVERY, LARGE SPLIT, INT. F/C
70% XC IN .5 SEC, ADAPT = -1

XA+1	5.0568549	XB+1	-5.6564609	XC+1	-.23656E-1	XP+1	3.5085098
THETAB	0.3639475	VKT	79.996625	PHIB	0.	VYB	-11.785136
XNGE	33718.472	NPINTE	7.3856667	VC	-2657.1674	WEIGHT	16638.000
OMRMR	1.1699999	NPMEAS	99.974205				

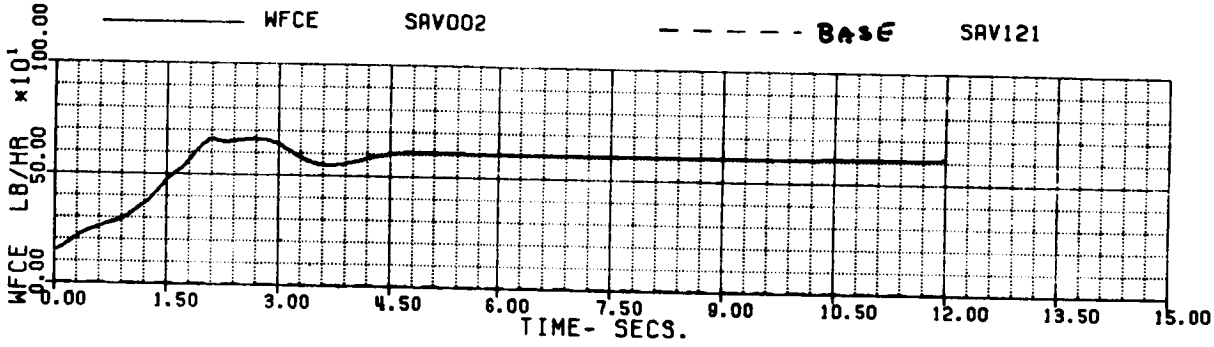

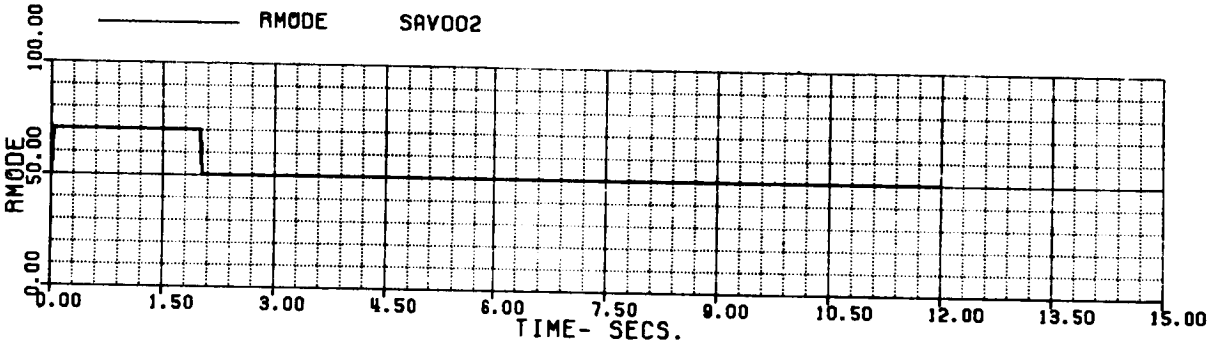

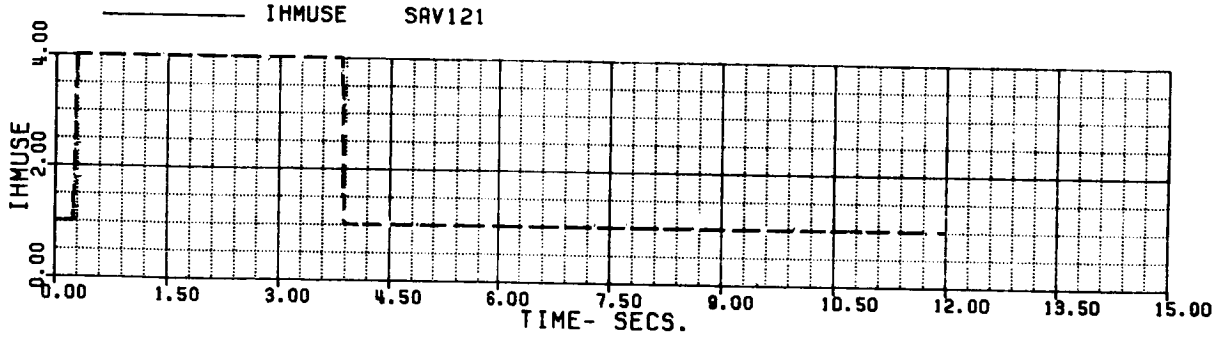

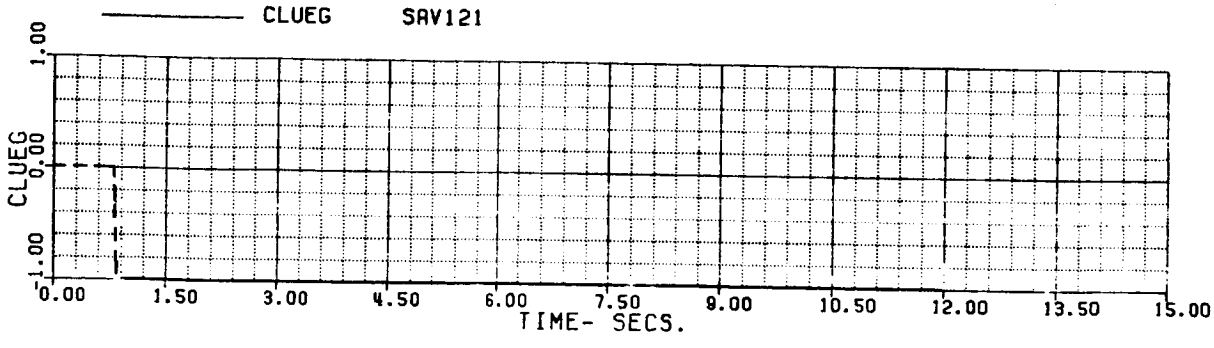

FIG 6.1.2 (h)

60A - BLACK HAWK

FAUTOL - AUTOROTATION RECOVERY, LARGE SPLIT, INT. F/C
70% XC IN .5 SEC, ADAPT = -1

XA+1	5.0568549	XB+1	-5.6564609	XC+1	-.23656E-1	XP+1	3.5085098
THETAB	0.3639475	VKT	79.996625	PHIB	0.	VTB	-11.785156
XNGE	33718.472	NPINTE	7.3856667	VC	-2657.1674	WEIGHT	16638.000
OMRMR	1.1699999	NPMEAS	99.974205				

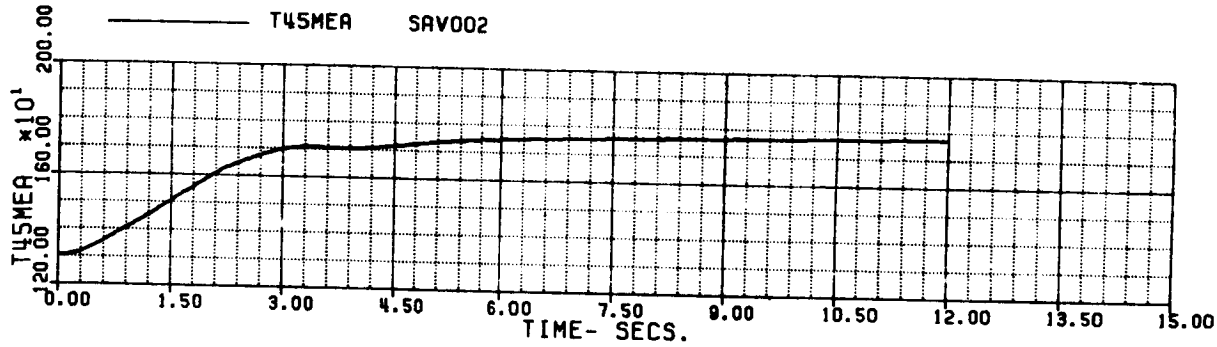

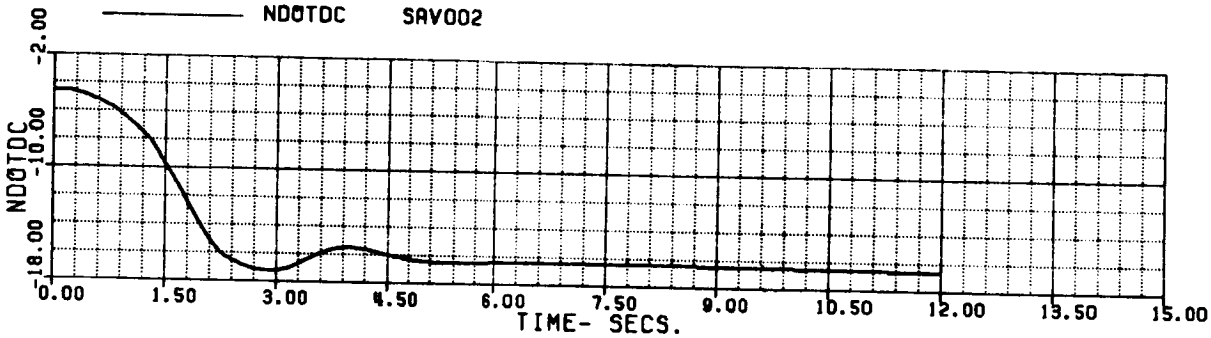

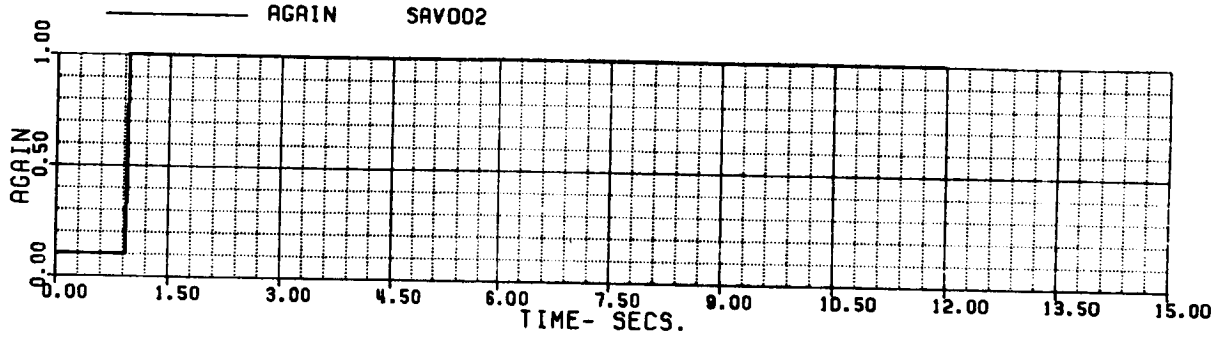

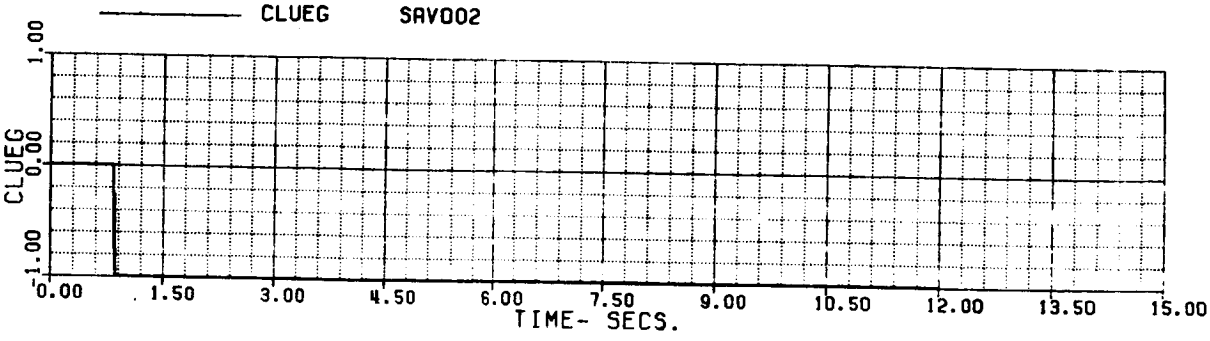

FIG 6.1.2 (i)

60A - BLACK HAWK

FAUTOL - AUTOROTATION RECOVERY, LARGE SPLIT, INT. F/C
70% XC IN .5 SEC, ADAPT = -1

XA+1	5.0568549	XB+1	-5.6564609	XC+1	-.23656E-1	XP+1	3.5085091
THETAB	0.3639475	VKT	79.996625	PHIB	0.	VYB	-11.7851
XNGE	33718.472	NPINTE	7.3856667	VC	-2657.1674	WEIGHT	16638.001
OMAMR	1.1699999	NPMEAS	99.974205				

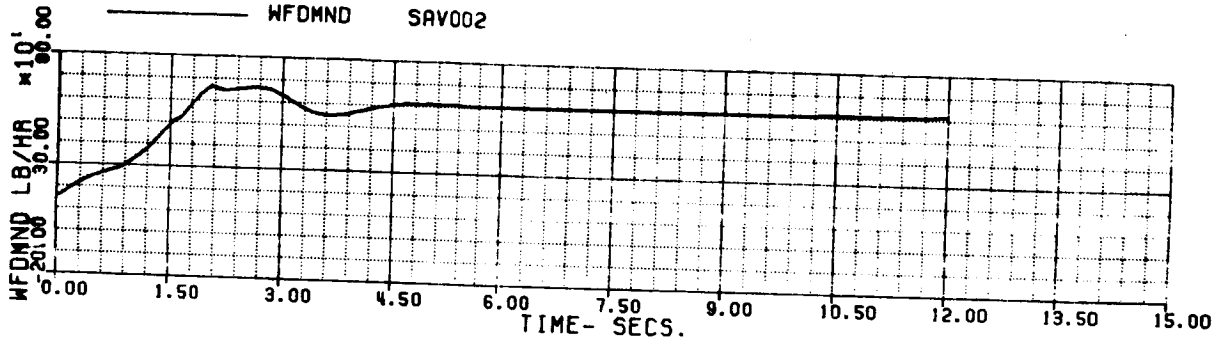

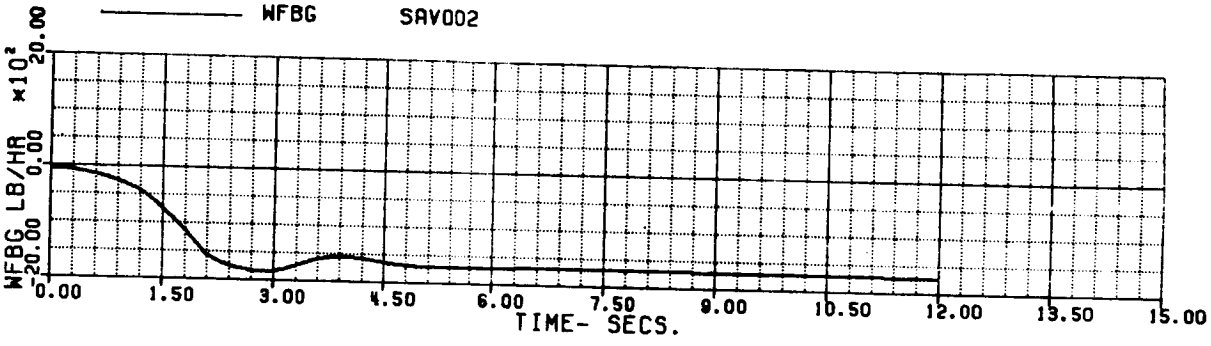

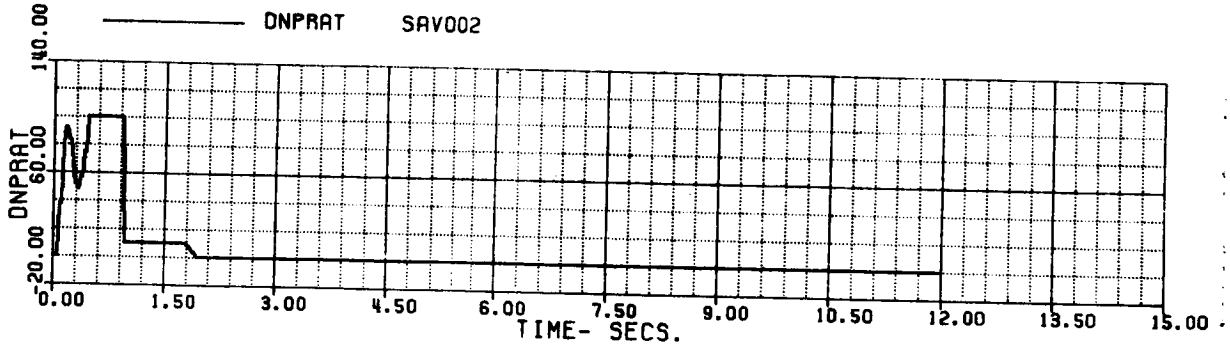

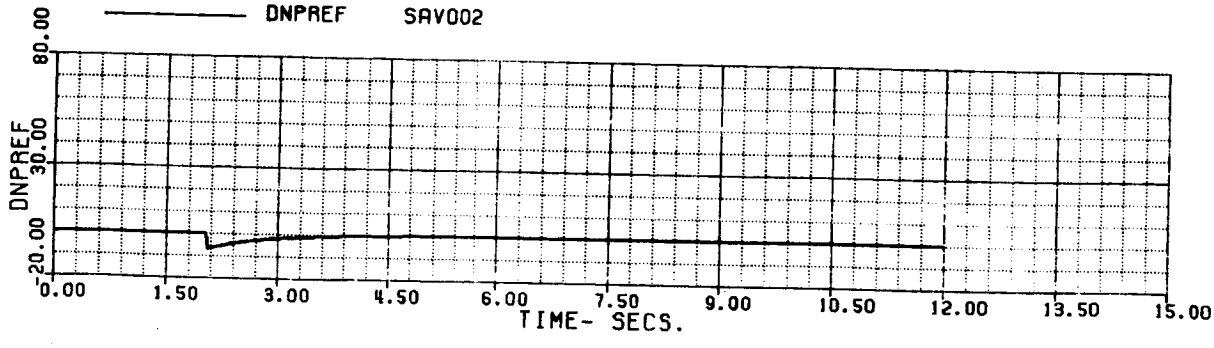

FIG 6.1.2 (j)

60A - BLACK HAWK

FAUTOL - AUTOROTATION RECOVERY, LARGE SPLIT, INT. F/C
70% XC IN .5 SEC, ADAPT = -1

XA+1	5.0568549	XB+1	-5.6564609	XC+1	-.23656E-1	XP+1	3.50850
THETAB	0.3639475	VKT	79.996625	PHIB	0.	VYB	-11.785
IGE	33718.472	NPINTE	7.3856667	VC	-2657.1674	WEIGHT	16638.0
IRMR	1.1699999	NPMEAS	99.974205				

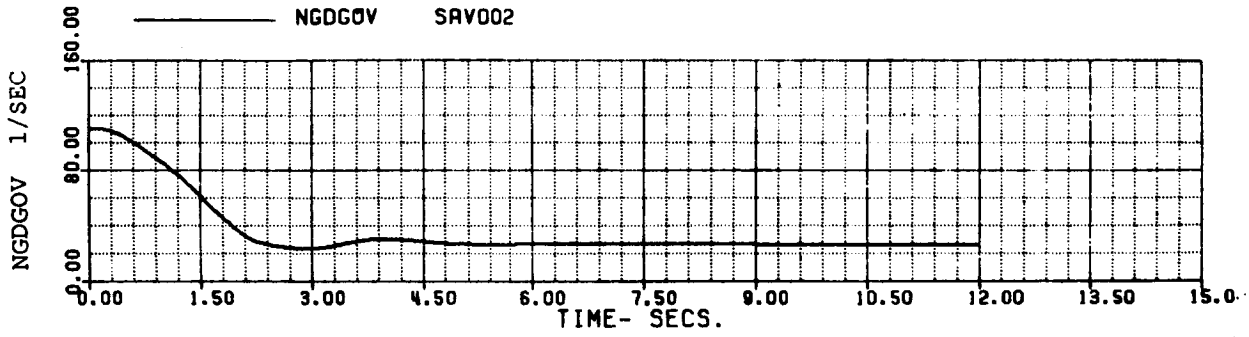

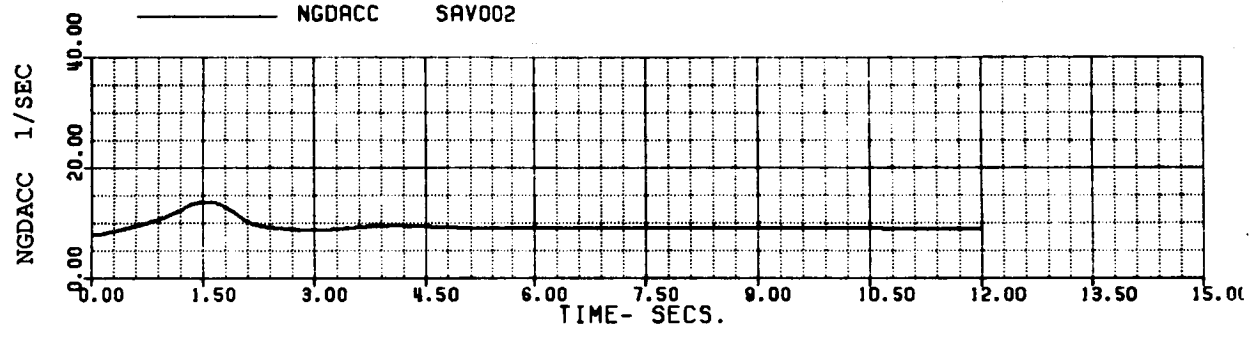

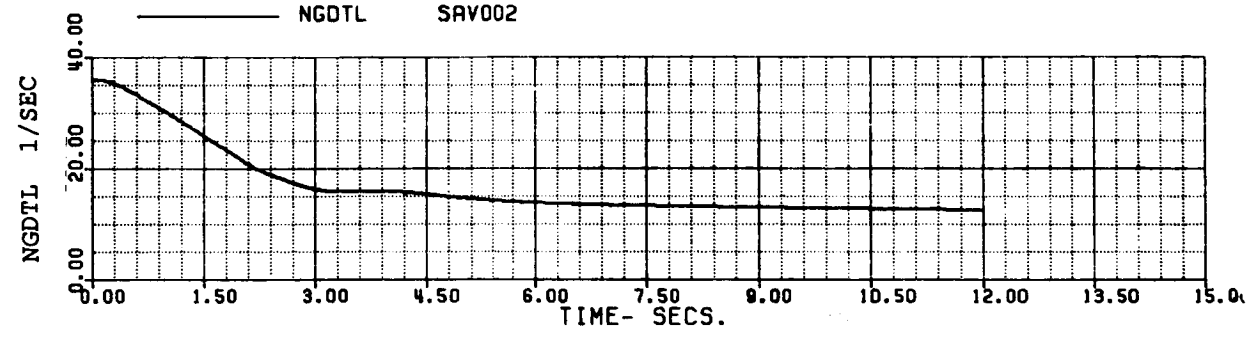

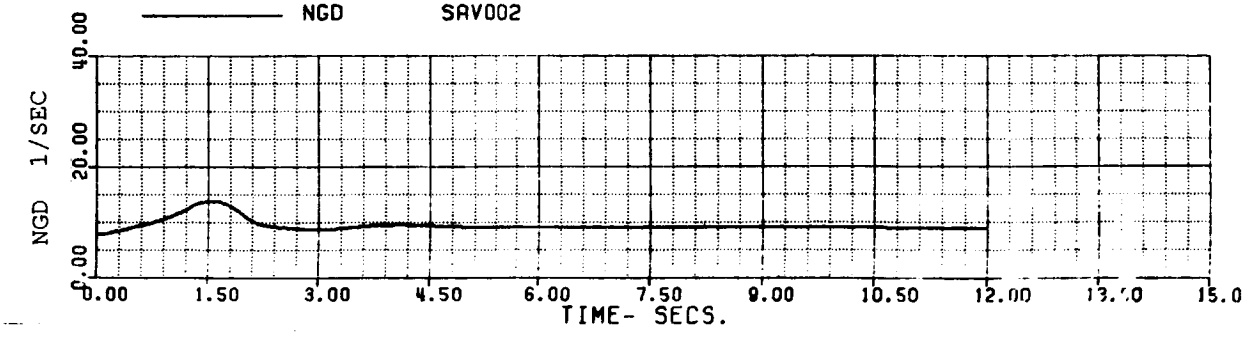

FIG 6.1.2 (k)

60A - BLACK HAWK

FAUTOS - AUTOROTATION RECOVERY, SMALL SPLIT, INT. F/C
70% XC IN 3 SEC, ADAPT=-1

XA+1	5.0207060	XB+1	-5.9170116	XC+1	-.17628E-2	XP+1	3.6171018
THETAB	0.8336849	VKT	79.993876	PHIB	0.	VTB	-12.509981
XNGE	33592.452	NPINTE	8.2866175	VC	-2775.6436	WEIGHT	16638.000
OMRMR	1.0199999	NPMEAS	99.974205				

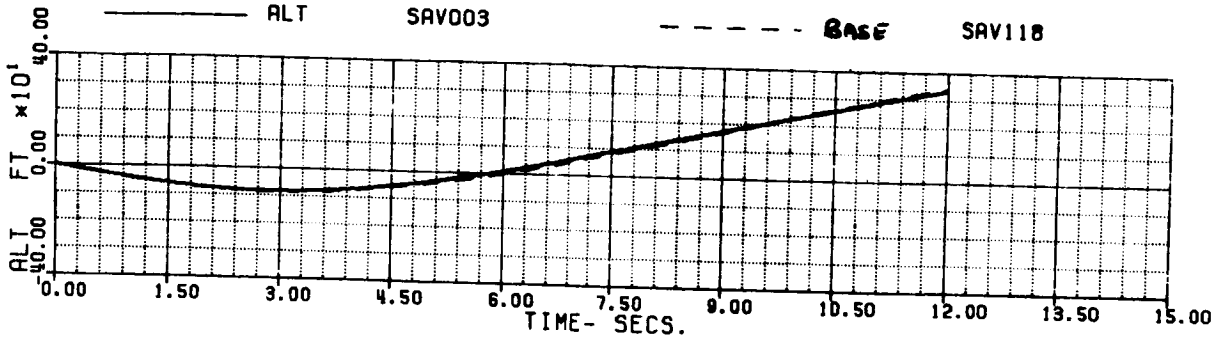

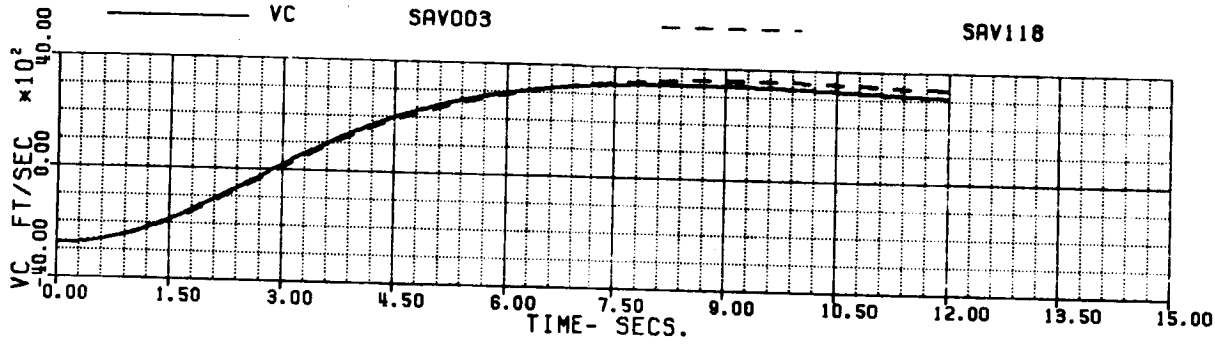

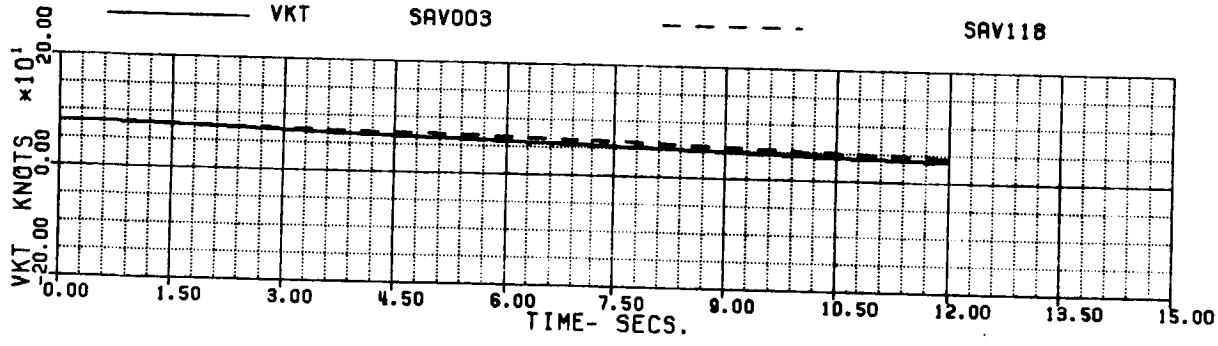

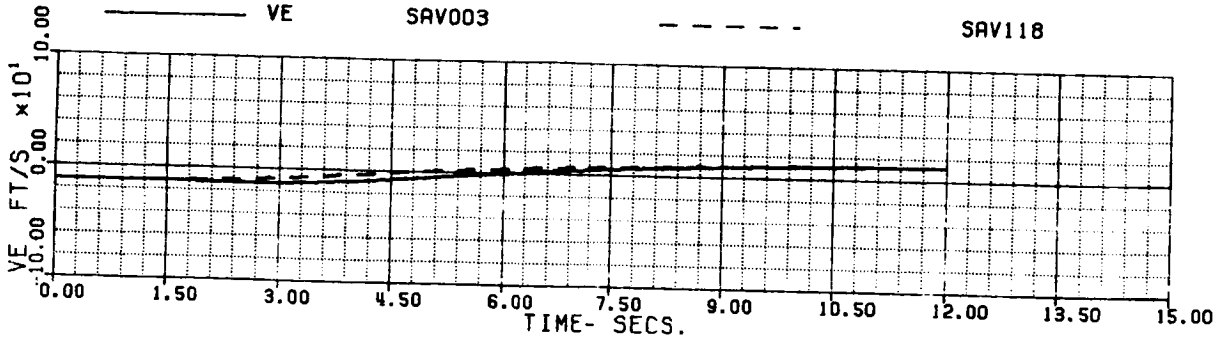

SIMULATED AUTOROTATION RECOVERY
(SMALL SPLIT, SLOW PULL)

FIG 6.1.3 (a)

60A - BLACK HAWK

FAUTOS - AUTOROTATION RECOVERY, SMALL SPLIT, INT. F/C
70% XC IN 3 SEC, ADAPT=-1

XA+1	5.0207060	XB+1	-5.9170116	XC+1	-.17628E-2	XP+1	3.6171018
THETAB	0.8336849	VKT	79.993876	PHIB	0.	VYB	-12.509981
XNGE	33592.452	NPINTE	8.2866175	VC	-2775.6436	WEIGHT	16638.000
OMRMR	1.0199999	NPMEAS	99.974205				

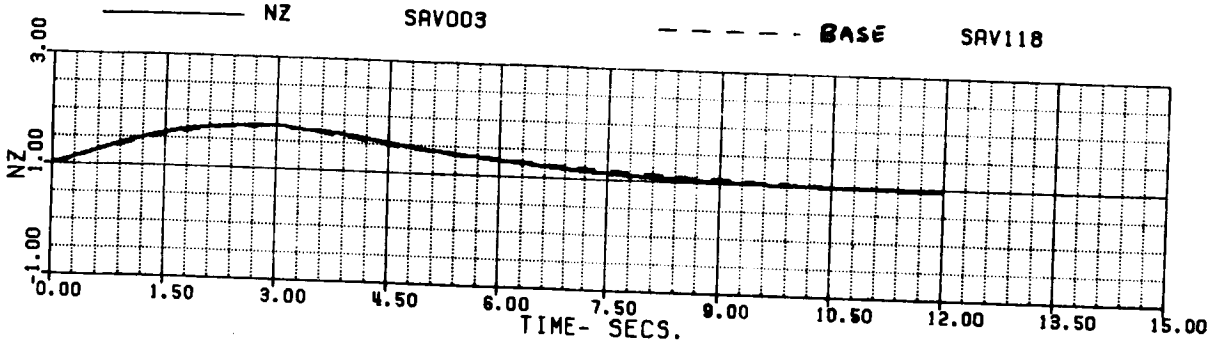

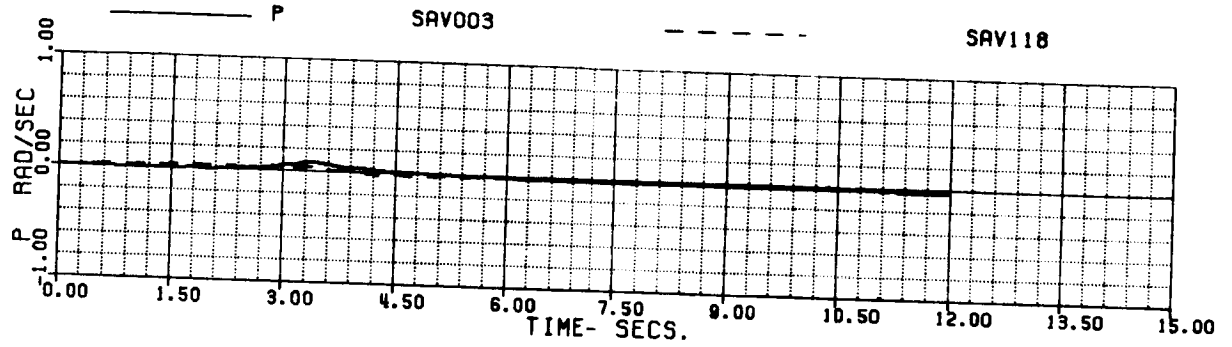

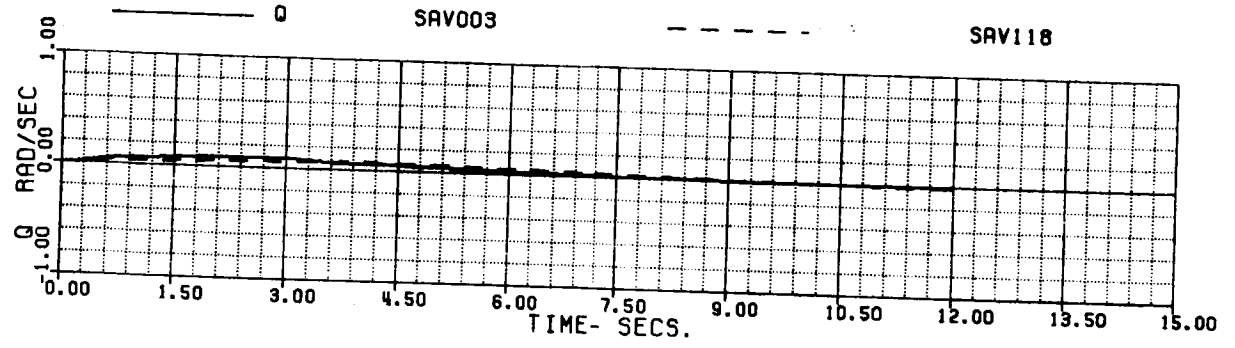

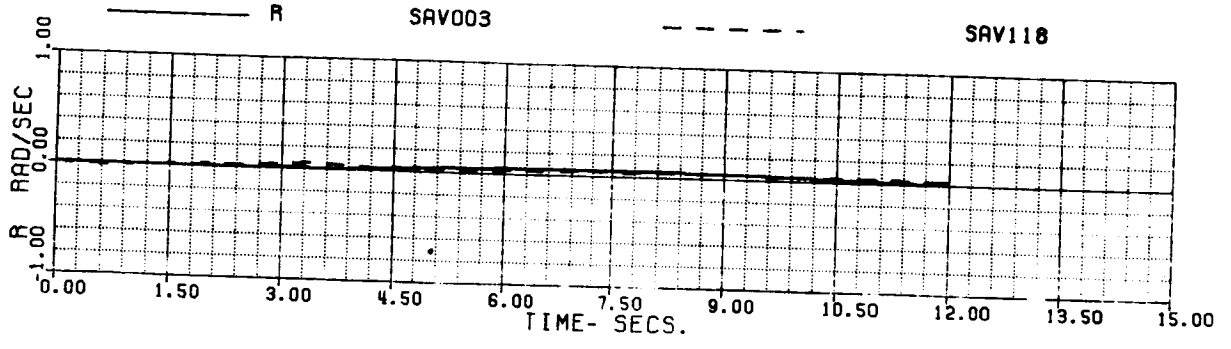

FIG 6.1.3 (b)

60A - BLACK HAWK

FAUTOS - AUTOROTATION RECOVERY, SMALL SPLIT, INT. F/C
70% XC IN 3 SEC, ADAPT=-1

XA+1	5.0207060	XB+1	-5.9170116	XC+1	-.17628E-2	XP+1	3.6171018
THETAB	0.8336849	VKT	79.993876	PHIB	0.	VYB	-12.509981
XNGE	33592.452	NPINTE	8.2866175	VC	-2775.6436	WEIGHT	16638.000
OMRMR	1.0199999	NPMEAS	99.974205				

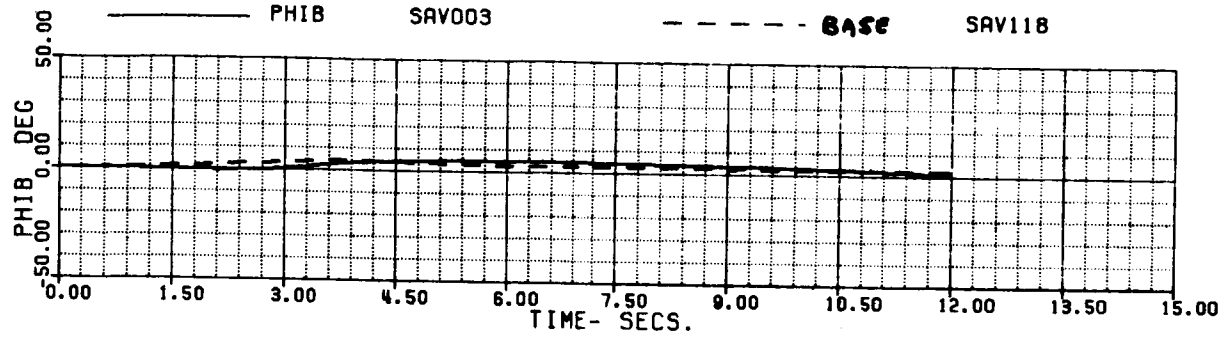

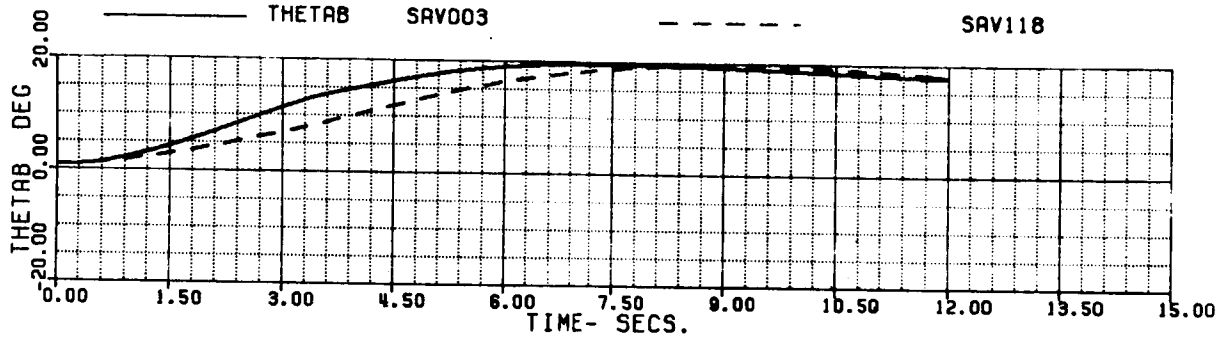

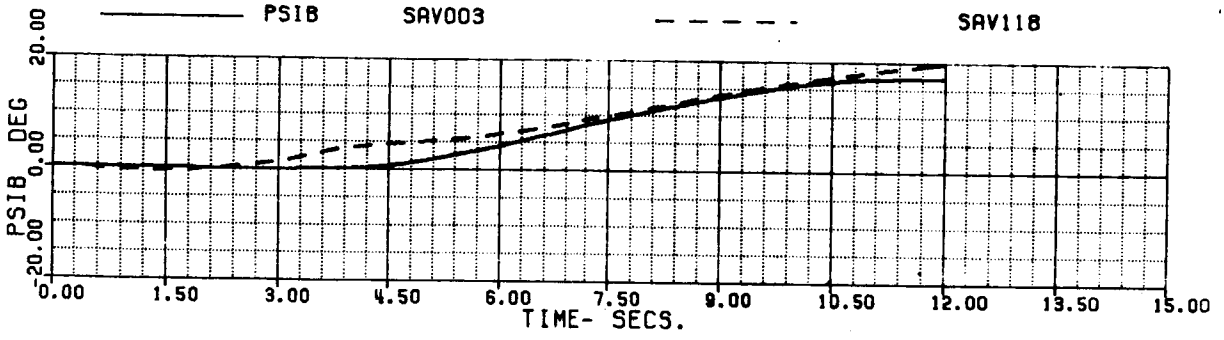

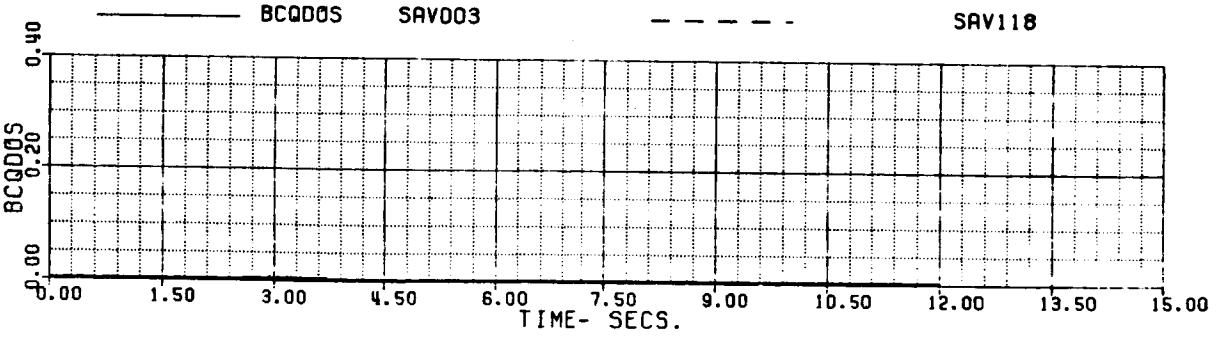

FIG 6.1.3 (c)

60A - BLACK HAWK

FAUTOS - AUTOROTATION RECOVERY, SMALL SPLIT, INT. F/C
70% XC IN 3 SEC, ADAPT=-1

XA+1	5.0207060	XB+1	-5.9170116	XC+1	-.17628E-2	XP+1	3.6171018
THETAB	0.8336849	VKT	79.993876	PHIB	0.	VYB	-12.509981
XNGE	33592.452	NPINTE	8.2866175	VC	-2775.6436	WEIGHT	16638.000
OMRMR	1.0199999	NPMEAS	99.974205				

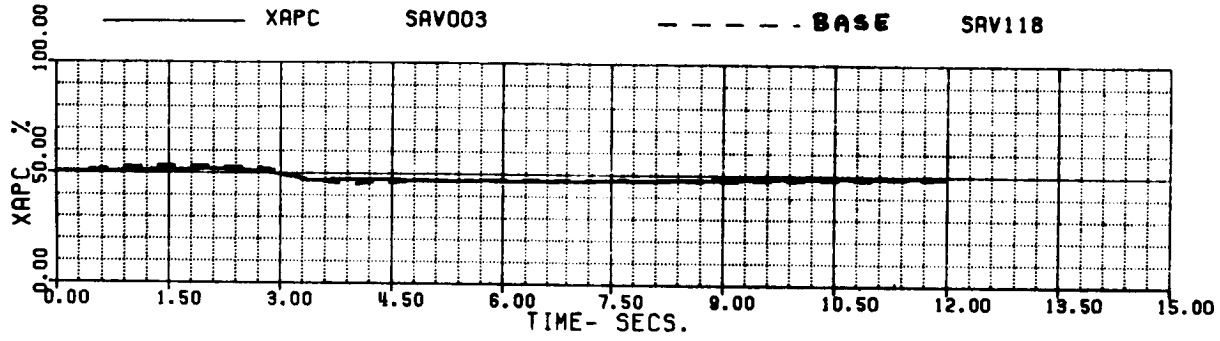

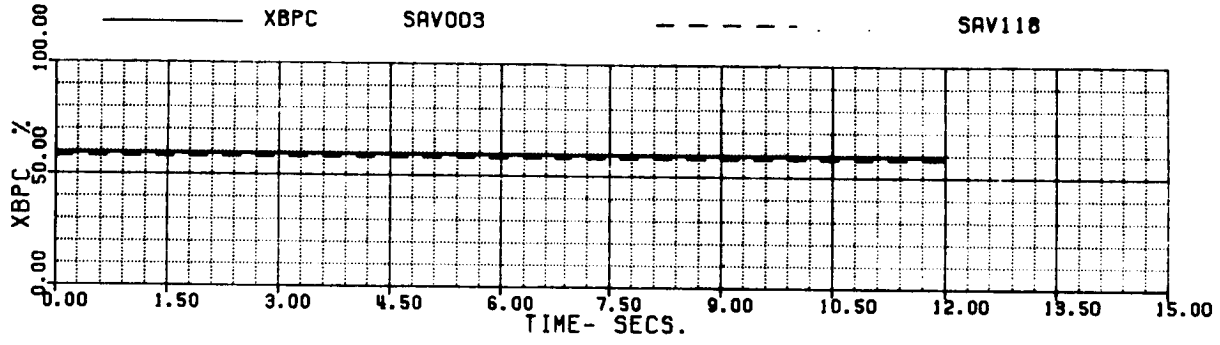

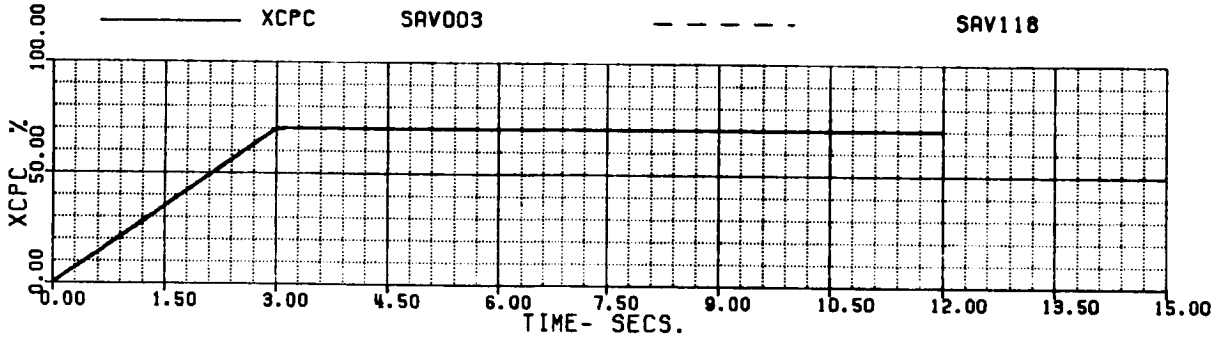

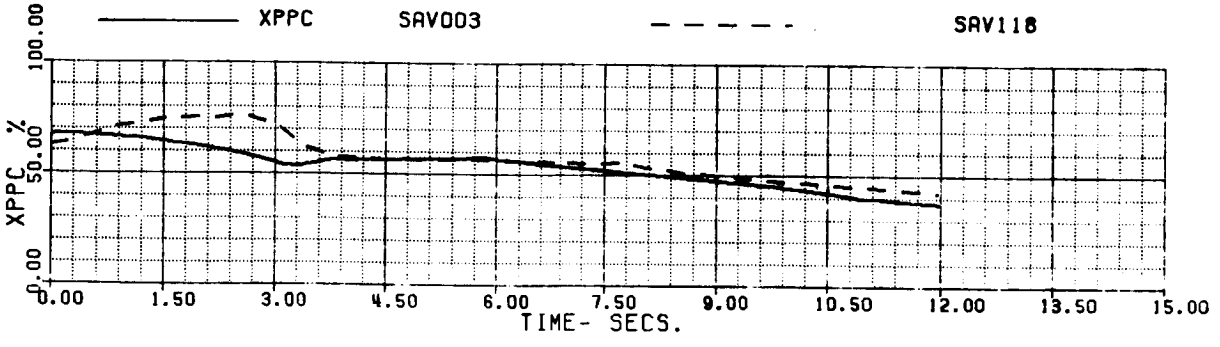

FIG 6.1.3 (d)

60A - BLACK HAWK

FAUTOS - AUTOROTATION RECOVERY, SMALL SPLIT, INT. F/C
70% XC IN 3 SEC, ADAPT=-1

XA+1	5.0207060	XB+1	-5.9170116	XC+1	-.17628E-2	XP+1	3.6171018
THETAB	0.8336849	VKT	79.993876	PHIB	0.	VYB	-12.509981
XNGE	33592.452	NPINTE	8.2866175	VC	-2775.6436	WEIGHT	16638.000
OMRMR	1.0199999	NPMEAS	99.974205				

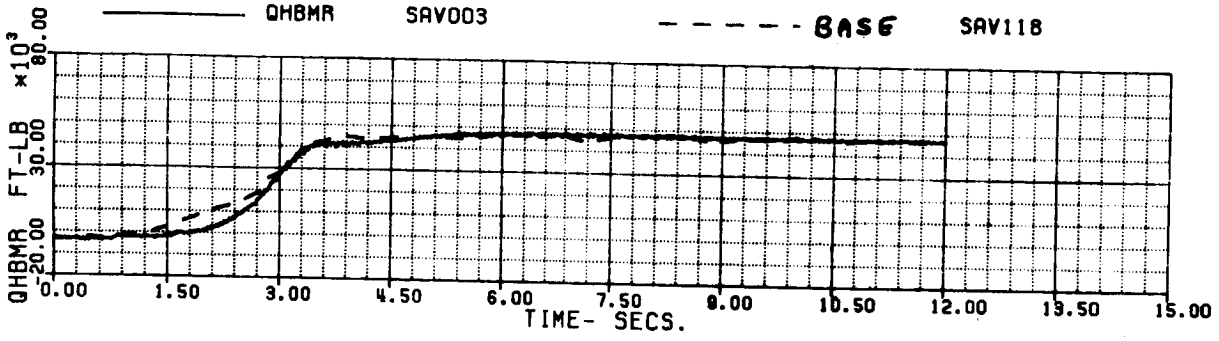

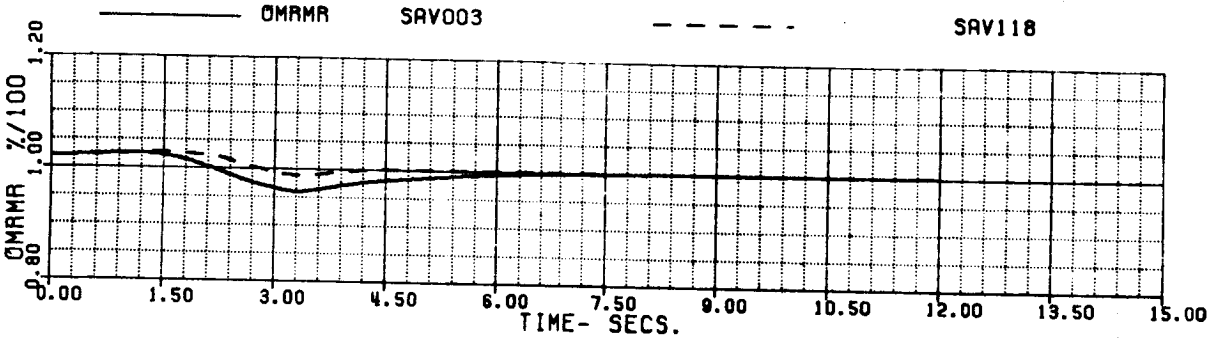

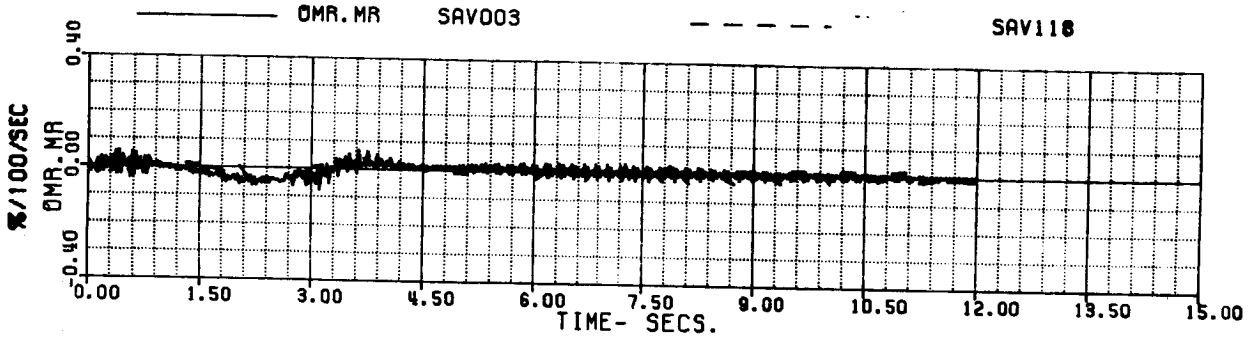

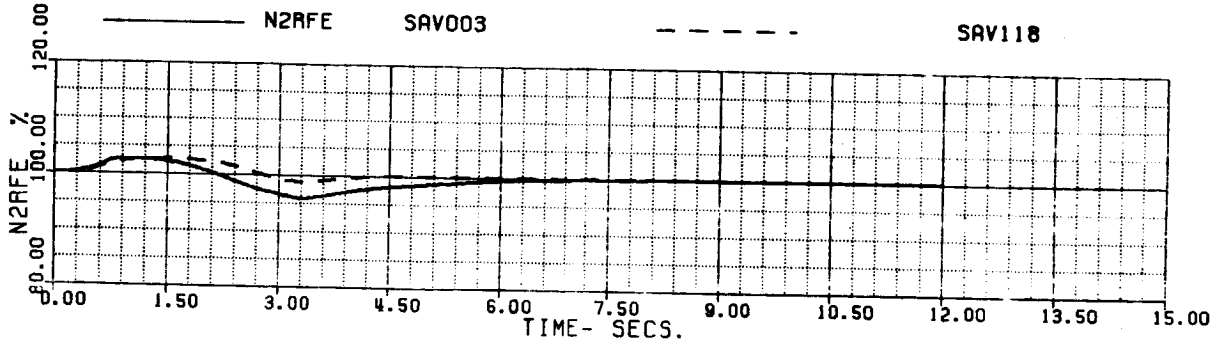

FIG 6.1.3 (e)

60A - BLACK HAWK

FAUTOS - AUTOROTATION RECOVERY, SMALL SPLIT, INT. F/C
70% XC IN 3 SEC, ADAPT=-1

XA+1	5.0207060	XB+1	-5.9170116	XC+1	-.17628E-2	XP+1	3.6171018
THETAB	0.8336849	VKT	79.993876	PHIB	0.	VTB	-12.509981
XNGE	33592.452	NPINTE	8.2866175	VC	-2775.6436	WEIGHT	16638.000
OMRMR	1.0199999	NPMEAS	99.974205				

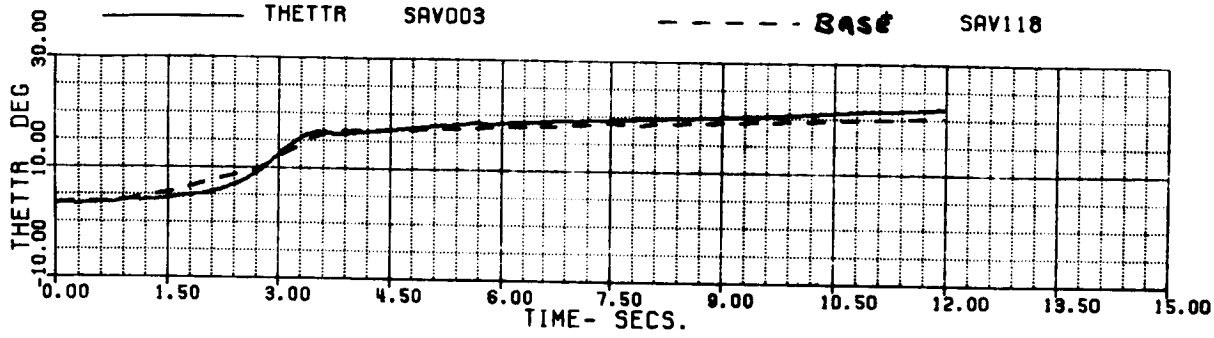

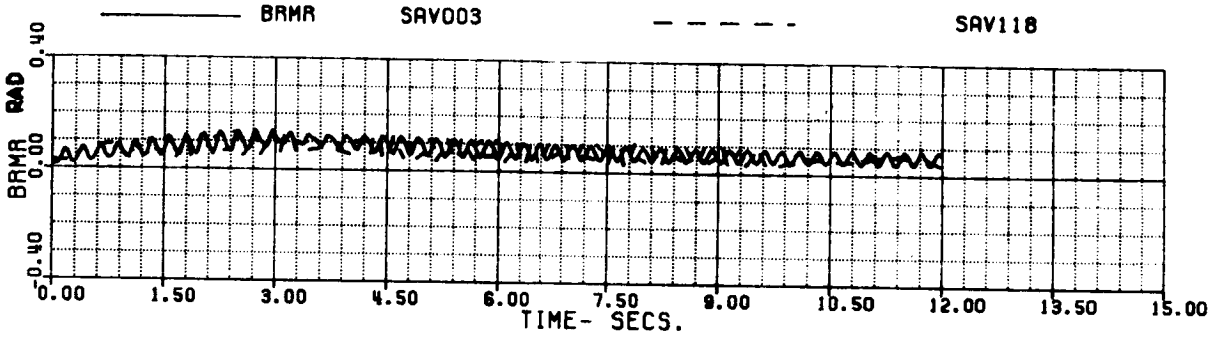

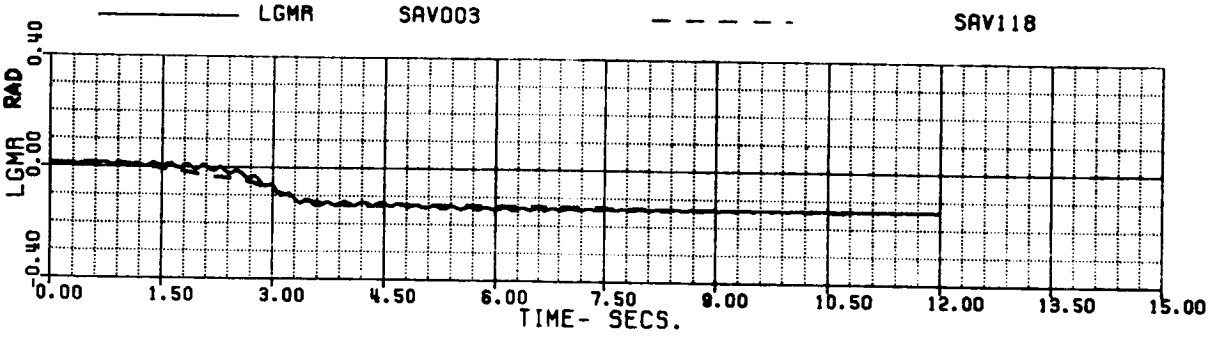

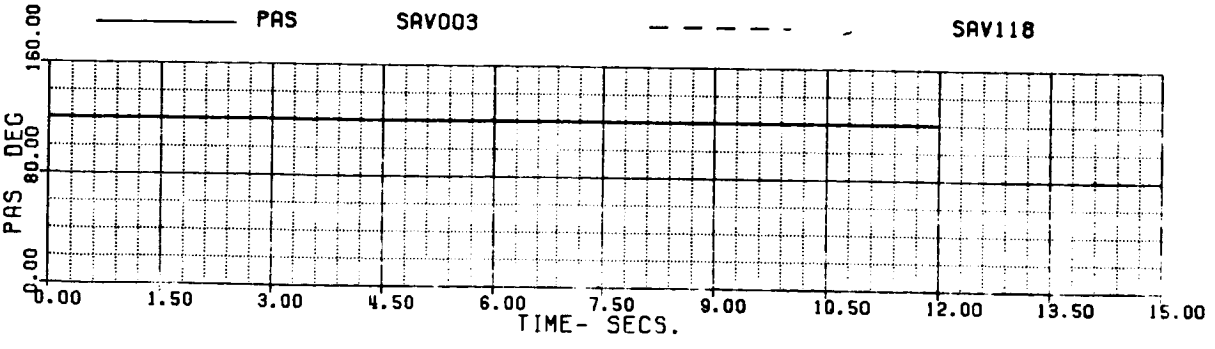

FIG 6.1.3 (f)

60A - BLACK HAWK .

FAUTOS - AUTOROTATION RECOVERY, SMALL SPLIT, INT. F/C
70% XC IN 3 SEC, ADAPT=-1

XA+1	5.0207060	XB+1	-5.9170116	XC+1	-.17628E-2	XP+1	3.6171018
THETAB	0.8336849	VKT	79.993876	PHIB	0.	VYB	-12.509981
XNGE	33592.452	NPINTE	8.2866175	VC	-2775.6436	WEIGHT	16638.000
OMAMR	1.0199999	NPMEAS	99.974205				

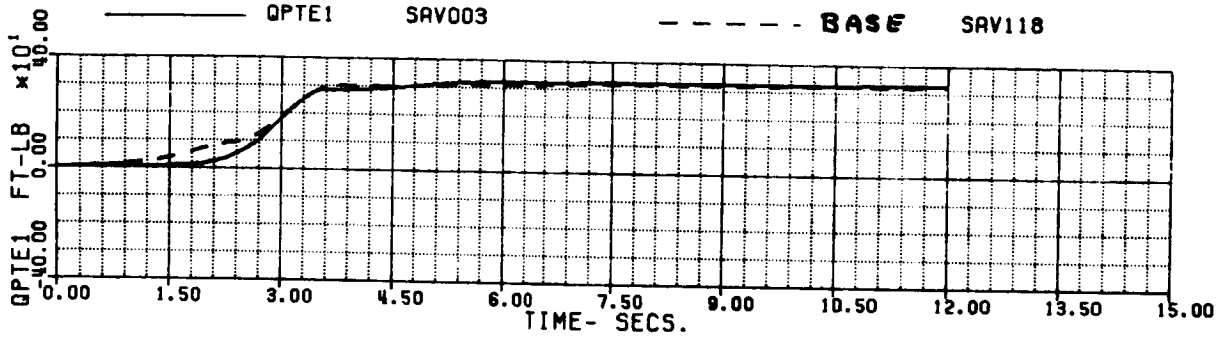

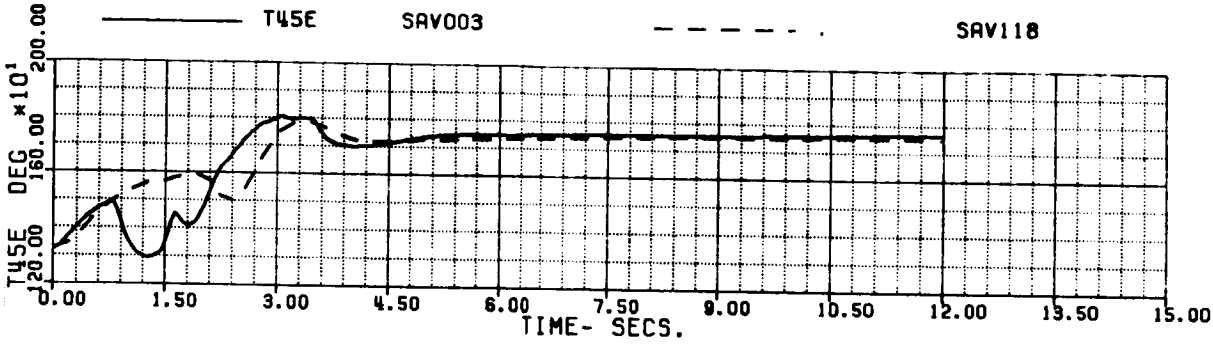

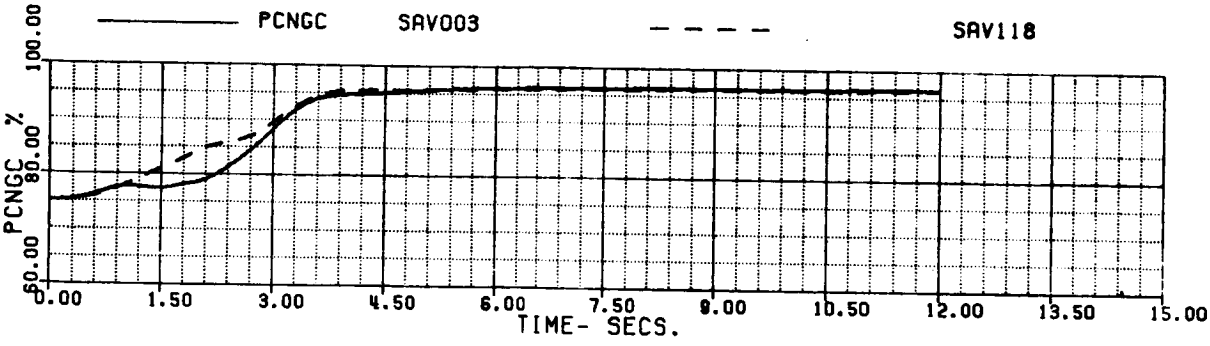

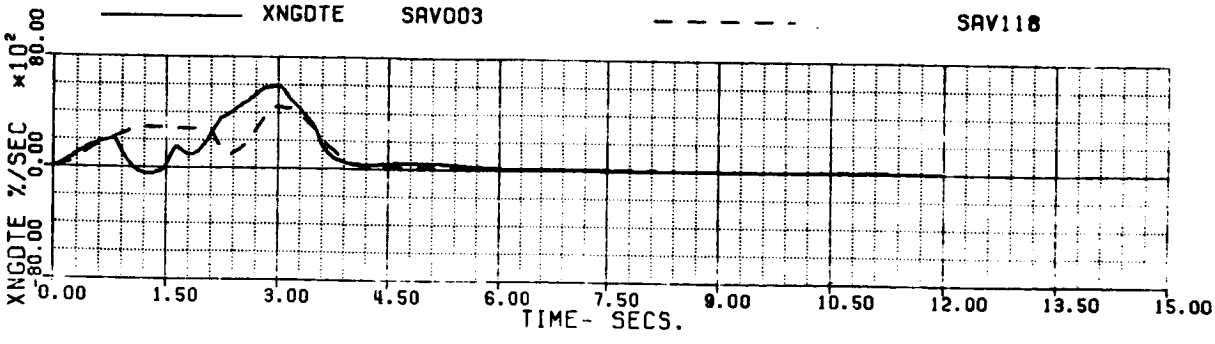

FIG 6.1.3 (g)

60A - BLACK HAWK

FAUTOS - AUTOROTATION RECOVERY, SMALL SPLIT, INT. F/C
70% XC IN 3 SEC, ADAPT=-1

XA+1	5.0207060	XB+1	-5.9170116	XC+1	-.17628E-2	XP+1	3.6171018
THETAB	0.8336849	VKT	79.993876	PHIB	0.	VYB	-12.509981
XNGE	33592.452	NPINTE	8.2066175	VC	-2775.6436	WEIGHT	16638.000
OMRMR	1.0199999	NPMEAS	99.974205				

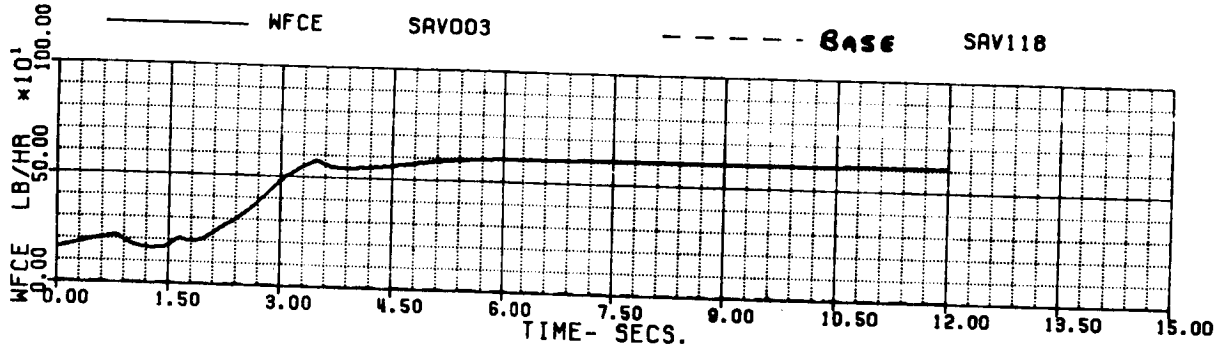

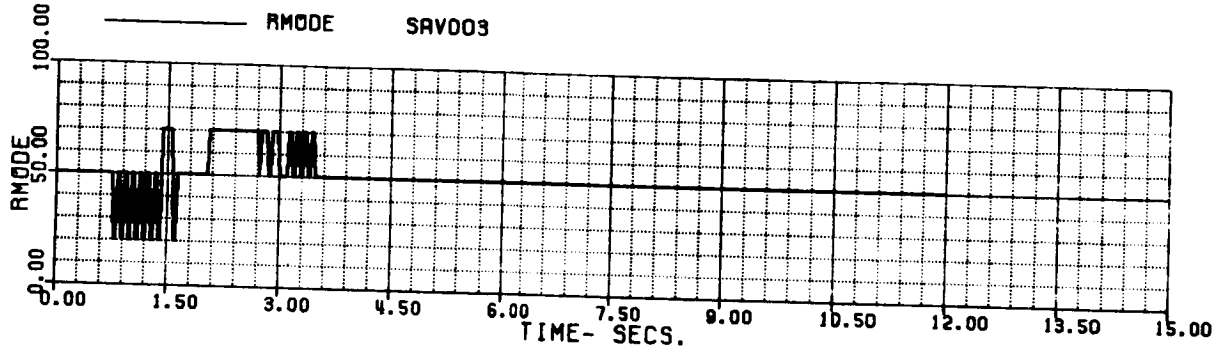

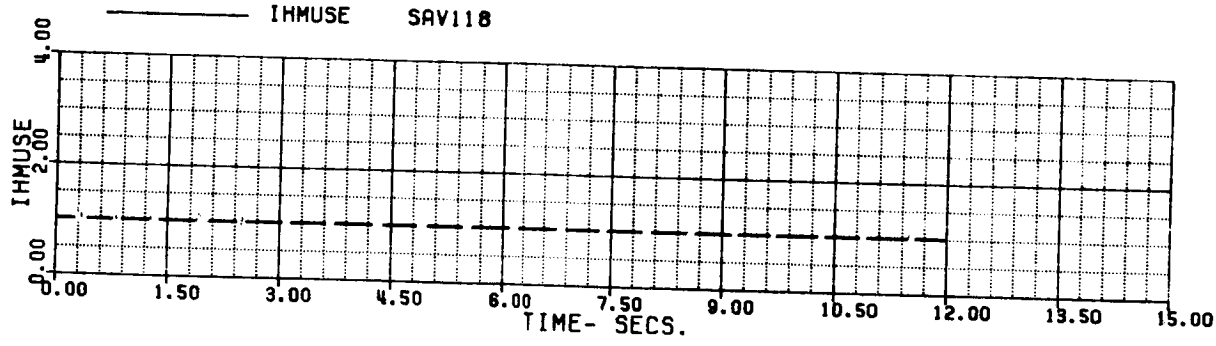

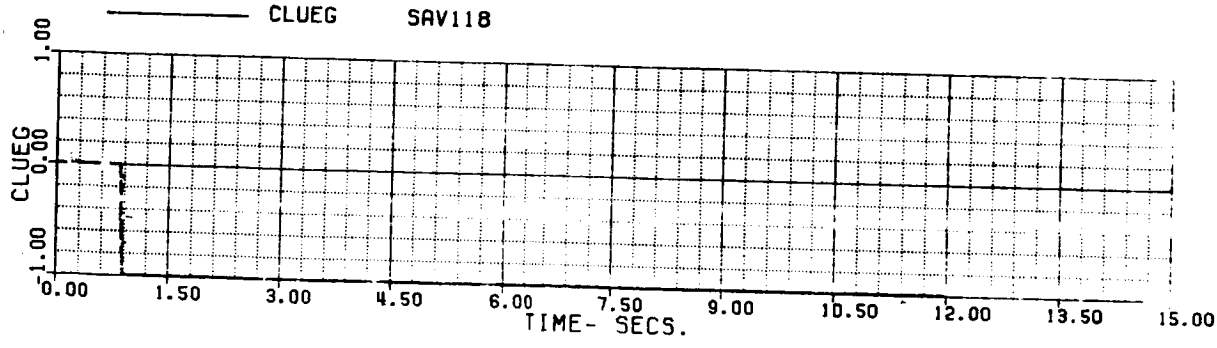

FIG 6.1.3 (h)

60A - BLACK HAWK

FAUTOS - AUTOROTATION RECOVERY, SMALL SPLIT, INT. F/C
70% XC IN 3 SEC, ADAPT=-1

XA+1	5.0207060	XB+1	-5.9170116	XC+1	-.17628E-2	XP+1	3.6171018
THETAB	0.8336849	VKT	79.993876	PHIB	0.	VYB	-12.509981
XNGE	33592.452	NPINTE	8.2866175	VC	-2775.6436	WEIGHT	16638.000
OMAMR	1.0199999	NPMEAS	99.974205				

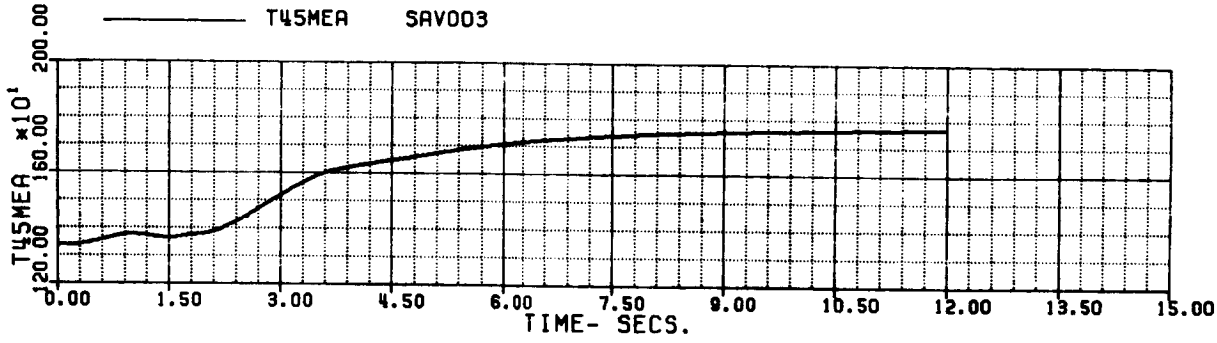

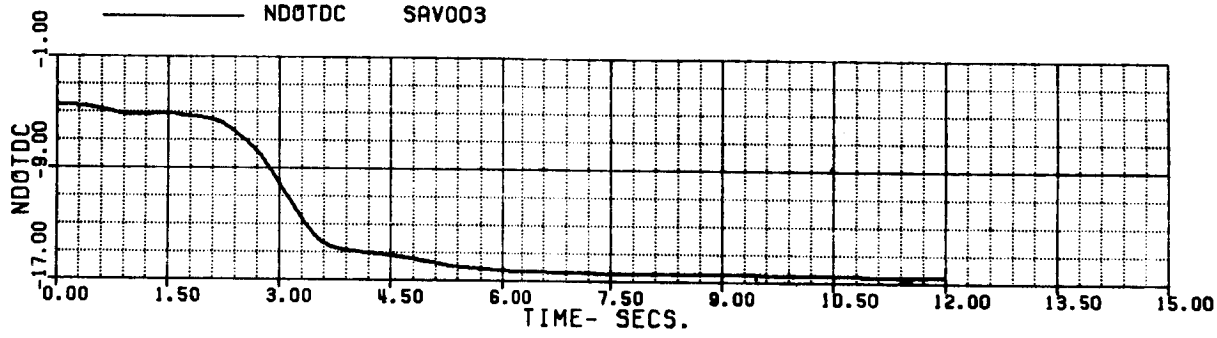

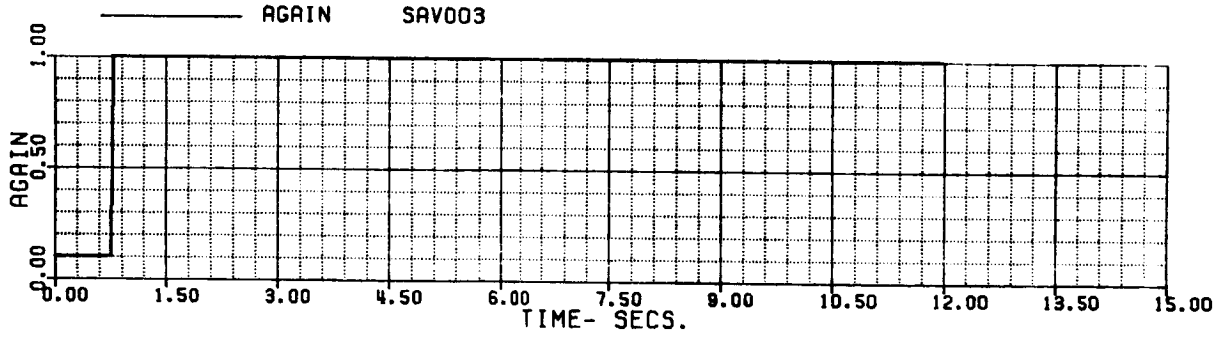

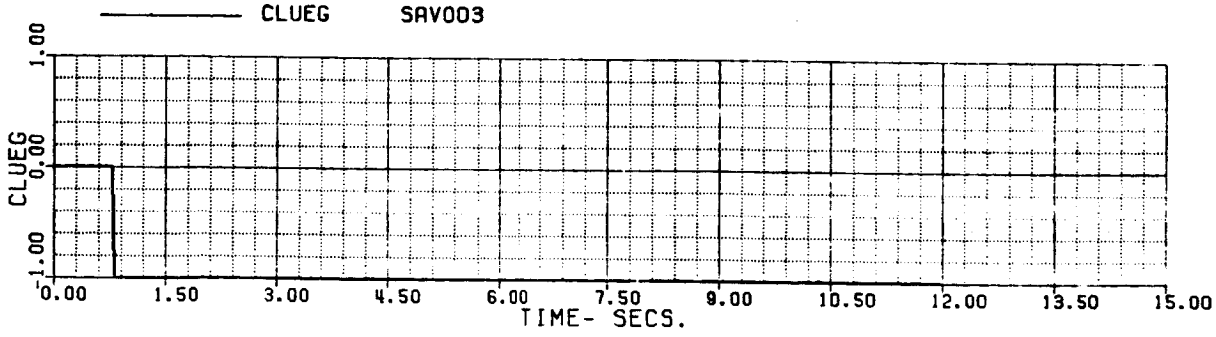

FIG 6.1.3 (i)

60A - BLACK HAWK

FAUTOS - AUTOROTATION RECOVERY, SMALL SPLIT, INT. F/C
70% XC IN 3 SEC, ADAPT=-1

XA+1	5.0207060	XB+1	-5.9170116	XC+1	-.17628E-2	XP+1	3.6171018
THETAB	0.8336849	VKT	79.993876	PHIB	0.	VTB	-12.509981
XNGE	33592.452	NPINTE	8.2866175	VC	-2775.6436	WEIGHT	16638.000
OMRMR	1.0199999	NPMEAS	99.974205				

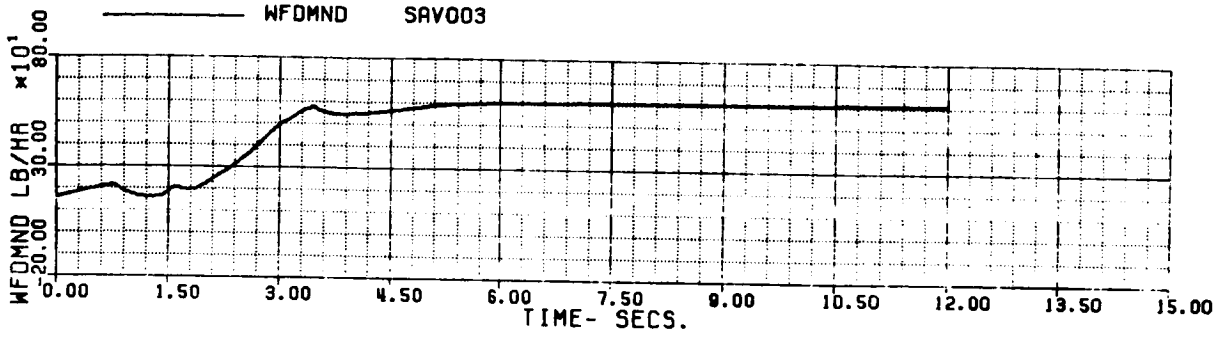

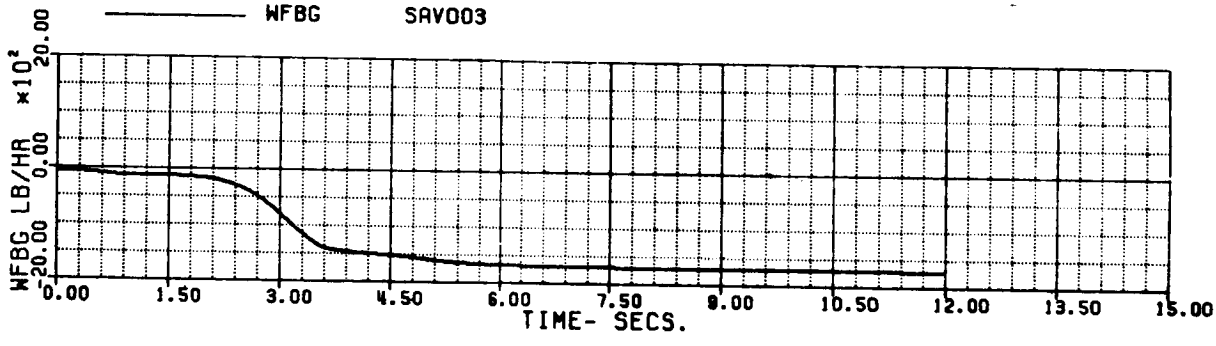

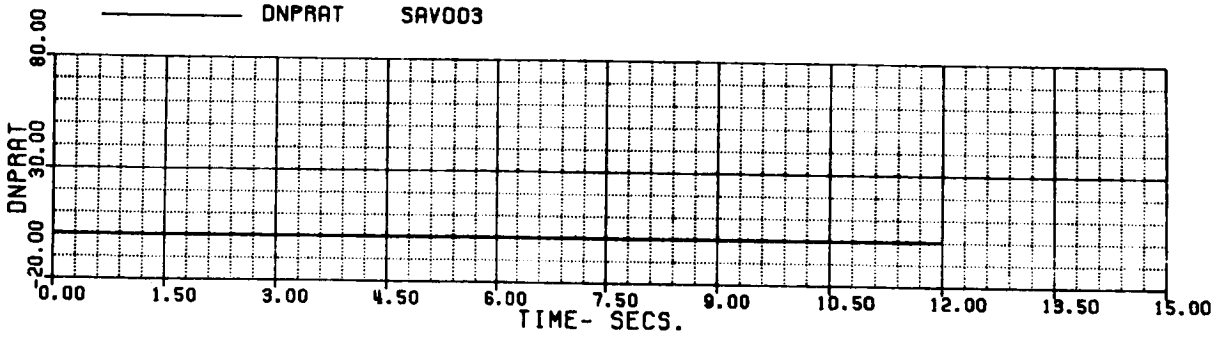

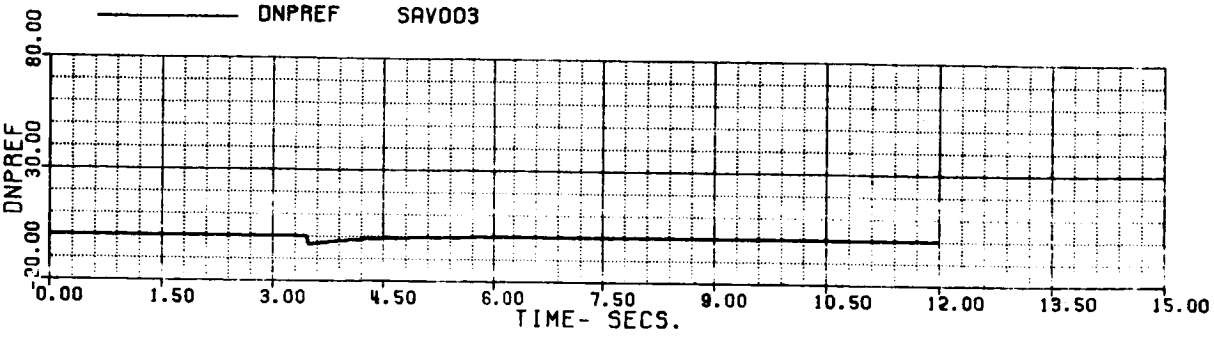

FIG 6.1.3 (j)

60A - BLACK HAWK

FAUTOS - AUTOROTATION RECOVERY, SMALL SPLIT, INT. F/C
70% XC IN 3 SEC, ADAPT=-1

XA+1	5.0207060	XB+1	-5.9170116	XC+1	-.17628E-2	XP+1	3.6171018
THETAB	0.8336849	VKT	79.993876	PHIB	0.	VYB	-12.509981
XNGE	33592.452	NPINTE	8.2866175	VC	-2775.6436	WEIGHT	16638.000
OMRMR	1.0199999	NPMEAS	99.974205				

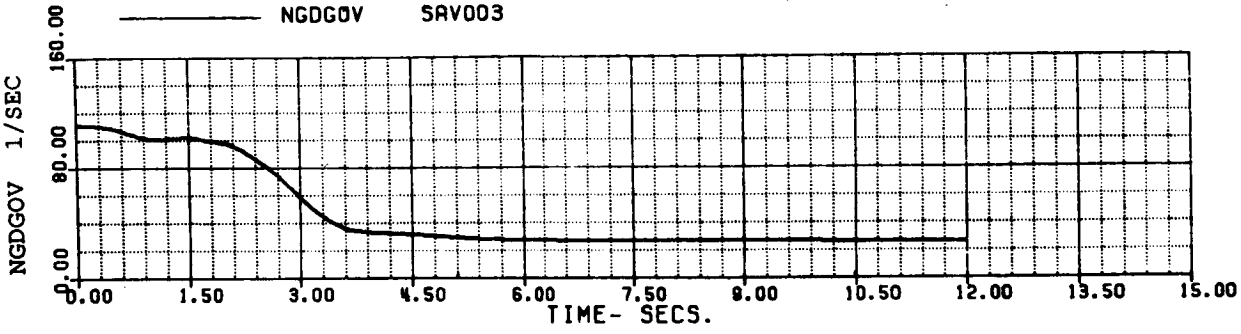

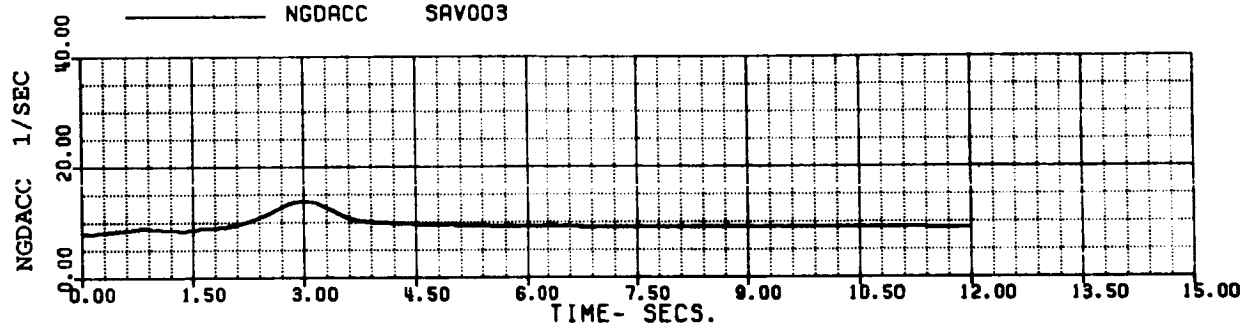

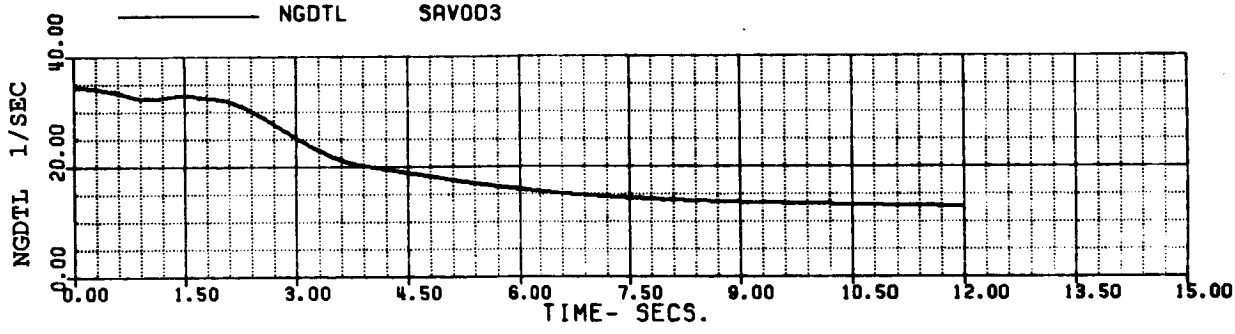

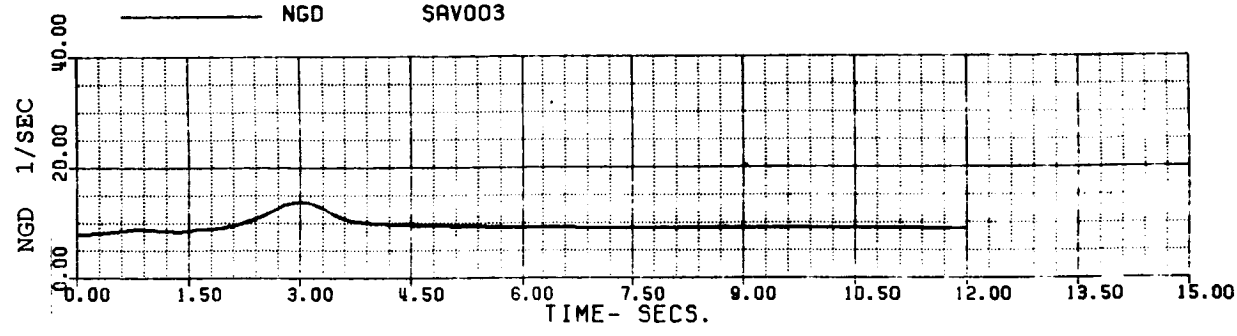

FIG 6.1.3 (k)

60A - BLACK HAWK

FAUTOS - AUTOROTATION RECOVERY, SMALL SPLIT, INT. F/C
70% XC IN .5 SEC, ADAPT=-1

XA+1	5.0205976	XB+1	-5.9173411	XC+1	-.22108E-2	XP+1	3.6171232
THETAB	0.8326049	VKT	79.993871	PHIB	0.	VYB	-12.509996
XNGE	33602.317	NPINTE	8.2332060	VC	-2775.9247	WEIGHT	16638.000
OMRMR	1.0199999	NPMEAS	99.974205				

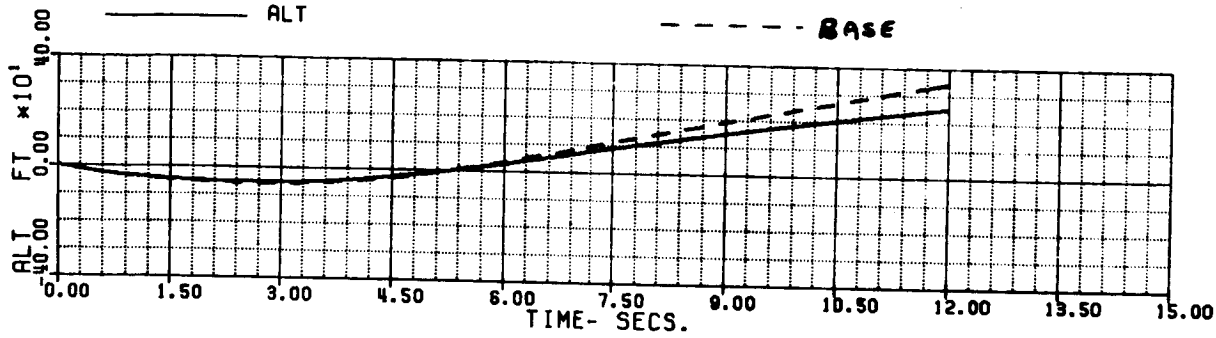

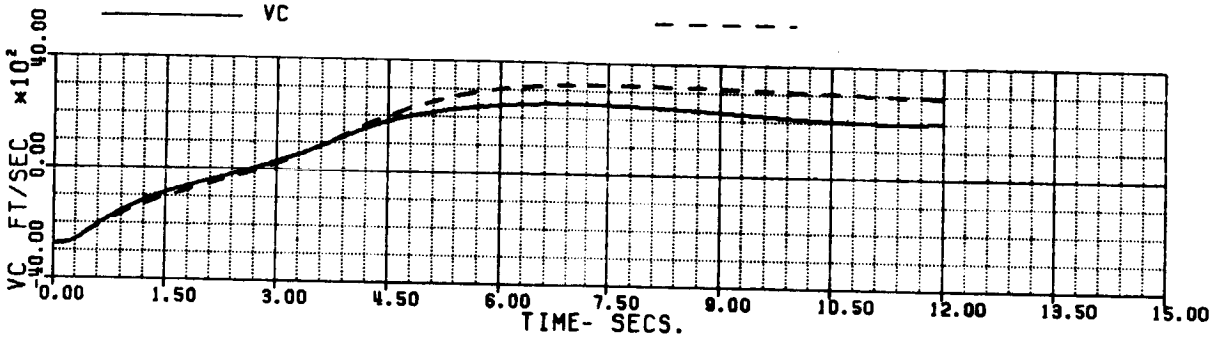

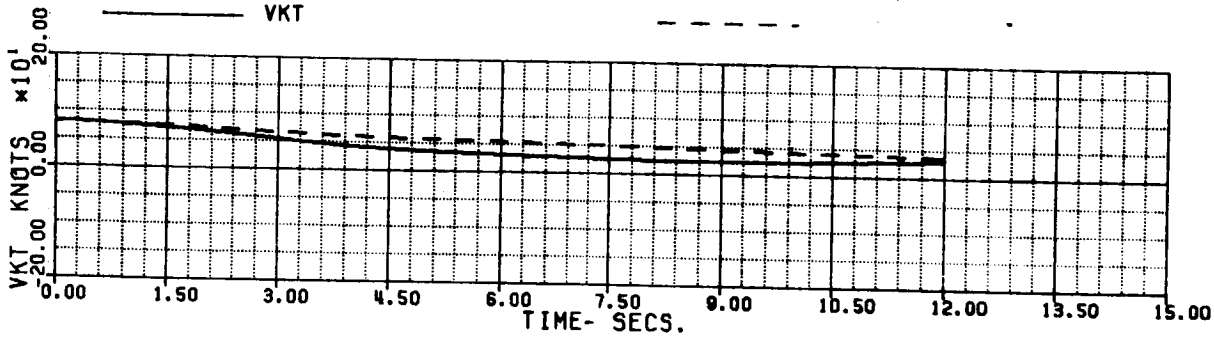

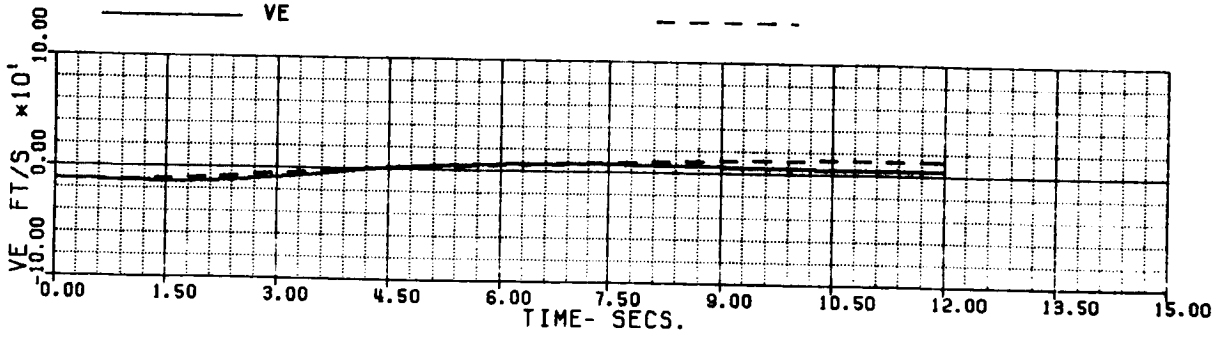

SIMULATED AUTOROTATION RECOVERY

(SMALL SPLIT, FAST PULL)

FIG 6.1.4 (a)

60A - BLACK HAWK

FAUTOS - AUTOROTATION RECOVERY, SMALL SPLIT, INT. F/C
70% XC IN .5 SEC, ADAPT=-1

XA+1	5.0205976	XB+1	-5.9173411	XC+1	-.22108E-2	XP+1	3.6171232
THETAB	0.8326049	VKT	79.993871	PHIB	0.	VYB	-12.509996
XNGE	33602.317	NPINTE	8.2332060	VC	-2775.9247	WEIGHT	16638.000
OMAMR	1.0199999	NPMEAS	99.974205				

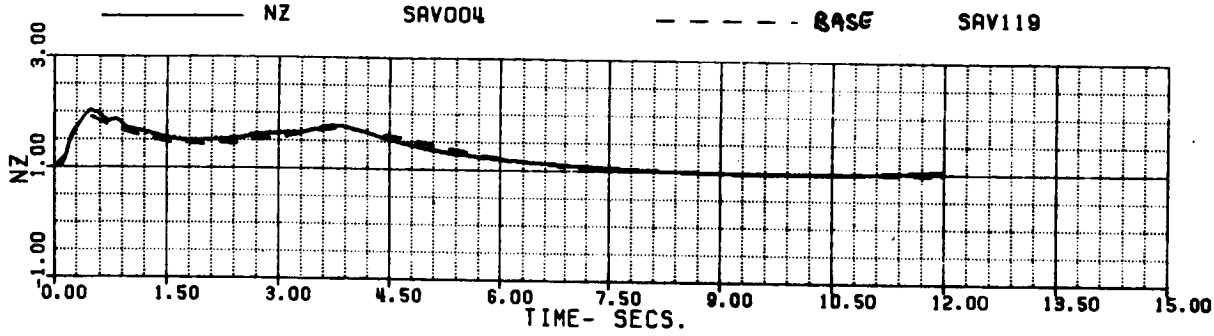

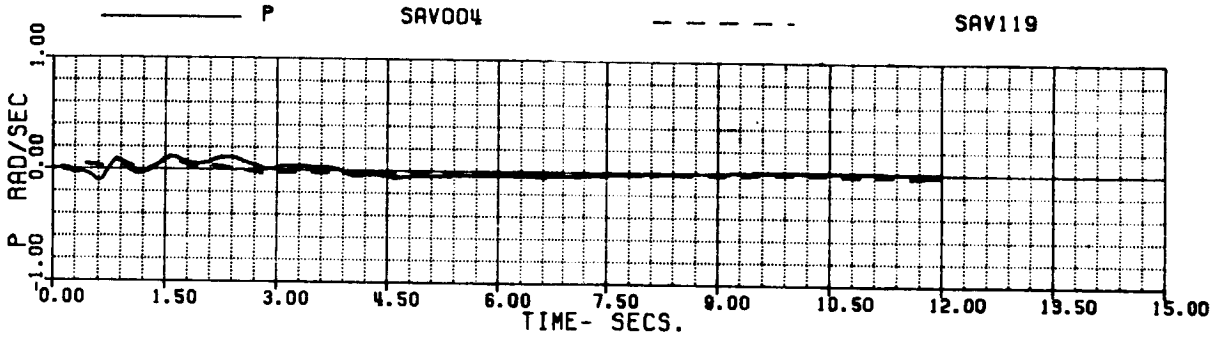

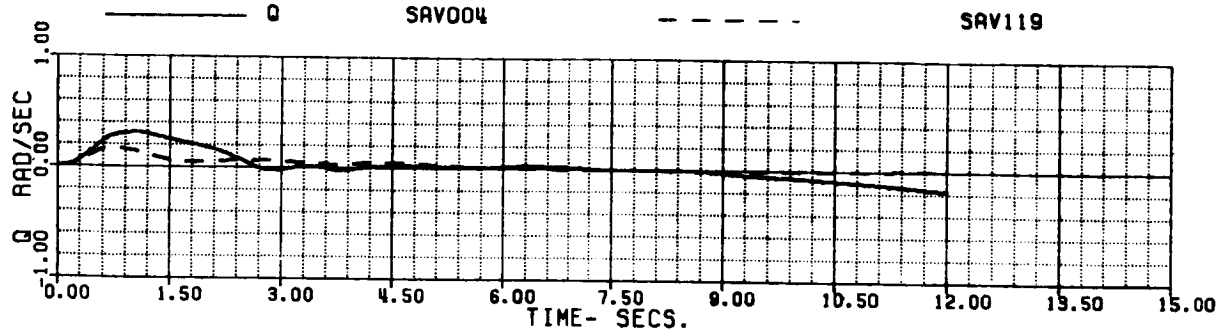

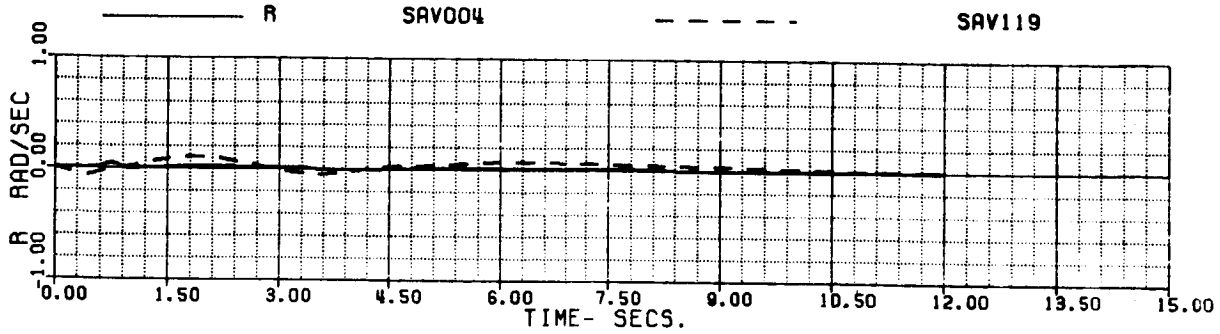

FIG 6.1.4 (b)

60A - BLACK HAWK

FAUTOS - AUTOROTATION RECOVERY, SMALL SPLIT, INT. F/C
70% XC IN .5 SEC, ADAPT=-1

XA+1	5.0205976	XB+1	-5.9173411	XC+1	-.22108E-2	XP+1	3.6171232
THETAB	0.8326049	VKT	79.993871	PHIB	0.	VYB	-12.509996
XNGE	33602.317	NPINTE	8.2332060	VC	-2775.9247	WEIGHT	16638.000
OMRMR	1.0199999	NPMEAS	99.974205				

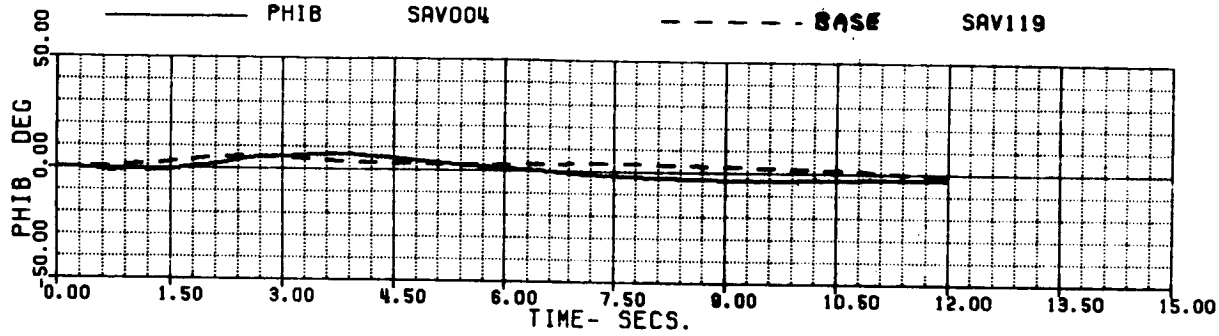

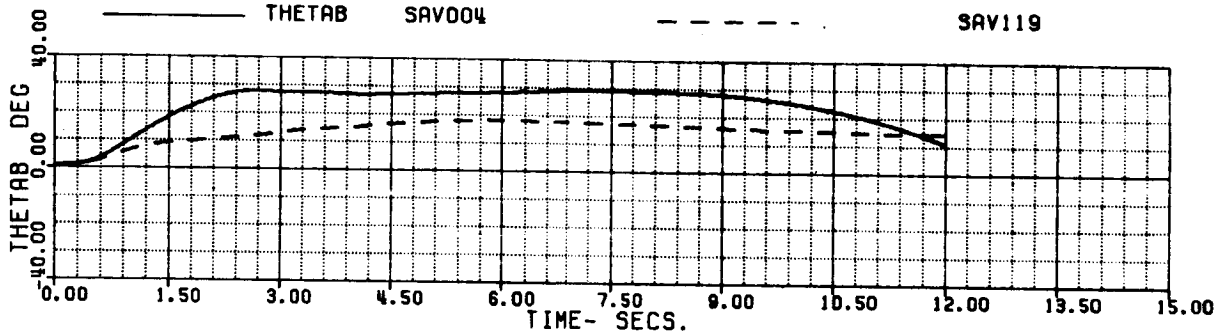

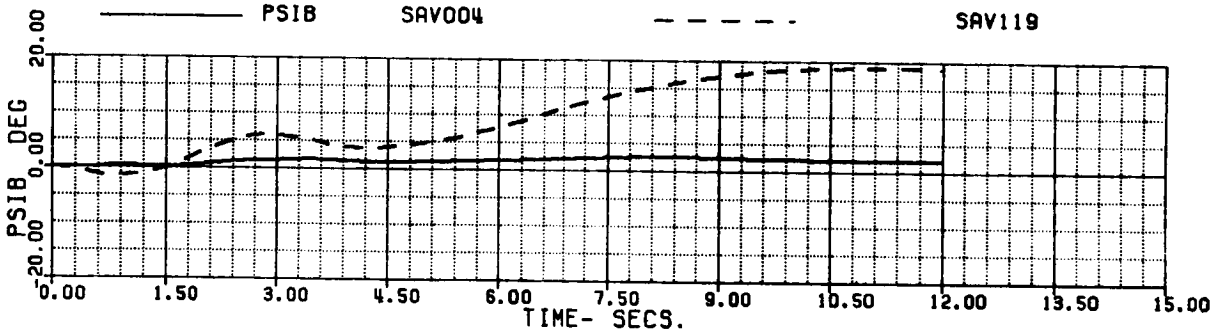

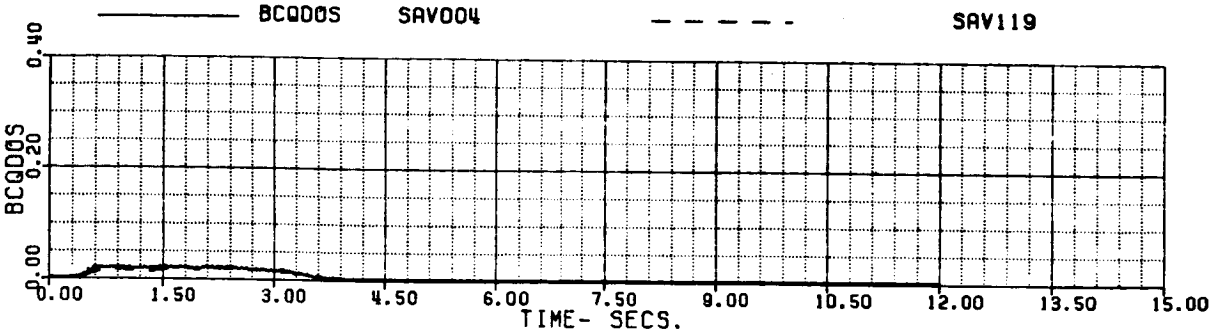

FIG 6.1.4 (c)

60A - BLACK HAWK

FAUTOS - AUTOROTATION RECOVERY, SMALL SPLIT, INT. F/C
70% XC IN .5 SEC, ADAPT=-1

XA+1	5.0205976	XB+1	-5.9173411	XC+1	-.22108E-2	XP+1	3.6171232
THETAB	0.8326049	VKT	79.993871	PHIB	0.	VYB	-12.509996
XNGE	33602.317	NPINTE	8.2332060	VC	-2775.9247	WEIGHT	16638.000
OMAMR	1.0199999	NPMEAS	99.974205				

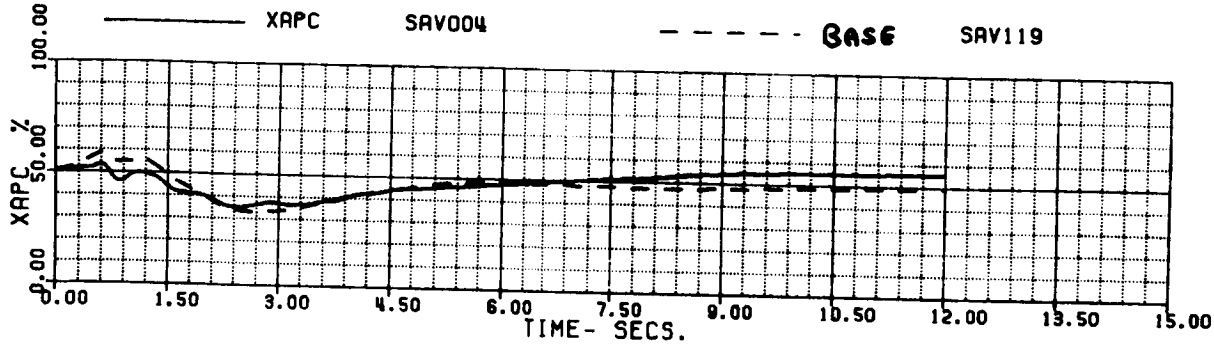

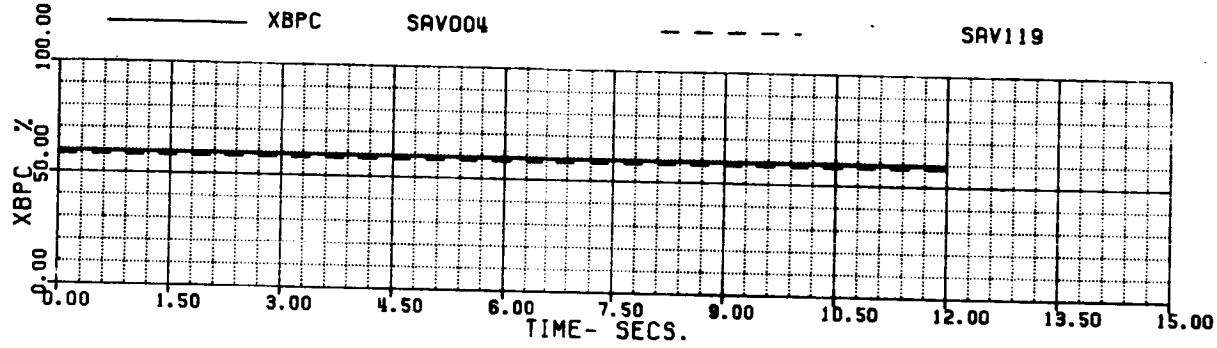

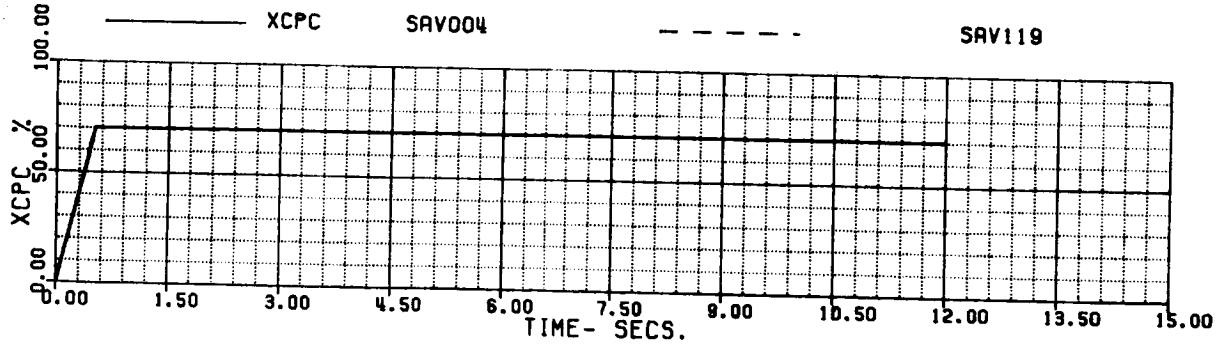

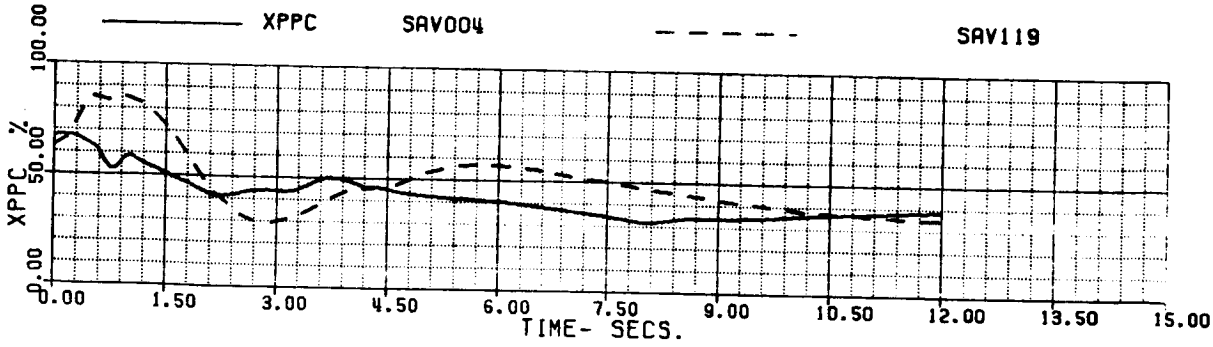

FIG 6.1.4 (d)

60A - BLACK HAWK

FAUTOS - AUTOROTATION RECOVERY, SMALL SPLIT, INT. F/C
70% XC IN .5 SEC, ADAPT=-1

XA+1	5.0205976	XB+1	-5.9173411	XC+1	-.22108E-2	XP+1	3.6171232
THETAB	0.8326049	VKT	79.993871	PHIB	0.	VYB	-12.509996
XNGE	33602.317	NPINTE	8.2332060	VC	-2775.9247	WEIGHT	16638.000
OMRMR	1.0199999	NPMEAS	99.974205				

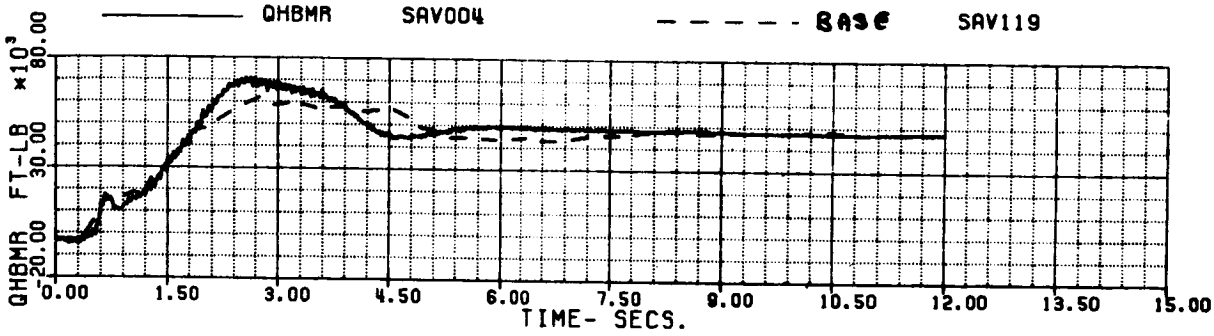

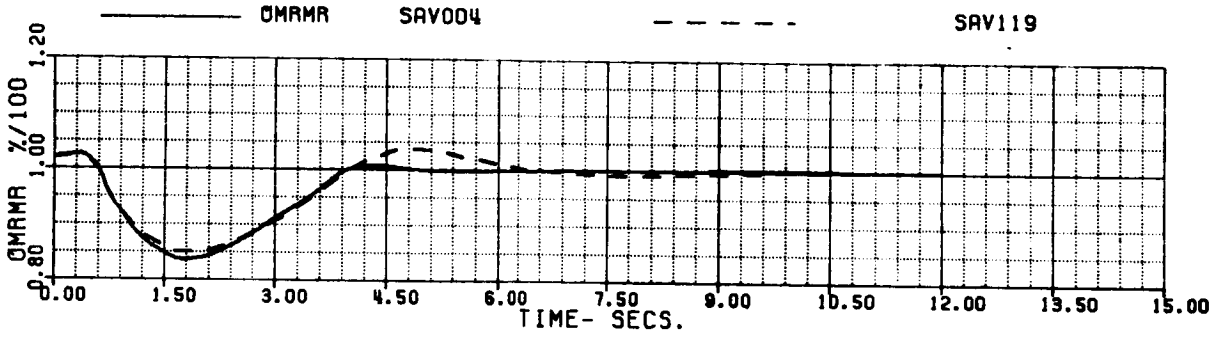

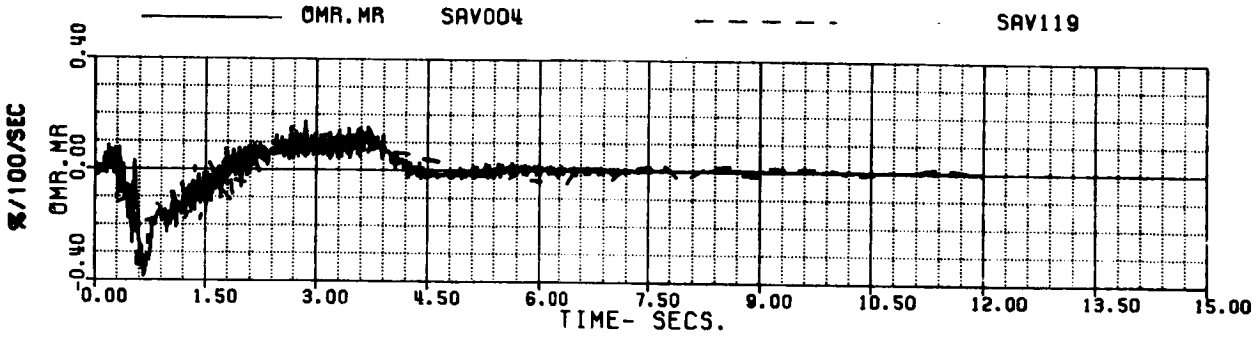

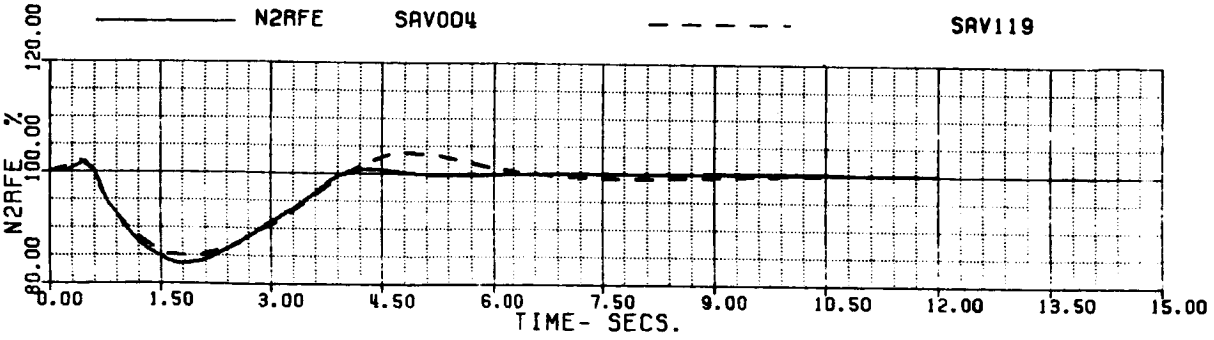

FIG 6.1.4 (e)

60A - BLACK HAWK

FAUTOS - AUTOROTATION RECOVERY, SMALL SPLIT, INT. F/C
70% XC IN .5 SEC, ADAPT=-1

XA+1	5.0205976	XB+1	-5.9173411	XC+1	-.22108E-2	XP+1	3.6171232
THETAB	0.8326049	VKT	79.993871	PHIB	0.	VYB	-12.509996
XNGE	33602.317	NPINTE	8.2332060	VC	-2775.9247	WEIGHT	16638.000
OMRMR	1.0199999	NPMEAS	99.974205				

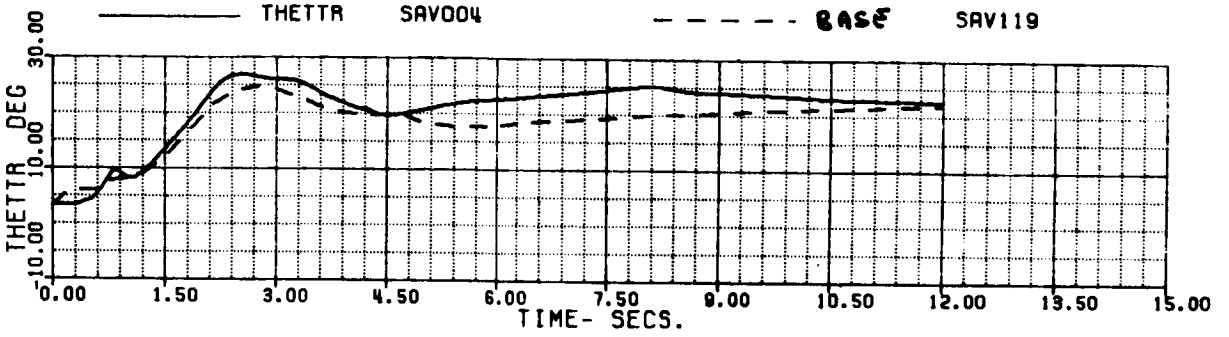

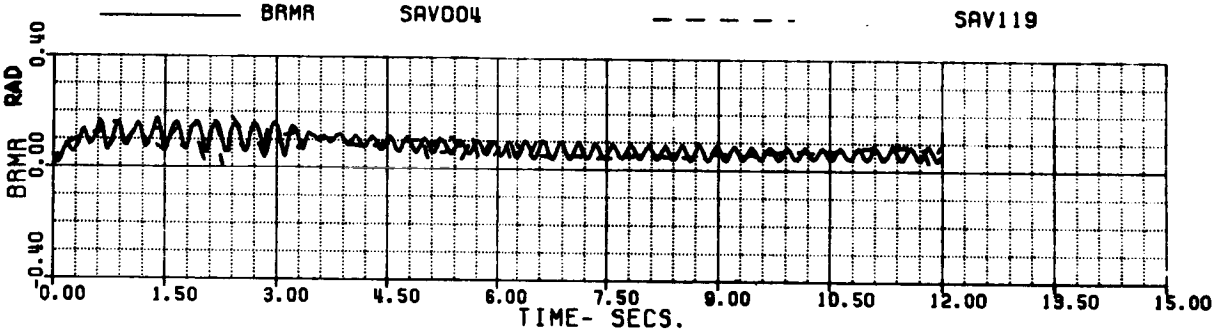

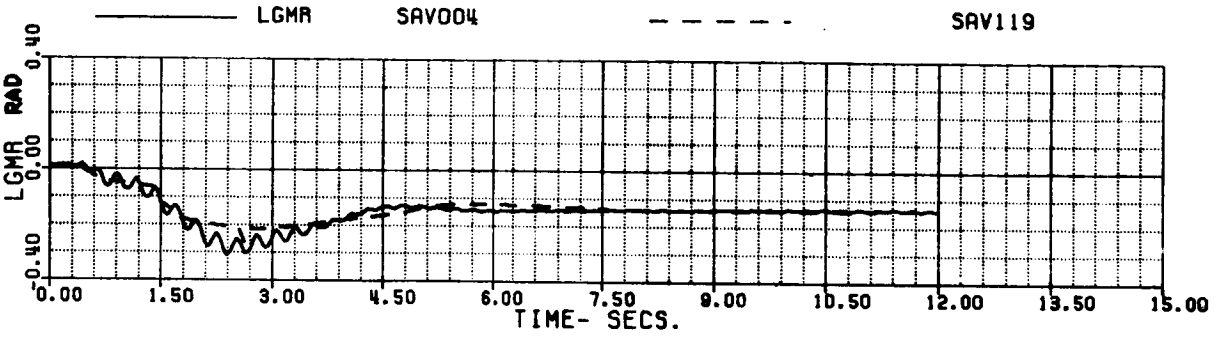

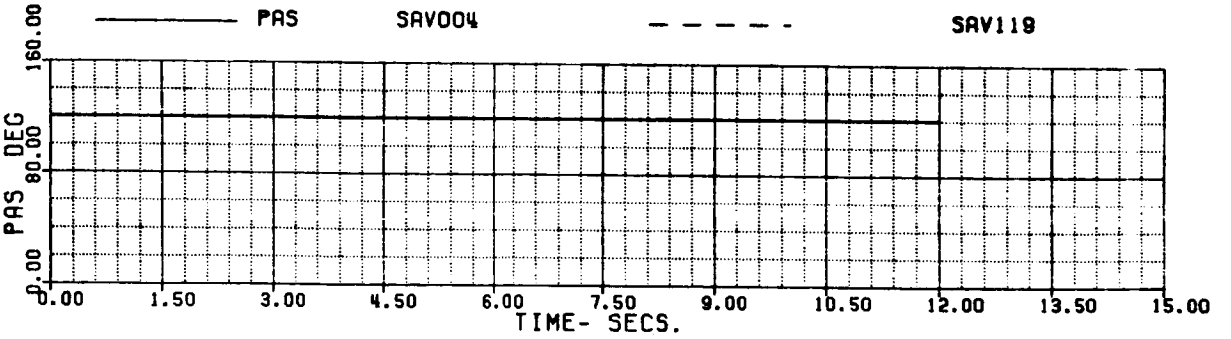

FIG 6.1.4 (f)

60A - BLACK HAWK

FAUTOS - AUTOROTATION RECOVERY, SMALL SPLIT, INT. F/C
70% XC IN .5 SEC, ADAPT=-1

XA+1	5.0205976	XB+1	-5.9173411	XC+1	-.22108E-2	XP+1	3.6171232
THETAB	0.8326049	VKT	79.993871	PHIB	0.	VYB	-12.509996
XNGE	33602.317	NPINTE	8.2332060	VC	-2775.9247	WEIGHT	16638.000
OMAMR	1.0199999	NPMEAS	99.974205				

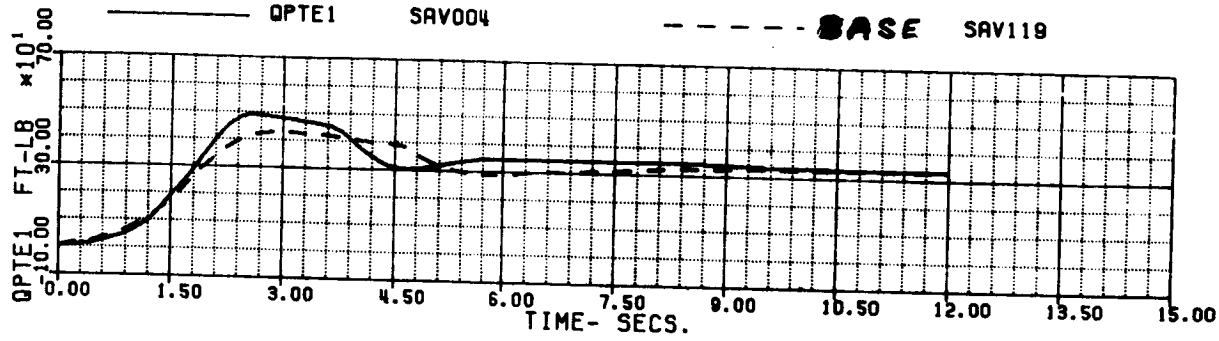

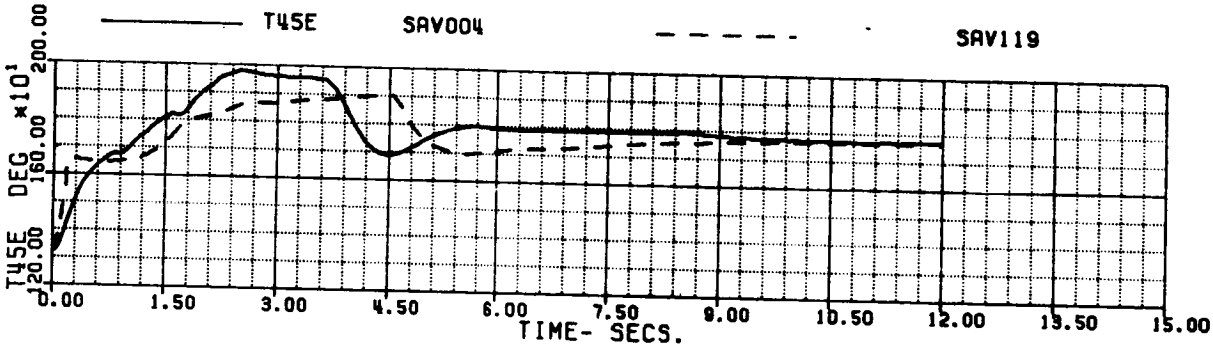

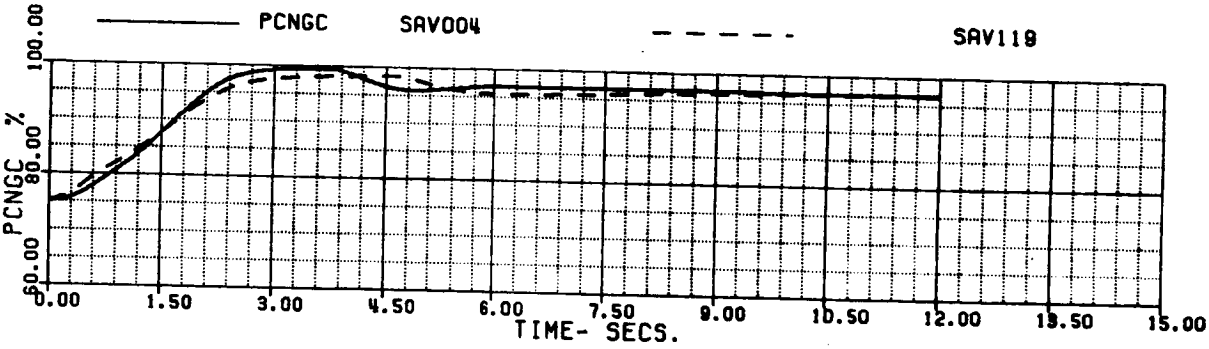

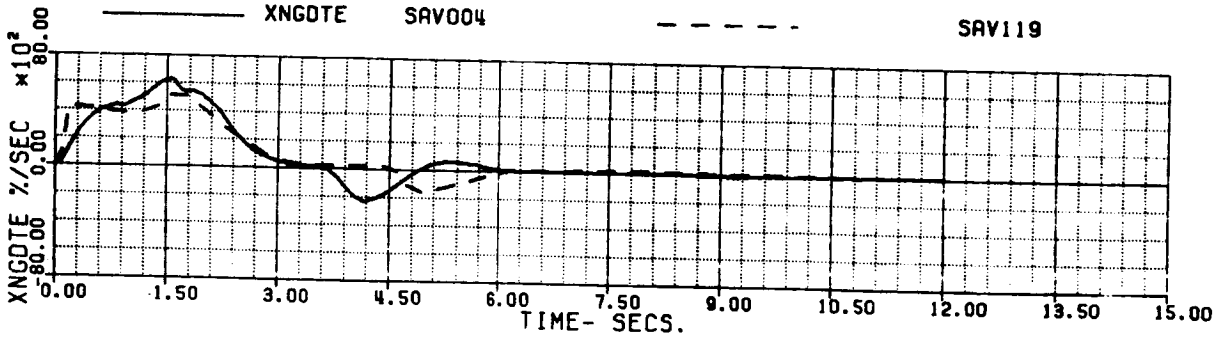

FIG 6.1.4 (g)

60A - BLACK HAWK

FAUTOS - AUTOROTATION RECOVERY, SMALL SPLIT, INT. F/C
70% XC IN .5 SEC, ADAPT=-1

XA+1	5.0205976	XB+1	-5.9173411	XC+1	-.22108E-2	XP+1	3.6171232
THETAB	0.8326049	VKT	79.993871	PHIB	0.	VTB	-12.509996
XNGE	33602.317	NPINTE	8.2332060	VC	-2775.9247	WEIGHT	16638.000
OMRMR	1.0199999	NPMEAS	99.974205				

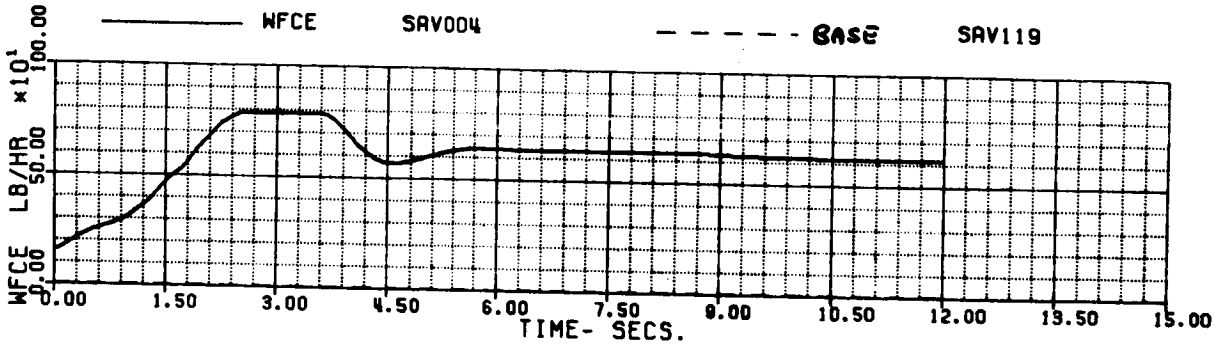

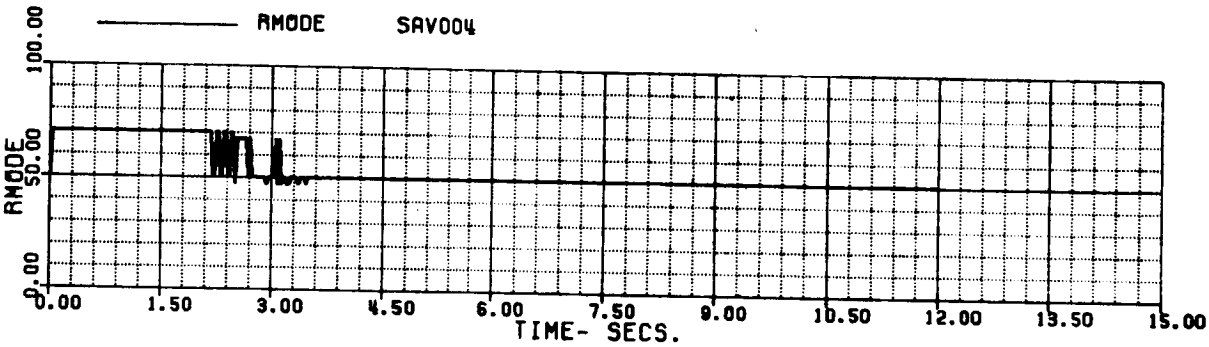

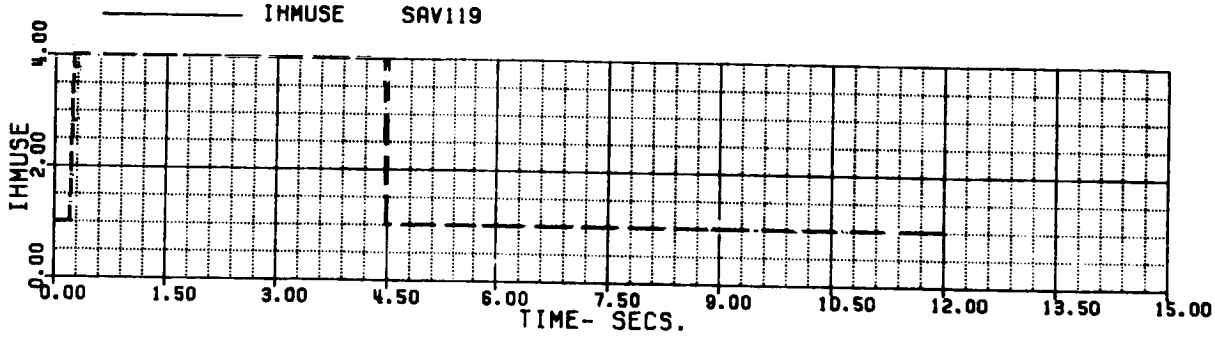

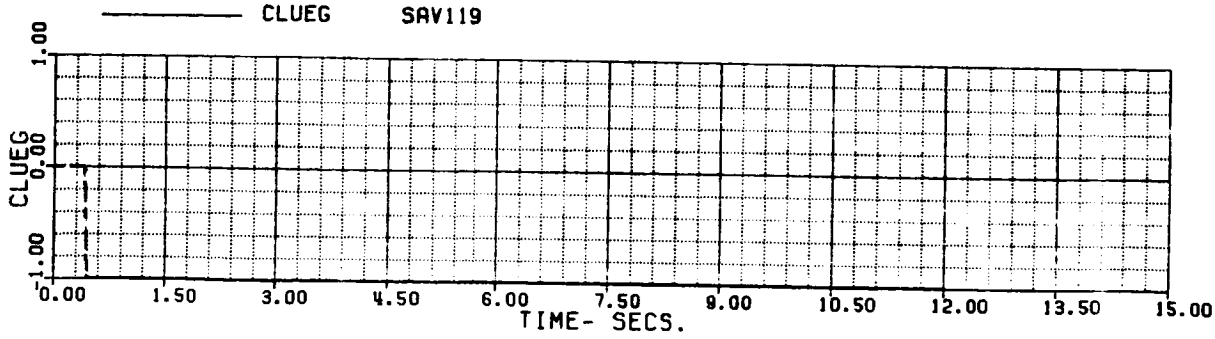

FIG 6.1.4 (h)

60A - BLACK HAWK

FAUTOS - AUTOROTATION RECOVERY, SMALL SPLIT, INT. F/C
70% XC IN .5 SEC, ADAPT=-1

XA+1	5.0205976	XB+1	-5.9173411	XC+1	-.22108E-2	XP+1	3.6171232
THETAB	0.8326049	VKT	79.993871	PHIB	0.	VYB	-12.509996
XNGE	33602.317	NPINTE	8.2332060	VC	-2775.9247	WEIGHT	16638.000
OMAMR	1.0199999	NPMEAS	99.974205				

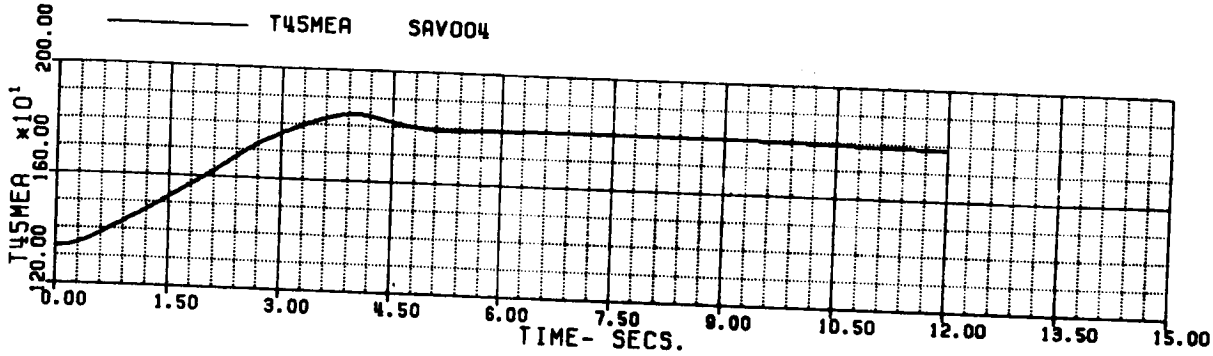

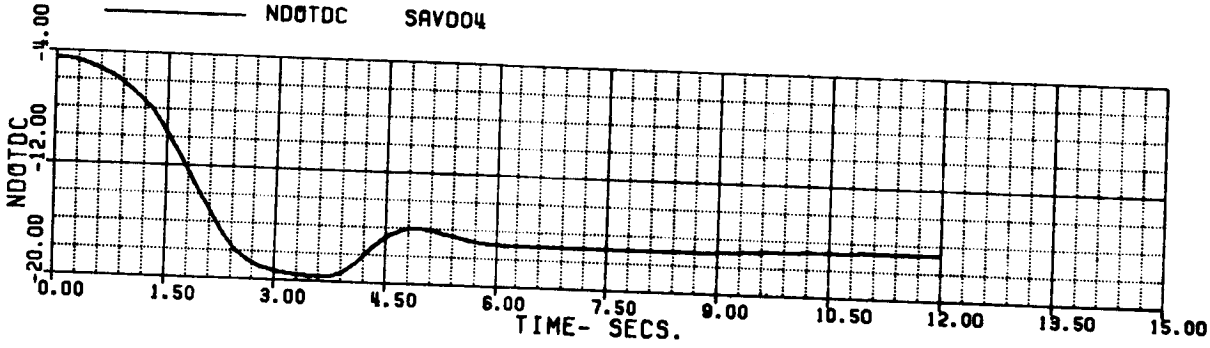

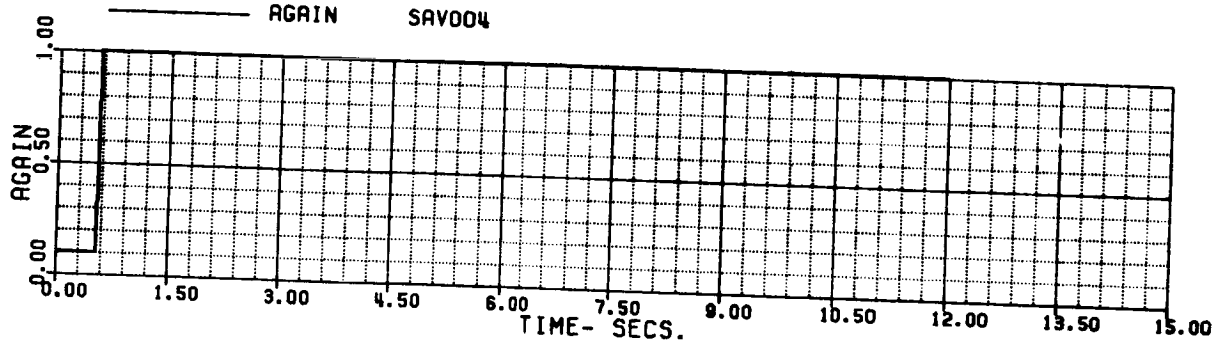

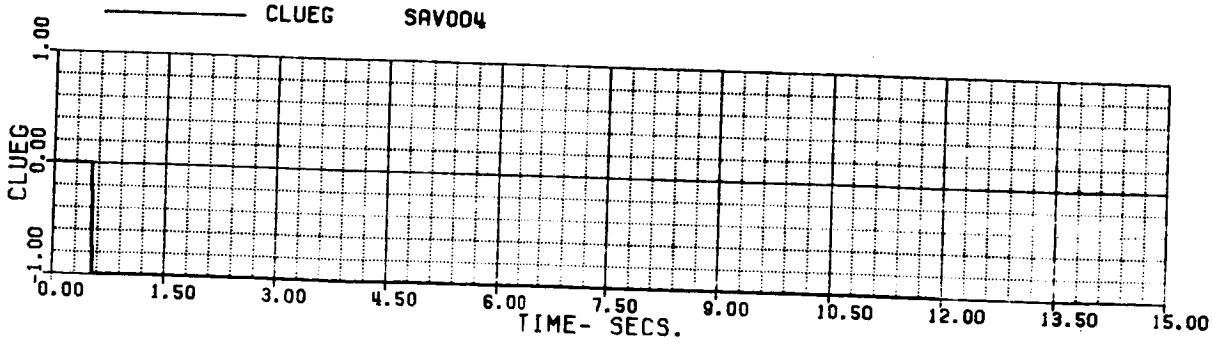

FIG 6.1.4 (i)

60A - BLACK HAWK

FAUTOS - AUTOROTATION RECOVERY, SMALL SPLIT, INT. F/C
70% XC IN .5 SEC, ADAPT=-1

XA+1	5.0205976	XB+1	-5.9173411	XC+1	-.22108E-2	XP+1	3.6171232
THETAB	0.8326049	VKT	79.993871	PHIB	0.	VYB	-12.50995
XNGE	33602.317	NPINTE	8.2332060	VC	-2775.9247	WEIGHT	16638.000
OMAMR	1.0199999	NPMEAS	99.974205				

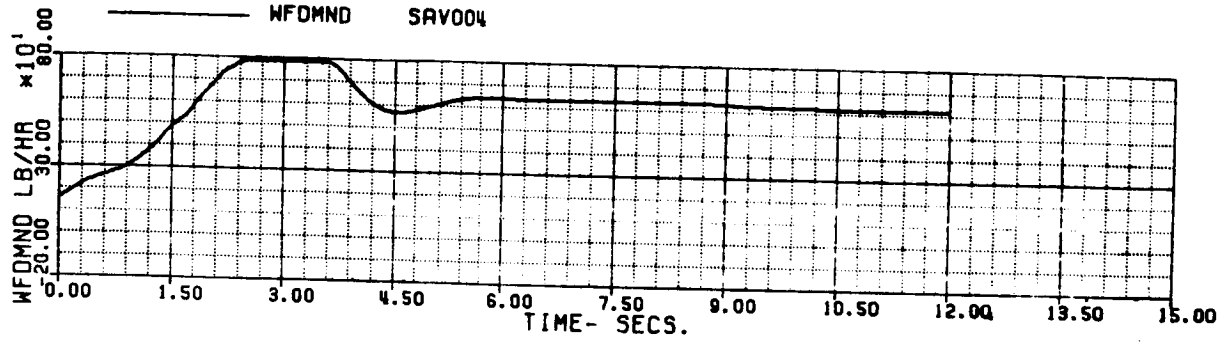

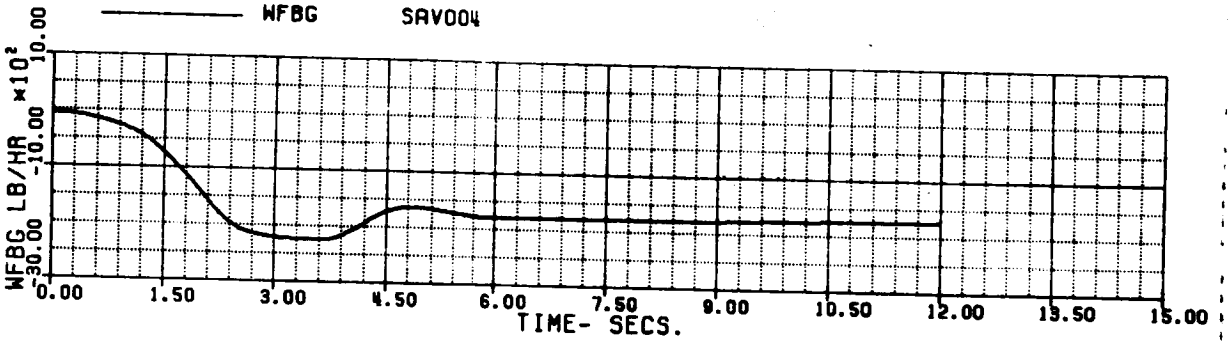

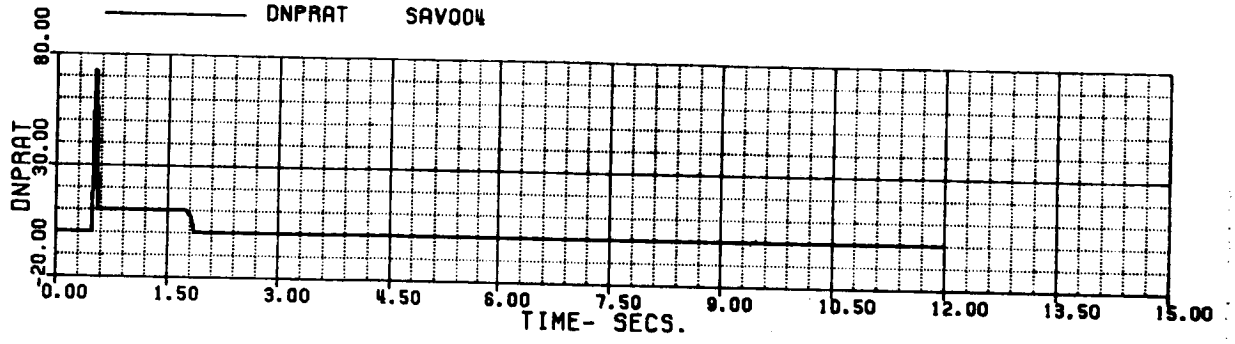

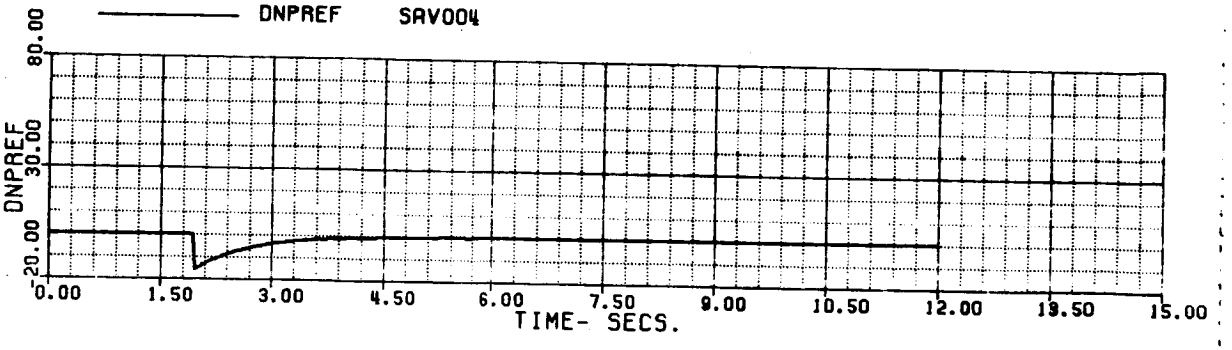

FIG 6.1.4 (j)

60A - BLACK HAWK

FAUTOS - AUTOROTATION RECOVERY, SMALL SPLIT, INT. F/C
70% XC IN .5 SEC, ADAPT=-1

XA+1	5.0205976	XB+1	-5.9173411	XC+1	-.22108E-2	XP+1	3.61712
THETAB	0.8326049	VKT	79.993871	PHIB	0.	VYB	-12.509
XNGE	33602.317	NPINTE	8.2332060	VC	-2775.9247	WEIGHT	16638.0
OMRMR	1.0199999	NPMEAS	99.974205				

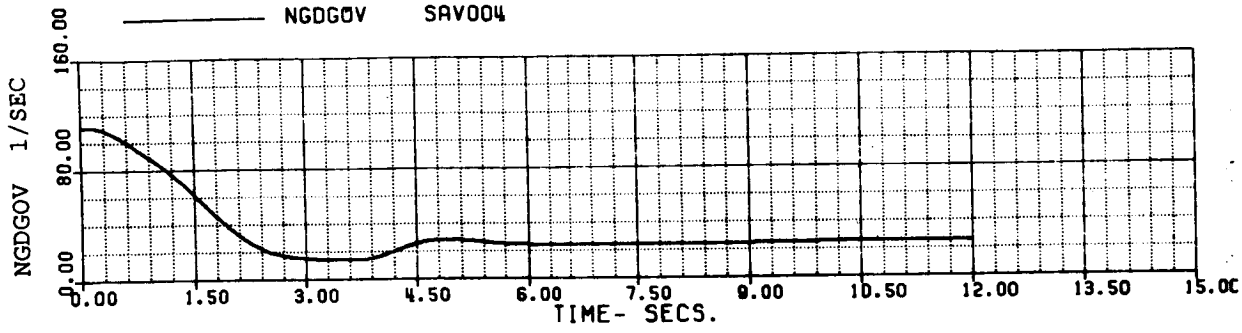

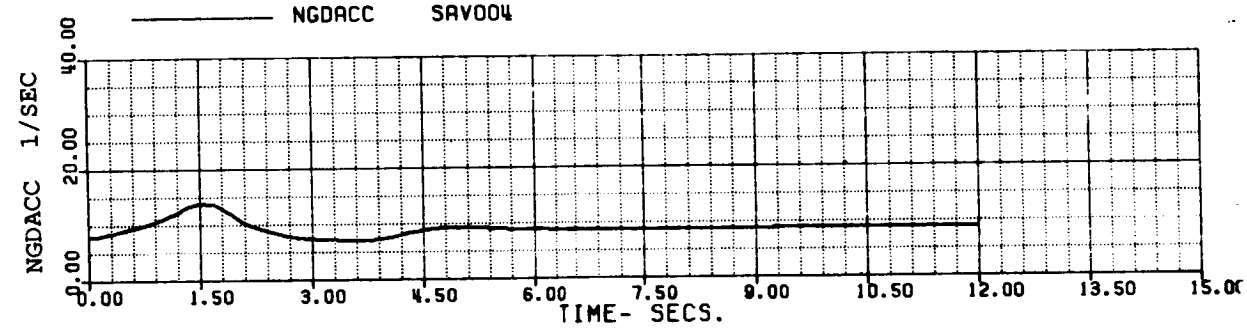

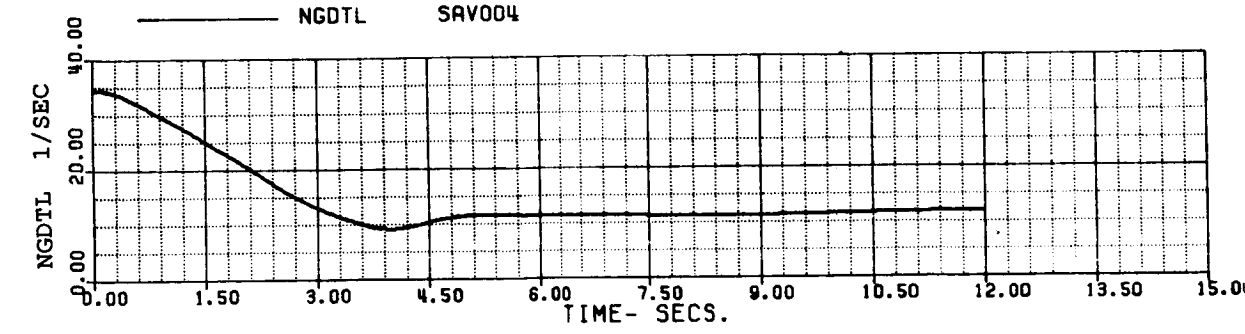

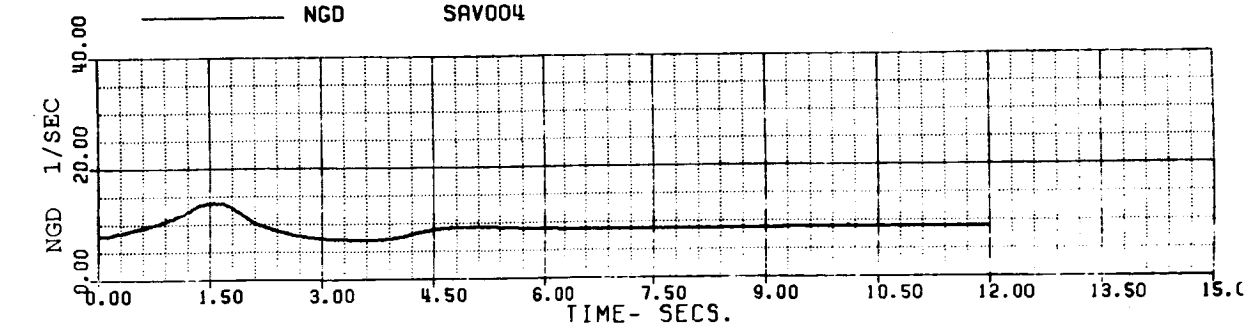

FIG 6.1.4 (k)

60A - BLACK HAWK
FBOBUP - POPUP/REMASK, INTEGRATED FUEL CONTROL

XA+1	5.3214099	XB+1	-5.7952079	XC+1	5.3291549	XP+1	1.9187516
THETAB	4.0996295	VKT	0.	PHIB	-2.5978147	VYB	0.
XNGE	41775.544	NPINTE	2.4556636	VC	0.	WEIGHT	16638.000
OMRMR	0.9999999	NPMEAS	99.999997				

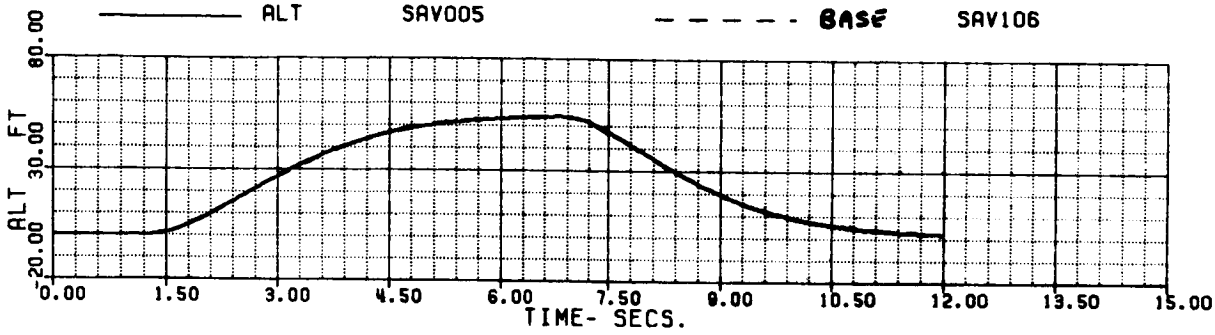

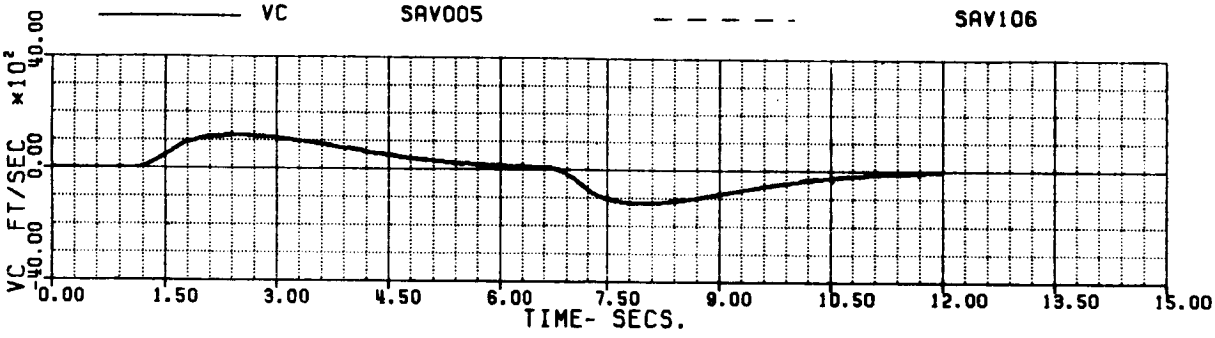

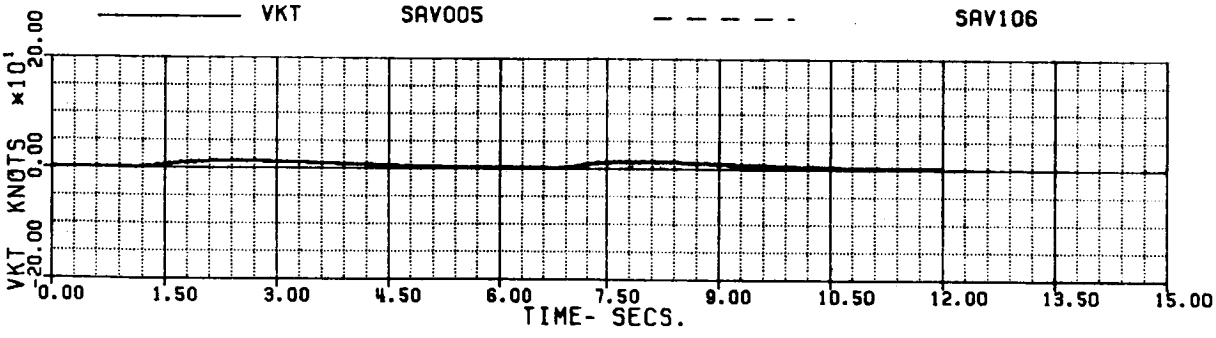

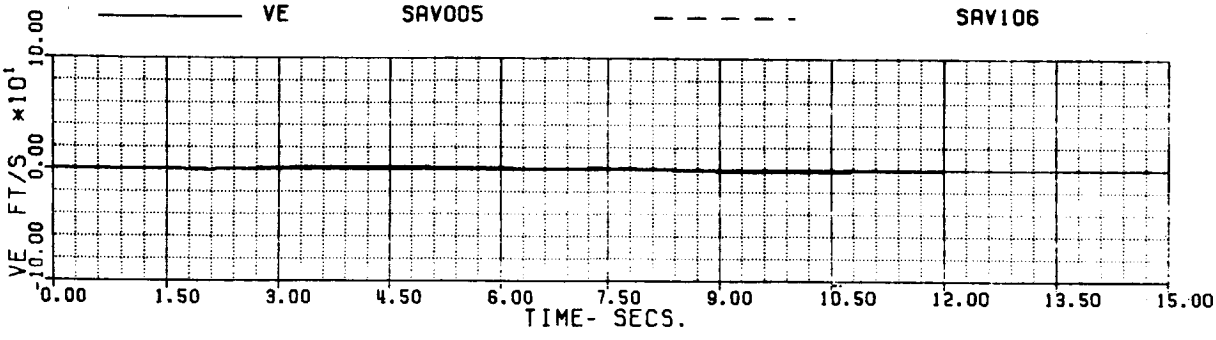

SIMULATED POP-UP & REMASK

FIG 6.1.5 (a)

60A - BLACK HAWK
FBOBUP - POPUP/REMASK, INTEGRATED FUEL CONTROL

XA+1	5.3214099	XB+1	-5.7952079	XC+1	5.3291549	XP+1	1.9187516
THETAB	4.0996295	VKT	0.	PHIB	-2.5978147	VYB	0.
XNGE	41775.544	NPINTE	2.4556636	VC	0.	WEIGHT	16638.000
OMRMR	0.9999999	NPMEAS	99.999997				

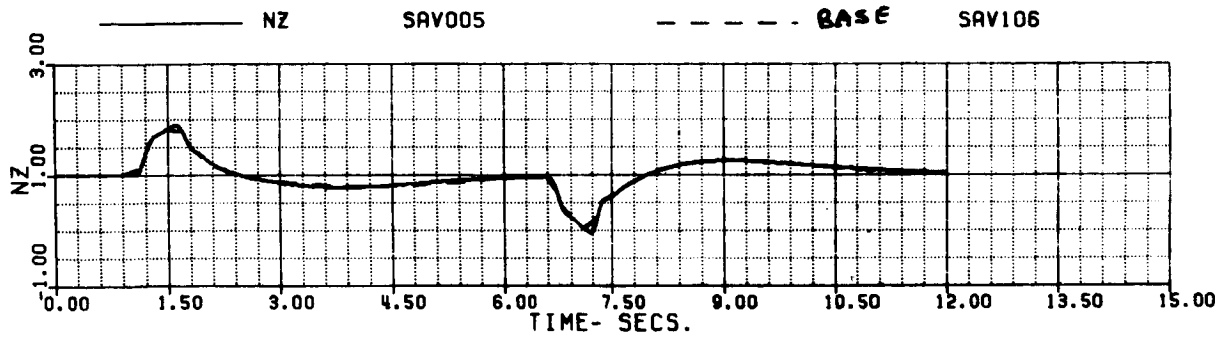

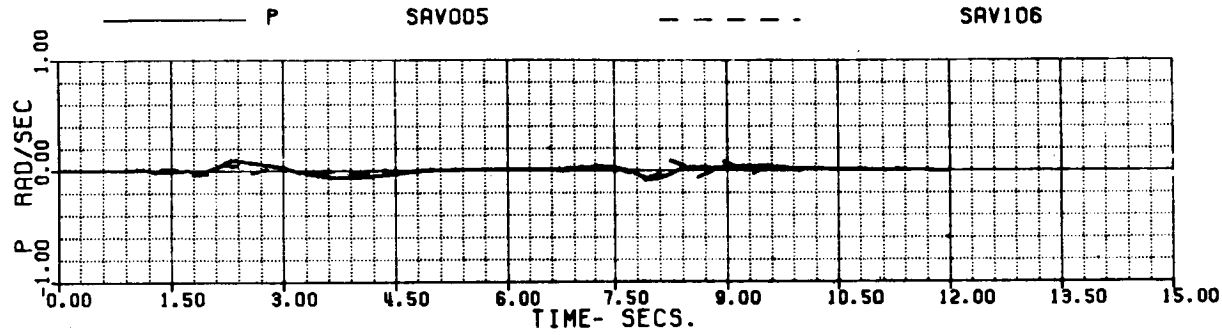

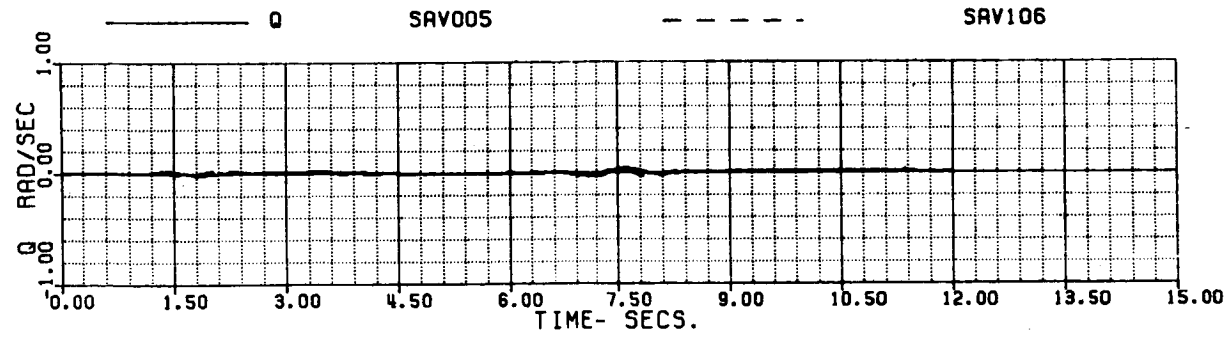

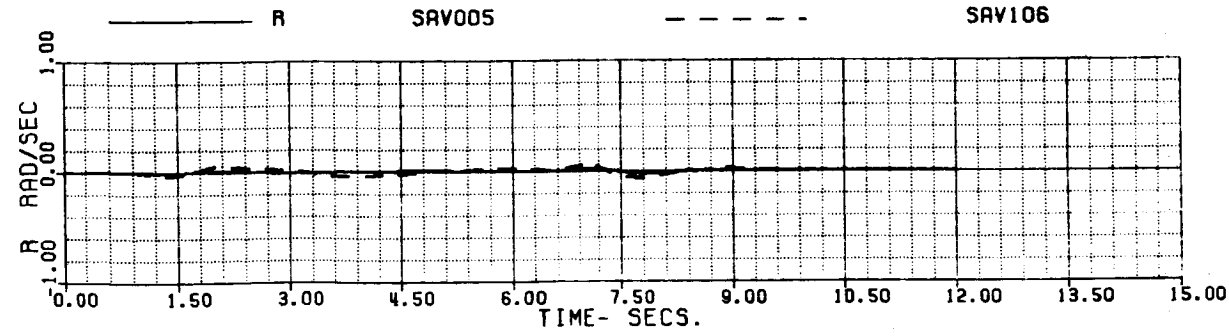

FIG 6.1.5 (b)

60A - BLACK HAWK .
FBOBUP - POPUP/REMASK, INTEGRATED FUEL CONTROL

XA+1	5.3214099	XB+1	-5.7952079	XC+1	5.3291549	XP+1	1.9187516
THETAB	4.0996295	VKT	0.	PHIB	-2.5978147	VTB	0.
XNGE	41775.544	NPINTE	2.4556636	VC	0.	WEIGHT	16638.000
OMAMR	0.9999999	NPMEAS	99.999997				

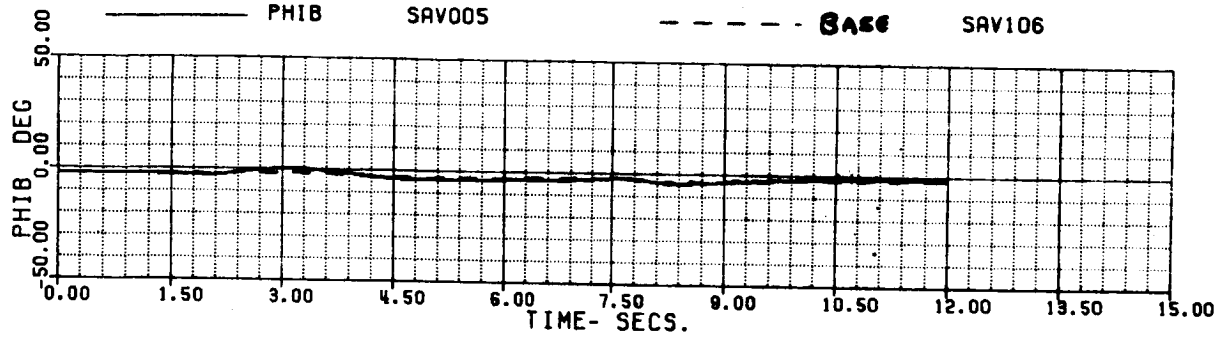

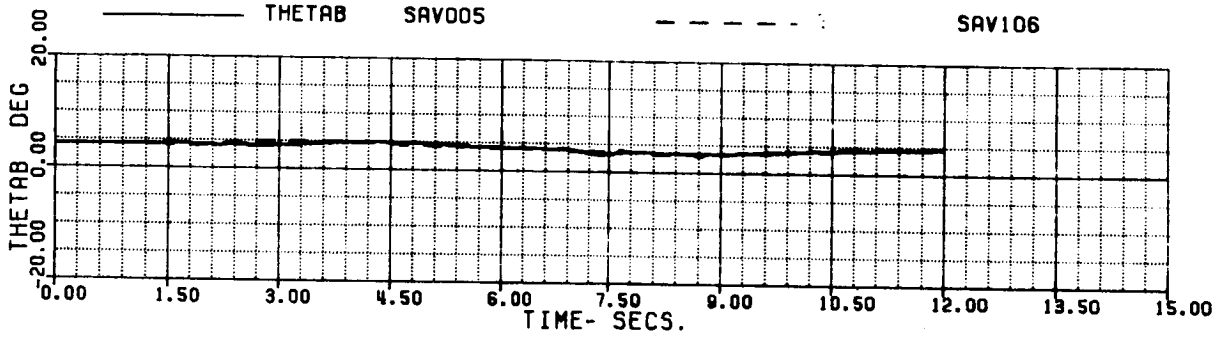

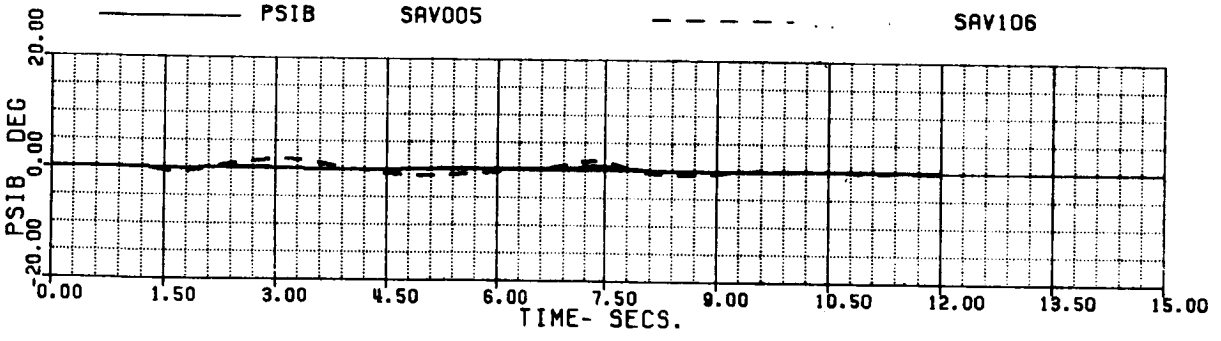

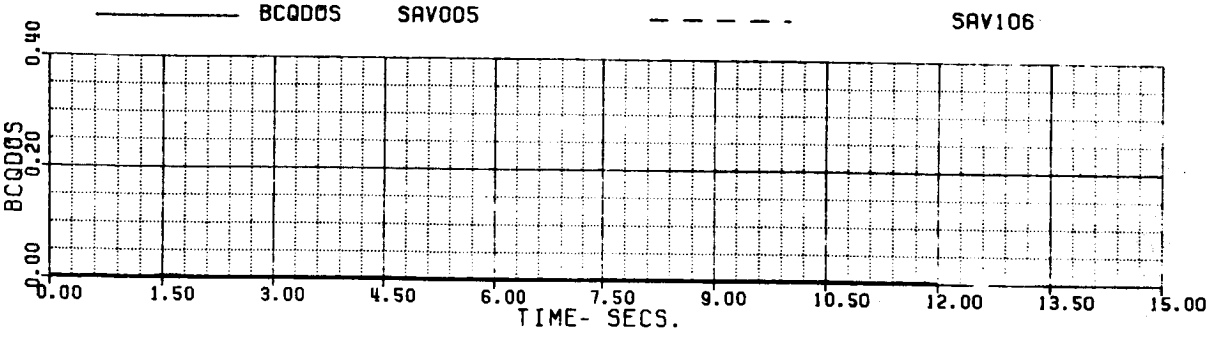

FIG 6.1.5 (c)

60A - BLACK HAWK
FBOBUP - POPUP/REMASK, INTEGRATED FUEL CONTROL

XA+1	5.3214099	XB+1	-5.7952079	XC+1	5.3291549	XP+1	1.9187516
THETAB	4.0996295	VKT	0.	PHIB	-2.5978147	VYB	0.
XNGE	41775.544	NPINTE	2.4556636	VC	0.	WEIGHT	16638.000
OMRMR	0.9999999	NPMEAS	99.999997				

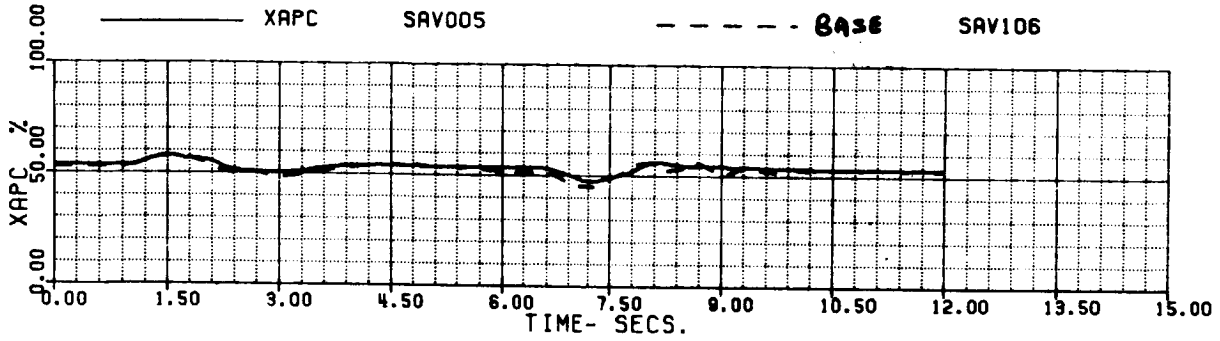

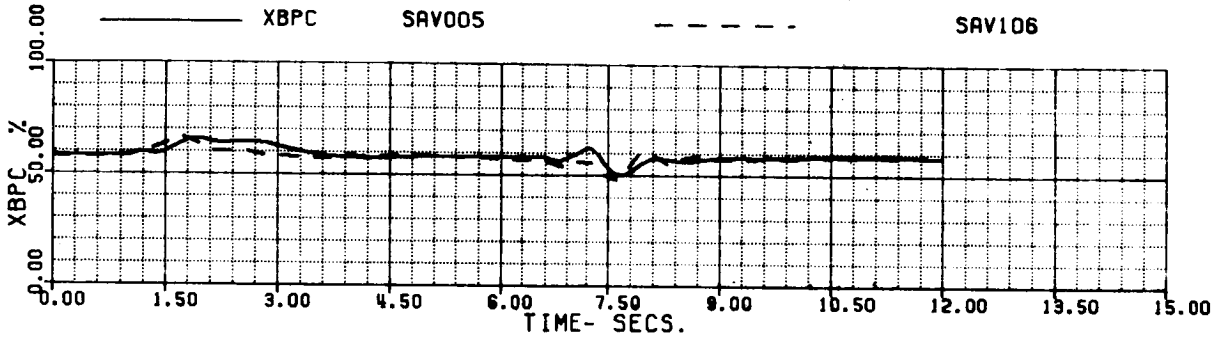

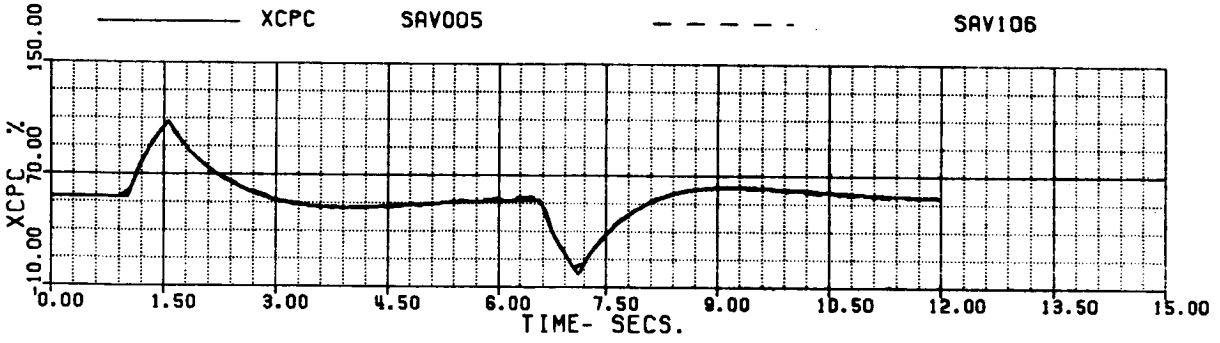

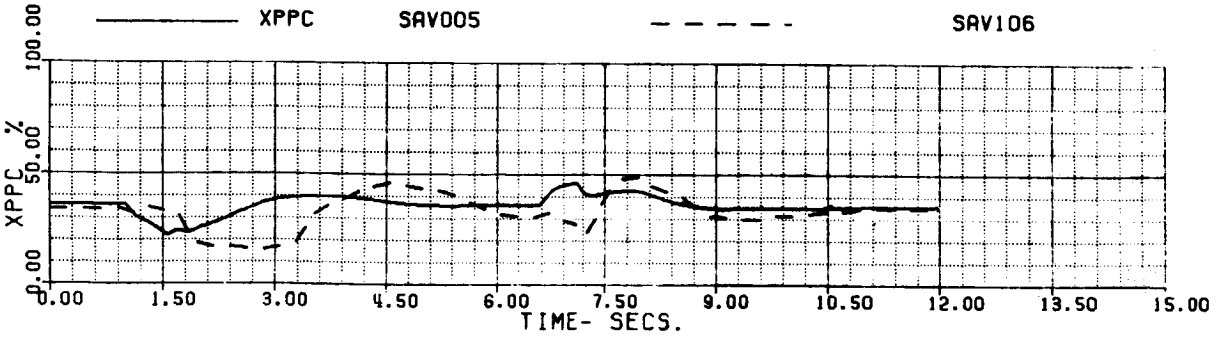

FIG 6.1.5 (d)

60A - BLACK HAWK
FBOBUP - POPUP/REMASK, INTEGRATED FUEL CONTROL

XA+1	5.3214099	XB+1	-5.7952079	XC+1	5.3291549	XP+1	1.9187516
THETAB	4.0996295	VKT	0.	PHIB	-2.5978147	VYB	0.
XNGE	41775.544	NPINTE	2.4556636	VC	0.	WEIGHT	16638.000
OMRMR	0.9999999	NPMEAS	99.999997				

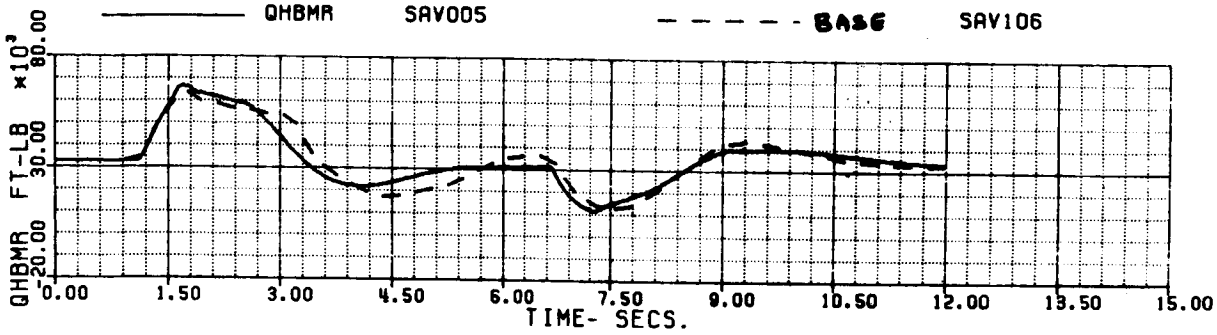

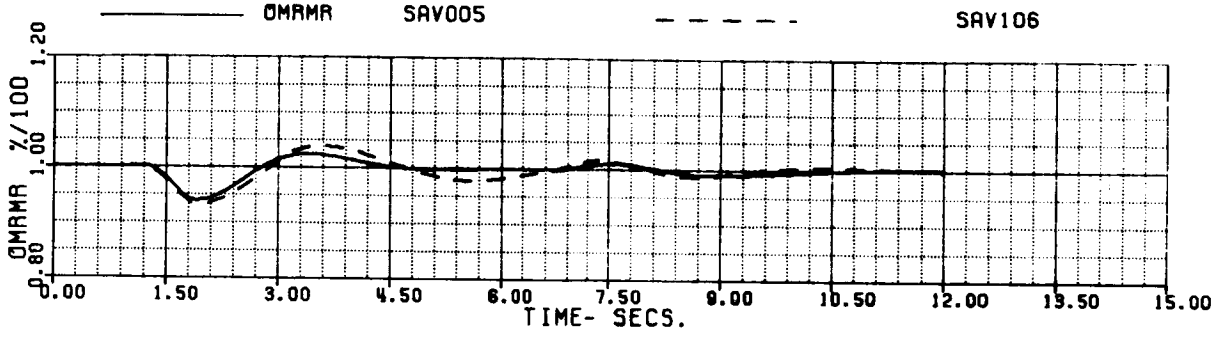

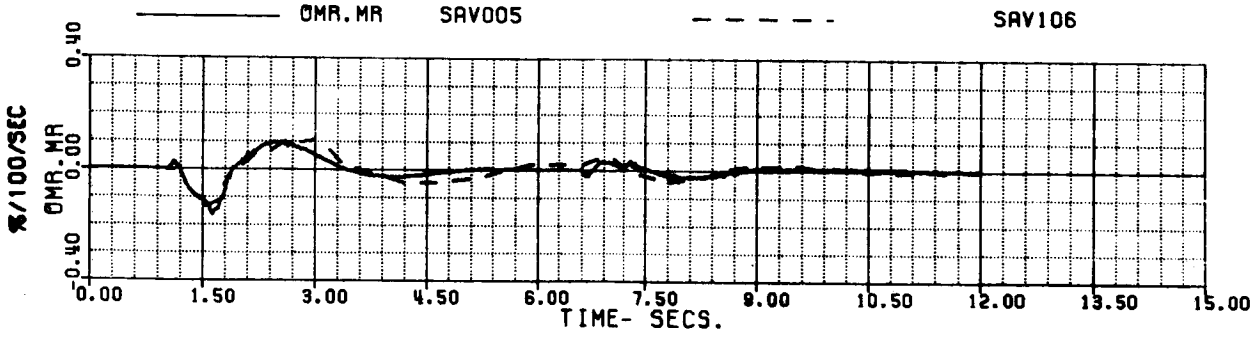

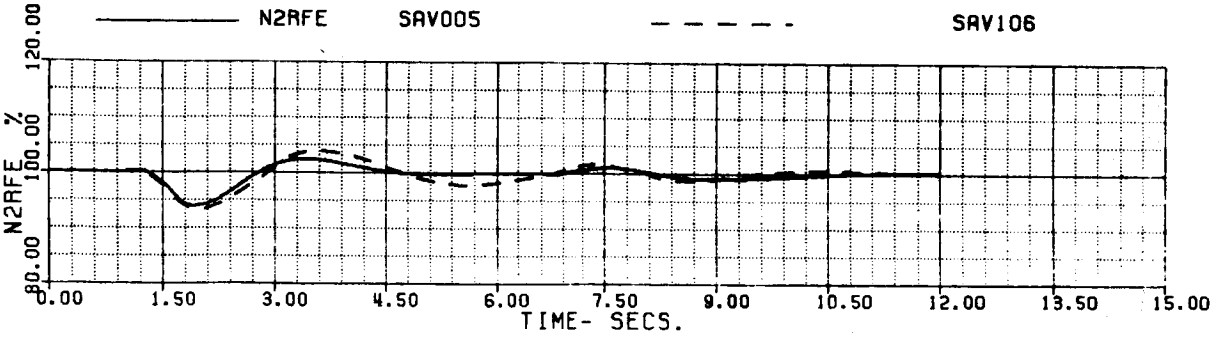

FIG 6.1.5 (e)

60A - BLACK HAWK

FBOBUP - POPUP/REMASK, INTEGRATED FUEL CONTROL

XA+1	5.3214099	XB+1	-5.7952079	XC+1	5.3291549	XP+1	1.9187516
THETAB	4.0996295	VKT	0.	PHIB	-2.5978147	VYB	0.
XNGE	41775.544	NPINTE	2.4556636	VC	0.	WEIGHT	16638.000
OMRMR	0.9999999	NPMEAS	99.999997				

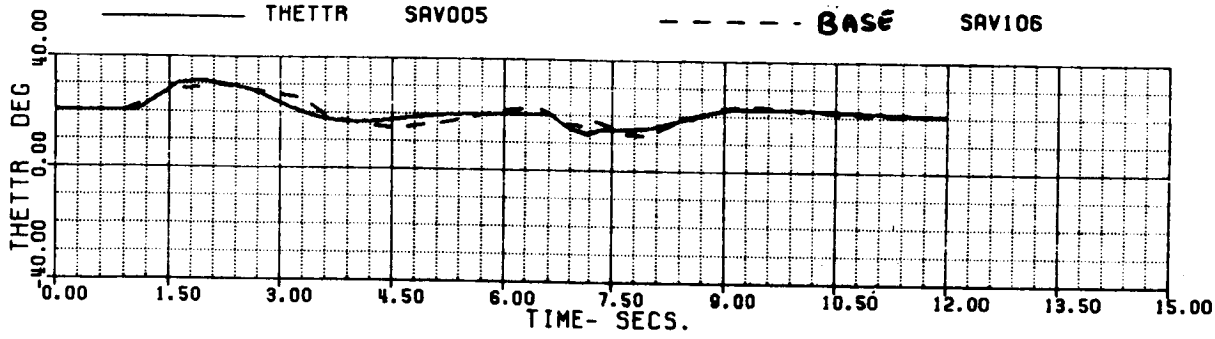

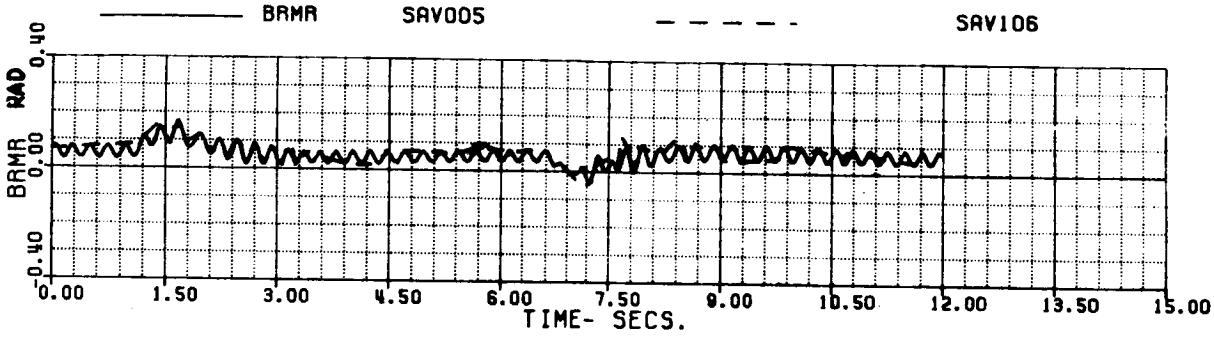

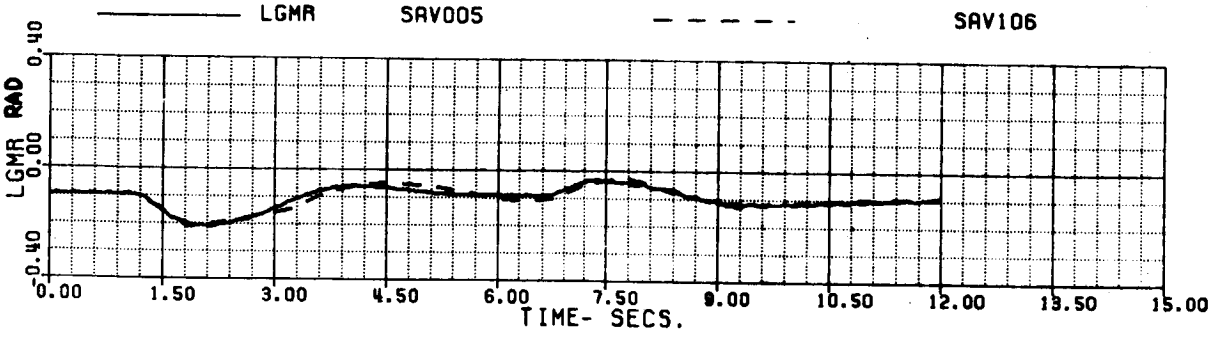

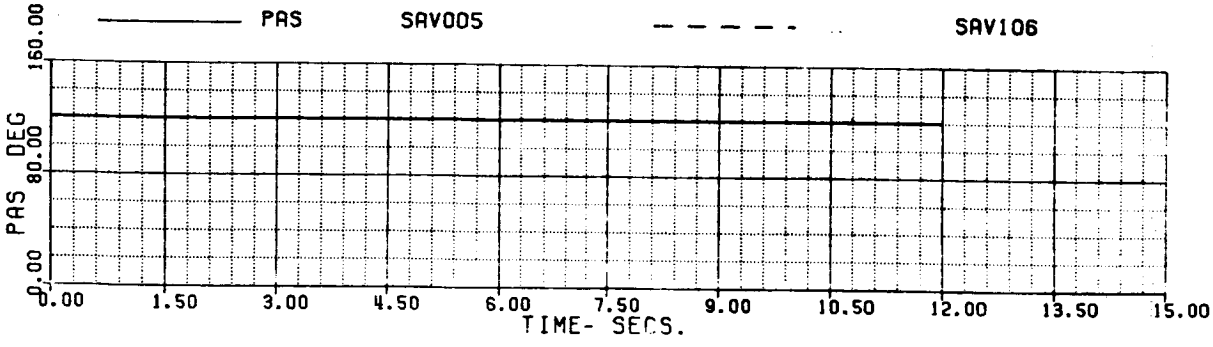

FIG 6.1.5 (f)

60A - BLACK HAWK

FBOBUP - POPUP/REMASK, INTEGRATED FUEL CONTROL

XA+1	5.3214099	XB+.	-5.7952079	XC+1	5.3291549	XP+1	1.9187516
THETAB	4.0996295	VKT	0.	PHIB	-2.5978147	VYB	0.
XNGE	41775.544	NPINTE	2.4556636	VC	0.	WEIGHT	16638.000
OMRMR	0.9999999	NPMEAS	99.999997				

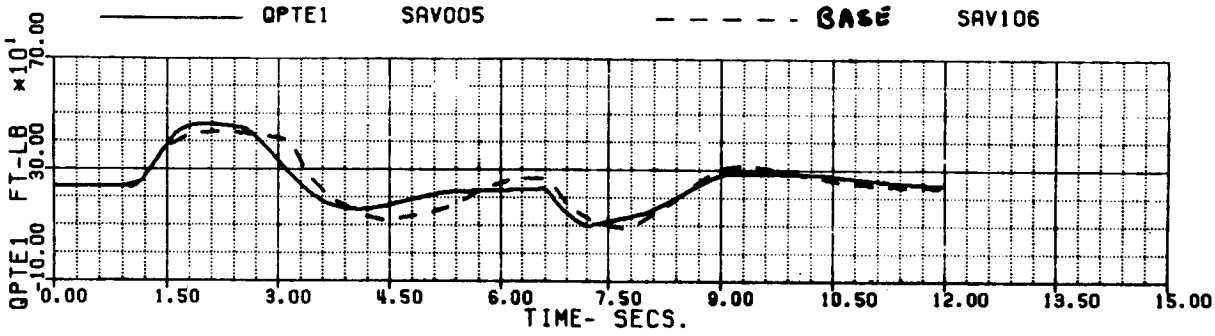

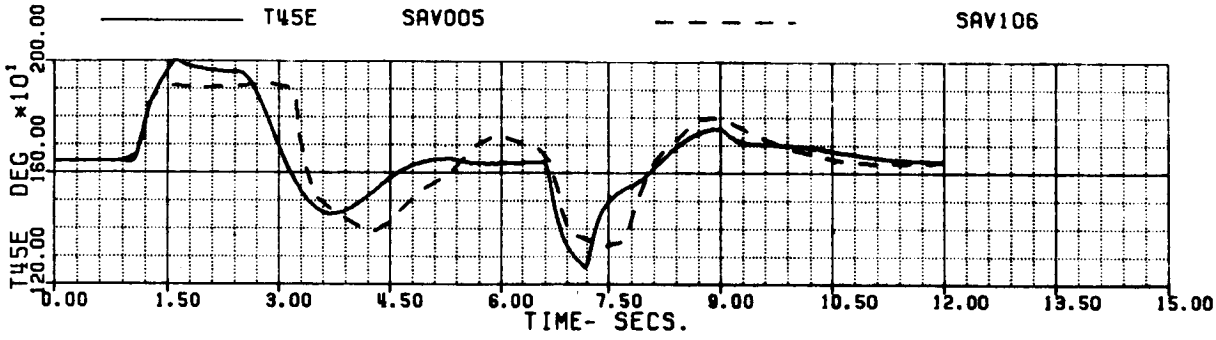

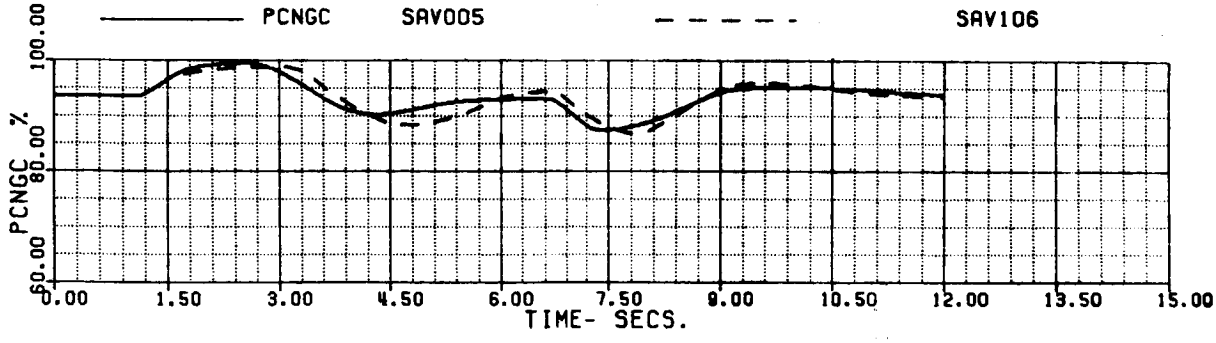

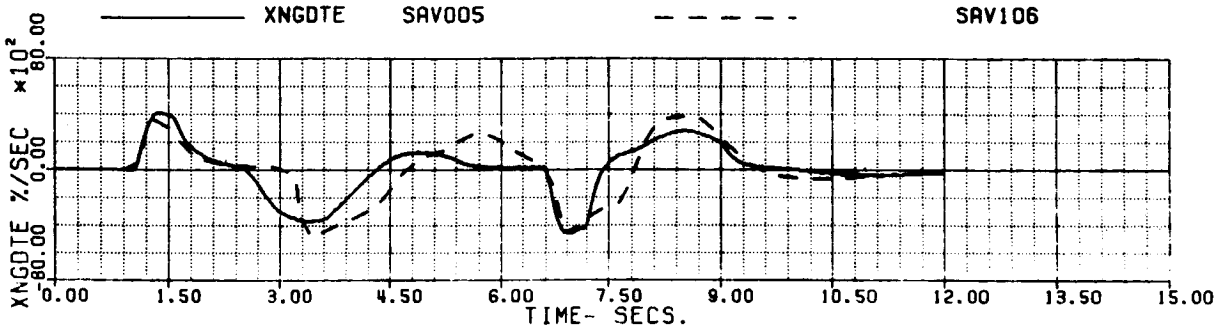

FIG 6.1.5 (g)

60A - BLACK HAWK

FBOBUP - POPUP/REMASK, INTEGRATED FUEL CONTROL

XA+1	5.3214099	XB+1	-5.7952079	XC+1	5.3291549	XP+1	1.9187516
THETAB	4.0996295	VKT	0.	PHIB	-2.5978147	VYB	0.
XNGE	41775.544	NPINTE	2.4556636	VC	0.	WEIGHT	16638.000
OMRMR	0.9999999	NPMEAS	99.999997				

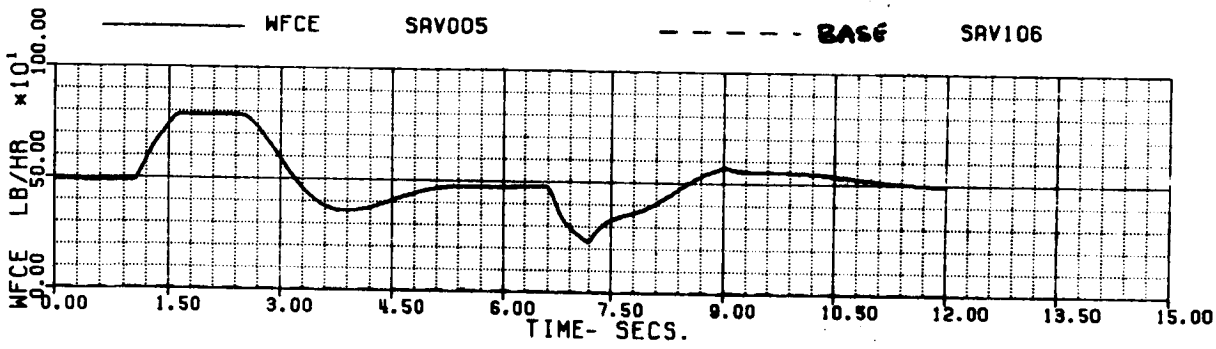

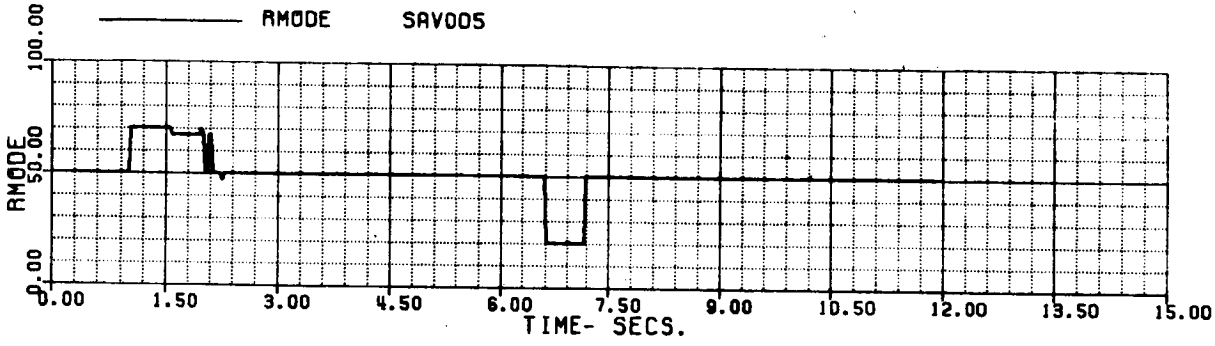

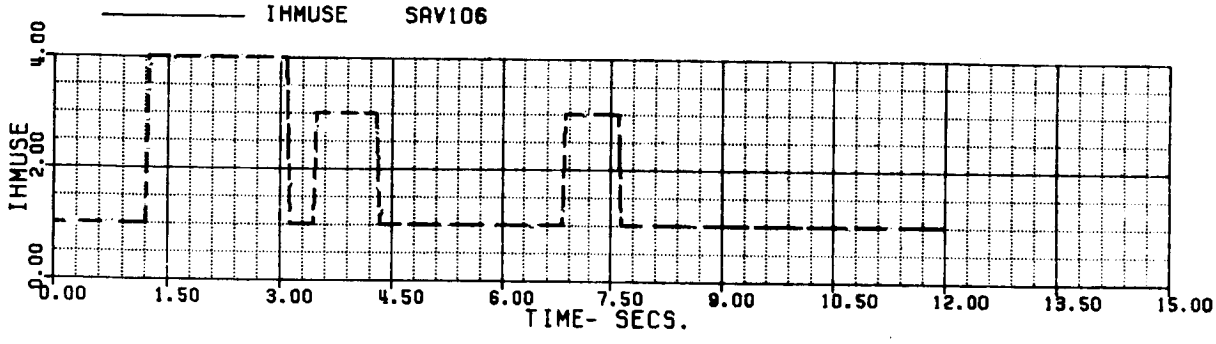

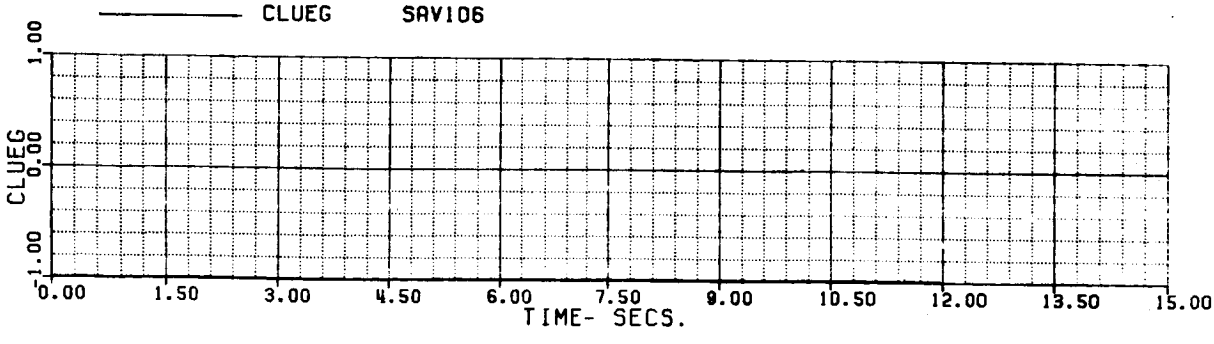

FIG 6.1.5 (h)

60A - BLACK HAWK

FB0BUP - POPUP/REMASK, INTEGRATED FUEL CONTROL

XA+1	5.3214099	XB+1	-5.7952079	XC+1	5.3291549	XP+1	1.9187516
THETAB	4.0996295	VKT	0.	PHIB	-2.5978147	VYB	0.
XNGE	41775.544	NPINTE	2.4556636	VC	0.	WEIGHT	16638.000
OMRMR	0.9999999	NPMEAS	99.999997				

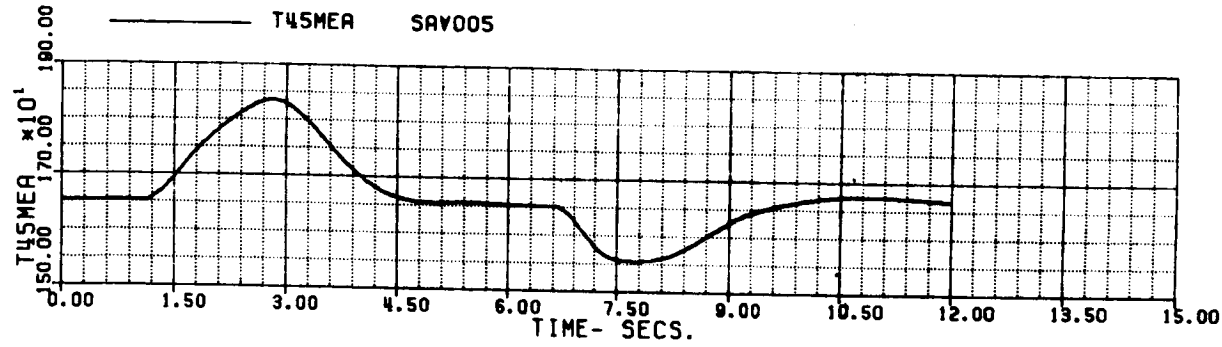

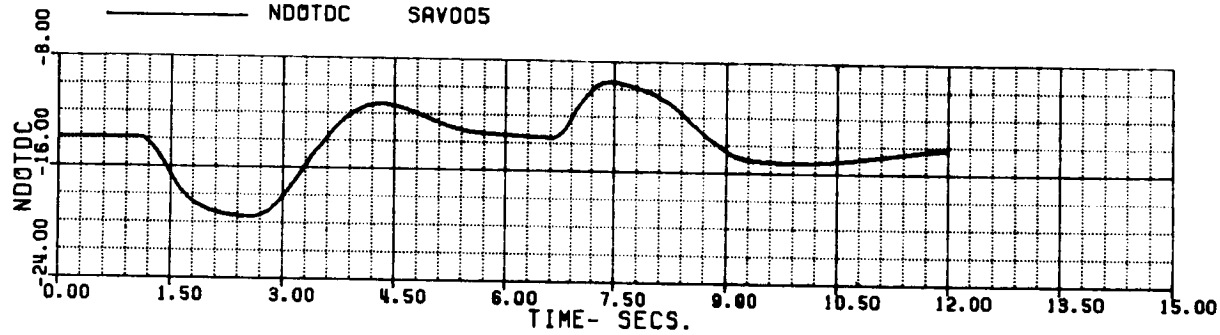

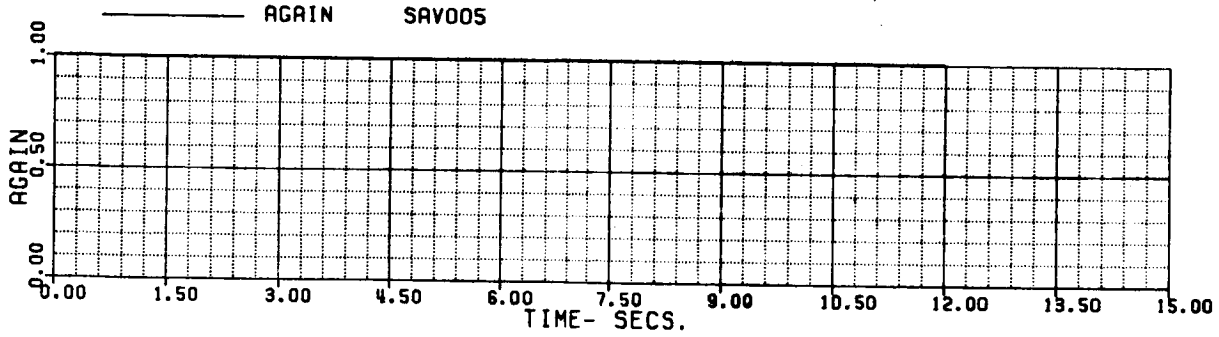

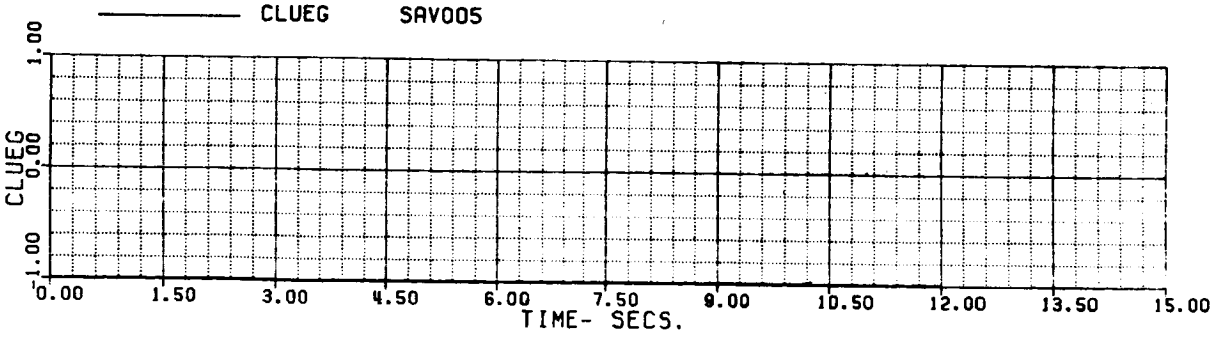

FIG 6.1.5 (i)

60A - BLACK HAWK
FBOBUP - POPUP/REMASK, INTEGRATED FUEL CONTROL

XA+1	5.3214099	XB+1	-5.7952079	XC+1	5.3291549	XP+1	1.9187516
THETAB	4.0996295	VKT	0.	PHIB	-2.5978147	VYB	0.
XNGE	41775.544	NPINTE	2.4556636	VC	0.	WEIGHT	16638.000
OMRMR	0.9999999	NPMEAS	99.999997				

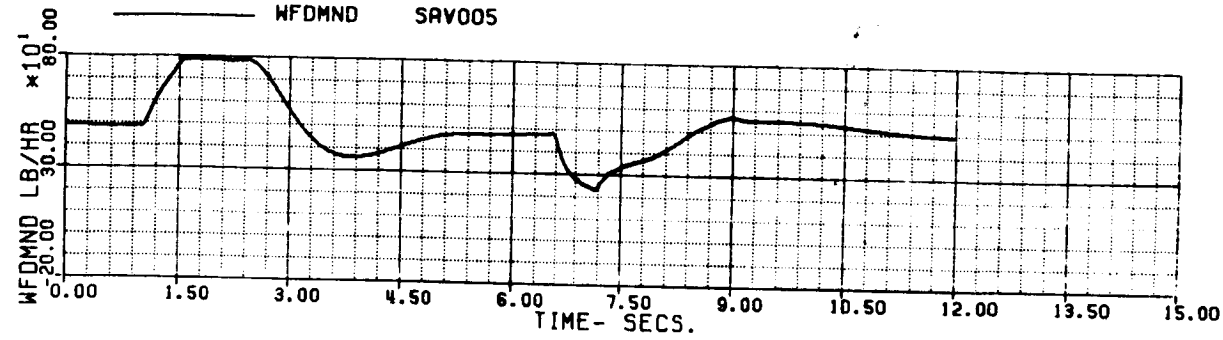

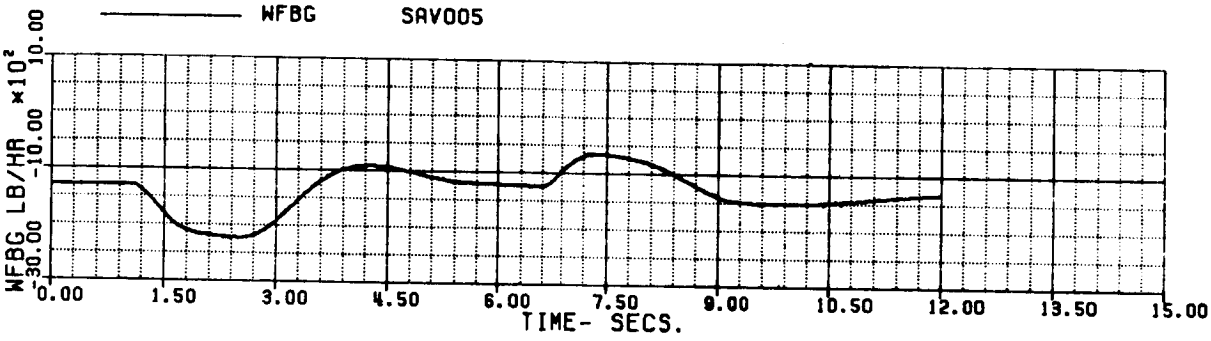

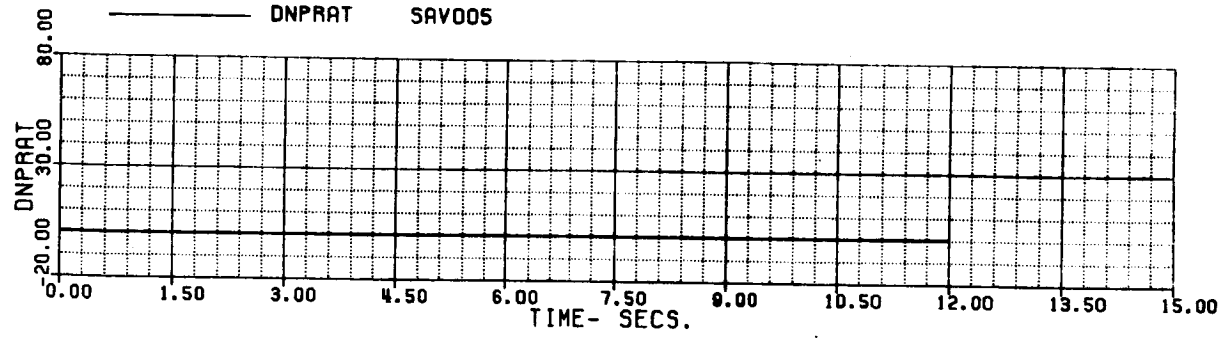

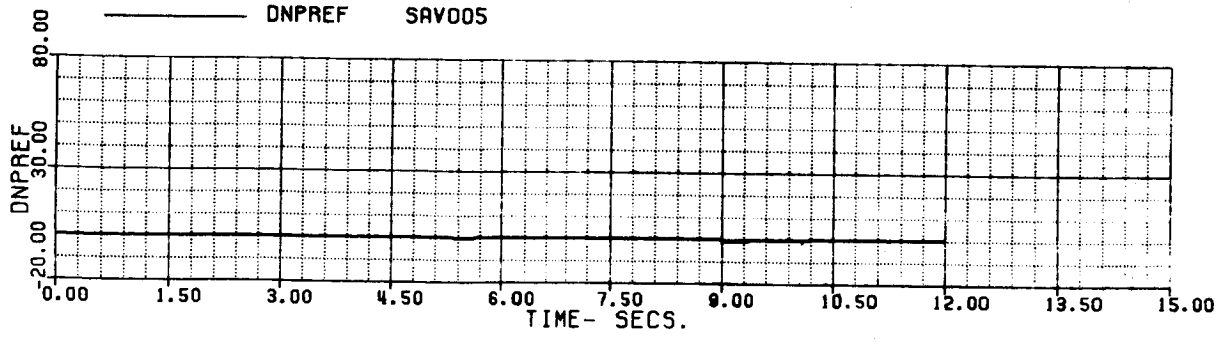

FIG 6.1.5 (j)

60A - BLACK HAWK
FBOBUP - POPUP/REMASK, INTEGRATED FUEL CONTROL

XA+1	5.3214099	XB+1	-5.7952079	XC+1	5.3291549	XP+1	1.9187516
THETAB	4.0996295	VKT	0.	PHIB	-2.5978147	VYB	0.
XNGE	41775.544	NPINTE	2.4556636	VC	0.	WEIGHT	16638.000
OMRMR	0.9999999	NPMEAS	99.999997				

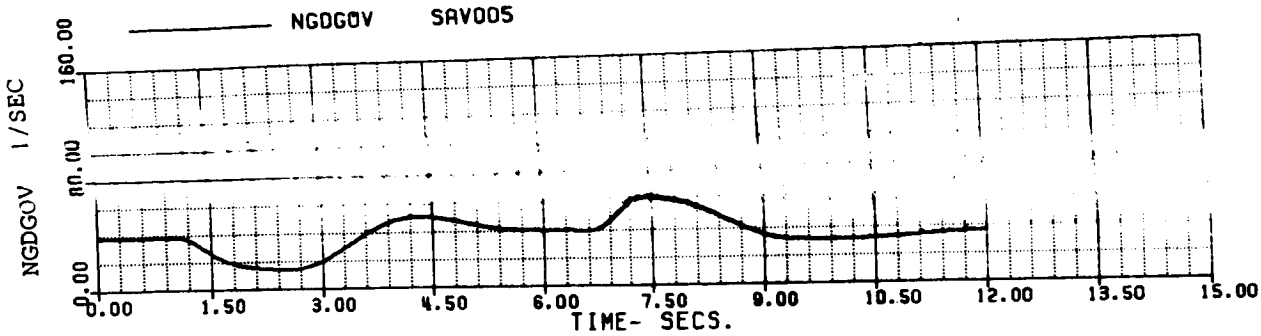

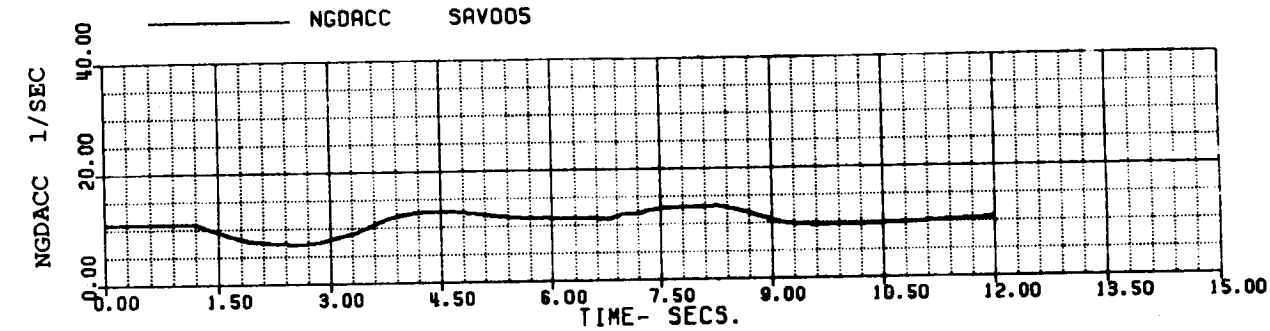

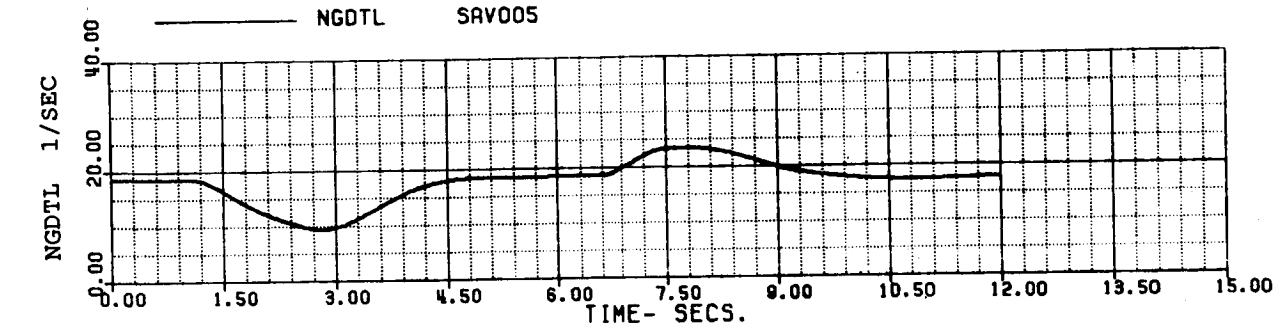

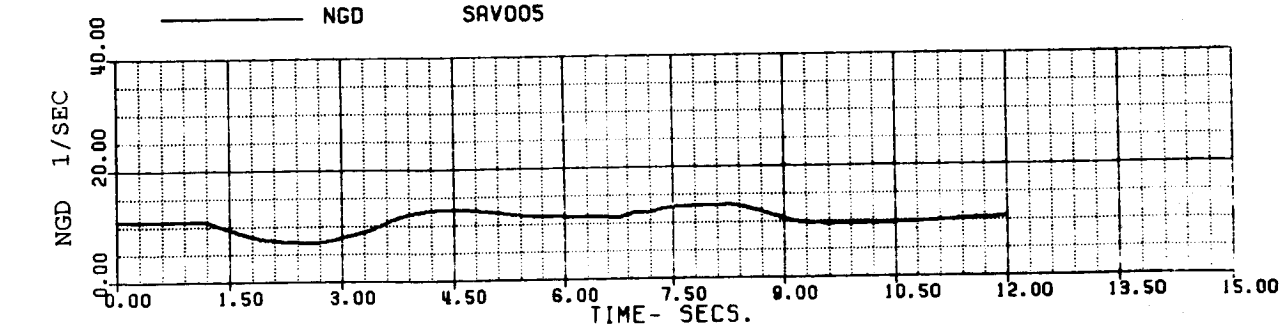

FIG 6.1.5 (k)

60A - BLACK HAWK

(1/12)

FQKSTQ - QUICK STOP, INTEGRATED FUEL CONTROL
135 KTS TO HOVER

XA+1	5.8210167	XB+1	-3.3724294	XC+1	6.5927867	XP+1	3.2154287
THETAB	-2.1868543	VKT	135.00311	PHIB	0.	VYB	-1.5475518
XNGE	41783.796	NPINTE	1.3112399	VC	-.45061E-3	WEIGHT	16638.000
OMRMR	0.9999999	NPMEAS	99.999999				

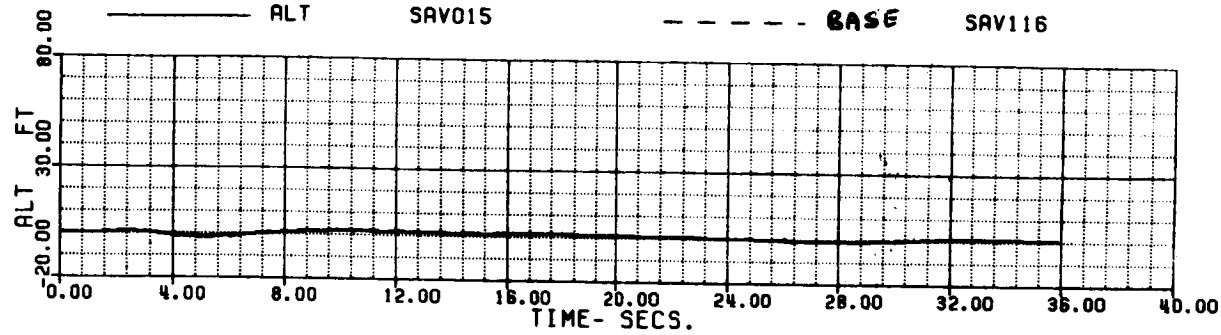

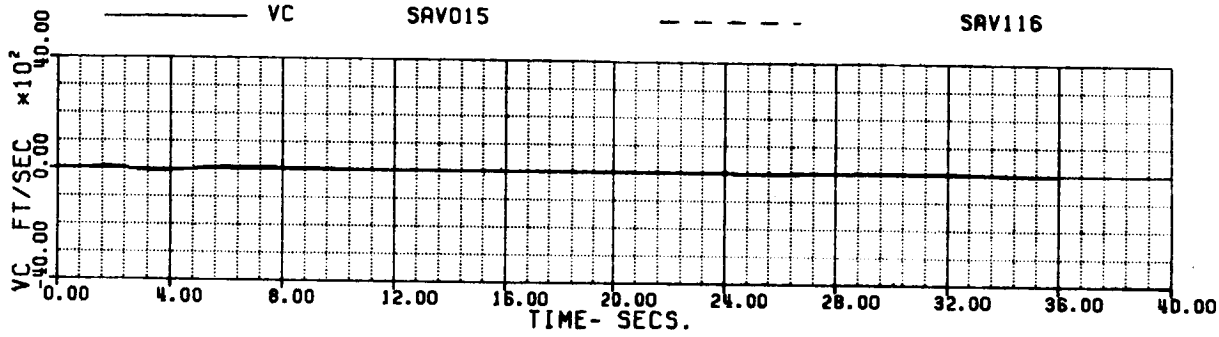

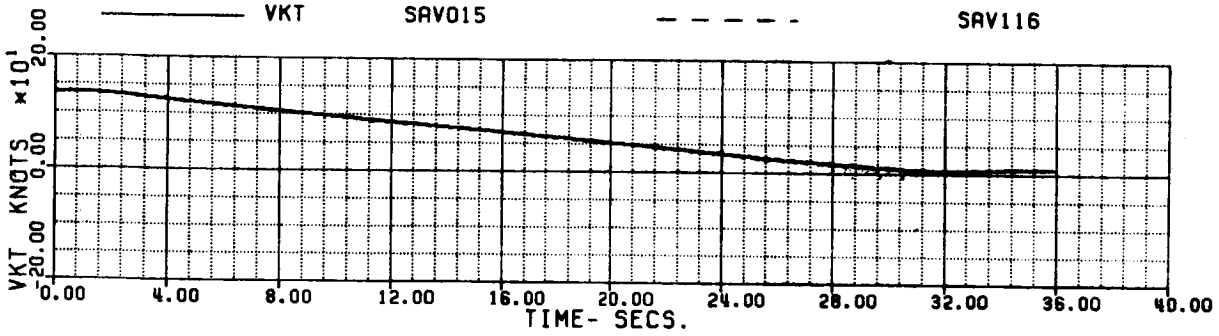

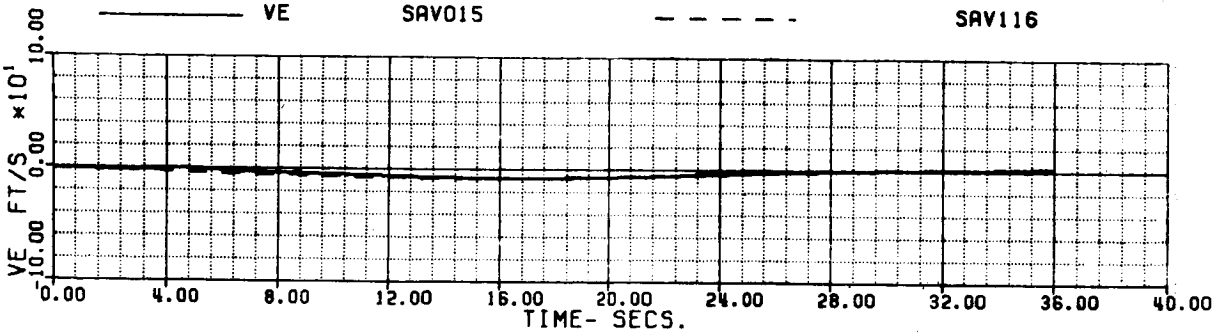

SIMULATED QUICK STOP

FIG 6.1.6 (a)

60A - BLACK HAWK

FQKSTO - QUICK STOP, INTEGRATED FUEL CONTROL
135 KTS TO HOVER

(2/12)

XA+1	5.8210167	XB+1	-3.3724294	XC+1	6.5927867	XP+1	3.2154287
THETAB	-2.1868543	VKT	135.00311	PHIB	0.	VYB	-1.5475518
XNGE	41783.796	NPINTE	1.3112399	VC	-.45061E-3	WEIGHT	16638.000
OMRMR	0.9999999	NPMEAS	99.999999				

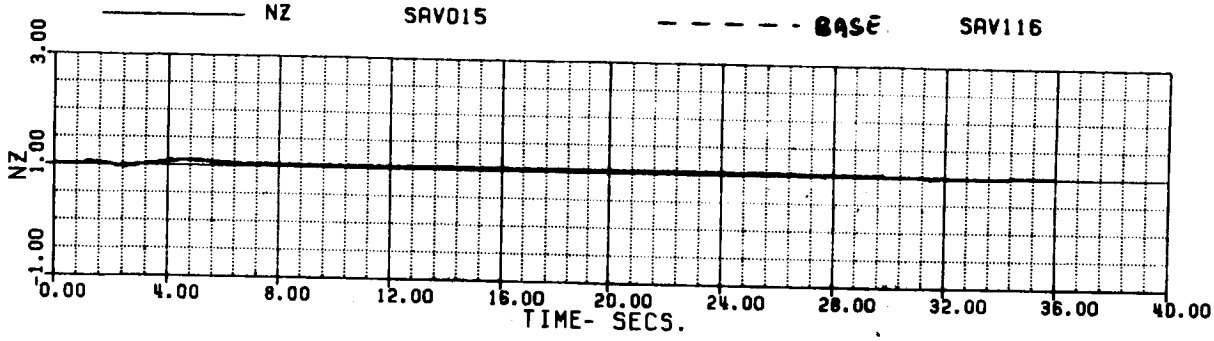

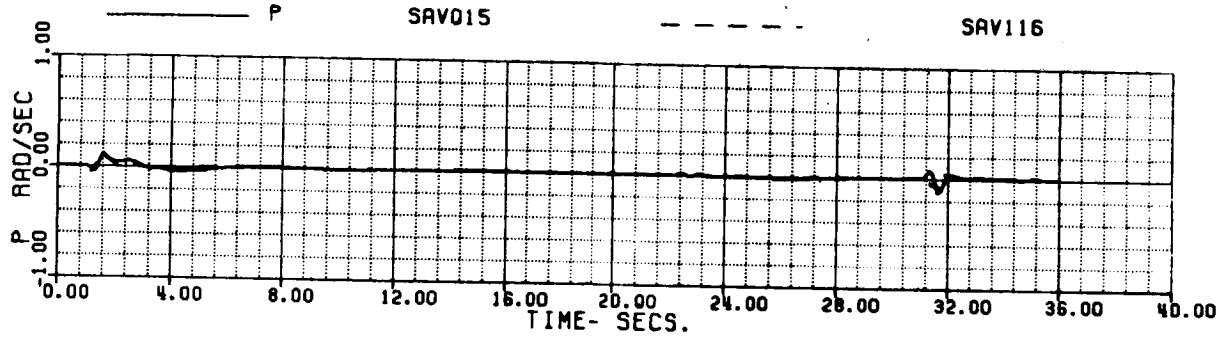

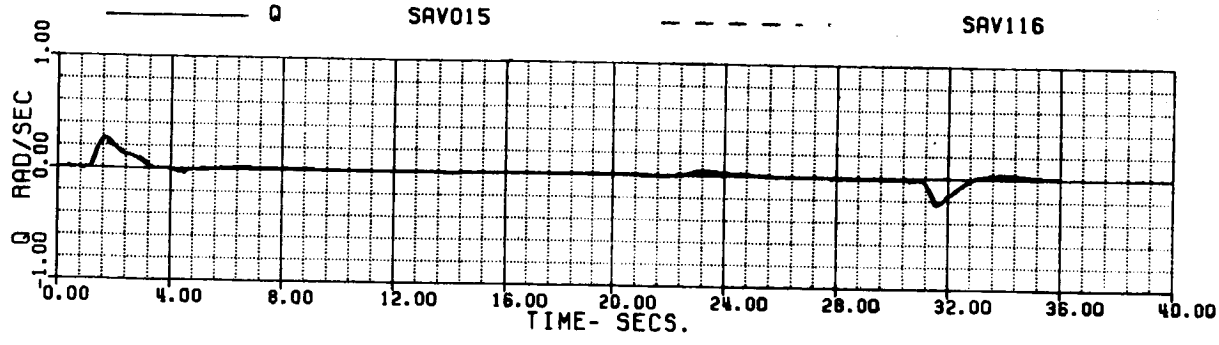

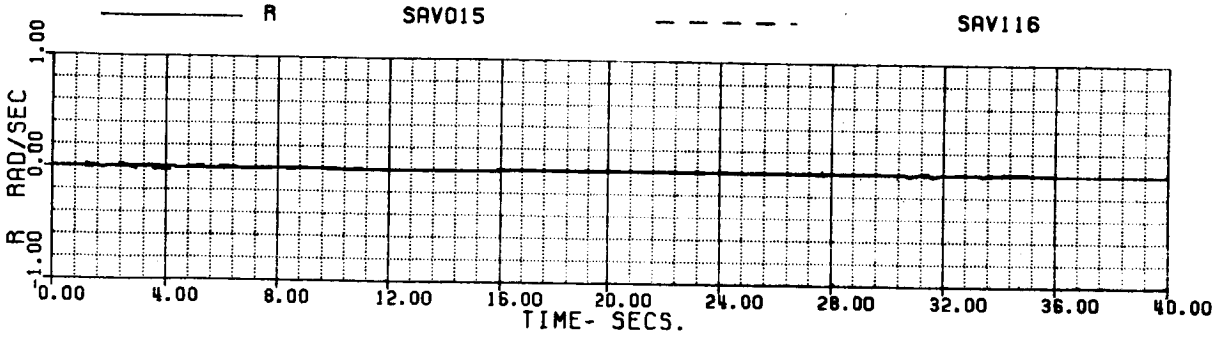

FIG 6.1.6 (b)

60A - BLACK HAWK (3/12)

FQKSTO - QUICK STOP, INTEGRATED FUEL CONTROL
135 KTS TO HOVER

XA+1	5.8210167	XB+1	-3.3724294	XC+1	6.5927867	XP+1	3.2154287
THETAB	-2.1868543	VKT	135.00311	PHIB	0.	VYB	-1.5475518
XNGE	41783.796	NPINTE	1.3112399	VC	-.45061E-3	WEIGHT	16638.000
OMRMR	0.9999999	NPMEAS	99.999999				

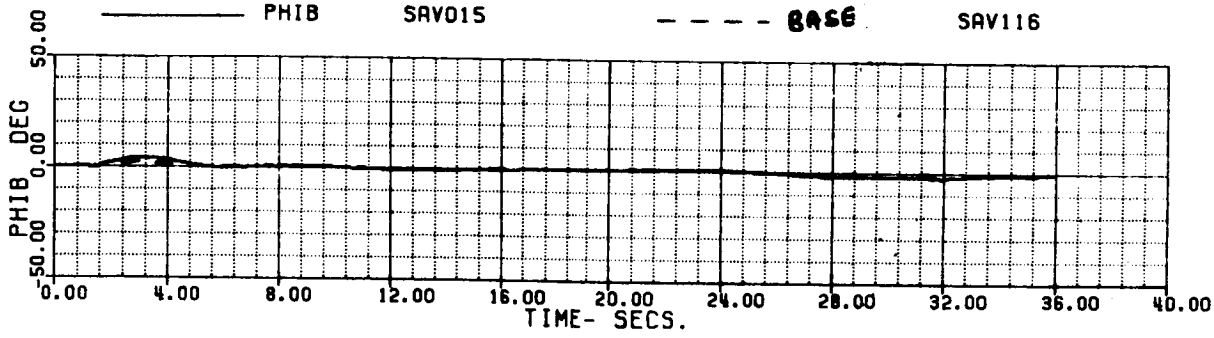

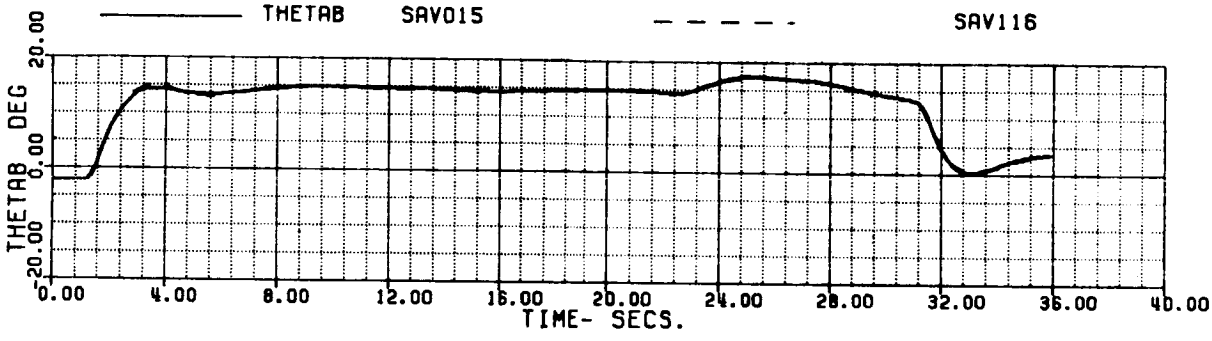

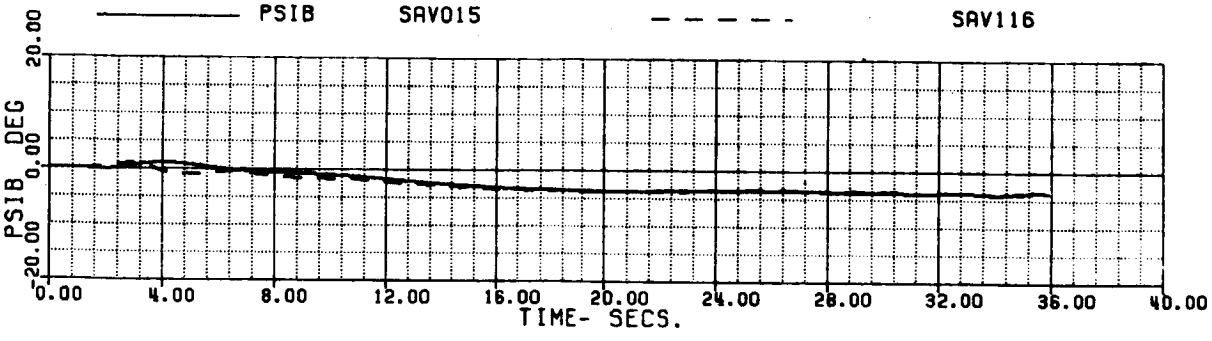

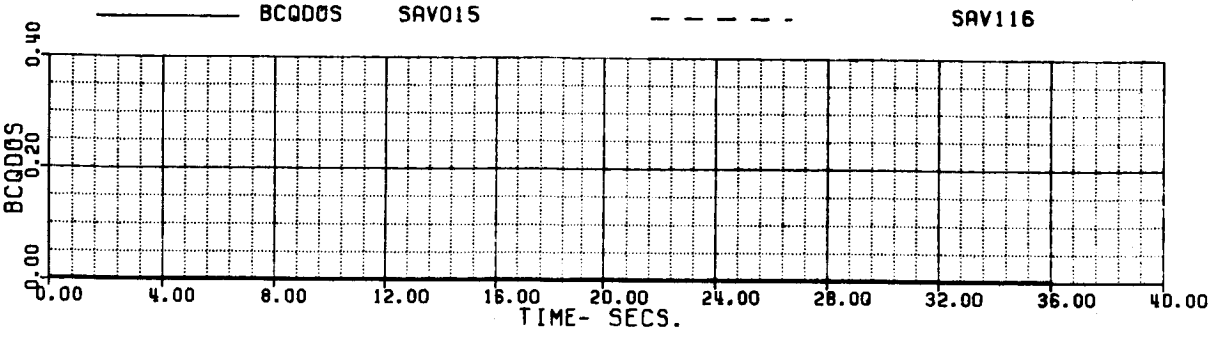

FIG 6.1.6 (c)

60A - BLACK HAWK (4/12)

FQKSTQ - QUICK STOP, INTEGRATED FUEL CONTROL
135 KTS TO HOVER

XA+1	5.8210167	XB+1	-3.3724294	XC+1	6.5927867	XP+1	3.2154287
THETAB	-2.1868543	VKT	135.00311	PHIB	0.	VYB	-1.5475518
XNGE	41783.796	NPINTE	1.3112399	VC	-.45061E-3	WEIGHT	16638.000
OMRMR	0.9999999	NPMEAS	99.999999				

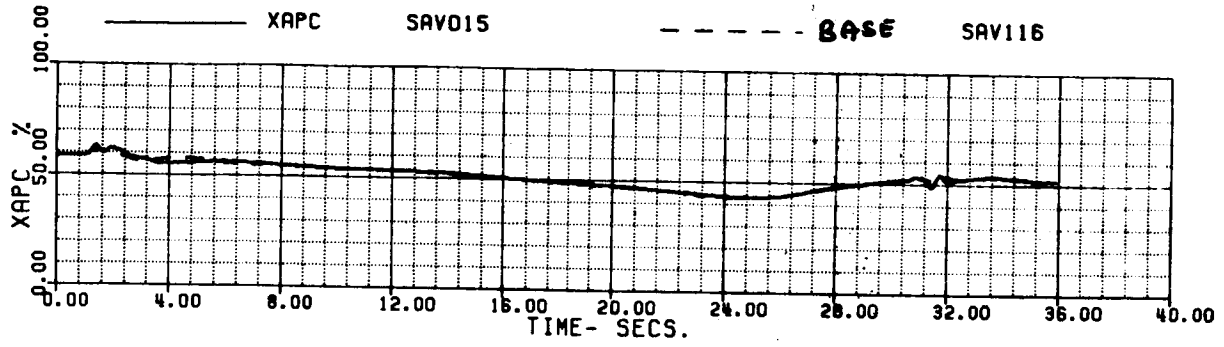

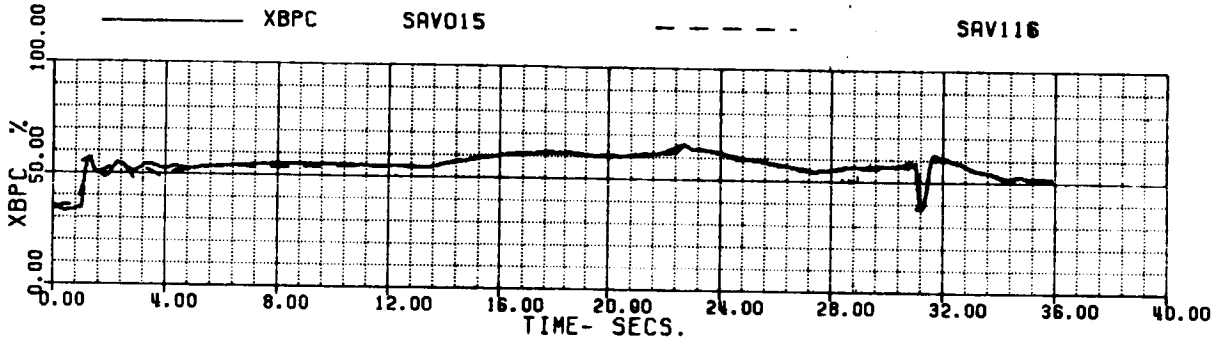

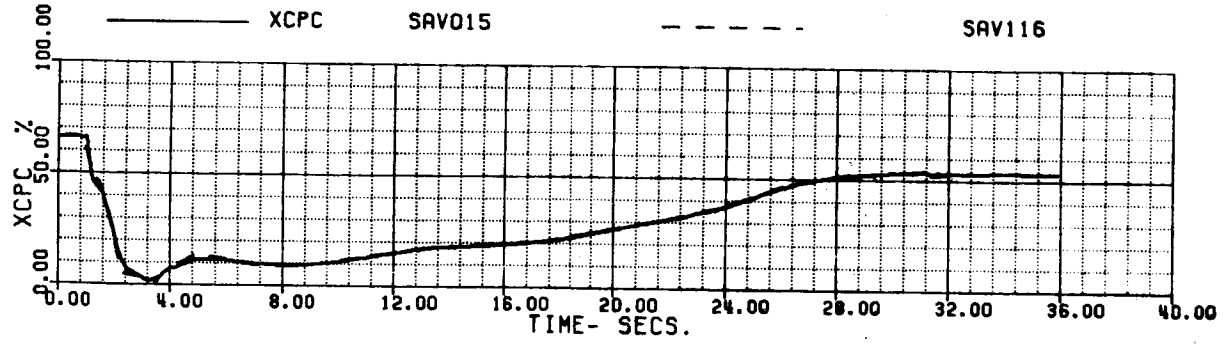

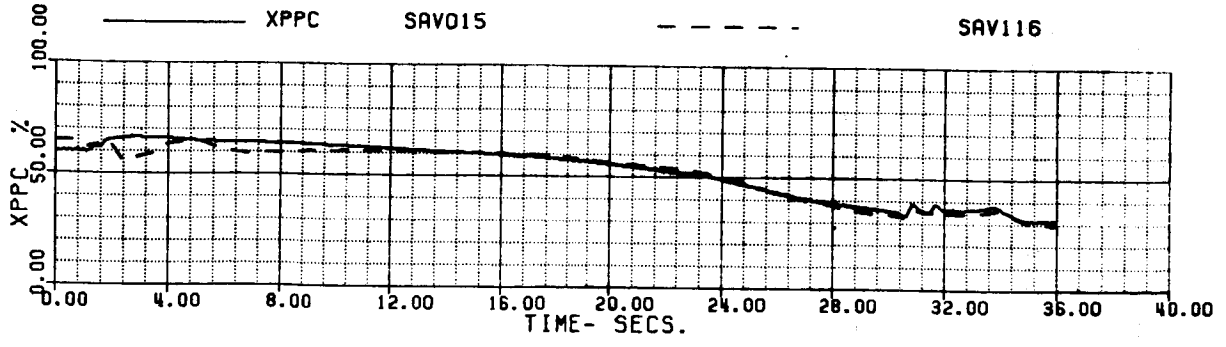

FIG 6.1.6 (d)

60A - BLACK HAWK

FQKSTQ - QUICK STOP, INTEGRATED FUEL CONTROL
135 KTS TO HOVER

(5/12)

XA+1	5.8210167	XB+1	-3.3724294	XC+1	6.5927867	XP+1	3.2154287
THETAB	-2.1868543	VKT	135.00311	PHIB	0.	VTB	-1.5475518
XNGE	41783.796	NPINTE	1.3112399	VC	-.45061E-3	WEIGHT	16638.000
OMRMR	0.9999999	NPMEAS	99.999999				

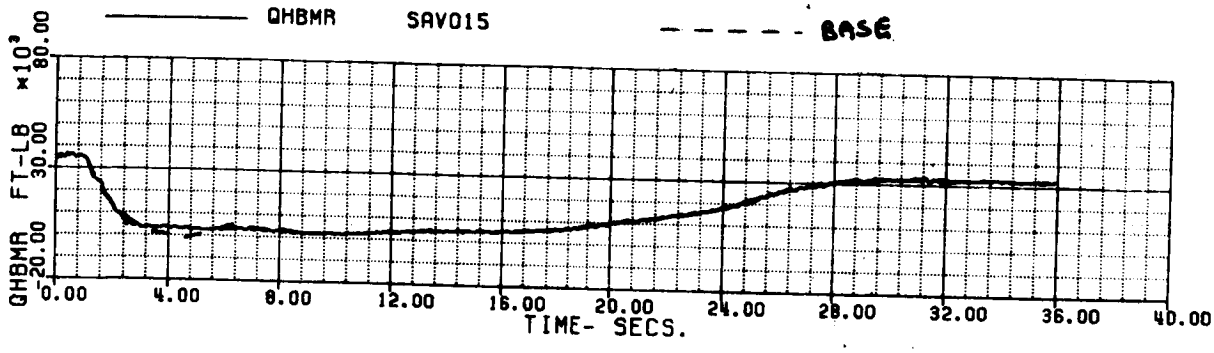

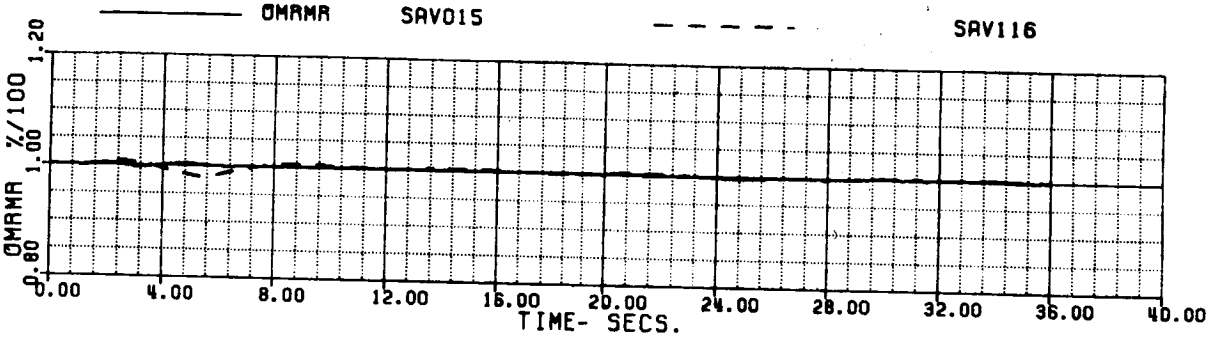

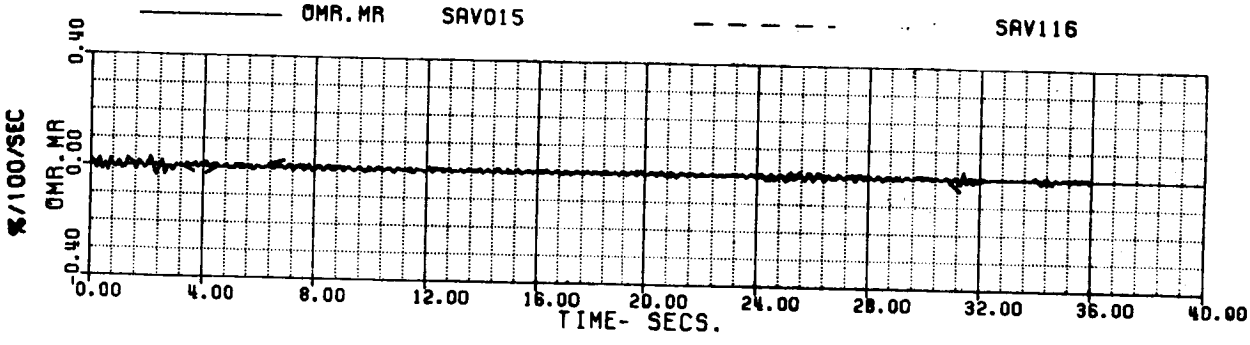

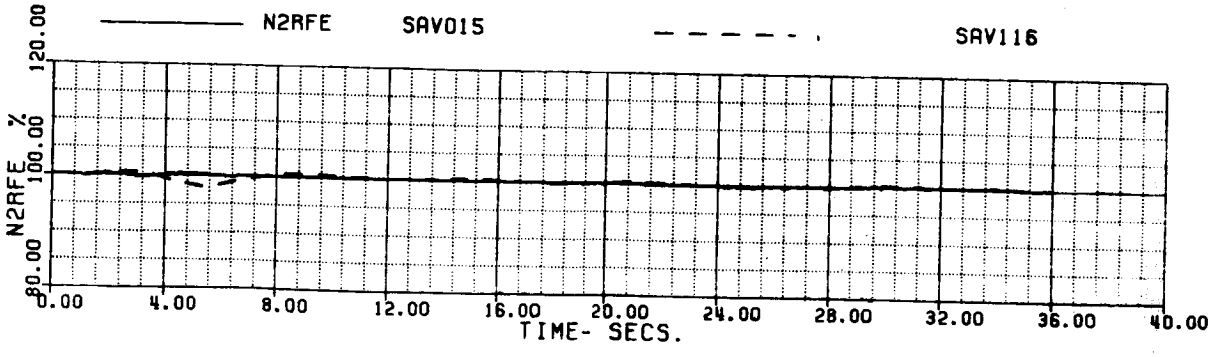

FIG 6.1.6 (e)

60A - BLACK HAWK (6/12)

FQKSTQ - QUICK STOP, INTEGRATED FUEL CONTROL
135 KTS TO HOVER

XA+1	5.8210167	XB+1	-3.3724294	XC+1	6.5927867	XP+1	3.2154287
THETAB	-2.1868543	VKT	135.00311	PHIB	0.	VYB	-1.5475518
XNGE	41783.796	NPINTE	1.3112399	VC	-.45061E-3	WEIGHT	16638.000
OMRMR	0.9999999	NPMEAS	99.999999				

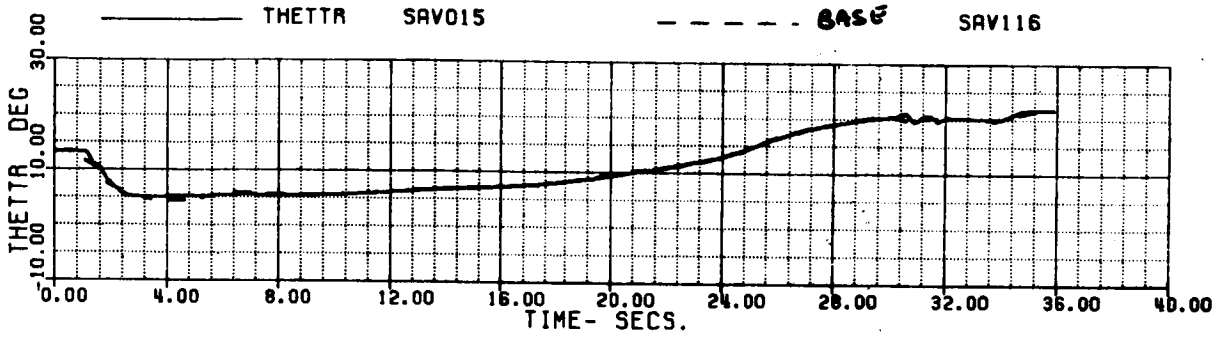

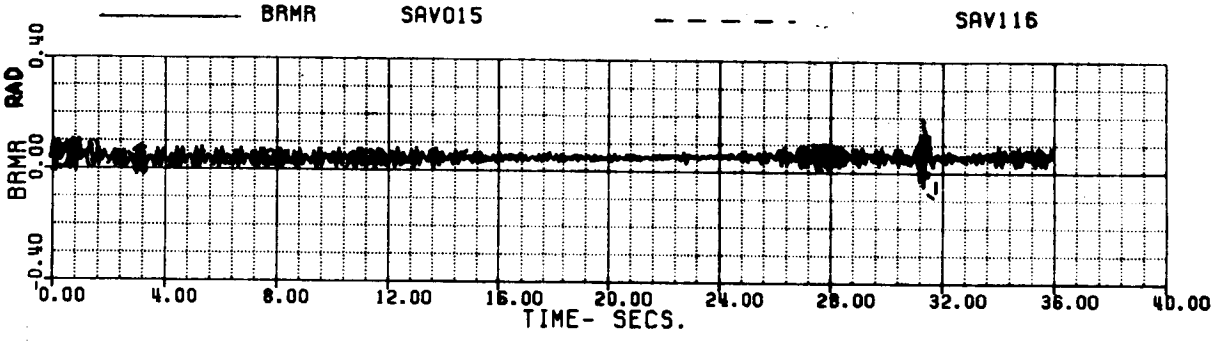

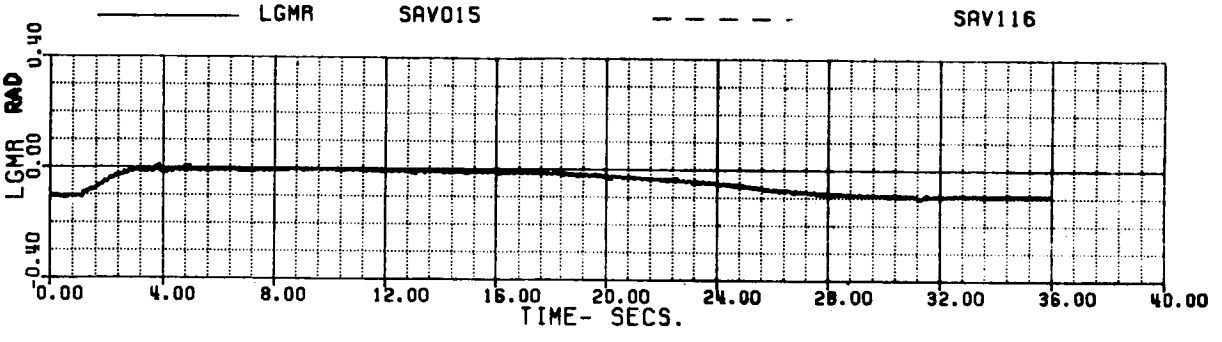

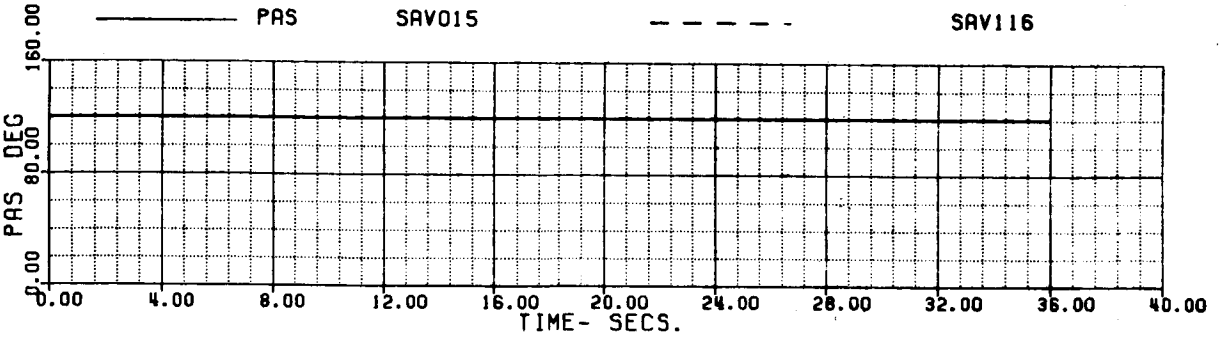

FIG 6.1.6 (f)

60A - BLACK HAWK

(7/12)

FQKSTO - QUICK STOP, ...EGRATED FUEL CONTROL
135 KTS TO HOVER

XA+1	5.8210167	XB+1	-3.3724294	XC+1	6.5927867	XP+1	3.2154287
THETAB	-2.1868543	VKT	135.00311	PHIB	0.	YTB	-1.5475518
XNGE	41783.796	NPINTE	1.3112399	VC	-.45061E-3	WEIGHT	16638.000
OMRMR	0.9999999	NPMEAS	99.999999				

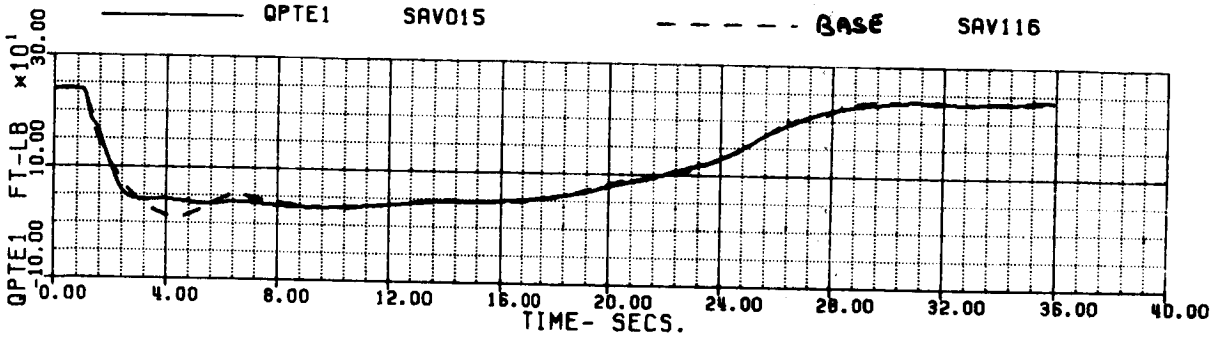

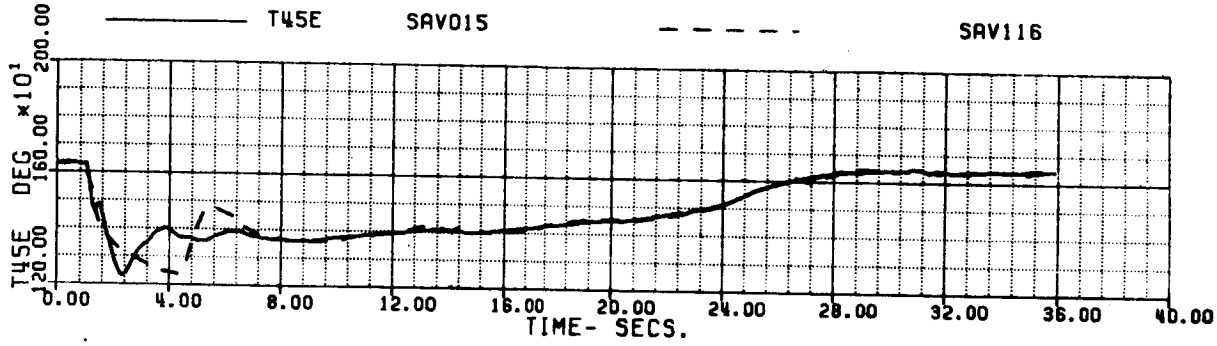

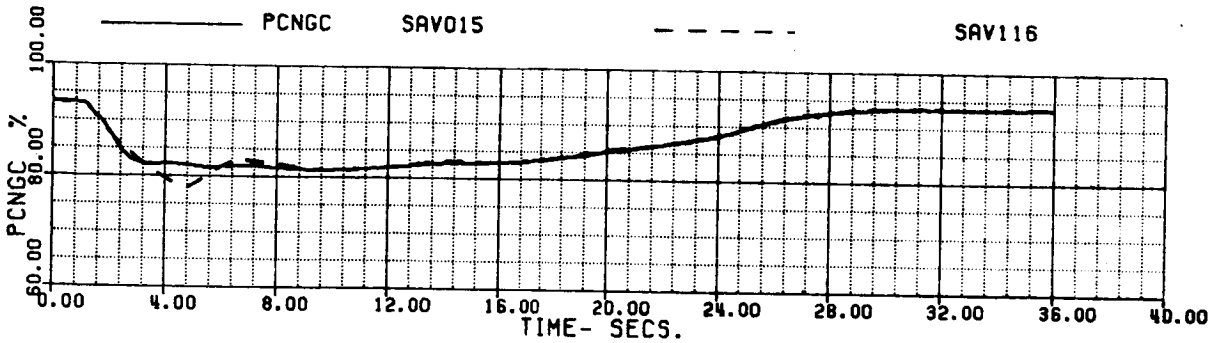

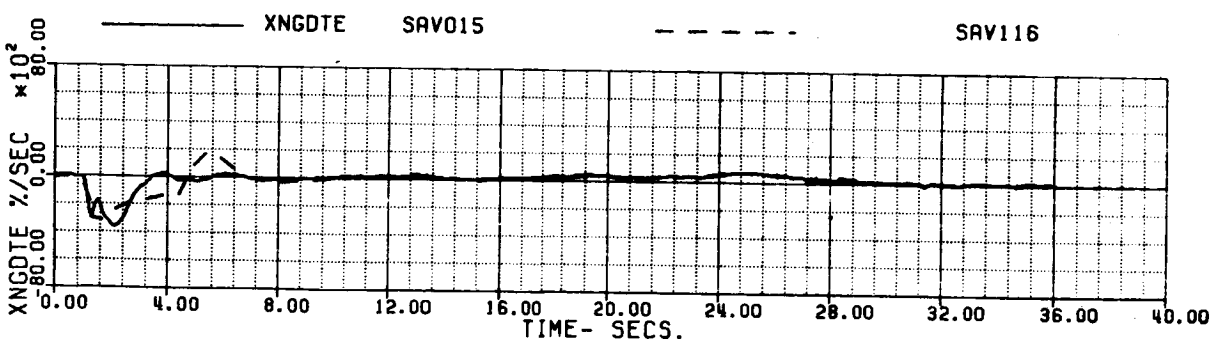

FIG 6.1.6 (g)

60A - BLACK HAWK (8/12)

FQKSTQ - QUICK STOP, INTEGRATED FUEL CONTROL
135 KTS TO HOVER

XA+1	5.8210167	XB+1	-3.3724294	XC+1	6.5927867	XP+1	3.2154287
THETAB	-2.1868543	VKT	135.00311	PHIB	0.	VYB	-1.5475518
XNGE	41783.796	NPINTE	1.3112399	VC	-.45061E-3	WEIGHT	16638.000
OMRMR	0.9999999	NPMEAS	99.999999				

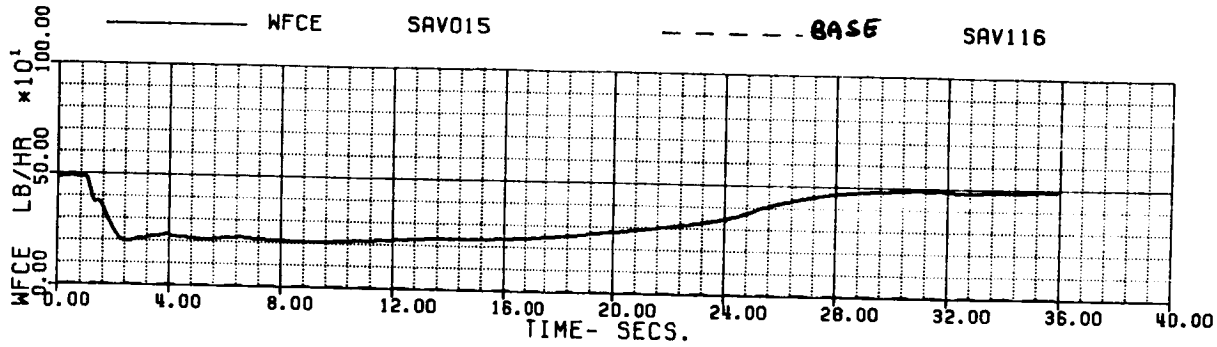

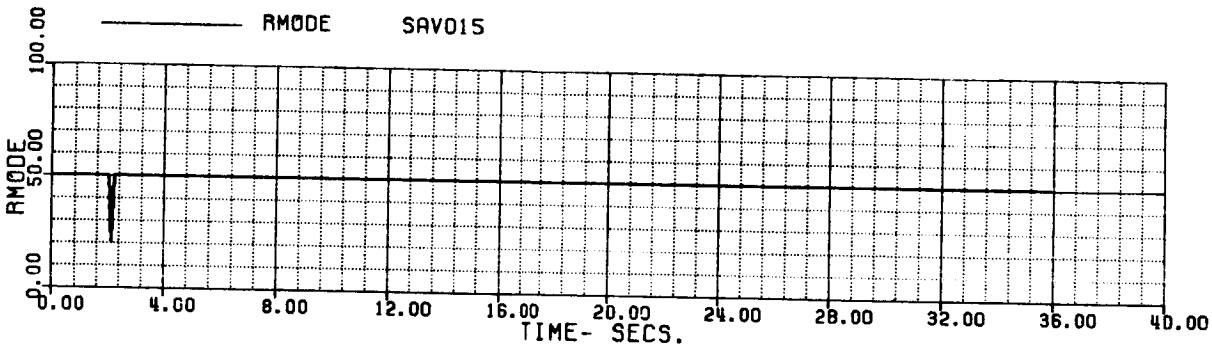

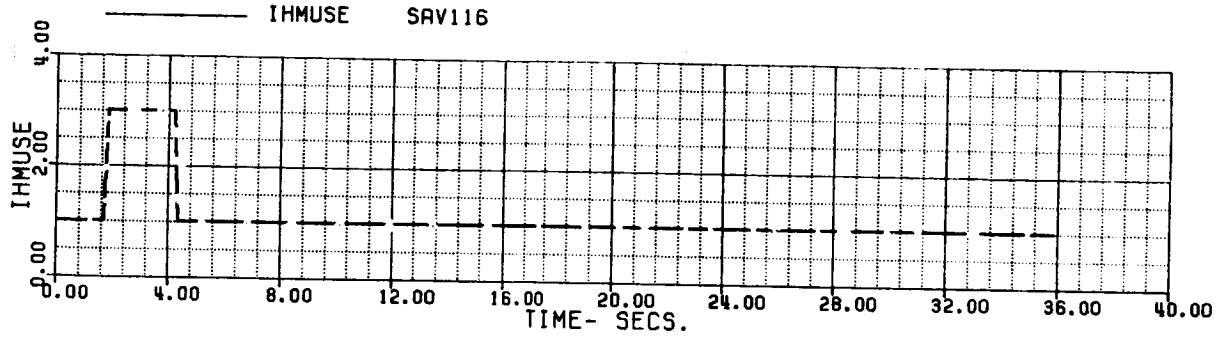

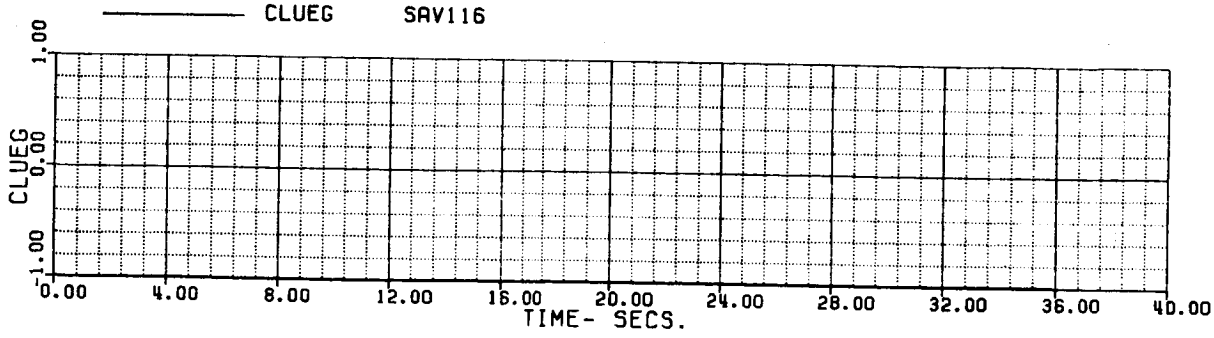

FIG 6.1.6 (h)

60A - BLACK HAWK (.

(9/12)

FQKSTO - QUICK STOP, INTEGRATED FUEL CONTROL
135 KTS TO HOVER

XA+1	5.8210167	XB+1	-3.3724294	XC+1	6.5927867	XP+1	3.2154287
THETAB	-2.1868543	VKT	135.00311	PHIB	0.	VYB	-1.5475518
XNGE	41783.796	NPINTE	1.3112399	VC	-.45061E-3	WEIGHT	16638.000
OMRMR	0.9999999	NPMEAS	99.999999				

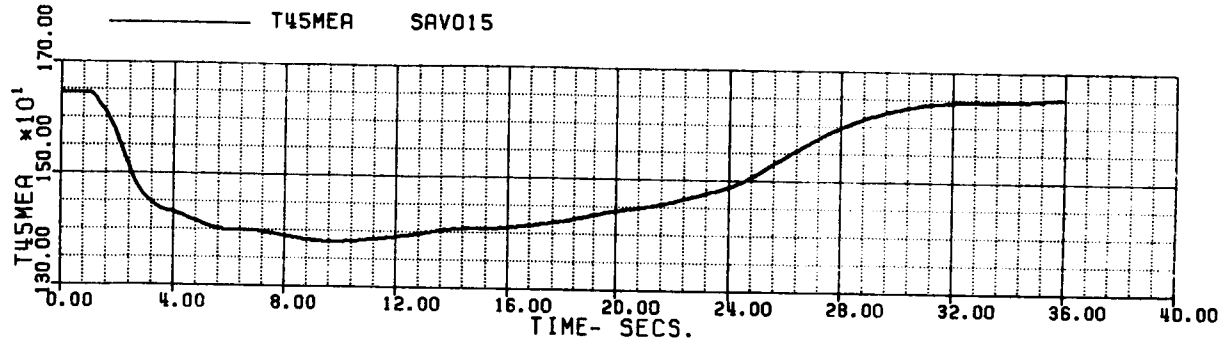

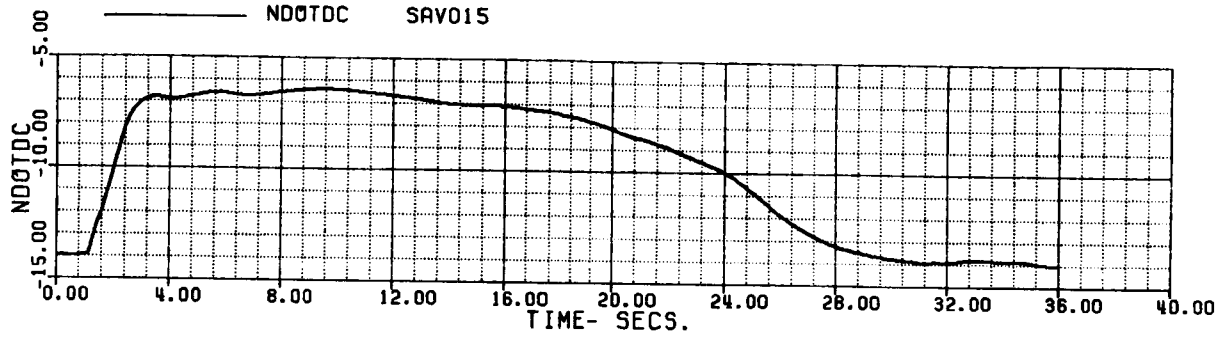

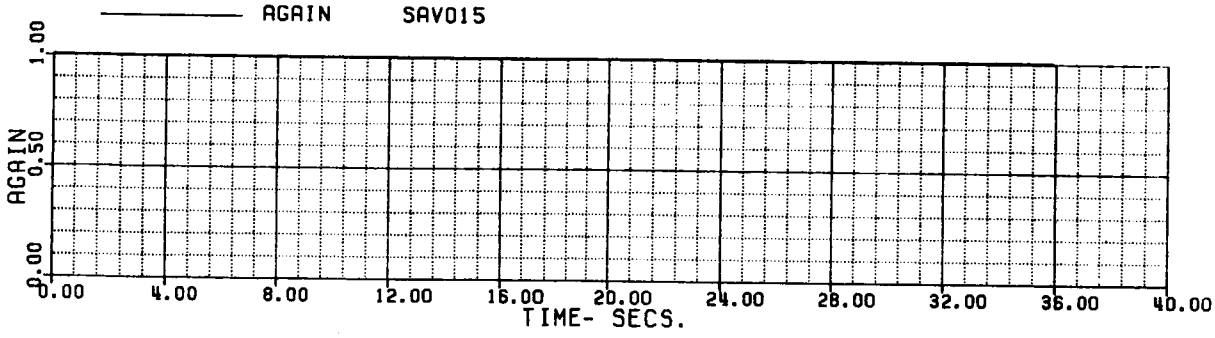

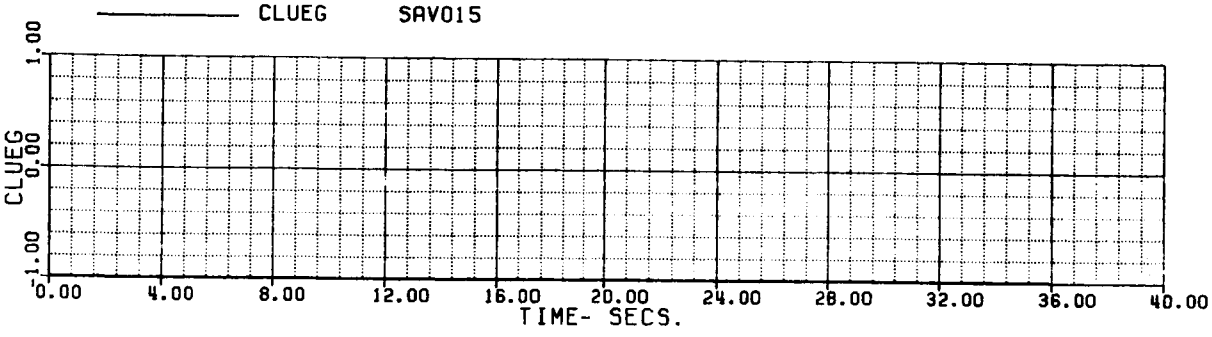

FIG 6.1.6 (i)

60A - BLACK HAWK

FQKSTQ - QUICK STOP, INTEGRATED FUEL CONTROL
135 KTS TO HOVER

XA+1	5.8210167	XB+1	-3.3724294	XC+1	6.5927867	XP+1	3.215428
THETAB	-2.1868543	VKT	135.00311	PHIB	0.	VYB	-1.54755
XNGE	41783.796	NPINTE	1.3112399	VC	-.45061E-3	WEIGHT	16638.00
OMRMR	0.9999999	NPMEAS	99.999999				

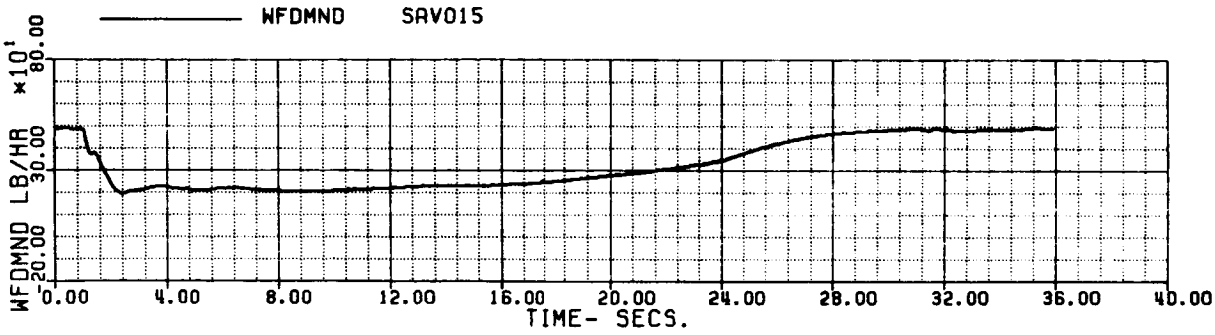

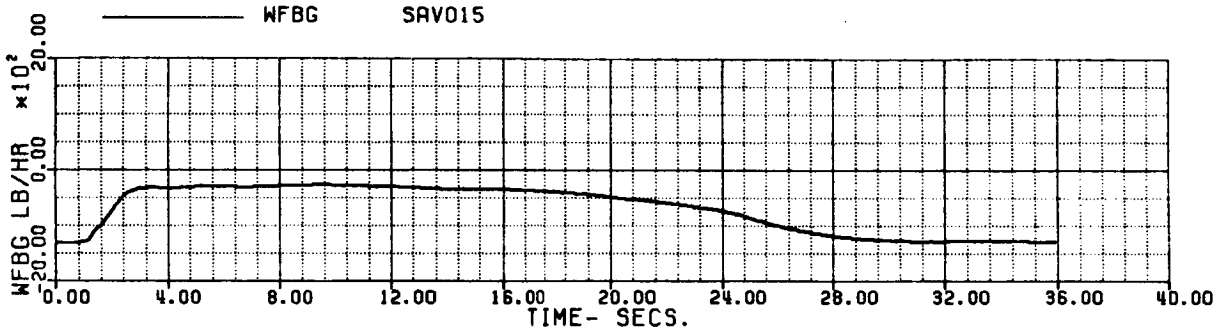

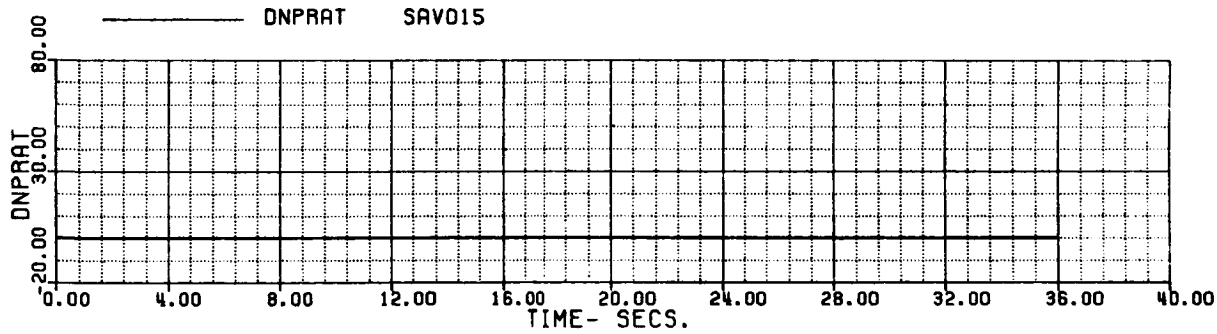

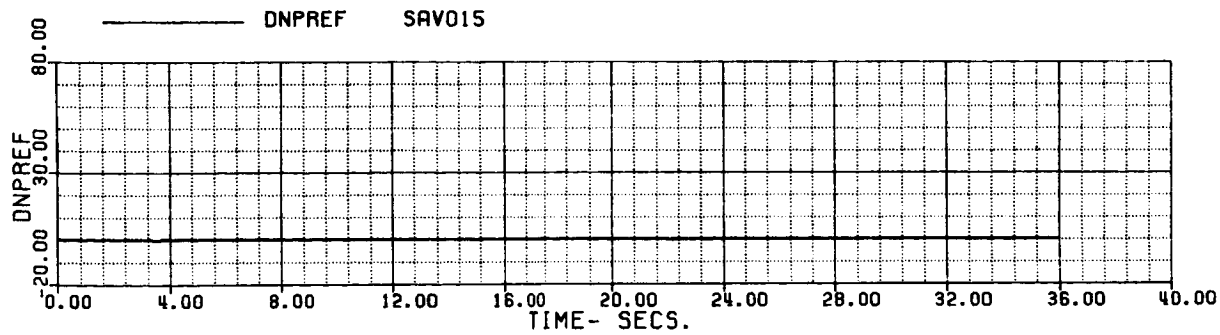

FIG 6.1.6 (j)

60A - BLACK HAWK . (12/1

FQKSTQ - QUICK STOP, INTEGRATED FUEL CONTROL
135 KTS TO HOVER

XA+1	5.8210167	XB+1	-3.3724294	XC+1	6.5927867	XP+1	3.215422
THETAB	-2.1868543	VKT	135.00311	PHIB	0.	VYB	-1.54752
XNGE	41783.796	NPINTE	1.3112399	VC	-.45061E-3	WEIGHT	16638.0
OMRMR	0.9999999	NPMEAS	99.999999				

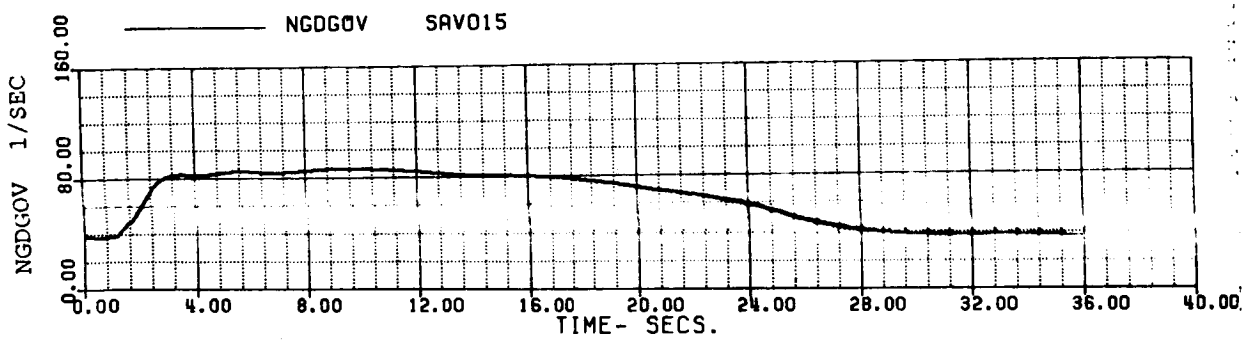

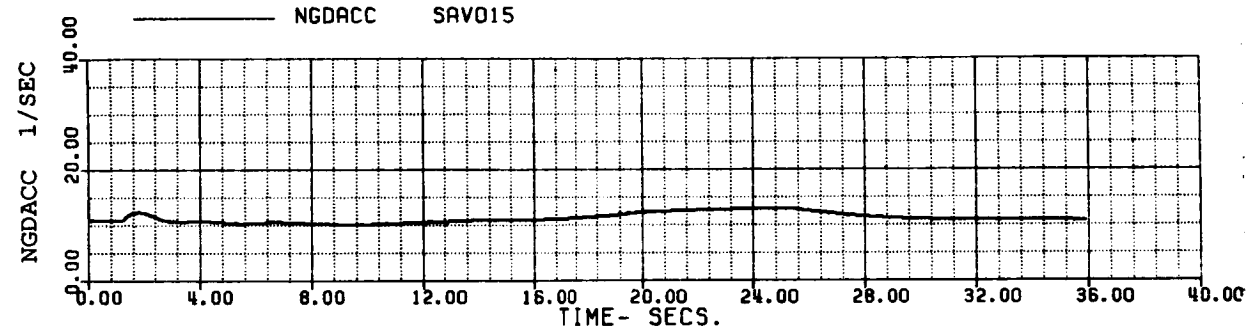

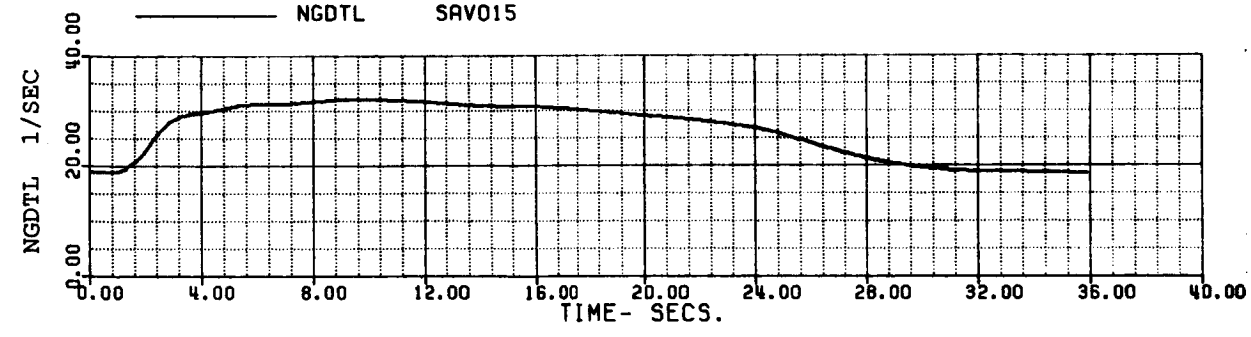

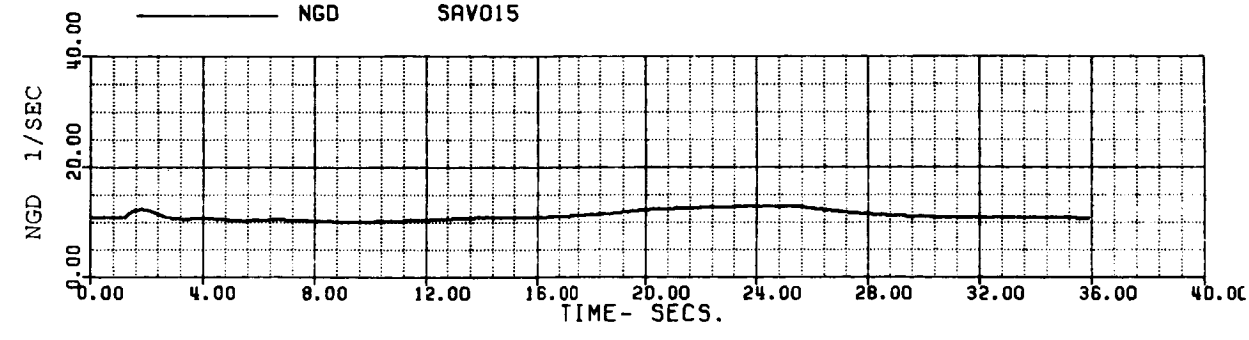

FIG 6.1.6 (k)

60A - BLACK HAWK

(1/12)

FSIDFL - SIDEWARD ACCEL/DECEL, INTEGRATED FUEL CONTROL
HOVER TO 35KTS TO HOVER

XA+1	5.3218404	XB+1	-5.7948286	XC+1	5.3279325	XP+1	1.9197290
THETAB	4.1039586	VKT	.100004E-1	PHIB	-2.5937968	VYB	0.
XNGE	41770.376	NPINTE	2.4467524	VC	.779656E-4	WEIGHT	16638.000
OMRMR	0.9999999	NPMEAS	99.999999				

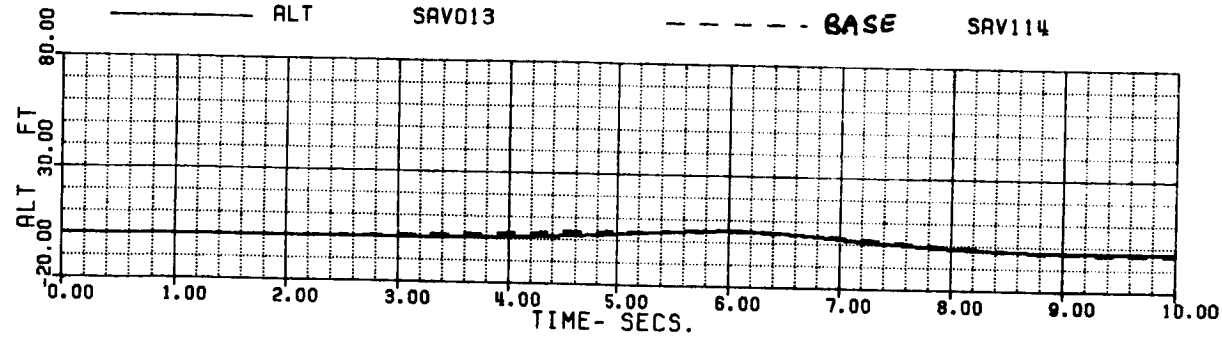

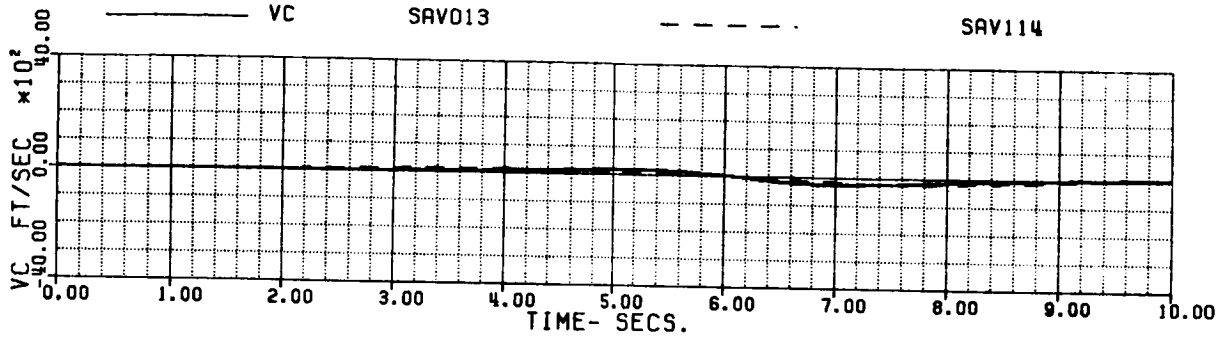

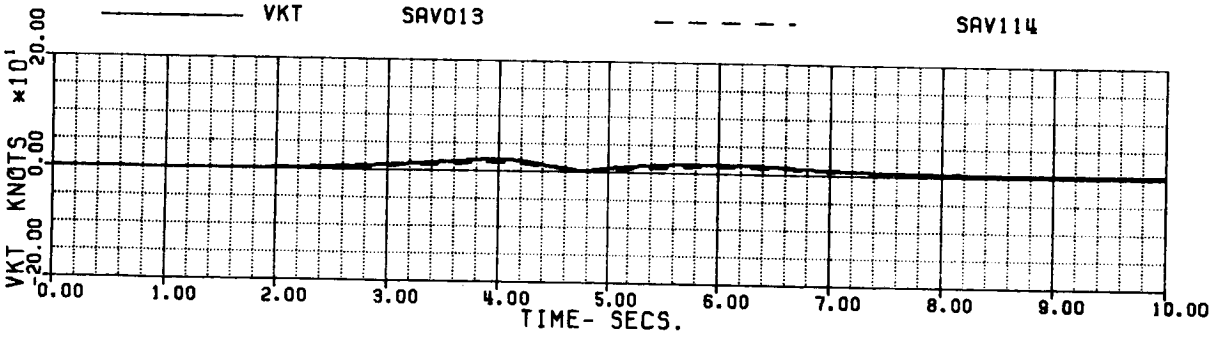

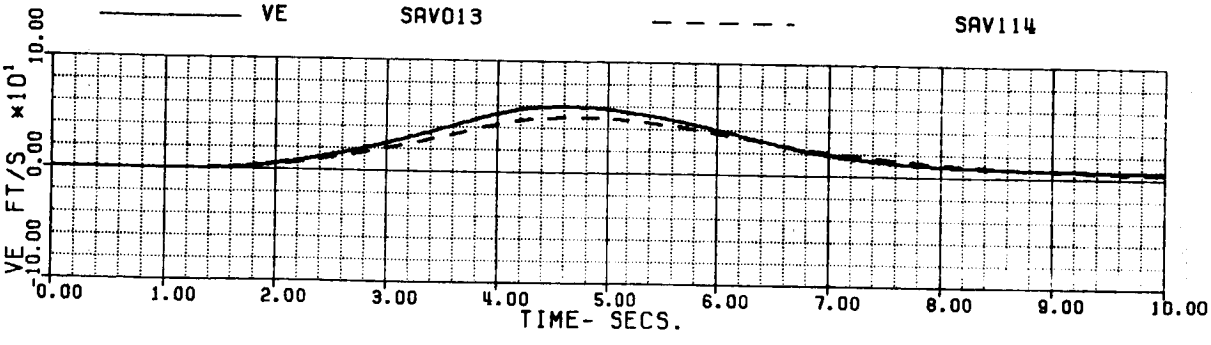

SIMULATED SIDEWARD ACCEL/DECEL

FIG 6.1.7 (a)

60A - BLACK HAWK (2/12)

FSIDFL - SIDEWARD ACCEL/DECEL, INTEGRATED FUEL CONTROL
HOVER TO 35KTS TO HOVER

XA+1	5.3218404	XB+1	-5.7948286	XC+1	5.3279325	XP+1	1.9197290
THETAB	4.1039586	VKT	.100004E-1	PHIB	-2.5937968	VYB	0.
XNGE	41770.376	NPINTE	2.4467524	VC	.779656E-4	WEIGHT	16638.000
OMRMR	0.9999999	NPMEAS	99.999999				

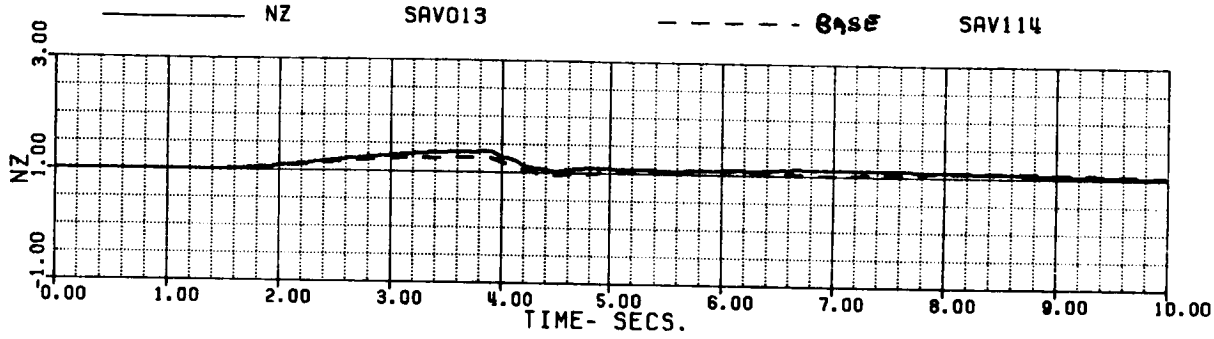

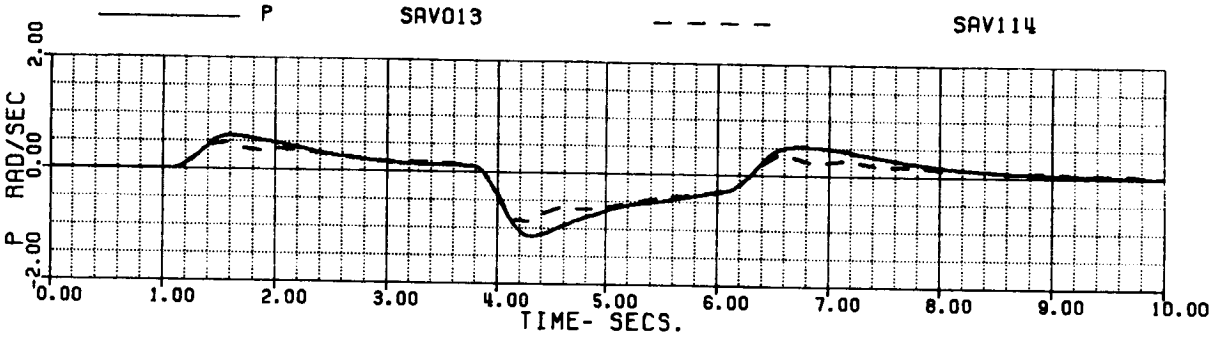

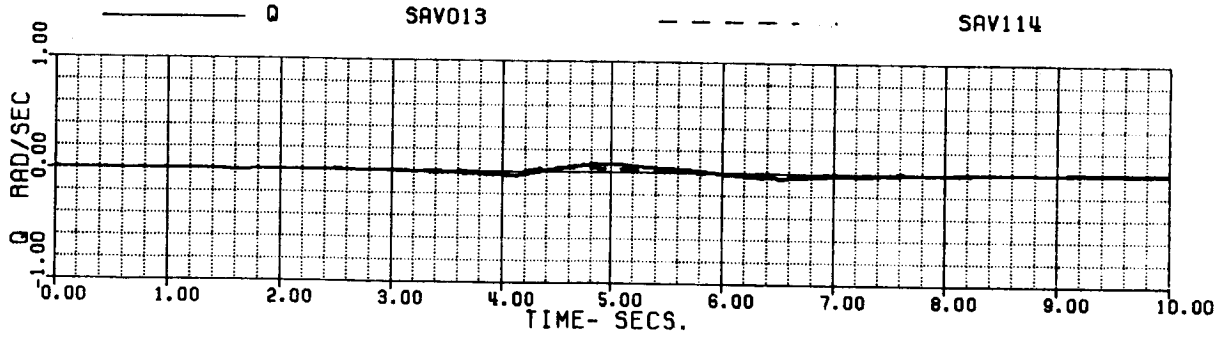

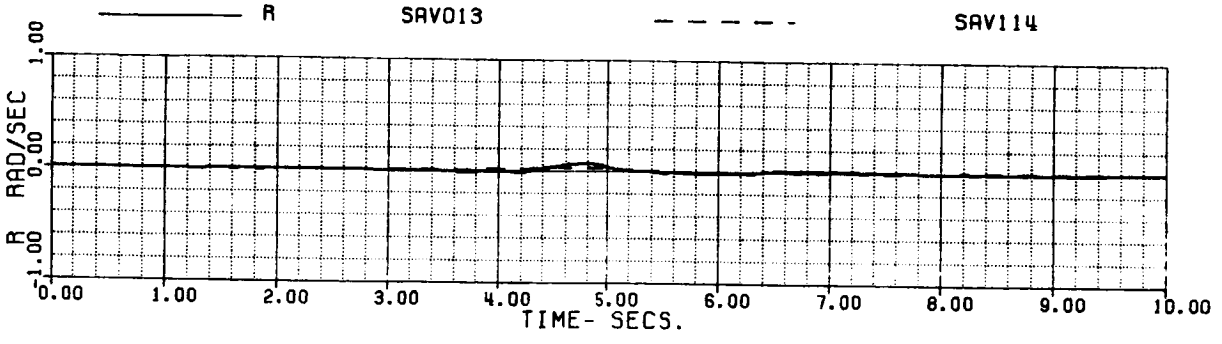

FIG 6.1.7 (b)

60A - BLACK HAWK (3/12)

FSIDFL - SIDEWARD ACCEL/DECEL, INTEGRATED FUEL CONTROL
HOVER TO 35KTS TO HOVER

XA+1	5.3218404	XB+1	-5.7948286	XC+1	5.3279325	XP+1	1.9197290
THETAB	4.1039586	VKT	.100004E-1	PHIB	-2.5937968	VYB	0.
XNGE	41770.376	NPINTE	2.4467524	VC	.779656E-4	WEIGHT	16638.000
OMRMR	0.9999999	NPMEAS	99.999999				

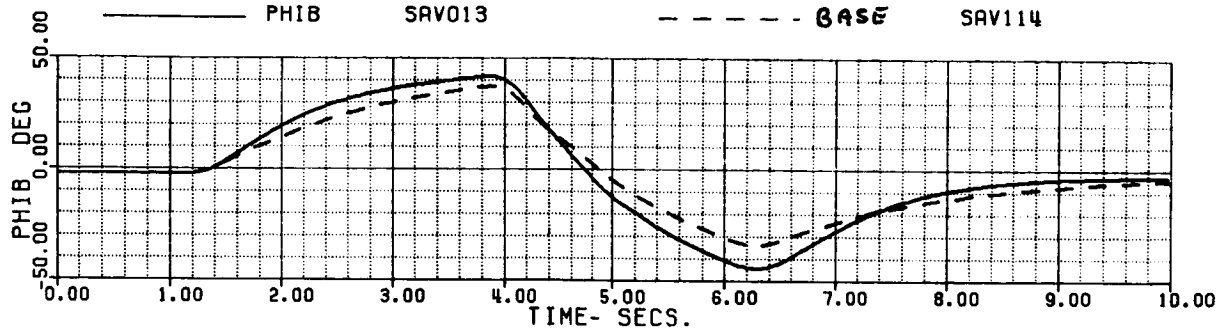

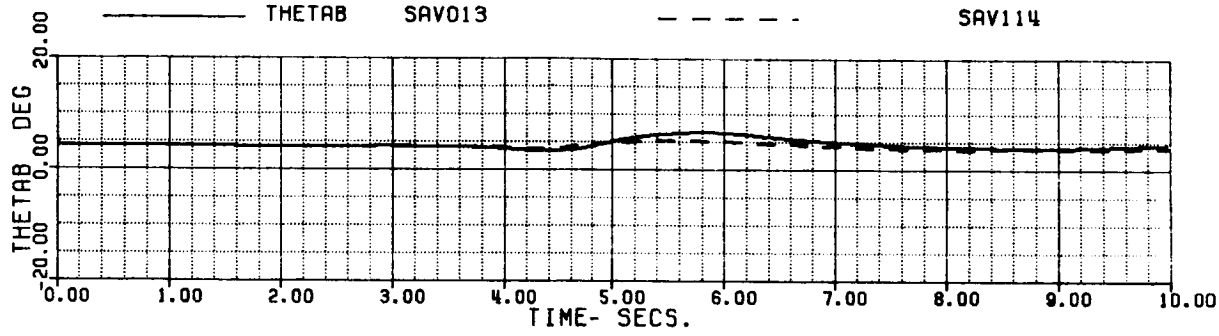

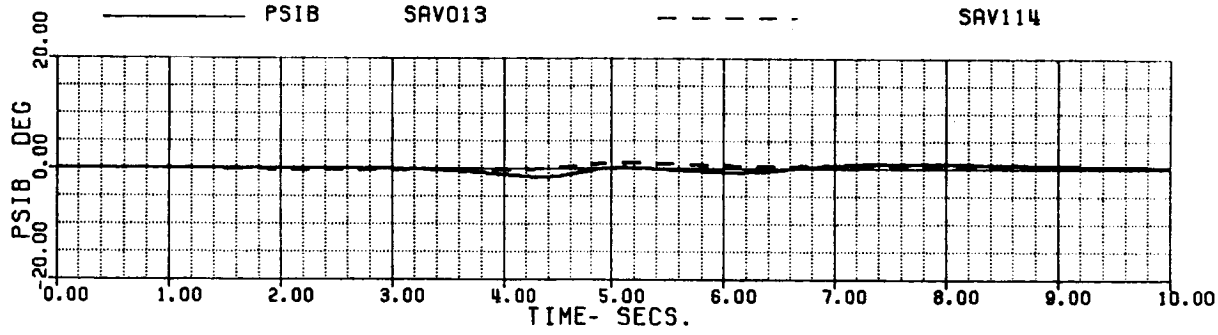

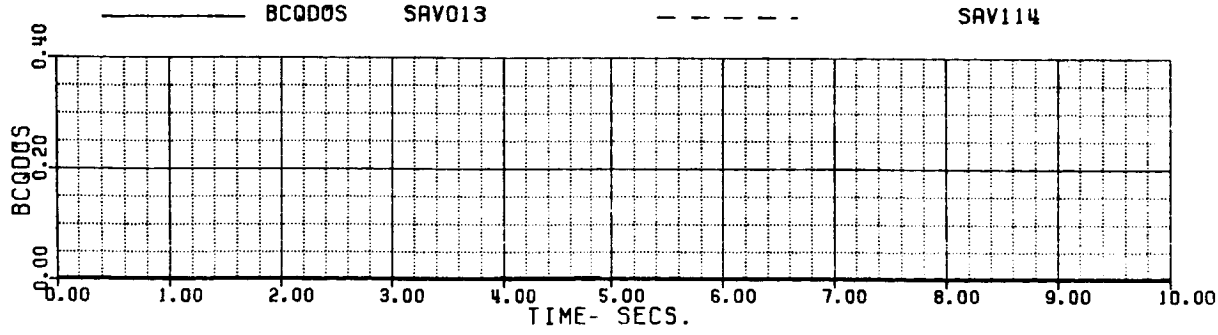

FIG 6.1.7 (c)

60A - BLACK HAWK (4/12)

FSIDFL - SIDEWARD ACCEL/DECEL, INTEGRATED FUEL CONTROL
HOVER TO 35KTS TO HOVER

XA+1	5.3218404	XB+1	-5.7948286	XC+1	5.3279325	XP+1	1.9197290
THETAB	4.1039586	VKT	.100004E-1	PHIB	-2.5937968	VYB	0.
XNGE	41770.376	NPINTE	2.4467524	VC	.779656E-4	WEIGHT	16638.000
OMRMR	0.9999999	NPMEAS	99.999999				

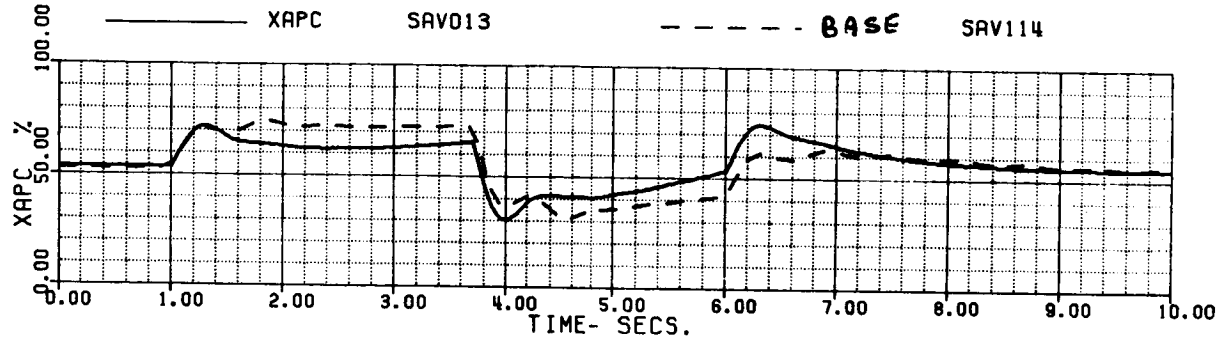

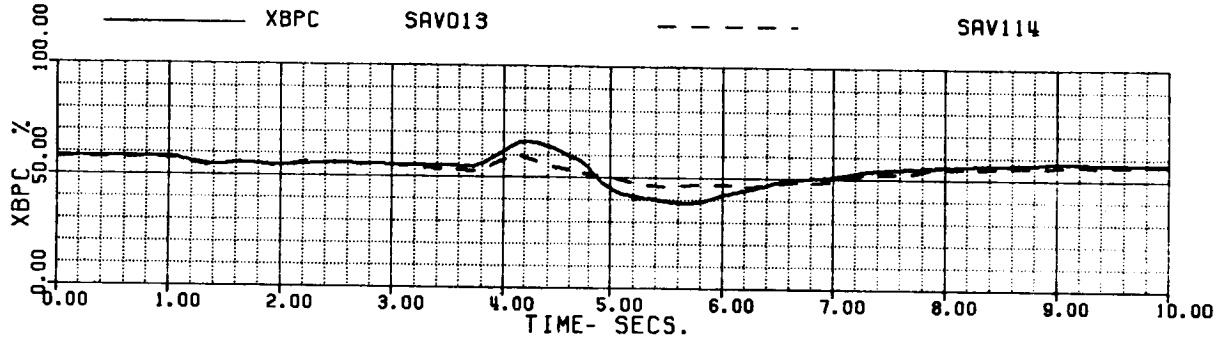

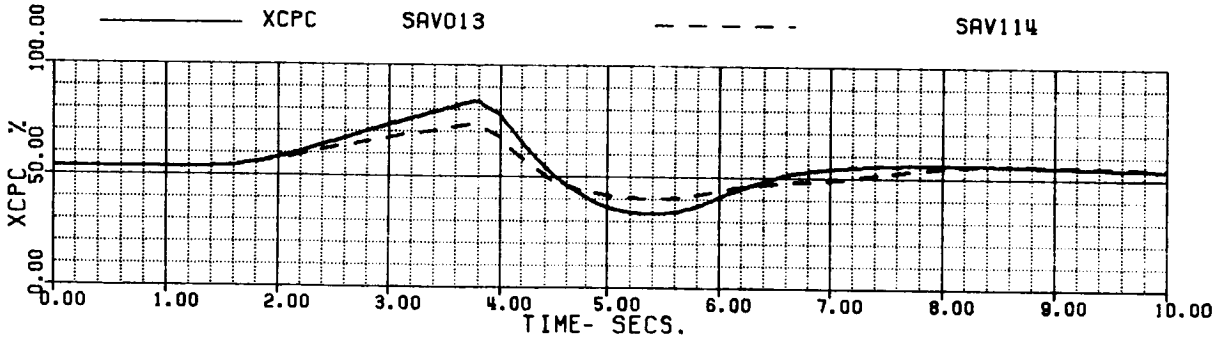

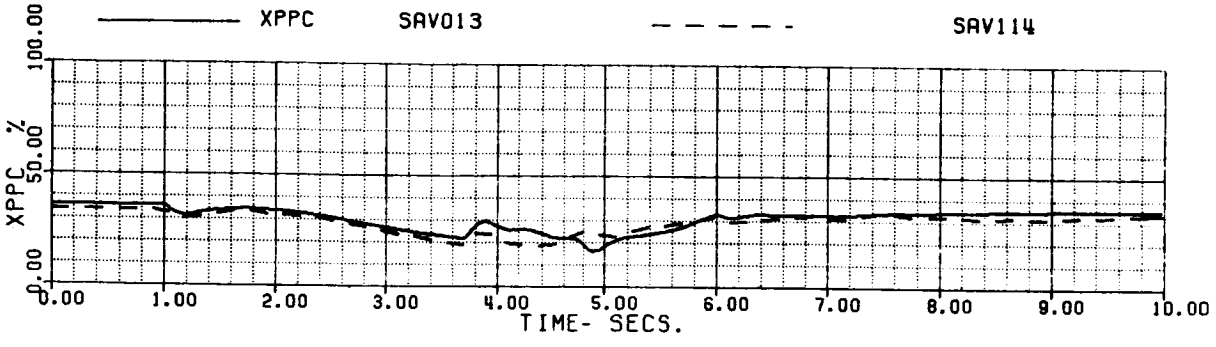

FIG 6.1.7 (d)

60A - BLACK HAWK (5/12)

FSIDFL - SIDEWARD ACCEL/DECEL, INTEGRATED FUEL CONTROL
HOVER TO 35KTS TO HOVER

XA+1	5.3218404	XB+1	-5.7948286	XC+1	5.3279325	XP+1	1.9197290
THETAB	4.1039586	VKT	.1000004E-1	PHIB	-2.5937968	VYB	0.
XNGE	41770.376	NPINTE	2.4467524	VC	.779656E-4	WEIGHT	16638.000
OMRMR	0.9999999	NPMEAS	99.999999				

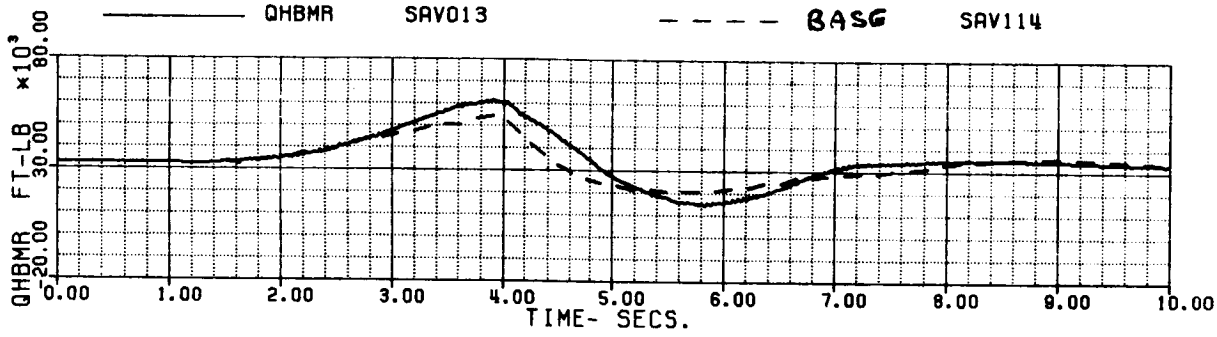

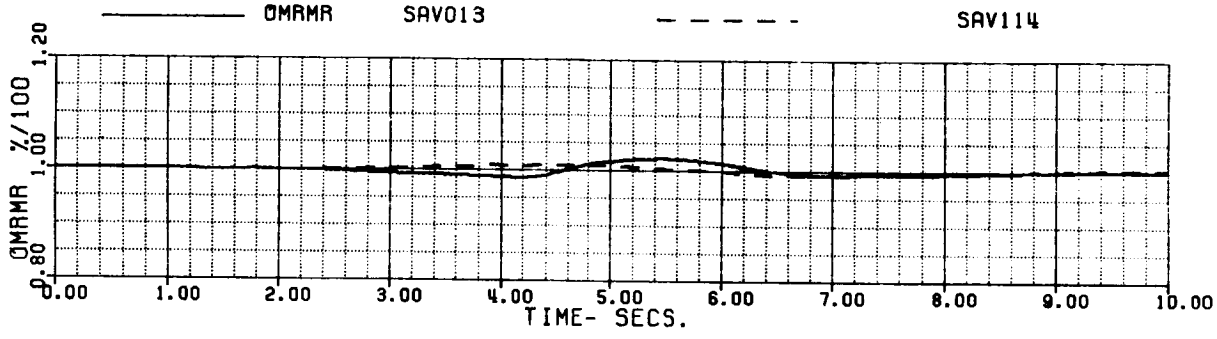

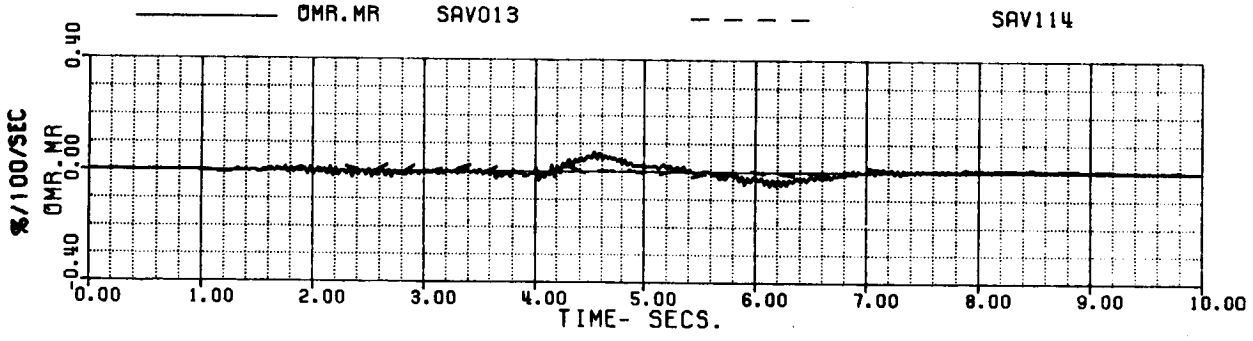

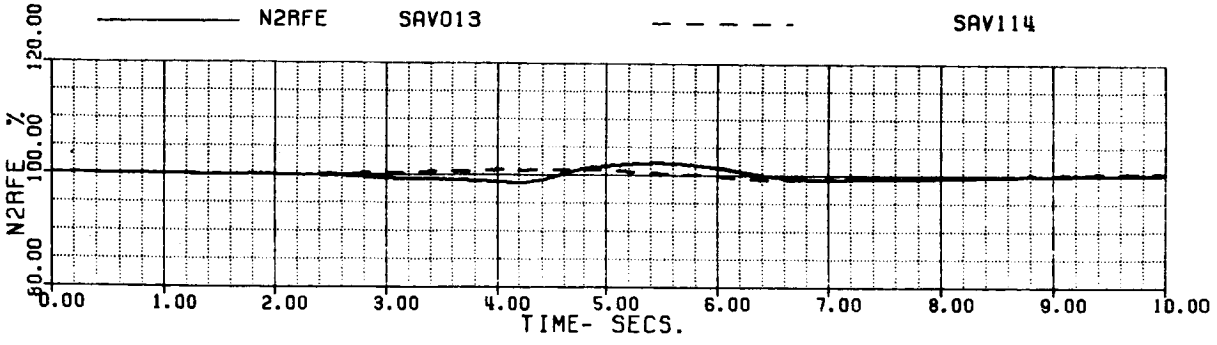

FIG 6.1.7 (e)

60A - BLACK HAWK (6/12)

FSIDFL - SIDEWARD ACCEL/DECEL, INTEGRATED FUEL CONTROL
HOVER TO 35KTS TO HOVER

XA+1	5.3218404	XB+1	-5.7948286	XC+1	5.3279325	XP+1	1.9197290
THETAB	4.1039586	VKT	.100004E-1	PHIB	-2.5937968	VYB	0.
XNGE	41770.376	NPINTE	2.4467524	VC	.779656E-4	WEIGHT	16638.000
OMRMR	0.9999999	NPMEAS	99.999999				

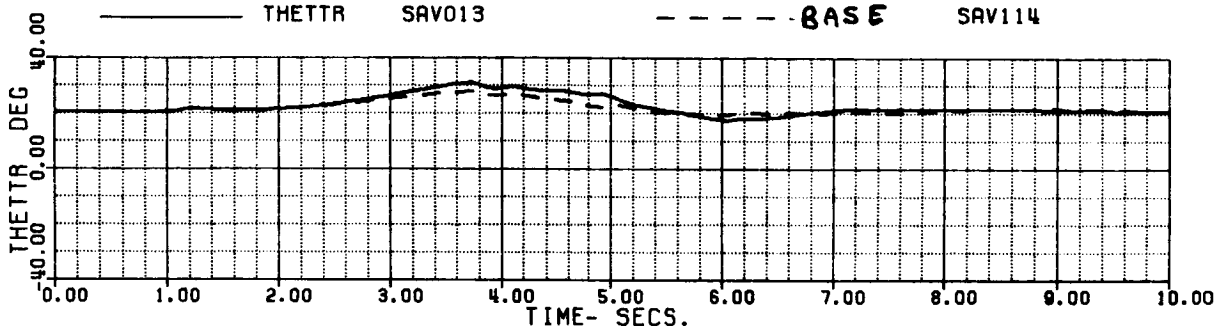

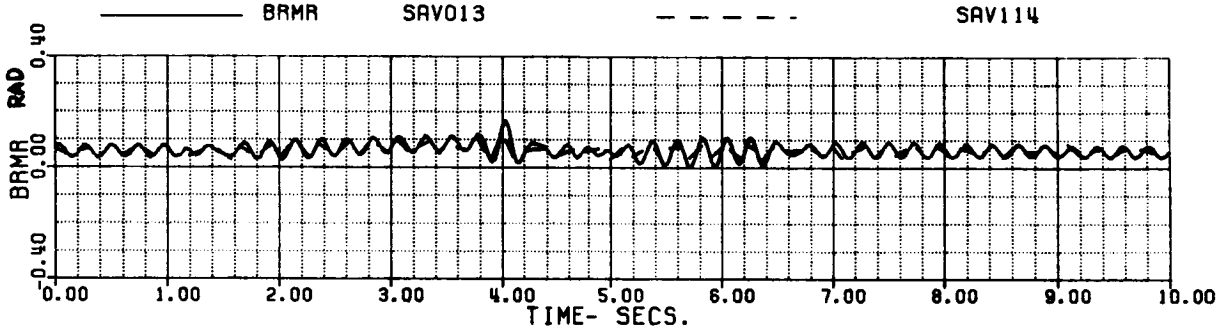

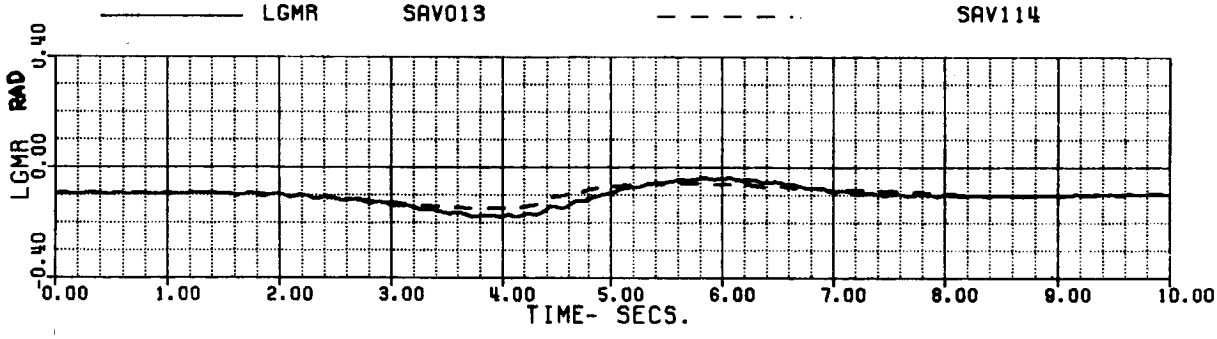

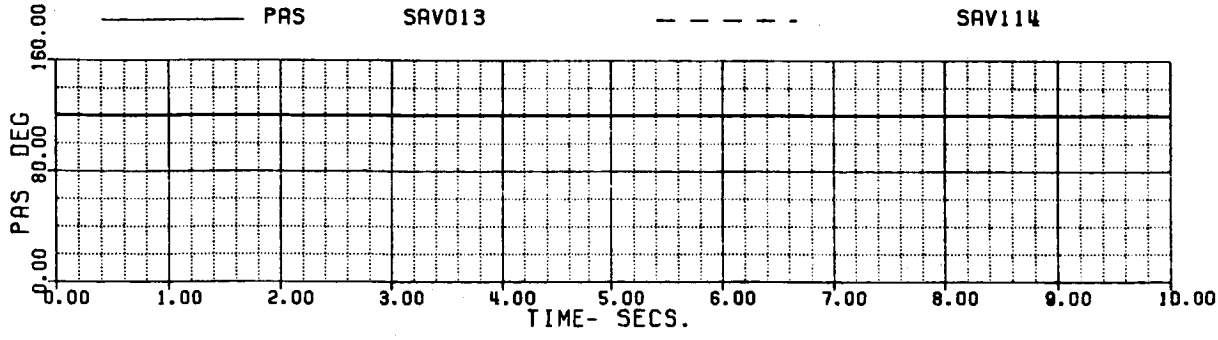

FIG 6.1.7 (f)

60A - BLACK HAWK (7/12)

FSIDFL - SIDEWARD ACCEL/DECEL, INTEGRATED FUEL CONTROL
HOVER TO 35KTS TO HOVER

XA+1	5.3218404	XB+1	-5.7948286	XC+1	5.3279325	XP+1	1.9197290
THETAB	4.1039586	VKT	.100004E-1	PHIB	-2.5937968	VYB	0.
XNGE	41770.376	NPINTE	2.4467524	VC	.779656E-4	WEIGHT	16638.000
OMAMR	0.9999999	NPMEAS	99.999999				

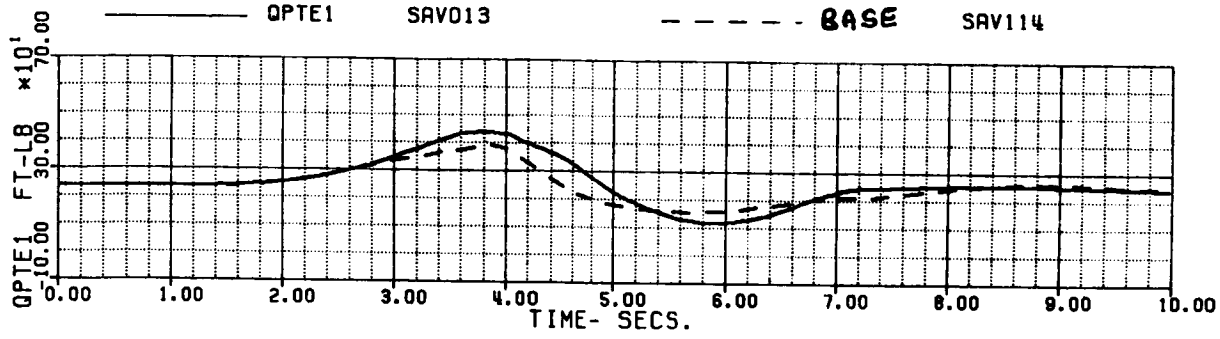

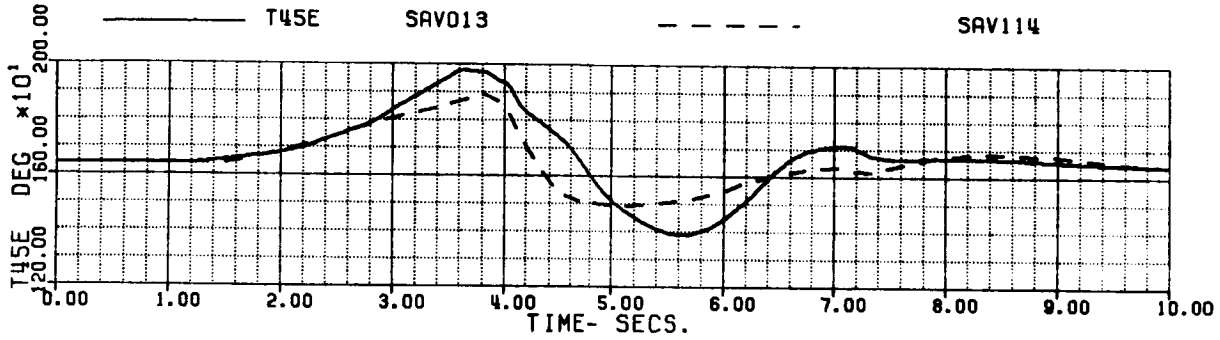

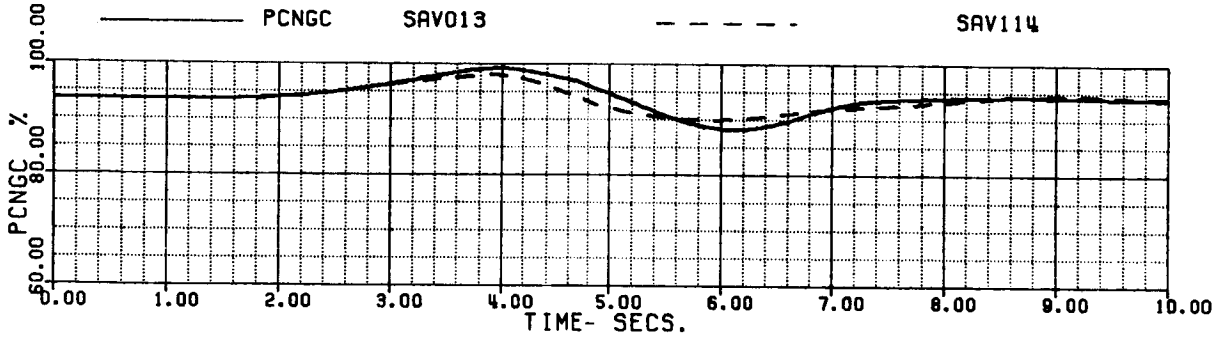

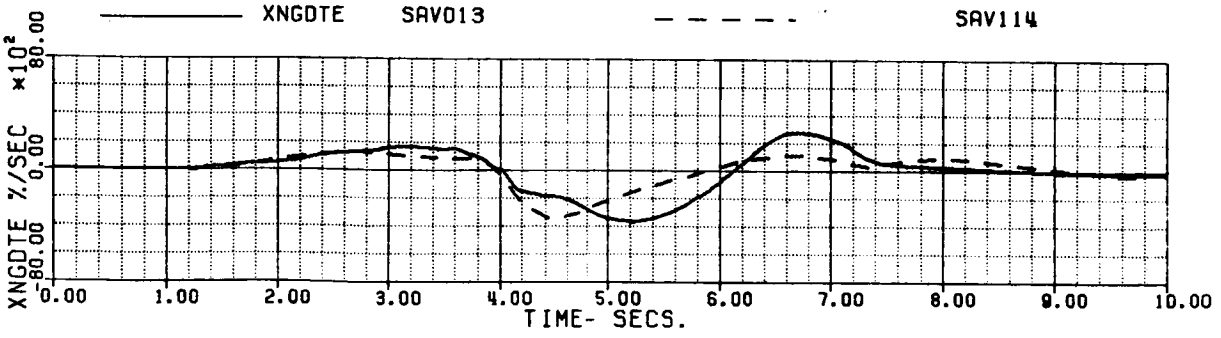

FIG 6.1.7 (g)

60A - BLACK HAWK (8/12)

FSIDFL - SIDEWARD ACCEL/DECEL, INTEGRATED FUEL CONTROL
HOVER TO 35KTS TO HOVER

XA+1	5.3218404	XB+1	-5.7948286	XC+1	5.3279325	XP+1	1.9197290
THETAB	4.1039586	VKT	.100004E-1	PHIB	-2.5937968	VYB	0.
XNGE	41770.376	NPINTE	2.4467524	VC	.779656E-4	WEIGHT	16638.000
OMRMR	0.9999999	NPMEAS	99.999999				

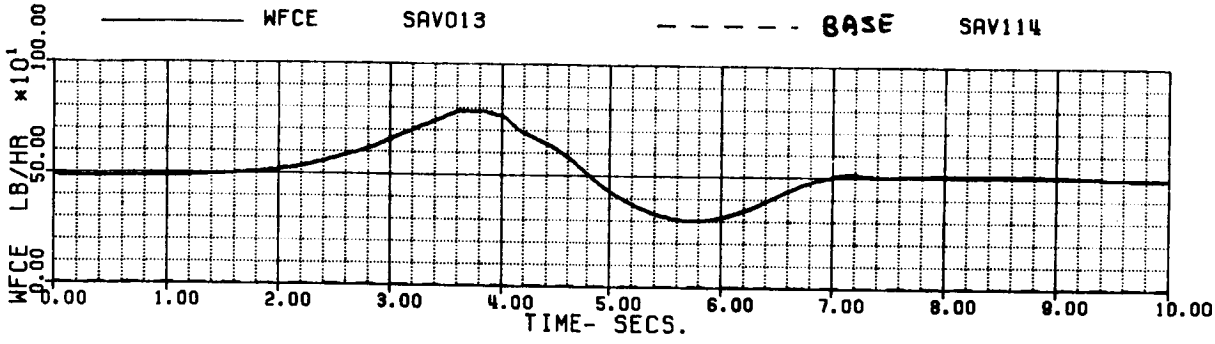

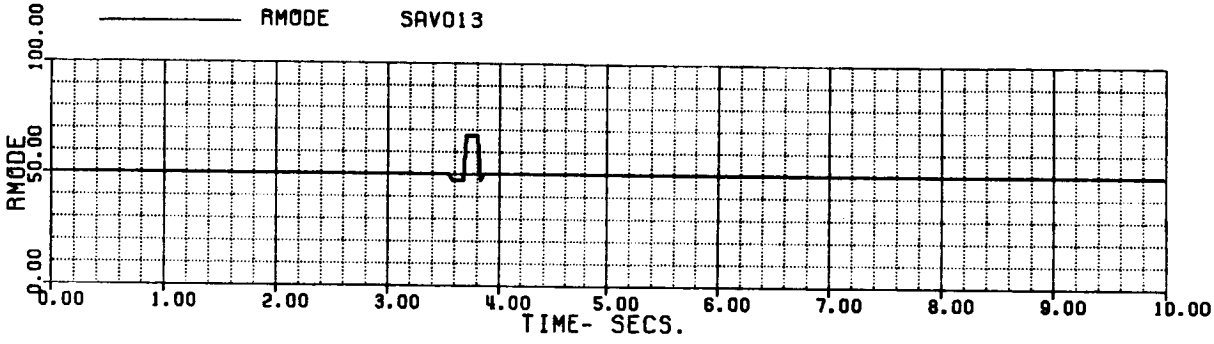

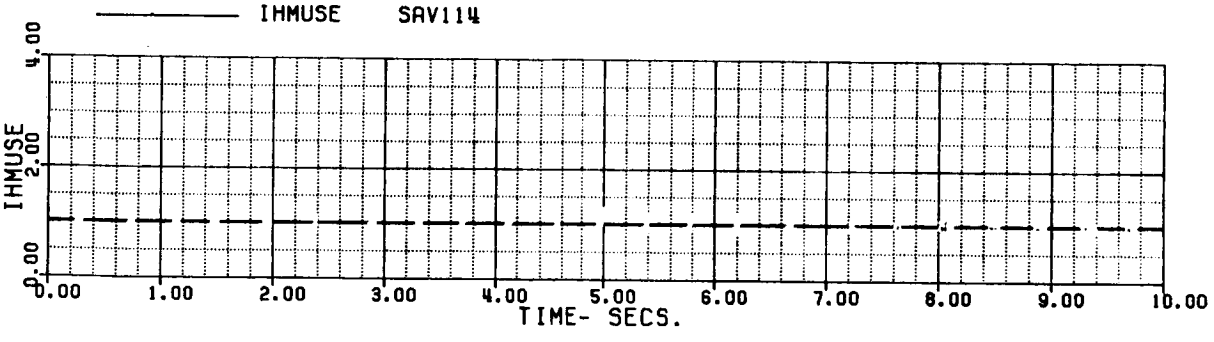

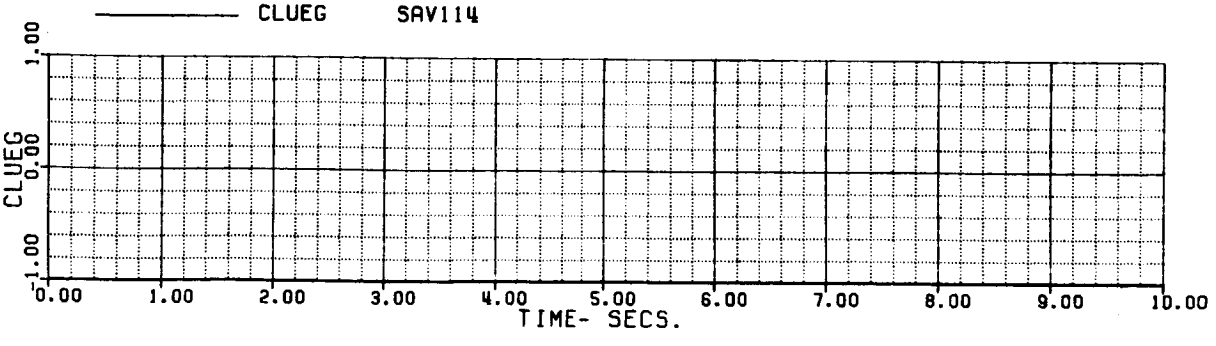

FIG 6.1.7 (h)

60A - BLACK HAWK (9/12)

FSIDFL - SIDEWARD ACCEL/DECEL, INTEGRATED FUEL CONTROL
HOVER TO 35KTS TO HOVER

XA+1	5.3218404	XB+1	-5.7948286	XC+1	5.3279325	XP+1	1.9197290
THETAB	4.1039586	VKT	.100004E-1	PHIB	-2.5937968	VYB	0.
XNGE	41770.376	NPINTE	2.4467524	VC	.779656E-4	WEIGHT	16638.000
OMRMR	0.9999999	NPMEAS	99.999999				

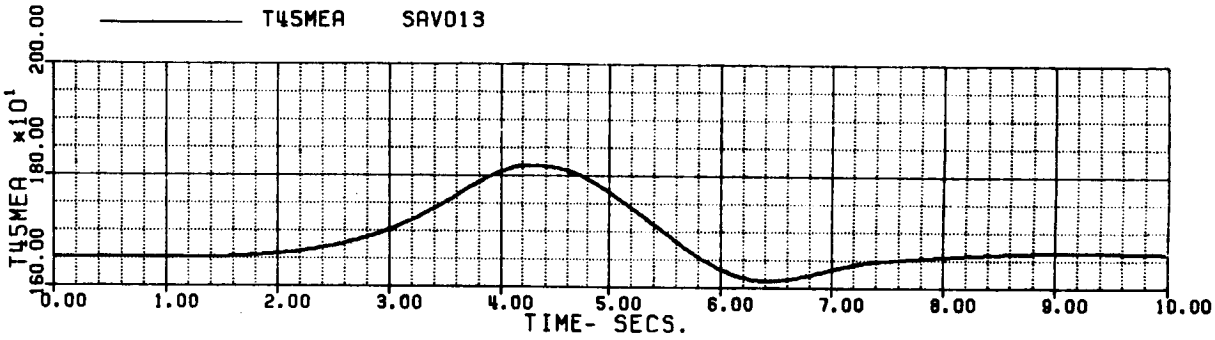

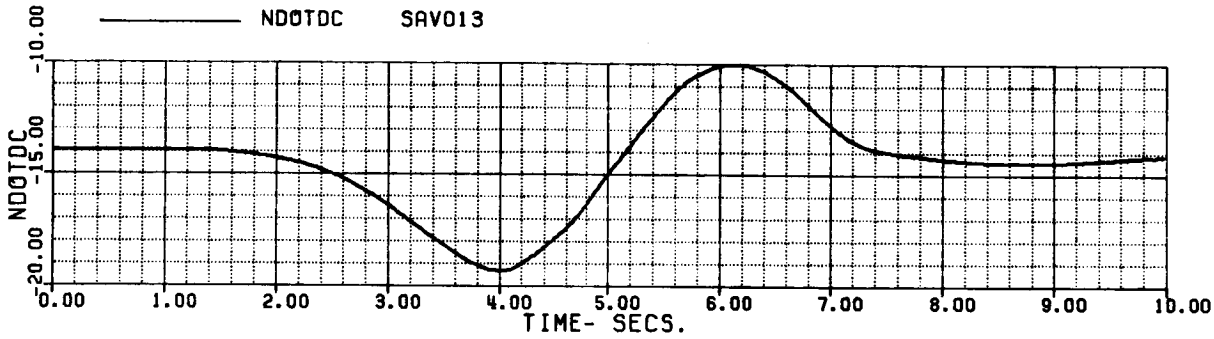

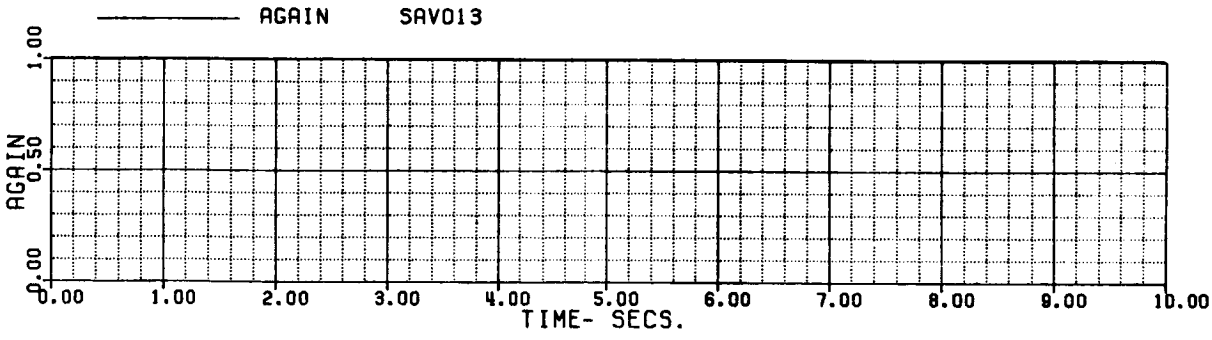

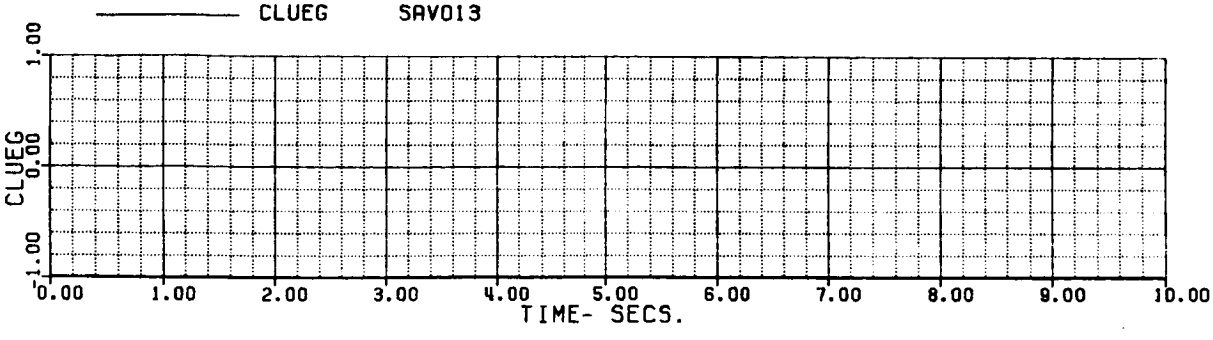

FIG 6.1.7 (i)

60A - BLACK HAWK (11/12)

FSIDFL - SIDEWARD ACCEL/DECEL, INTEGRATED FUEL CONTROL
HOVER TO 35KTS TO HOVER

XA+1	5.3218404	XB+1	-5.7948286	XC+1	5.3279325	XP+1	1.9197290
THETAB	4.1039586	VKT	.1000046E-1	PHIB	-2.5937968	VYB	0.
XNGE	41770.376	NPINTE	2.4467524	VC	.779656E-4	WEIGHT	16638.000
OMRMR	0.9999999	NPMEAS	99.999999				

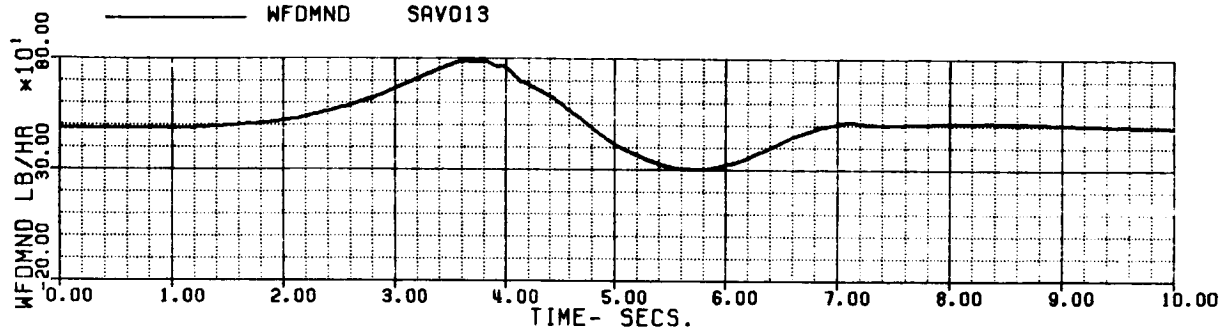

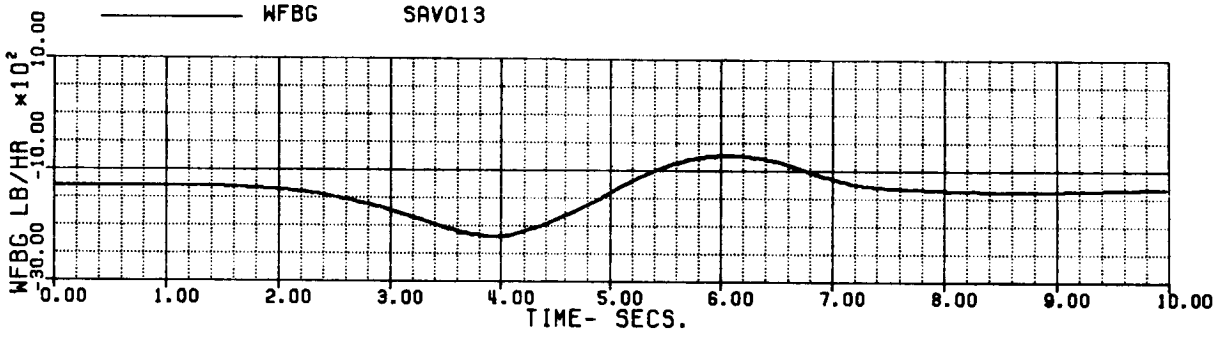

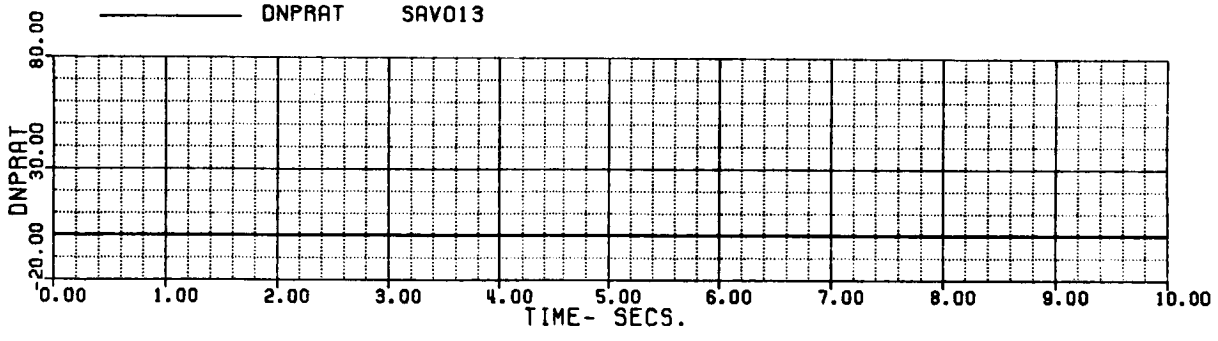

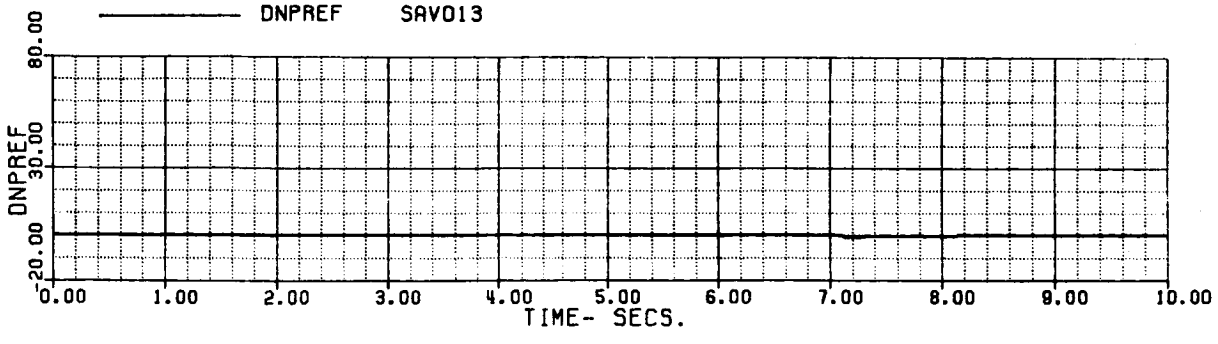

FIG 6.1.7 (j)

(12/12)

60A - BLACK HAWK

FSIDFL - SIDEWARD ACCEL/DECEL, INTEGRATED FUEL CONTROL
HOVER TO 35KTS TO HOVER

XA+1	5.3218404	XB+1	-5.7948286	XC+1	5.3279325	XP+1	1.9197290
THETAB	4.1039586	VKT	.100004E-1	PHIB	-2.5937968	VYB	0.
XNGE	41770.376	NPINTE	2.4467524	VC	.779656E-4	WEIGHT	16638.000
OMRMR	0.9999999	NPMEAS	99.999999				

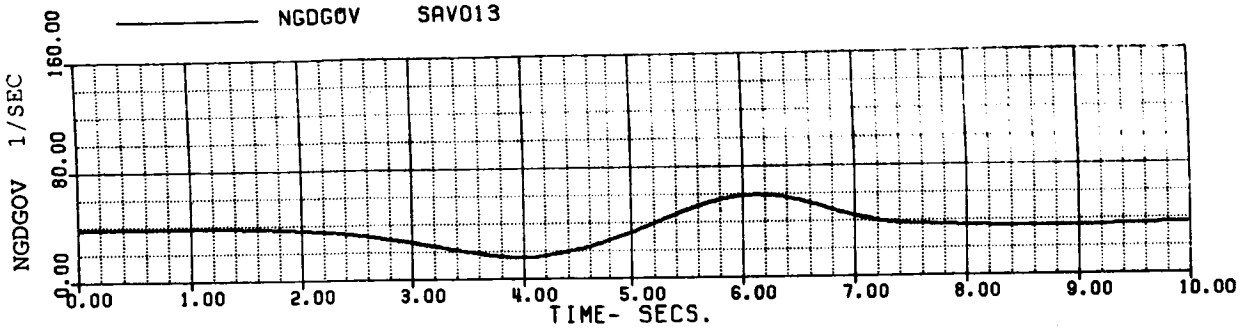

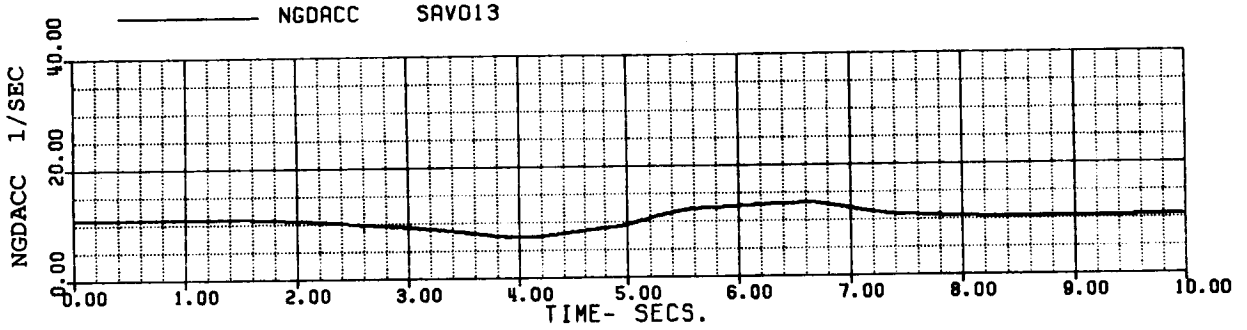

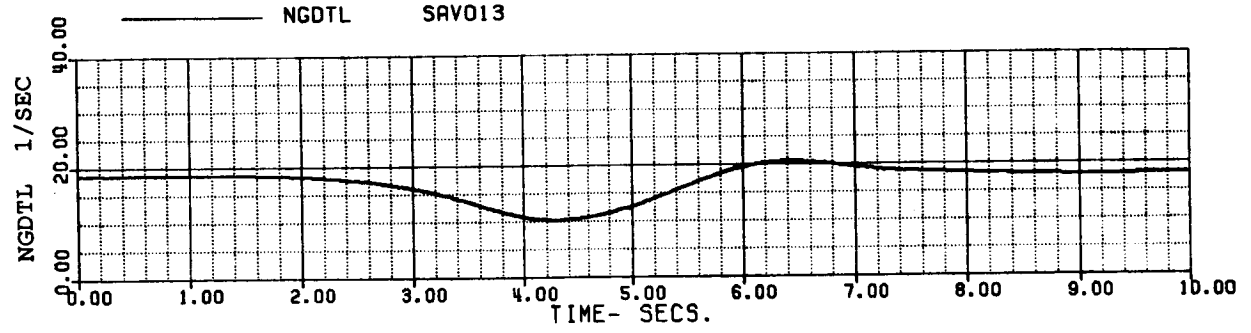

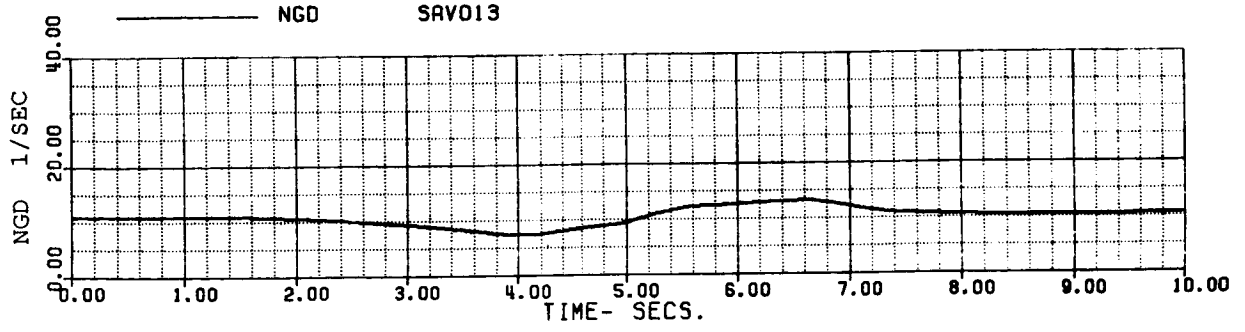

FIG 6.1.7 (k)

60A - BLACK HAWK (1/12)

FHIGTR - HIGH G TURN INT FUEL CONTROL
NZ FED TO NPREF

XA+1	5.7903764	XB+1	-3.5056055	XC+1	6.2289388	XP+1	3.1971333
THETAB	-1.7157311	VKT	129.99868	PHIB	0.	VYB	-1.5099977
XNGE	41524.665	NPINTE	1.3490933	VC	.175952E-2	WEIGHT	16638.000
OMRMR	0.9999999	NPMEAS	99.999997				

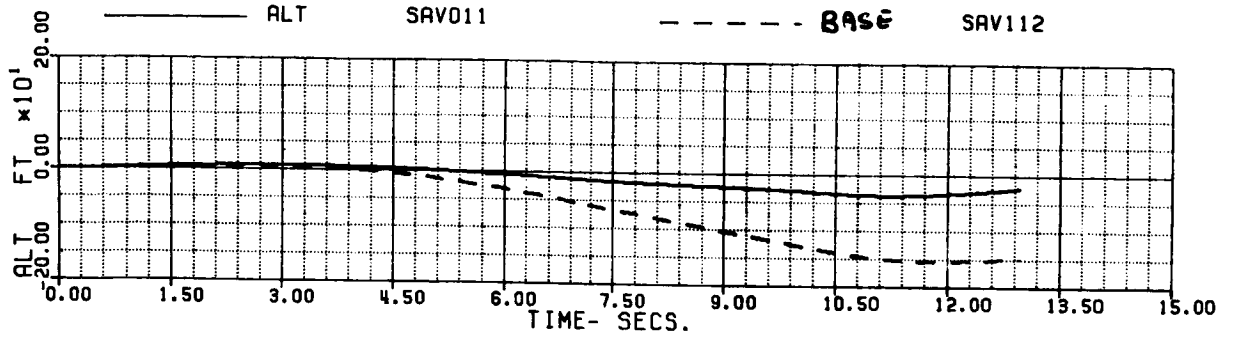

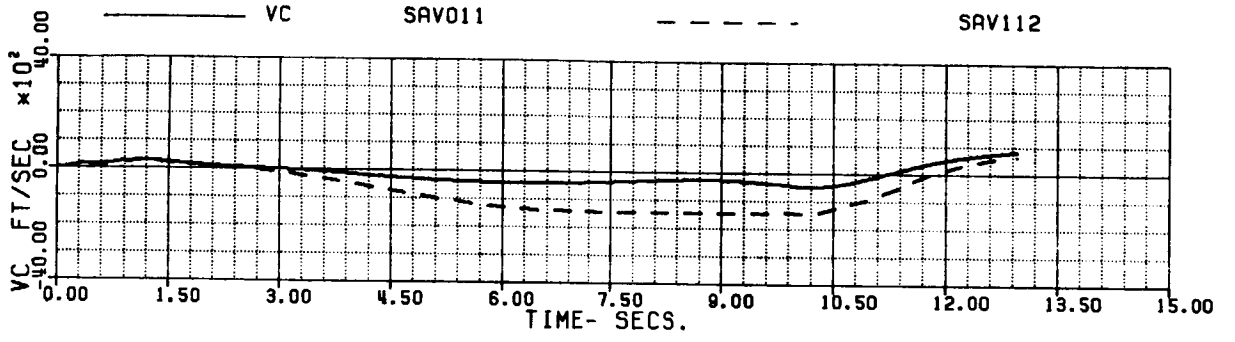

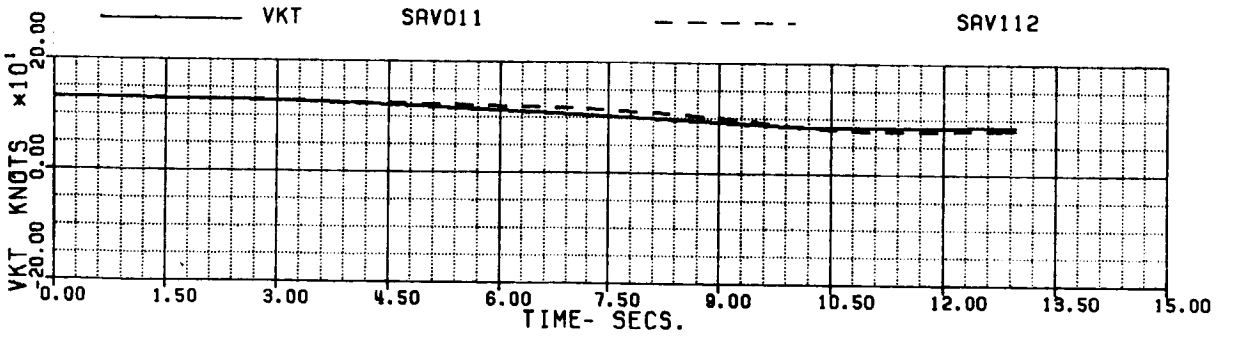

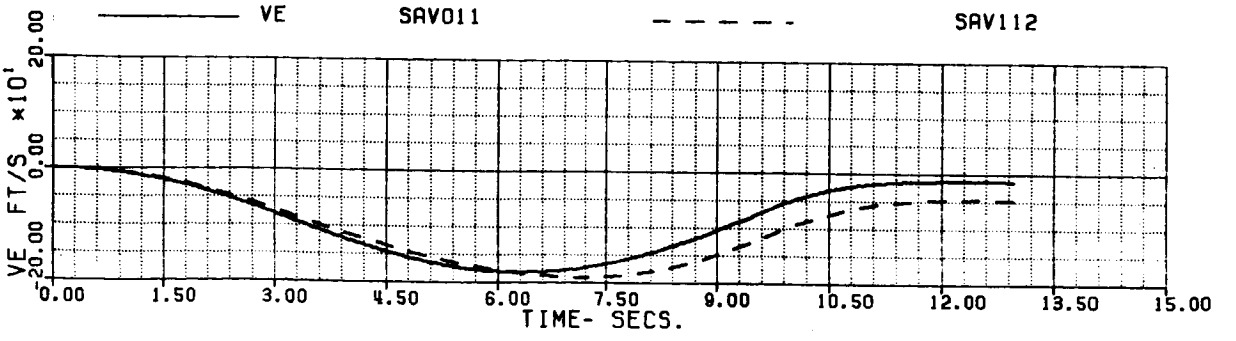

SIMULATED HIGH G TURN/DECEL

FIG 6.1.8 (a)

60A - BLACK HAWK (2/12)

FHIGTR - HIGH G TURN INT FUEL CONTROL
NZ FED TO NPREF

XA+1	5.7903764	XB+1	-3.5056055	XC+1	6.2289388	XP+1	3.1971333
THETAB	-1.7157311	VKT	129.99868	PHIB	0.	VTB	-1.5099977
XNGE	41524.665	NPINTE	1.3490933	VC	.175952E-2	WEIGHT	16638.000
OMAMR	0.9999999	NPMEAS	99.999997				

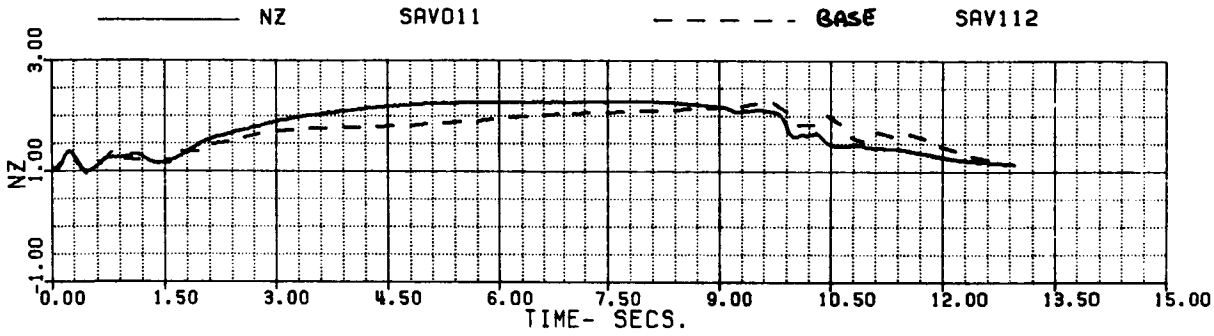

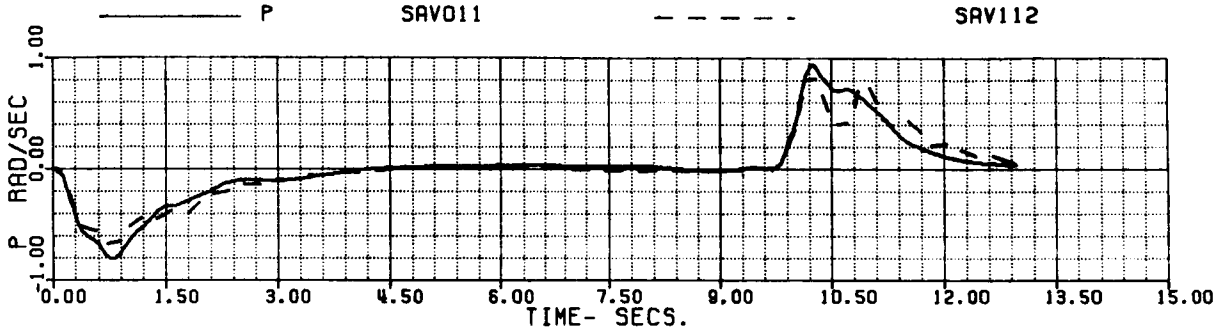

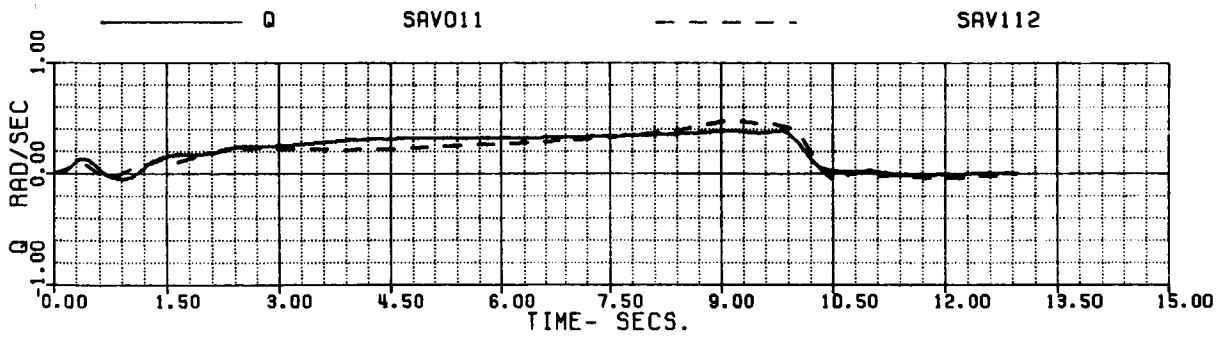

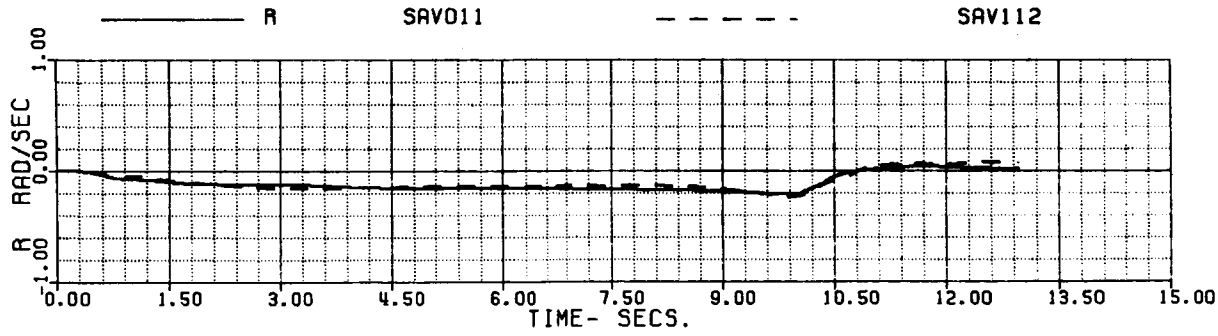

FIG 6.1.8 (b)

60A - BLACK HAWK (3/12)

FHIGTR - HIGH G TURN INT FUEL CONTROL
NZ FED TO NPREF

XA+1	5.7903764	XB+1	-3.5056055	XC+1	6.2289388	XP+1	3.1971333
THETAB	-1.7157311	VKT	129.99868	PHIB	0.	YB	-1.5099977
XNGE	41524.665	NPINTE	1.3490933	VC	.175952E-2	WEIGHT	16638.000
OMRMR	0.9999999	NPMEAS	99.999997				

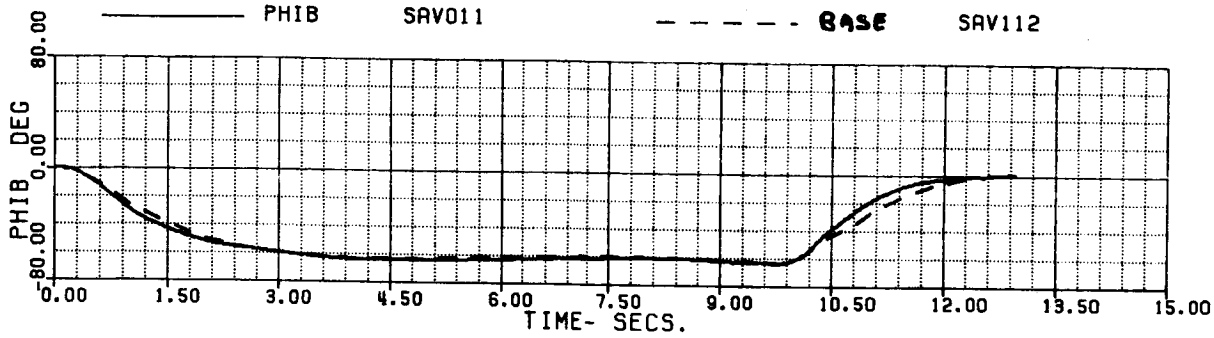

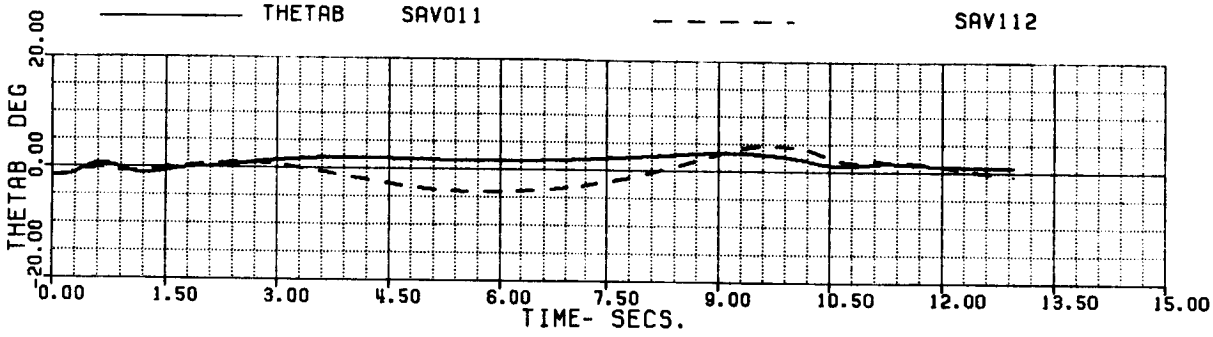

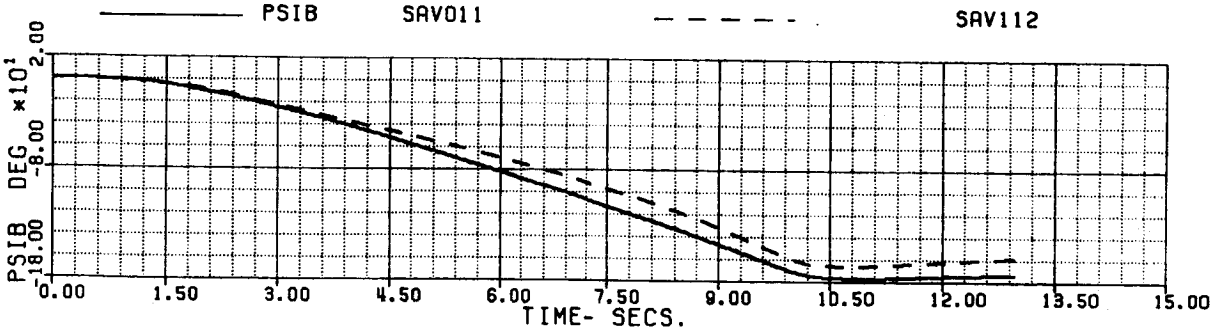

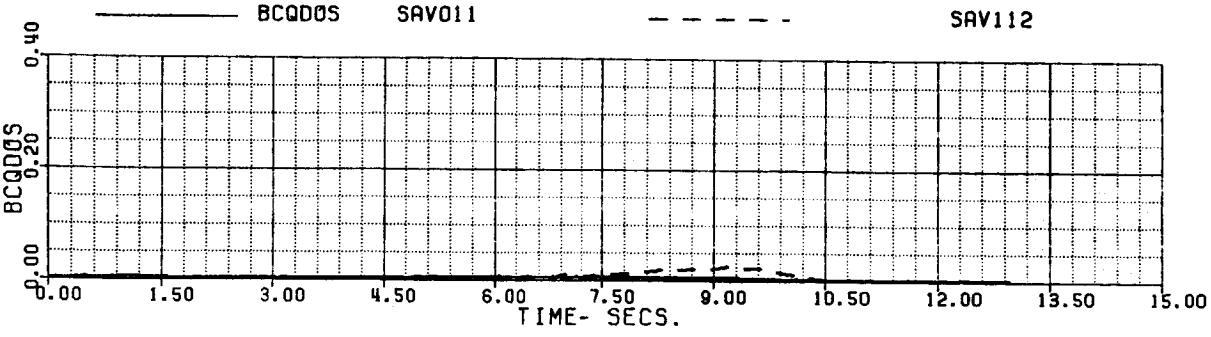

FIG 6.1.8 (c)

60A - BLACK HAWK (4/12)

FHIGTR - HIGH G TURN INT FUEL CONTROL
NZ FED TO NPREF

XA+1	5.7903764	XB+1	-3.5056055	XC+1	6.2289388	XP+1	3.1971333
THETAB	-1.7157311	VKT	129.99868	PHIB	0.	VYB	-1.5099977
XNGE	41524.665	NPINTE	1.3490933	VC	.175952E-2	WEIGHT	16638.000
OMRMR	0.9999999	NPMEAS	99.999997				

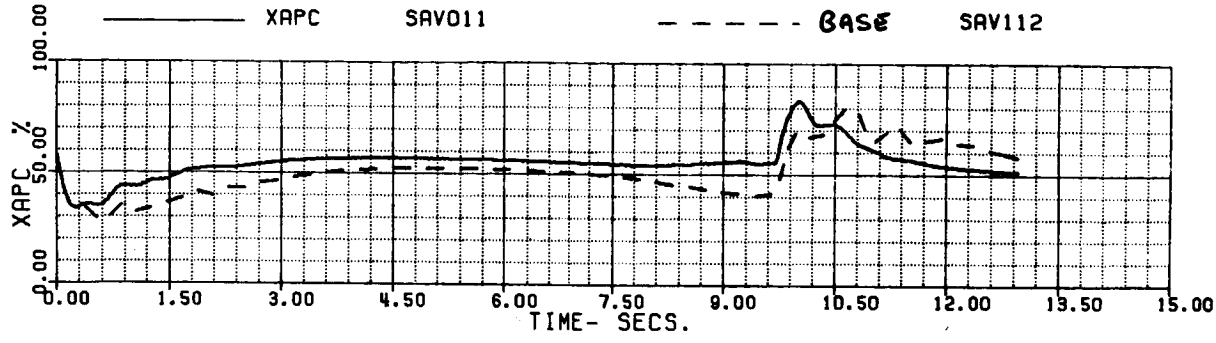

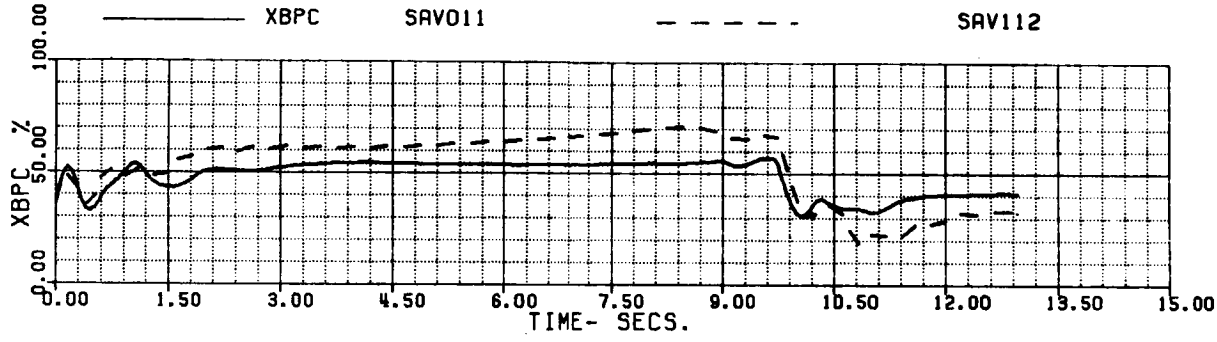

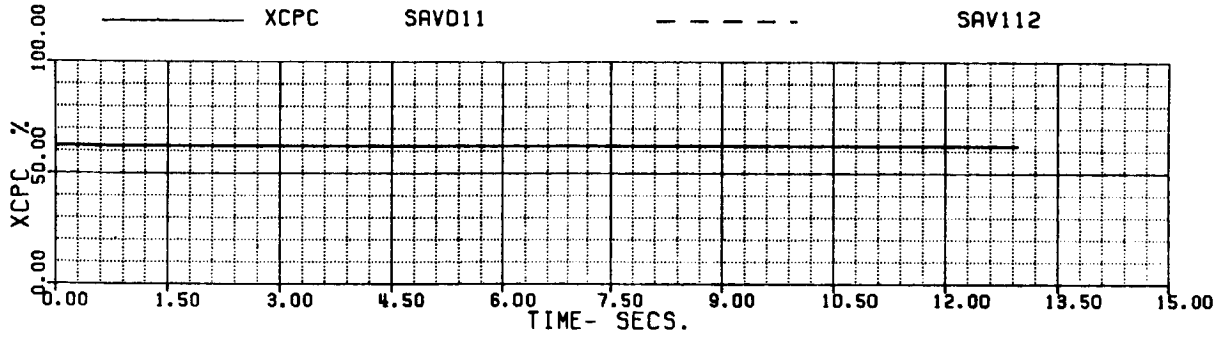

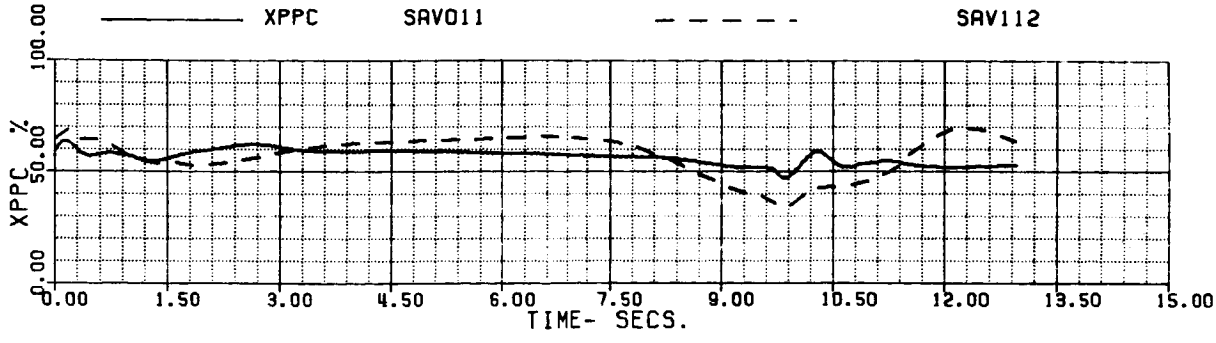

FIG 6.1.8 (d)

60A - BLACK HAWK (5/12)

FHIGTR - HIGH G TURN INT FUEL CONTROL
NZ FED TO NPREF

XA+1	5.7903764	XB+1	-3.5056055	XC+1	6.2289388	XP+1	3.1971333
THETAB	-1.7157311	VKT	129.99868	PHIB	0.	VTB	-1.5099977
XNGE	41524.665	NPINTE	1.3490933	VC	.175952E-2	WEIGHT	16638.000
OMRMR	0.9999999	NPMEAS	99.999997				

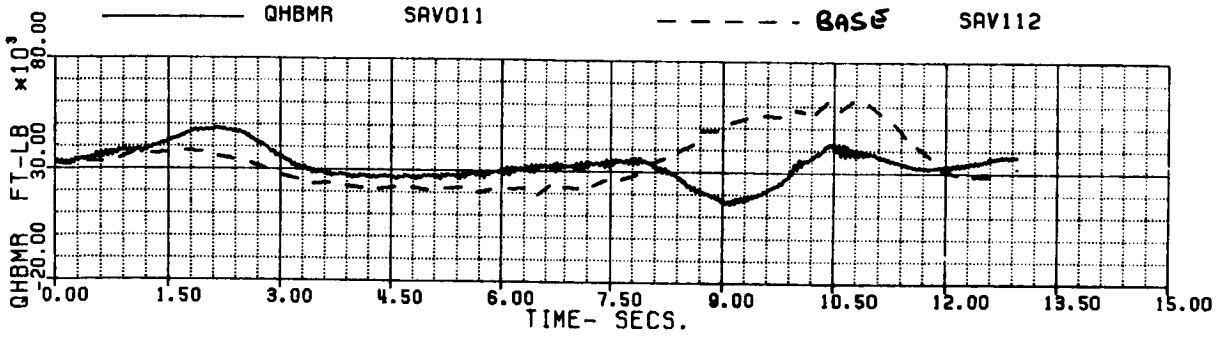

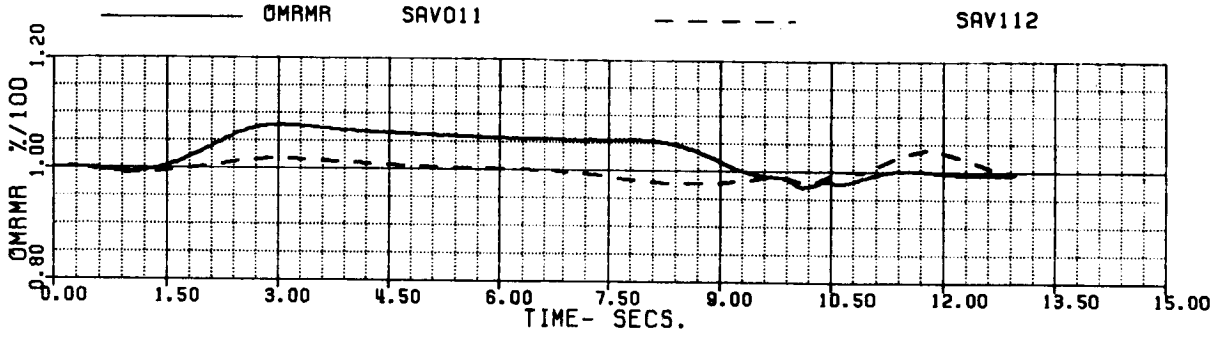

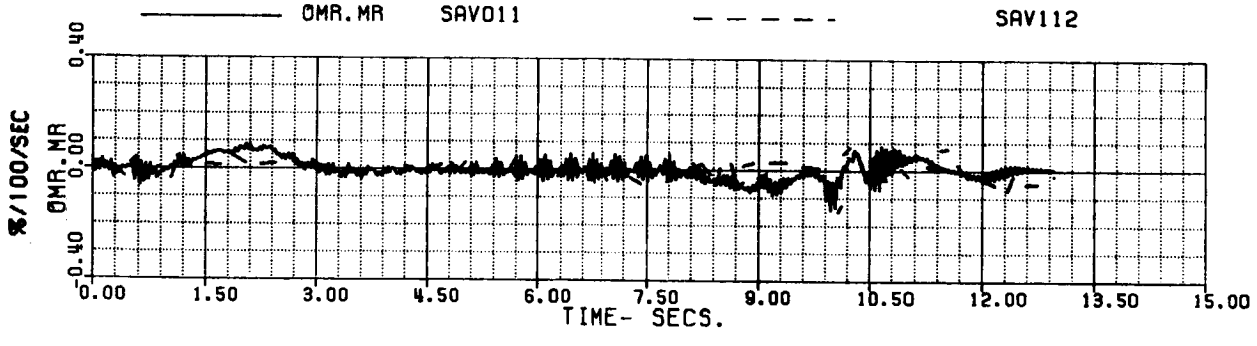

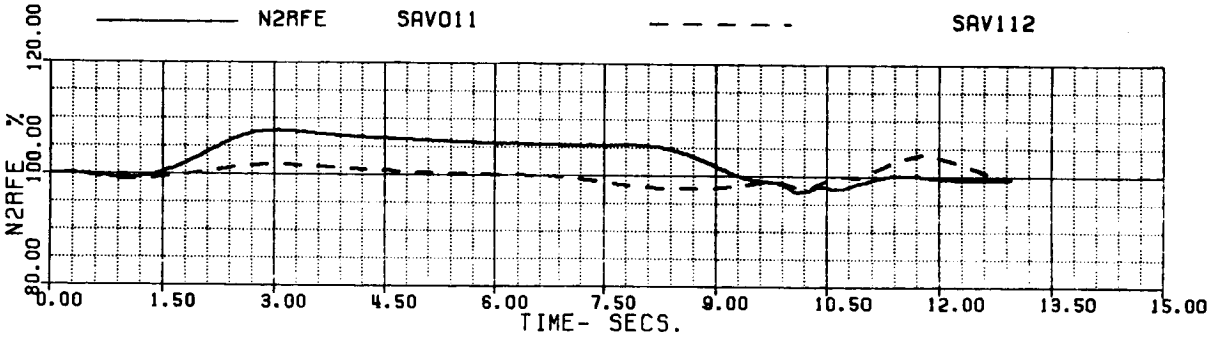

FIG 6.1.8 (e)

60A - BLACK HAWK

FHIGTR - HIGH G TURN INT FUEL CONTROL
NZ FED TO NPREF

(6/12)

XA+1	5.7903764	XB+1	-3.5056055	XC+1	6.2289388	XP+1	3.1971333
THETAB	-1.7157311	VKT	129.99868	PHIB	0.	VYB	-1.5099977
XNGE	41524.665	NPINTE	1.3490933	VC	.175952E-2	WEIGHT	16638.000
OMRMR	0.9999999	NPMEAS	99.999997				

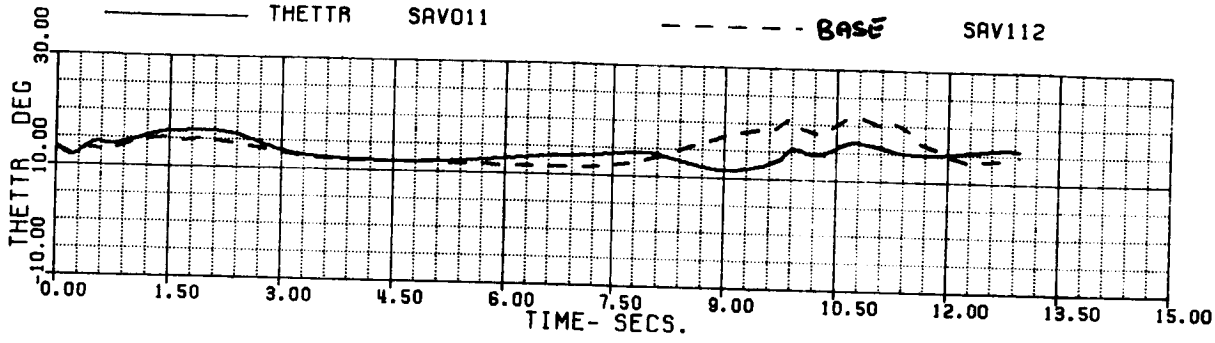

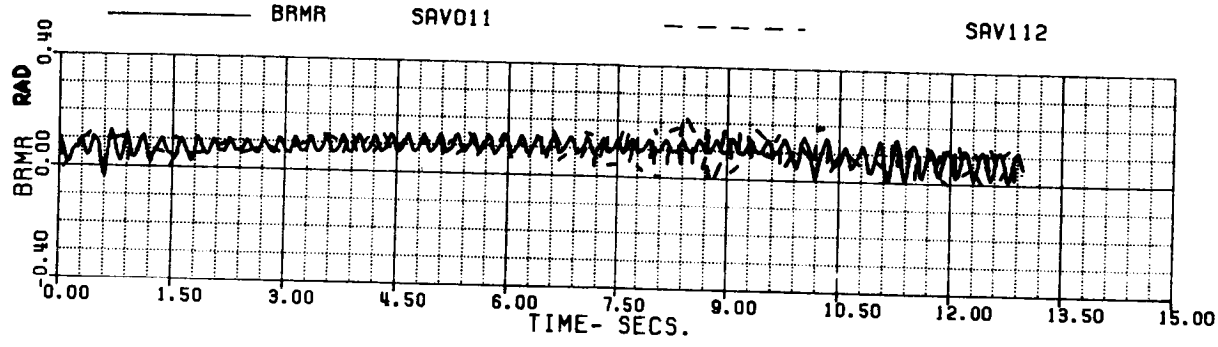

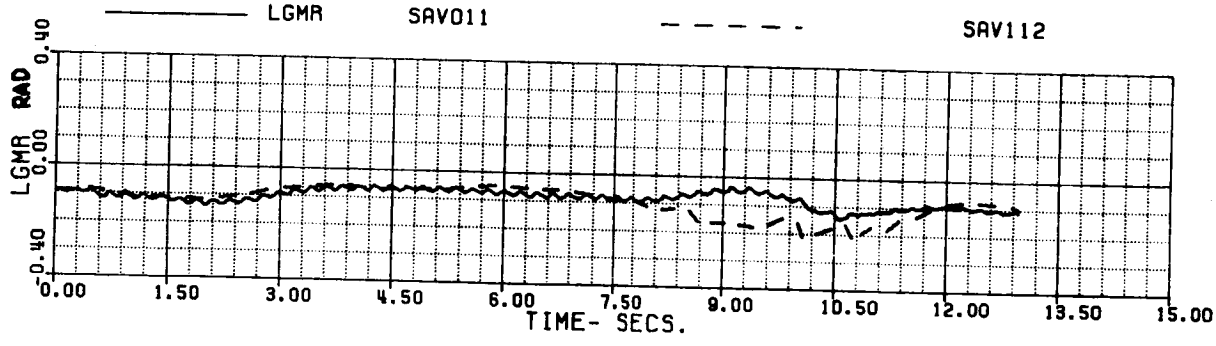

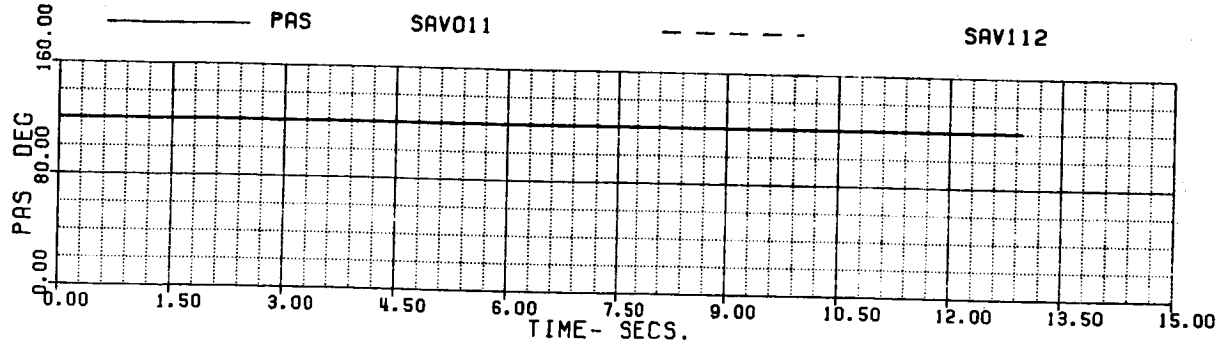

FIG 6.1.8 (f)

60A - BLACK HAWK

FHIGTR - HIGH G TURN INT FUEL CONTROL
NZ FED TO NPREF

(7/12)

XA+1	5.7903764	XB+1	-3.5056055	XC+1	6.2289388	XP+1	3.1971333
THETAB	-1.7157311	VKT	129.99868	PHIB	0.	VYB	-1.5099977
XNGE	41524.665	NPINTE	1.3490933	VC	.175952E-2	WEIGHT	16638.000
OMRMR	0.9999999	NPMEAS	99.999997				

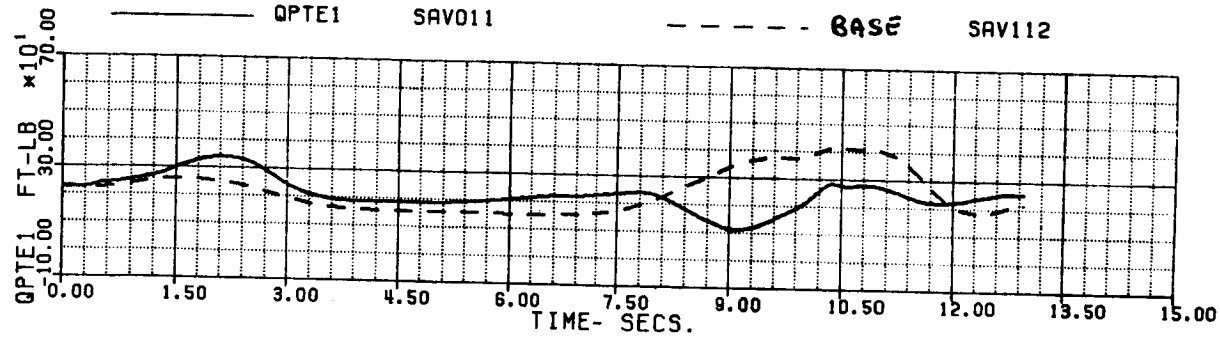

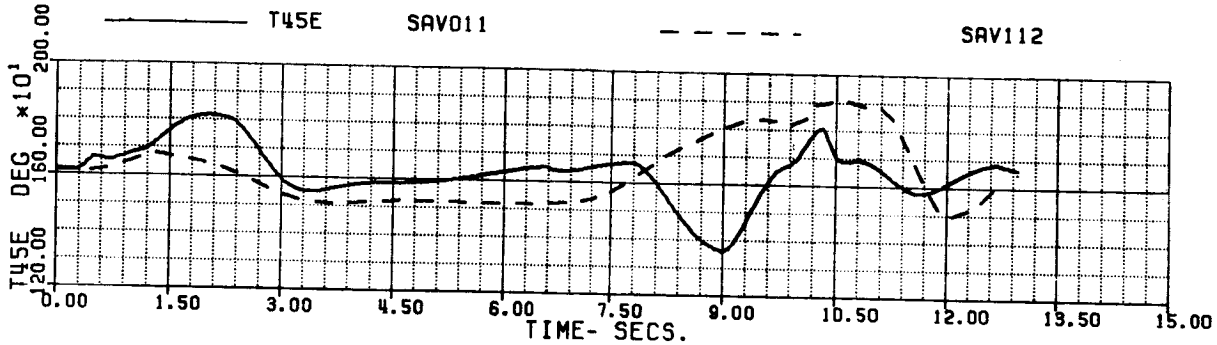

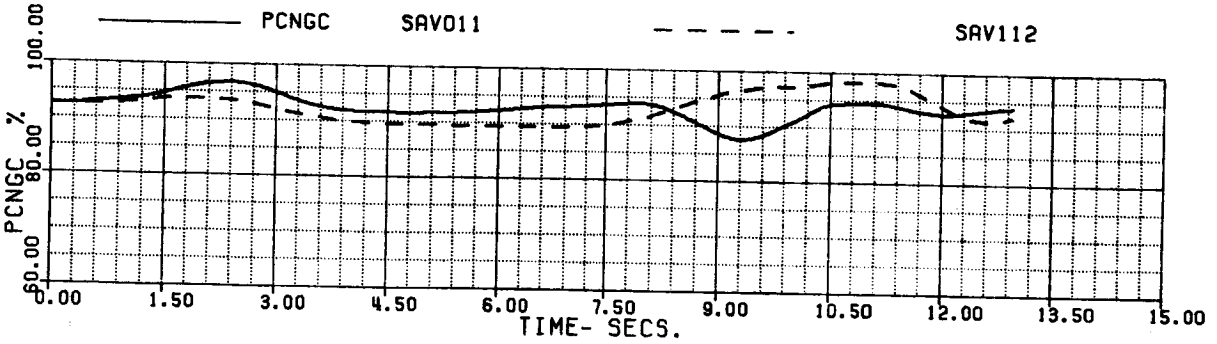

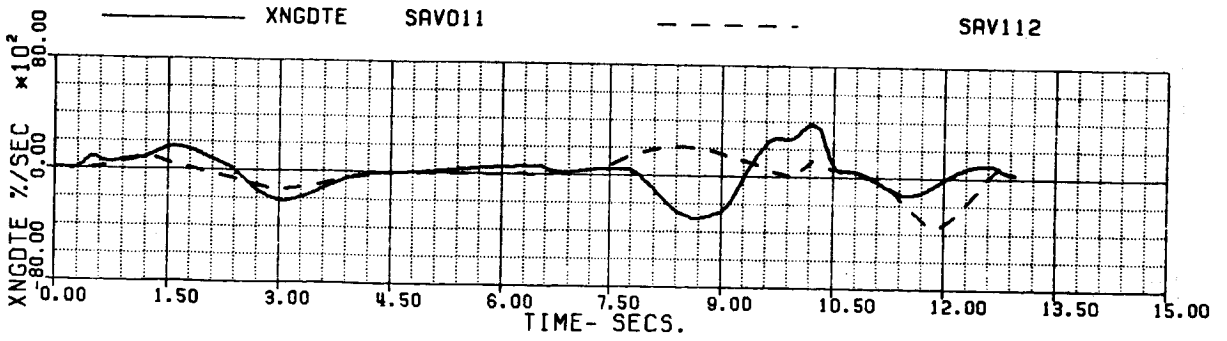

FIG 6.1.8 (g)

60A - BLACK HAWK (8/12)

FHIGTR - HIGH G TURN INT FUEL CONTROL
NZ FED TO NPREF

XA+1	5.7903764	XB+1	-3.5056055	XC+1	6.2289388	XP+1	3.1971333
THETAB	-1.7157311	VKT	129.99868	PHIB	0.	VYB	-1.5099977
XNGE	41524.665	NPINTE	1.3490933	VC	.175952E-2	WEIGHT	16638.000
OMRMR	0.9999999	NPMEAS	99.999997				

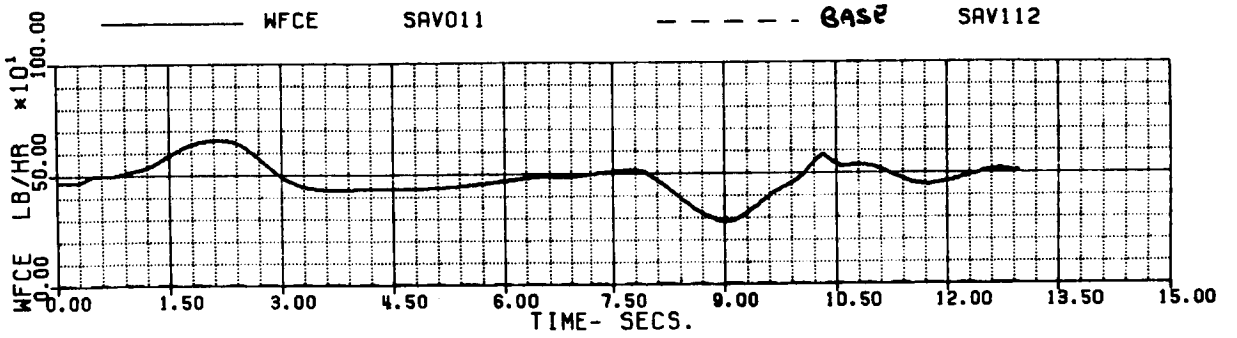

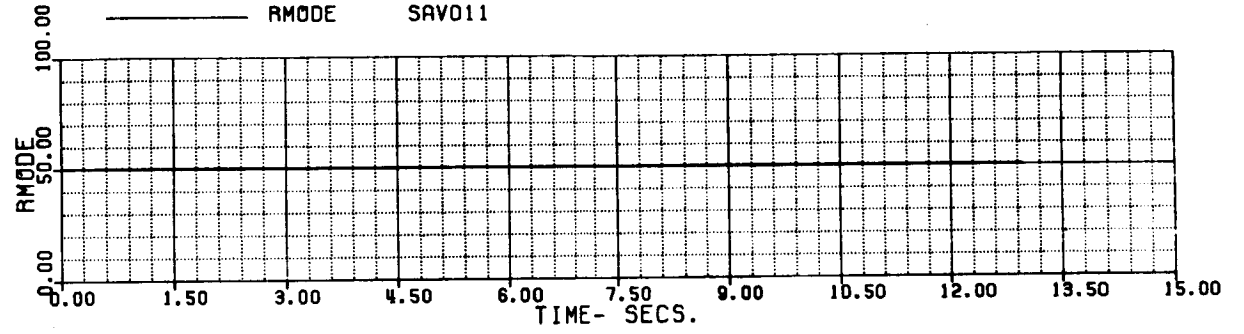

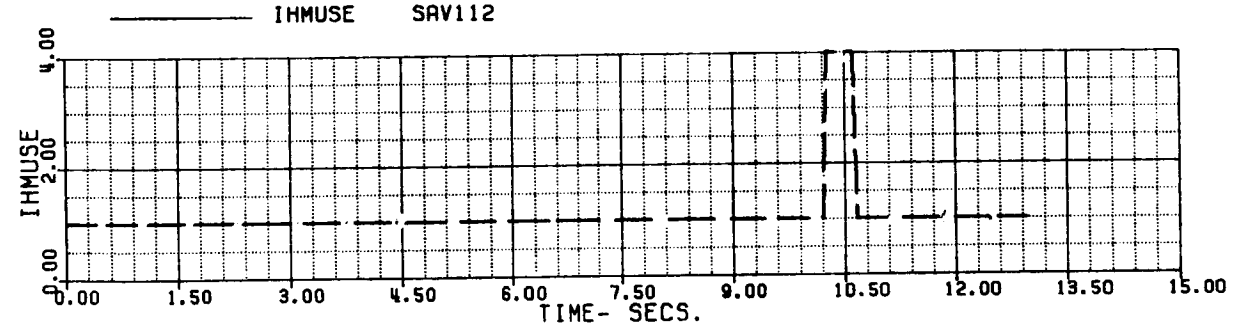

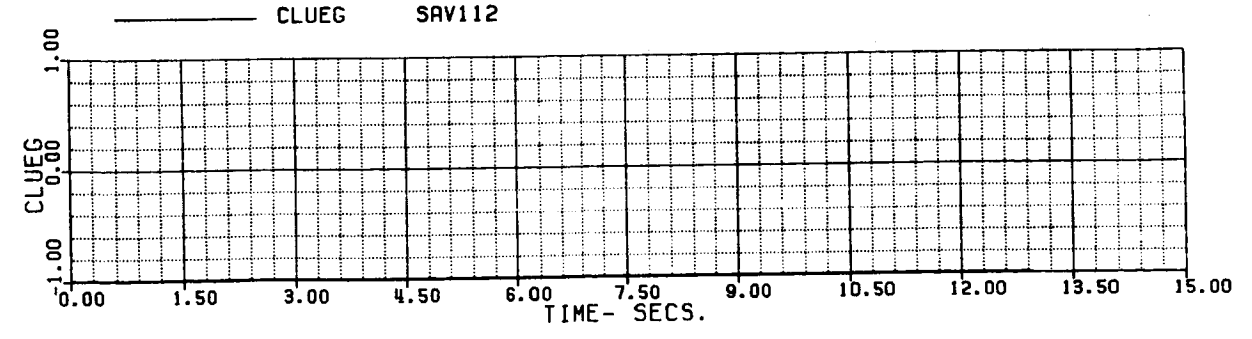

FIG 6.1.8 (h)

60A - BLACK HAWK 12:40 (9/12)
FHIGTR - HIGH G TURN INT FUEL CONTROL
NZ FED TO NPREF

XA+1	5.7903764	XB+1	-3.5056055	XC+1	6.2289388	XP+1	3.1971333
THETAB	-1.7157311	VKT	129.99868	PHIB	0.	YTB	-1.5099977
XNGE	41524.665	NPINTE	1.3490933	VC	.175952E-2	WEIGHT	16638.000
OMRMR	0.9999999	NPMEAS	99.999997				

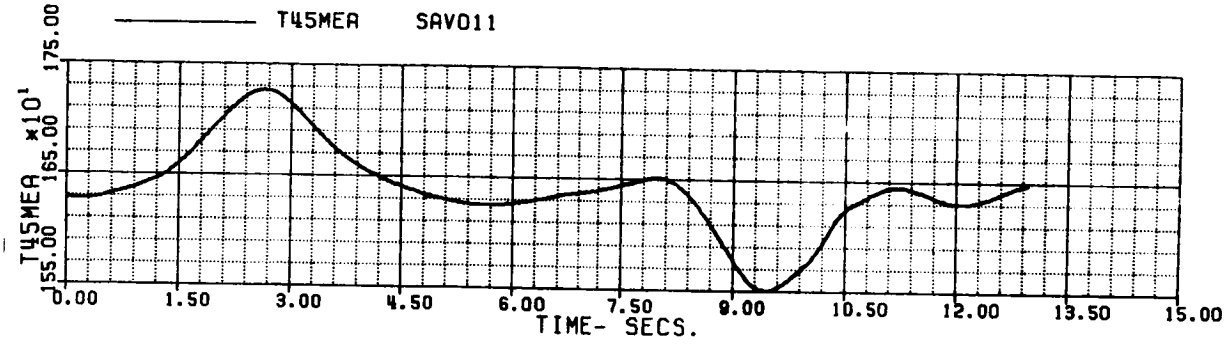

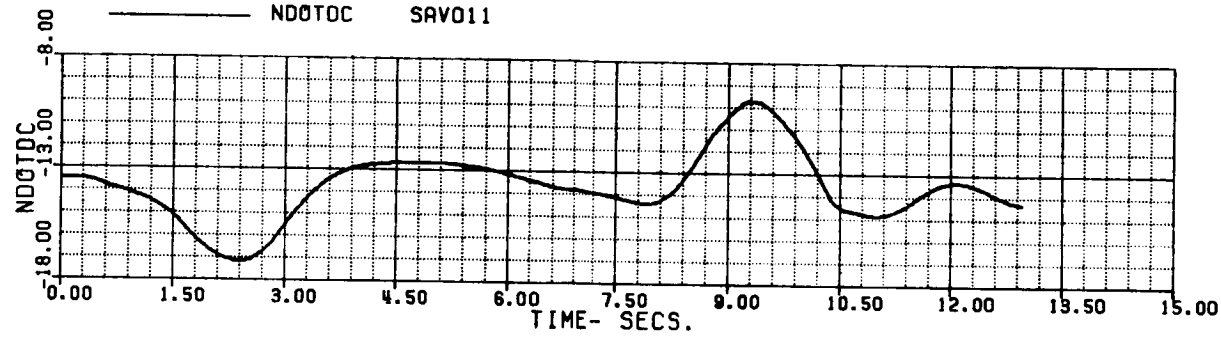

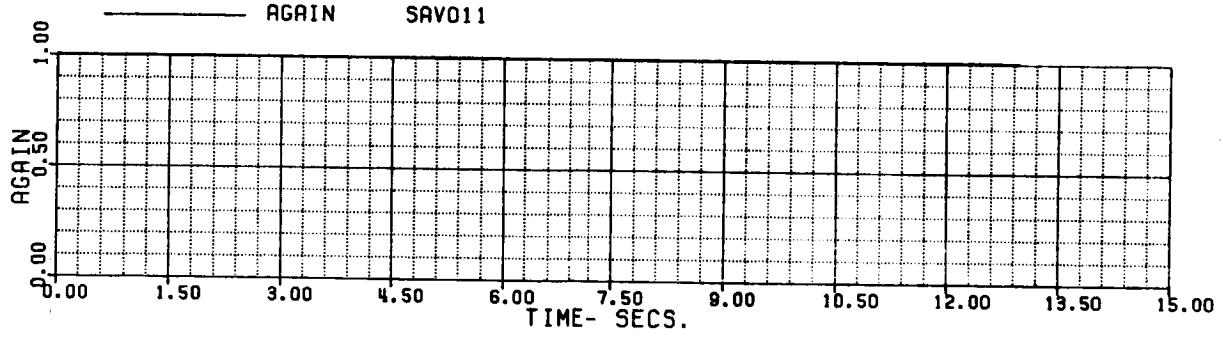

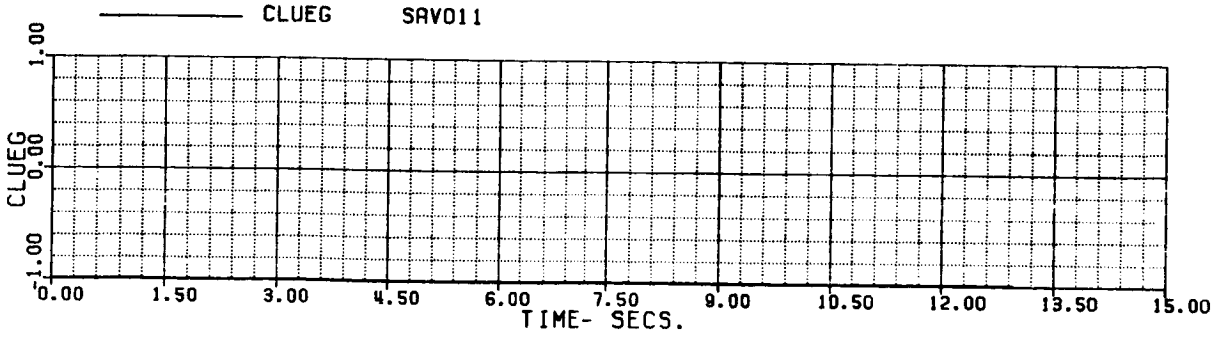

FIG 6.1.8 (i)

60A - BLACK HAWK (11/12

FHIGTR - HIGH G TURN INT FUEL CONTROL
NZ FED TO NPREF

XA+1	5.7903764	XB+1	-3.5056055	XC+1	6.2289388	XP+1	3.1971333
THETAB	-1.7157311	VKT	129.99868	PHIB	0.	VYB	-1.509997
XNGE	41524.665	NPINTE	1.3490933	VC	.175952E-2	WEIGHT	16638.000
OMRMR	0.9999999	NPMEAS	99.999997				

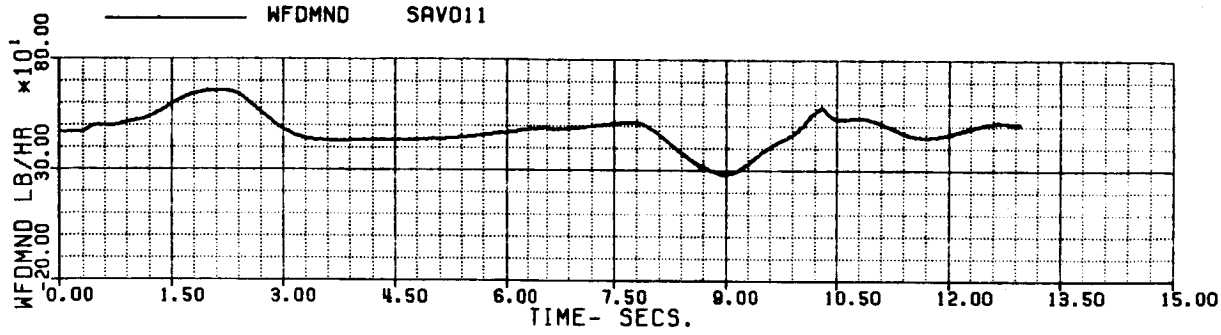

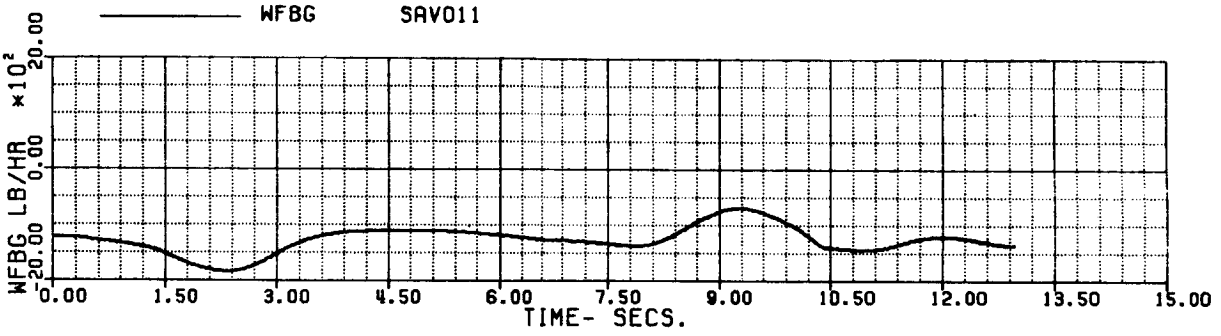

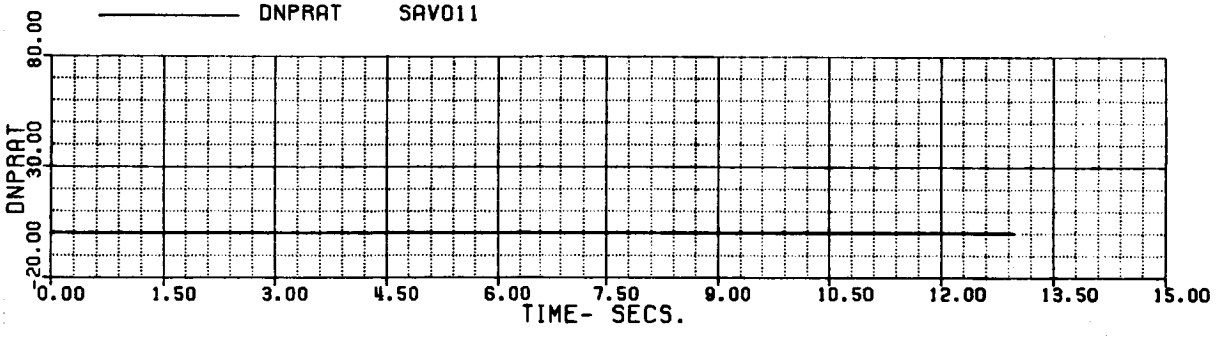

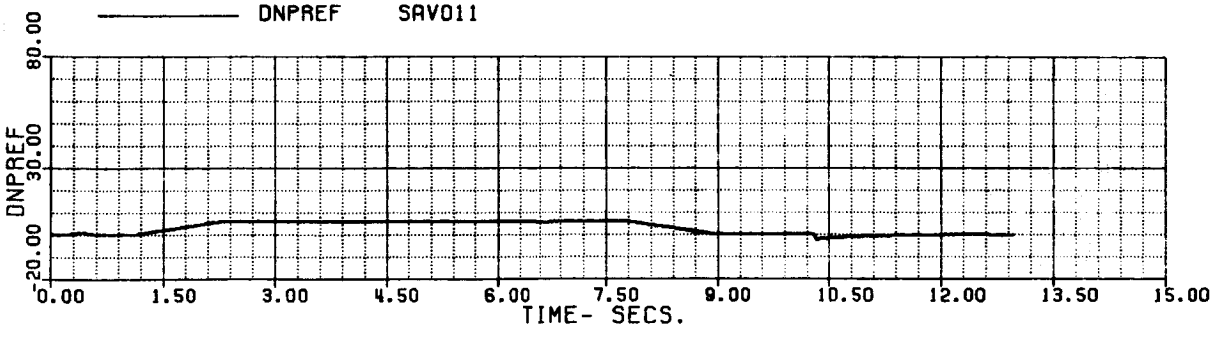

FIG 6.1.8 (j)

60A - BLACK HAWK (12/1

FHIGTR - HIGH G TURN INT FUEL CONTROL
NZ FED TO NPREF

XA+1	5.7903764	XB+1	-3.5056055	XC+1	6.2289388	XP+1	3.197135
THETAB	-1.7157311	VKT	129.99868	PHIB	0.	VYB	-1.50995
XNGE	41524.665	NPINTE	1.3490933	VC	.175952E-2	WEIGHT	16638.0C
OMRMR	0.9999999	NPMEAS	99.999997				

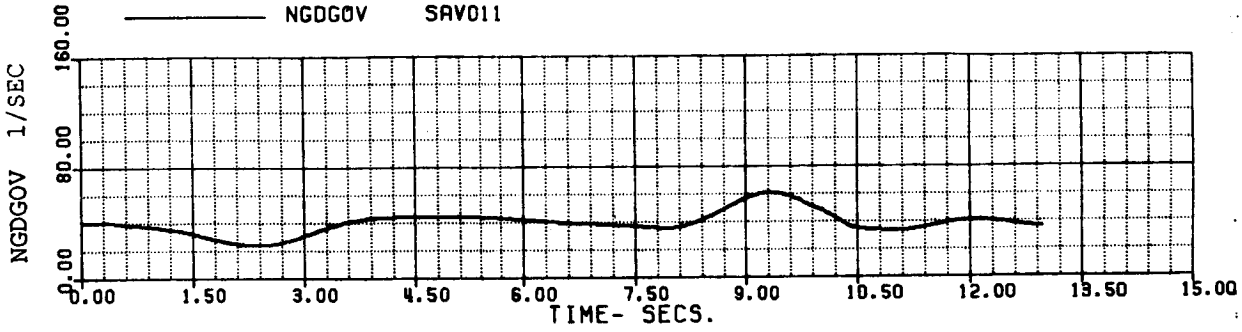

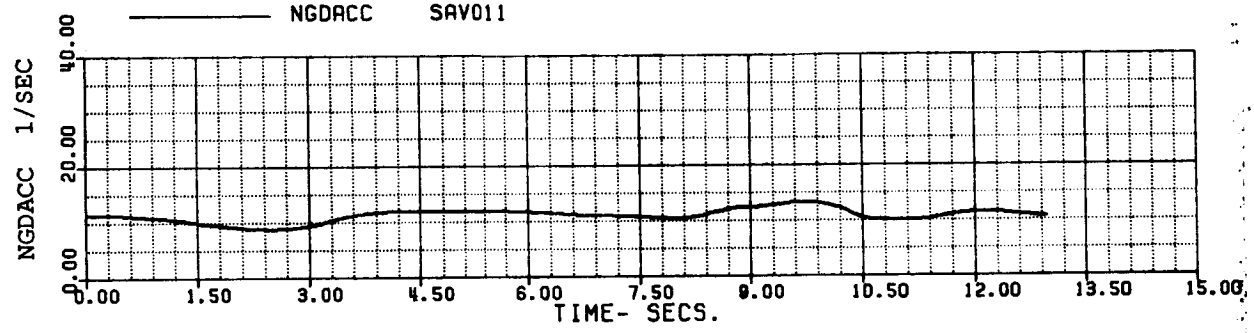

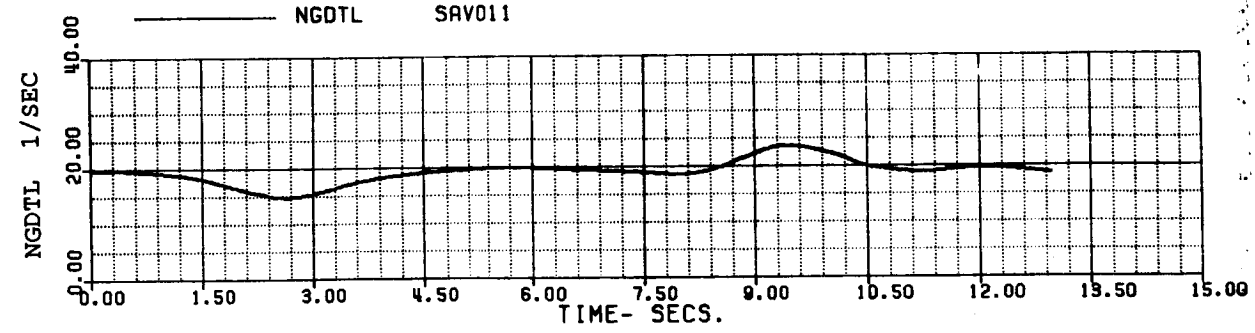

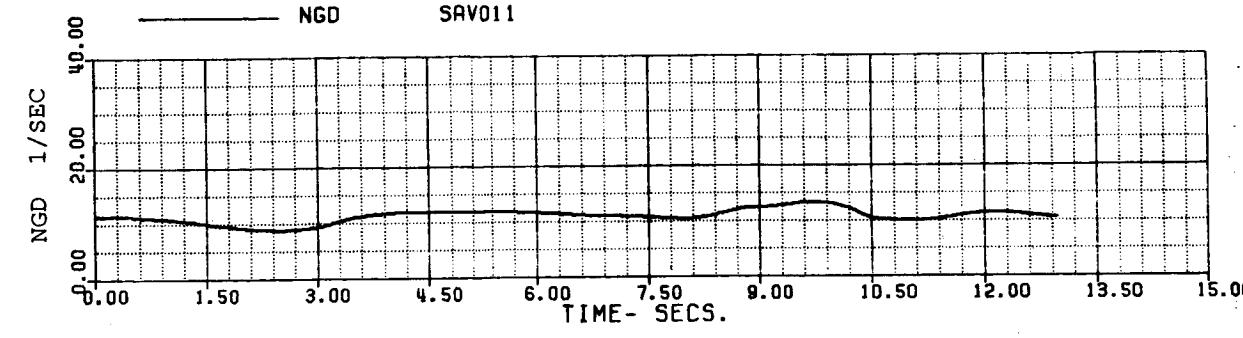

FIG 6.1.8 (k)

60A - BLACK HAWK (1/12)

FROLRE - ROLL REVERSAL, INTEGRATED FUEL CONTROL
ROLL RIGHT THEN LEFT

XA+1	5.8205497	XB+1	-3.3702563	XC+1	6.5933595	XP+1	3.2153668
THETAB	-2.1869954	VKT	135.00311	PHIB	0.	VYB	-1.5477484
XNGE	41784.030	NPINTE	1.3116747	VC	.116586E-2	WEIGHT	16638.000
OMRMR	0.9999999	NPMEAS	99.999997				

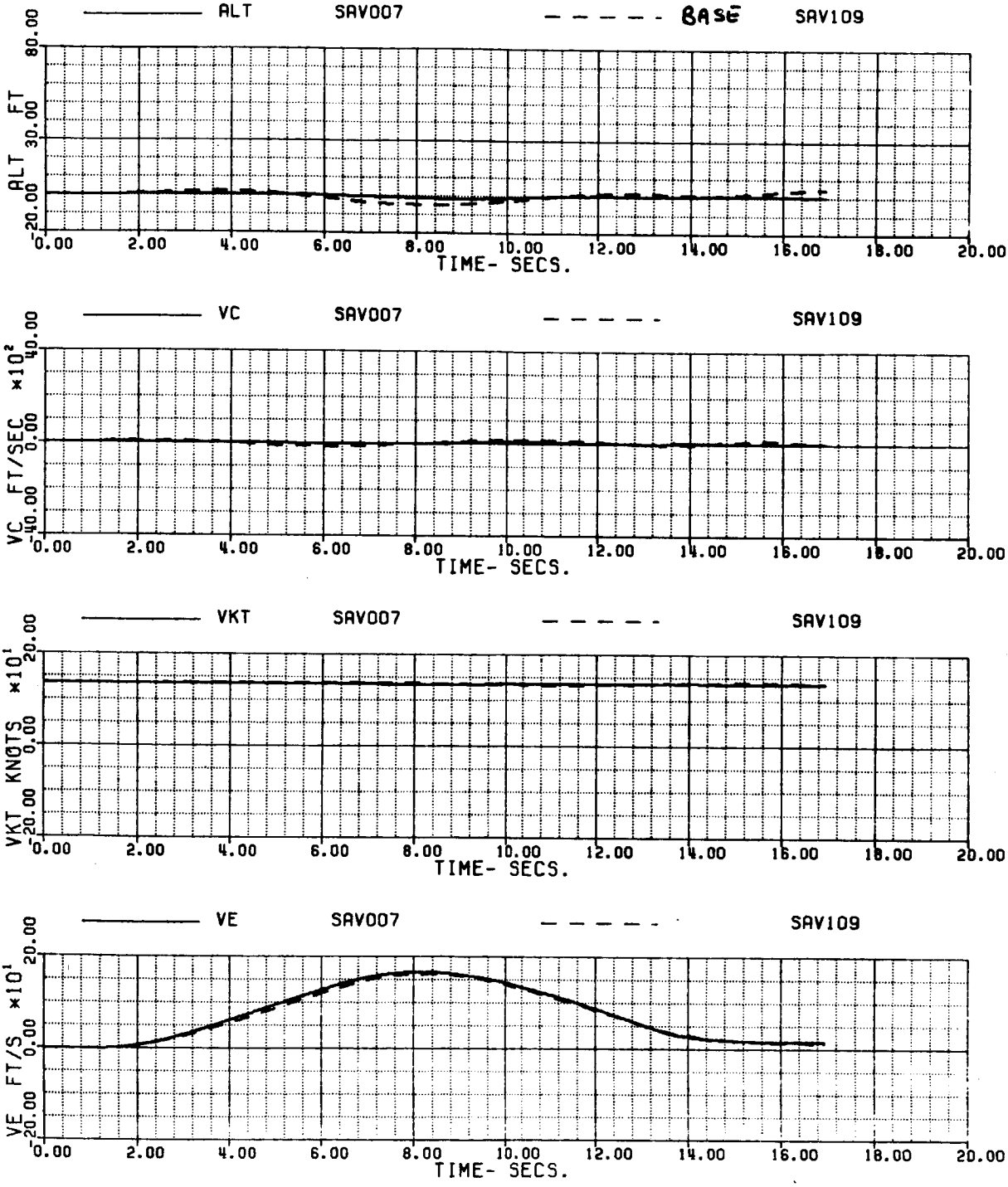

SIMULATED ROLL REVERSAL (RIGHT-LEFT-RIGHT)

FIG 6.1.9 (a)

60A - BLACK HAWK (2/12)

FROLRE - ROLL REVERSAL, INTEGRATED FUEL CONTROL
ROLL RIGHT THEN LEFT

XA+1	5.8205497	XB+1	-3.3702563	XC+1	6.5933595	XP+1	3.2153668
THETAB	-2.1869954	VKT	135.00311	PHIB	0.	VYB	-1.5477484
XNGE	41784.030	NPINTE	1.3116747	VC	.116586E-2	WEIGHT	16638.000
OMRMR	0.9999999	NPMEAS	99.999997				

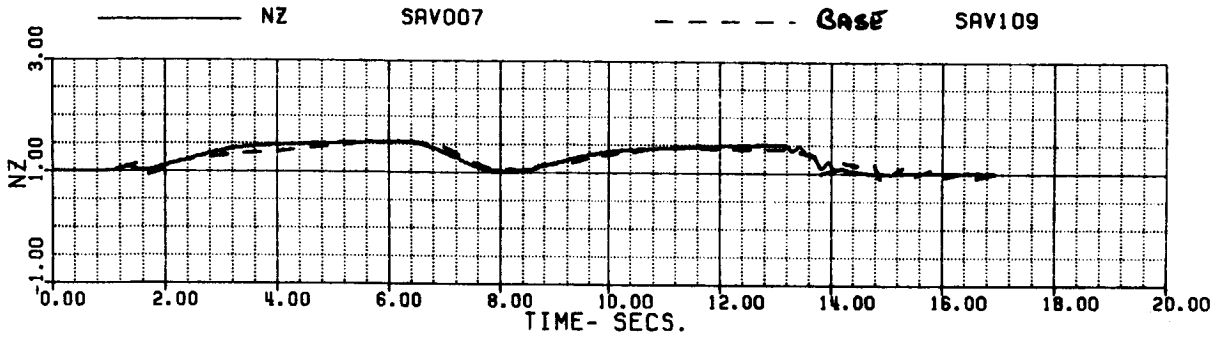

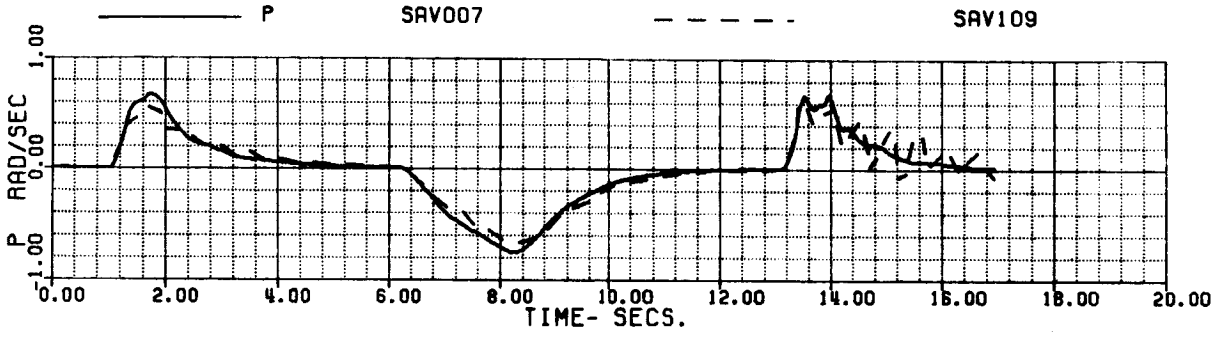

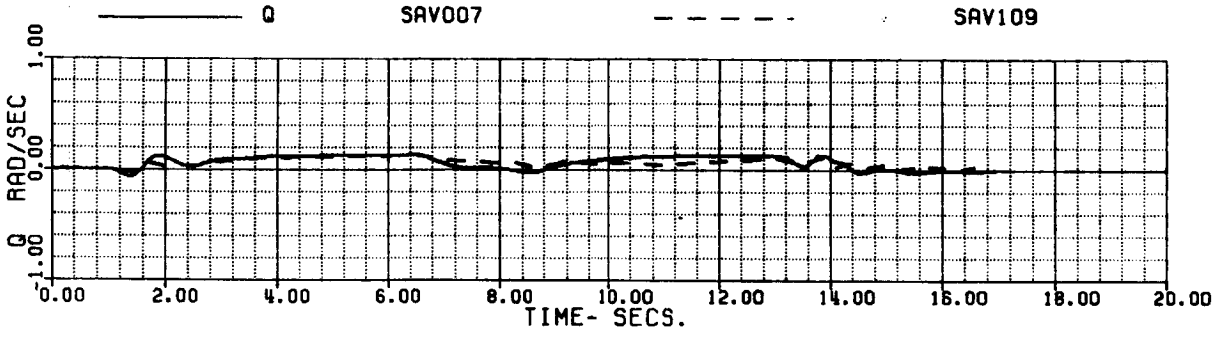

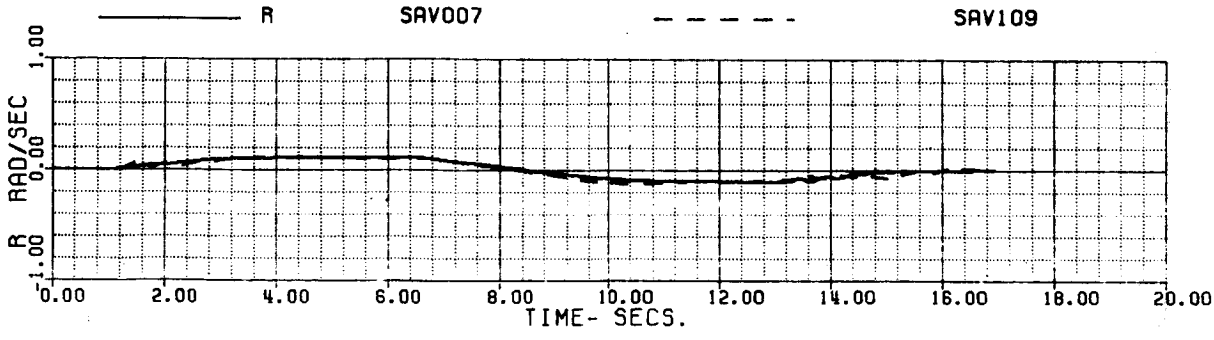

FIG 6.1.9 (b)

60A - BLACK HAWK (3/12)

FROLRE - ROLL REVERSAL, INTEGRATED FUEL CONTROL
ROLL RIGHT THEN LEFT

XA+1	5.8205497	XB+1	-3.3702563	XC+1	6.5933595	XP+1	3.2153668
THETAB	-2.1869954	VKT	135.00311	PHIB	0.	VYB	-1.5477484
XNGE	41784.030	NPINTE	1.3116747	VC	.116586E-2	WEIGHT	16638.000
OMRMR	0.9999999	NPMEAS	99.999997				

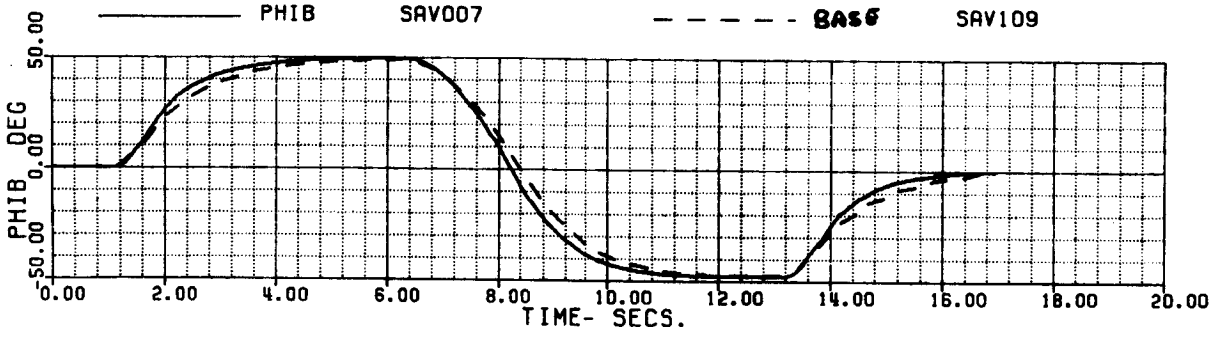

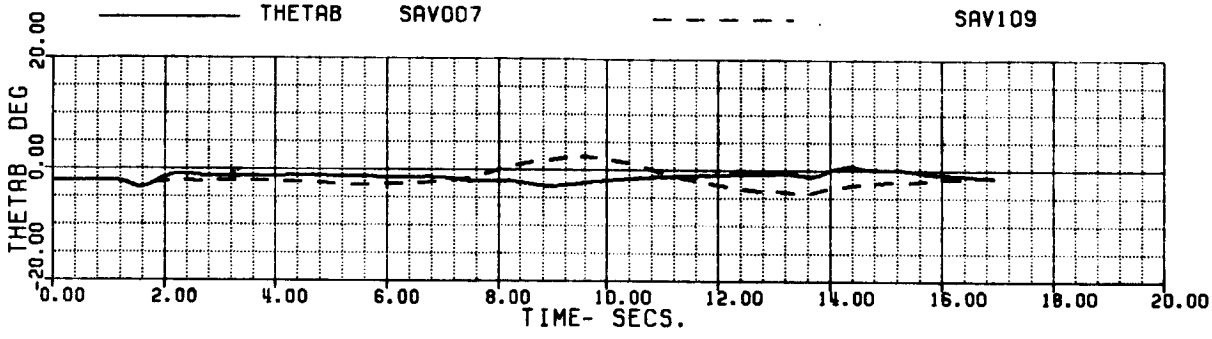

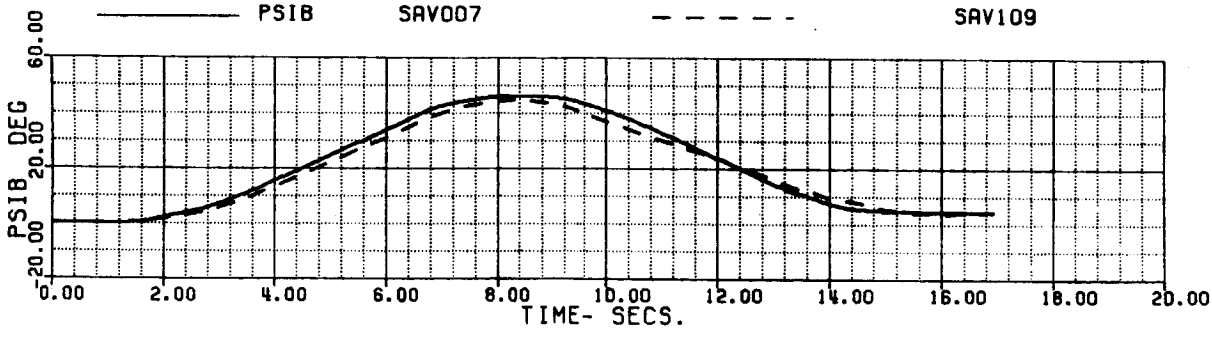

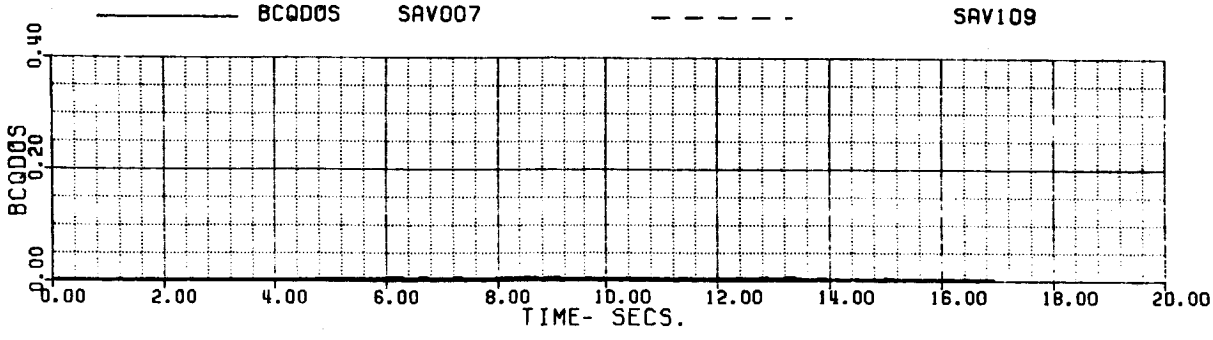

FIG 6.1.9 (c)

60A - BLACK HAWK (4/12)

FROLRE - ROLL REVERSAL, INTEGRATED FUEL CONTROL
ROLL RIGHT THEN LEFT

XA+1	5.8205497	XB+1	-3.3702563	XC+1	6.5933595	XP+1	3.2153668
THETAB	-2.1869954	VKT	135.00311	PHIB	0.	VYB	-1.5477484
XNGE	41784.030	NPINTE	1.3116747	VC	.116586E-2	WEIGHT	16638.000
OMRMR	0.9999999	NPMEAS	99.999997				

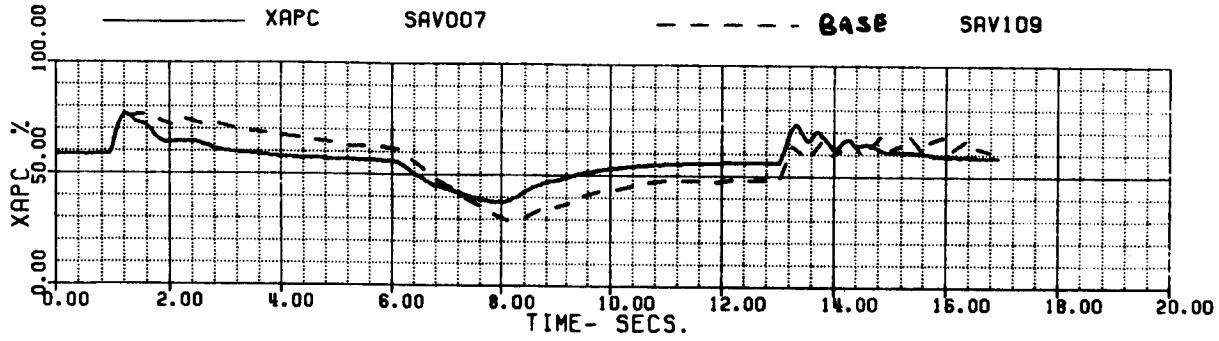

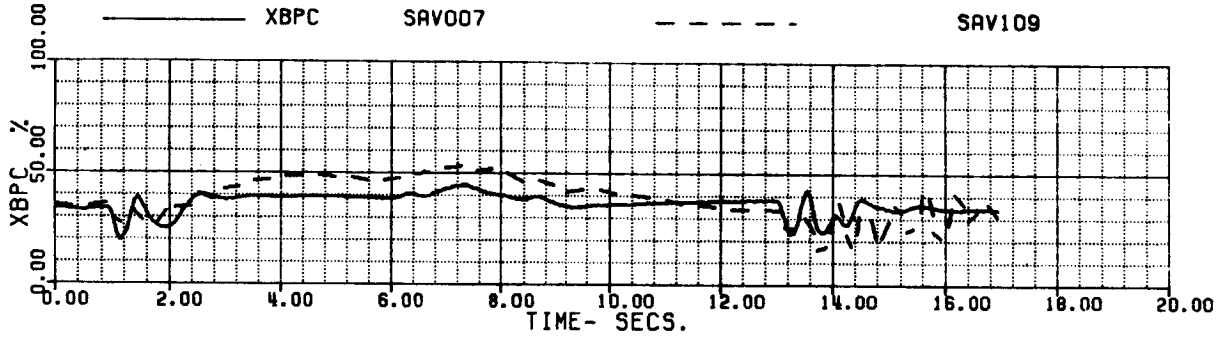

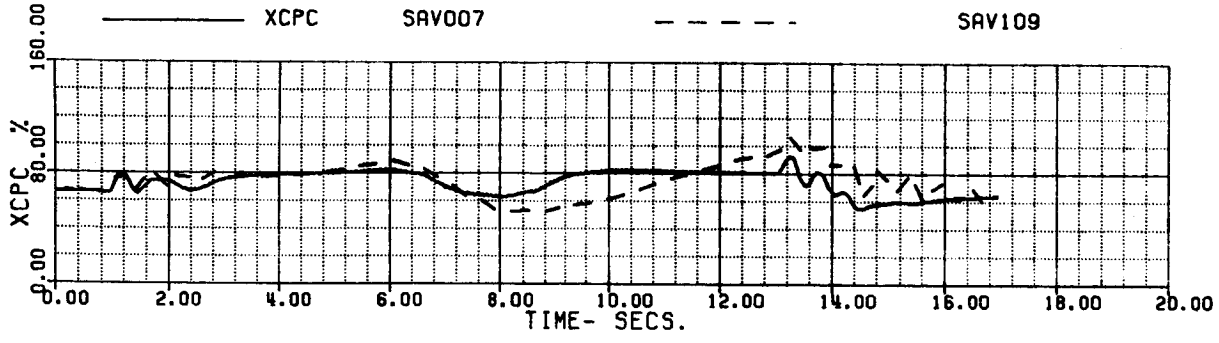

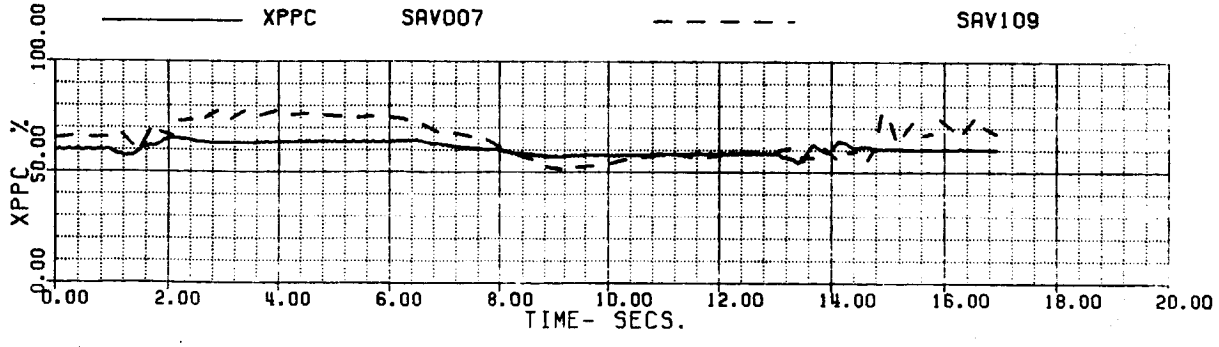

FIG 6.1.9 (d)

60A - BLACK HAWK (5/12)

FROLRE - ROLL REVERSAL, INTEGRATED FUEL CONTROL
ROLL RIGHT THEN LEFT

XA+1	5.8205497	XB+1	-3.3702563	XC+1	6.5933595	XP+1	3.2153668
THETAB	-2.1869954	VKT	135.00311	PHIB	0.	VTB	-1.5477484
XNGE	41784.030	NPINTE	1.3116747	VC	.116586E-2	WEIGHT	16638.000
OMRMR	0.9999999	NPMEAS	99.999997				

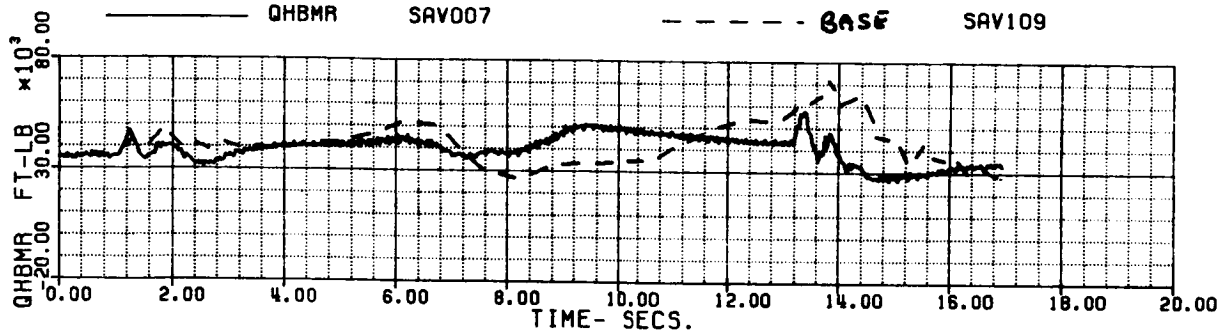

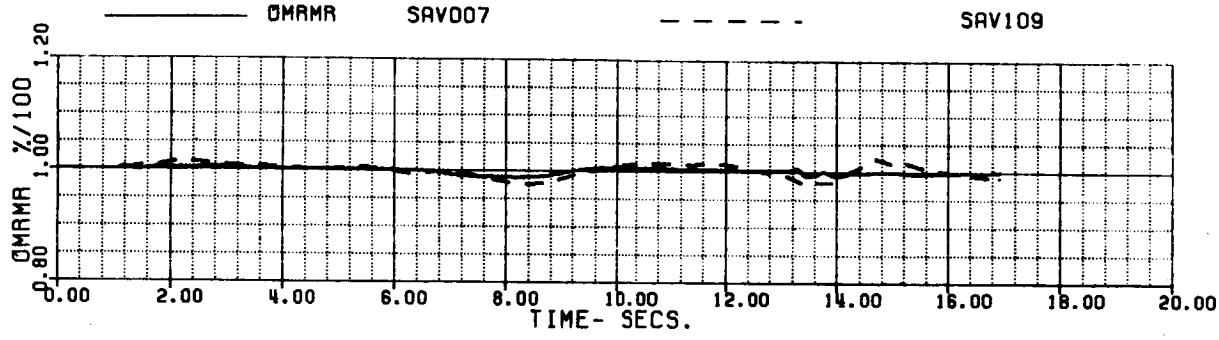

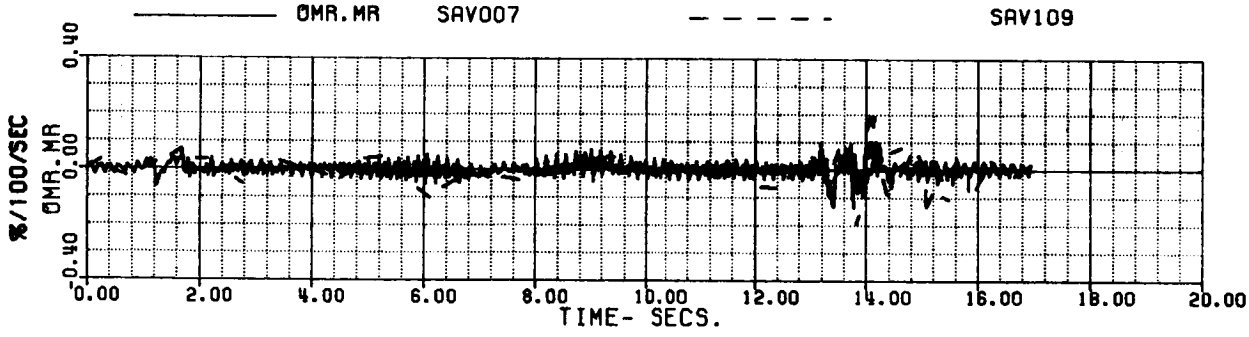

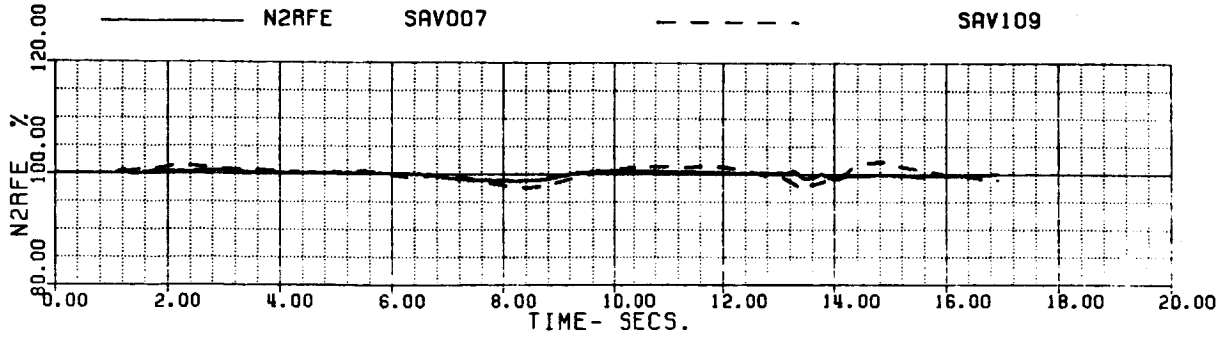

FIG 6.1.9 (e)

60A - BLACK HAWK (6/12)

FROLRE - ROLL REVERSAL, INTEGRATED FUEL CONTROL
ROLL RIGHT THEN LEFT

XA+1	5.8205497	XB+1	-3.3702563	XC+1	6.5933595	XP+1	3.2153668
THETAB	-2.1869954	VKT	135.00311	PHIB	0.	VYB	-1.5477484
XNGE	41784.030	NPINTE	1.3116747	VC	.116586E-2	WEIGHT	16638.000
OMRMR	0.9999999	NPMEAS	99.999997				

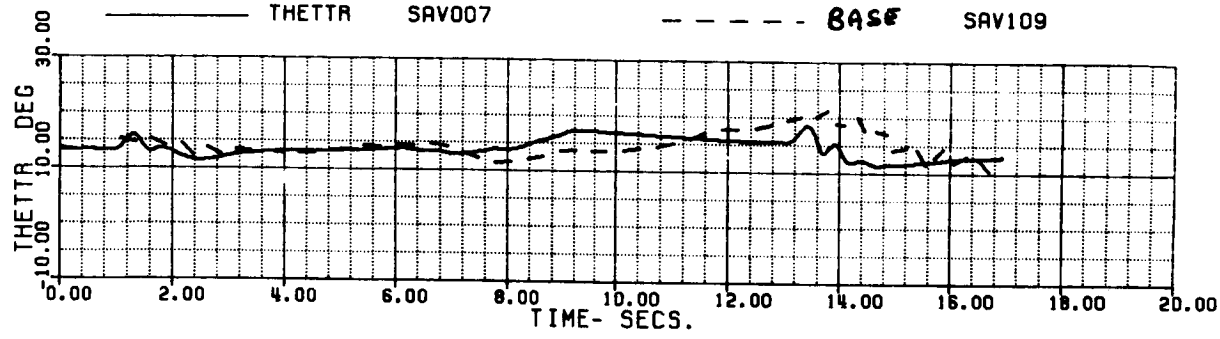

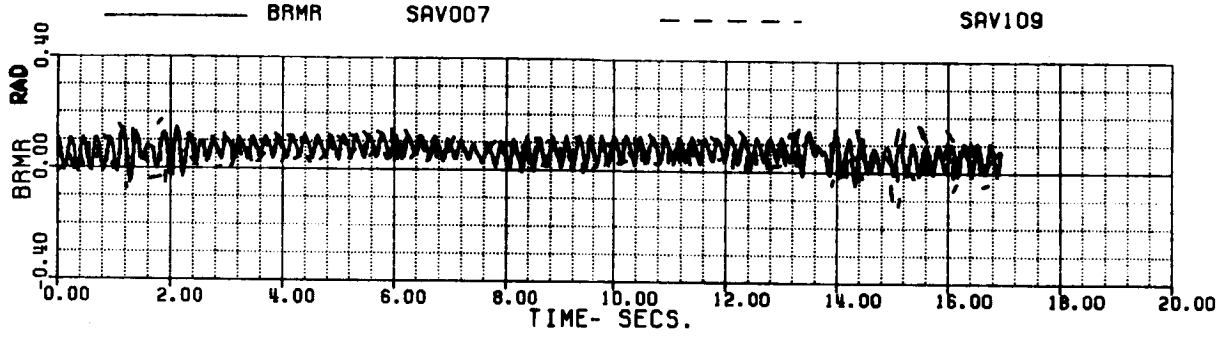

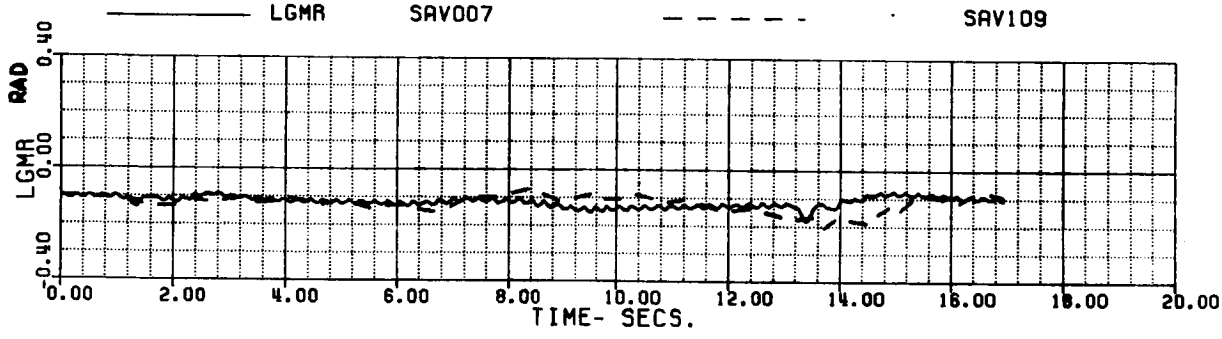

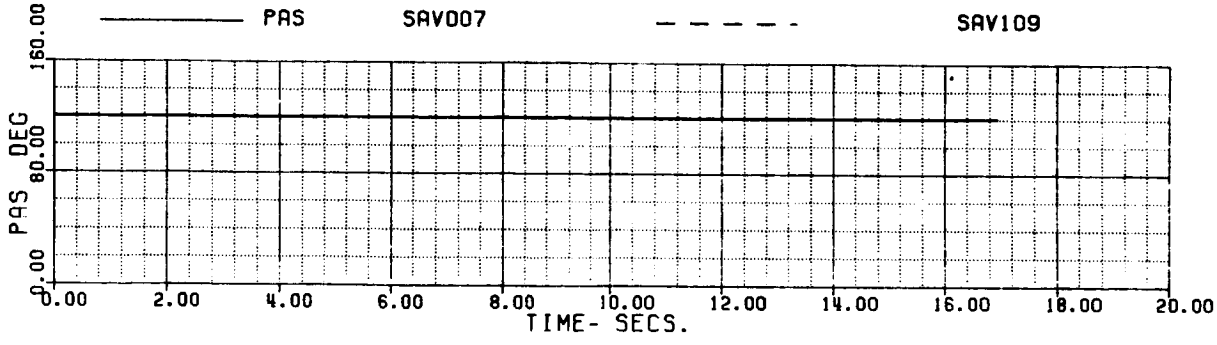

FIG 6.1.9 (f)

60A - BLACK HAWK

(7/12)

FROLRE - ROLL REVERSAL, INTEGRATED FUEL CONTROL
ROLL RIGHT THEN LEFT

XA+1	5.8205497	XB+1	-3.3702563	XC+1	6.5933595	XP+1	3.2153668
THETAB	-2.1869954	VKT	135.00311	PHIB	0.	VTB	-1.5477484
XNGE	41784.030	NPINTE	1.3116747	VC	.116586E-2	WEIGHT	16638.000
OMRMR	0.9999999	NPMEAS	99.999997				

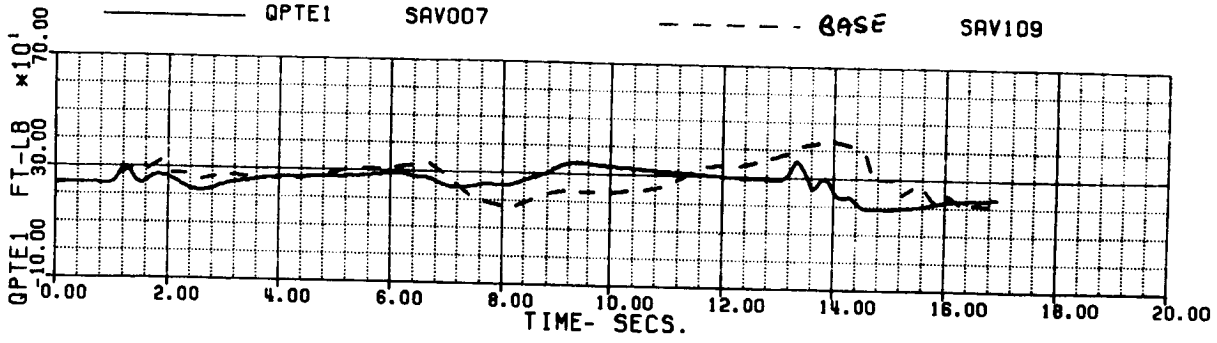

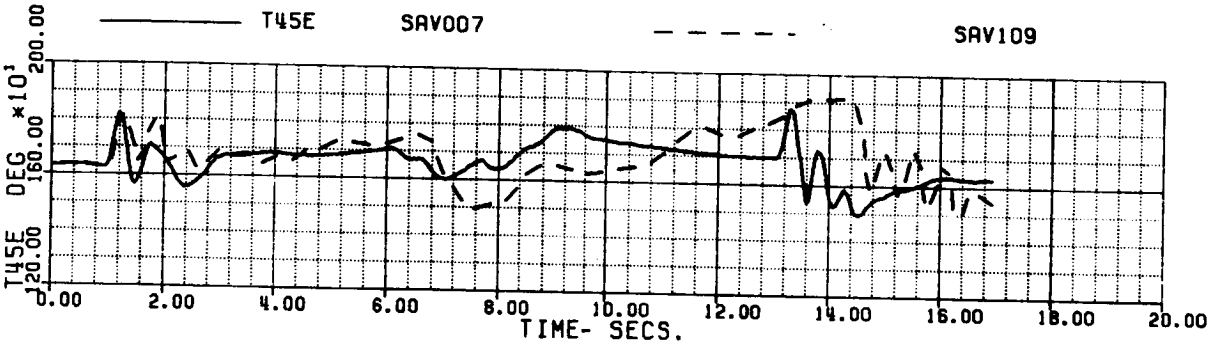

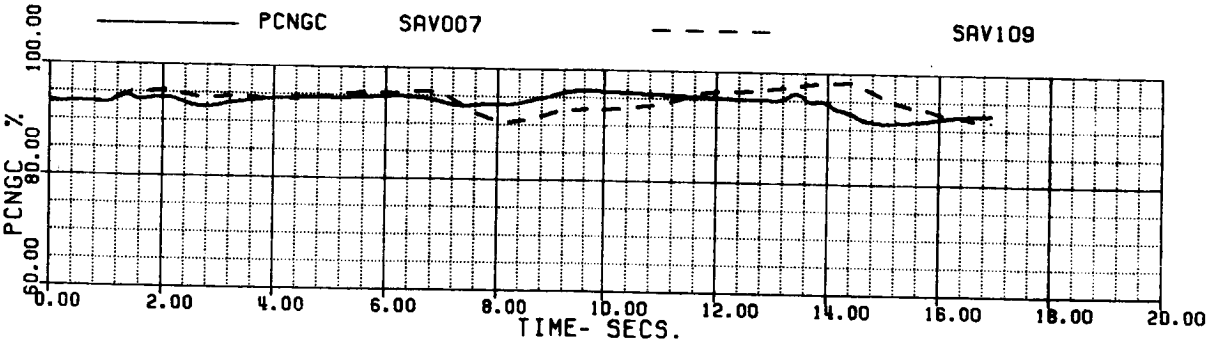

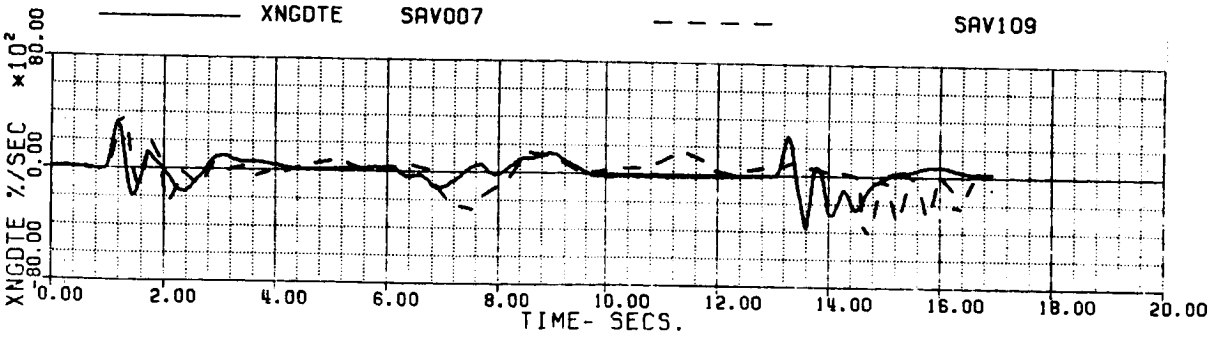

C-3

FIG 6.1.9 (g)

60A - BLACK HAWK (8/12)

FROLRE - ROLL REVERSAL, INTEGRATED FUEL CONTROL
ROLL RIGHT THEN LEFT

XA+1	5.8205497	XB+1	-3.3702563	XC+1	6.5933595	XP+1	3.2153668
THETAB	-2.1869954	VKT	135.00311	PHIB	0.	VYB	-1.5477484
XNGE	41784.030	NPINTE	1.3116747	VC	.116586E-2	WEIGHT	16638.000
OMRMR	0.9999999	NPMEAS	99.999997				

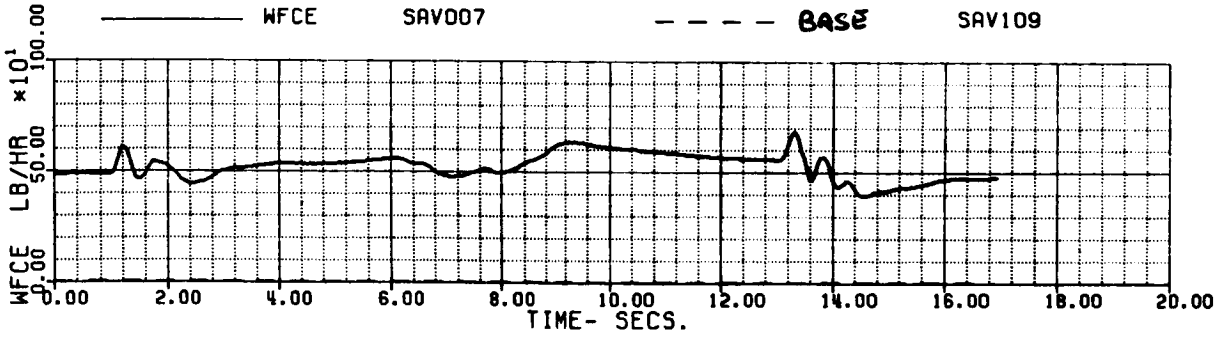

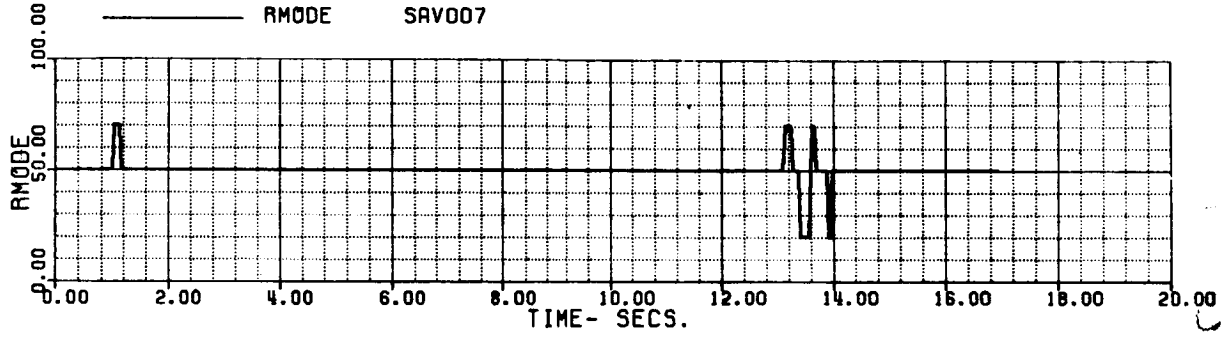

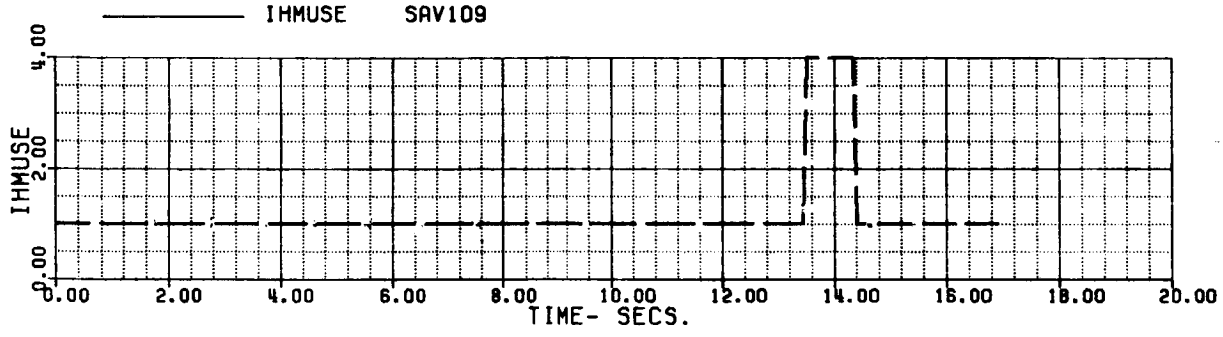

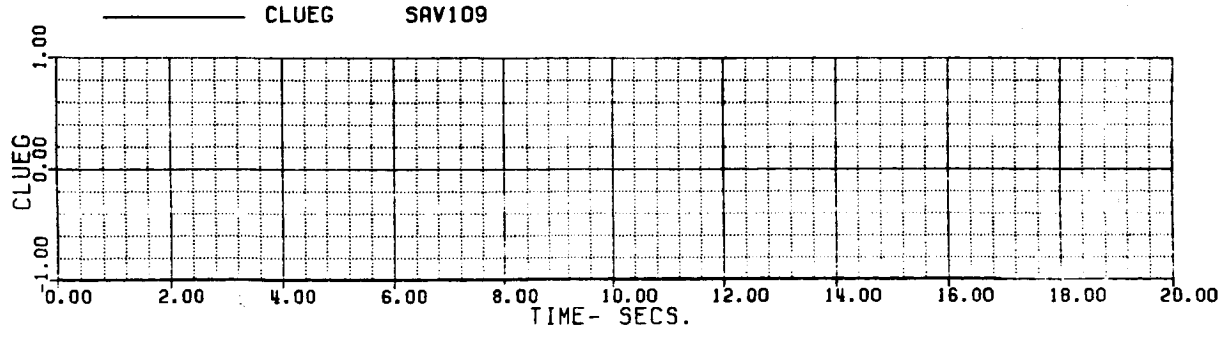

FIG 6.1.9 (h)

60A - BLACK HAWK (9/12)

FROLRE - ROLL REVERSAL, INTEGRATED FUEL CONTROL
ROLL RIGHT THEN LEFT

XA+1	5.8205497	XB+1	-3.3702563	XC+1	6.5933595	XP+1	3.2153668
THETAB	-2.1869954	VKT	135.00311	PHIB	0.	VYB	-1.5477484
XNGE	41784.030	NPINTE	1.3116747	VC	.116586E-2	WEIGHT	16638.000
OMRMR	0.9999999	NPMEAS	99.999997				

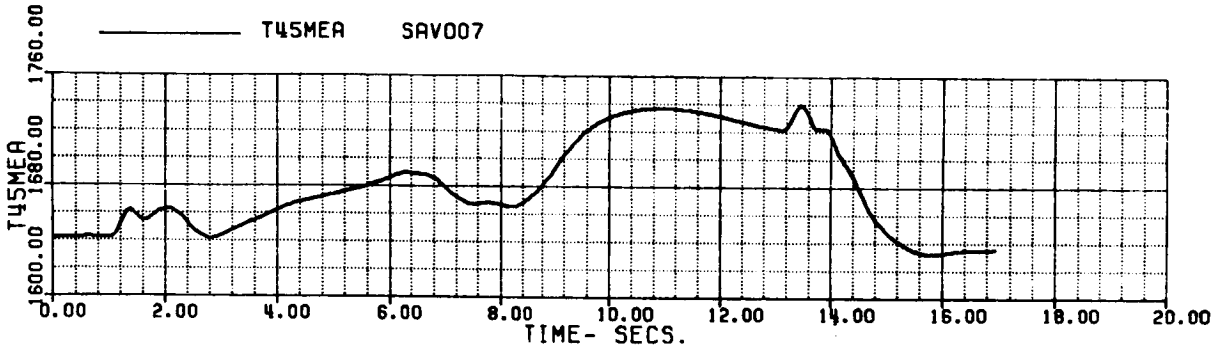

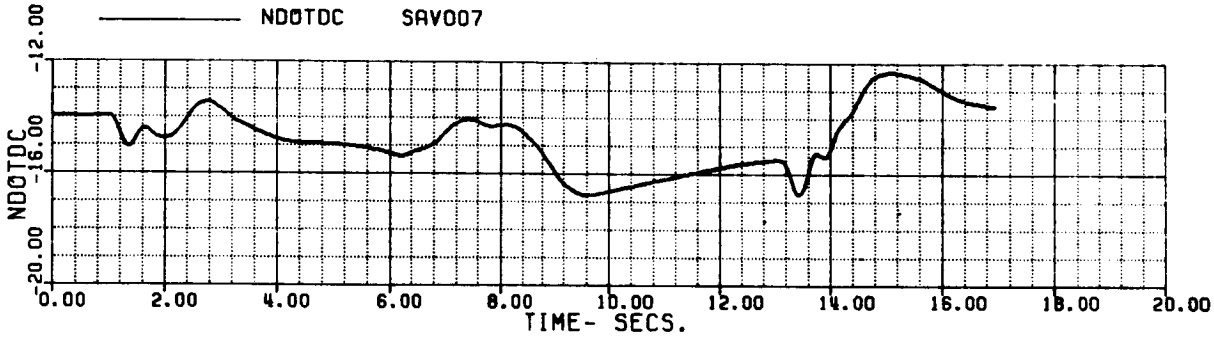

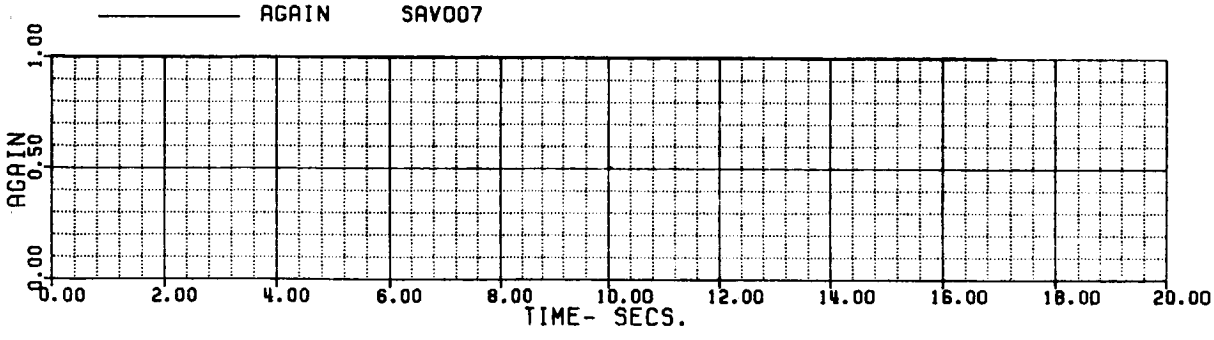

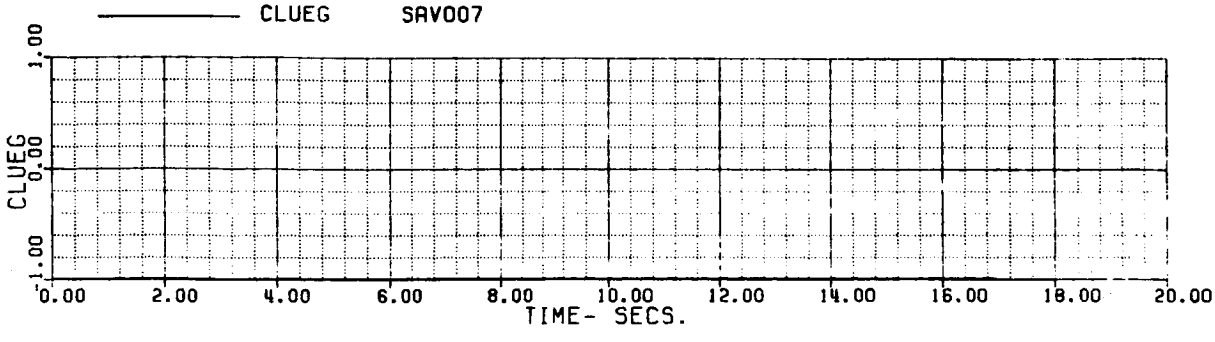

FIG 6.1.9 (i)

60A - BLACK HAWK

(11/12

FROLRE - ROLL REVERSAL, INTEGRATED FUEL CONTROL
ROLL RIGHT THEN LEFT

XA+1	5.8205497	XB+1	-3.3702563	XC+1	6.5933595	XP+1	3.215366
THETAB	-2.1869954	VKT	135.00311	PHIB	0.	VYB	-1.54774
XNGE	41784.030	NPINTE	1.3116747	VC	.116586E-2	WEIGHT	16638.00
OMRMR	0.9999999	NPMEAS	99.999997				

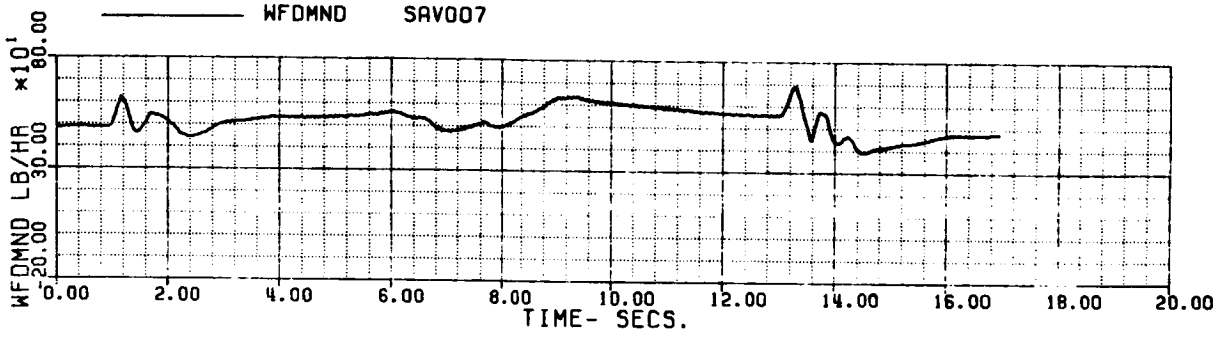

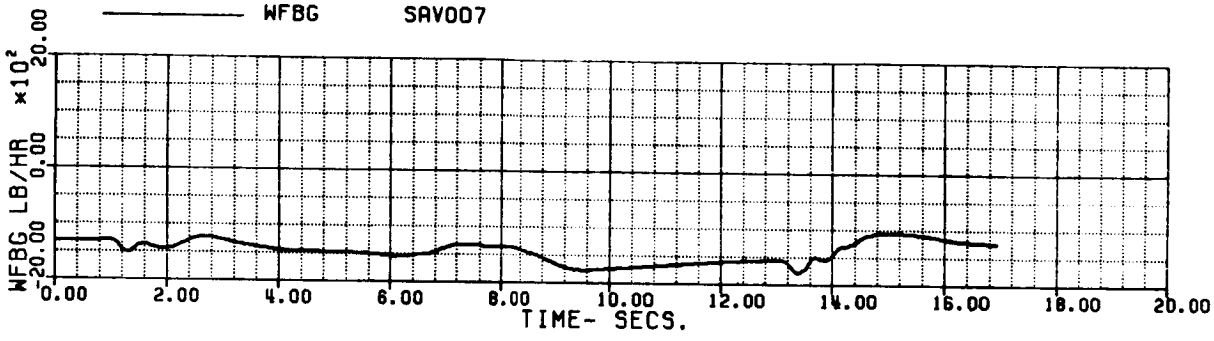

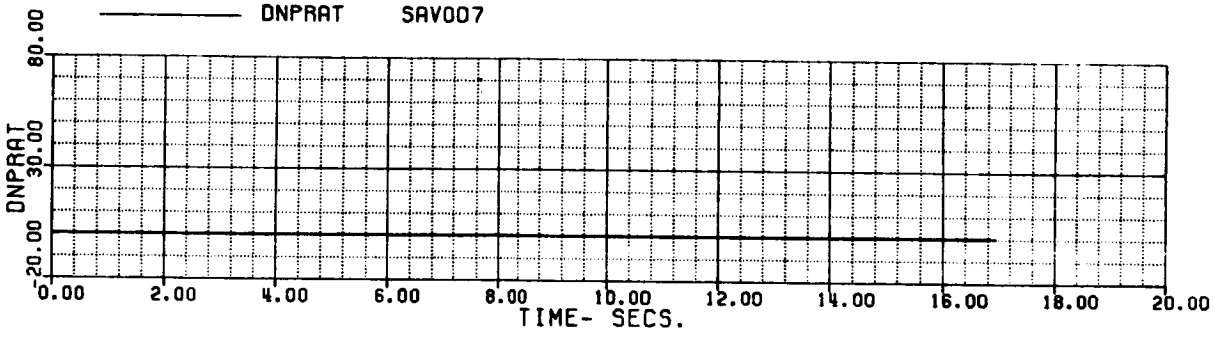

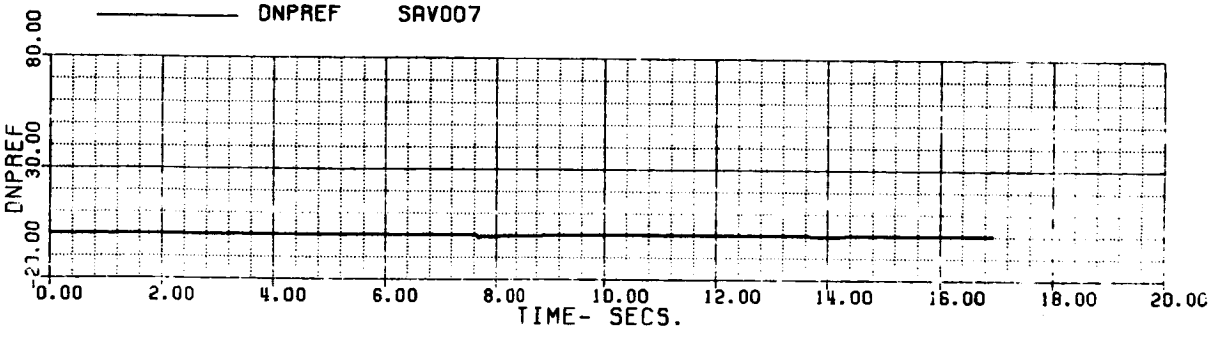

FIG 6.1.9 (j)

60A - BLACK HAWK

(12/1

FROLRE - ROLL REVERSAL, INTEGRATED FUEL CONTROL
ROLL RIGHT THEN LEFT

XA+1	5.8205497	XB+1	-3.3702563	XC+1	6.5933595	XP+1	3.21536
THETAB	-2.1869954	VKT	135.00311	PHIB	0.	VYB	-1.5477
XNGE	41784.030	NPINTE	1.3116747	VC	.116586E-2	WEIGHT	16638.0
OMRMR	0.9999999	NPMEAS	99.999997				

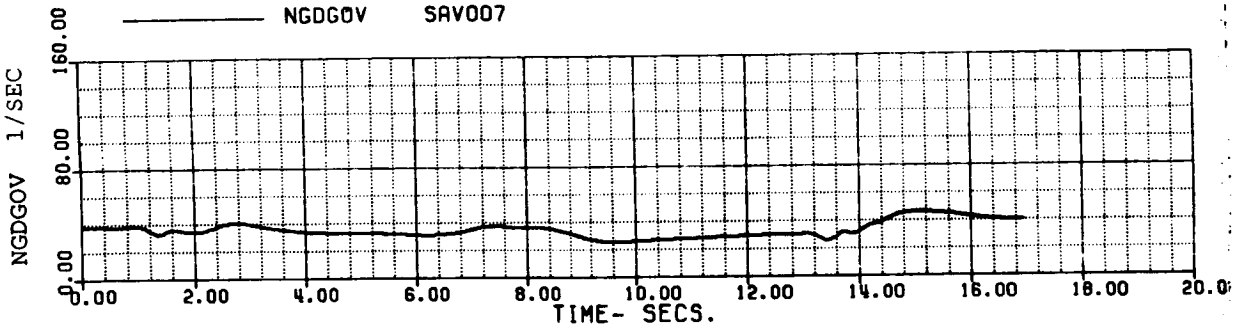

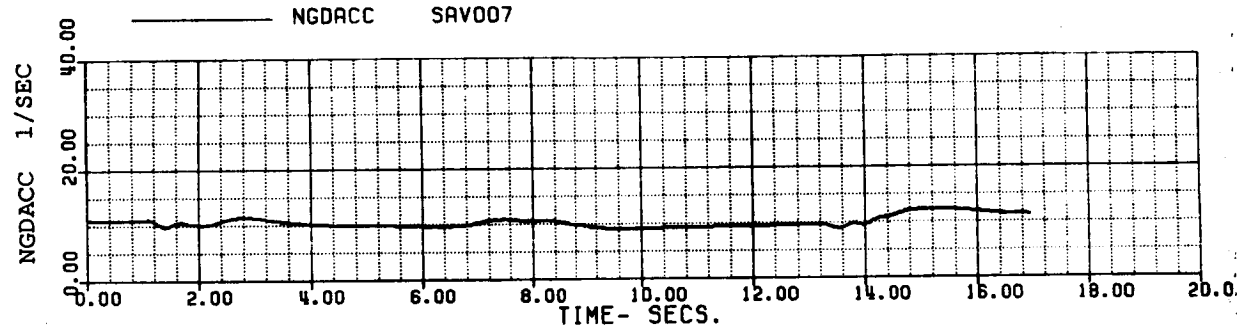

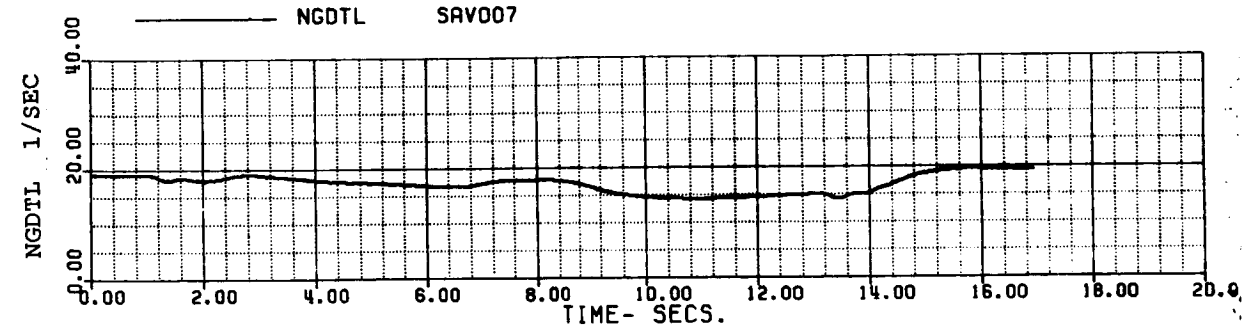

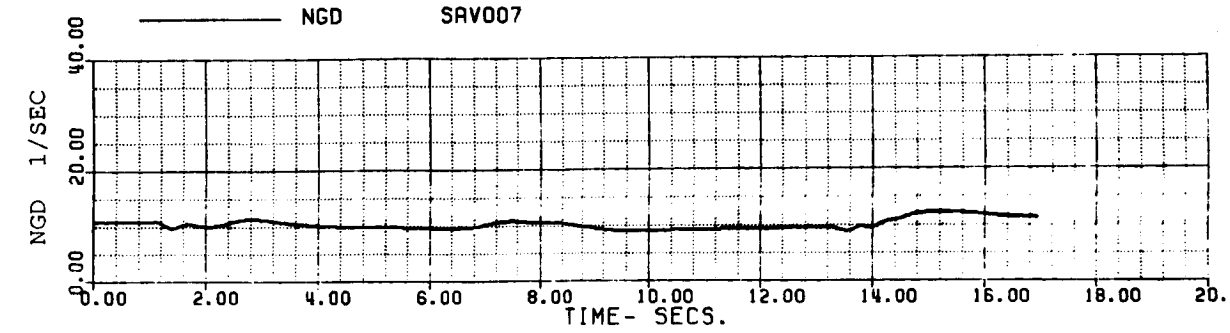

FIG 6.1.9 (k)

60A - BLACK HAWK (1/12)

FROLRE - ROLL REVERSAL, INTEGRATED FUEL CONTROL
ROLL LEFT THEN RIGHT

XA+1	5.8194404	XB+1	-3.3697050	XC+1	6.5937374	XP+1	3.2156306
THETAB	-2.1831187	VKT	135.00324	PHIB	0.	VYB	-1.5407037
XNGE	41781.880	NPINTE	1.3166568	VC	.550746E-3	WEIGHT	16638.000
OMRMR	0.9999999	NPMEAS	99.999994				

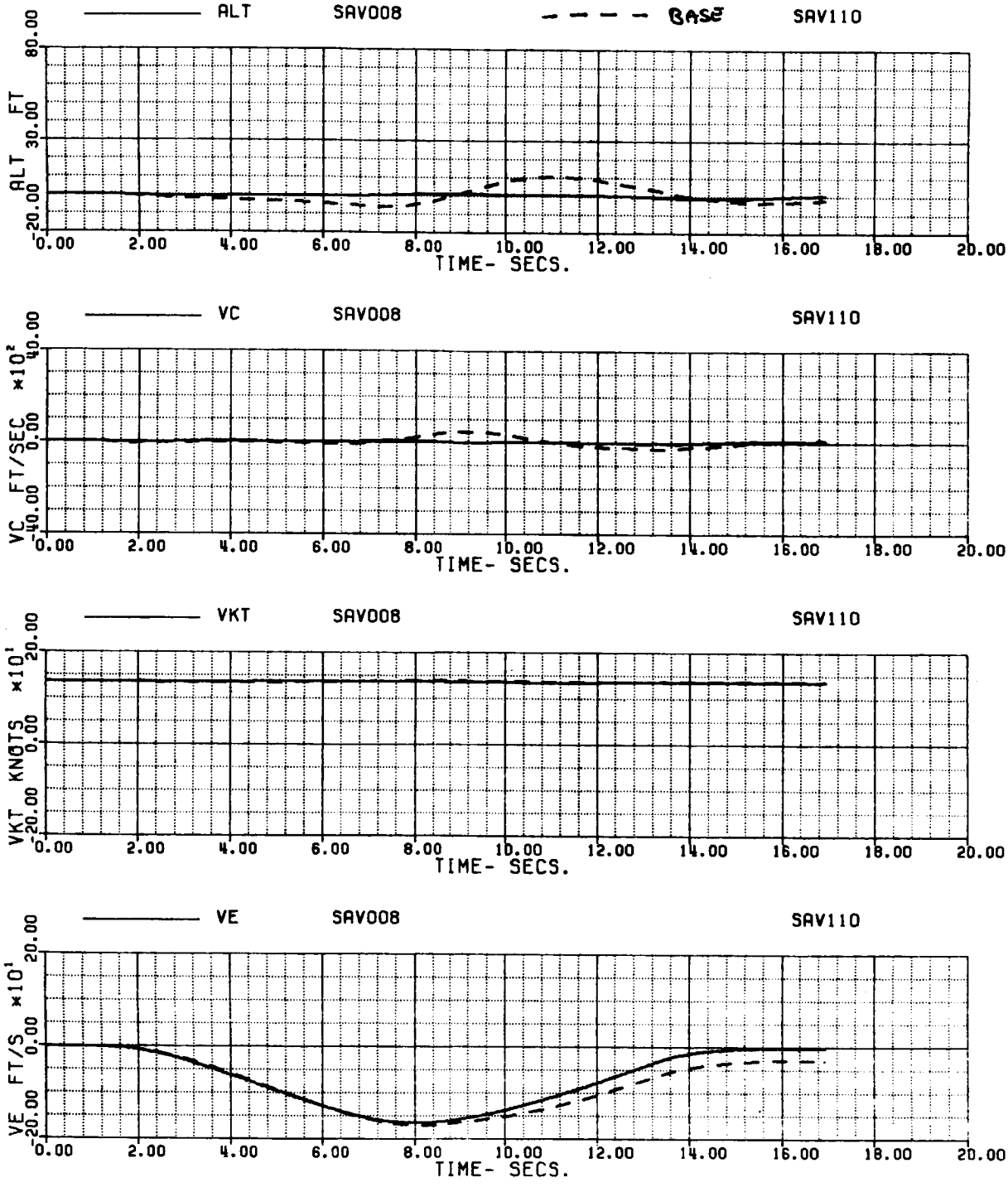

SIMULATED ROLL REVERSAL (LEFT-RIGHT-LEFT)

FIG 6.1.10 (a)

60A - BLACK HAWK (2/12)

FRQLRE - ROLL REVERSAL, INTEGRATED FUEL CONTROL
ROLL LEFT THEN RIGHT

XA+1	5.8194404	XB+1	-3.3697050	XC+1	6.5937374	XP+1	3.2156306
THETAB	-2.1831187	VKT	135.00324	PHIB	0.	YTB	-1.5407037
XNGE	41781.880	NPINTE	1.3166568	VC	.550746E-3	WEIGHT	16638.000
OMRMR	0.9999999	NPMEAS	99.999994				

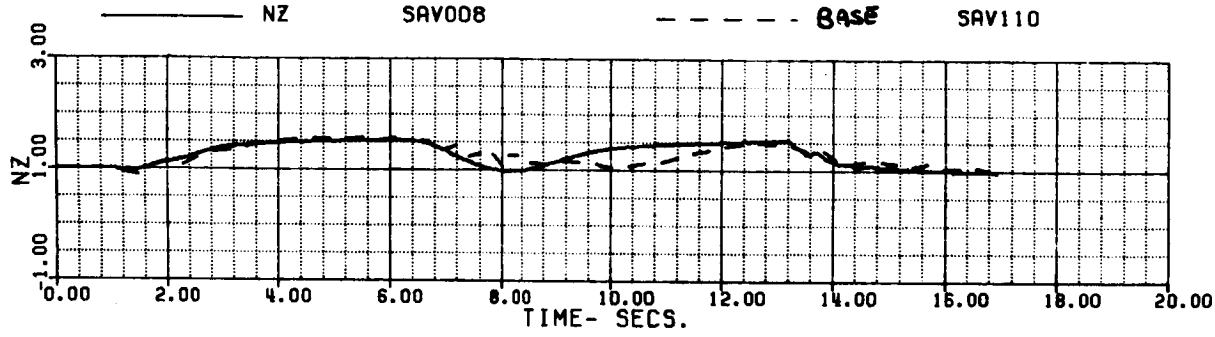

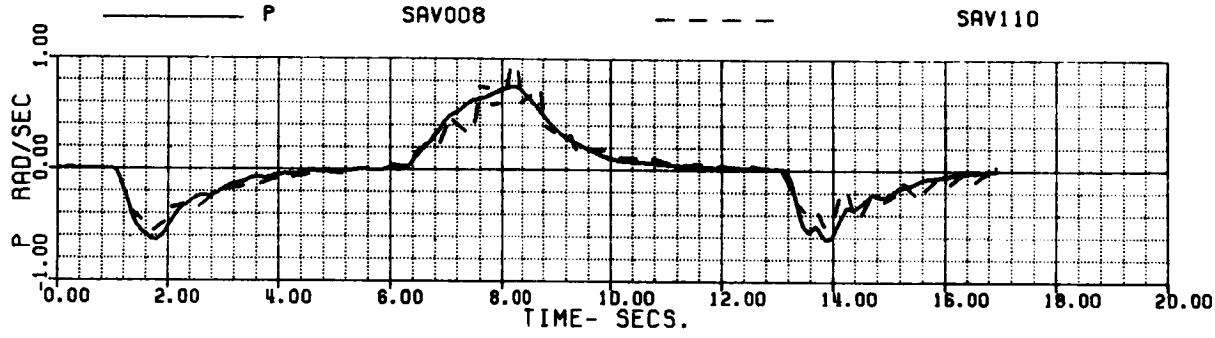

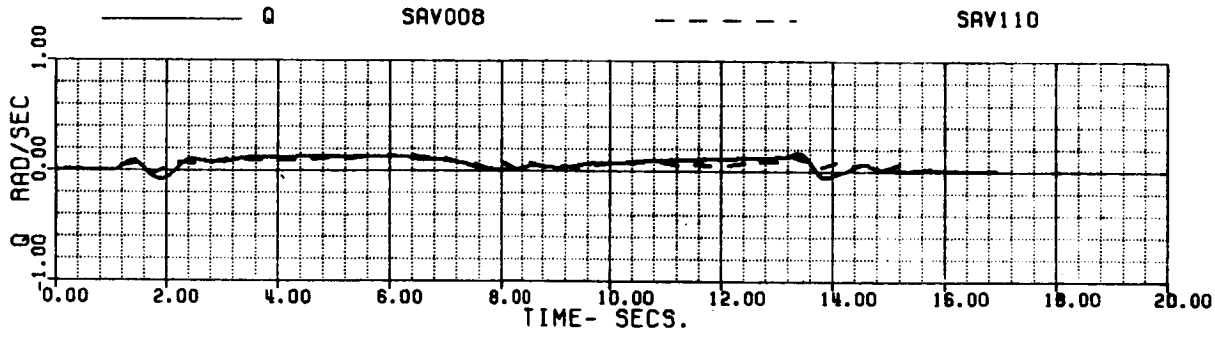

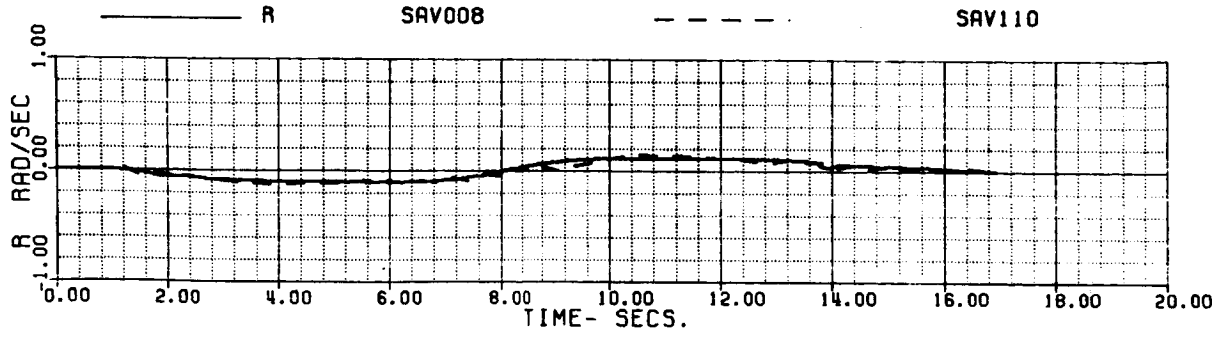

FIG 6.1.10 (b)

60A - BLACK HAWK (3/12)

FROLRE - ROLL REVERSAL, INTEGRATED FUEL CONTROL
ROLL LEFT THEN RIGHT

XA+1	5.8194404	XB+1	-3.3697050	XC+1	6.5937374	XP+1	3.2156306
THETAB	-2.1831187	VKT	135.00324	PHIB	0.	VYB	-1.5407037
XNGE	41781.880	NPINTE	1.3166568	VC	.550746E-3	WEIGHT	16638.000
OMAMR	0.9999999	NPMEAS	99.999994				

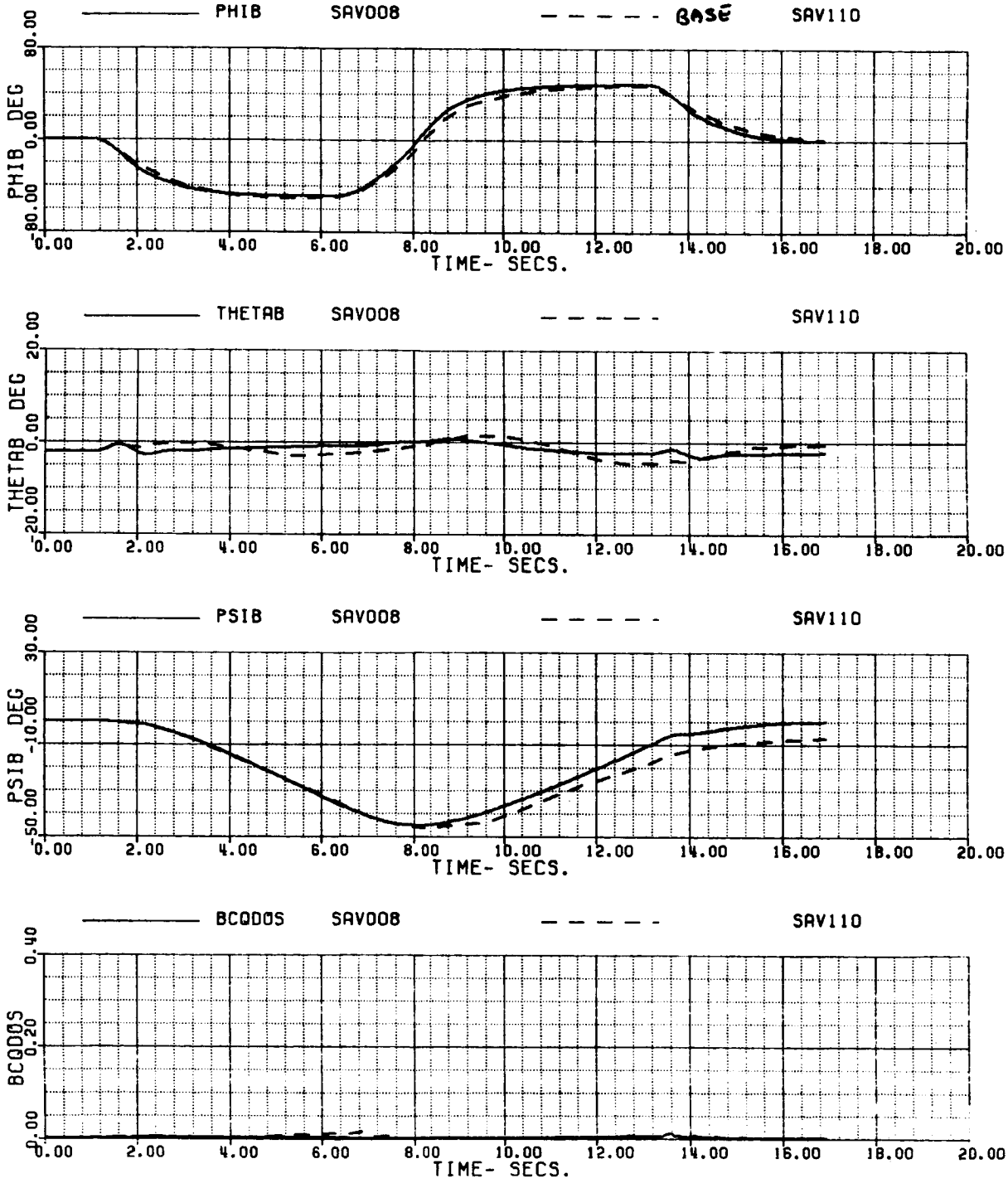

FIG 6.1.10 (c)

60A - BLACK HAWK (4/12)

FROLRE - ROLL REVERSAL, INTEGRATED FUEL CONTROL
ROLL LEFT THEN RIGHT

XA+1	5.8194404	XB+1	-3.3697050	XC+1	6.5937374	XP+1	3.2156306
THETAB	-2.1831187	VKT	135.00324	PHIB	0.	VYB	-1.5407037
XNGE	41781.880	NPINTE	1.3166568	VC	.550746E-3	WEIGHT	16638.000
OMRMR	0.9999999	NPMEAS	99.999994				

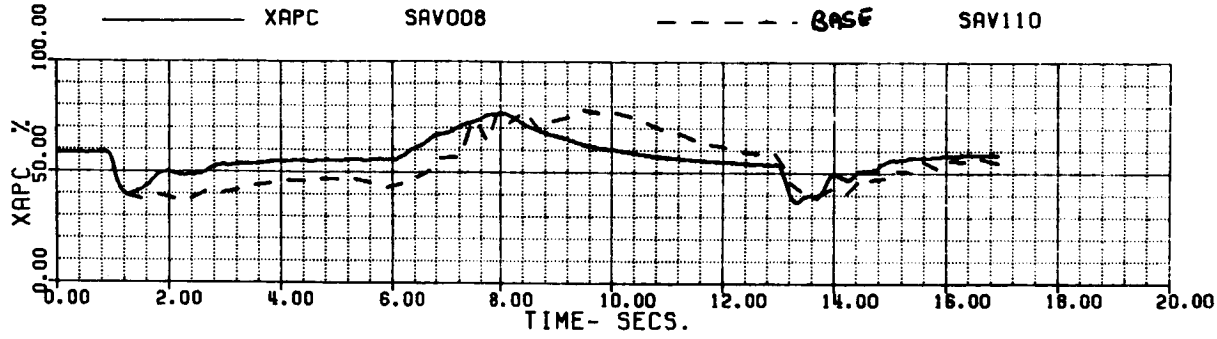

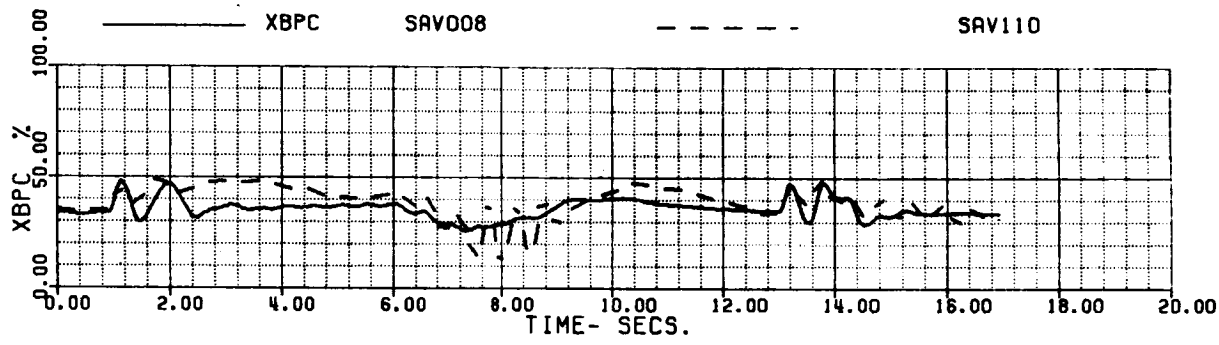

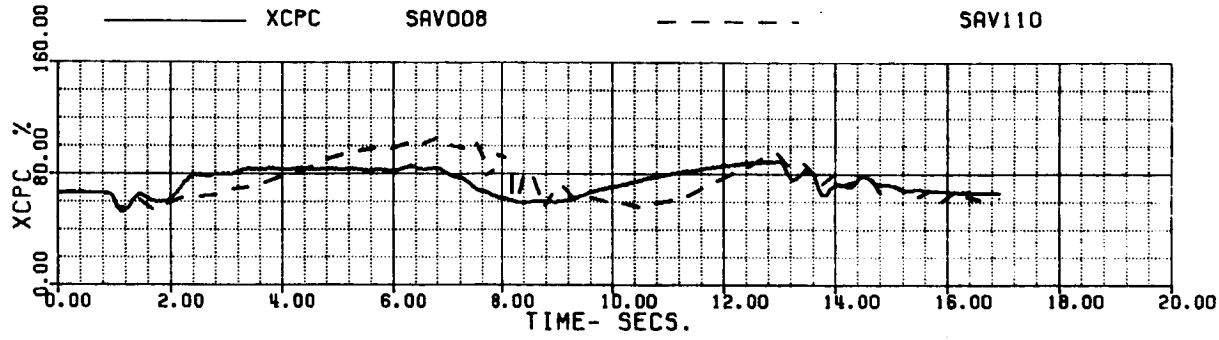

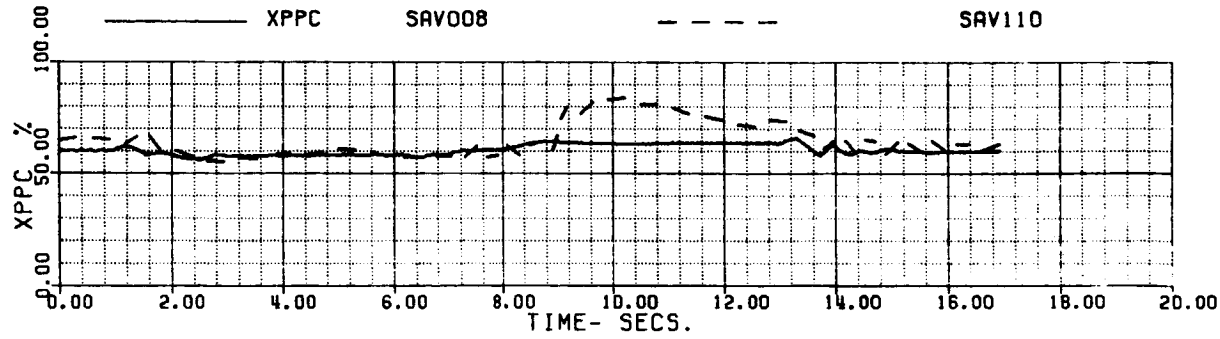

FIG 6.1.10 (d)

60A - BLACK HAWK (5/12)

FAILRE - ROLL REVERSAL, INTEGRATED FUEL CONTROL
ROLL LEFT THEN RIGHT

XA+1	5.8194404	XB+1	-3.3697050	XC+1	6.5937374	XP+1	3.2156306
THETAB	-2.1831187	VKT	135.00324	PHIB	0.	YTB	-1.5407037
XNGE	41781.880	NPINTE	1.3166568	VC	.550746E-3	WEIGHT	16638.000
OMRMR	0.9999999	NPMEAS	99.999994				

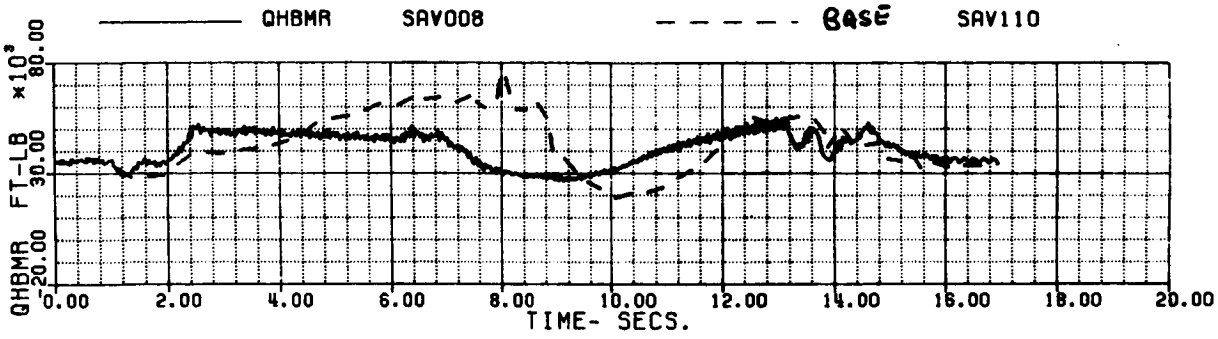

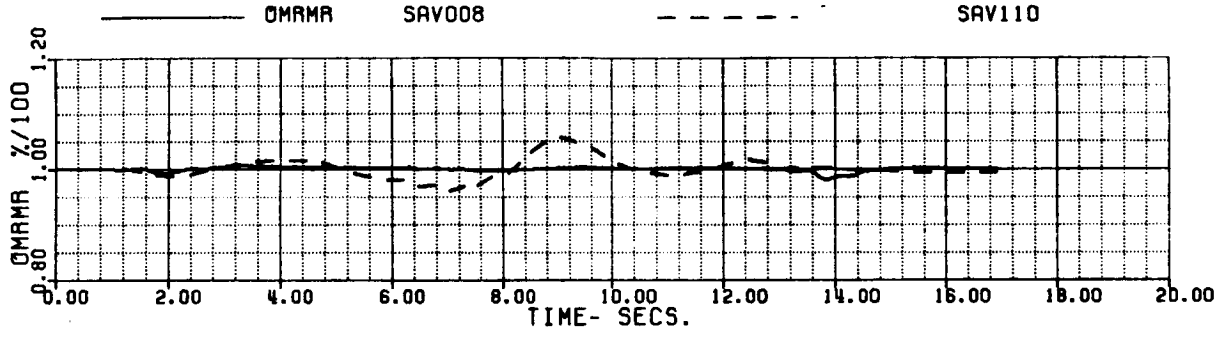

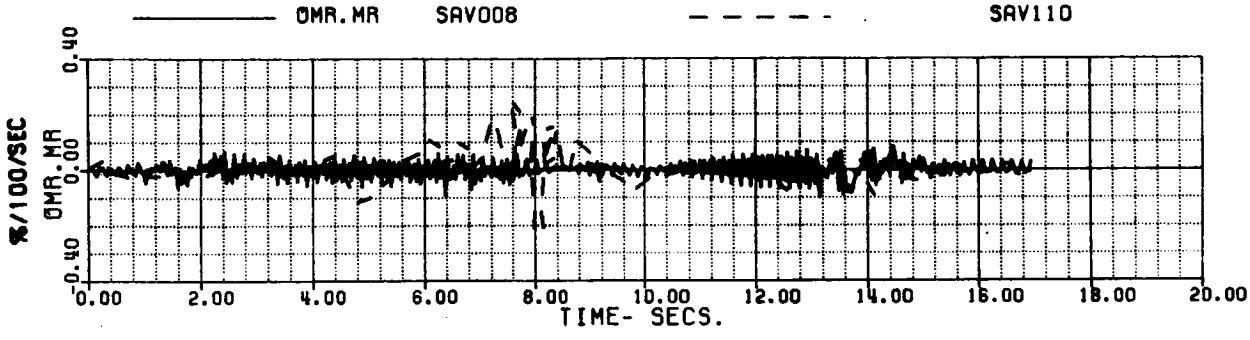

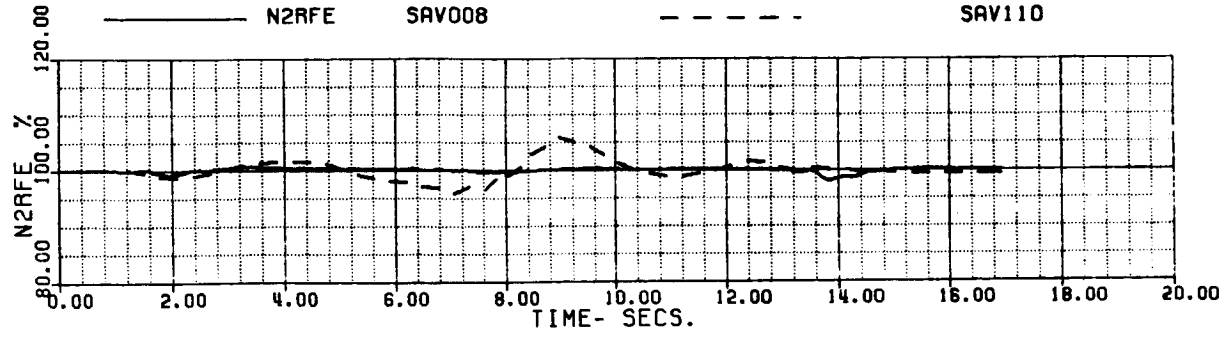

FIG 6.1.10 (e)

60A - BLACK HAWK

(6/12)

FROLRE - ROLL REVERSAL, INTEGRATED FUEL CONTROL
ROLL LEFT THEN RIGHT

XA+1	5.8194404	XB+1	-3.3697050	XC+1	6.5937374	XP+1	3.2156306
THETAB	-2.1831187	VKT	135.00324	PHIB	0.	VYB	-1.5407037
XNGE	41781.880	NPINTE	1.3166568	VC	.550746E-3	WEIGHT	16638.000
OMRMR	0.9999999	NPMEAS	99.999994				

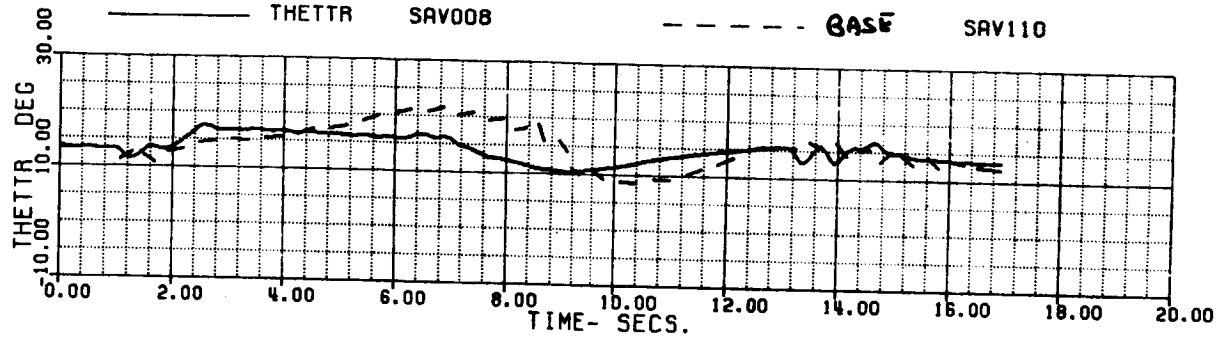

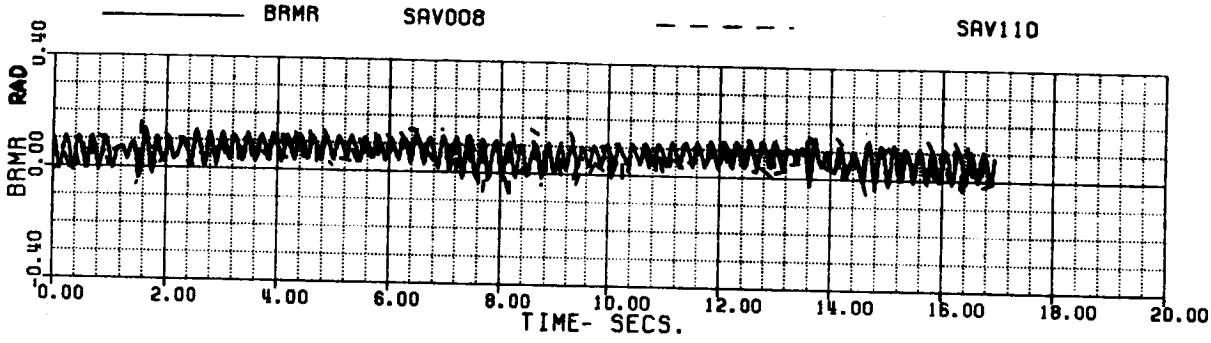

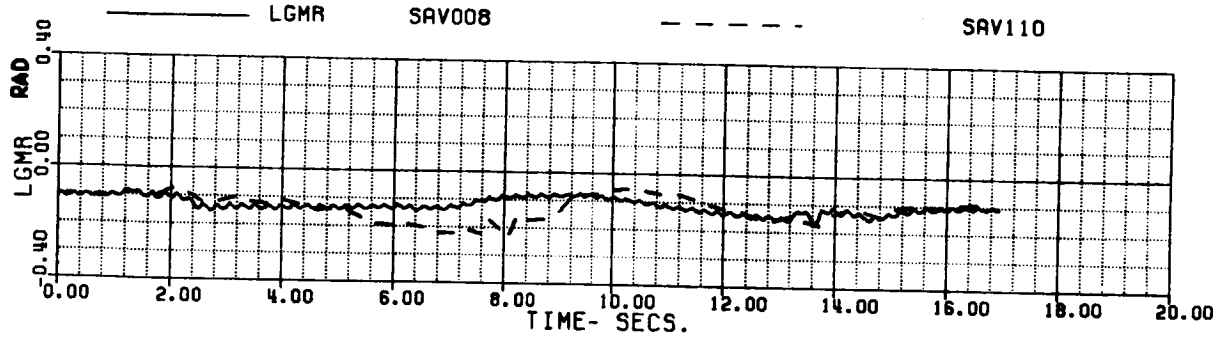

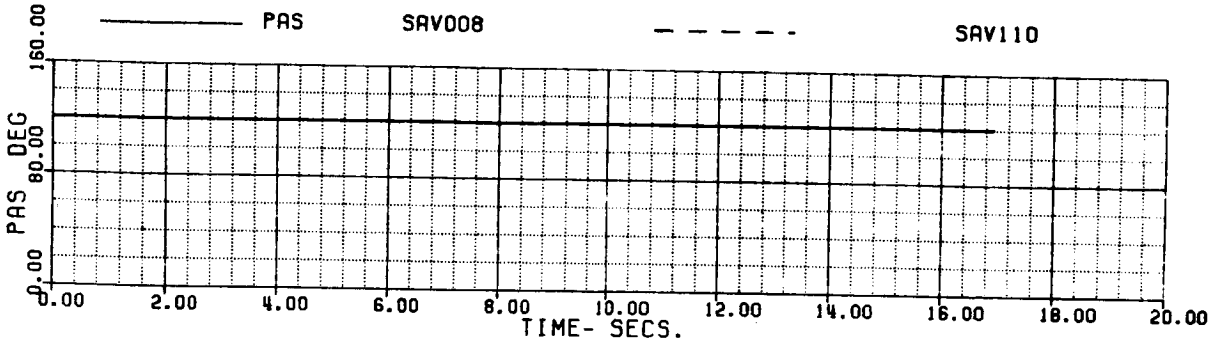

FIG 6.1.10 (f)

60A - BLACK HAWK

09:33 (7/12)

FROLRE - ROLL REVERSAL. INTEGRATED FUEL CONTROL
ROLL LEFT THEN RIGHT

XA+1	5.8194404	XB+1	-3.3697050	XC+1	6.5937374	XP+1	3.2156306
THETAB	-2.1831187	VKT	135.00324	PHIB	0.	VYB	-1.5407037
XNGE	41781.880	NPINTE	1.3166568	VC	.550746E-3	WEIGHT	16638.000
OMAMR	0.9999999	NPMEAS	99.999994				

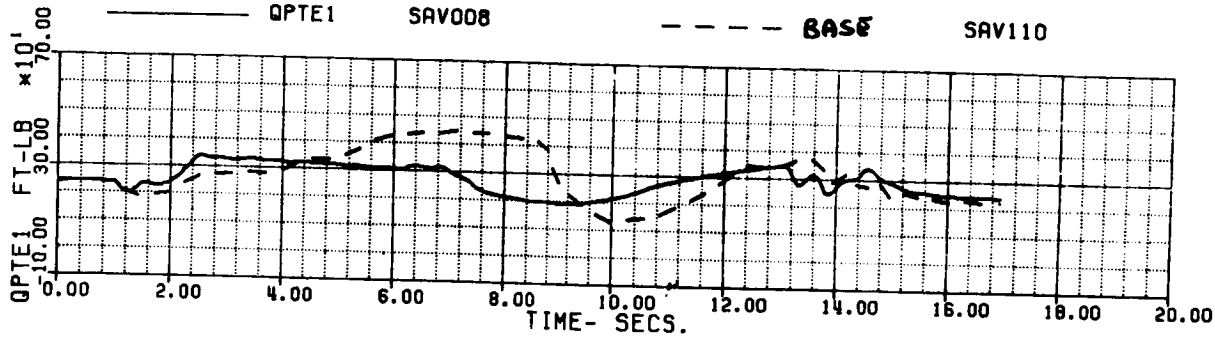

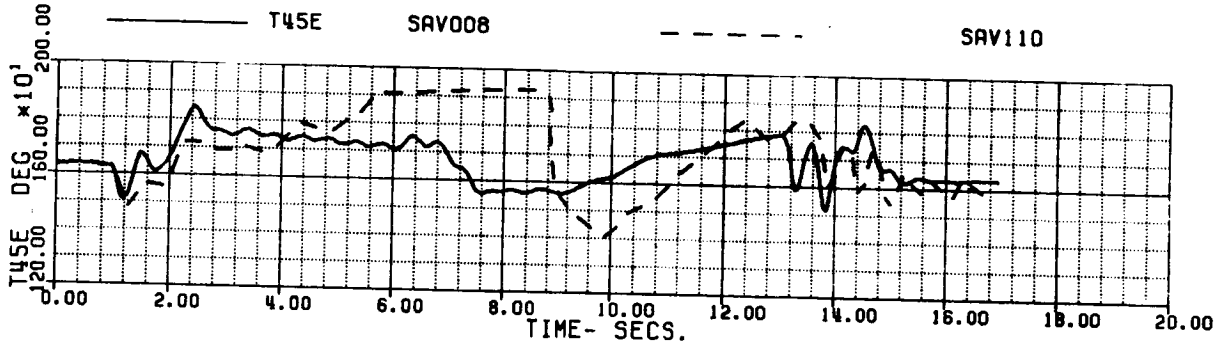

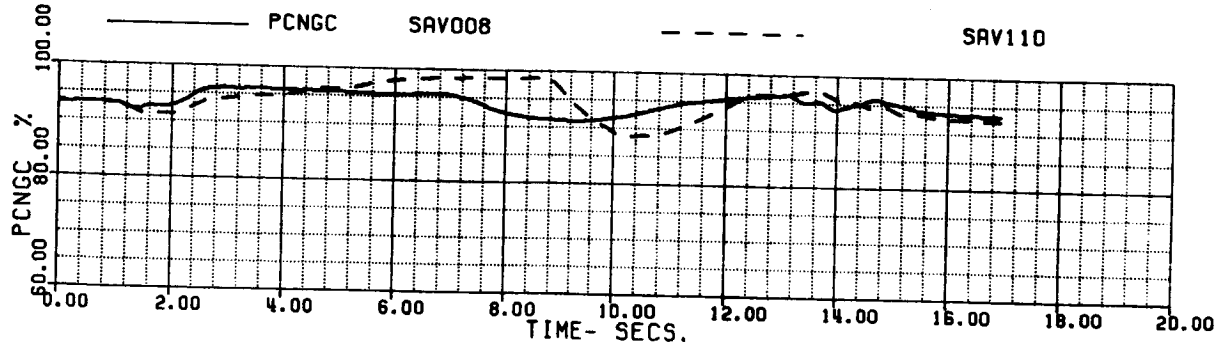

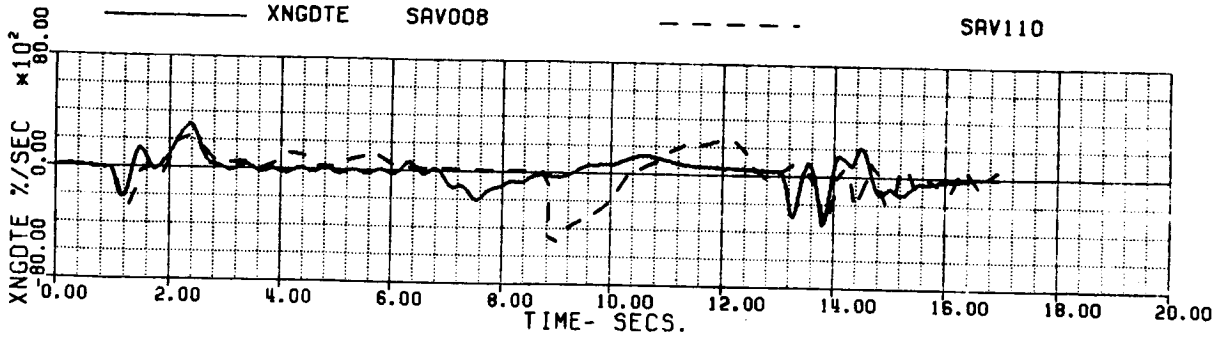

FIG 6.1.10 (g)

60A - BLACK HAWK (8/12)

FROLRE - ROLL REVERSAL, INTEGRATED FUEL CONTROL
ROLL LEFT THEN RIGHT

XA+1	5.8194404	XB+1	-3.3697050	XC+1	6.5937374	XP+1	3.2156306
THETAB	-2.1831187	VKT	135.00324	PHIB	0.	VYB	-1.5407037
XNGE	41781.880	NPINTE	1.3166568	VC	.550746E-3	WEIGHT	16638.000
OMAMR	0.9999999	NPMEAS	99.999994				

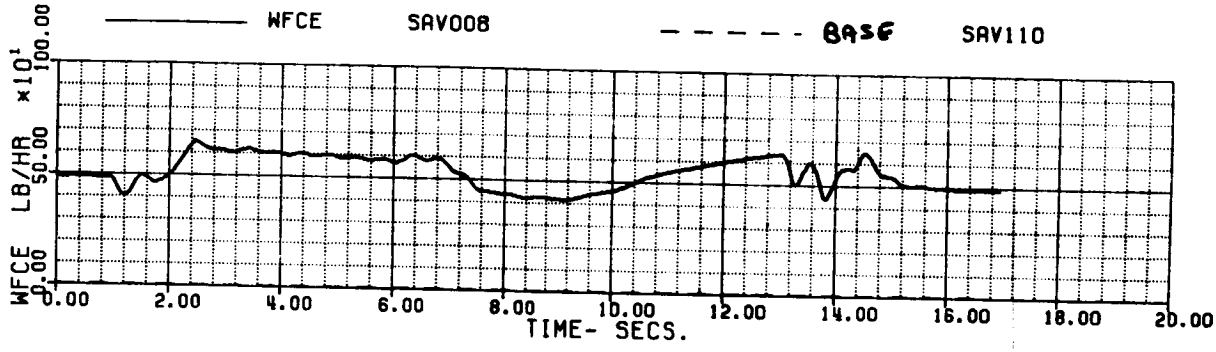

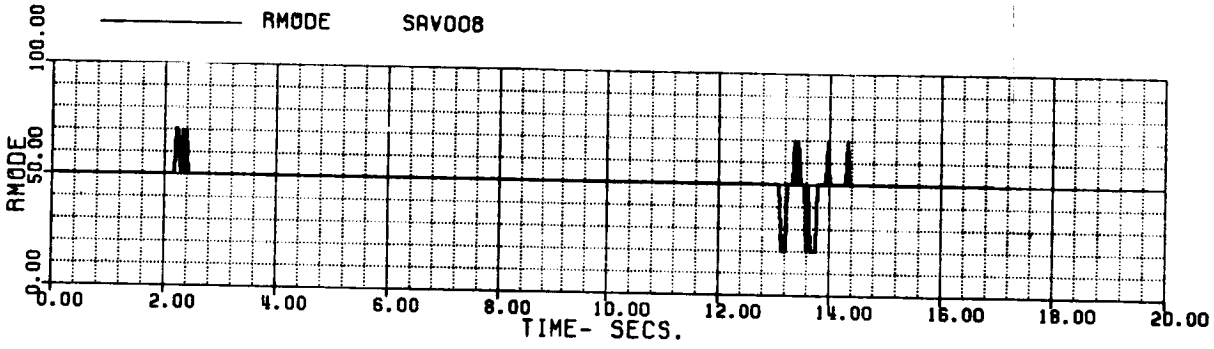

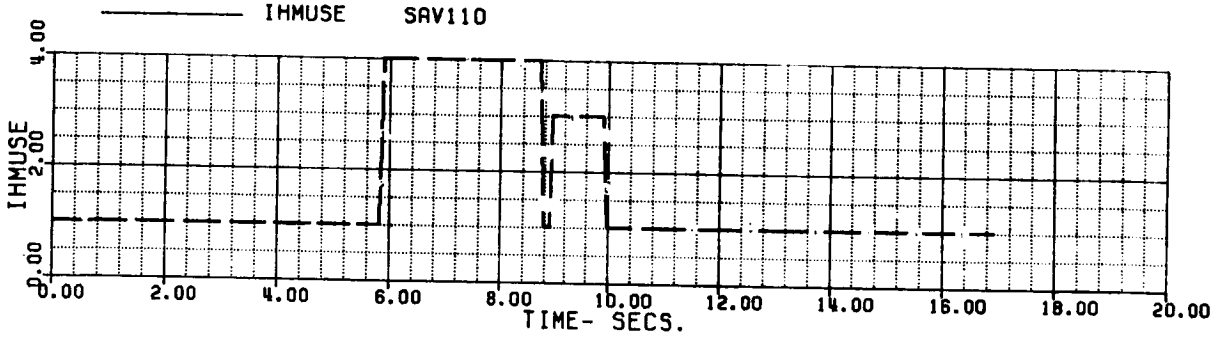

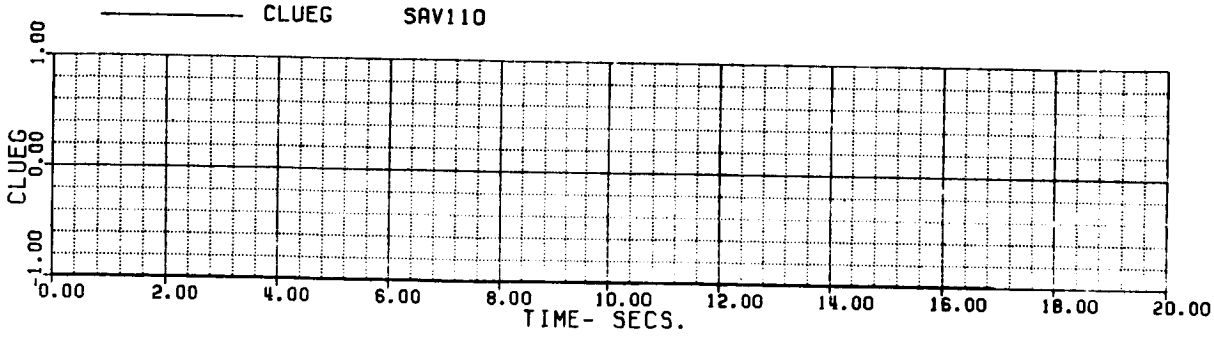

FIG 6.1.10 (h)

60A - BLACK HAWK

FROLRE - ROLL REVERSAL, INTEGRATED FUEL CONTROL
ROLL LEFT THEN RIGHT

(9/12)

XA+1	5.8194404	XB+1	-3.3697050	XC+1	6.5937374	XP+1	3.2156306
THETAB	-2.1831187	VKT	135.00324	PHIB	0.	VYB	-1.5407037
XNGE	41781.880	NPINTE	1.3166568	VC	.550746E-3	WEIGHT	16638.000
OMRMR	0.9999999	NPMEAS	99.999994				

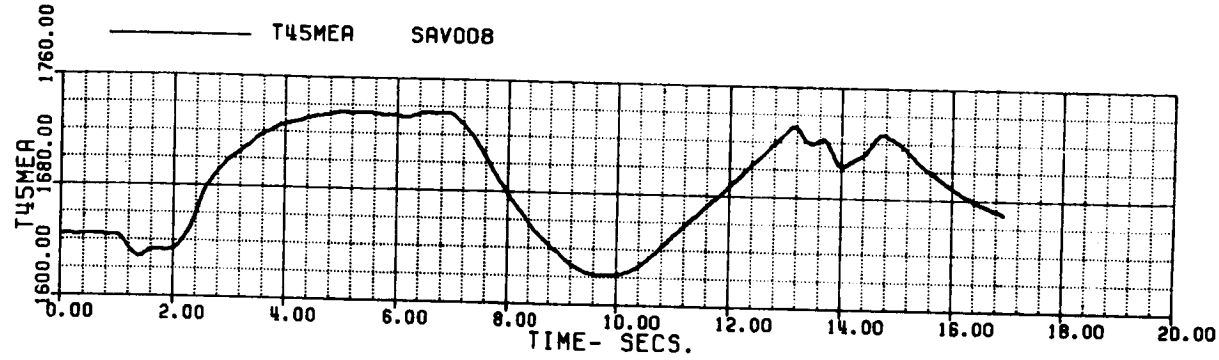

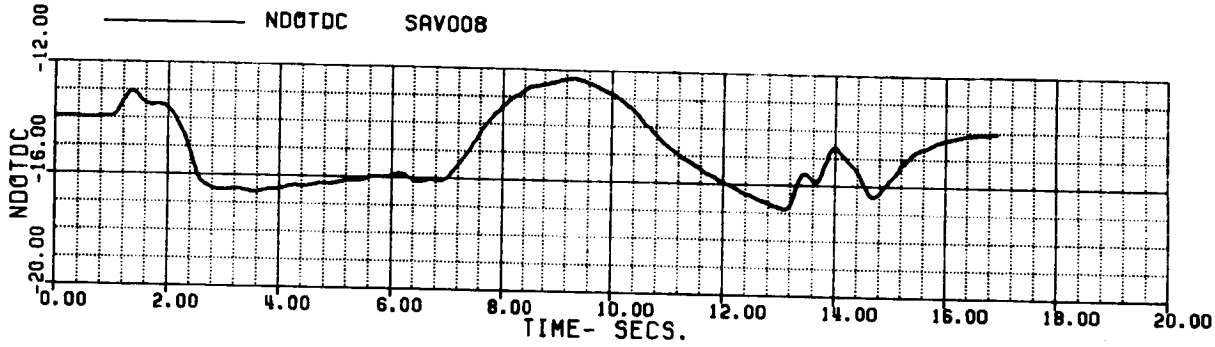

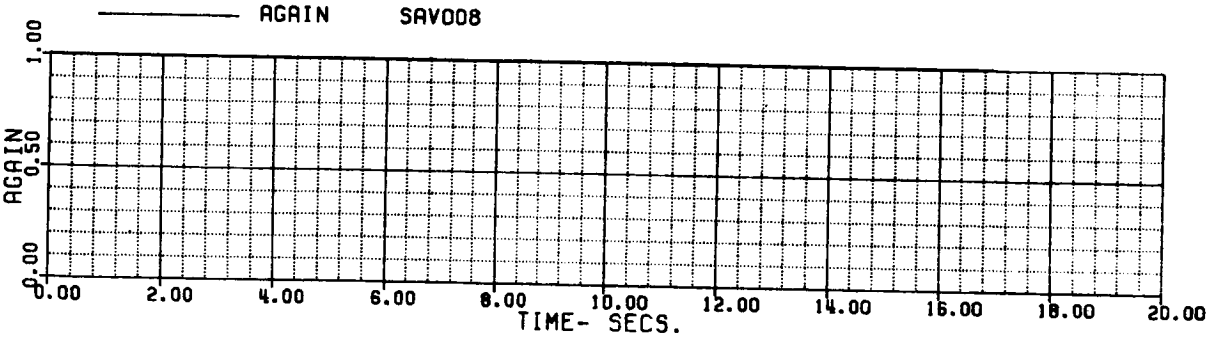

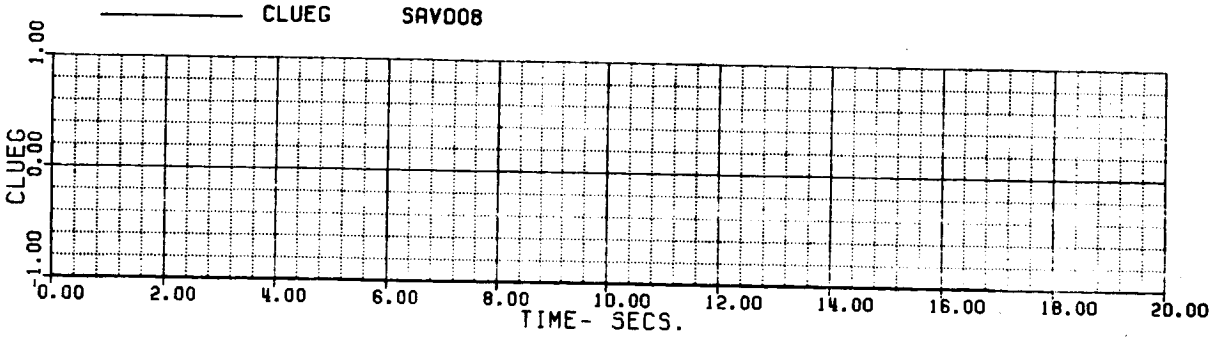

FIG 6.1.10 (i)

60A - BLACK HAWK 09:33 (11/1

FRQLRE - ROLL REVERSAL. INTEGRATED FUEL CONTROL
ROLL LEFT THEN RIGHT

XA+1	5.8194404	XB+1	-3.3697050	XC+1	6.5937374	XP+1	3.215630
THETAB	-2.1831187	VKT	135.00324	PHIB	0.	VYB	-1.54070
XNGE	41781.880	NPINTE	1.3166568	VC	.550746E-3	WEIGHT	16638.00
OMRMR	0.9999999	NPMEAS	99.999994				

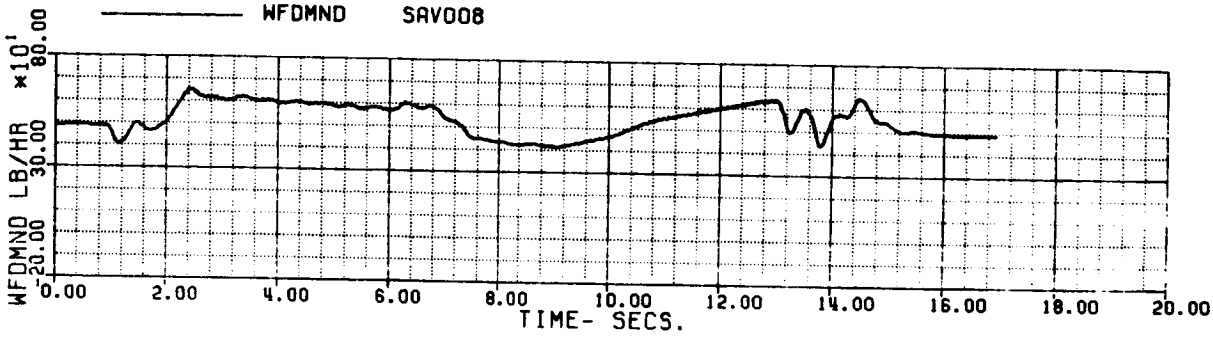

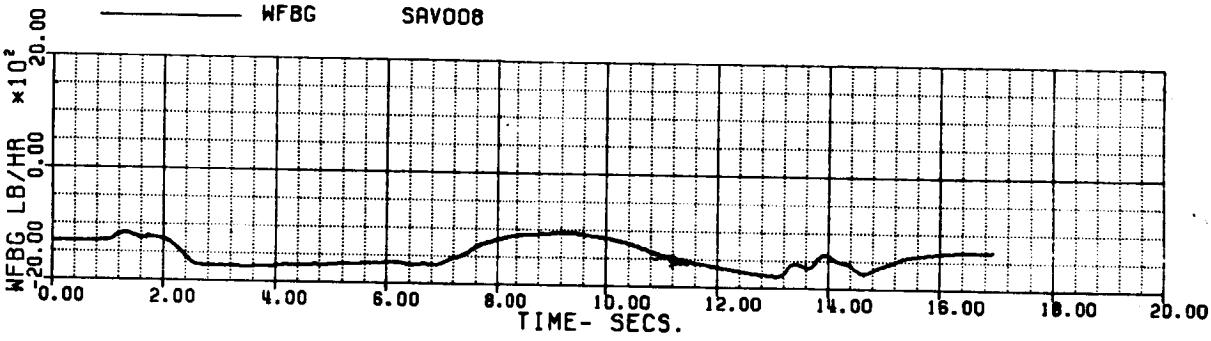

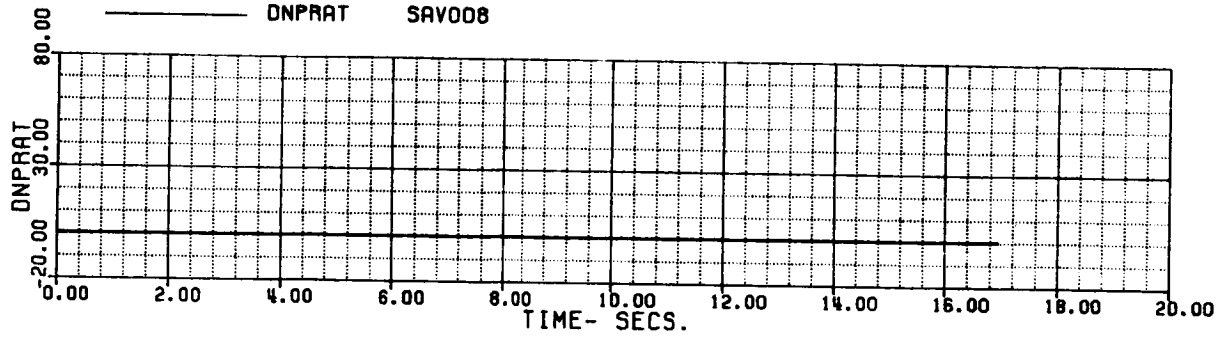

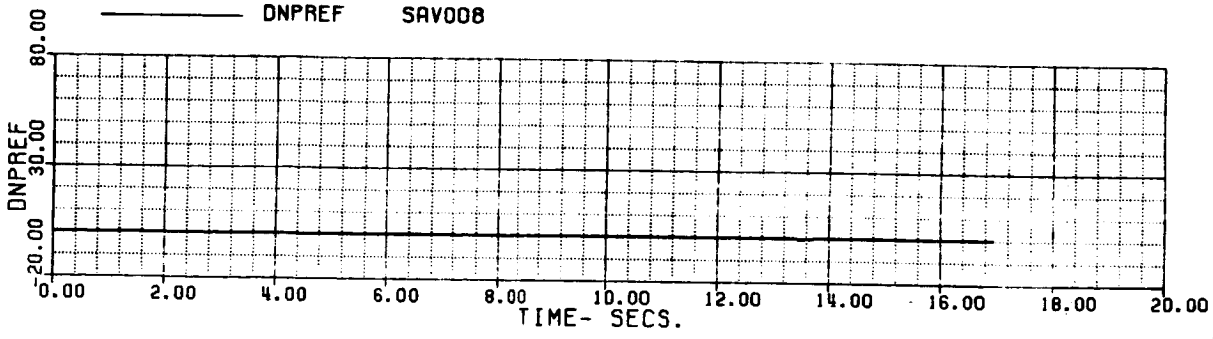

FIG 6.1.10 (j)

60A - BLACK HAWK (12/1

FROLRE - ROLL REVERSAL, INTEGRATED FUEL CONTROL
ROLL LEFT THEN RIGHT

XA+1	5.8194404	XB+1	-3.3697050	XC+1	6.5937374	XP+1	3.21563
THETAB	-2.1831187	VKT	135.00324	PHIB	0.	VYB	-1.5407
XNGE	41781.880	NPINTE	1.3166568	VC	.550746E-3	WEIGHT	16638.0
OMRMR	0.9999999	NPMEAS	99.999994				

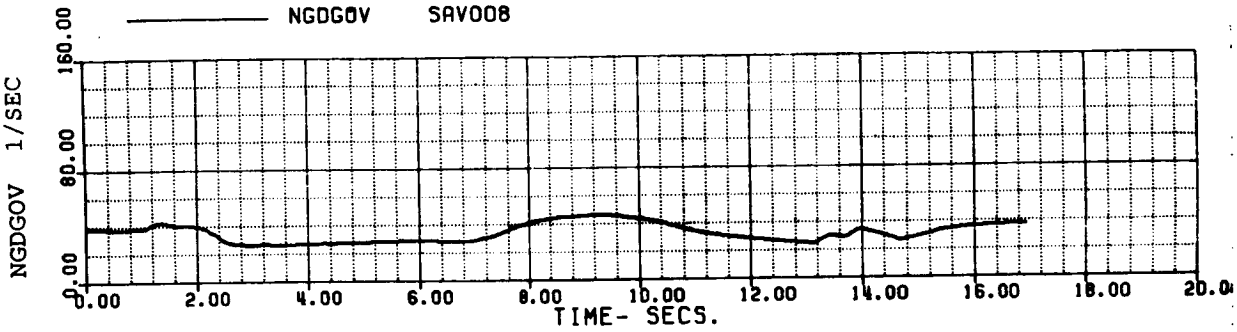

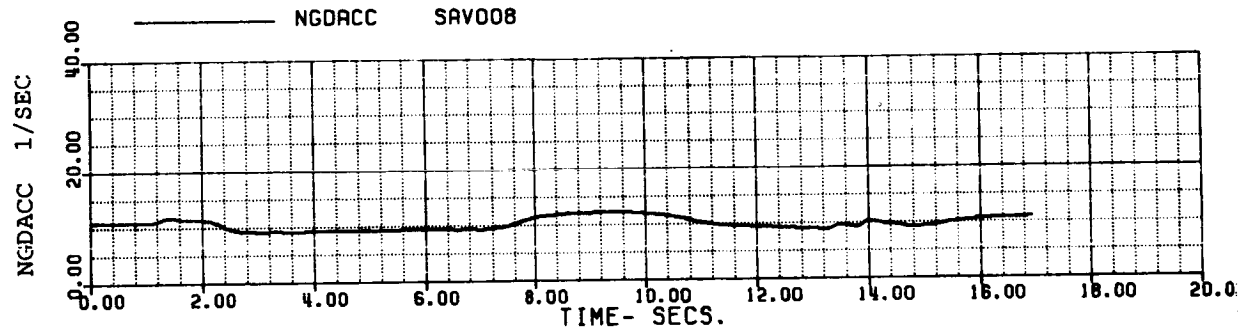

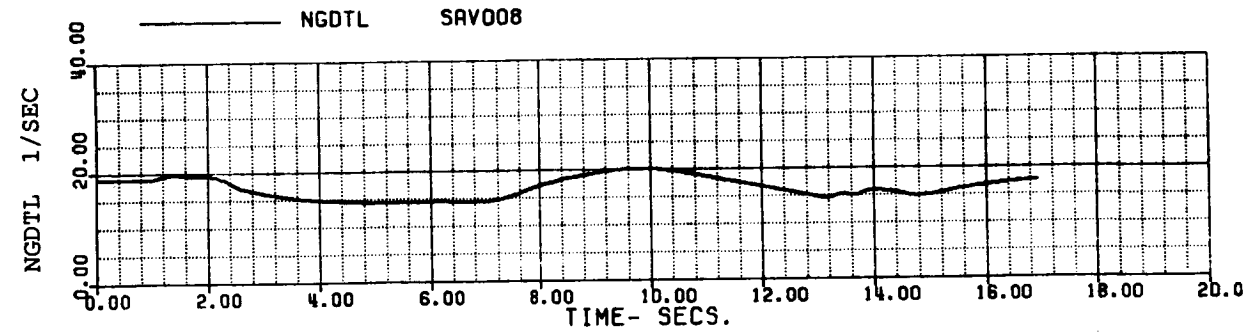

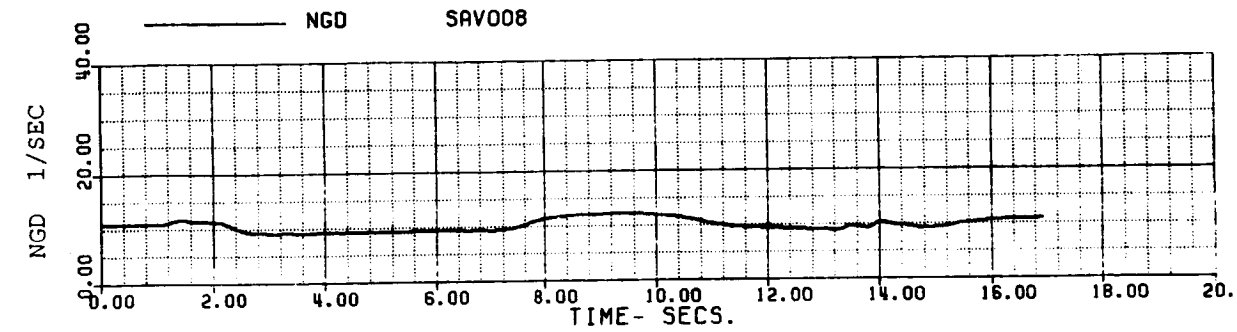

FIG 6.1.10 (k)

60A - BLACK HAWK (12/1

FROLRE - ROLL REVERSAL, INTEGRATED FUEL CONTROL
ROLL LEFT THEN RIGHT

XA+1	5.8194404	XB+1	-3.3697050	XC+1	6.5937374	XP+1	3.21563
THETAB	-2.1831187	VKT	135.00324	PHIB	0.	VYB	-1.5407
XNGE	41781.880	NPINTE	1.3166568	VC	.550746E-3	WEIGHT	16638.0
OMRMR	0.9999999	NPMEAS	99.999994				

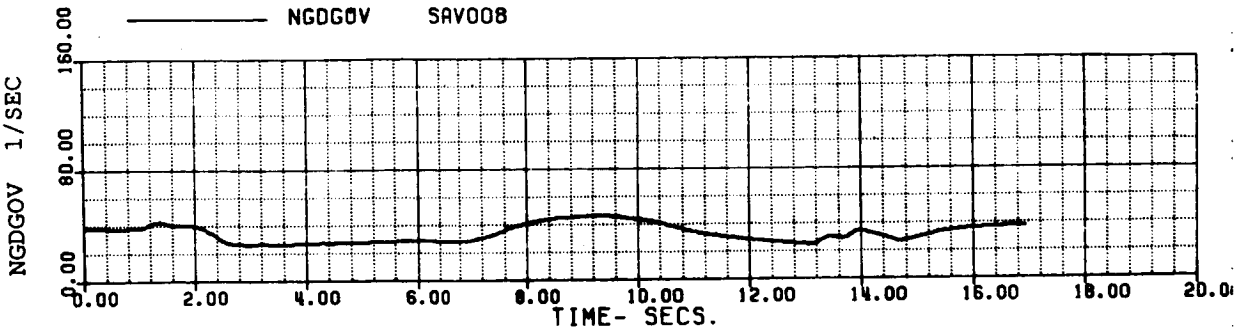

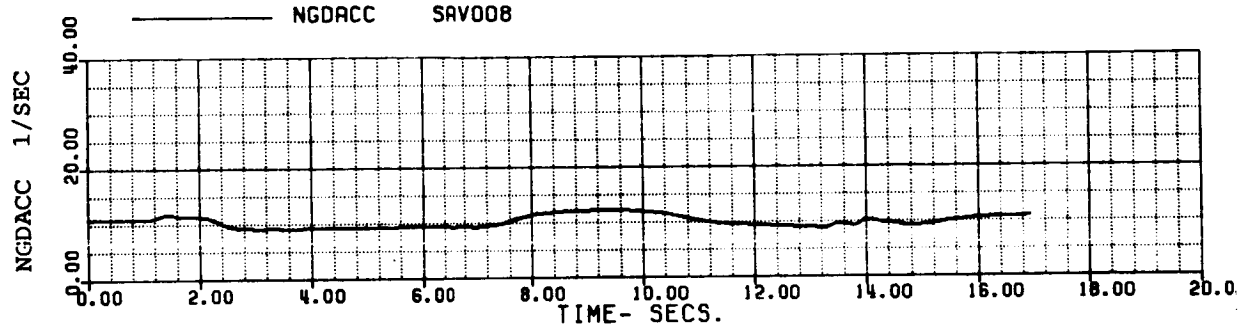

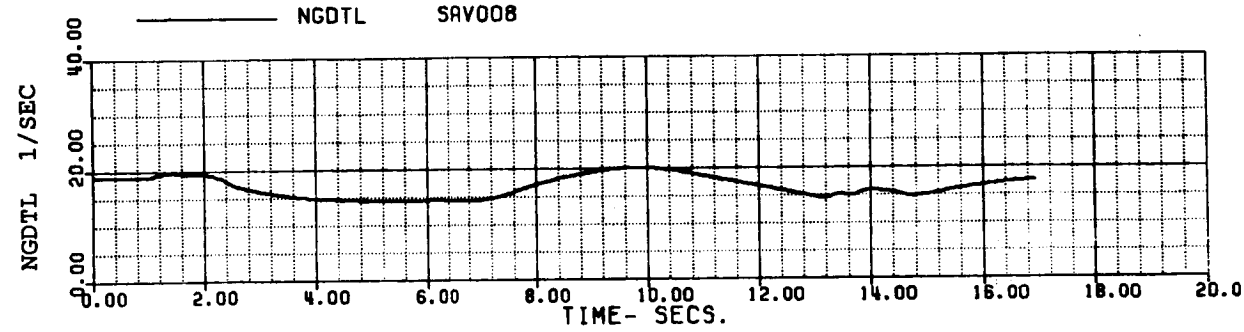

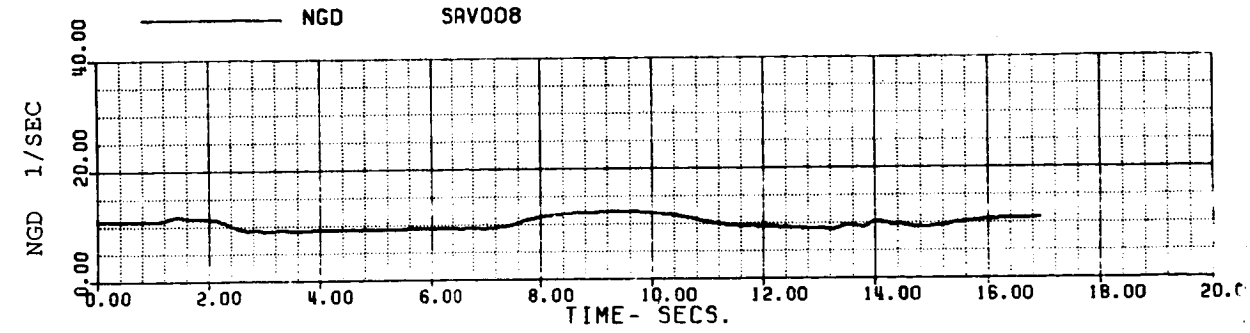

FIG 6.1.10 (k)